frontiers | Research Topics

Insights in plant-pathogen interactions 2023

Edited by
Brigitte Mauch-Mani and Choong-Min Ryu

Published in
Frontiers in Plant Science

ISSN 1664-8714
ISBN 978-2-8325-5987-1
DOI 10.3389/978-2-8325-5987-1

About Frontiers

Frontiers is more than just an open access publisher of scholarly articles: it is a pioneering approach to the world of academia, radically improving the way scholarly research is managed. The grand vision of Frontiers is a world where all people have an equal opportunity to seek, share and generate knowledge. Frontiers provides immediate and permanent online open access to all its publications, but this alone is not enough to realize our grand goals.

Frontiers journal series

The Frontiers journal series is a multi-tier and interdisciplinary set of open-access, online journals, promising a paradigm shift from the current review, selection and dissemination processes in academic publishing. All Frontiers journals are driven by researchers for researchers; therefore, they constitute a service to the scholarly community. At the same time, the *Frontiers journal series* operates on a revolutionary invention, the tiered publishing system, initially addressing specific communities of scholars, and gradually climbing up to broader public understanding, thus serving the interests of the lay society, too.

Dedication to quality

Each Frontiers article is a landmark of the highest quality, thanks to genuinely collaborative interactions between authors and review editors, who include some of the world's best academicians. Research must be certified by peers before entering a stream of knowledge that may eventually reach the public - and shape society; therefore, Frontiers only applies the most rigorous and unbiased reviews. Frontiers revolutionizes research publishing by freely delivering the most outstanding research, evaluated with no bias from both the academic and social point of view. By applying the most advanced information technologies, Frontiers is catapulting scholarly publishing into a new generation.

What are Frontiers Research Topics?

Frontiers Research Topics are very popular trademarks of the *Frontiers journals series*: they are collections of at least ten articles, all centered on a particular subject. With their unique mix of varied contributions from Original Research to Review Articles, Frontiers Research Topics unify the most influential researchers, the latest key findings and historical advances in a hot research area.

Find out more on how to host your own Frontiers Research Topic or contribute to one as an author by contacting the Frontiers editorial office: frontiersin.org/about/contact

Insights in plant-pathogen interactions: 2023

Topic editors

Brigitte Mauch-Mani — Université de Neuchâtel, Switzerland

Choong-Min Ryu — Korea Research Institute of Bioscience and Biotechnology (KRIBB), Republic of Korea

Citation

Mauch-Mani, B., Ryu, C.-M., eds. (2025). *Insights in plant-pathogen interactions: 2023*. Lausanne: Frontiers Media SA. doi: 10.3389/978-2-8325-5987-1

Table of contents

frontiers | Frontiers in Plant Science

TYPE Editorial
PUBLISHED 28 January 2025
DOI 10.3389/fpls.2025.1547600

OPEN ACCESS

EDITED AND REVIEWED BY
Chun-Ming Liu,
Peking University, China

*CORRESPONDENCE
Choong-Min Ryu
cmryu@kribb.re.kr

RECEIVED 18 December 2024
ACCEPTED 13 January 2025
PUBLISHED 28 January 2025

CITATION
Ryu C-M and Mauch-Mani B (2025) Editorial: Insights in plant-pathogen interactions: 2023. *Front. Plant Sci.* 16:1547600. doi: 10.3389/fpls.2025.1547600

Editorial: Insights in plant-pathogen interactions: 2023

Choong-Min Ryu[1,2]* and Brigitte Mauch-Mani[3]

[1]Infectious Disease Research Center, Korea Research Institute of Bioscience and Biotechnology (KRIBB), Daejeon, Republic of Korea, [2]Department of Biosystems and Bioengineering, KRIBB School, University of Science and Technology, Daejeon, Republic of Korea, [3]Department of Biology, Université de Neuchâtel, Neuchâtel, Switzerland

KEYWORDS

plant pathology, pathogen, defense signaling, resistance, plant immunity

Editorial on the Research Topic
Insights in plant-pathogen interactions: 2023

Introduction

We are now well into the second decade of the 21st Century, and, especially in recent years, the achievements made by scientists have been exceptional, leading to major advancements in the fast-growing field of plant science. To reflect this development, a Research Topics highlighting the latest advancements in this research field, with articles by members of the accomplished editorial board of Frontiers in Plant Science, section Plant-Pathogen Interactions, was initiated. This Research Topic of particular relevance was led by the two Specialty Chief Editors of the Plant-Pathogen Interactions section. It focusses on new insights, novel developments, current challenges, latest discoveries, recent advances, and future perspectives in the field of Plant-Pathogen Interactions. This Research Topic will inspire, inform, and provide direction and guidance to researchers in the field.

What are the causes of plant diseases?

In the field of plant-pathogen interactions, the study on virulence and pathogenicity of microbial pathogens has always been of special interest. Not surprisingly, in this Research Topic too, many of the submitted papers focused on this area addressing diseases caused by oomycetes, fungi, bacteria and viruses.

Deng et al., reported on a new virulence factor, the cell wall degrading enzyme pectinesterase (PE) secreted by *Phytophthora infestans*, the well-known Oomycete that caused the Irish famine I the mid 19th century. PE activity and gene expression were shown to be positively correlated to the increased pathogenicity of *P. infestans* on potato.

Several reports focused on how fungi cause diseases on their hosts. The grapevine trunk disease, Botryosphaeria dieback, is the cause of large economic losses in France for lack of effective treatments. Moret et al. demonstrated that members of the *Botrysphaeriaceae*

family present in the vascular system in the basal internodes of stems in grapevine impact on the physiology and development of xylem and phloem of basal stem internodes resulting in an obstruction of the sieve plates by callose and symptoms such as leaf drop and premature plant death.

Colletotrichum viniferum, the causal pathogen of grape ripe rot and leaf spot, also has an important impact on grape production. Dou et al. evaluated the differences between highly sensitive, moderately resistant and resistant grapevine cultivars at the cytological upon infection with this pathogen and analyzed changes in the transcriptome of susceptible and resistant grapevine cultivars following *C. viniferum* challenge. They identified 236 differentially expressed *C. viniferum* genes encoding among others effector proteins. On the plant side differentially expressed grape genes showed differences in hormone signaling, phytoalexin production or disease-related genes.

The effector proteins secreted during another foliar disease, Brown rot, caused by necrotrophic plant pathogens *Monilinia* spp. in many stone fruits were evaluated to elicit cell-death phenotype on the non-host plants tobacco and tomato and the host plant *Prunus* spp. (Lopez et al.). This proceeding allows the screening of *Prunus* germplasm to identify susceptibility to brown rot.

Besides above-ground pathogens, the soil-borne pathogens are a further challenge affecting crop productivity. One of the serious soil-borne pathogens, *Fusarium* species makes devastating damages to the roots and stalks of maize in the field. Xiong et al. investigated which plant organs such as ears, stalks, and roots could be the place where the highest symptom-genotype correlation occurred. Out of 43 *Fusarium* spp. isolates, *Fusarium verticillioides* showed a strong correlation with stalk and root rot, but not with ear rot, indicating the main battlefield for the coevolution between maize and *F. verticillioides* is in the stalks and roots of maize.

In the interaction between pathogenic bacteria and host plants, studies on effector proteins to understand the gene-for-gene theory and immune response and modulation made significant progress in last three decades. Here, the first identified bacterial effector *AvrRps4* and its family was reviewed by Horton and Gassmann as the 30th anniversary of the discovery and cloning of *avrRps4* approaches.

Interesting data on the bacterial effector gene *eop1* from *Erwinia amylovora* and the FB_Mar12 resistance locus of apple point to a putative relationship between the two. This could be exploited to generate fire blight resistant apple varieties (Emeriewen et al.).

Because of global warming and globalization, new and re-emerging virus diseases occur due to the expanding habitat of insect vectors. Wang et al. demonstrated that the coat protein of Citrus yellow vein clearing virus interacts with the ascorbate peroxidase 1 (ClAPX1) from lemon plants resulting in an increased virus accumulation and a decreased expression of most genes involved in jasmonic acid signaling.

A study on the virulence factor of Mungbean yellow mosaic virus in mung bean (*Vigna radiata*) validated the infectivity of a series of infectious clones (Balasubramaniam et al.). In the future, this information can be used to identify cultivars susceptible and resistant to yellow mosaic disease.

How do plants interact with pathogen and protect themselves?

In nature, plants need to recognize potential pathogens and act appropriately to pathogen attacks. Plant defense response and resistance mechanisms are an important topic in the plant-pathogen interaction field. Here, the critical review of a novel signaling molecule, the CLAVATA3/EMBRYO SURROUNDING REGION-RELATED (CLE) peptide derived from the *CLE* gene in many plant species was shown to play a role during nodulation, immunity, and symbiosis with arbuscular mycorrhizal fungi. This sheds light on the role of regulatory networks on trade-off between plant defense and growth (Nakagami et al.).

The analysis of PR proteins in the cocoa tree apoplastome during infection by *Moniliophthora perniciosa* shows the defense dynamics occurring during this interaction. This could help designing novel control strategies for witches' broom disease (De Oliveira et al.).

Leucine-rich repeat receptor-like kinases are also prominent actors in plant defense. Yan et al. showed that the *Sesamum indicum* SiLRR-RLKs play a vital role in biotic stress and contribute to the sesame plant resistance to *Macrophomina phaseolina*.

How can plant diseases be managed?

The major objective to study plant-microbe interaction and plant pathology is to protect crops against pathogens. In this Research Topic, novel biological and synthetic materials are shown to control foliar and soil-borne pathogens. Intriguingly, amphibian skin bacteria application inhibits gray mold caused by *Botrytis cinerea* on tomato and post-harvest blueberries as well as the model plant *Arabidopsis thaliana* (Romero-Conttreras et al.) and root-associated bacteria (rhizobacteria) were shown to activate soybean chitinases and defense mechanism against *Fusarium oxypsorum* (Chen et al.).

Chitosan, a biopolymer extracted from crustacean exoskeletons has been used to control downy and powdery mildews in grapevine. The authors show that chitosans with a low degree of polymerization are effective inducers of defense in grapevine and also exhibit strong pesticidal effects against *Botrytis cinerea and Plasmopara viticola* (Brule et al.).

An ecological point of view can give hints on how to manage plant diseases. Investigation on the microbial transition and network studies between phyllosphere and rhizosphere suggest that interactions among bacteria of the genera *Caulobacter* and *Bosea* could help to manage wildfire disease in hydroponic systems (Liu et al.).

Novel data on salicylic acid-dependent plant signaling in age-related resistance of *Arabidopsis* suggest that salicylic acid accumulation and response are transiently increased during leaf maturation. A similar pattern was observed in cotton plants (Hu et al.).

High Ca2+ influx was shown to regulate ferroptotic cell death in rice. It triggered iron-dependent ROS accumulation, lipid peroxidation, and subsequent hypersensitive response cell death (Wang et al.).

Outlook

The Research Topic solicited brief, forward-looking contributions from the editorial board members that describe the state of the art, outlining recent developments and major accomplishments that have been achieved and that need to occur to move the field forward for the first time in our section. The goal of this special edition Research Topic was to shed light on the progress made in the past decade in the Plant-Pathogen Interactions field, and on its future challenges to provide a thorough overview of the field. The current Research Topic was successful and timely provides the global research field trends in the plant -pathogen interaction area.

Author contributions

C-MR: Conceptualization, Writing – original draft, Writing – review & editing. BM-M: Conceptualization, Writing – original draft, Writing – review & editing.

Funding

The author(s) declare financial support was received for the research, authorship, and/or publication of this article. This work was carried out with support from the Cooperative Research Program for Agriculture Science and Technology Development (Project No. RS-2022-RD010288) of the Rural Development Administration, Bio & Medical Technology Development Program of the National Research Foundation (NRF), funded by the Ministry of Science & ICT (NRF-2021M3A9I5021439); and the Korea Research Institute of Bioscience and Biotechnology (KRIBB) Initiative Program, Republic of Korea (for C-MR).

Conflict of interest

The authors declare that the research was conducted in the absence of any commercial or financial relationships that could be construed as a potential conflict of interest.

The author(s) declared that they were an editorial board member of Frontiers, at the time of submission. This had no impact on the peer review process and the final decision.

Publisher's note

frontiers | Frontiers in Plant Science

TYPE Original Research
PUBLISHED 28 November 2023
DOI 10.3389/fpls.2023.1306580

OPEN ACCESS

EDITED BY
Brigitte Mauch-Mani,
Université de Neuchâtel, Switzerland

REVIEWED BY
Katarzyna Otulak-Koziel,
Warsaw University of Life Sciences, Poland
Ram Prasnna Meena,
ICAR Central Institute of Arid Horticulture (CIAH), India

*CORRESPONDENCE
Zhen Song
songzhen@cric.cn

†These authors share first authorship

RECEIVED 04 October 2023
ACCEPTED 10 November 2023
PUBLISHED 28 November 2023

CITATION
Wang C, Zhang Q, Li J, Wang X, Li C, Bin Y and Song Z (2023) The coat protein of citrus yellow vein clearing virus directly targets the ascorbate peroxidase 1 in lemon (ClAPX1) to facilitate virus accumulation. *Front. Plant Sci.* 14:1306580. doi: 10.3389/fpls.2023.1306580

The coat protein of citrus yellow vein clearing virus directly targets the ascorbate peroxidase 1 in lemon (ClAPX1) to facilitate virus accumulation

Chunqing Wang[1,2†], Qi Zhang[1,2†], Jiaxin Li[1,2], Xinliang Wang[1,2], Chuxin Li[1,2], Yu Bin[1,2] and Zhen Song[1,2*]

[1]Citrus Research Institute, Southwest University, Chongqing, China, [2]Southwest University, Integrative Science Center of Germplasm Creation in Western China, Chongqing, China

Reactive oxygen species (ROS) are closely related to the antiviral immune response of plants, while virus can regulate ROS through various pathways to facilitate their own infection or replication. Citrus yellow vein clearing virus (CYVCV) is one of the most devastating viruses affecting lemon (*Citrus limon*) industry worldwide. However, the pathogenesis of CYVCV remains poorly understood. In this study, direct interaction between the coat protein (CP) of CYVCV and the ascorbate peroxidase 1 of lemon (ClAPX1) was confirmed for the first time by yeast two-hybrid, Bimolecular Fluorescence Complementation, and Co-immunoprecipitation assays. Transient expression of CP in lemon and *Nicotiana benthamiana* significantly enhanced the enzyme activity of the ClAPX1, and then inhibited the accumulation of H_2O_2. In addition, overexpression of ClAPX1 in lemon by transgene significantly promoted CYVCV accumulation and depressed the expression of most genes involved in jasmonic acid (JA) signaling pathway. Correspondingly, ClAPX1 silencing by RNA interference inhibited CYVCV accumulation and increased the expression of most genes involved in JA signaling pathway. To our knowledge, this is the first report that viruses regulate ROS by targeting APX directly, thereby suppressing host immune response and promoting viral accumulation, which may be mediated by JA signaling pathway.

KEYWORDS

reactive oxygen species, ascorbate peroxidase, citrus yellow vein clearing virus, coat protein, jasmonic acid

1 Introduction

Reactive oxygen species (ROS), including superoxide (O_2^-), hydroxyl radicals (·OH), hydrogen peroxide (H_2O_2), is critical for plant development, response to abiotic and biotic stresses. Studies have shown that a local ROS burst can directly limit virus spread and ROS also act as signaling molecules to induce or trigger antivital immune responses, including pathogen-associated molecular pattern-triggered immunity (PTI), effector-triggered immunity (ETI), and systemic acquired resistance (SAR) (Durrant and Dong, 2004; Mittler, 2017; Li et al., 2021). On the other hand, virus can also promote their own infection or replication by regulating ROS via various pathways. The p27 protein of red clover necrotic mosaic virus (RCNMV) utilizes a respiratory burst oxidase homologue (RBOH) of *Nicotiana benthamiana* (*N. benthamiana*) to induce an intracellular ROS burst, which promoting viral RNA replication (Hyodo et al., 2017). The interaction between the helper component proteinase (HCPro) of chilli veinal mottle virus (ChiVMV) and the catalase (CAT) of *N. benthamiana*, induces a ROS burst to facilitate viral infection (Yang et al., 2020). In addition, the 2b protein of cucumber mosaic virus (CMV) directly interacted with CATs and inhibited their activities to facilitate ROS accumulation, thereby promotes its accumulation in host (Yang et al., 2022). The P31 protein of maize chlorotic mottle virus (MCMV) hijacks maize CAT1 resulting in H_2O_2 accumulation and enhanced viral multiplication. Further studies showed that P31 attenuated the expression of salicylic acid (SA)-responsive pathogenesis-related (PR) genes by inhibiting CAT activity during MCMV infection (Jiao et al., 2021). Barley stripe mosaic virus (BSMV) gb interacts with glycolate oxidase and inhibits peroxisomal ROS production to facilitate virus infection (Yang et al., 2018).

Ascorbate peroxidase (APX) is a key enzyme in ROS-scavenging system and plays a significant role in plant responding to abiotic and biotic stresses. APX distributed in various cellular compartment as cytoplasm, chloroplast and microbody, can be divided into four isoforms, such as: thylakoid membrane-bound APX (tAPX), microbody (including glyoxysome and peroxisome) membrane-bound APX (mAPX), stromal APX (sAPX), and cytosolic APX (cAPX) (Panchuk et al., 2005; Shigeoka et al., 2014). In abiotic stress, overexpression of the APX1 enhances ascorbate content and drought resistance in *Arabidopsis* (Liu et al., 2019). Overexpression of APX induces orchestrated ROS scavenging and enhances cold and heat tolerances in tobacco (Wang et al., 2017). Overexpression of thylakoid APX in tomatoes shows enhanced resistance to chilling stress (Duan et al., 2012). Stromal *OsAPX7* modulates drought stress tolerance in rice (*Oryza sativa*) (Jardim et al., 2023). In biotic stress, overexpression of the OsAPX8 increases tolerance to bacterial blight (Jiang et al., 2016). *Zea mays* APX1 overexpression resulted in lower H_2O_2 accumulation and enhanced resistance against *B. maydis* (Zhang et al., 2022). Tomato seedlings subject to 2,6-Dichloroisonicotinic acid (INA) treatment that significantly increase APX2 enzyme activity and enhanced resistance to *Xanthomonas perforans* (Chandrashekar and Umesha, 2014). Studies on citrus have also reported that APX enzyme activity remains at high levels after citrus tristeza virus infection of citrus (Pérez-Clemente et al., 2015). Mittler reported that tobacco mosaic virus infection did not affects the transcription of APX, but inhibits the translational extension of APX and down-regulates enzyme activity, leading to H_2O_2 accumulation and inducing an immune response in tobacco (Mittler et al., 1998). To date, the direct interaction between APX and protein of plant virus has not been reported.

Citrus yellow vein clearing virus (CYVCV) is an emerging virus that causes serious economic damage to the lemon industry worldwide. The virus was first identified in Pakistan in 1988 (Catara et al., 1993), and later spread rapidly into India, Turkey. In China, CYVCV was first identified in Eureka lemon (C. limon Burm. f.) in 2009 in Yunnan province (Chen et al., 2014), and spread rapidly in other citrus producing regions (Zhou et al., 2017). The virus is usually asymptomatic in most citrus species, cultivars and hybrids, but severe leaf distortion and yellow vein clearing are found in lemon (Citrus limon Burm. f.) and sour orange (C. aurantium L.) (Alshami et al., 2003; Önelge et al., 2007; Iftikhar et al., 2010; Loconsole et al., 2012). It caused particularly serious damage, resulting in reduced tree vigor, lower yields, and decreased marketability of fruit production. and it is easily transmitted by grafting, contaminated tools, Dialeurodes citri, and several aphid species (Zhang et al., 2018; Zhang, et al., 2019; Afloukou et al., 2021), which may further make the spread of the disease quick and extensive. Therefore, it is necessary to pay attention to the virus and exploit useful methods to control this virus.

CYVCV is a positive-sense single-stranded virus that belongs to genus *Mandarivirus* in the family *Alphafexiviridae* (Loconsole et al., 2012)The viral genome is about 7.5 kb, contains six predicted open reading frames (ORF) (Loconsole et al., 2012; Song et al., 2015). ORF1 encodes a putative RNA-dependent RNA polymerase (RdRp). ORF2-ORF4 encodes the triple gene block proteins (TGB1, TGB2, TGB3). ORF5 encodes the coat protein (CP), which considered to be a stronger RNA silencing suppressor (RSS), and associated with the pathogenicity of CYVCV (Rehmana et al., 2019; Bin et al., 2019). ORF6 encodes a 23 kDa protein of unknown function. Until now, the pathogenesis of CYVCV remains unclear. The CP of CYVCV can interact with its own TGB1, TGB3 and TGB triple gene block proteins, which may be involved in virus movement (Rehmana et al., 2019). Additionally, the CP exhibits a stronger RSS activity. Previous studies have demonstrated that plant viruses can utilize encoded RSS as pathogenic or symptomatic determinant (Ma et al., 2019). Additionally, the titer of CYVCV is positively associated with the severity of symptoms in infected citrus seedings (Bin et al., 2022). Furthermore, CP plays a crucial role in the infection and pathogenicity of CYVCV (Bin et al., 2019). However, there have been few studies on the interaction between CYVCV and host factors. Previously, a total of 32 host factors that interact with the CP of CYVCV were initially screened from the cDNA library of Eureka lemon by Bin Yu et al. (Bin et al., 2023a); however, the precise mechanism underlying these interactions remains unknown. A previous study has reported that the activity of APX1 enzyme increased significantly in CYVCV-infected lemons, ClAPX1 was identified as a cellular protein (Zhang et al., 2022), and

the APX that interact with CP of CYVCV was initially identified by Bin Yu et al. (Bin et al., 2023a), but its function and mechanism still need to be clarified. Therefore, it is essential to explore the interaction between CYVCV and host factors, which may provide efficient strategies for disease control.

In this study, in order to clarify the pathogenesis of CYVCV, explore the interaction between CYVCV and host factors, to exploit resistant varieties for effective virus control, we confirm that there is a direct interaction between CP of CYVCV and ClAPX1 for the first time. The transient expression of CP promoted the enzyme activity of ClAPX1 and reduced the accumulation of H_2O_2. In addition, overexpression of ClAPX1 facilitates the CYVCV accumulation and inhibited the expression of most genes associated with JA signaling pathway, the accumulation of CYVCV was reduced and the expression level of most genes involved with JA signaling pathway were elevated in ClAPX1-silenced plants.

2 Materials and methods

2.1 Plant material and growth conditions

A CYVCV infectious cDNA clone, pCY-AY221, was constructed by Cui et al. (Cui et al., 2018). *N. benthamiana* were grown in a greenhouse at 25°C under a 16 h/8 h light/dark cycle. Eureka lemon (*Citrus limon (L.) Osbeck*) seeds were maintained in a greenhouse at 25°C under a 16 h/8 h light/dark cycle.

2.2 Yeast two-hybrid assay

The cDNA library was constructed by the Genecreate company using Eureka lemon leaves infected with CYVCV. The coding sequence (CDS) of the CP was cloned into the pGBKT7 vector to generate the pGBKT7-CP vector. Subsequently, The CDS of ClAPX1 was cloned and fused with the pGADT7 vector to generate the pGADT7-ClAPX1 vector. The generated bait and prey plasmids were co-transformed into yeast cells (Y2H Gold) and cultured on SD-Leu/-Trp medium for 2-3 days post inoculation (dpi). Then, they were plated onto SD-Leu/-Trp/-His medium to analyze the interaction. The primers used for vector construction are listed in Supplementary Table S1.

2.3 Bimolecular fluorescence complementation

The CDS of CP and ClAPX1 were inserted into the pSPYNE and pSPYCE vectors, respectively, to generate the pSPYNE-CP and pSPYCE-ClAPX1 constructs. The obtained vectors were transformed into *A. tumefaciens* strain GV3101 and cultured overnight. The cultures were collected and resuspended with infiltration buffer (10 mM MES, 10 mM $MgCl_2$, 200 μM acetosyringone) with OD_{600} = 1.0. *Agrobacterium* strain GV3101 with pSPYNE-CP and pSPYCE-ClAPX1 were mixed (1:1 ratio), followed by incubation at 25°C for 3 h. Subsequently, the mixture was infiltrated into *N. benthamiana* leaves. The infiltrated leaves were collected using a 5 mm diameter punch and observed under an Olympus FV3000 confocal microscope at 2-3 dpi. The primers used for vector construction are listed in Supplementary Table S1.

2.4 Co-immunoprecipitation assay

The CDS of CP and ClAPX1 were cloned into the pBI121 vector to generate pBI121-CP-RFP and pBI121-ClAPX1-CFP, respectively. *A. tumefaciens* harboring pBI121-CP-RFP and pBI121-ClAPX1-CFP were co-agroinfiltrated in *N. benthamiana* leaves. The infiltrated leaves were harvested at 2 dpi, frozen with liquid nitrogen, and subsequently ground into a powder. Total protein was then extracted using IP buffer (0.15 M NaCl, 0.05 M Tris-HCl, pH 7.5, 1 mM EDTA, 0.1% (v/v) Triton X-100, 10% (v/v) glycerol, 1×protease inhibitor cocktail and 1 mM phenylmethylsulfonyl fluoride (PMSF)). After being incubated for 20 min, the mixture was centrifuged at 12000 g, 4°C for 20 min. The supernatant was then incubated with anti-GFP beads. The immunoprecipitated proteins were separated by 12.5% SDS-PAGE and analyzed using the corresponding antibodies. The primers used for vector construction are listed in Supplementary Table S1.

2.5 Subcellular localization in *N. benthamiana*

The pBI121-CP-RFP and pBI121-ClAPX1-CFP vectors were used for the subcellular localization assay, and pBI121-CFP was used for control. The pBI121-ClAPX1-CFP construct was subsequently co-infiltrated into the leaves of *N. benthamiana* along with agrobacterial cells harboring the plasma membrane marker PM-GFP and the nuclear marker H2B-GFP. pBI121-CP-RFP and pBI121-ClAPX1-CFP were also co-infiltrated into *N. benthamiana* leaves. Green fluorescence protein (GFP), blue fluorescent protein (BFP) and red fluorescence (RFP) were observed using confocal laser scanning microscope FV3000 at 2-3 dpi.

2.6 Transient expression in *N. benthamiana* and citrus

A. tumefaciens GV3101, which harbors the pBI121-CP-RFP and pBI121-ClAPX1-CFP plasmids, were mixed in a 1:1 ratio for co-infiltration into *N. benthamiana* and one-year-old virus-free Eureka lemon seedlings, respectively. At 2-3 dpi, the infiltrated leaves of *N. benthamiana* were collected for CYVCV accumulation and additional analysis. At 10 and 20 dpi, the infiltrated lemon leaves were collected for observation of CYVCV accumulation and further analysis.

2.7 Citrus hairy root transformation

Citrus hairy root transformation was performed according to the methods reported by Ma et al. (2022). The CDS of ClAPX1 was amplified and inserted into the plant binary expression vector pLGN, which is driven by a 35S promoter. A fragment of about 400 bp from ClAPX1 was chosen as the target for silencing and cloned into the RNAi vector to generate the pLGN-RNAi-ClAPX1 vector. The plasmids were then transformed into *A. rhizogenes* strain K599 and cultured overnight at 28°C using TY liquid medium. The resuspended cell at final concentration (OD600 = 0.6-0.8) with the MES buffer (10 mM MgCl2, 10 mM MES [pH 5.6], and 200 μM AS) followed by incubated at 28°C for 3 h. Subsequently, Eureka lemon branches were soaked in the resuspended *A. rhizogenes* strains K599 and subjected to vacuum infiltration for approximately 25 min using a standard vacuum. The stem sections were cultured in a dome tray filled with vermiculite-mixed soil in the greenhouse at 26°C, with 90% relative humidity and a 16 h/8 h (light/dark) photoperiod. To identify the transgenic roots, GUS histochemical staining and reverse transcription-PCR (RT-PCR) assays were used. The obtained transgenic roots were used for gene expression analysis and subsequent evaluation. The primers used for vector construction are listed in Supplementary Table S1.

2.8 Tolerance of transgenic and silenced Eureka lemons to CYVCV

Transgene and silencing citrus were graft inoculated with CYVCV positive bark by RT-qPCR detection. Subsequently, root samples were collected one month after virus inoculation for gene expression and CYVCV accumulation analysis. The primers used for vector construction are listed in Supplementary Table S1.

2.9 Western blot

The total protein of *N. benthamiana* leaves, Eureka lemon leaves and roots were extracted according to Plant Total Protein Extraction Kit (Solarbio Life Sciences). The extracted proteins were then separated using 10% SDS-PAGE and then transferred to the PVDF membrane. The PVDF membranes were incubated with monoclonal anti-CP of CYVCV, monoclonal anti-GFP (Sigma), followed by a horseradish peroxidase (HRP)-conjugated secondary antibody (Proteintech). Blots were visualized using a chemiluminescence detection kit (Everbright Inc.).

2.10 Biochemical analysis

The hydrogen peroxide (H_2O_2) contents were measured using the micro method kit following the manufacturer's instructions (Nanjing molfarming Biotech Co., Ltd., Nanjing, China). Three biological replicates were maintained in each group. The ClAPX1 activity was measured using a micro method kit following the manufacturer's instructions (Beijing Solarbio Science & Technology Co., Ltd., Beijing, China).

2.11 Total RNA extraction and RT-qPCR analysis

The total RNA was isolated from *N. benthamiana* or citrus leaves or roots using the RNAiso plus, 1st Strand cDNA Synthesis SuperMix (Novoprotein, Japan) was used to generate the first-strand cDNA. RT-qPCR was conducted using BlasTaq^{TM} 2 × qPCR mixes, *N. benthamiana* and citrus actin gene were used as an internal reference. The results were analyzed by the $2^{-\Delta\Delta Ct}$ method and shown as means ± SD (n = 3). At least three biological repeats were conducted for all experiments. Different letters indicate significant differences at $P \leq 0.05$.

2.12 Statistical analysis

Each experiment was repeated at least three times, and data are represented as the mean. Values are presented as means ± SD. Statistical significance was determined using Student's t-test, * $P < 0.05$; ** $P<0.01$, *** $P<0.001$. All analyses were performed with the GraphPad Prism 8.0 software.

3 Results

3.1 CP of CYVCV interacts with ClAPX1 both *in vivo* and *in vitro*

In order to verify the direct interaction between CP and ClAPX1, Y2H, BiFC, and CO-IP assays were conducted. The Y2H assay demonstrated that PGBKT7-CP and PGADT-ClAPX1 exhibited natural growth on the SD/−Trp/−Leu/−His (TDO) medium, while the negative control did not show any growth (Figures 1A, B), indicating a direct interaction between CP and ClAPX1. To further confirm this interaction, BiFC assay was conducted on plants epidermis tissue. At 2 dpi, GFP was observed in the plasma membrane of *N. benthamiana* co-infiltrated with *Agrobacterium* carrying pSPYNE-CP and pSPYCE-ClAPX1 plasmids, but not in those co-infiltrated with pSPYNE-CP and pSPYNE or pSPYCE-ClAPX1 and pSPYCE plasmids (Figure 1D). These findings provide evidence that CP interacts with ClAPX1 in the plasma membrane *in vivo*. Additionally, Co-IP results also confirmed the interaction between CP and ClAPX1 (Figure 1C). Taken together, these results unequivocally establish that CP of CYVCV directly interacts with ClAPX1 both *in vivo* and *in vitro*.

3.2 Subcellular location of CP of CYVCV and ClAPX1

The subcellular location of CP and ClAPX1 were investigated in epidermis tissue of *N. benthamiana*. When expressed individually,

10.3389/fpls.2023.1306580

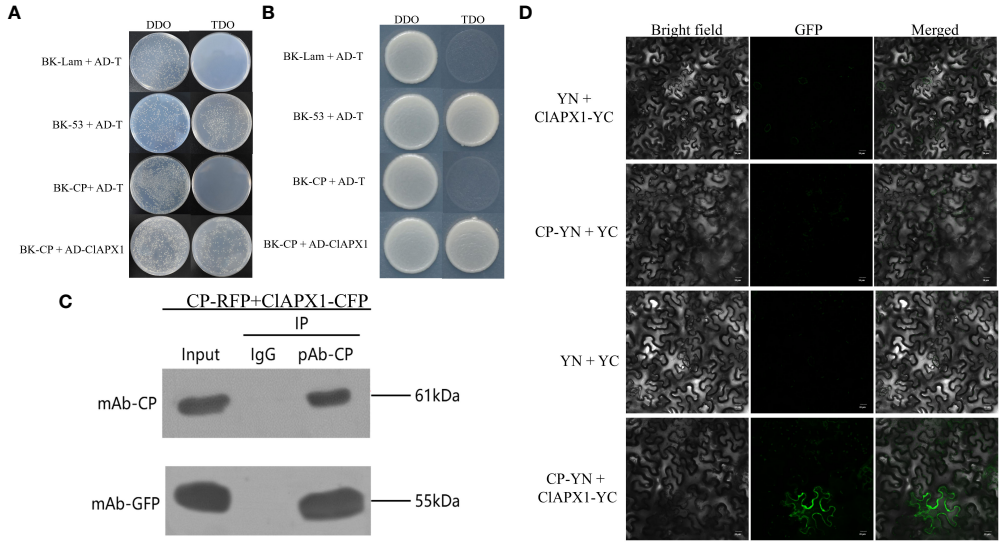

FIGURE 1
The coat protein (CP) of citrus yellow vein clearing virus (CYVCV) directly interacts with Ascorbate peroxidase 1 of lemon (ClAPX1) *in vitro* and *in vivo*. **(A–D)**. **(A, B)** Yeast two-hybrid (Y2H) analysis. Plasmid combinations are indicated on the left. **(A)** represent cells of yeast strain Y2H Gold co-expressing the indicated plasmid combinations were spotted onto yeast synthetic defined (SD) medium SD/-Trp/-Leu and SD/-Trp/-Leu/-His. The yeast cells harboring BK-CP + AD-T, and BK-Lam + AD-T were used as negative controls, and BK-53 + AD-T was used as positive control. **(B)** represent a single clone was select from **(A)** and plate on to the (SD) medium SD/-Trp/-Leu and SD/-Trp/-Leu/-His. **(C)** Coimmunoprecipitation (co-IP) assay. The pBI121-CP-RFP construct was transiently co-expressed with pBI121-ClAPX1-CFP in *Nicotiana benthamiana* (*N. benthamiana*) leaves by agroinfiltration, total protein was extracted at 3 days post inoculation (dpi) and immunoprecipitated with anti-CP and anti-GFP beads. Input and IP immunoprecipitation were analyzed by immunoblotting with anti-GFP or anti-CP antibodies. **(D)** Bimolecular fluorescence complementation (BiFC) assay, the experiments was conducted on plants epidermis tissue. Plasmid combinations were co-infiltrated into *N. benthamiana* leaves; GFP fluorescence was visualized by confocal microscopy at 2 dpi. The Green fluorescence indicates an interaction between CP and ClAPX1. Scale bars=20 μm.

CP was found to be localized in the nucleus and the plasma membrane (Figure 2A), while ClAPX1 was localized solely in the plasma membrane (Figure 2B). In contrast, co-expression of both proteins resulted in their localization on the plasma membrane (Figure 2C). These findings further support the interaction between CP and ClAPX1 on the plasma membrane as demonstrated by BiFC analysis.

3.3 CP enhanced the H_2O_2 scavenging activity of ClAPX1

To investigate the biological function of the interaction between CP and ClAPX1, both proteins were transiently expressed individually and co-expressed on *N. benthamiana* through *Agrobacterium* mediated injection. At 3 dpi, the enzyme activity of ClAPX1 and the H_2O_2 content of the inoculated leaves were measured. The findings revealed a significant increase in enzyme activity and a significant decrease in H_2O_2 content in leaves expressing ClAPX1, while no changes were observed in leaves expressing CP (Figures 3A, B). These results suggest that ClAPX1 possesses the ability to scavenge ROS.

Furthermore, compared to expression of ClAPX1 alone, the co-expression of CP and ClAPX1 resulted in a significant increase in enzyme activity and a decrease in H_2O_2 content, as observed in Figures 3A, B. This suggests that CP has a positive effect on enhancing the enzyme activity of ClAPX1. Additionally, the transcriptional analysis confirmed the expression of CP and ClAPX1, indicating that CP negatively regulates the expression of ClAPX1, while ClAPX1 does not affect the expression of CP, as shown in Figures 3C, D. Overall, these findings suggest that CP likely enhances the H_2O_2 scavenging activity of ClAPX1 through direct interaction.

3.4 Transient expression of ClAPX1 enhanced CYVCV accumulation in *N. benthamiana* and citrus

To investigate the impact of ClAPX1 on CYVCV accumulation, *Agrobacterium* carrying pBI121-ClAPX1-CFP or pCY-AY221, an infectious clone of CYVCV, were co-infiltrated into *N. benthamiana* plants. At 3 dpi, the expression level of the *ClAPX1* gene and the titer of CYVCV were quantified using RT-qPCR and western blotting, respectively. The results demonstrated a significant increase in CYVCV titer (Figure 4A) upon overexpression of *ClAPX1* gene (Figure 4B), indicating that elevated levels of ClAPX1 enhance CYVCV accumulation. Additionally, a similar experiment was conducted on lemon leaves. At 10 dpi, both the expression level of *ClAPX1* and the titer of CYVCV showed significant increases compared to control

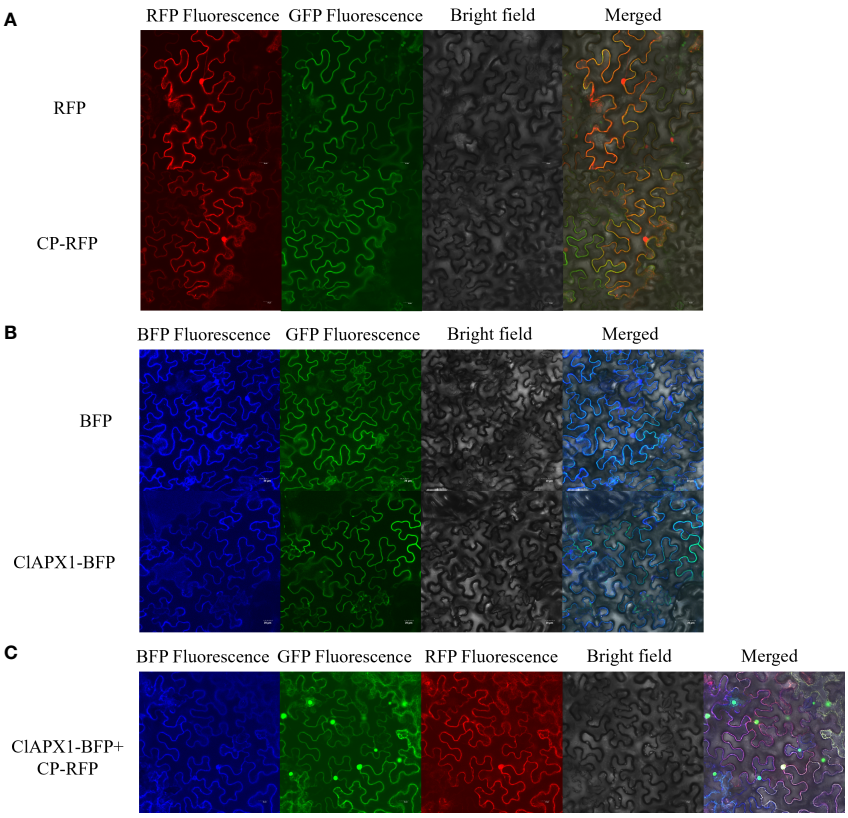

FIGURE 2
Subcellular localization of CP of CYVCV and ClAPX1 in *N. benthamiana* leaves. **(A–C)**. **(A)** CP of CYVCV fused with RFP and empty RFP-containing vectors were transiently expressed. **(B)** ClAPX1 fused with BFP and empty BFP-containing vectors were transiently expressed. **(C)** CP fused with RFP and ClAPX1 fused with BFP were transiently co-expressed. Scale bars=20 μm. the experiments was conducted on plants epidermis tissue.

samples (Figure 4C). Even at 20 dpi, there was still higher accumulation level of CYVCV compared to controls (Figure 4D). These findings highlight that transient expression of ClAPX1 promotes accumulation of CYVCV.

3.5 Over-expression of ClAPX1 enhanced the accumulation of CYVCV in transgenic lemon while ClAPX1 silencing depressed the virus

To further elucidate the role of ClAPX1 in CYVCV accumulation, transgenic lemon lines overexpressing and silencing ClAPX1 in roots were generated and subsequently subjected to CYVCV inoculation via grafting. At 30 dpi, samples were collected from the infected roots for subsequent analysis using RT-qPCR and western blotting techniques.

The results revealed a significant increased levels of both CP mRNA and protein (Figures 5A, B) in roots with *ClAPX1* over-expression (Figure 5C) compared to the empty vector control. Conversely, silencing *ClAPX1* resulted in a significant downregulation of both CP mRNA and protein levels in roots (Figures 6A–C). These findings provide compelling evidence that the enhanced expression of ClAPX1 promotes increased accumulation of CYVCV in transgenic lemon plants, while silence of ClAPX1 restrains accumulation of CYVCV.

3.6 ClAPX1 negatively regulates genes involved in the JA signaling pathway during CYVCV infection

To elucidate the mechanism underlying ClAPX1-mediated facilitation of CYVCV accumulation, we examined the relative expression levels of ten genes involved in jasmonic acid (JA) biosynthesis and immune response, including allene oxide synthase (*CsAOS*), allene oxide cyclase (*CsAOC*), coronatine insensitive 1 (*CsCOI1*), lipoxygenase 3 (CsLOX3), lipoxygenase 1 (CsLOX1), jasmonic acid-amido synthetase 1 (CsJAR1), myelocytomatosis proteins 2 (CsMYC2), mitogen-activated protein kinase (*CsMAPKs*), plant defensin 1.2 (*CsPDF1.2*), and pathogenesis-related protein 3 (*CsPR3*) in transgenic lemon roots.

The results revealed that the expression levels of six genes, namely *CsAOS*, *CsLOX3*, *CsJARl*, *CsLOX1*, *CsMYC2*, and *CsPDF1.2*, significantly downregulated in ClAPX1-overexpressing plants (Figure 5D). Conversely, the expression levels of seven genes were significantly upregulated in ClAPX1-silenced roots, including *CsAOS*, *CsAOC*, *CsCOI1*, *CsJAR1*, *CsLOX3*, *CsMAPKs* and

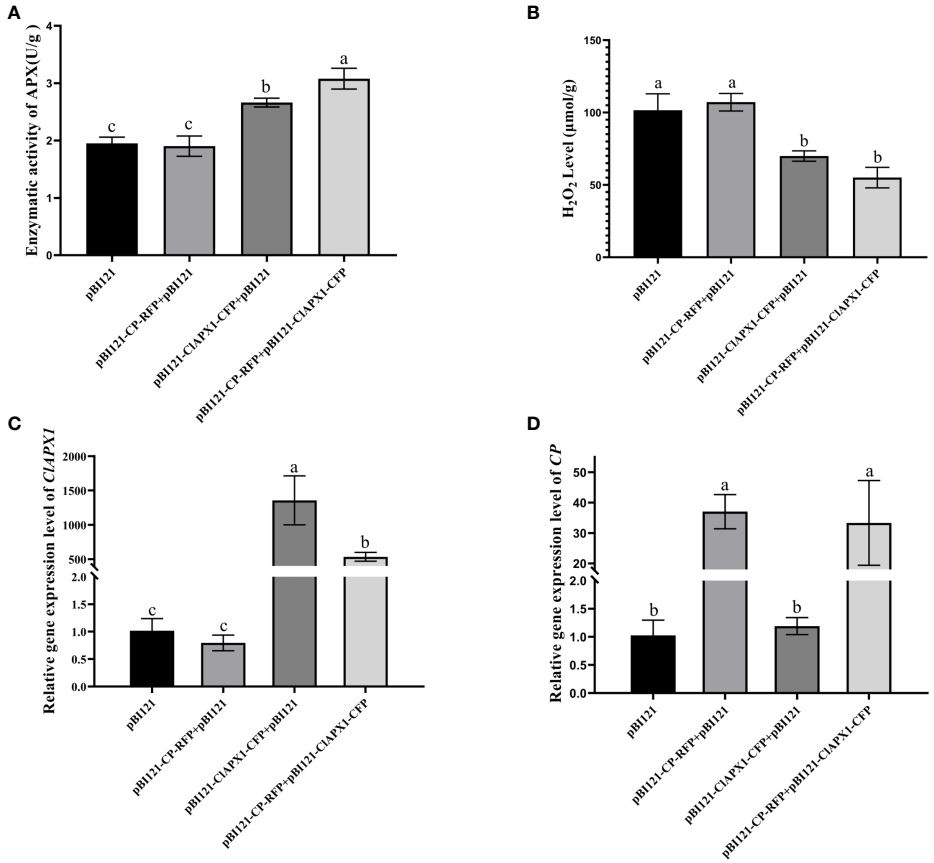

FIGURE 3
CP enhanced the H_2O_2 scavenging activity of ClAPX1 through transient expression CP and ClAPX1 in *N. benthamiana* leaves at 3 dpi. **(A–D)** The CP and ClAPX1 were cloned into the pBI121 vector to generate pBI121-CP-RFP and pBI121-ClAPX1-CFP for transient expression, respectively. The three groups pBI121-CP-RFP+pBI121, pBI121-ClAPX1-CFP+pBI121, pBI121-CP-RFP+pBI121-ClAPX1-CFP represented *A. tumefaciens* harboring pBI121-CP-RFP mixed with pBI121, pBI121-ClAPX1-CFP mixed with pBI121, pBI121-CP-RFP mixed with pBI121-ClAPX1-CFP were co-agroinfiltrated in *N. benthamiana* leaves, respectively. The pBI121 was used as the control. **(A)** Quantification of ClAPX1 enzyme activity. **(B)** Quantification of H_2O_2 accumulation. **(C)** the relative expression level of *ClAPX1* gene. **(D)** the relative expression level of CP of CYVCV. Error bars represented standard error of the means, letters represent significant differences between samples, one-way ANOVA with a p-value of 0.05 by least significant method (LSD) *post hoc* test was performed.

CsMYC2 (Figure 6D). Thus, ClAPX1 negatively regulates genes involved in the JA signaling pathway during CYVCV infection. This may lead to a suppression of the immune response that facilitates the accumulation of the virus.

4 Discussion

ROS plays a crucial role in plant defense responses. However, plant viruses interfere with host ROS signaling to evade plant's immunity response and promote virus infection or replication. A previous study has shown a significant increase in the H_2O_2 content in lemons infected with CYVCV (Zhang et al., 2023), suggesting a competitive relationship between the virus and ROS. However, the underlying mechanism and function remain unknown. In this study, it was found that CP of CYVCV directly targets the host protein ClAPX1, thereby enhancing its ROS scavenging activity in plants. This subsequently suppresses the host immune response and facilitates viral accumulation, potentially through modulation of the JA signaling pathway (Figure 7).

APX plays a major role in scavenging ROS. It is involved in the response to various stresses, including high light, drought, heat, bacterial and fungal infection (Chin et al., 2014; Bonifacio et al., 2016; Jiang et al., 2016; Du et al., 2023). However, the effects of APX in response to plant viruses remain largely unknown. The previous study has reported that the relative expression level of ClAPX1 and enzyme activity of CIAPX1 were higher when induced by the CYVCV-infected Eureka lemons (Zhang et al., 2023). These findings suggested that ClAPX1 may play a role in modulating the host-virus interaction. In this study, we demonstrate that the direct interaction between CP and ClAPX1 both *in vitro* and *in vivo*, thereby enhancing its activities and mitigating ROS accumulation. This study represents the first report to elucidate the direct interaction between CP and ClAPX1 in regulating ROS, thereby establishing a fundamental basis for unraveling the pathogenesis of CYVCV.

ROS burst is a plant defense response that limits the spread of viruses. To evade the immune mechanism of plants, viruses use their encoded protein to regulate ROS production or accumulation in order to manipulate host factors and promote infection. The interaction between Triple gene block protein 1 (TGBp1) of Pepino

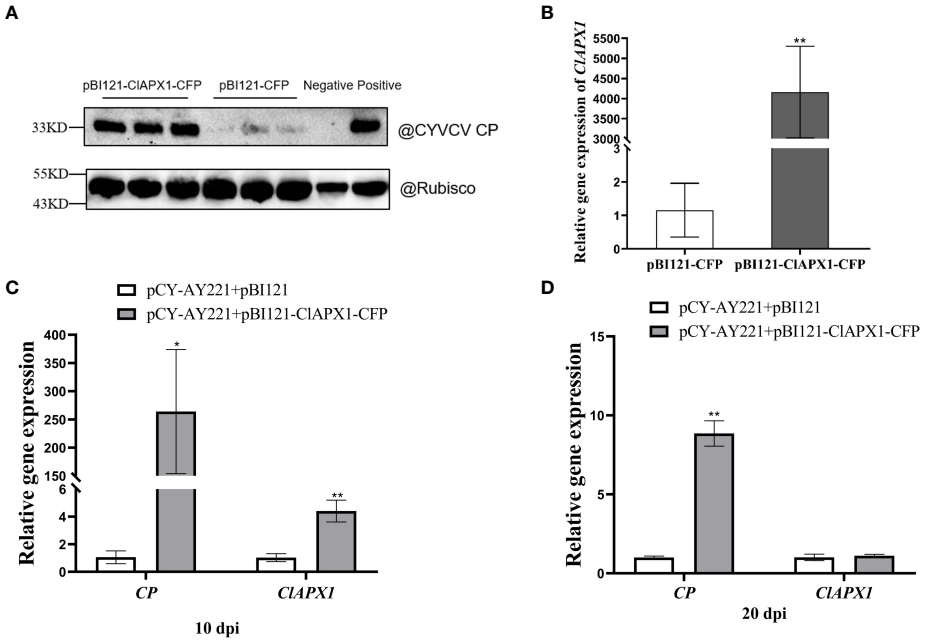

FIGURE 4
Transient expression of ClAPX1 facilitate CYVCV accumulation in *N. benthamiana* and lemon. **(A–D)** The ClAPX1 was cloned into the pBI121-CFP to generated the pBI121-ClAPX1-CFP for the transient expression. The pBI121-CP-RFP and pBI121-ClAPX1-CFP were co-infiltrated into the *N. benthamiana*. The pBI121 vector was used as a control. **(A)** quantification of CYVCV accumulation by western blot analysis after transient ClAPX1 expression in *N. benthamiana* at 3dpi. Rubisco was used as a loading control. **(B)** the relative expression level of *ClAPX1* gene after transient ClAPX1 expression in *N. benthamiana* at 3dpi. The pCY-AY221, a CYVCV infectious clone, pBI121-ClAPX1-CFP were co-infiltrated into *N. benthamiana*. **(C)** and **(D)** the relative expression level of *ClAPX1* and CYVCV accumulation after transient expression in lemon at 10 dpi and 20 dpi. Bars represent standard deviation values, statistical significance was determined using Student's t-test (* $P < 0.05$, ** $P < 0.01$).

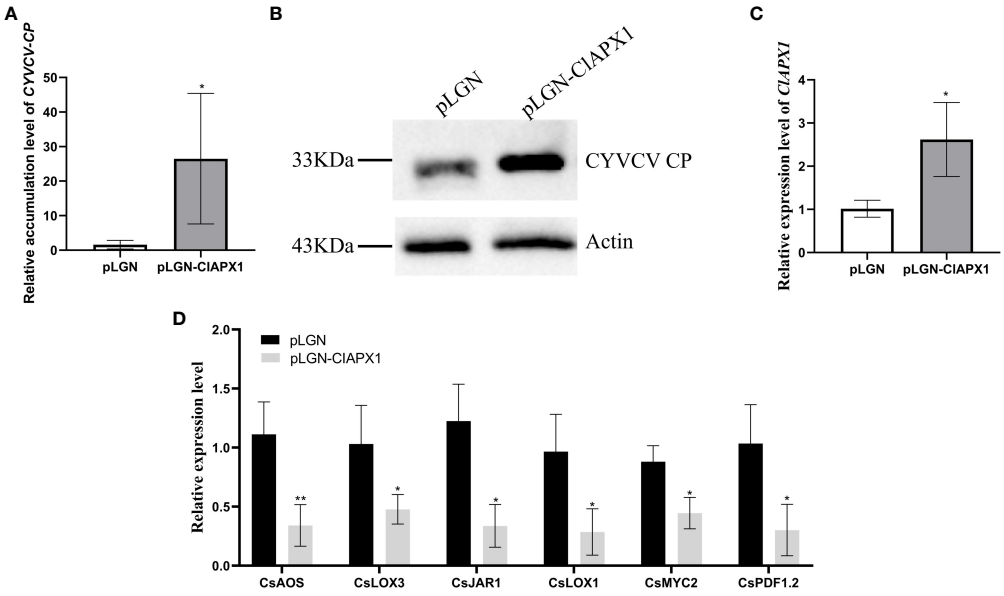

FIGURE 5
Overexpression of ClAPX1 facilitates CYVCV accumulation in transgenic lemon. **(A–D)**. **(A)** The relative accumulation level of CYVCV in transgenic citrus roots in mRNA level. **(B)** the accumulation level of CYVCV in transgenic citrus roots by western blot analysis, Actin served as loading control. **(C)** the relative expression level of *ClAPX1* gene in transgenic citrus roots. **(D)** the relative transcript levels of the jasmonic acid (JA) biosynthesis and responsive genes in the transgene citrus roots. Bars represent standard deviation values, statistical significance was determined using Student's t-test (* $P < 0.05$, ** $P < 0.01$).

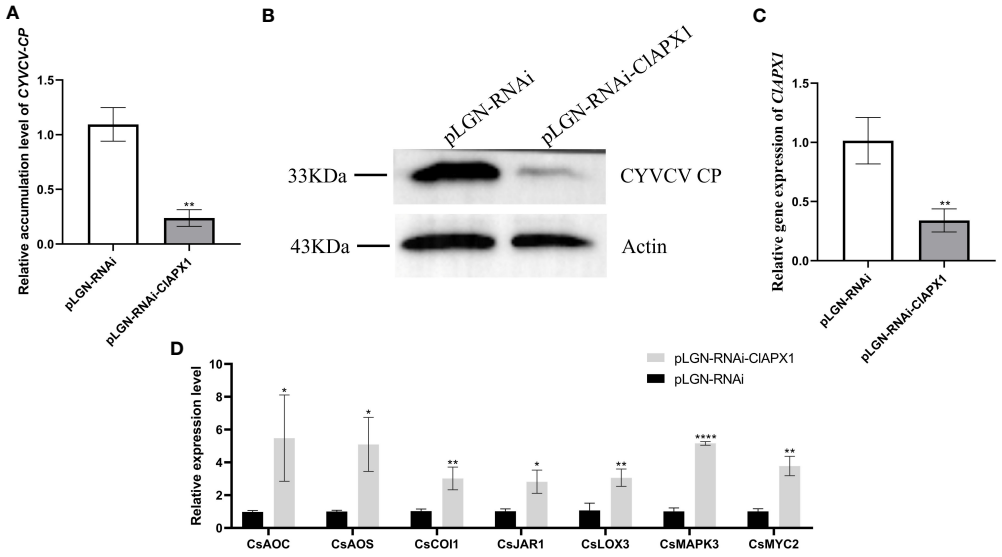

FIGURE 6
Silence of *ClAPX1* inhibits CYVCV accumulation in silenced citrus. **(A–D)**. **(A)** The relative accumulation level of CYVCV in silenced citrus roots by RT-qPCR. **(B)** the accumulation level of CYVCV in silenced citrus roots by western blot analysis, Actin served as loading control. **(C)** the relative expression level of *ClAPX1* gene in silenced citrus roots. **(D)** relative transcript levels of JA biosynthesis and responsive genes in silenced citrus roots. Bars represent standard deviation values, statistical significance was determined using Student's t-test (* $P < 0.05$, ** $P < 0.01$, **** $P < 0.0001$).

mosaic virus (PepMV) and tomato CAT1 increases its activity and promotes virus accumulation (Mathioudakis et al., 2013). In this study, we have demonstrated that transient expression and overexpression of ClAPX1 in citrus promote the CYVCV accumulation, while silencing ClAPX1 in citrus decreases CYVCV accumulation. This finding suggest that ClAPX1 may be a susceptible gene for CYVCV infection. A study has reported that engineering canker-resistant plants through CRISPR/Cas9-targeted editing of the susceptibility gene *CsLOB1* promoter in citrus (Peng et al., 2017), suggesting that it is possible to mutate or silence the APX gene either using the CRISPR-Cas9 system or RNAi system, thereby exploring resistant varieties for effective virus control.

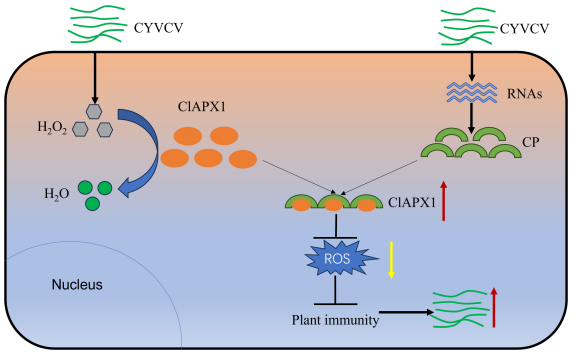

FIGURE 7
Proposed model. In plants, APX plays crucial roles in H_2O_2 scavenging and ROS homeostasis maintaining. When CYVCV infection, the CP directly targets ClAPX1 to promotes its enzyme activity and reduce ROS content in plant, thereby inhibiting the immunity of host plants and facilitate CYVCV accumulation, which may be mediated by JA signaling pathway.

The role of APX in pathogen infection has been extensively studied; however, the underlying mechanism by which APX responds to biological stress remains elusive. One study revealed that the cytosolic localized protein ZmAPX1 induces resistance to SCLB in maize by reducing H_2O_2 accumulation and activating a JA-mediated defense signaling pathway (Zhang et al., 2022). CAT, which has the same effect as APX, was inhibited during viral infection, and ROS species in plants were increased, while the expression of SA and PR pathway genes were reduced. Consequently, plant defenses were weakened and viral protein accumulation were enhanced (Jiao et al., 2021). In this study, we found that the interaction between CP and ClAPX1 enhances the enzyme activity of the ClAPX1, promoting CYVCV accumulation. However, the mechanism underlying plant susceptibility remains unclear. In a previous study, we found that the JA contents decreased, implying that JA maybe participate in the process of CYVCV infection (Bin et al., 2023b). In order to investigate the impact of ClAPX1 on the JA signaling pathway, the expression levels of ten JA biosynthesis and response genes were analyzed in transgenic and silenced citrus roots. It was found that the expression level of six genes (*AOS, LOX3, JAR1, LOX1, MYC2, PDF1.2*) were decreased in the transgenic roots, while the expression levels of seven genes (*AOS, LOX3, JAR1, MYC2, AOC, COI1, MAPK3*) were increased in the silenced roots. These results suggest that the interaction of CP with ClAPX1 may affect the JA signaling pathway, while further studies are needed to elucidate the mechanism by which APX promotes CYVCV accumulation.

In summary, our study confirmed that the CP of CYVCV can directly interact with the host protein ClAPX1, thereby promoting its activity and reducing ROS accumulation. Furthermore, the interaction between CP and ClAPX1 suppresses plant immunity, thereby facilitating CYVCV accumulation, which may be involved with JA signaling pathway. The present study represents the first report to clarify the direct interaction of CP with ClAPX1 via regulating ROS.

This finding lays a foundation for future investigations aimed at unraveling the functional role of APX in plant-pathogen interactions and exploring potential resistant varieties.

Data availability statement

The raw data supporting the conclusions of this article will be made available by the authors, without undue reservation.

Author contributions

CW: Investigation, Validation, Writing – original draft, Writing – review & editing. QZ: Investigation, Writing – review & editing. JL: Writing – review & editing. XW: Writing – review & editing. CL: Writing – review & editing. YB: Writing – review & editing. ZS: Supervision, Writing – review & editing.

Funding

The author(s) declare financial support was received for the research, authorship, and/or publication of this article. This work was supported by Natural Science Foundation of Chongqing (CSTB2022NSCQ-MSX0752), the National Key R&D Program of China (Grant no. 2021YFD1400800), Innovation Research 2035 Pilot Plan of Southwest University, and China Agriculture Research System (CARS-26-05B).

Acknowledgments

We thanks Professor X. P. Zou for providing vector pLGN and pLGN-RNAi (Citrus Research Institute, SWU/CAAS).

Conflict of interest

The authors declare that the research was conducted in the absence of any commercial or financial relationships that could be construed as a potential conflict of interest.

Publisher's note

Supplementary material

The Supplementary Material for this article can be found online at: https://www.frontiersin.org/articles/10.3389/fpls.2023.1306580/full#supplementary-material

References

Afloukou, F. M., Caliskan, F., and Önelge, N. (2021). Aphis gossypii glover is a vector of citrus yellow vein clearing virus. *J. Gen. Plant Pathol.* 87, 83–86. doi: 10.1007/s10327-020-00976-6

Alshami, A., Ahlawat, Y., and Pant, R. (2003). A hitherto unreported yellow vein clearing disease of citrus in india and its viral etiology. *Indian Phytopathology.* 4, 422–427.

Bin, Y., Song, Z., Cui, T., and Zhou, C. (2019). Citrus yellow vein clearing virus mutant and its construction method. ZL201910939750.8.

Bin, Y., Xu, J., Duan, Y., Ma, Z., Zhang, Q., Wang, C., et al. (2022). The titer of citrus yellow vein clearing virus is positively associated with the severity of symptoms in infected citrus seedlings. *Plant Disease.* 106, 828–834. doi: 10.1094/PDIS-02-21-0232-RE

Bin, Y., Zhang, Q., Su, Y., Wang, C., Jiang, Q., and Song, Z. (2023b). Transcriptome analysis of citrus limon infected with citrus yellow vein clearing virus. *BMC Genomics* 24, 65. doi: 10.1186/s12864-023-09151-5

Bin, Y., Zhang, Q., Wang, C., Zhao, X., Song, Z., and Zhou, C. (2023a). Screening of the host factors interacting with CP of Citrus yellow vein clearing virus by yeast two-hybrid System. *Scientia Agricultura Sinica.* 10, 1881–1892.

Bonifacio, A., Carvalho, F. E. L., Martins, M. O., Lima Neto, M. C., Cunha, J. R., Ribeiro, C. W., et al. (2016). Silenced rice in both cytosolic ascorbate peroxidases displays pre-acclimation to cope with oxidative stress induced by 3-aminotriazole-inhibited catalase. *Plant Physiol.* 201, 17–27. doi: 10.1016/j.jplph.2016.06.015

Catara, A., Azzaro, A., Davino, M., and Polizzi, G. (1993). "Yellow vein clearing of lemon in pakistan," in *Proceedings of the 12th conference of the international organization of citrus virologists: 1993* (Riverside: IOCV), 364–367.

Chandrashekar, S., and Umesha, S. (2014). 2, 6-Dichloroisonicotinic acid enhances the expression of defense genes in tomato seedlings against *Xanthomonas perforans*. *Physiol. Mol. Plant P.* 86, 49–56. doi: 10.1016/j.pmpp.2014.03.003

Chen, H., Li, Z., Wang, X., Zhou, Y., Tang, K., Zhou, C., et al. (2014). First report of citrus yellow vein clearing virus on lemon in yunnan, china. *Plant Dis.* 12, 1747. doi: 10.1094/PDIS-04-14-0343-PDN

Chin, D. C., Shen, C. H., SenthilKumar, R., and Yeh, K. W. (2014). Prolonged exposure to elevated temperature induces floral transition via up-regulation of cytosolic ascorbate peroxidase 1 and subsequent reduction of the ascorbate redox ratio in Oncidium hybrid orchid. *Plant Cell Physiol.* 55, 2164–2176. doi: 10.1093/pcp/pcu146

Cui, T., Bin, Y., Yan, J., Mei, P., Li, Z., Zhou, C., et al. (2018). Development of infectious cDNA clones of citrus yellow vein clearing virus using a novel and rapid strategy. *Phytopathology.* 108, 1212–1218. doi: 10.1094/PHYTO-02-18-0029-R

Du, J., Wang, Q., Shi, H., Zhou, C., He, J., and Wang, X. (2023). A prophage-encoded effector from "*Candidatus* Liberibacter asiaticus" targets ASCORBATE PEROXIDASE6 in citrus to facilitate bacterial infection. *Mol. Plant Pathol.* 24, 302–316. doi: 10.1111/mpp.13296

Duan, M., Feng, H., Wang, L., Li, D., and Meng, Q. (2012). Overexpression of thylakoidal ascorbate peroxidase shows enhanced resistance to chilling stress in tomato. *J. Plant Physiol.* 169, 867–877. doi: 10.1016/j.jplph.2012.02.012

Durrant, W. E., and Dong, X. (2004). Systemic acquired resistance. *Annu. Rev. Phytopathol.* 42, 185–209. doi: 10.1146/annurev.phyto.42.040803.140421

Hyodo, K., Hashimoto, K., Kuchitsu, K., Suzuki, N., and Okuno, T. (2017). Harnessing host ROS-generating machinery for the robust genome replication of a plant RNA virus. *Proc. Natl. Acad. Sci.* 114, E1282–E1290. doi: 10.1073/pnas.1610212114

Iftikhar, Y., Ibal, Z., Ahmed, S., Awan, A. R., Saleem, U., and Sarwar, G. (2010). Effect of environmental factors on yellow vein clearing virus incidence in lemon. *J. Agric. Res.* 48, 87–92.

Jardim-Messeder, D., Caverzan, A., Balbinott, N., Menguer, P. K., Paiva, A. L. S., Lemos, M., et al. (2023). Stromal ascorbate peroxidase (OsAPX7) modulates drought stress tolerance in rice (Oryza sativa). *Antioxidants (Basel)* 12, 387. doi: 10.3390/antiox12020387

Jiang, G., Yin, D., Zhao, J., Chen, H., Guo, L., Zhu, L., et al. (2016). The rice thylakoid membrane-bound ascorbate peroxidase OsAPX8 functions in tolerance to bacterial blight. *Sci. Rep.* 6, 26104. doi: 10.1038/srep26104

Jiao, Z., Tian, Y., Cao, Y., Wang, J., Zhan, B., Zhao, Z., et al. (2021). A novel pathogenicity determinant hijacks maize catalase 1 to enhance viral multiplication and infection. *New Phytol.* 230, 1126–1141. doi: 10.1111/nph.17206

Li, P., Zhao, L., Qi, F., Htwe, N., Li, Q., Zhang, D., et al. (2021). The receptor-like cytoplasmic kinase RIPK regulates broad-spectrum ROS signaling in multiple layers of plant immune system. *Mol. Plant* 14, 1652–1667. doi: 10.1016/j.molp.2021.06.010

Liu, J., Feng, K., Duan, A., Li, H., Yang, Q., Xu, Z., et al. (2019). Isolation, purification and characterization of an ascorbate peroxidase from celery and overexpression of the AgAPX1 gene enhanced ascorbate content and drought tolerance in Arabidopsis. *BMC Plant Biol.* 19, 488. doi: 10.1186/s12870-019-2095-1

Loconsole, G., Onelge, N., Potere, O., Giampetruzzi, A., Bozan, O., Satar, S., et al. (2012). Identification and characterization of citrus yellow vein clearing virus, a putative new member of the genus *Mandarivirus*. *Phytopathology.* 102, 1168–1175. doi: 10.1094/PHYTO-06-12-0140-R

Ma, H., Meng, X., Xu, K., Li, M., Gmitter, F., Liu, N., et al. (2022). Highly efficient hairy root genetic transformation and applications in citrus. *Front. Plant Sci.* 13. doi: 10.3389/fpls.2022.1039094

Ma, X., Hong, N., Moffett, P., Zhou, Y., and Wang, G. (2019). Functional analysis of apple stem pitting virus coat protein variants. *Virol. J.* 16, 20. doi: 10.1186/s12985-019-1126-8

Mathioudakis, M. M., Veiga, R. S., Canto, T., Medina, V., Mossialos, D., Makris, A. M., et al. (2013). Pepino mosaic virus triple gene block protein 1 (TGBp1) interacts with and increases tomato catalase 1 activity to enhance virus accumulation. *Mol. Plant Pathol.* 14, 589–601. doi: 10.1111/mpp.12034

Mittler, R. (2017). ROS are good. *Trends Plant Sci.* 22, 11–19. doi: 10.1016/j.tplants.2016.08.002

Mittler, R., Feng, X., and Cohen, M. (1998). Post-transcriptional suppression of cytosolic ascorbate peroxidase expression during pathogen-induced programmed cell death in tobacco. *Plant Cell.* 10, 461–473. doi: 10.1105/tpc.10.3.461

Önelge, N., Bozan, O., Gök, M., and Satar, S. (2007). "Yellow vein clearing of lemons in turkey," in *Proceedings of the 17th Conference of the International Organization of Citrus Virologists*, Turkey. 227–228.

Panchuk, I. I., Zentgraf, U., and Volkov, R. A. (2005). Expression of the apx gene family during leaf senescence of arabidopsis thaliana. *Planta* 222, 926–932. doi: 10.1007/s00425-005-0028-8

Peng, A., Chen, S., Lei, T., Xu, L., He, Y., Wu, L., et al. (2017). Engineering canker-resistant plants through CRISPR/Cas9-targeted editing of the susceptibility gene *CsLOB1* promoter in citrus. *Plant Biotechnol. J.* 15, 1509–1519. doi: 10.1111/pbi.12733

Pérez-Clemente, R. M., Montoliu, A., Vives, V., López-Climent, M. F., and Gómez-Cadenas, A. (2015). Photosynthetic and antioxidant responses of Mexican lime (Citrus aurantifolia) plants to Citrus tristeza virus infection. *Plant Pathol.* 64, 16–24. doi: 10.1111/ppa.12241

Rehmana, A. U., Li, Z., Yang, Z., Waqas, M., Wang, G., Xu, W., et al. (2019). The coat protein of citrus yellow vein clearing virus interacts with viral movement proteins and serves as an RNA silencing suppressor. *Viruses-Basel.* 11, 329. doi: 10.3390/v11040329

Shigeoka, S., Ishikawa, T., Tamoi, M., Miyagawa, Y., Takeda, T., Yabuta, Y., et al. (2014). Simultaneous over-expression of PaSOD and RaAPX in transgenic *Arabidopsis thaliana* confers cold stress tolerance through increase in vascular lignifications. *PloS One* 9, e110302. doi: 10.1371/journal.pone.0110302

Song, Z., Kurth, E. G., Peremyslov, V. V., Zhou, C., and Dolja, V. V. (2015). Molecular characterization of a citrus yellow vein clearing virus strain from China. *Arch.Virol.* 160, 1811–1813. doi: 10.1007/s00705-015-2423-1

Wang, J., Wu, B., Yin, H., Fan, Z., Li, X., Ni, S., et al. (2017). Overexpression of CaAPX induces orchestrated reactive oxygen scavenging and enhances cold and heat tolerances in tobacco. *BioMed. Res. Int.* 2017, 4049534. doi: 10.1155/2017/4049534

Yang, M., Li, Z., Zhang, K., Zhang, X., Zhang, Y., Wang, X., et al. (2018). Barley stripe mosaic virus γb interacts with glycolate oxidase and inhibits peroxisomal ROS production to facilitate virus infection. *Mol. Plant* 11, 338–341. doi: 10.1016/j.molp.2017.10.007

Yang, T., Peng, Q., Lin, H., and Xi, D. (2022). Alpha-momorcharin preserves catalase activity to inhibit viral infection by disrupting the 2b-CAT interaction in *Solanum lycopersicum*. *Mol. Plant Pathol.* 24, 107–122. doi: 10.1111/mpp.13279

Yang, T., Qiu, L., Huang, W., Xu, Q., Zou, J., Peng, Q., et al. (2020). Chilli veinal mottle virus HCPro interacts with catalase to facilitate virus infection in Nicotiana tabacum. *J. Exp. Bot.* 71, 5656–5668. doi: 10.1093/jxb/eraa304

Zhang, J., Jia, X., Wang, G., Ma, S., Wang, S., Yang, Q., et al. (2022). Ascorbate peroxidase 1 confers resistance to southern corn leaf blight in maize. *J. Integr. Plant Biol.* 64, 1196–1211. doi: 10.1111/jipb.13254

Zhang, Q., Song, C., Cao, P., Su, Y., Jiang, Q., Wang, C., et al. (2023). Identification of citrus APX gene family and their response to CYVCV infection. *J. Plant Res.* 136, 371–382. doi: 10.1007/s10265-023-01447-7

Zhang, Y., Wang, Y., Wang, Q., Cao, M., Zhou, C., and Zhou, Y. (2018). Identification of aphis spiraecola as a vector of citrus yellow vein clearing virus. *Eur. J. Plant Pathol.* 152, 841–844. doi: 10.1007/s10658-018-1523-7

Zhang, Y., Liu, Y., Wang, Y., Wang, Q., He, S., Li, X., et al. (2019). Transmissibility of Citrus yellow vein clearing virus by contaminated tools. *J. Plant Pathol.* 101, 169–171. doi: 10.1007/s42161-018-0141-8

Zhou, Y., Chen, H., Cao, M., Wang, X., Jin, X., Liu, K., et al. (2017). Occurrence, distribution, and molecular characterization of citrus yellow vein clearing virus in china. *Plant Dis.* 101, 137–143. doi: 10.1094/PDIS-05-16-0679-RE

frontiers | Frontiers in Plant Science

TYPE Original Research
PUBLISHED 07 February 2024
DOI 10.3389/fpls.2024.1360254

OPEN ACCESS

EDITED BY
Brigitte Mauch-Mani,
Universitéde Neuchâtel,
Switzerland

REVIEWED BY
Porfirio Gutierrez-Martinez,
Instituto Tecnológico de Tepic, Mexico
Sylvain Cordelier,
Universitéde Reims Champagne-Ardenne,
France

*CORRESPONDENCE
Benoit Poinssot
benoit.poinssot@inrae.fr

RECEIVED 22 December 2023
ACCEPTED 22 January 2024
PUBLISHED 07 February 2024

CITATION
Brulé D, Héloir M-C, Roudaire T, Villette J, Bonnet S, Pascal Y, Darblade B, Crozier P, Hugueney P, Coma V and Poinssot B (2024) Increasing vineyard sustainability: innovating a targeted chitosan-derived biocontrol solution to induce grapevine resistance against downy and powdery mildews.
Front. Plant Sci. 15:1360254.
doi: 10.3389/fpls.2024.1360254

Increasing vineyard sustainability: innovating a targeted chitosan-derived biocontrol solution to induce grapevine resistance against downy and powdery mildews

Daphnée Brulé[1], Marie-Claire Héloir[1], Thibault Roudaire[1], Jérémy Villette[1], Silvère Bonnet[2], Yoann Pascal[2], Benoît Darblade[2], Philippe Crozier[3], Philippe Hugueney[4], Véronique Coma[5] and Benoit Poinssot[1]*

[1]UMR Agroécologie, INRAE, Institut Agro Dijon, Université de Bourgogne, Dijon, France, [2]Elicityl, Crolles, France, [3]Phyteurop, Paris, France, [4]UMR-A 1131 Santé de la Vigne et Qualité du Vin (SVQV), Université de Strasbourg, INRAE, Colmar, France, [5]Laboratoire de Chimie des Polymères Organiques, Université de Bordeaux, CNRS, Bordeaux INP, UMR 5629, Pessac, France

The European Green Deal aims to reduce the pesticide use, notably by developing biocontrol products to protect crops from diseases. Indeed, the use of significant amounts of chemicals negatively impact the environment such as soil microbial biodiversity or groundwater quality, and human health. Grapevine (*Vitis vinifera*) was selected as one of the first targeted crop due to its economic importance and its dependence on fungicides to control the main damaging diseases worldwide: grey mold, downy and powdery mildews. Chitosan, a biopolymer extracted from crustacean exoskeletons, has been used as a biocontrol agent in many plant species, including grapevine, against a variety of cryptogamic diseases such as downy mildew (*Plasmopara viticola*), powdery mildew (*Erysiphe necator*) and grey mold (*Botrytis cinerea*). However, the precise molecular mechanisms underlying its mode of action remain unclear: is it a direct biopesticide effect or an indirect elicitation activity, or both? In this study, we investigated six chitosans with diverse degrees of polymerization (DP) ranging from low to high DP (12, 25, 33, 44, 100, and 470). We scrutinized their biological activities by evaluating both their antifungal properties and their abilities to induce grapevine immune responses. To investigate their elicitor activity, we analyzed their ability to induce MAPKs phosphorylation, the activation of defense genes and metabolite changes in grapevine. Our results indicate that the chitosans with a low DP are more effective in inducing grapevine defenses and possess the strongest biopesticide effect against *B. cinerea* and *P. viticola*. We identified chitosan with DP12 as the most efficient resistance inducer. Then, chitosan DP12 has been tested against downy and powdery mildews in the vineyard trials performed during the last three years. Results obtained indicated that a chitosan-based biocontrol product could be sufficiently efficient when the amount of pathogen inoculum is quite low and could be combined with only two

fungicide treatments during whole season programs to obtain a good protection efficiency. On the whole, a chitosan-based biocontrol product could become an interesting alternative to meet the chemicals reduction targeted in sustainable viticulture.

KEYWORDS

Vitis vinifera, induced resistance, biocontrol product, chito-oligosaccharides, chitosan, degree of polymerization

Introduction

Plants are in constant interaction with a variety of microorganisms, including pathogens like bacteria, fungi, oomycetes, and viruses. These crop pathogens significantly diminish the agricultural yields and product quality, resulting in substantial financial losses (Savary et al., 2019). To ensure both satisfactory yield and harvest quality, plant protection necessitates numerous chemical treatments, which can have detrimental impacts on the environment and human health. The present regulations in France and Europe aim to reduce the pesticide use in agriculture by 50% and phase out the most harmful substances by 2025 to help recover the Europe's biodiversity by 2030.

Viticulture holds great agricultural and economic importance in many countries. However, the most commonly cultivated grapevine (*Vitis vinifera*) is highly susceptible to cryptogamic diseases like downy mildew (caused by the oomycete *Plasmopara viticola*), grey mold (*Botrytis cinerea*), and powdery mildew (*Erysiphe necator*). These destructive diseases frequently occur, impacting yield, wine flavor, and quality. Their control heavily relies on frequent fungicide applications. Beyond resistant cultivars, an interesting alternative involves stimulating the plant immune system with elicitors, natural molecules that mimic pathogen attacks. Plants possess the ability to detect various microbe-associated molecular patterns (MAMPs; Dodds and Rathjen, 2010) initiating diverse defense mechanisms. The recognition of these consistent microbial markers by pattern recognition receptors (PRRs; Boller and Felix, 2009; Boutrot and Zipfel, 2017) triggers plant defense responses (Jones and Dangl, 2006). These responses encompass generating reactive oxygen species (ROS), phosphorylating mitogen-activated protein kinases (MAPKs), synthesizing phytoalexins, and expressing defense-related genes (Yu et al., 2017).

In the last two decades, the significance of chito-oligosaccharides as novel biopesticides has garnered attention (Ait Barka et al., 2004; Aziz et al., 2006; Trotel-Aziz et al., 2006; Chandra et al., 2017). Among these compounds, chitosan has gained notable traction in plant protection as a natural fungicide and elicitor of plant immunity. This compound, a polycationic β-1,4-linked D-glucosamine biopolymer, is obtained through deacetylation of chitin derived from crustacean shells and fungal cell walls. Due to its biocompatibility, biosafety, biodegradability, and accessibility, chitosan finds widespread applications in many fields, ranging from food packaging to cosmetics, medical industry, and agriculture (Meynaud et al., 2023). The antifungal and antibacterial properties of chitosan against various pathogens are well-established, as it reduces infections in different crops like pea, grapevine, wheat, cucumber, tobacco and barley (Vander et al., 1998; Ben-Shalom et al., 2003; Aziz et al., 2006; Iriti et al., 2006; Faoro et al., 2008; Iriti and Varoni, 2015; Kheiri et al., 2016; Romanazzi et al., 2016).

In laboratory, chitosan triggers grapevine defense responses, including phytoalexin production, MAPKs phosphorylation, and defense gene expression, resulting in resistance against *B. cinerea* and *P. viticola* (Aziz et al., 2006; Brulé et al., 2019). While chitosan shows promising results under controlled conditions, its adoption in plant protection practices remains limited, likely due to its variable effectiveness in vineyards (Dagostin et al., 2011). Some studies have also highlighted chitosan's effectiveness and utilization in postharvest decay control of fruits (Romanazzi et al., 2018; Duan et al., 2019). However, despite the numerous advantageous properties and agricultural applications of chitosan, the precise molecular mechanisms underlying its elicitation potential remain unclear. This lack of clarity hinders establishing a direct correlation between defense elicitation and plant protection. The biological impact of chitosan hinges on physicochemical attributes such as the deacetylation degree (DDA), and the molecular weight (MW), directly depending on the polymerization degree (DP). Notably, chitosan oligomers with lower MW have been proven more effective in inducing defense responses compared to higher MW counterparts (Lin et al., 2005; Aziz et al., 2006).

The aim of this study was to harness the complete phytosanitary potential of chitosan by using an optimized structure, with the aim of introducing a biocontrol product that surpasses the effectiveness of current solutions against grapevine downy and powdery mildews. Our investigation centered around six chitosan variants with diverse degrees of polymerization (DP) ranging from low to high (12, 25, 33, 44, 100, 470), all featuring a robust deacetylation degree (DDA) exceeding 93%. We scrutinized their biological activities by evaluating both their antifungal properties and their abilities to elicit grapevine immune responses in controlled settings and real vineyard conditions.

From these evaluations, we concluded that all chitosans do not possess the same biological activities. Thus, we identified the chitosan of DP12 as the most potent and comprehensively characterized candidate. We have also investigated the protection efficiency of combining chitosan with only two fungicide treatments, with the additional goal of reducing the excessive chemical applications.

Materials and methods

Plant and fungal materials

Grapevine (*V. vinifera* cv. Marselan) herbaceous cuttings were grown in a greenhouse until they had developed 6–8 leaves. The first and second youngest adult leaves from each plant were used for experiments, as previously indicated (Steimetz et al., 2012).

Grapevine samples (*V. vinifera* cv. Chardonnay, roodstock 3309C), collected from the Marsannay-la-Côte vineyard of the University of Burgundy (France), were used for *P. viticola* infection tests on leaf discs and qRT-PCR.

Grapevine downy mildew (*P. viticola*) was routinely maintained on *V. vinifera* cv. Marselan plants as previously described (Lemaître-Guillier et al., 2017).

The BMM strain of *B. cinerea* used (Zimmerli et al., 2001) was grown on Petri dishes containing V8 medium ½ diluted, KH_2PO_4 5 g/L, agar 30 g/L, pH 6.0 for two weeks in the dark (22°C). Conidia were collected with water, filtered to remove mycelia, counted and kept at 4°C prior to infection assays.

Chitosans and chemicals

Chitosans were provided by Elicityl (Crolles, France). Their origin is the exoskeletons of crustaceans. They were hydrolyzed, purified by chromatography and finally their degrees of polymerization (DP) and deacetylation degree (DDA) were evaluated by ^{1}H NMR analysis (Table 1). The chitosan with the lowest DP was more deeply characterized in terms of molecular weight by size exclusion chromatography (SEC) and thermal resistance (according to Meynaud et al., 2023). Chitosans with low DPs (12 and 25) were dissolved in sterile ultrapure water and those with medium or high DPs (33, 44, 100, 470) were dissolved in acetic acid pH 4.5 (0.1%, 0.1%, 0.2% and 0.3% respectively).

Chitooligosaccharides and Oligogalacturonides (COS-OGA) mixture solution has been used as a positive control with the homologated biocontrol product "BLASON" provided by Cerience. Chemicals provided by Phyteurop have also been used as positive controls in vineyard trials: the homologated copper mixture solution "Bouillie Bordelaise CAFFARO WG" and the sulfur solution "LUCIFERE" to protect grapevine against downy or powdery mildew, respectively.

MAPKs activation

Discs of grapevine leaves from greenhouse cuttings were first vacuum-infiltrated with water, then floated on water (lower leaf surface facing the solution) during 3h before adding elicitor solutions. Discs were treated with the various chitosans (1 mg/mL), COS-OGA (62.5 mg/L) or water (as control) and harvested 20 min post-treatment. MAPKs activation was detected after immunoblotting of the extracted proteins using anti-p42/44-phospho-ERK antibody (Cell Signaling, Danvers, MA), as previously described (Brulé et al., 2019; De Bona et al., 2019). Transfer quality and homogeneous loading were checked by Ponceau red staining.

Analysis of defense gene expression by quantitative polymerase chain reaction

For greenhouse assays, grapevine leaf discs were floated on water during 3h, then treated with the different chitosans (1 g/L), COS-OGA (62.5 mg/L) or water (as control) and harvested 3h post-treatment. Total RNA was extracted by using the Spectrum™ Plant Total RNA Kit (Sigma), according to the manufacturer's instructions.

For vineyard grapevine assays, plants were sprayed with chitosans of different DPs (2 g/L), COS-OGA (125 mg/L) or control solutions with a knapsack sprayer and two youg adult

TABLE 1 Characterization of the different chitosans.

Name	Deacetylation degree (DDA)	Polymerization degree (DP)	Polymerization degree (DP)
	(^{1}H-RMN) [a]	(^{1}H-RMN) [b]	(NDS)
DP12	98.2%	9.9	23
DP25	98.4%	28	25.2
DP33	97.8%	40	33
DP44	97.4%	78.1	44.7
DP100	93.4%	na	93/110
DP470	92.8%	na	~500

a- Deacetylation degrees from ^{1}H-NMR (1H NMR 400 MHz (Bruker, Condition: chitosan (10 mg/ml) in D2O/DCl at 80°C, n=3).
b- Polymerization degree from ^{1}H-NMR at room temperature in D20: DCl mixture (n=3).
NDS (3, 5 Dinitrosalicylic acid) is an acid reagent used for the determination of reducing sugars.

leaves were harvested and frozen 10h post-treatment (hpt). RNA extraction was then carried out by the addition of TRIzol® (Invitrogen, Life Technologies, Saint-Aubin, France) following the manufacturer's instructions.

For both, reverse transcription was performed using Superscript IV (Invitrogen) following the manufacturer's protocol. Real-time qPCR was carried out as described previously (Trdá et al., 2014). The relative transcript level was calculated using the ΔΔCt method (Livak and Schmittgen, 2001) with the validated grapevine reference gene *VvVATP16* (Gamm et al., 2011) whose primers are described Table 2.

Metabolomic analysis by LCMS

Leaf discs of grapevine cuttings grown in greenhouse were floated on water (lower leaf surface facing the solution) during 3h before adding elicitor solutions of the different chitosans (1 g/L), COS-OGA (62.5 mg/L) or water (as control). Twenty four h after treatment, discs were harvested, freeze-dried and ground in a mortar to obtain a fine powder. Thirty to 40 mg of powder was extracted with methanol (50 µL/dry mg) containing 5 µg/mL of chloramphenicol used as an internal standard. Analyses were performed on Dionex Ultimate 3000 ultra-high performance liquid chromatography (UHPLC) equipment coupled to a Thermo Exactive high-resolution mass spectrometer (HRMS). The analyses were carried out in positive and negative mode. The methods used have been previously described (Martin et al., 2021).

Botrytis cinerea and downy mildew assays

For *B. cinerea* growth inhibition assays, the direct antifungal activity of chitosans was assessed by growing 270 µL of *B. cinerea* conidia (2.10^5 c/mL) in Potato Dextrose Broth (PDB) 6 g/L, with 30 µL of different final concentrations of chitosans (25, 50, 250 and 500 mg/L), in a 100-wells microplate honeycomb Bioscreen. The growth of *B. cinerea* was followed by optical density at 492 nm using the Thermo Labsystem Bioscreen C system (cyan filter) with a reading every 2 hours during 60h (20°C, dark, continuous agitation).

For *P. viticola* infection on grapevine cuttings, the lower leaf surface was sprayed in greenhouse with elicitors (30 mg/L). Two days post-treatment (dpt), treated leaves were sprayed with a freshly prepared suspension of sporangia (2.10^4 sp/mL) and plants were maintained in 100% relative humidity for 4h in darkness. Leaf discs were punched 5 dpi and transferred on moist Whatman paper in a plastic box maintained in 100% relative humidity under a 10/14h day/night cycle at 20/18°C. Infection intensity was assessed 7 dpi by measuring the sporulating area by using the image analysis Visilog 6.9 software (Kim Khiook et al., 2013).

For *P. viticola* infection on leaves harvested in vineyard 3 dpt, the leaf discs were punched in the laboratory, transferred on moist Whatman paper in a plastic box, inoculated and maintained in the same conditions as previously. Infection intensity was assessed 7 dpi by image analysis previously described.

For toxicity assays on *P. viticola* zoospores, a suspension of *P. viticola* sporangia (1.10^5 sp/mL) was treated with different concentrations of chitosan. One hour and a half later, released zoospores, moving on a 1 mm^2 square of a Malassez hemocytometer, were counted during one minute.

For *B. cinerea* infection on leaves harvested in vineyard 2 dpt, the leaf discs were punched in the laboratory, transferred on moist Whatman paper in a plastic box, inoculated on the upper surface with 1000 conidia in a 20 µL-droplet of 6 g/L PDB and maintained in the same conditions as previously. Infection intensity was quantified at 5 dpi by measuring the macerated lesion diameter.

Vineyard experimental trials

The vineyard experimental trials have been realized between 2020 and 2023 on different grapevine cultivars (Merlot, Cabernet franc, Pinot Noir, Carignan, Chardonnay) in different locations (Nohic, Laruscade, Allones, Nimes, Cardet, Villevieille, Marsannay) to be representative of the different french vineyards. The experimental trials have been designed with four Fisher complet randomized blocks per modality. For downy mildew assays, the vineyards were brumerized with water and artificially inoculated. For powdery mildew assays, vineyard trials were realized in natural conditions. All product applications were realized preventively every 7 to 9 days during the entire period of grapevine susceptibility. Spraying was carried out with a knapsack sprayer (airblast) by treating each side of the grapevine row with a volume of slurry between 150 and 300 L/ha, depending on the vegetative stage of the plant and the spacing between rows in the vineyard plot.

Observations are made daily and complete notations are triggered when the disease is significantly present on the observed organs (leaves and clusters). In general, two to three notations on leaves and bunches are carried out between fruit set (BBCH 71) and the beginning of veraison (BBCH 81). The ratings consist of assessing the intensity (severity) of the disease on leaves or on clusters from a sample of 100 leaves or 50 clusters per elementary plot, i.e. 400 leaves and 200 clusters per modality. From the values observed in the untreated control plot, the protection efficiency of

TABLE 2 List of the primers used.

Name		Forward Primer (5'->3')	Reverse Primer (5'->3')
VATP16	V-type proton ATPase 16kDa subunit	CTTCTCCTGTATGGGAGCTG	CCATAACAACTGGTACAATCGAC
ROMT	Resveratrol O-methyltransferase	TGCCTCTAGGCTCCTTCTAA	TTTGAAACCAAGCACTCAGA
STS1.2	Stilbene synthase	AGGAAGCAGCATTGAAGGCTC	TGCACCAGGCATTTCTACACC
PR3.4C	Endochitinase (*PR3*)	TCGAATGCGATGGTGGAAA	CGTCGCCCTAGCAAGTGAG

10.3389/fpls.2024.1360254

each modality is calculated for each block by the Abott formula (((untreated control – modality)/untreated control) x 100) followed by the mean efficacy +/- SE of the 4 blocks.

Results

The chitosan's degree of polymerization influences its biopesticide effect

A wide range of chitosans was used in this study (Table 1). The characterization of these chitosans based on their size and degree of deacetylation using various methods such as ^{1}H NMR analysis and assessment of reducing sugars, revealed that the selected chitosans were nearly completely deacetylated. Moreover, their DP ranged from 10 to 500, thereby validating the earlier characterization of some among them (Huet et al., 2023). The direct biopesticide activity of the different chitosans were investigated on the necrotrophic fungus *B. cinerea* and the biotrophic oomycete *P. viticola*. The anti-*Botrytis* activity was determined by following the mycelial growth of *B. cinerea in vitro*. After a 60-hour treatment period, all the chitosans inhibited the growth of *B. cinerea* at low concentrations; however, variations were observed based on their DP. Chitosans DP12, 25 and 33 exhibited the highest fungitoxic effects, as they almost completely inhibited the growth of *B. cinerea* at the lowest concentration of 25 mg/L, with rates of inhibition reaching 95%, 98%, and 97%, respectively (Figure 1A). Chitosan DP44 and 100 showed an intermediate antifungal activity with 81% and 91% of growth inhibition at 50 mg/L while chitosan DP470 was more variable and less toxic on *B. cinerea*, and reached 88% of growth inhibition only at 500 mg/L (Figure 1A).

Their biopesticide activity was then assessed on the motility of *P. viticola* zoospores. All the different chitosans are toxic at very low concentrations as they totally inhibited the release and the motility of *P. viticola* zoospores from 1000 to 10 mg/L (Figure 1B). At 5 mg/L, chitosans DP12, 25, 33 and 470 always prevent the motility of

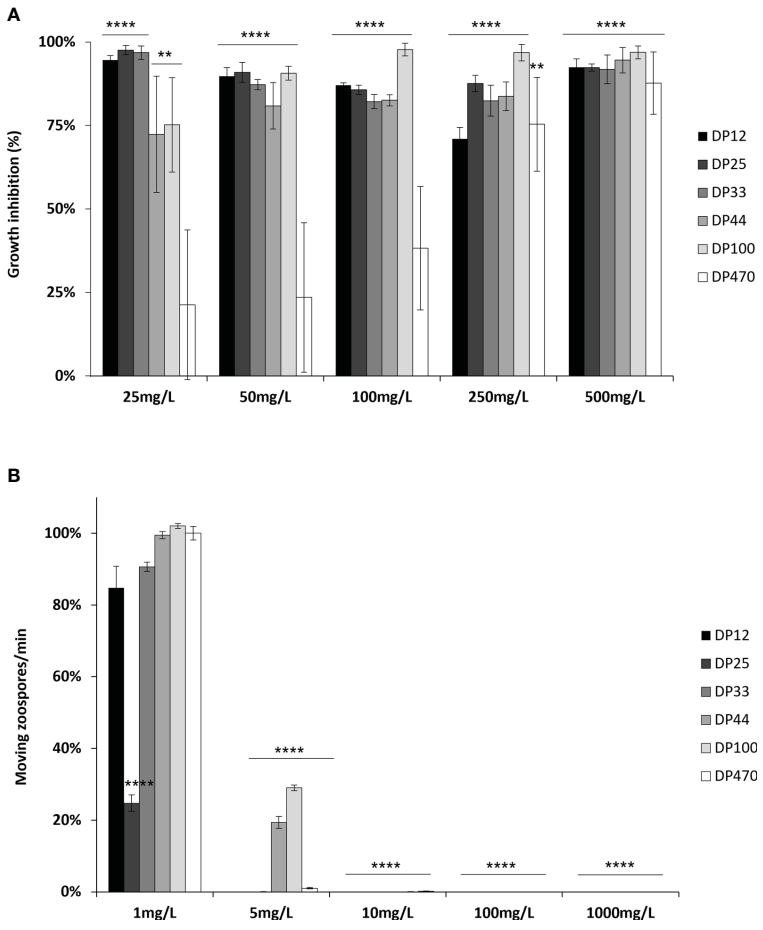

FIGURE 1
Biopesticide effects of chitosan with different DPs on *Botrytis cinerea* and *Plasmopara viticola*. **(A)** *B. cinerea* conidia were treated with increasing concentrations of chitosan DP12 to DP470 and mycelial growth was followed by optical density at 492 nm. Values represent the mean of growth inhibition ± standard error (SE) of triplicate data obtained in three independent experiments (n=9) at 60 hours and are expressed as a percentage of the control, set as 0%. Asterisks (*) indicate significant differences relative to the control using an unpaired heteroscedastic Student's *t* test (**, P<0.01, ****, P<0.0001). **(B)** *P. viticola* sporangia were treated with increasing concentrations of chitosan DP12 to DP470 and released moving zoospores were counted for one minute on a 1 mm^2 square of a Malassez hemocytometer. Values represent the mean ± SE of triplicate data obtained in three independent experiments (n=9) and are expressed as a percentage of the control, set as 100%. Asterisks indicate significant differences relative to the control using an unpaired heteroscedastic Student's *t* test (****, P<0.0001).

10.3389/fpls.2024.1360254

zoospores while 19% and 29% moving zoospores are still observed after treatment with chitosans DP44 and 100, respectively. At 1 mg/L, there are as many moving zoospores as in the control for all the different chitosans, except for DP25, which is the most toxic. Although different bioactivities have been observed between chitosans depending on their DP, these results indicate a strong biocide effect of chitosans.

Effects of the chitosan's DP on the elicitation of grapevine immune responses

The importance of the chitosan's DP for its elicitor activity was investigated on the grapevine immune responses such as MAPKs phosphorylation, defense gene expression and production of defense metabolites such as phytoalexins.

Similar to the positive control COS-OGA, a rapid phosphorylation of two MAPKs with relative molecular masses of 45 and 49 kDa, has been observed 20 min after treatment with the different chitosans, whatever their DP (Figure 2A). These 2 MAPKs were almost not activated in water- and solvent-treated control leaf discs (Figure 2A).

In response to the chitosans of different DP, the expression of defense genes known to be induced by different MAMPs in grapevine (Poinssot et al., 2003; Dubreuil-Maurizi et al., 2010; Trdá et al., 2014; Brulé et al., 2019) was quantified by qPCR. Three hours post-treatment (hpt), the positive control COS-OGA and all the chitosans markedly induced the expression of two selected defense genes encoding a stilbene synthase (*STS1.2* encoding the last enzyme of the stilbene phytoalexins pathway) and an acidic chitinase (*PR3.4c*). The results showed that chitosan DP12 was always the most active molecule (Figures 2B, C).

Metabolomic analyzes were then carried out 24 hpt and the heatmap presented Figure 2D indicates the compounds significantly different between the water control and the tested conditions. If the acidic solvent 0.3% (negative control) did not induce the production

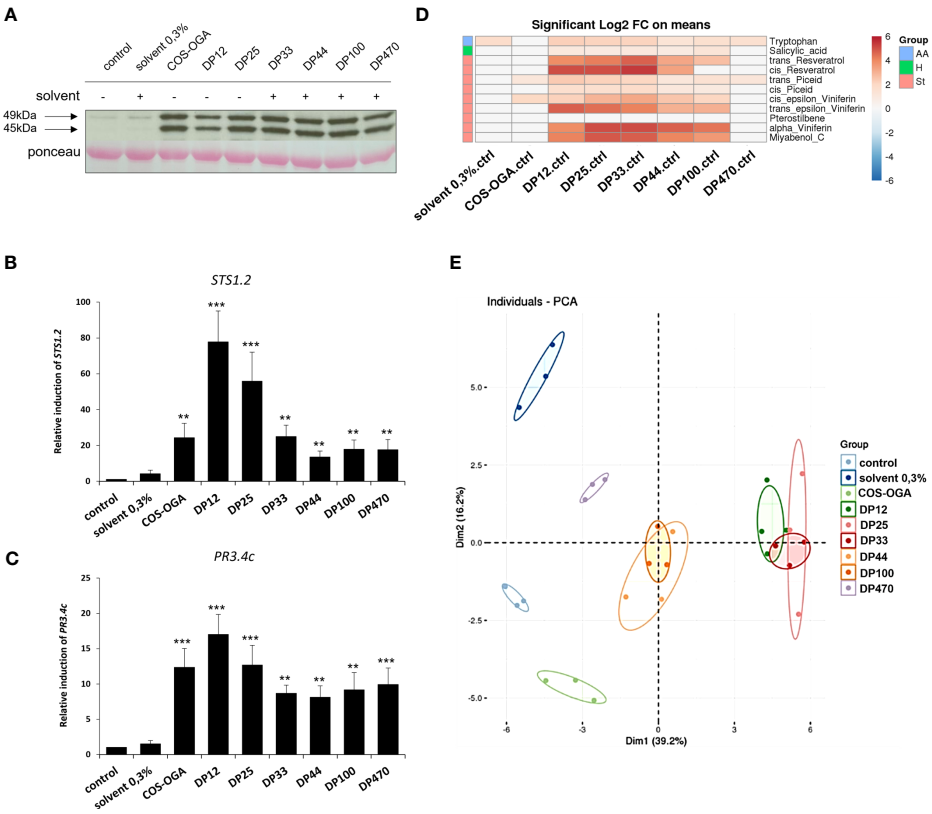

FIGURE 2
Defense response-induced with the different chitosans in grapevine. Leaf discs were floated on chitosan solutions (1g/L). Chitosan DP12 to DP470 were tested and compared to the negative control (water) and the previously characterized COS-OGA (62,5mg/L) as positive control. **(A)** Activation of two mitogen-activated protein kinases (MAPKs) in grapevine leaf discs, 20 min after elicitor treatment, detected by immunoblotting with α-pERK1/2 (Brulé et al., 2019). **(B, C)** Expression of defense genes encoding a stilbene synthase (*STS1.2*, **B**) and a chitinase (*PR3.4c*, **C**) measured by qPCR in grapevine leaf discs, 3h after treatment with the different chitosans. Values represent the mean ± SE of triplicate data obtained in three independant experiments (n=9). Asterisks indicate statistically significant differences between water and chitosan treatment, using an unpaired heteroscedastic Student's *t* test (**, P<0.01, ***, P<0.001). **(D)** Log2 of significant metabolite fold changes 24 hpt. Indicated pairwise comparisons are given by shades of red or blue colors according to the scale bar. Metabolites were grouped according to their chemical family as amino acids (AA), hormones (H) and stilbenes (St). Data represent mean values of three biological replicates for each condition. Statistical analyses were performed using Tukey's Honest Significant Difference method followed by a false discovery rate (FDR) correction, with FDR < 0.05. For FDR ≥ 0.05, Log2 fold changes were set to 0. **(E)** Global grapevine leaf disc metabolite changes 24 h after treatment with the different chitosans or control treatments. Principal component analysis (PCA) was performed on all quantified compounds in all conditions. Data represent mean values of three biological replicates for each treatment.

10.3389/fpls.2024.1360254

of defense compounds, the COS-OGA (positive control) slightly elicit the production of the two phytoalexins ε-viniferin and piceid at the concentration used and at the selected time point. The most marked significant differences concerned the production of stilbene phytoalexins such as resveratrol, α- and ε-viniferins, myabenol C and to a lesser extent piceid, the defense-related phytohormone salicylic acid, and the tryptophan amino acid (Figure 2D). Compared to water control, the differences at the level of stilbenes were strongly marked for chitosans DP12, 25 and 33, moderately for DP44 and 100, and low for DP470. These observations are corroborated by the principal component analysis (PCA, Figure 2E) which highlighted three groups related to the chitosan's DP: highly elicitor (DP12, 25, 33), intermediate (DP44 and 100) and weakly active (DP470). COS-OGA and the acidic solvent 0.3% were separated from the control (Figure 2E).

Taken together, these results confirmed that chitosans with smaller DPs are most effective in eliciting grapevine immune responses in plants grown in greenhouse-controlled conditions.

Effect of the chitosan's DP on the induced resistance against downy mildew in grapevine plants grown in greenhouse

The efficiency of the different chitosans to induce grapevine resistance was also investigated against downy mildew using a low dose of chitosan (30 mg/L). In greenhouse, grapevine leaves were treated with the different chitosans 48h prior to inoculation with *P. viticola*. Compared to the water control, showing a very important sporulation of *P. viticola* (0% protection), chitosan treatment with low DPs (12, 25 and 33) significantly reduced its sporulation with 95%, 91% and 89% of protection efficiency, respectively, while treatment with intermediate DPs (44 and 100) or high DP (470) only induced a partial resistance against downy mildew with respectively 45%, 47%, and 35% of protection (Figure 3).

Chitosan with a low DP better elicits defense gene expression in grapevine plants from vineyard

The abilities of three chitosans with different DPs (12, 100 and 470) to induce defense gene expression was also investigated in grapevine plants grown in vineyard, 10h after treatment by using a manual knapsack sprayer. Figure 4A indicated that only chitosan DP12 and the positive control COS-OGA led to the expression of the defense gene *STS1.2* in grapevine leaves. Figure 4B showed that all chitosans significantly induced the expression of the defense gene *ROMT* which encodes the enzyme catalyzing the biosynthesis of pterostilbene from resveratrol. As previously shown on grapevine plants grown in greenhouse, among the chitosans with different DPs, DP12 was also the best elicitor in vineyard conditions. The fact that, in the same experiements and at the same timepoint (10 hpt), defense genes in different pathways such as *STS1.2* and *PR3.4C* were

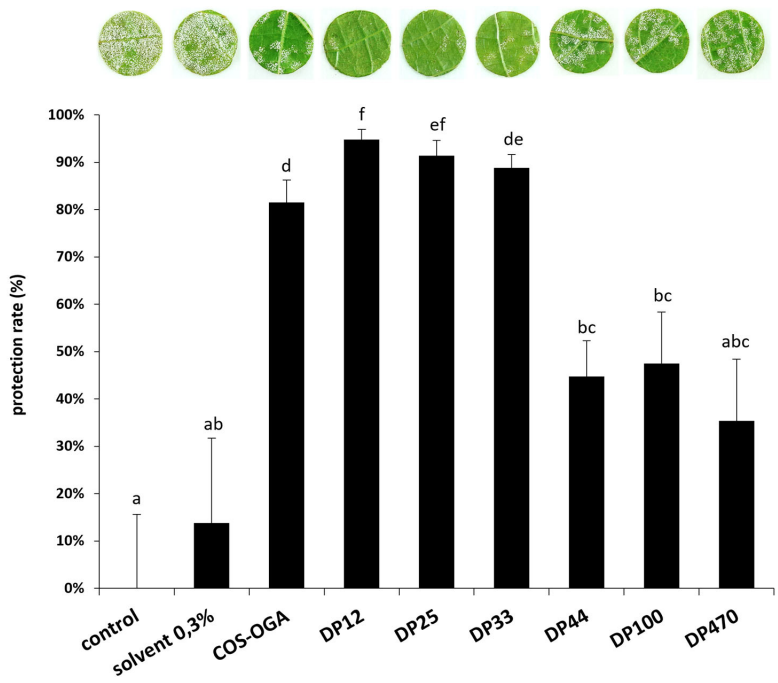

FIGURE 3
Chitosan-induced resistance against *Plasmopara viticola* under greenhouse conditions. Grapevine cuttings were sprayed with chitosan solutions (30 mg/L) 48 h before inoculation. Leaf discs were punched 5 dpi and the disease caused by *P. viticola* was assessed at 7 dpi. Sporulating leaf area was evaluated by image analysis Visilog 6.9 software (Kim Khiook et al., 2013). Values represent the mean of protection rate ± SE (n=36 discs from 3 different plants/condition) from one representative experiment out of three. Different letters indicate a statistically significant difference between treatments (Kruskal Wallis followed by Mann Whitney *post hoc* with P< 0 05).

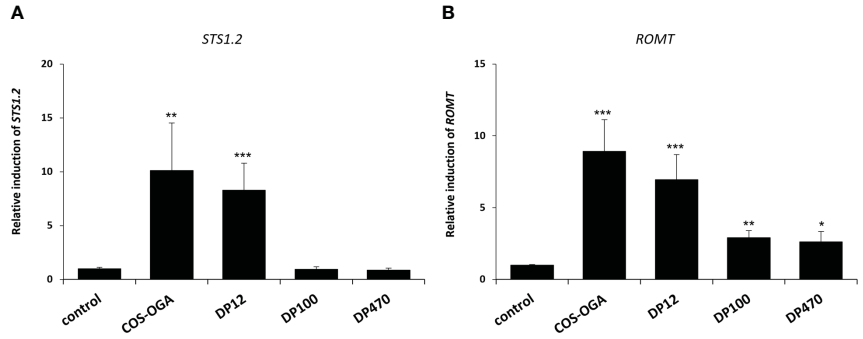

FIGURE 4
Chitosan-induced defense gene expression in grapevine leaves treated in vineyard. For both **(A, B)**, the expression of defense genes encoding a stilbene synthase (*STS1.2*) and a resveratrol O-methyltransferase (*ROMT*) measured by qPCR in grapevine leaves 10 h after being sprayed in vineyard. Values represent the mean ± SE of quadriplicate data (4 independent blocks) obtained in one experiment (n=4). Asterisks indicate statistically significant differences between water and chitosan treatment, using an unpaired heteroscedastic Student's *t* test (*, P<0.05, **, P<0.01, ***, P<0.001).

not induced in chitosan-treated young green berries (Supplementary Figure S1) suggests that the elicitation of plant immunity in leaves or fruits seems to be different, depending on the plant organ.

Chitosan with a low DP better induces grapevine resistance against downy mildew in vineyard-treated plants

Thereafter, the ability of chitosans to trigger grapevine resistance against downy mildew was tested in vineyard, using one chitosan with the lowest DP (DP12) and one with the highest DP (DP470). Grapevine plants were treated in the vineyard using a knapsack sprayer with these two chitosans and then artificially inoculated in the lab with *P. viticola*. In vineyard-treated plants, the disease intensity of downy mildew was similar with DP470 (20.2%) compared to the untreated control (21.9%) whereas DP12 showed the lowest disease intensity of 4.4% (Figure 5A). Interestingly protection against downy mildew triggered by chitosan DP12 was higher than that obtained with DP470 and reached 80% or 8%, respectively (Figure 5B). In the same vineyard experiments, chitosan-treated leaves were also artificially inoculated in the lab with *B. cinerea*. Similarly to the results obtained with downy mildew, chitosan DP12 induced a better protection against gray mold than DP470 (Supplementary Figure S2). These data indicate that chitosans can induce grapevine resistance not only in greenhouse conditions but also in vineyard-treated plants. Altogether, these results led us to select chitosan DP12 as the most efficient resistance inducer to further evaluate its ability to

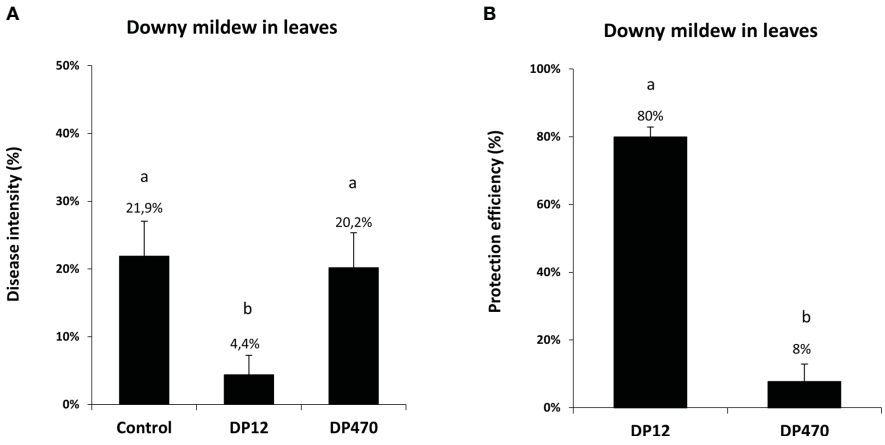

FIGURE 5
Comparison of the disease intensity and protection efficiency against downy mildew from grapevine leaves treated in vineyard with chitosan DP12 or DP470. Grapevine leaves from vineyard plants were sprayed with chitosan DP12 or DP470 (2 g/L) or untreated (control). Three days after treatment, leaves were harvested and leaf discs were punched and inoculated in the lab by *P. viticola* at 2.10^4 sp./mL. **(A)** Disease intensity was quantified by measuring the sporulating area at 7 dpi with image analysis Visilog 6.9 software. Data represent the mean ± SE of quintuplicate data (5 blocks) obtained in three independent experiments (n=15) realized in 2020 in the experimental vineyard of Marsannay. **(B)** The protection efficiency against downy mildew has been calculated for chitosan DP12 vs DP470 using the Abott formula (see materials and methods). Different letters indicate significant differences between treatments using the Kruskal Wallis test followed by Dunn's *post hoc* with P<0.05.

protect grapevine against powdery and downy mildews in different vineyard conditions.

Chitosan DP12 induces grapevine resistance against downy and powdery mildews in vineyard

To evaluate the ability of chitosan DP12 to protect grapevine against downy mildew, experimental trials were performed in independent vineyards on three different locations in France (Nohic, Laruscade, Allones). Four modalities were tested: untreated control as negative control, treatment with the copper mixture solutionat 500g Cu/ha (Bouillie Bordelaise CAFFARO WG at 2.5 kg/ha with 200g Cu/kg) used as positive control, treatment with the homologated dose of the biocontrol product COS-OGA at 25g/ha (BLASON at 2L/ha with 12.5 g COS-OGA/L) and chitosan DP12 at 400 g/ha. Our results indicate that the mean protection efficiency quantified in grapevine leaves against downy mildew, between the physiological stages BBCH73 and BBCH79, was 15% with COS-OGA, 52% with chitosan DP12 and 72% with the copper mixture solution used as positive control (Figure 6A; Supplementary Figure S3). Similar results were obtained on grapevine berries with a protection efficiency of 27% for COS-OGA, 54% for chitosan DP12 and 80% for the copper mixture solution (Figure 6B; Supplementary Figure S3).

The efficiency of chitosan DP12 was also investigated to protect grapevine berries against powdery mildew in experimental trials realized in three independent vineyards on different locations in France (Nîmes, Cardet and Villevieille). Our results showed that the protection efficiency against powdery mildew was 38% with COS-OGA, 47% with chitosan DP12 and 73% with the sulfur treatment (Lucifere at 2400g S/ha) used as a positive control (Figure 6C; Supplementary Figure S3).

Interestingly these results were obtained in independent vineyards where the disease intensities in control plants were quite different (Supplementary Figure S4).

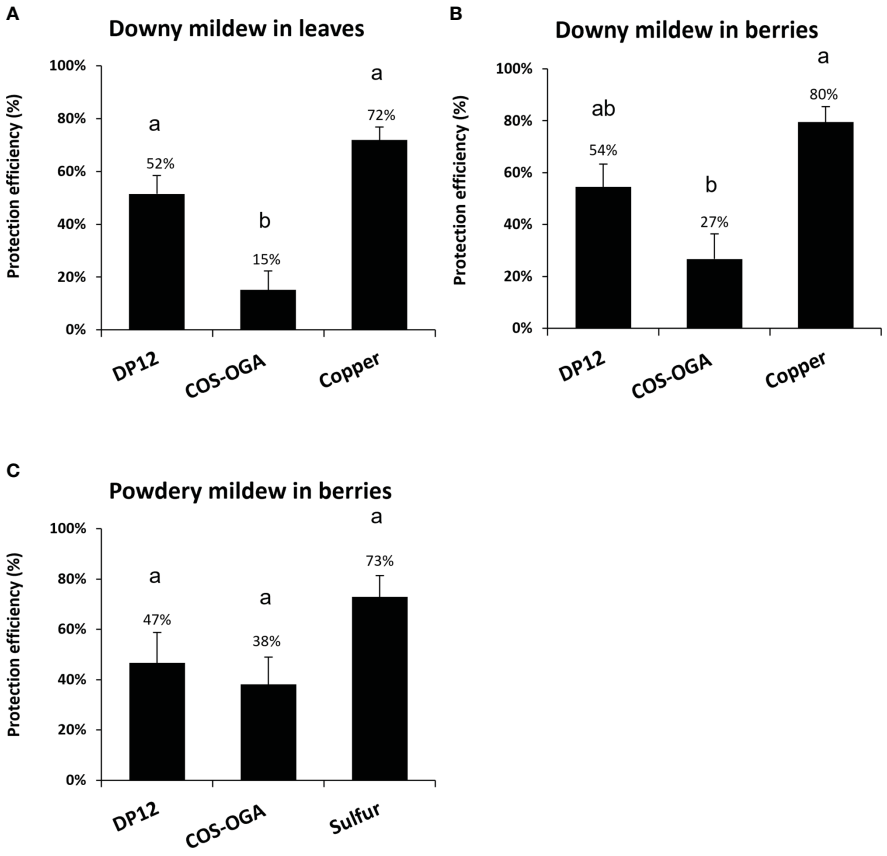

FIGURE 6
Protection efficiency of chitosan DP12 in grapevine leaves and berries against downy and powdery mildew in vineyard. Grapevine were sprayed with chitosan DP12 (400g/ha), COS-OGA (25g/ha; BLASON at 2 L/ha), copper mixture solution at 500g Cu/ha (Bouillie Bordelaise CAFFARO WG 20% Cu at 2,5 Kg/ha), sulfur solution at 2400g S/ha (LUCIFERE 3 L/ha at 800g S/L) or untreated (control). Protection efficiency of chitosan DP12 against downy mildew in leaves **(A)** and berries **(B)**, or against powdery mildew in berries **(C)**. Depending on the vineyard, between five to eight applications were carried out every 7 to 9 days and the protection efficiency was assessed 4 days after the last application between stages BBCH73 and 79. Values represent the mean of protection efficiency ± SE of quadriplicate data (4 blocks) obtained in three independent experiments (n=12) realized in 2023 in independent experimental vineyards on three different locations in France (i) (Nohic, Laruscade, Allonnes) on different grapevine cv (Cabernet franc, Merlot or Pinot noir, respectively) for downy mildew, and (ii) (Nîmes, Cardet and Villevieille) on different grapevine cv (Carignan, Chardonnay or Chardonnay, respectively) for powdery mildew. Different letters indicate significant differences between treatments using the Kruskal Wallis test followed by Dunn's *post hoc* ($P<0.05$).

Combination between chitosan DP12 and low amount of fungicides protects grapevine leaves and berries against downy mildew in vineyard

To evaluate the ability of chitosan DP12 to protect grapevine against downy mildew on a whole season program in vineyard, experimental trials were performed with 10 treatments per year. Three modalities were tested between physiological stages BBCH 35 to BBCH79: untreated control, 10 consecutive treatments with the copper mixture solution (Bouillie Bordelaise CAFFARO WG) with the following program: 4 times at 300g Cu/ha, 2 times at 500g Cu/ha at the flowering stage, and 4 times at 300g Cu/ha until veraison) used as positive control, or 4 treatments of chitosan DP12 (400 g/ha) followed by 2 treatments with the copper mixture solution (Bouillie Bordelaise CAFFARO WG at 500g Cu/ha) at the flowering stage, before the last 4 treatments with chitosan DP12 (400 g/ha). Our results indicated that the reduction of the chemical treatments by 80% (2 vs 10 treatments with the copper mixture solution) only decreases the protection efficiency from 67% to 58% on grapevine leaves (Figure 7A; Supplementary Figure S5) and from 70% to 48% on grapevine berries (Figure 7B; Supplementary Figure S5). Comparing the annual amount of copper used, 1000g Cu/ha were used in the program "DP12-Copper-DP12" compared to 3400g Cu/ha in the "Copper" program. Thus, the reduction by ~70% of the annual copper amount in the chitosan-based program (1000g Cu/ha vs 3400g Cu/ha) did not significantly decrease the protection efficiency (Figure 7).

Discussion

Chitosan is well known for its antimicrobial and antifungal properties that can be used in plant protection (Ait Barka et al., 2004; Dagostin et al., 2011; Kheiri et al., 2016). This antimicrobial effect is largely influenced by the molecular weight, the degree of acetylation as well as the preparation methods used (Verlee et al., 2017). Despite the amount of literature available, the variety of chitosan used and their incomplete characterization make comparison almost impossible. In a previous work, we have shown that chitosan treatments lead to grapevine resistance against *Botrytis cinerea* and *Plasmopara viticola* in laboratory conditions (Brulé et al., 2019). However, the efficiency of chitosan to confer a good protection level in grapevine leaves in laboratory and greenhouse settings greatly varies compared to the results obtained in vineyard (Dagostin et al., 2011). The reasons for this discrepancy remain unclear but several hypotheses can be made: (i) all chitosans do not possess the same biological activity to induce grapevine resistance, (ii) the leaching of chitosan by rainfall, (iii) the photo-oxidation of chitosan due to sunlight exposure and (iv) its degradation by enzymes secreted by the microbial community of the phyllosphere. Recently, Meynaud et al. demonstrated that UV irradiation of chitosan is ineffective in degrading chitosan, indicating that the lower effectiveness of chitosan in open fields cannot be attributed to sunlight exposure (Meynaud et al., 2023).

In the present study, we showed that a well characterized chitosan, highly deacetylated with a low DP, is more efficient in protecting grapevine plants grown in greenhouse and vineyard, as previously demonstrated in laboratory conditions (Aziz et al., 2006; Younes et al., 2014). Additionally, it is interesting to note that the part of the elicitation and the anti-microbial effect in the biological activity of chitosan remain poorly reported in the literature and seems to be difficult to estimate. Our results suggest that elicitation of the plant immunity has a synergistic effect with the anti-microbial properties of chitosan, at least in laboratory and greenhouse conditions. The present data highlight the induction of defense genes in chitosan-treated leaves of grapevine plants grown under greenhouse as in vineyard, indicating that these

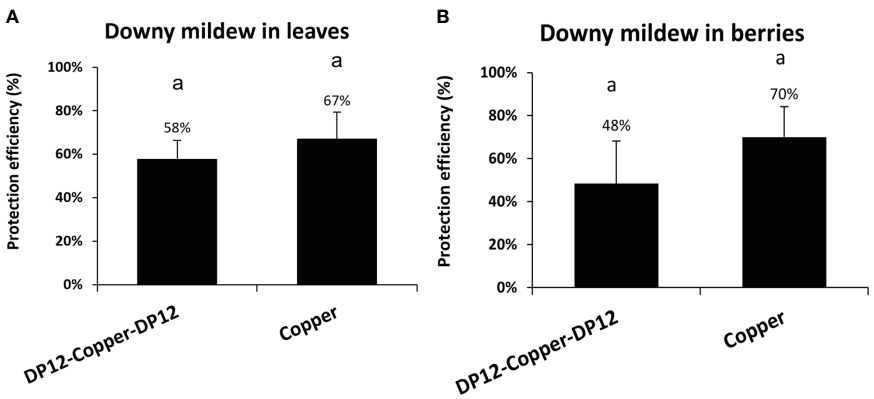

FIGURE 7
Protection efficiency of chitosan DP12 combined with low amount of fungicides in grapevine leaves **(A)** and berries **(B)** against downy mildew in vineyard. Ten applications were carried out every 7 to 9 days: either 4 times chitosan DP12 (400 g/ha) – 2 times copper mixture solution (Bouillie Bordelaise CAFFARO 500g Cu/ha) – 4 times chitosan DP12 (400 g/ha) or 10 times copper mixture solution (Bouillie Bordelaise CAFFARO) with 4 times (300g Cu/ha) – 2 times (500g Cu/ha) – 4 times (300g Cu/ha). The protection efficiency was assessed 4 days after the last application. Data represent the protection efficiency from one season program ± SE of quadriplicate data from 4 blocks (n=4) realized in 2021 in the French experimental vineyard of Allonnes on the Pinot noir cv. The annual amount of copper used was 1000g Cu/ha in the program "DP12-Copper-DP12" compared to 3400g Cu/ha in the "Copper" program. Similar letters indicate no significant differences between treatments using the Kruskal Wallis test followed by Dunn's post hoc with $P<0.05$.

defense genes could be used as molecular markers of the elicitation of plant immune responses. Interestingly, the tested defense genes were not induced at 10, 24 and 48 hpt (additional time points realized with no significant differences) in chitosan-treated young berries suggesting that the elicitation of the plant immunity could be different in leaves or fruits and thus could depend on the plant organ. So far, it might be interesting to discover the chitosan receptor to know its expression profile in the different plant organs. We have previously identified the two grapevine LysM receptor-like kinases VvLYK1-1 and VvLYK1-2 which participate in the chitosan perception (Brulé et al., 2019) whereas VvLYK5-1 or VvLYK5-2 are not involed (Roudaire et al., 2023). Interestingly, the expression of *VvLYK1-1* and *VvLYK 1-2* is quite low in the skin of young berries, suggesting that these co-receptors might be present in low amounts during the early development of this organ (Roudaire et al., 2023). Nevertheless, if the chitosan receptor is present in low quantity, we cannot exclude that these defense genes might be transiently induced at time points where samples were not harvested.

If the results obtained in the vineyard over several years were very interesting we also noticed that chitosan was less effective during rainy weather suggesting that chitosan might be rapidly leached. Thus, additional work is needed to find an appropriate formulation to still increase the protection efficiency of chitosan in vineyard conditions. Complementary trials conducted in different areas under real conditions have shown that chitosan efficiently protects grapevine leaves against downy or powdery mildew when the disease pressure is relatively low but that there was not a clear dose effect between 200, 300, 400 and 600 g/ha of chitosan. Thus, in a disease control program (against downy or powdery mildew), chitosan treatments can be inserted when the grapevine susceptibility to the disease is less strong, with a dose ranging from 200 to 400 g/ha depending on the quality of the spraying. When the disease pressure increases, the treatments with chitosan during the whole season with only two treatments of fungicides around the flowering stage offer a good vineyard protection to maintain the harvest. Finally, the association between chitosan and only two copper- or sulfur-based treatments during whole season programs could become an interesting alternative to greatly reduce the use of chemicals to improve the vineyards sustainability.

Data availability statement

The original contributions presented in the study are included in the article/Supplementary Material. Further inquiries can be directed to the corresponding author.

Author contributions

DB: Conceptualization, Data curation, Investigation, Methodology, Visualization, Writing – original draft. M-CH: Investigation, Methodology, Supervision, Writing – review & editing. TR: Investigation, Writing – review & editing. JV: Investigation, Writing – review & editing. SB: Data curation, Investigation, Methodology, Validation, Writing – review & editing. YP: Data curation, Investigation, Methodology, Writing – review & editing. BD: Data curation, Methodology, Supervision, Writing – review & editing. PC: Conceptualization, Investigation, Methodology, Supervision, Writing – review & editing. PH: Data curation, Formal analysis, Investigation, Methodology, Software, Supervision, Writing – review & editing. VC: Data curation, Investigation, Software, Supervision, Writing – review & editing. BP: Conceptualization, Funding acquisition, Investigation, Methodology, Project administration, Resources, Supervision, Validation, Writing – original draft, Writing – review & editing.

Funding

The author(s) declare financial support was received for the research, authorship, and/or publication of this article. This work has been financially supported by Agence Nationale de la Recherche (ANR) and Office Français de la Biodiversiteí (OFB) ("ChitoProtect" project, grant # ANR-19-ECOM-0008 and "BioSprayTech" project, grant # ANR-23-ECOM-0004).

Acknowledgments

The authors want to express gratitude to Dr Christian Gardrat from LCPO that provided its expertise in chitosan characterization. INRAE team would like to thank Agnès Klinguer for her help in the bioactivity assays.

Conflict of interest

The authors declare that the research was conducted in the absence of any commercial or financial relationships that could be construed as a potential conflict of interest.

Publisher's note

Supplementary material

The Supplementary Material for this article can be found online at: https://www.frontiersin.org/articles/10.3389/fpls.2024.1360254/full#supplementary-material

References

Ait Barka, E., Eullaffroy, P., Clément, C., and Vernet, G. (2004). Chitosan improves development, and protects Vitis vinifera L. against Botrytis cinerea. *Plant Cell Rep.* 22 (8), 608–614. doi: 10.1007/s00299-003-0733-3

Aziz, A., Trotel-Aziz, P., Dhuicq, L., Jeandet, P., Couderchet, M., and Vernet, G. (2006). Chitosan oligomers and copper sulfate induce grapevine defense reactions and resistance to gray mold and downy mildew. *Phytopathology* 96 (11), 1188–1194. doi: 10.1094/PHYTO-96-1188

Ben-Shalom, N., Ardi, R., Pinto, R., Aki, C., and Fallik, E. (2003). Controlling gray mould caused by Botrytis cinerea in cucumber plants by means of chitosan. *Crop Prot.* 22 (2), 285–290. doi: 10.1016/S0261-2194(02)00149-7

Boller, T., and Felix, G. (2009). A renaissance of elicitors: Perception of microbe-associated molecular patterns and danger signals by pattern-recognition receptors. *Annu. Rev. Plant Biol.* 60, 379–406. doi: 10.1146/annurev.arplant.57.032905.105346

Boutrot, F., and Zipfel, C. (2017). Function, discovery, and exploitation of plant pattern recognition receptors for broad-spectrum disease resistance. *Annu. Rev. Phytopathol.* 55, 257–286. doi: 10.1146/annurev-phyto-080614-120106

Brulé, D., Villano, C., Davies, L. J., Trdá, L., Claverie, J., Héloir, M. C., et al. (2019). The grapevine (Vitis vinifera) LysM receptor kinases VvLYK1-1 and VvLYK1-2 mediate chitooligosaccharide-triggered immunity. *Plant Biotechnol. J.* 17 (4), 812–825. doi: 10.1111/pbi.13017

Chandra, S., Chakraborty, N., Panda, K., and Acharya, K. (2017). Chitosan-induced immunity in Camellia sinensis (L.) O. Kuntze against blister blight disease is mediated by nitric-oxide. *Plant Physiol. Biochem.* 115, 298–307. doi: 10.1016/j.plaphy.2017.04.008

Dagostin, S., Schärer, H.-J., Pertot, I., and Tamm, L. (2011). Are there alternatives to copper for controlling grapevine downy mildew in organic viticulture? *Crop Prot.* 30 (7), 776–788. doi: 10.1016/j.cropro.2011.02.031

De Bona, G. S., Adrian, M., Negrel, J., Chiltz, A., Klinguer, A., Poinssot, B., et al. (2019). Dual Mode of Action of Grape Cane Extracts against Botrytis cinerea. *J. Agric. Food Chem.* 67 (19), 5512–5520. doi: 10.1021/acs.jafc.8b07098

Dodds, P., and Rathjen, J. (2010). Plant immunity: towards an integrated view of plant-pathogen interactions. *Nat. Rev. Genet.* 11 (8), 539–548. doi: 10.1038/nrg2812

Duan, C., Meng, X., Meng, J., Khan, M. I. H., Dai, L., Khan, A., et al. (2019). Chitosan as A preservative for fruits and vegetables: A review on chemistry and antimicrobial properties. *J. Bioresources Bioproducts* 4 (1), 11–21. doi: 10.21967/jbb.v4i1.189

Dubreuil-Maurizi, C., Trouvelot, S., Frettinger, P., Pugin, A., Wendehenne, D., and Poinssot, B. (2010). beta-aminobutyric acid primes an NADPH oxidase-dependent reactive oxygen species production during grapevine-triggered immunity. *Mol. Plant-Microbe Interact.* 23 (8), 1012–1021. doi: 10.1094/mpmi-23-8-1012

Faoro, F., Maffi, D., Cantu, D., and Iriti, M. (2008). Chemical-induced resistance against powdery mildew in barley: the effects of chitosan and benzothiadiazole. *BioControl* 53 (2), 387–401. doi: 10.1007/s10526-007-9091-3

Gamm, M., Héloir, M. C., Kelloniemi, J., Poinssot, B., Wendehenne, D., and Adrian, M. (2011). Identification of reference genes suitable for qRT-PCR in grapevine and application for the study of the expression of genes involved in pterostilbene synthesis. *Mol. Genet. Genomics* 285 (4), 273–285. doi: 10.1007/s00438-011-0607-2

Huet, G., Wang, Y., Gardrat, C., Brulé, D., Vax, A., Le Coz, C., et al. (2023). Deep chemical and physico-chemical characterization of antifungal industrial chitosans-biocontrol applications. *Molecules* 28 (3), 966. doi: 10.3390/molecules28030966

Iriti, M., Sironi, M., Gomarasca, S., Casazza, A. P., Soave, C., and Faoro, F. (2006). Cell death-mediated antiviral effect of chitosan in tobacco. *Plant Physiol. Biochem.* 44 (11-12), 893–900. doi: 10.1016/j.plaphy.2006.10.009

Iriti, M., and Varoni, E. M. (2015). Chitosan-induced antiviral activity and innate immunity in plants. *Environ. Sci. pollut. Res. Int.* 22 (4), 2935–2944. doi: 10.1007/s11356-014-3571-7

Jones, J. D. G., and Dangl, J. L. (2006). The plant immune system. *Nature* 444 (7117), 323–329. doi: 10.1038/nature05286

Kheiri, A., Moosawi Jorf, S. A., Malihipour, A., Saremi, H., and Nikkhah, M. (2016). Application of chitosan and chitosan nanoparticles for the control of Fusarium head blight of wheat (Fusarium graminearum) in *vitro* and greenhouse. *Int. J. Biol. Macromol* 93 (Pt A), 1261–1272. doi: 10.1016/j.ijbiomac.2016.09.072

Kim Khiook, I. L., Schneider, C., Heloir, M. C., Bois, B., Daire, X., Adrian, M., et al. (2013). Image analysis methods for assessment of H2O2 production and Plasmopara viticola development in grapevine leaves: application to the evaluation of resistance to downy mildew. *J. Microbiol. Methods* 95 (2), 235–244. doi: 10.1016/j.mimet.2013.08.012

Lemaître-Guillier, C., Hovasse, A., Schaeffer-Reiss, C., Recorbet, G., Poinssot, B., Trouvelot, S., et al. (2017). Proteomics towards the understanding of elicitor induced resistance of grapevine against downy mildew. *J. Proteomics* 156, 113–125. doi: 10.1016/j.jprot.2017.01.016

Lin, W., Hu, X., Zhang, W., Rogers, W. J., and Cai, W. (2005). Hydrogen peroxide mediates defence responses induced by chitosans of different molecular weights in rice. *J. Plant Physiol.* 162 (8), 937–944. doi: 10.1016/j.jplph.2004.10.003

Livak, K. J., and Schmittgen, T. D. (2001). Analysis of relative gene expression data using real-time quantitative PCR and the 2(T)(-Delta Delta C) method. *Methods* 25 (4), 402–408. doi: 10.1006/meth.2001.1262

Martin, I. R., Vigne, E., Velt, A., Hily, J. M., Garcia, S., Baltenweck, R., et al. (2021). Severe stunting symptoms upon nepovirus infection are reminiscent of a chronic hypersensitive-like response in a perennial woody fruit crop. *Viruses* 13 (11), 2138. doi: 10.3390/v13112138

Meynaud, S., Huet, G., Brulé, D., Gardrat, C., Poinssot, B., and Coma, V. (2023). Impact of UV irradiation on the chitosan bioactivity for biopesticide applications. *Molecules* 28 (13), 4954. doi: 10.3390/molecules28134954

Poinssot, B., Vandelle, E., Bentéjac, M., Adrian, M., Levis, C., Brygoo, Y., et al. (2003). The endopolygalacturonase 1 from Botrytis cinerea activates grapevine defense reactions unrelated to its enzymatic activity. *Mol. Plant Microbe Interact.* 16 (6), 553–564. doi: 10.1094/MPMI.2003.16.6.553

Romanazzi, G., Feliziani, E., and Sivakumar, D. (2018). Chitosan, a biopolymer with triple action on postharvest decay of fruit and vegetables: eliciting, antimicrobial and film-forming properties. *Front. Microbiol.* 9. doi: 10.3389/fmicb.2018.02745

Romanazzi, G., Mancini, V., Feliziani, E., Servili, A., Endeshaw, S., and Neri, D. (2016). Impact of alternative fungicides on grape downy mildew control and vine growth and development. *Plant Dis.* 100 (4), 739–748. doi: 10.1094/PDIS-05-15-0564-RE

Roudaire, T., Marzari, T., Landry, D., Löffelhardt, B., Gust, A. A., Jermakow, A., et al. (2023). The grapevine LysM receptor-like kinase VvLYK5-1 recognizes chitin oligomers through its association with VvLYK1-1. *Front. Plant Sci.* 14. doi: 10.3389/fpls.2023.1130782

Savary, S., Willocquet, L., Pethybridge, S. J., Esker, P., McRoberts, N., and Nelson, A. (2019). The global burden of pathogens and pests on major food crops. *Nat. Ecol. Evol.* 3 (3), 430–439. doi: 10.1038/s41559-018-0793-y

Steimetz, E., Trouvelot, S., Gindro, K., Bordier, A., Poinssot, B., Adrian, M., et al. (2012). Influence of leaf age on induced resistance in grapevine against Plasmopara viticola. *Physiol. Mol. Plant Pathol.* 79, 89–96. doi: 10.1016/j.pmpp.2012.05.004

Trdá, L., Fernandez, O., Boutrot, F., Héloir, M. C., Kelloniemi, J., Daire, X., et al. (2014). The grapevine flagellin receptor VvFLS2 differentially recognizes flagellin-derived epitopes from the endophytic growth-promoting bacterium Burkholderia phytofirmans and plant pathogenic bacteria. *New Phytol.* 201 (4), 1371–1384. doi: 10.1111/nph.12592

Trotel-Aziz, P., Couderchet, M., Vernet, G., and Aziz, A. (2006). Chitosan stimulates defense reactions in grapevine leaves and inhibits development of botrytis cinerea. *Eur. J. Plant Pathol.* 114 (4), 405–413. doi: 10.1007/s10658-006-0005-5

Vander, P., V rum, K. M., Domard, A., Eddine El Gueddari, N., and Moerschbacher, B. M. (1998). Comparison of the ability of partially N-acetylated chitosans and chitooligosaccharides to elicit resistance reactions in wheat leaves. *Plant Physiol.* 118 (4), 1353–1359. doi: 10.1104/pp.118.4.1353

Verlee, A., Mincke, S., and Stevens, C. V. (2017). Recent developments in antibacterial and antifungal chitosan and its derivatives. *Carbohydr Polym* 164, 268–283. doi: 10.1016/j.carbpol.2017.02.001

Younes, I., Sellimi, S., Rinaudo, M., Jellouli, K., and Nasri, M. (2014). Influence of acetylation degree and molecular weight of homogeneous chitosans on antibacterial and antifungal activities. *Int. J. Food Microbiol.* 185, 57–63. doi: 10.1016/j.ijfoodmicro.2014.04.029

Yu, X., Feng, B., He, P., and Shan, L. (2017). From chaos to harmony: Responses and signaling upon microbial pattern recognition. *Annu. Rev. Phytopathol.* 55, 109–137. doi: 10.1146/annurev-phyto-080516-035649

Zimmerli, L., Metraux, J., and Mauch-Mani, B. (2001). beta-aminobutyric acid-induced protection of Arabidopsis against the necrotrophic fungus Botrytis cinerea. *Plant Physiol.* 126 (2), 517–523. doi: 10.1104/pp.126.2.517

frontiers | Frontiers in Plant Science

TYPE Original Research
PUBLISHED 09 February 2024
DOI 10.3389/fpls.2024.1341181

OPEN ACCESS

EDITED BY
Choong-Min Ryu,
Korea Research Institute of Bioscience and Biotechnology (KRIBB), Republic of Korea

REVIEWED BY
Ahsan Rizvi,
Institute of Advanced Research (IAR), India
Veerendra Sharma,
Kansas State University, United States

*CORRESPONDENCE
Hao-Xun Chang
hxchang@ntu.edu.tw

RECEIVED 20 November 2023
ACCEPTED 08 January 2024
PUBLISHED 09 February 2024

CITATION
Chen J-Y, Sang H, Chilvers MI, Wu C-H and Chang H-X (2024) Characterization of soybean chitinase genes induced by rhizobacteria involved in the defense against *Fusarium oxysporum*.
Front. Plant Sci. 15:1341181.
doi: 10.3389/fpls.2024.1341181

Characterization of soybean chitinase genes induced by rhizobacteria involved in the defense against *Fusarium oxysporum*

Jheng-Yan Chen[1], Hyunkyu Sang[2], Martin I. Chilvers[3], Chih-Hang Wu[4] and Hao-Xun Chang[1,5,6]*

[1]Department of Plant Pathology and Microbiology, National Taiwan University, Taipei, Taiwan, [2]Department of Integrative Food, Bioscience and Biotechnology, Chonnam National University, Gwangju, Republic of Korea, [3]Department of Plant, Soil and Microbial Sciences, Michigan State University, East Lansing, MI, United States, [4]Institute of Plant and Microbial Biology, Academia Sinica, Taipei, Taiwan, [5]Master Program of Plant Medicine, National Taiwan University, Taipei, Taiwan, [6]Center of Biotechnology, National Taiwan University, Taipei, Taiwan

Rhizobacteria are capable of inducing defense responses via the expression of pathogenesis-related proteins (PR-proteins) such as chitinases, and many studies have validated the functions of plant chitinases in defense responses. Soybean (*Glycine max*) is an economically important crop worldwide, but the functional validation of soybean chitinase in defense responses remains limited. In this study, genome-wide characterization of soybean chitinases was conducted, and the defense contribution of three chitinases (GmChi01, GmChi02, or GmChi16) was validated in *Arabidopsis* transgenic lines against the soil-borne pathogen *Fusarium oxysporum*. Compared to the *Arabidopsis* Col-0 and empty vector controls, the transgenic lines with GmChi02 or GmChi16 exhibited fewer chlorosis symptoms and wilting. While GmChi02 and GmChi16 enhanced defense to *F. oxysporum*, GmChi02 was the only one significantly induced by *Burkholderia ambifaria*. The observation indicated that plant chitinases may be induced by different rhizobacteria for defense responses. The survey of 37 soybean chitinase gene expressions in response to six rhizobacteria observed diverse inducibility, where only 10 genes were significantly upregulated by at least one rhizobacterium and 9 genes did not respond to any of the rhizobacteria. Motif analysis on soybean promoters further identified not only consensus but also rhizobacterium-specific transcription factor-binding sites for the inducible chitinase genes. Collectively, these results confirmed the involvement of GmChi02 and GmChi16 in defense enhancement and highlighted the diverse inducibility of 37 soybean chitinases encountering *F. oxysporum* and six rhizobacteria.

KEYWORDS

Bacillus amyloliquefaciens*, *Bradyrhizobium japonicum*, *Burkholderia ambifaria*, *Lysobacter enzymogenes*, *Pseudomonas fluorescens*, *Rhizobium rhizogenes*, *Glycine max

Introduction

The composition of soil microbial communities varies depending on numerous factors, including the plant species or variety present. Plants release root exudates, which can attract beneficial microbes moving from bulk soil into the rhizosphere (Lugtenberg and Kamilova, 2009; Martinez-Medina et al., 2016; Lundberg and Teixeira, 2018). Many rhizobacteria, such as plant growth-promoting rhizobacteria (PGPR), can stimulate plant growth, and these rhizobacteria may enhance plant health by interacting directly or indirectly with soil-borne pathogens. The interactions can be generalized into three types: antagonism (Elnahal et al., 2022), parasitism (Tian et al., 2007), and induced systemic resistance (ISR) (Zhu et al., 2022). In terms of antagonism, rhizobacteria may secrete antibiotics or siderophores to antagonize or compete for nutrients with pathogens. Rhizobacteria such as *Bacillus amyloliquefaciens* and *Streptomyces* sp. exhibit these capabilities, and some strains have been developed into commercial products (Boubekri et al., 2022; Luo et al., 2022). Regarding parasitism, rhizobacteria may secrete enzymes such as chitinases that degrade fungal cell walls. Rhizobacteria such as *Burkholderia ambifaria* and *Enterobacter* sp. also possess predatory behaviors on fungi, thereby reducing fungal pathogens in the rhizosphere (Mousa et al., 2016; Stopnisek et al., 2016; Chang et al., 2021). Furthermore, due to the presence of microbe-associated molecular patterns (MAMPs) in most rhizobacteria, such as *Pseudomonas fluorescens* (Orozco-Mosqueda et al., 2023), pattern-triggered immunity (PTI) and ISR can be activated in the absence of soil-borne pathogens, leading to a phenomenon known as defense priming (Mauch-Mani et al., 2017; Salwan et al., 2023). Accordingly, the diverse mechanisms and interactions between plants and the rhizosphere microbes together contribute to the overall plant health and support agricultural sustainability.

The expression of pathogenesis-related protein (PR-protein) genes is one of the important responses in defense responses to combat pathogens, and many PR-protein genes have been confirmed to enhance defense responses in various mechanisms (Huang et al., 2016; Su et al., 2016; Luo et al., 2023; Wang Y et al., 2021). Among 17 families of PR-proteins (van Loon et al., 2006), the PR-3, PR-4, PR-8, and PR-11 proteins all encode plant chitinases, which contain the glycosyl hydrolases (GH) domain capable of breaking the β-1,4-glycosidic linkages of chitin, leading to disruption of fungal cell walls (Vaghela et al., 2022). These chitinases can be classified into GH18 and GH19 based on the similarity of their catalytic domains (CatD) (Kawase et al., 2004; Funkhouser and Aronson, 2007). The GH18 chitinases exhibit a barrel-like structure consisting of eight α-helices and eight β-sheets (Yang et al., 2010), and the GH19 chitinases possess a lysozyme-like domain composed of several α-helices (Kezuka et al., 2006). Plant chitinases have been further grouped into five classes (classes I–V) according to characteristics such as N-terminal sequences. While classes III and V belong to GH18, classes I, II, and IV belong to GH19 (Grover, 2012). Class I chitinases possess a chitin-binding domain (CBD) in their N-terminal region (Tang et al., 2004), and the C-terminal region of class I chitinases contains seven extended amino acids that facilitate their targeting to vacuolar and intracellular transport (Vaghela et al., 2022). Class II chitinases lack CBD in the N-terminal, and they are typically acidic proteins induced by pathogen infection and secreted to the extracellular space (Patil et al., 2000). Class III chitinases exhibit lysozyme activity without sequence similarity to classes I and II chitinases (Xu et al., 2016; Ma et al., 2017). Class IV chitinases possess both CBD and CatD similar to class I; however, due to deletions in the CBD and CatD domains, class IV chitinases are usually smaller than class I (Xu et al., 2016). Class V chitinases have a C-terminal extension for vacuolar targeting and may contain CBD (Taira et al., 2009; Grover, 2012). Accordingly, plant chitinases have evolved with diverse domains and variations.

The importance of plant chitinases in defense responses has been studied in several cases. For example, it was shown that 11 chitinase genes of rice were upregulated by *R. solani* infection. These rice chitinases were secreted into extracellular spaces, resulting in the degradation of fungal cell walls (Richa et al., 2016). Overexpression of the rice chitinase gene LOC_Os03g30470 enhanced defense against *Botrytis cinerea* and *Diplocarpon rosae* (Marchant et al., 1998; Núñez de Cáceres González et al., 2015). Overexpression of another rice chitinase gene, LOC_Os05g33130, increased defense responses to many diseases, and many studies have also demonstrated the defense contribution of various plant chitinases in different plant systems (Table 1). Other than the overexpression approach, gene silencing of the chili pepper chitinase gene CaChiIII7 resulted in larger foliar symptoms, less ROS accumulation in leaves, and reduced expression of defense-related genes (Ali et al., 2020). Collectively, the importance of plant chitinases in defense responses has been confirmed through overexpression and silencing approaches in different plant systems.

The advancement of high-throughput sequencing technology in the past decade has completed about 800 plant genomes (Marks et al., 2021; Sun et al., 2022), which speeded up the genome-wide characterization of plant chitinases in apple, *Arabidopsis thaliana*, *Brassica rapa*, cotton, cucumber, mulberry, rice, and tea (Grover, 2012; Xu et al., 2016; Chen et al., 2018; Bartholomew et al., 2019; Mir et al., 2020; Bordoloi et al., 2021; Haxim et al., 2022; Xin et al., 2022). For example, seven of the 24 chitinase genes discovered in the *A. thaliana* genome, such as AT1G19810, AT2G43570, AT2G43580, AT2G4359, and AT3G47540, were found to be upregulated upon infection by *B. cinerea* and *Pseudomonas syringae*. In the case of rice, 49 chitinase genes were characterized, and transcriptome analysis identified Os01g18400, Os01g19750, Os10g28050, and Os11g47510 being upregulated in response to *Magnaporthe grisea* infection (Grover, 2012). In the genomes of *B. rapa* and tea, 33 and 49 chitinase genes were discovered, respectively. Upregulation of several chitinase genes was also found during infections of the clubroot pathogen and three tea pathogens (Chen et al., 2018; Bordoloi et al., 2021). These findings demonstrate the power of high-throughput sequencing in genome-wide identification of plant chitinases, which also enable investigations for their expressions to different microbes.

Soybean (*Glycine max*) is one of the most important crops worldwide, and soybean diseases have been one of the major yield-limiting stresses for decades (Bandara et al., 2020; Bradley et al., 2021; Allen et al., 2022). However, there were limited studies on the functional validation of soybean chitinases (Lv et al., 2022) and their expressions induced by rhizobacteria. Therefore, this study

TABLE 1 Literature review of functionally characterized plant chitinases against fungal diseases.

Donor species	Gene ID	CAZy family	Class	Annotation	Recipient species	Targeting fungus	Ref.
Balsam pear	DQ407723.1 ABD66068.1	19	I	Mcchit1	Rice	*Magnaporthe grisea* *Rhizoctonia solani*	Li et al. (2009)
					Cotton	*Verticillium dahliae*	Xiao et al. (2007)
Barley	AJ276226.1 CAB99486.1	19	II	Chi2	Potato	*Alternaria solani*	Khan et al. (2017)
	AAA56786.1	19	II	CHI	Blackgram	*Corynespora cassiicola*	Chopra and Saini (2014)
					Tobacco	*Rhizoctonia solani*	Jach et al. (1995)
	M62904.1 AAA32941.1	19	II	Chi26	Wheat	*Fusarium graminearum*	Shin et al. (2008)
						Puccinia recondite *Puccinia striiformis* f. sp. *tritici* *Blumeria graminis*	Eissa et al. (2017)
	AAD28730.1	19	VII	Chi194	Tomato	*Fusarium oxysporum* f. sp. *lycopersici*	Girhepuje and Shinde (2011)
	KC899774.1 AGS38341.1	19	II	CEMB-chiII	Sugarcane	*Colletotrichum falcatum*	Tariq et al. (2018)
Bean	S43926.1 AAB23263.1	–	–	Chi CH5B	Cotton	*Verticillium dahliae*	Tohidfar et al. (2005)
					Canola	*Rhizoctonia solani*	Benhamou et al. (1993)
					Tobacco	*Rhizoctonia solani*	Brogue et al. (1991)
					Strawberry	*Botrytis cinerea*	Vellicce et al. (2006)
Chinese wild strawberry	MN709779 QLY89005.1	18	V	FnCHIT2	*Arabidopsis*	*Colletotrichum higginsianum*	Wen et al. (2020)
Cocoa	U30324 AAA80656.1	19	I	TcChi1	Cocoa	*Colletotrichum gloeosporioides*	Maximova et al. (2006)
Cucumber	NM_001308904.2 NP_001295833.1	18	III	CHI2	Cucumber	*Botrytis cinerea*	Kishimoto et al. (2004)
Eucommia ulmoides	KJ413009.1 AHX74093.1	19	I	EuCHIT2	Tobacco	*Erysiphe cichoracearum*	Dong et al. (2017)
Hanfu apple	LOC103401024 NP_001280823.1	19	II	MdCHI1	GL-3 apple	*Colletotrichum gloeosporioides* *Alternaria alternata*	Wang F et al. (2021)
Indian mustard	EF586206 ABQ57389.1	19	IV	Bj chitinase IV	Indian mustard	*Alternaria brassica*	Mir et al. (2021)
Mulberry	EXB55192.1	19	IV	MnChi18	*Arabidopsis*	*Botrytis cinerea*	Xin et al. (2022)
Maize	MG017374.1 AYK28286.1	19	I	Chit2	Maize	*Fusarium graminearum*	Dowd et al. (2018)
Pepper	KJ649334.1 AJF11981.1	19	IV	CaChitIV	*Arabidopsis*	*Hyaloperonospora arabidopsidis*	Kim et al. (2015)
Rice	LOC_Os03g30470 XP_015629397.1	–	–	RCH10	Rose	*Diplocarpon rosae*	Marchant et al. (1998)
					Lily	*Botrytis cinerea*	Núñez de Cáceres González et al. (2015)
	LOC_Os05g33130 XP_015640432.1	19	I	Chitinase2 Cht-2 RCC2 RCG3 RC7	Banana	*Mycosphaerella fijiensis*	Kovács et al. (2013)
					Chrysanthemum	*Botrytis cinerea*	Takatsu et al. (1999)
					Cucumber	*Botrytis cinerea*	Tabei et al. (1998)
					Cucumber	*Botrytis cinerea*	Kishimoto et al. (2002)

(Continued)

TABLE 1 Continued

Donor species	Gene ID	CAZy family	Class	Annotation	Recipient species	Targeting fungus	Ref.
				ChtBD1 RC24	Grape	*Uncinula necator*	Yamamoto et al. (2000)
					Italian ryegrass	*Puccinia coronata*	Takahashi et al. (2005)
					Indica rice	*Rhizoctonia solani*	Datta et al. (2001)
					Peanut	*Cercospora arachidicola*	Iqbal et al. (2012)
					Rice	*Magnaporthe grisea*	Nishizawa et al. (1999)
					Strawberry	*Sphaerotheca humuli*	Asao et al. (1997)
					Tomato	*Alternaria solani* *Fusarium oxysporum* f. sp. *lycopersici*	Jabeen et al. (2015)
					Wheat	*Puccinia striiformis* f. sp. *tritici*	Huang et al. (2013)
	X54367.1 CAA38249.1	19	I	Chil1 RCC11 RChit	Finger millet	*Pyricularia grisea*	Ignacimuthu and Ceasar (2012)
					Grapevine	*Uncinula necator*	Nirala et al. (2010)
					Litchi	*Phomopsis* sp.	Das and Rahman (2018)
					Peanut	*Aspergillus flavus*	Prasad et al. (2013)
					Rice	*Rhizoctonia solani*	Rajesh et al. (2016)
	LOC_Os11g47510 ABA95474.1	18	–	–	Rice	*Rhizoctonia solani*	Richa et al. (2017)
Round-leaved sundew	KU516826.1 AMM76171.1	19	I	DrChit	Tobacco	*Trichoderma viride*	Durechova et al. (2019)
Strawberry	OQ211094.1 WGF83129.1	19	II	FvChi-14	*Arabidopsis*	*Colletotrichum higginsianum*	He et al. (2023)
Sweet potato	MN971588.1 QOD94995.1	19	II	IbChiA	Sweet potato	*Ceratocystis fimbriata*	Liu et al. (2020)
Sugar beet	A23392.1 CAA01677.1	19	IV	Chitinase IV	Silver birch	*Melampsoridium betulinum*	Pasonen et al. (2004)
						Pyrenopeziza betulicola	Pappinen et al. (2002)
Tobacco	X16938.1 CAA34812.1	19	I	Tob CHI	Tobacco	*Rhizoctonia solani*	Vierheilig et al. (1993)
					Peanut	*Cercospora arachidicola*	Rohini and Sankara Rao (2001)
Wild rice	EU850802.1 ACJ24349.1	19	IV	OgChitIVa	*Arabidopsis*	*Botrytis cinerea*	Pak et al. (2009)
Wild tomato	LOC107008831 XP_015063508.1	–	–	pcht28	Strawberry	*Verticillium dahliae*	Chalavi et al. (2003)
					Tomato	*Verticillium dahliae* race 2	Tabaeizadeh et al. (1999)
Zoysiagrass	–	19	II	Zjchi2	Zoysiagrass	*Rhizoctonia solani* AG2-2	Kang et al. (2017)

performed a genome- and transcriptome-wide identification of soybean chitinases induced by *B. ambifaria* and validated the potential of soybean chitinases in defense against *Fusarium oxysporum*. In addition, transcriptomic analyses were conducted to profile soybean chitinases induced by six rhizobacteria, including *B. amyloliquefaciens*, *Bradyrhizobium japonicum*, *B. ambifaria*, *Lysobacter enzymogenes*, *P. fluorescens*, and *Rhizobium rhizogenes* (previously known as *Agrobacterium rhizogenes*). The study not only completed a comprehensive identification and validation of soybean chitinases induced by rhizobacteria but also highlighted the regulatory consensus and diversity among soybean chitinases to different rhizobacteria.

Results

Genome-wide identification of soybean chitinase genes

A search of the GH18 (PF00704) and GH19 (PF00182) domains identified 37 chitinase genes in the soybean genome, and all of them were predicted with an N-terminal signal peptide. Following the classification system of *Arabidopsis* chitinase genes, the soybean chitinase genes can be further divided into five genes in class I, four genes in class II, nineteen genes in class III, three genes in class IV, and six genes in class V (Figure 1). Using MEME analyses for characterizing motifs, the conserved GH18 motifs were identified in classes III and V, and the GH19 motifs were identified in classes I, II, and IV. As reported in the previous literature (Ma et al., 2017), class III chitinases harbor both GH18 motifs and GH19 lysozyme domain (motifs 3 and 8) as a classification signature. These results together confirmed that the HMMER method in genome-wide identification of soybean chitinase genes is robust and precise.

One controversial classification appeared for Glyma.01G160100, Glyma.02G007400, and Glyma.19G221800, which should be classified as class II for the absence of CBD (motif 15) if they followed the conventional classification for *Arabidopsis* chitinase genes (Patil et al., 2000). Although the presence or absence of CBD has been used to identify class I or IV chitinases (Patil et al., 2000; Grover, 2012; Xu et al., 2016), the MEME analyses found exceptions not only in soybean but also in *Arabidopsis*. For example, AT3G47540 was recognized as class IV chitinase because CBD was absent. In addition, although AT1G02360 and AT4G01700 were grouped as class II chitinases based on the absence of CBD, both phylogenetic and MEME analyses suggested that their sequences and motif structures were closer to the class I chitinases. Therefore, this study suggests a phylogeny-based classification for soybean chitinase genes (Figure 1), where classes II, III, and V chitinase genes do not contain CBD motif,

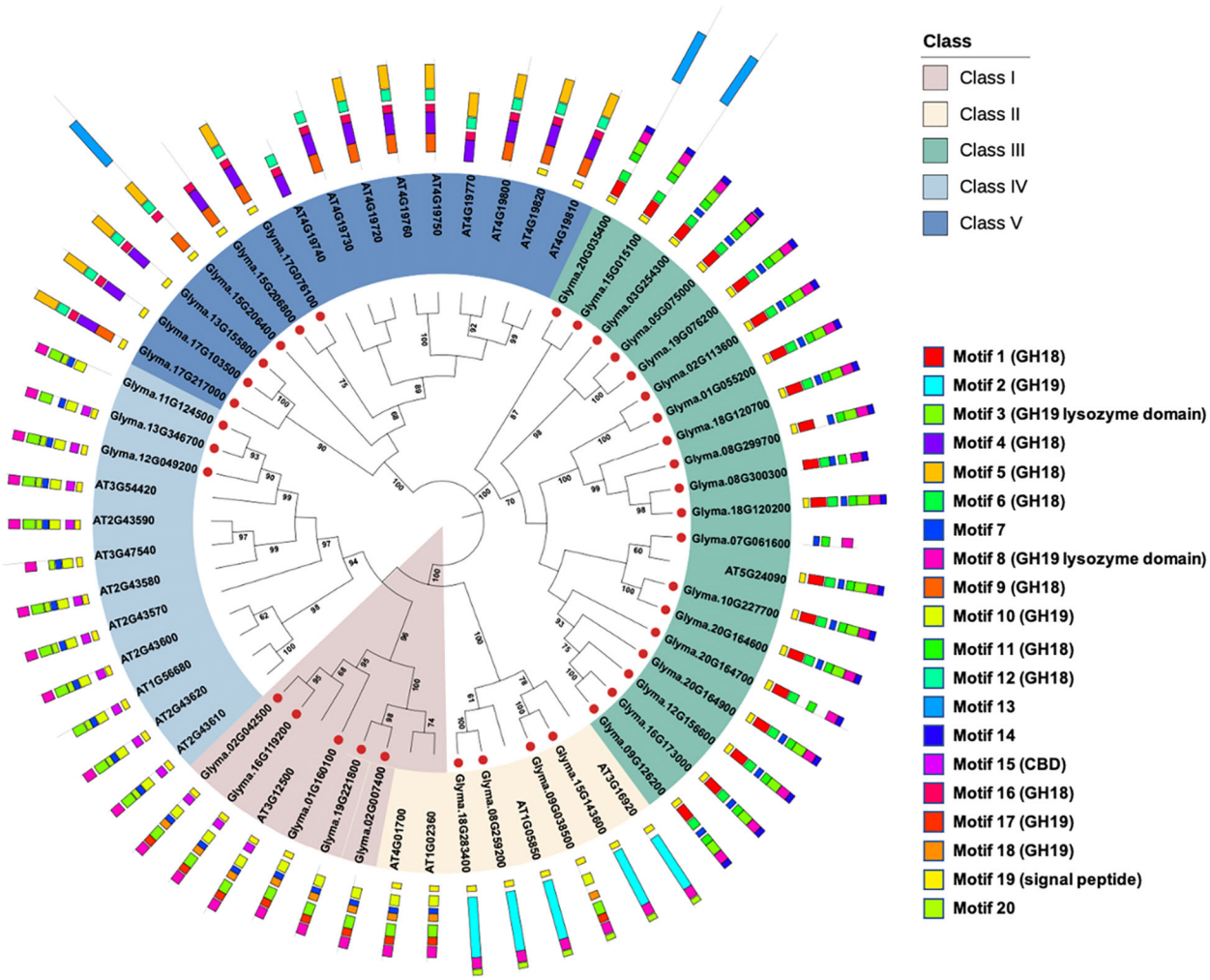

FIGURE 1
Genome-wide identification of soybean chitinase genes. The conserved HMM domains of the glycosyl hydrolase (GH) GH18 (PF00704) and GH19 (PF00182) chitinases were used as templates to identify soybean chitinases in the soybean reference genome. The 37 putative chitinases were further grouped using the neighbor-joining method into five classes according to the classification system built on *Arabidopsis thaliana* chitinases. There were 5, 4, 19, 3, and 6 chitinase genes in classes I, II, III, IV, and V, respectively, and there were 20 conserved motifs detected in the soybean chitinases. Bootstrap values above 60 were shown in the nodes.

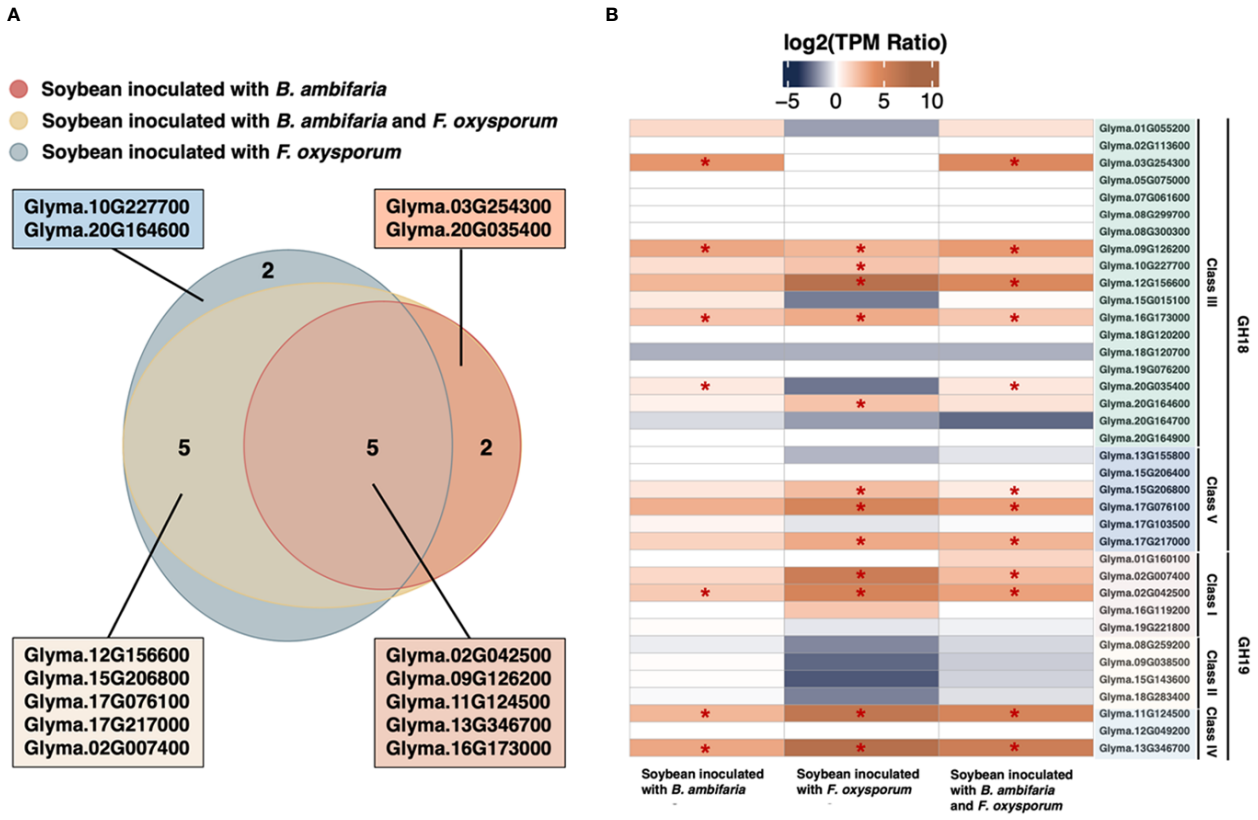

FIGURE 2
Soybean chitinase genes in response to the inoculation of *Burkholderia ambifaria*, *Fusarium oxysporum*, and co-inoculation. **(A)** Venn diagram suggests 12 chitinases being upregulated in response to *F. oxysporum* inoculation, while 7 chitinase genes were significantly induced by *B. ambifaria* in the absence of *F. oxysporum*. There were 5 consensus responding to the inoculation of *B. ambifaria*, *F. oxysporum*, and co-inoculation. **(B)** Gene expression of the 37 soybean chitinases, and the asterisk indicated the statistical significance of differential expression at a *q*-value of 0.05.

while classes I and IV chitinase genes may contain CBD motif. According to such criteria, Glyma.01G160100, Glyma.02G007400, and Glyma.19G221800 were classified as class I chitinases.

Gene expression of soybean chitinases in a tritrophic RNA-Seq experiment

Among the soybean chitinase genes, 12 genes exhibited upregulation in response to inoculation with *F. oxysporum* (Figure 2A). The top 5 upregulated genes included Glyma.13G346700, Glyma.12G156600, Glyma.11G124500, Glyma.02G007400, and Glyma.02G024500, which displayed a $\log_2$ fold change of 7.27, 7.23, 6.44, 5.89, and 4.97, respectively. Meanwhile, three among these five genes (Glyma.13G346700, Glyma.11G124500, and Glyma.02G024500) were also upregulated by the inoculation of rhizobacterium *B. ambifaria* in the absence of *F. oxysporum* (Table 2). In addition, Glyma.16G173000 and Glyma.09G126200 were also induced by *B. ambifaria*, but the upregulation of these two genes by *F. oxysporum* was not as high as the others. These results highlighted that these five soybean chitinase genes (Glyma.02G024500, Glyma.09G126200, Glyma.11G124500, Glyma.13G346700, and Glyma.16G173000) participated in the defense responses induced by *B. ambifaria*, and three of the five genes were listed in the top 5 important chitinase genes in the defense responses to *F. oxysporum* infection (Figure 2B). Indeed, upon the co-inoculation of *F. oxysporum* and *B. ambifaria*, for which the biomass of *F. oxysporum* was reduced by the antagonism of *B. ambifaria* (Chang et al., 2021), the upregulation of Glyma.13G346700, Glyma.11G124500, and Glyma.02G024500 was about 20% to 33% reduced compared to inoculation with *F. oxysporum* alone (Table 2). Collectively, Glyma.13G346700, Glyma.11G124500, and Glyma.02G024500 became the research focus not only for their inducibility but also for their expression trends reflecting the biotic stress created by the inoculation of *F. oxysporum*.

Phylogenetic analysis for soybean chitinases in defense responses

In order to assess the potentials of Glyma.13G346700, Glyma.11G124500, and Glyma.02G024500 in defense responses, a phylogenetic analysis for the 37 soybean chitinase genes was performed together with functionally validated plant chitinases from the literature (Table 1). For GH 18 chitinases, there were only three functionally validated plant chitinases, including cucumber, Chinese wild strawberry, and rice that can enhance

TABLE 2 Soybean chitinase genes induced by the inoculation of *Fusarium oxysporum*, *Burkholderia ambifaria*, and co-inoculation.

Gene ID	*F. oxysporum*		*B. ambifaria*		Co-inoculation	
	Log_2FC	*q*-value	Log_2FC	*q*-value	Log_2FC	*q*-value
Glyma.02G007400	**5.89**	**3.59E−18**	**n.s.**	**n.s.**	**2.64**	**4.28E−04**
Glyma.02G042500	**4.97**	**1.15E−50**	**1.87**	**2.17E−04**	**3.32**	**1.86E−22**
Glyma.03G254300	n.s.	n.s.	3.13	3.30E−02	3.92	9.04E−04
Glyma.09G126200	2.57	7.85E−08	3.12	5.88E−51	3.57	7.64E−91
Glyma.10G227700	2.08	6.45E−05	n.s.	n.s.	n.s.	n.s.
Glyma.11G124500	**6.44**	**8.66E−125**	**2.69**	**3.39E−06**	**5.07**	**4.81E−73**
Glyma.12G156600	**7.23**	**1.73E−22**	**n.s.**	**n.s.**	**4.82**	**4.41E−04**
Glyma.13G346700	**7.27**	**9.46E−69**	**3.28**	**1.12E−17**	**5.77**	**9.76E−69**
Glyma.15G206800	2.35	1.73E−25	n.s.	n.s.	0.71	5.09E−05
Glyma.16G173000	3.00	2.42E−05	2.12	8.11E−06	1.99	7.85E−05
Glyma.17G076100	4.88	1.36E−08	n.s.	n.s.	3.12	5.07E−04
Glyma.17G217000	3.09	1.46E−06	n.s.	n.s.	2.72	2.23E−04
Glyma.20G035400	n.s.	n.s.	0.88	8.63E−03	0.98	3.90E−04
Glyma.20G164600	2.43	1.96E−02	n.s.	n.s.	n.s.	n.s.

n.s., genes that were not being significantly upregulated. Bold values are the top 5-upregulated chitinase genes in response to *F. oxysporum*

defense responses to *B. cinerea*, *Colletotrichum higginsianum*, and *R. solani*, respectively (Kishimoto et al., 2004; Richa et al., 2017; Wen et al., 2020) (Figure 3A). There were more studies that confirmed the function of GH19 plant chitinases, and 27 functionally validated plant chitinases from apple, barley, cocoa, common bean, cucumber, maize, pepper, rice, and wheat were included in the phylogenetic analysis together with 12 GH19 soybean chitinases. These 12 soybean genes can be categorized into three groups (Figure 3B). The first group contains three soybean chitinase genes (Glyma.11G124500, Glyma.12G049200, and Glyma.13G346700), and the closest ortholog gene is the pepper CaChitIV, which enhances defense responses to *Arabidopsis* downy mildew (Kim et al., 2015). The second group includes four soybean chitinase genes, but only a strawberry gene, FvChi-14, which enhances *Arabidopsis* defense responses to *C. higginsianum*, is phylogenetically neighboring to these four genes (He et al., 2023). The last group with Glyma.01G160100, Glyma.02G024500, and Glyma.16G119200 clustered with apple, barley, bitter melon, cucumber, wild tomato, and zoysiagrass that were previously shown to contribute to the defense responses against multiple fungal pathogens, including many soil-borne fungi such as *F. oxysporum*, *R. solani*, and *Verticillium dahliae* (Table 1). In addition, two chitinase genes (Glyma.02G007400 and Glyma19G221800) were in the same clade but located distantly from the three soybean chitinase genes abovementioned. Among these genes, Glyma.02G024500 is the one that responded to the inoculation of *F. oxysporum* and *B. ambifaria*. On the other hand, the phylogenetically closed Glyma.01G160100 and Glyma.16G119200 did not seem to participate in the defense responses at least to *F. oxysporum*, nor be induced by *B. ambifaria*. The observation raised a question whether Glyma.01G160100, Glyma.02G024500, and Glyma.16G119200 (hereafter referred to a GmChi01, GmChi02, and GmChi16) all contain antifungal capability or if only Glyma.02G024500 remains antifungal. Accordingly, GmChi01, GmChi02, and GmChi16 were selected for functional validation.

Functional validation for soybean chitinases in defense responses

The homozygous transgenic *Arabidopsis* lines overexpressing empty vector (EV), GmChi01, GmChi02, or GmChi16, respectively, were validated for the expression of soybean chitinases (Supplementary Figure S1) before using their T_4 generation for experiments. For seedling root length, rosette leaves, and plant height, the transgenic lines (EV_6-8, GmChi01_6-8, GmChi01_7-1, GmChi02_3-7, GmChi02_6-3, GmChi16_4-3, and GmChi16_7-1) exhibited no difference in phenotypes (Figures 4A–C). However, the area under the disease progress curve (AUDPC) of these lines inoculated with *F. oxysporum* exhibited significant differences. The AUDPC of transgenic *Arabidopsis* overexpressing GmChi02 and GmChi16 were significantly lower than the controls (Figures 4D, E). Although transgenic *Arabidopsis* overexpressing GmChi01 exhibited reduced AUDPC in appearance, statistical analysis did not detect a significant difference. Meanwhile, identical results can be observed in soil inoculation with the conidial suspension of *F. oxysporum*, where transgenic *Arabidopsis* overexpressing GmChi02 and GmChi16 exhibited less seedling wilt. Transgenic *Arabidopsis* overexpressing GmChi01 again showed better survival in appearance, but the statistical analysis did not detect any significance (Figures 4F, G). These results indicate that GmChi02

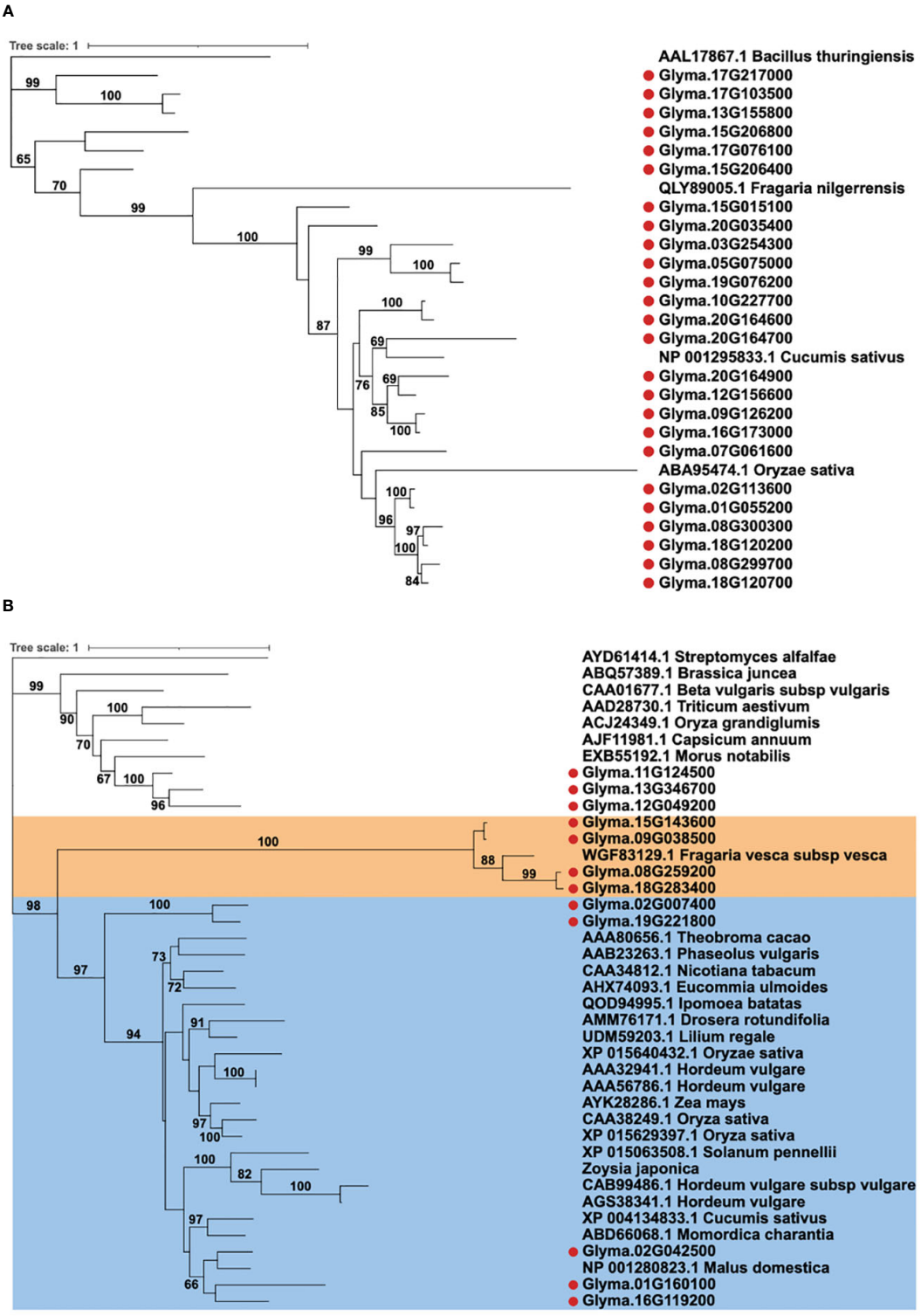

FIGURE 3
Phylogenetic analysis of soybean chitinase genes with functionally validated plant chitinases. **(A)** Soybean GH18 chitinases were analyzed with 3 functionally validated chitinases from Chinese wild strawberries, cucumber, and rice. **(B)** Soybean GH19 chitinases were analyzed with 27 functionally validated chitinases from multiple plant species. Soybean chitinase GmChi02, GmChi01, and GmChi16 (Glyma.02G042500, Glyma.01G160100, and Glyma.16G119200) are phylogenetically close to each other and grouped with most functionally validated plant chitinases. Unlike GmChi02, GmChi01 and GmChi16 were not upregulated by *F. oxysporum* nor induced by *B. ambifaria*. Bootstrap values above 60 in the Maximum likelihood tree are shown.

10.3389/fpls.2024.1341181

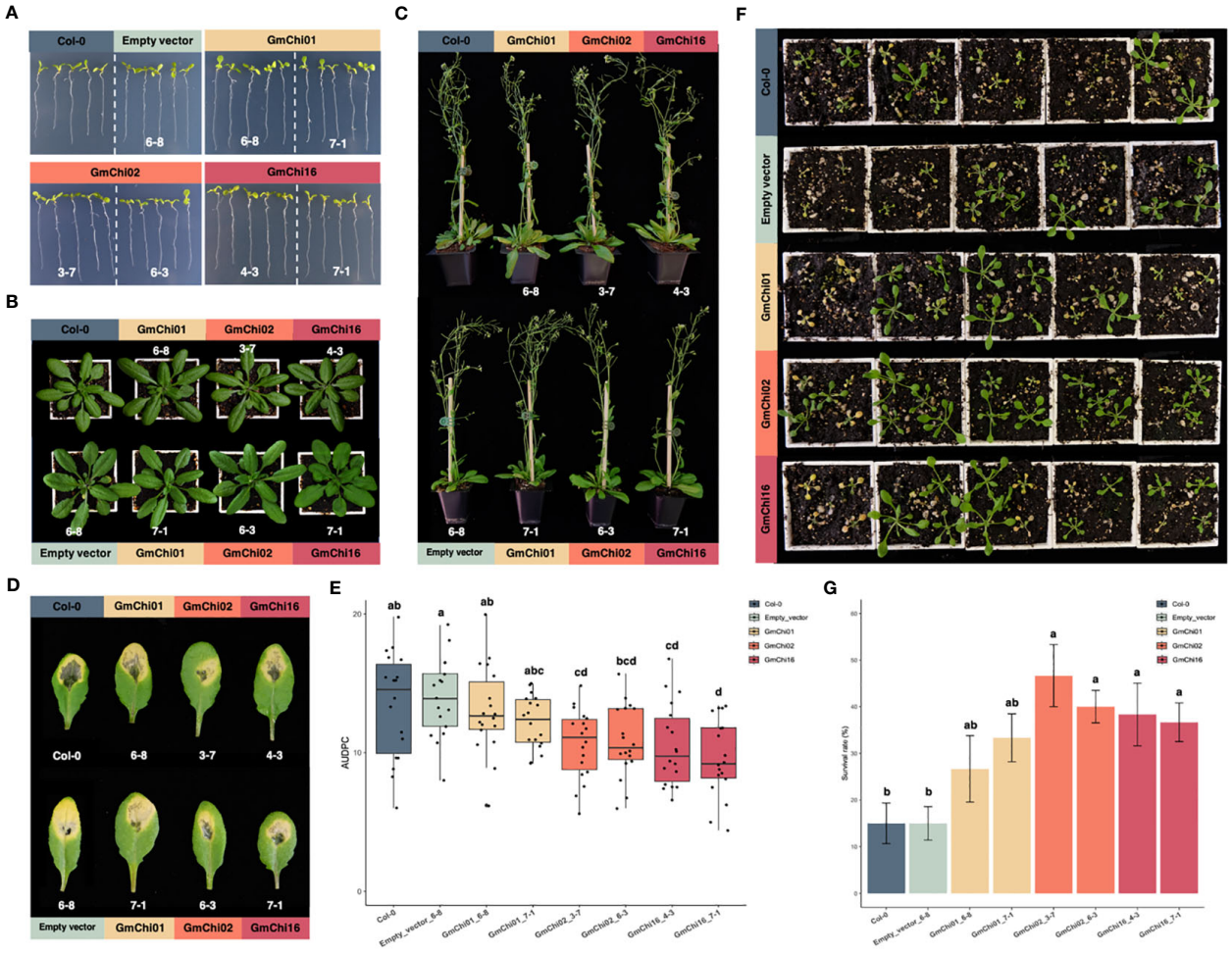

FIGURE 4
Phenotypes of *Arabidopsis* transgenic lines with GmChi01, GmChi02, or GmChi16. **(A)** Seedling root length, **(B)** Rosette leaves, and **(C)** Plant height of *Arabidopsis* transgenic lines exhibited no significant difference to the wild type Col-0 or *Arabidopsis* transgenic line with empty vector. **(D)** *Arabidopsis* transgenic lines with GmChi02 or GmChi16 exhibited mild symptoms after the inoculation of *F. oxysporum*. **(E)** Quantification of foliar symptoms after the inoculation of *F. oxysporum*. **(F)** *Arabidopsis* transgenic lines with GmChi02 or GmChi16 exhibited better seedling survival rates after the inoculation of *F. oxysporum*. **(G)** Quantification of seedling survival rates after the inoculation of *F. oxysporum*. Different letters indicate significant difference among the *Arabidopsis* transgenic lines (P< 0.05).

and GmChi16 were indeed phylogenetically and functionally close, and these two soybean chitinases enhanced defense responses to *F. oxysporum* infection. However, the gene regulation of GmChi01, GmChi02, and GmChi16 appeared to be diversified, and only GmChi02 exhibited inducibility in response to *B. ambifaria*.

Gene preference induced by different rhizobacteria on soybean chitinases

In order to survey the inducibility of soybean chitinase genes, six rhizobacteria from different genera were applied to soybean taproot to characterize gene expressions. As a result, *Bacillus amyloliquefaciens*, *Bradyrhizobium japonicum*, *B. ambifaria*, *Lysobacter enzymogenes*, *Pseudomonas fluorescens*, and *Rhizobium rhizogenes* upregulated zero, one, eight, one, six, and zero chitinase genes, respectively. Although there were some chitinase genes showing upregulation based on the average $\log_2$ fold change, variation within biological replicates may reduce the confidence in detecting statistical significance for cases such as GmChi02 (Glyma.02G024500) in response to *P. fluorescens*. Nonetheless, the survey confirmed that soybean chitinase genes responded differently to various rhizobacteria, where the expression of 10 chitinase genes (Glyma.02G007400, Glyma.02G042500, Glyma.10G227700, Glyma.11G124500, Glyma.12G156600, Glyma.13G155800, Glyma.13G346700, Glyma.16G173000, Glyma.17G217000, and Glyma.20G035400) were significantly induced by at least one rhizobacterium, and the expression of nine chitinase genes (Glyma.07G061600, Glyma.08G299700, Glyma.08G300300, Glyma.12G049200, Glyma.15G206400, Glyma.15G206800, Glyma.17G076100, Glyma.18G120200, and Glyma.20G164900) remain unchanged to all rhizobacteria (Figure 5).

Specifically, GmChi02 can be significantly induced by *B. diazoefficiens*, *B. ambifaria*, and *L. enzymogenes*. On the other hand, GmChi01 or GmChi16 did not reach statistical significance

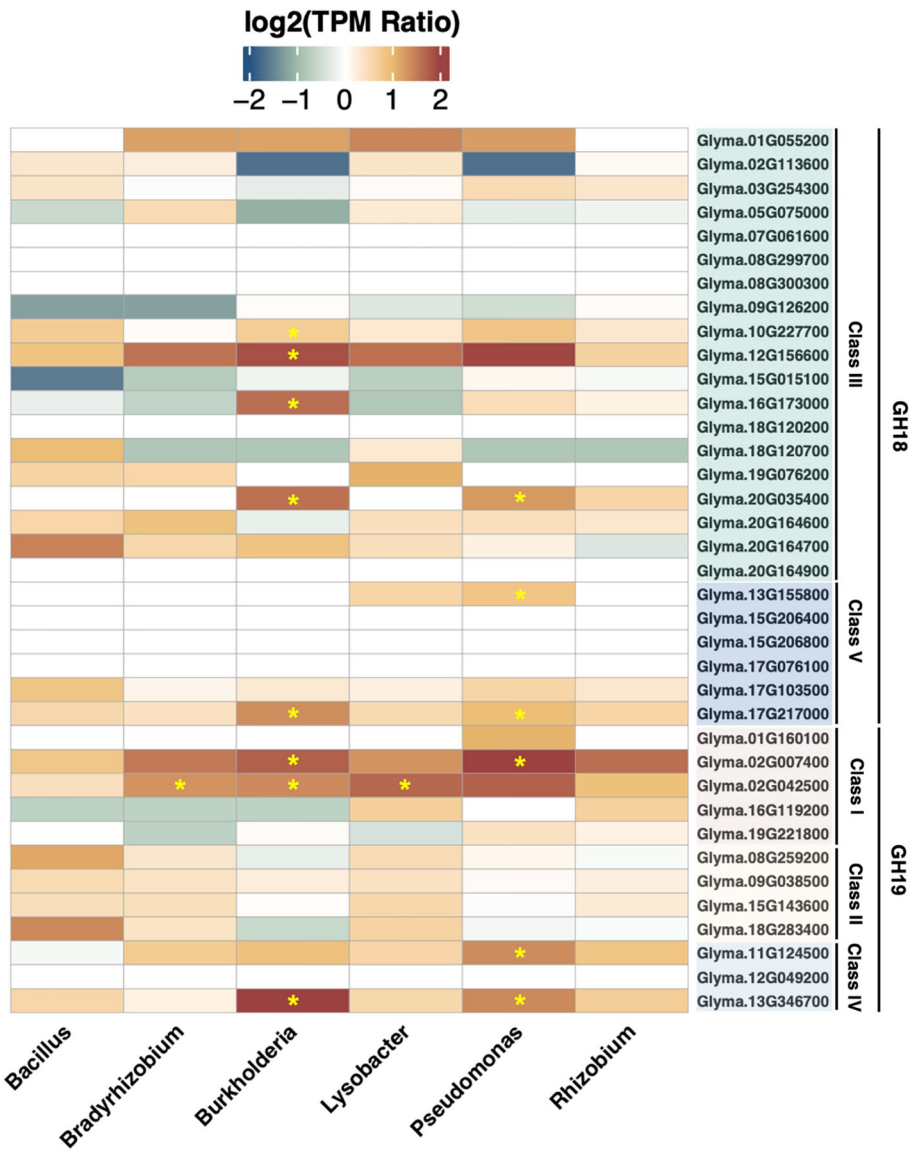

FIGURE 5
Gene expression of soybean chitinases in response to six rhizobacteria. Asterisks highlight the significant upregulation induced by the inoculation of each rhizobacterium. GmChi02 responded to all rhizobacteria, and the inoculation of *B. japonicum*, *B. ambifaria*, and *L. enzymogenes* reached statistical significance. GmChi01 only responded to *P. fluorescens* without statistical significance, and GmChi16 was upregulated by *L. enzymogenes* and *R. rhizogenes* without statistical significance.

for any rhizobacteria. As for other chitinase genes such as Glyma.13G346700, Glyma.12G156600, Glyma.11G124500, and Glyma.02G007400 that were induced by *F. oxysporum* infection (Figure 2B), Glyma.13G346700 and Glyma.02G007400 can be significantly induced by *B. ambifaria* and *P. fluorescens*. On the other hand, Glyma.12G156600 was upregulated by *B. ambifaria*, while Glyma.11G124500 was upregulated by *P. fluorescens*. These results suggest that soybean chitinase genes upregulated in the defense responses to *F. oxysporum* infection all interacted with at least one of the six rhizobacteria. Therefore, transcription factor-binding sites may have emerged during the co-evolution between soybeans and these rhizobacteria.

Identification of transcription factor and transcription factor-binding sites for the rhizobacteria-inducible soybean chitinase genes

In order to identify the potential regulatory motifs, the 5′ UTR and 3′ UTR of soybean chitinase genes that responded to the six rhizobacteria were analyzed. There were 94, 62, 76, 59, 125, and 90 soybean transcription factor-binding sites (TFBSs) associated with transcription factors (TFs) for soybean chitinase genes induced by *B. amyloliquefaciens*, *B. japonicum*, *B. ambifaria*, *L. enzymogenes*, *P. fluorescens*, and *R. rhizogenes*, respectively (Figure 6A). Among

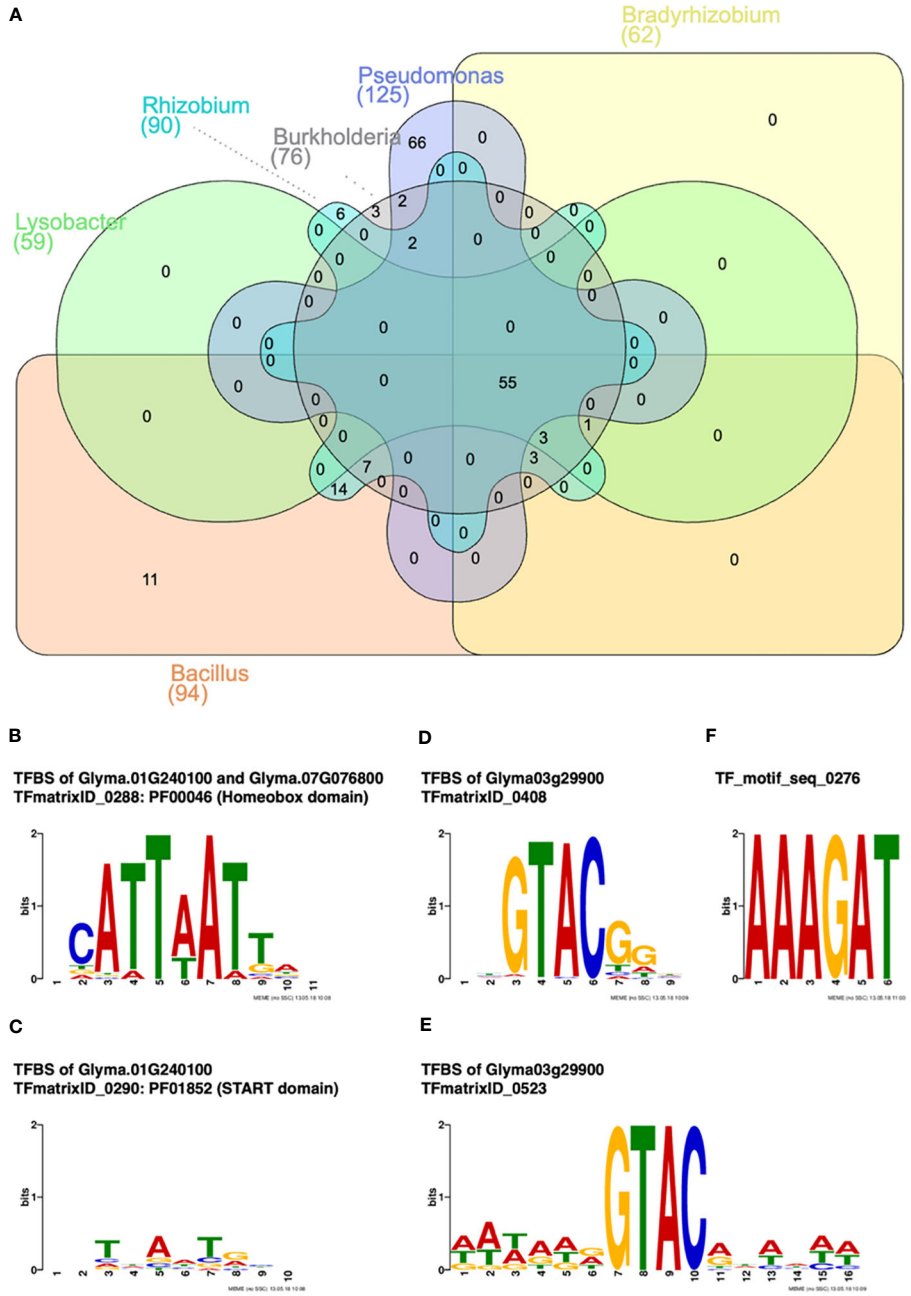

FIGURE 6
Transcription factor (TF) and TF-binding site (TFBS) analysis for rhizobacteria-inducible soybean chitinase genes. **(A)** Venn diagram of inducible soybean chitinase genes by *Bacillus amyloliquefaciens*, *Bradyrhizobium japonicum*, *Burkholderia ambifaria*, *Lysobacter enzymogenes*, *Pseudomonas fluorescens*, and *Rhizobium rhizogenes*. Only three soybean TFs responded to *B. ambifaria*, specifically. **(B)** Two TFs containing the homeobox domain in response to the inoculation of *B. ambifaria*, specifically. **(C)** One TF containing the START domain in response to the inoculation of *B. ambifaria*, specifically. **(D, E)** One TF containing the SQUAMOSA promoter-binding (SPB) domain in response to the inoculation of *B. ambifaria*, specifically. **(F)** The nodule-specific *cis*-regulatory motif was found in response to *B. amyloliquefaciens*, *B. japonicum*, *B. ambifaria*, *L. enzymogenes*, and *R. rhizogenes*.

these genes, there were 55 TFBSs associated with TFs consensually identified for all rhizobacteria, while there were only 11, zero, three, zero, 66, and six TFs exhibiting a specificity to *B. amyloliquefaciens*, *B. japonicum*, *B. ambifaria*, *L. enzymogenes*, *P. fluorescens*, and *R. rhizogenes*, respectively. Focusing on the TF enriched for interacting with *B. ambifaria*, there were three unique TFs, including two homeobox domain TFs (Glyma.01G240100 and Glyma.07G076800) and one SQUAMOSA promoter-binding protein (SBP)-box TF (Glyma03g29900) (Figures 6B–E).

As for TFBS without associated TFs, only one *cis*-regulatory element, NODCON1GM1, was found for *B. amyloliquefaciens*, *B. japonicum*, *B. ambifaria*, *L. enzymogenes*, and *R. rhizogenes* in contrast to the inducible and noninducible chitinase genes (Figure 6F). Based on the consensus and diversified inducibility of

soybean chitinase genes, the results indicated that the regulatory mechanism of chitinase genes may have co-evolved with soybean–rhizobacteria interaction.

Discussion

The benefits of rhizobacteria for plant health have been greatly recognized in different aspects. Other than direct antagonism against soil-borne pathogens, rhizobacteria may stimulate defense responses to provide sustainable plant protection. However, some scholars have pointed out that crops grown in fields may already be in a constant defense priming and/or induced systemic resistance (ISR) state because they are persistently interacting with rhizobacteria, and simply applying or exposure to rhizobacteria may not be sufficient to combat pathogens (Pieterse et al., 2014). Other literature indicates the density of rhizobacteria is a crucial key for defense priming, or ISR. For example, the minimum bacterial density required for *P. fluorescens* alone to induce ISR in laboratory conditions required 10^5 (Raaijmakers, 1995), and it may need to be higher in field conditions. Therefore, it could be challenging to achieve a sufficient population density of rhizobacteria for defense priming or ISR throughout the entire growing season (Walters et al., 2013). An alternative strategy is molecular breeding for important defense genes to bypass the reliance on bacterial density. For example, Rushanaedy et al. (2012) found the koa tree chitinase genes AKchit1a and AKchit1b were significantly upregulated in the resistant cultivars against *F. oxysporum* compared to susceptible cultivars, providing a screening criterion for disease resistance. Another application of plant chitinase genes is the early detection of biotic stresses. For example, the chitinase activity of papaya fruits was significantly increased upon *Colletotrichum gloeosporioides* infection during both the preharvest and storage stages. Since *C. gloeosporioides* is a pathogen exhibiting a latent infection stage, the expression of chitinase genes may serve as diagnostic biomarkers for asymptomatic fruits (Lucas-Bautista et al., 2020). Regardless of being selected as breeding targets or diagnosis biomarkers, the characterization of plant chitinase genes can provide novel insights and a comprehensive understanding of defense responses for a plant species.

This study performed genome- and transcriptome-wide identifications of soybean chitinases and functionally validated three phylogenetically close-related genes (GmChi01, GmChi02, and GmChi16) for their involvement in defense responses. The results showed that GmChi02 and GmChi16 enhanced defense responses to *F. oxysporum*, but only GmChi02 can be induced by *B. ambifaria*. In the transcriptomic characterization of GmChi02 in different rhizobacteria, the results confirmed a significant upregulation by *B. ambifaria* and *P. fluorescens*, and the expression of GmChi02 also responded to the inoculation of *B. amyloliquefaciens*, *B. japonicum*, *L. enzymogenes*, as well as *R. rhizogenes*. The observation indicates that GmChi02 may have co-evolved with multiple rhizobacteria to induce defense responses against soil-borne pathogens. On the other hand, although GmChi16 exhibited an equivalent defense effect as GmChi02, the expression of GmChi16 only responded to the inoculation of *L. enzymogenes* and *R. rhizogenes*. Collectively, these observations indicate that the regulatory mechanism of soybean chitinase genes may have diversity not only in the coding sequence level for functionality but also in the expression level in terms of inducibility.

Several TFs and TFBSs have been shown to regulate plant chitinase expression. For example, the homeodomain leucine zipper III TF CsHB15 of cucumber was found to bind the promoter of CsChi23 and induce gene expression in response to *F. oxysporum* (Bartholomew et al., 2022). The R2R3-MYB TF of brown mustard was shown to recognize the W-box-like-4 (Wbl-4) element to activate BjCHI1 in response to *B. cinerea* (Gao et al., 2016). Another example is the LrWRKY2 of lily, which induced LrCHI2 expression in response to *F. oxysporum* (Li et al., 2021). However, whether plant chitinase genes harbor conserved TF and TFBS in response to rhizobacteria has not been assessed. In this study, several TF genes and motifs were highlighted by contrasting the TFs and TFBS motifs between the inducible and non-inducible soybean chitinase genes in each rhizobacterium (Supplementary Table S2). One with particular interest would be the NODCON1GM, which has been known to be a nodule-specific regulatory element (Wang et al., 2022). Mutation and deletion of NODCON1GM (5′-AAAGAT) or another regulatory element, NODCON2GM (5′-CTCTT), were shown to decrease the number of nodule formations (Jørgensen et al., 1991). The presence of NODCON1GM in the promoters of rhizobacteria-inducible chitinase genes suggests a possibility that the regulatory mechanism to drive chitinase genes may rely on a similar manner as the regulatory element NODCON1GM. Additional studies on the emergence of NODCON1GM in some but not all soybean chitinase genes, along with studies on the presence of NODCON1GM in the promoters of other soybean PR-protein genes, may further illuminate the evolution of rhizobacteria-induced defense responses.

Research has shown that soybean has diverse rhizobacteria, including *Bradyrhizobium*, *Bacillus*, *Burkholderia*, and *Rhizobium* species (Biate et al., 2014; Zhong et al., 2019; Han et al., 2020; Yamazaki et al., 2021), that could affect soybean yield and disease incidence (Chang et al., 2017; Hussain et al., 2018). Future studies may focus on the selection pressure derived from soybean rhizobacteria on the expressions of PR-protein genes and the regulatory mechanisms of defense responses induced by different rhizobacteria. These research advances may provide a broad knowledge of the application of beneficial rhizobacteria to enhance plant health.

Materials and methods

Plant and microbial materials

For routine cultivation of *Arabidopsis thaliana*, the seeds were surface-sterilized using 70% ethanol and 50% Clorox bleach (Oakland, CA, USA). After rinsing five times with sterile water, the seeds were placed in the dark at 4°C for 48 h for vernalization. Subsequently, the seeds were planted in a soil mixture (peat moss: vermiculite:perlite = 6:1:1) and cultured in a long-day condition (16 h light/8 h dark) at 22°C.

For routine growth of rhizobacteria, *Bradyrhizobium japonicum* USDA6 (BCRC 80814^T) was cultured in yeast mannitol broth (0.2 g/L K_2HPO_4, 0.2 g/L $MgSO_4{\cdot}7H_2O$, 10.0 g/L mannitol, 0.05 g/L NaCl, 0.3 g/L yeast extract; pH 6.2). The other bacterial species, including *Bacillus amyloliquefaciens* ATCC23350 (BCRC 11601^T), *Burkholderia ambifaria* AMMD ATCCBAA-244 (NRRL B-23395^T), *Lysobacter enzymogenes* ATCC29487 (BCRC 11654^T), *Pseudomonas fluorescens* ATCC 13525 (BCRC 11028^T), and *Rhizobium rhizogenes* K599 (Lifeasible, Shirley, NY 11967, USA) were cultured in Nutrient Broth (HiMedia, Mumbai, India). All rhizobacteria were cultured at 28°C with 125 rpm shaking. To establish the correlation between optical density (OD) 600 and colony-forming units (CFU), bacterial suspensions at OD600 value of 0.5 were diluted and quantified on plates, and linear regression was applied in the later experiment for estimating CFU of bacterial suspensions.

For routine growth of *Fusarium oxysporum* f.sp. *rapae* (BCRC FU31513), the fungus was subcultured on potato dextrose agar (PDA) at 28°C without light every 7 days. For producing conidia, the fungus was cultured in synthetic nutrient-poor broth (SNB) (0.5 g/L $MgSO_4{\cdot}7H_2O$, 1 g/L KH_2PO_4, 1 g/L KNO_3, 0.5 g/L KCl, 0.2 g/L glucose, and 0.2 g/L sucrose) (Moura et al., 2020) in the dark at 28°C and 125 rpm for 7 days. The conidia suspension was adjusted to a concentration of 1×10^6 conidia/ml.

Genome-wide identification and phylogenetic analysis of soybean chitinases

To identify chitinase genes in the soybean genome, the HMMs of the GH18 (PF00704) and GH19 (PF00182) protein domains were downloaded from the Pfam database (Mistry et al., 2021). Subsequently, HMMER v3.3.2 was applied to search PF00704 and PF00182 in the 'Williams 82' (W82) (Gmax_508_Wm82.a4.v1.protein) at a threshold of 1^{-10} *E*-value (Finn et al., 2011). The presence of GH18 or GH19 domain was double-checked using the NCBI Conserved Domain Database at a threshold of 1^{-20} *E*-value. In addition, protein tertiary structure was assessed by predicting the folded structure of each soybean chitinase gene protein sequence using ColabFold (Mirdita et al., 2022). Furthermore, MEME v5.4.1 was utilized at a setting of a maximum motif length of 300 and a number of motifs of 20 to identify conserved motifs within the protein sequences (Bailey and Elkan, 1994). The Protparam (Gasteiger et al., 2005), SignalP5.0 (Almagro Armenteros et al., 2019), and DeepLoc-1.0 (Almagro Armenteros et al., 2017) webtools were employed to investigate the amino acid composition, molecular weight, and isoelectric point of soybean chitinase proteins.

The protein sequences of soybean chitinases were aligned with 24 *Arabidopsis thaliana* chitinases sourced from the TAIR database (Lamesch et al., 2012). Alignment was performed using MAFFT v7 (Katoh et al., 2019), and the phylogenetic tree was constructed using the neighbor-joining (NJ) method in MEGA-X (Kumar et al., 2018). Additionally, the protein sequences of soybean chitinases were aligned with functionally validated chitinase sequences from 21 plant species (Table 1). The phylogenetic tree was constructed using the maximum likelihood (ML) method in IQ-TREE v2.2.0 (Nguyen et al., 2015). The visualization of the phylogenetic trees was generated using iTOL (Letunic and Bork, 2021).

Transcriptomic analysis of soybean chitinases

The tritrophic RNA-Seq data were obtained from a previous study on the gene expression of *F. oxysporum* in the roots of the soybean variety 'Jack' under the influence of the antagonistic bacterium *B. ambifaria* (Chang et al., 2021). The data can be categorized into four treatments: (1) soybean roots without *B. ambifaria* or *F. oxysporum*, (2) soybean roots inoculated with *B. ambifaria*, (3) soybean roots inoculated with *F. oxysporum*, and (4) soybean roots simultaneously inoculated with both *B. ambifaria* and *F. oxysporum*. Each treatment consisted of three biological replicates, totaling 12 samples. The RNA-Seq was performed using the Illumina HiSeq 4000 platform (Illumina, San Diego, CA, USA). The raw data underwent quality control to keep reads with a Phred score ≥ 30 using the FASTQC and FASTX-ToolKit v0.0.14. The soybean W82 transcriptome (Gmax_508_Wm82.a4.v1.cds.fa) was used as a template for Kallisto v0.46.1 (Bray et al., 2016). Subsequently, differential gene expression analysis was conducted using the R package Sleuth v0.30 (Pimentel et al., 2017) at a threshold of 0.05 *q*-value. Transcript per million (TPM) measurements of the 37 soybean chitinase genes were presented in a heatmap using the R package ComplexHeatmap v2.13.1 (Gu et al., 2016).

In the RNA-Seq experiment of soybean root inoculated by six rhizobacteria, the W82 soybean seeds were sterilized in 1% bleach for 15 min, followed by five rinses with sterile water. The sterilized seeds were vernalized in sterile water at 28°C without light to better synchronize the germination rate. The next day, the seed coats were removed, and the seeds were placed on 1.5% water agar plates in a growth chamber at 28°C without light for 3 days. After the seeds germinated and the hypocotyls elongated to approximately 3 cm to 5 cm, the seedlings were transferred to new water agar (WA) plates, where 100 µl (approximately 1×10^7 CFU/ml) of bacterial suspension was inoculated onto the soybean hypocotyls. The control group was inoculated with ddH_2O.

The inoculated soybean seedlings were further incubated in a growth chamber at 28°C without light. After incubating for 2 days, the frozen taproot samples were homogenized in liquid nitrogen with Invitrogen™ TRIzol™ Reagent (Thermo Fisher Scientific, Waltham, MA, USA), followed by the extraction workflow using chloroform and isopropanol. With two biological replicates per rhizobacteria and control, a total of 14 samples were sent to RNA-Seq using the Illumina NovaSeq 6000 platform in a 150-bp pair-ended platform (Biotools, New Taipei City, Taiwan).

Molecular cloning of GmChi01, GmChi02, and GmChi16

Three chitinase genes, namely Glyma.01G160100 (GmChi01), Glyma.02G042500 (GmChi02), and Glyma.16G119200

(GmChi16), were PCR amplified from the soybean W82 genomic DNA using primers with a SpeI site at the 3′ end (GmChi01_F_SpeI/GmChi01_R_SpeI; GmChi02_F_SpeI/GmChi02_R_SpeI; GmChi16_F_SpeI/GmChi16_R_SpeI) (Supplementary Table S1) via the Phusion® High-Fidelity DNA Polymerase (New England Biolabs, Ipswich, MA, USA). The PCR sizes of three chitinase genes were 2227 bp (GmChi01), 2243 bp (GmChi02), and 1417 bp (GmChi16), and the amplicons were treated with SpeI before being cleaned up using the GenepHlowTW Gel/PCR Kit (Geneaid, New Taipei City, Taiwan). The T4 DNA Ligase (NEB) was used to ligate chitinase amplicons into the pCAMBIA1302 vector pretreated with shrimp alkaline phosphatase (rSAP) (NEB). The ligation mixture was heat-shock transformed into *Escherichia coli* DH5α competent cells (Yeastern Biotech, New Taipei City, Taiwan) and selected on kanamycin. Colony PCR was performed using specific primers for each chitinase gene (Table 2) using the SMB All-1 DNA Polymerase Premix (StarMoonBio, New Taipei City, Taiwan). The constructs (pCAMBIA1302::GmChi01, pCAMBIA1302::GmChi02, and pCAMBIA1302::GmChi16) were purified using the EasyPure Plasmid DNA Mini Kit (Bioman, New Taipei City, Taiwan) before being sent for Sanger sequencing (Genomics Co., New Taipei City, Taiwan).

Generation of *Arabidopsis* transgenic lines using *Agrobacterium* floral dipping

The *Agrobacterium tumefaciens* GV3101 was cultured in the 523 liquid medium (8 g/L casein hydrolysate, 2 g/L K_2HPO_4, 0.3 g/L $MgSO_4{\cdot}7H_2O$, 10 g/L sucrose, 4 g/L yeast extract; pH 6.9) supplemented with rifampicin (50 mg/L) and streptomycin (100 mg/L) at 125 rpm shaking for 24 h at 28°C. Upon the optical density (OD600) reaching 1.0 to 1.5, the *Agrobacterium* suspension was centrifuged at 4,500 rpm at 4°C. The bacterial pellet was resuspended in 20 mM $CaCl_2$ as competent cells. Three soybean chitinase constructs and an empty vector were individually transformed into *A. tumefaciens* GV3101 using the freeze–thaw method, including a 30-s liquid nitrogen immersion and a 37°C water bath for 5 min. The transformed bacterial cells were selected by kanamycin (50 mg/L). Colony PCR, using gene-specific primer pairs, was used for validation. The *Agrobacterium* strains were stored in 523/Kan+/Rif+/Strep+ medium with 50% glycerol at −80°C.

For *Agrobacterium* floral dipping, the desired *Agrobacterium* strains were freshly prepared in the 523/Kan+/Rif+/Strep+ medium, and the bacterial pellets were resuspended in a 5% sucrose solution containing 0.02% Silwet L-77 (PhytoTech Lab, Lenexa, KS, USA) to OD600 = 0.6 as inoculum. The floral dipping procedure followed the protocol by Zhang et al. (2006) with slight modifications; in brief, the siliques and pollinated flowers were removed from 6-week-old *A. thaliana* ecotype Col-0, and the unopened *Arabidopsis* inflorescences were immersed in the *Agrobacterium* inoculum for 20 s. After immersion, the plants were kept in humid chambers before being routinely cultured at 22°C.

The *Arabidopsis* seeds harvested after floral dipping represented the T_1 generation. The T_1 seeds were selected on the MS medium containing 40 ppm hygromycin. The T_1 plants with hygromycin resistance were further PCR-confirmed before generating the T_2 seeds. The T_2 seeds were selected on hygromycin to estimate the Mendelian segregation (3:1) for each T_1 lineage. T_1 lineages with a single T-DNA insertion were propagated into the T_3 generation. Approximately 100 T_3 seeds of each lineage were screened on hygromycin. If the T_3 germination rate was approximately 100%, the lineage was considered to be homozygous. On the other hand, if the germination rate was around 75%, the lineage was considered to be heterozygous at the T_2 generation. Phenotyping and pathogenicity assay were only performed using the progenies of homozygous T_2 lineages (Supplementary Figure S1).

For the *Arabidopsis* transgenic lines, the expressions of soybean chitinase (GmChi01, GmChi02, or GmChi16) were confirmed via RT-qPCR. In brief, foliar RNA of transgenic lines was extracted by the TRIzol procedure described above. The raw RNA was treated with the TURBO DNase (Thermo Fisher Scientific) before cDNA synthesis using the SuperScript IV Reverse Transcriptase (Thermo Fisher Scientific) and oligo d(T)18 primer (Bioman). RT-qPCR was performed using the iQ™ SYBR® Green Supermix (Bio-RAD, Hercules, CA, USA) with the primers (GmChi01_qPCR; GmChi02_qPCR; GmChi16_qPCR; AtACT7) (Supplementary Table S1) on the CFX ConnectTM Real-Time PCR Detection System (Bio-RAD). Three-step thermocycling conditions were set: initial denaturation at 95°C for 5 min, 40 cycles of denaturation at 95°C for 15 s, annealing at 62°C for 10 s, and extension at 72°C for 10 s. The gene expression was presented using the formula $\Delta Ct = Ct_{\text{target gene}} - Ct_{AtACT7}$. The melty curve of each RT-qPCR amplicon was assessed to confirm specificity, and the amplification efficiencies of primers were optimized to ensure the use of $2^{-\Delta Ct}$ (Livak and Schmittgen, 2001).

Phenotyping and pathogenicity assay on *Arabidopsis* transgenic lines

The hypocotyl length, radical length, rosette area, and stem length were measured for the wild-type *A. thaliana* Col-0 and the *Arabidopsis* transgenic lines. Hypocotyl and radical lengths were measured after 1 week of growth on MS medium, while rosette area was calculated using the software Easy Leaf Area (Easlon and Bloom, 2014) after another 3 weeks in pots. Stem length measurements were conducted at the 6-week growth stage. The experiments were repeated twice, and there were 15 biological replicates each time. These data were collected for statistical analyses.

The detached leaf assay was applied to evaluate the defense responses of *Arabidopsis* lines. A 5-mm-diameter PDA plug with the mycelial edge of *F. oxysporum* f.sp. *rapae* was inoculated onto *Arabidopsis* leaves with a needle wound on the leaf surface. The inoculated leaves were grown for 4 weeks. An ordinal disease index (DI) was measured daily for 1 week, for which the index at 0, 1, 2, 3, 4, and 5 indicates 0%, 1%–10%, 11%–25%, 25%–50%, 51%–75%, and 76%–100% of leaf yellowing, and index at 6 indicates a

complete wilt and dead leaf (Supplementary Figure S2). The area under the disease progress curve (AUDPC) was calculated (Sparks et al., 2008). The experiments were repeated three times, and there were nine biological replicates each time.

In addition, soil inoculation was performed by spreading the conidial suspension of *F. oxysporum* f. sp. *rapae* onto the 1-week-old *Arabidopsis* lines. After inoculation, the pots were covered with plastic lids to maintain humidity and placed in the greenhouse at room temperature (25°C ± 2°C). The plastic lids were removed after 10 days postinoculation. The experiments were repeated three times, and there were four biological replicates each time. These data were collected for statistical analyses.

Statistical analysis for phenotypic data

The R v4.0.5 environment and RStudio v1.4.17 were used for statistical analyses. All data were analyzed using the nonparametric Kruskal–Wallis rank sum test, and Dunn's test was applied for mean separation at a threshold of $\alpha = 0.05$.

Identification of TF and TFBS for the rhizobacteria-inducible soybean chitinase genes

Soybean chitinase genes were grouped into two categories, including rhizobacteria-inducible chitinase genes (regardless of up- or downregulation) and nonrhizobacteria-inducible chitinase genes (Supplementary Table S2). The upstream 2,000 bp 5′UTR and downstream 500 bp 3′UTR of these genes were subjected to PlantPAN3.0 analysis (Chow et al., 2019) using soybean as the model plant for searching TF and TFBS at 90% frequency of support.

Data availability statement

The RNA-Seq data were deposited in the NCBI BioProject PRJNA987518 and the analyses also included the previously published data in the NCBI BioProject PRJNA512928.

Author contributions

J-YC: Conceptualization, Data curation, Formal analysis, Investigation, Methodology, Resources, Software, Validation, Visualization, Writing – original draft, Writing – review & editing. HS: Conceptualization, Investigation, Methodology, Writing – review & editing. MC: Conceptualization, Investigation, Methodology, Writing – review & editing. C-HW: Conceptualization, Investigation, Methodology, Writing – review & editing. H-XC: Conceptualization, Data curation, Funding acquisition, Investigation, Methodology, Project administration, Supervision, Visualization, Writing – original draft, Writing – review & editing.

Funding

The author(s) declare financial support was received for the research, authorship, and/or publication of this article. This project was supported by the Yushan Young Scholar Program (Ministry of Education, Taiwan) to Dr. Hao-Xun Chang.

Conflict of interest

The authors declare that the research was conducted in the absence of any commercial or financial relationships that could be construed as a potential conflict of interest.

Publisher's note

Supplementary material

The Supplementary Material for this article can be found online at: https://www.frontiersin.org/articles/10.3389/fpls.2024.1341181/full#supplementary-material

SUPPLEMENTARY FIGURE 1
RT-PCR validation for the expression of GmChi01, GmChi02, and GmChi16 in the *Arabidopsis* transgenic lines.

SUPPLEMENTARY FIGURE 2
The disease index scale for detached leaf assay.

SUPPLEMENTARY TABLE 1
Primer sequences.

SUPPLEMENTARY TABLE 2
Soybean chitinase genes inducible or non-inducible by six rhizobacteria.

References

Ali, M., Li, Q.-H., Zou, T., Wei, A.-M., Gombojab, G., Lu, G., et al. (2020). Chitinase gene positively regulates hypersensitive and defense responses of pepper to *Colletotrichum acutatum* infection. *Int. J. Mol. Sci.* 21, 6624. doi: 10.3390/ijms21186624

Allen, T., Mueller, D., and Sisson, A. (2022). *Soybean disease loss estimates from the United States and Ontario* (Canada: Crop Protection Network). doi: 10.31274/cpn-20230421-1

Almagro Armenteros, J. J., Sønderby, C. K., Sønderby, S. K., Nielsen, H., and Winther, O. (2017). DeepLoc: prediction of protein subcellular localization using deep learning. *Bioinformatics* 33, 3387–3395. doi: 10.1093/bioinformatics/btx431

Almagro Armenteros, J. J., Tsirigos, K. D., Sønderby, C. K., Peterson, T. N., Winther, O., Brunak, S., et al. (2019). SignalP 5.0 improves signal peptide predictions using deep neural networks. *Nat. Biotechnol.* 37, 420–423. doi: 10.1038/s41587-019-0036-z

Asao, H., Nishizawa, Y., Arai, S., Sato, T., Hirai, M., Yoshida, K., et al. (1997). Enhanced resistance against a fungal pathogen *Sphaerotheca humuli* in transgenic strawberry expressing a rice chitinase gene. *Plant Biotechnol.* 14, 145–149. doi: 10.5511/plantbiotechnology.14.145

Bailey, T. L., and Elkan, C. (1994). Fitting a mixture model by expectation maximization to discover motifs in biopolymers. *Proc. Int. Conf Intell. Syst. Mol. Biol.* 2, 28–36.

Bandara, A. Y., Weerasooriya, D. K., Bradley, C. A., Allen, T. W., and Esker, P. D. (2020). Dissecting the economic impact of soybean diseases in the United States over two decades. *PloS One* 15, e0231141. doi: 10.1371/journal.pone.0231141

Bartholomew, E. S., Black, K., Feng, Z., Liu, W., Shan, N., Zhang, X., et al. (2019). Comprehensive analysis of the chitinase gene family in cucumber (*Cucumis sativus* L.): From gene identification and evolution to expression in response to *Fusarium oxysporum*. *Int. J. Mol. Sci.* 20, 5309. doi: 10.3390/ijms20215309

Bartholomew, E. S., Xu, S., Zhang, Y., Yin, S., Feng, Z., Chen, S., et al. (2022). A chitinase CsChi23 promoter polymorphism underlies cucumber resistance against *Fusarium oxysporum* f. sp. *cucumerinum*. *New Phytol.* 236, 1471–1486. doi: 10.1111/nph.18463

Benhamou, N., Broglie, K., Chet, I., and Broglie, R. (1993). Cytology of infection of 35S-bean chitinase transgenic canola plants by *Rhizoctonia solani*: cytochemical aspects of chitin breakdown in *vivo*. *Plant J.* 4, 295–305. doi: 10.1046/j.1365-313X.1993.04020295.x

Biate, D. L., Kumar, L. V., Ramadoss, D., Kumari, A., Naik, S., Reddy, K. K., et al. (2014). "Genetic diversity of soybean root nodulating bacteria," in *Bacterial diversity in sustainable agriculture, sustainable development and biodiversity*. Ed. D. K. Maheshwari (Cham: Springer International Publishing), 131–145.

Bordoloi, K. S., Krishnatreya, D. B., Baruah, P. M., Borah, A. K., Mondal, T. K., and Agarwala, N. (2021). Genome-wide identification and expression profiling of chitinase genes in tea (*Camellia sinensis* (L.) O. Kuntze) under biotic stress conditions. *Physiol. Mol. Biol. Plants* 27, 369–385. doi: 10.1007/s12298-021-00947-x

Boubekri, K., Soumare, A., Mardad, I., Lyamlouli, K., Ouhdouch, Y., Hafidi, M., et al. (2022). Multifunctional role of Actinobacteria in agricultural production sustainability: A review. *Microbiol. Res.* 261, 127059. doi: 10.1016/j.micres.2022.127059

Bradley, C. A., Allen, T. W., Sisson, A. J., Bergstrom, G. C., Bissonnette, K. M., Bond, J., et al. (2021). Soybean yield loss estimates due to diseases in the United States and Ontario, Canada, from 2015 to 2019. *Plant Health Progress.* 22, 483–495. doi: 10.1094/PHP-01-21-0013-RS

Bray, N. L., Pimentel, H., Melsted, P., and Pachter, L. (2016). Near-optimal probabilistic RNA-seq quantification. *Nat. Biotechnol.* 34, 525–527. doi: 10.1038/nbt.3519

Brogue, K., Chet, I., Holliday, M., Cressman, R., Biddle, P., Knowlton, S., et al. (1991). Transgenic plants with enhanced resistance to the fungal pathogen. *Rhizoctonia solani. Science.* 254, 1194–1197. doi: 10.1126/science.254.5035.1194

Chalavi, V., Tabaeizadeh, Z., and Thibodeau, P. (2003). Enhanced resistance to *Verticillium dahliae* in transgenic strawberry plants expressing a *Lycopersicon Chilense* chitinase gene. *J. Am. Soc Hortic. Sci.* 128, 747–753. doi: 10.21273/JASHS.128.5.0747

Chang, H.-X., Haudenshield, J. S., Bowen, C. R., and Hartman, G. L. (2017). Metagenome-wide association study and machine learning prediction of bulk soil microbiome and crop productivity. *Front. Microbiol.* 8, 519. doi: 10.3389/fmicb.2017.00519

Chang, H.-X., Noel, Z. A., and Chilvers, M. I. (2021). A β-lactamase gene of *Fusarium oxysporum* alters the rhizosphere microbiota of soybean. *Plant J.* 106, 1588–1604. doi: 10.1111/tpj.15257

Chen, J., Piao, Y., Liu, Y., Li, X., and Piao, Z. (2018). Genome-wide identification and expression analysis of chitinase gene family in *Brassica rapa* reveals its role in clubroot resistance. *Plant Sci.* 270, 257–267. doi: 10.1016/j.plantsci.2018.02.017

Chopra, R., and Saini, R. (2014). Transformation of blackgram (*Vigna mungo* (L.) Hepper) by barley chitinase and ribosome-inactivating protein genes towards improving resistance to Corynespora leaf spot fungal disease. *Appl. Biochem. Biotechnol.* 174, 2791–2800. doi: 10.1007/s12010-014-1226-2

Chow, C.-N., Lee, T.-Y., Hung, Y.-C., Li, G.-Z., Tseng, K.-C., Liu, Y.-H., et al. (2019). PlantPAN3.0: a new and updated resource for reconstructing transcriptional regulatory networks from ChIP-seq experiments in plants. *Nucleic Acids Res.* 47, D1155–D1163. doi: 10.1093/nar/gky1081

Das, D. K., and Rahman, A. (2018). Expression of a rice chitinase gene enhances antifungal response in transgenic litchi (cv. Bedana). *Am. J. Plant Sci.* 9, 2256–2275. doi: 10.4236/ajps.2018.911163

Datta, K., Tu, J., Oliva, N., Ona, I., Velazhahan, R., Mew, T. W., et al. (2001). Enhanced resistance to sheath blight by constitutive expression of infection-related rice chitinase in transgenic elite indica rice cultivars. *Plant Sci.* 160, 405–414. doi: 10.1016/S0168-9452(00)00413-1

Dong, X., Zhao, Y., Ran, X., Guo, L., and Zhao, D. G. (2017). Overexpression of a new chitinase gene *EuCHIT2* enhances resistance to *Erysiphe cichoracearum* DC. @ in Tobacco Plants. *Int. J. Mol. Sci.* 18, 2361. doi: 10.3390/ijms18112361

Dowd, P. F., Naumann, T. A., Price, N. P. J., and Johnson, E. T. (2018). Identification of a maize (*Zea mays*) chitinase allele sequence suitable for a role in ear rot fungal resistance. *Agric. Gene.* 7, 15–22. doi: 10.1016/j.aggene.2017.10.001

Durechova, D., Jopcik, M., Rajninec, M., Moravcikova, J., and Libantova, J. (2019). Expression of *Drosera rotundifolia* chitinase in transgenic tobacco plants enhanced their antifungal potential. *Mol. Biotechnol.* 61, 916–928. doi: 10.1007/s12033-019-00214-1

Easlon, H. M., and Bloom, A. J. (2014). Easy leaf area: Automated digital image analysis for rapid and accurate measurement of leaf area. *App. Plant Sci.* 2, 1400033. doi: 10.3732/apps.1400033

Eissa, H. F., Hassanien, S. E., Ramadan, A. M., El-Shamy, M. M., Saleh, O. M., Shokry, A. M., et al. (2017). Developing transgenic wheat to encounter rusts and powdery mildew by overexpressing barley chi26 gene for fungal resistance. *Plant Methods* 13, 41. doi: 10.1186/s13007-017-0191-5

Elnahal, A. S. M., El-Saadony, M. T., Saad, A. M., Desoky, E.-S. M., El-Tahan, A. M., Rady, M. M., et al. (2022). The use of microbial inoculants for biological control, plant growth promotion, and sustainable agriculture: A review. *Eur. J. Plant Pathol.* 162, 759–792. doi: 10.1007/s10658-021-02393-7

Finn, R. D., Clements, J., and Eddy, S. R. (2011). HMMER web server: interactive sequence similarity searching. *Nucleic Acids Res.* 39, W29–W37. doi: 10.1093/nar/gkr367

Funkhouser, J. D., and Aronson, N. N. (2007). Chitinase family GH18: evolutionary insights from the genomic history of a diverse protein family. *BMC Evol. Biol.* 7, 96. doi: 10.1186/1471-2148-7-96

Gao, Y., Jia, S., Wang, C., Wang, F., Wang, F., and Zhao, K. (2016). BjMYB1, a transcription factor implicated in plant defence through activating BjCHI1 chitinase expression by binding to a W-box-like element. *J. Exp. Bot.* 67, 4647–4658. doi: 10.1093/jxb/erw240

Gasteiger, E., Hoogland, C., Gattiker, A., Duvaud, S., Wilkins, M. R., Appel, R. D., et al. (2005). "Protein identification and analysis tools on the ExPASy server," in *The proteomics protocols handbook*. Eds. J. M. Walker and N. J. Totowa (Totowa, NJ: Humana Press US), 571–607. doi: 10.1385/1-59259-890-0:571

Girhepuje, P. V., and Shinde, G. B. (2011). Transgenic tomato plants expressing a wheat endochitinase gene demonstrate enhanced resistance to *Fusarium oxysporum* f. sp. *lycopersici. Plant Cell Tiss. Organ. Cult.* 105, 243–251. doi: 10.1007/s11240-010-9859-5

Grover, A. (2012). Plant chitinases: Genetic diversity and physiological roles. *Crit. Rev. Plant Sci.* 31, 57–73. doi: 10.1080/07352689.2011.616043

Gu, Z., Eils, R., and Schlesner, M. (2016). Complex heatmaps reveal patterns and correlations in multidimensional genomic data. *Bioinform.* 32, 2847–2849. doi: 10.1093/bioinformatics/btw313

Han, Q., Ma, Q., Chen, Y., Tian, B., Xu, L., Bai, Y., et al. (2020). Variation in rhizosphere microbial communities and its association with the symbiotic efficiency of rhizobia in soybean. *ISME J.* 14, 1915–1928. doi: 10.1038/s41396-020-0648-9

Haxim, Y., Kahar, G., Zhang, X., Si, Y., Waheed, A., Liu, X., et al. (2022). Genome-wide characterization of the chitinase gene family in wild apple (*Malus sieversii*) and domesticated apple (*Malus domestica*) reveals its role in resistance to *Valsa Mali*. *Front. Plant Sci.* 13, 1007936. doi: 10.3389/fpls.2022.1007936

He, T., Fan, J., Jiao, G., Liu, Y., Zhang, Q., Luo, N., et al. (2023). Bioinformatics and expression analysis of the chitinase genes in strawberry (*Fragaria vesca*) and functional study of FvChi-14. *Plants.* 12, 1543. doi: 10.3390/plants12071543

Huang, L.-F., Lin, K.-H., He, S.-L., Chen, J.-L., Jiang, J.-Z., Chen, B.-H., et al. (2016). Multiple patterns of regulation and overexpression of a ribonuclease-like pathogenesis-related protein gene, OsPR10a, conferring disease resistance in rice and Arabidopsis. *PloS One* 11, e0156414. doi: 10.1371/journal.pone.0156414

Huang, X., Wang, J., Du, Z., Zhang, C., Li, L., and Xu, Z. (2013). Enhanced resistance to stripe rust disease in transgenic wheat expressing the rice chitinase gene RC24. *Transgenic Res.* 22, 939–947. doi: 10.1007/s11248-013-9704-9

Hussain, M., Hamid, M. I., Tian, J., Hu, J., Zhang, X., Chen, J., et al. (2018). Bacterial community assemblages in the rhizosphere soil, root endosphere and cyst of soybean cyst nematode-suppressive soil challenged with nematodes. *FEMS Microbiol. Ecol.* 94, fiy142. doi: 10.1093/femsec/fiy142

Ignacimuthu, S., and Ceasar, S. A. (2012). Development of transgenic finger millet (*Eleusine coracana* (L.) Gaertn.) resistant to leaf blast disease. *J. Biosci.* 37, 135–147. doi: 10.1007/s12038-011-9178-y

Iqbal, M. M., Nazir, F., Ali, S., Asif, M. A., Zafar, Y., Iqbal, J., et al. (2012). Over expression of rice chitinase gene in transgenic peanut (*Arachis hypogaea* L.) improves resistance against leaf spot. *Mol. Biotechnol.* 50, 129–136. doi: 10.1007/s12033-011-9426-2

Jabeen, N., Chaudhary, Z., Gulfraz, M., Rashid, H., and Mirza, B. (2015). Expression of rice chitinase gene in genetically engineered tomato confers enhanced resistance to Fusarium wilt and early blight. *Plant Pathol. J.* 31, 252–258. doi: 10.5423/PPJ.OA.03.2015.0026

Jach, G., Görnhardt, B., Mundy, J., Logemann, J., Pinsdorf, E., Leah, R., et al. (1995). Enhanced quantitative resistance against fungal disease by combinatorial expression of different barley antifungal proteins in transgenic tobacco. *Plant J.* 8, 97–109. doi: 10.1046/j.1365-313X.1995.08010097.x

Jørgensen, J. E., Stougaard, J., and Marcker, K. A. (1991). A two-component nodule-specific enhancer in the soybean N23 gene promoter. *Plant Cell* 3, 819–827. doi: 10.1105/tpc.3.8.819

Kang, J.-N., Park, M.-Y., Kim, W.-N., Kang, H.-G., Sun, H.-J., Yang, D.-H., et al. (2017). Resistance of transgenic zoysiagrass overexpressing the zoysiagrass class II chitinase gene Zjchi2 against *Rhizoctonia solani* AG2-2 (IV). *Plant Biotechnol. Rep.* 11, 229–238. doi: 10.1007/s11816-017-0445-8

Katoh, K., Rozewicki, J., and Yamada, K. D. (2019). MAFFT online service: multiple sequence alignment, interactive sequence choice and visualization. *Brief. Bioinform.* 20, 1160–1166. doi: 10.1093/bib/bbx108

Kawase, T., Saito, A., Sato, T., Kanai, R., Fujii, T., Nikaidou, N., et al. (2004). Distribution and phylogenetic analysis of family 19 chitinases in Actinobacteria. *Appl. Environ. Microbiol.* 70, 1135–1144. doi: 10.1128/AEM.70.2.1135-1144.2004

Kezuka, Y., Ohishi, M., Itoh, Y., Watanabe, J., Mitsutomi, M., Watanabe, T., et al. (2006). Structural studies of a two-domain chitinase from *Streptomyces griseus* HUT6037. *J. Mol. Biol.* 358, 472–484. doi: 10.1016/j.jmb.2006.02.013

Khan, A., Nasir, I. A., Tabassum, B., Aaliya, K., Tariq, M., and Rao, A. Q. (2017). Expression studies of chitinase gene in transgenic potato against *Alternaria solani*. *Plant Cell Tiss Organ Cult.* 128, 563–576. doi: 10.1007/s11240-016-1134-y

Kim, D. S., Kim, N. H., and Hwang, B. K. (2015). The *Capsicum annuum* class IV chitinase ChitIV interacts with receptor-like cytoplasmic protein kinase PIK1 to accelerate PIK1-triggered cell death and defence responses. *J. Exp. Bot.* 66, 1987–1999. doi: 10.1093/jxb/erv001

Kishimoto, K., Nishizawa, Y., Tabei, Y., Hibi, T., Nakajima, M., and Akutsu, K. (2002). Detailed analysis of rice chitinase gene expression in transgenic cucumber plants showing different levels of disease resistance to gray mold (*Botrytis cinerea*). *Plant Sci.* 162, 655–662. doi: 10.1016/S0168-9452(01)00602-1

Kishimoto, K., Nishizawa, Y., Tabei, Y., Nakajima, M., Hibi, T., and Akutsu, K. (2004). Transgenic cucumber expressing an endogenous class III chitinase gene has reduced symptoms from *Botrytis cinerea*. *J. Gen. Plant Pathol.* 70, 314–320. doi: 10.1007/s10327-004-0152-5

Kovács, G., Sági, L., Jacon, G., Arinaitwe, G., Busogoro, J.-P., Thiry, E., et al. (2013). Expression of a rice chitinase gene in transgenic banana ('Gros Michel', AAA genome group) confers resistance to black leaf streak disease. *Transgenic Res.* 22, 117–130. doi: 10.1007/s11248-012-9631-1

Kumar, S., Stecher, G., Li, M., Knyaz, C., and Tamura, K. (2018). MEGA X: Molecular evolutionary genetics analysis across computing platforms. *Mol. Biol. Evol.* 35, 1547–1549. doi: 10.1093/molbev/msy096

Lamesch, P., Berardini, T. Z., Li, D., Swarbreck, D., Wilks, C., Sasidharan, R., et al. (2012). The Arabidopsis information resource (TAIR): Improved gene annotation and new tools. *Nucleic Acids Res.* 40, D1202–D1210. doi: 10.1093/nar/gkr1090

Letunic, I., and Bork, P. (2021). Interactive tree of life (iTOL) v5: An online tool for phylogenetic tree display and annotation. *Nucleic Acids Res.* 49, W293–W296. doi: 10.1093/nar/gkab301

Li, P., Pei, Y., Sang, X., Ling, Y., Yang, Z., and He, G. (2009). Transgenic indica rice expressing a bitter melon (*Momordica charantia*) class I chitinase gene (McCHIT1) confers enhanced resistance to *Magnaporthe grisea* and *Rhizoctonia solani*. *Eur. J. Plant Pathol.* 125, 533–543. doi: 10.1007/s10658-009-9501-8

Li, S., Hai, J., Wang, Z., Deng, J., Liang, T., Su, L., et al. (2021). *Lilium regale* Wilson WRKY2 regulates chitinase gene expression during the response to the root rot pathogen *Fusarium oxysporum*. *Front. Plant Sci.* 12, 741463. doi: 10.3389/fpls.2021.741463

Liu, M., Gong, Y., Sun, H., Zhang, J., Zhang, L., Sun, J., et al. (2020). Characterization of a novel chitinase from sweet potato and its fungicidal effect against *Ceratocystis fimbriata*. *J. Agric. Food Chem.* 68, 7591–7600. doi: 10.1021/acs.jafc.0c01813

Livak, K. J., and Schmittgen, T. D. (2001). Analysis of relative gene expression data using real-time quantitative PCR and the $2^{-\Delta\Delta CT}$ method. *Methods.* 25, 402–408. doi: 10.1006/meth.2001.1262

Lucas-Bautista, J. A., Ventura-Aguilar, R. I., Bautista-Baños, S., Corona-Rangel, M. L., and Guillén-Sánchez, D. (2020). Evaluation of the chitinase activity in papaya fruit at different phenological stages as a possible biomarker for the detection of Colletotrichum gloeosporioides infection. *Curr. Plant Biol.* 23, 100165. doi: 10.1016/j.cpb.2020.100165

Lugtenberg, B., and Kamilova, F. (2009). Plant-growth-promoting rhizobacteria. *Annu. Rev. Microbiol.* 63, 541–556. doi: 10.1146/annurev.micro.62.081307.162918

Lundberg, D. S., and Teixeira, P. J. P. L. (2018). Root-exuded coumarin shapes the root microbiome. *PNAS.* 115, 5629–5631. doi: 10.1073/pnas.1805944115

Luo, X., Tian, T., Feng, L., Yang, X., Li, L., Tan, X., et al. (2023). Pathogenesis-related protein 1 suppresses oomycete pathogen by targeting against AMPK kinase complex. *J. Adv. Res.* 43, 13–26. doi: 10.1016/j.jare.2022.02.002

Luo, L., Zhao, C., Wang, E., Raza, A., and Yin, C. (2022). *Bacillus amyloliquefaciens* as an excellent agent for biofertilizer and biocontrol in agriculture: An overview for its mechanisms. *Microbiol. Res.* 259, 127016. doi: 10.1016/j.micres.2022.127016

Lv, P., Zhang, C., Xie, P., Yang, X., El-Sheikh, M. A., Hefft, D. I., et al. (2022). Genome-wide identification and expression analyses of the chitinase gene family in response to white mold and drought stress in soybean (*Glycine max*). *Life* 12, 1340. doi: 10.3390/life12091340

Ma, X. L., Milne, R. I., Zhou, H. X., Fang, J. Y., and Zha, H. G. (2017). Floral nectar of the obligate outcrossing *Canavalia gladiata* (Jacq.) DC. (Fabaceae) contains only one predominant protein, a class III acidic chitinase. *Plant Biol.* 19, 749–759. doi: 10.1111/plb.12583

Marchant, R., Davey, M. R., Lucas, J. A., Lamb, C. J., Dixon, R. A., and Power, J. B. (1998). Expression of a chitinase transgene in rose (*Rosa hybrida* L.) reduces development of blackspot disease (*Diplocarpon rosae* Wolf). *Mol. Breeding.* 4, 187–194. doi: 10.1023/A:1009642707505

Marks, R. A., Hotaling, S., Frandsen, P. B., and VanBuren, R. (2021). Representation and participation across 20 years of plant genome sequencing. *Nat. Plants* 7, 1571–1578. doi: 10.1038/s41477-021-01031-8

Mauch-Mani, B., Baccelli, I., Luna, E., and Flors, V. (2017). Defense priming: An adaptive part of induced resistance. *Annu. Rev. Plant Biol.* 68, 485–512. doi: 10.1146/annurev-arplant-042916-041132

Martinez-Medina, A., Flors, V., Heil, M., Mauch-Mani, B., Pieterse, C. M. J., Pozo, M. J., et al. (2016). Recognizing Plant Defense Priming. *Trends Plant Sci.* 21, 818–822. doi: 10.1016/j.tplants.2016.07.009

Maximova, S. N., Marelli, J.-P., Young, A., Pishak, S., Verica, J. A., and Guiltinan, M. J. (2006). Over-expression of a cacao class I chitinase gene in *Theobroma cacao* L. enhances resistance against the pathogen, *Colletotrichum gloeosporioides*. *Planta.* 224, 740–749. doi: 10.1007/s00425-005-0188-6

Mir, Z. A., Ali, S., Shivaraj, S. M., Bhat, J. A., Singh, A., Yadav, P., et al. (2020). Genome-wide identification and characterization of chitinase gene family in *Brassica juncea* and *Camelina sativa* in response to *Alternaria brassicae*. *Genomics.* 112, 749–763. doi: 10.1016/j.ygeno.2019.05.011

Mir, Z. A., Ali, S., Singh, A., Yadav, P., Tyagi, A., Chaturani, G. D. G., et al. (2021). *In silico* analysis and overexpression of chitinase class IV gene in *Brassica juncea* improves resistance against *Alternaria brassicae*. *Ind. Crops Prod.* 169, 113555. doi: 10.1016/j.indcrop.2021.113555

Mirdita, M., Schütze, K., Moriwaki, Y., Heo, L., Ovchinnikov, S., and Steinegger, M. (2022). ColabFold: making protein folding accessible to all. *Nat. Methods* 19, 679–682. doi: 10.1038/s41592-022-01488-1

Mistry, J., Chuguransky, S., Williams, L., Qureshi, M., Salazar, G. A., Sonnhammer, E. L. L., et al. (2021). Pfam: The protein families database in 2021. *Nucleic Acids Res.* 49, D412–D419. doi: 10.1093/nar/gkaa913

Moura, R. D., de Castro, L. A. M., Culik, M. P., Fernandes, A. A. R., Fernandes, P. M. B., and Ventura, J. A. (2020). Culture medium for improved production of conidia for identification and systematic studies of *Fusarium* pathogens. *J. Microbiol. Meth.* 173, 105915. doi: 10.1016/j.mimet.2020.105915

Mousa, W. K., Shearer, C., Limay-Rios, V., Ettinger, C. L., Eisen, J. A., and Raizada, M. N. (2016). Root-hair endophyte stacking in finger millet creates a physicochemical barrier to trap the fungal pathogen *Fusarium graminearum*. *Nat. Microbiol.* 1, 1–12. doi: 10.1038/nmicrobiol.2016.167

Nguyen, L.-T., Schmidt, H. A., von Haeseler, A., and Minh, B. Q. (2015). IQ-TREE: A fast and effective stochastic algorithm for estimating maximum-likelihood phylogenies. *Mol. Biol. Evol.* 32, 268–274. doi: 10.1093/molbev/msu300

Nirala, N. K., Das, D. K., Srivastava, P. S., Sopory, S. K., and Upadhyaya, K. C. (2010). Expression of a rice chitinase gene enhances antifungal potential in transgenic grapevine (*Vitis vinifera* L.). *Vitis.* 49 (4), 181–187. doi: 10.5073/vitis.2010.49.181-187

Nishizawa, Y., Nishio, Z., Nakazono, K., Soma, M., Nakajima, E., Ugaki, M., et al. (1999). Enhanced resistance to blast (*Magnaporthe grisea*) in transgenic Japonica rice by constitutive expression of rice chitinase. *Theor. Appl. Genet.* 99, 383–390. doi: 10.1007/s001220051248

Núñez de Cáceres González, F. F., Davey, M. R., Cancho Sanchez, E., and Wilson, Z. A. (2015). Conferred resistance to *Botrytis cinerea* in *Lilium* by overexpression of the RCH10 chitinase gene. *Plant Cell Rep.* 34, 1201–1209. doi: 10.1007/s00299-015-1778-9

Orozco-Mosqueda, M d.C., Fadiji, A. E., Babalola, O. O., and Santoyo, G. (2023). Bacterial elicitors of the plant immune system: An overview and the way forward. *Plant Stress.* 7, 100138. doi: 10.1016/j.stress.2023.100138

Pak, J.-H., Chung, E.-S., Shin, S.-H., Jeon, E.-H., Kim, M.-J., Lee, H.-Y., et al. (2009). Enhanced fungal resistance in Arabidopsis expressing wild rice PR-3 (OgChitIVa) encoding chitinase class IV. *Plant Biotechnol. Rep.* 3, 147–155. doi: 10.1007/s11816-009-0084-9

Pappinen, A., Degefu, Y., Syrjälä, L., Keinonen, K., and von Weissenberg, K. (2002). Transgenic silver birch (*Betula pendula*) expressing sugarbeet chitinase 4 shows enhanced resistance to *Pyrenopeziza betulicola*. *Plant Cell Rep.* 20, 1046–1051. doi: 10.1007/s00299-002-0449-9

Pasonen, H.-L., Seppänen, S.-K., Degefu, Y., Rytkönen, A., von Weissenberg, K., and Pappinen, A. (2004). Field performance of chitinase transgenic silver birches (*Betula pendula*): Resistance to fungal diseases. *Theor. Appl. Genet.* 109, 562–570. doi: 10.1007/s00122-004-1650-8

Patil, R. S., Ghormade, V., and Deshpande, M. V. (2000). Chitinolytic enzymes: An exploration. *Enzyme Microb. Tech.* 26, 473–483. doi: 10.1016/S0141-0229(00)00134-4

Pieterse, C. M. J., Zamioudis, C., Berendsen, R. L., Weller, D. M., Van Wees, S. C. M., and Bakker, P. A. H. M. (2014). Induced systemic resistance by beneficial microbes. *Annu. Rev. Phytopathol.* 52, 347–375. doi: 10.1146/annurev-phyto-082712-102340

Pimentel, H., Bray, N. L., Puente, S., Melsted, P., and Pachter, L. (2017). Differential analysis of RNA-seq incorporating quantification uncertainty. *Nat. Methods* 14, 687–690. doi: 10.1038/nmeth.4324

Prasad, K., Bhatnagar-Mathur, P., Waliyar, F., and Sharma, K. K. (2013). Overexpression of a chitinase gene in transgenic peanut confers enhanced resistance

to major soil borne and foliar fungal pathogens. *J. Plant Biochem. Biotechnol.* 22, 222–233. doi: 10.1007/s13562-012-0155-9

Raaijmakers, J. M., Leeman, M., van Oorschot, M. M. P., van der Sluis, I., Schippers, B., and Bakker, P. A. H. M. (1995). Dose-response relationships in biological control of Fusarium wilt of radish by Pseudomonas spp. *Phytopathology* 85, 1075–1081. doi: 10.1094/Phyto-85-1075

Rajesh, T., Maruthasalam, S., Kalpana, K., Poovannan, K., Kumar, K. K., Kokiladevi, E., et al. (2016). Stability of sheath blight resistance in transgenic ASD16 rice lines expressing a rice *chi11* gene encoding chitinase. *Biol. Plant* 60, 749–756. doi: 10.1007/s10535-016-0594-6

Richa, K., Tiwari, I. M., Devanna, B. N., Botella, J. R., Sharma, V., and Sharma, T. R. (2017). Novel chitinase gene LOC_Os11g47510 from indica rice Tetep provides enhanced resistance against sheath blight pathogen *Rhizoctonia solani* in rice. *Front. Plant Sci.* 8, 596. doi: 10.3389/fpls.2017.00596

Richa, K., Tiwari, I. M., Kumari, M., Devanna, B. N., Sonah, H., Kumari, A., et al. (2016). Functional characterization of novel chitinase genes present in the sheath blight resistance QTL: qSBR11-1 in rice line Tetep. *Front. Plant Sci.* 7, 244. doi: 10.3389/fpls.2016.00244

Rohini, V. K., and Sankara Rao, K. (2001). Transformation of peanut (*Arachis hypogaea* L.) with tobacco chitinase gene: variable response of transformants to leaf spot disease. *Plant Sci.* 160, 889–898. doi: 10.1016/S0168-9452(00)00462-3

Rushanaedy, I., Jones, T. C., Dudley, N. S., Liao, R. J. F., Agbayani, R., and Borthakur, D. (2012). Chitinase is a potential molecular biomarker for detecting resistance to Fusarium oxysporum in Acacia koa. *Trop. Plant Biol.* 5, 244–252. doi: 10.1007/s12042-012-9108-7

Salwan, R., Sharma, M., Sharma, A., and Sharma, V. (2023). Insights into plant beneficial microorganism-triggered induced systemic resistance. *Plant Stress* 7, 100140. doi: 10.1016/j.stress.2023.100140

Shin, S., Mackintosh, C. A., Lewis, J., Heinen, S. J., Radmer, L., Dill-Macky, R., et al. (2008). Transgenic wheat expressing a barley class II chitinase gene has enhanced resistance against *Fusarium graminearum*. *J. Exp. Bot.* 59, 2371–2378. doi: 10.1093/jxb/ern103

Sparks, A. H., Esker, P. D., Bates, M., Dall' Acqua, W., Guo, Z., Segovia, V., et al. (2008). Ecology and epidemiology in R: Disease progress over time. *Plant Health Instructor*. doi: 10.1094/PHI-A-2008-0129-02

Stopnisek, N., Zühlke, D., Carlier, A., Barberán, A., Fierer, N., Becher, D., et al. (2016). Molecular mechanisms underlying the close association between soil *Burkholderia* and fungi. *ISME J.* 10, 253–264. doi: 10.1038/ismej.2015.73

Su, Y., Wang, Z., Liu, F., Li, Z., Peng, Q., Guo, J., et al. (2016). Isolation and characterization of ScGluD2, a new sugarcane beta-1,3-glucanase D family gene induced by *Sporisorium scitamineum*, ABA, H_2O_2, NaCl, and $CdCl_2$ stresses. *Front. Plant Sci.* 7, 1348. doi: 10.3389/fpls.2016.01348

Sun, Y., Shang, L., Zhu, Q.-H., Fan, L., and Guo, L. (2022). Twenty years of plant genome sequencing: achievements and challenges. *Trends Plant Sci.* 27, 391–401. doi: 10.1016/j.tplants.2021.10.006

Tabaeizadeh, Z., Agharbaoui, Z., Harrak, H., and Poysa, V. (1999). Transgenic tomato plants expressing a *Lycopersicon Chilense* chitinase gene demonstrate improved resistance to *Verticillium dahliae* race 2. *Plant Cell Rep.* 19, 197–202. doi: 10.1007/s002990050733

Tabei, Y., Kitade, S., Nishizawa, Y., Kikuchi, N., Kayano, T., Hibi, T., et al. (1998). Transgenic cucumber plants harboring a rice chitinase gene exhibit enhanced resistance to gray mold (*Botrytis cinerea*). *Plant Cell Rep.* 17, 159–164. doi: 10.1007/s002990050371

Taira, T., Hayashi, H., Tajiri, Y., Onaga, S., Uechi, G., Iwasaki, H., et al. (2009). A plant class V chitinase from a cycad (*Cycas revoluta*): Biochemical characterization, cDNA isolation, and posttranslational modification. *Glycobiol.* 19, 1452–1461. doi: 10.1093/glycob/cwp119

Takahashi, W., Fujimori, M., Miura, Y., Komatsu, T., Nishizawa, Y., Hibi, T., et al. (2005). Increased resistance to crown rust disease in transgenic Italian ryegrass (*Lolium multiflorum* Lam.) expressing the rice chitinase gene. *Plant Cell Rep.* 23, 811–818. doi: 10.1007/s00299-004-0900-1

Takatsu, Y., Nishizawa, Y., Hibi, T., and Akutsu, K. (1999). Transgenic chrysanthemum (*Dendranthema grandiflorum* (Ramat.) Kitamura) expressing a rice chitinase gene shows enhanced resistance to gray mold (*Botrytis cinerea*). *Sci. Hortic.* 82, 113–123. doi: 10.1016/S0304-4238(99)00034-5

Tang, C. M., Chye, M.-L., Ramalingam, S., Ouyang, S.-W., Zhao, K.-J., Ubhayasekera, W., et al. (2004). Functional analyses of the chitin-binding domains and the catalytic domain of *Brassica juncea* chitinase BjCHI1. *Plant Mol. Biol.* 56, 285–298. doi: 10.1007/s11103-004-3382-1

Tariq, M., Khan, A., Tabassum, B., Toufiq, N., Bhatti, M., Riaz, S., et al. (2018). Antifungal activity of chitinase II against *Colletotrichum falcatum* Went. causing red rot disease in transgenic sugarcane. *Turk. J. Biol.* 42, 45–53. doi: 10.3906/biy-1709-17

Tian, B., Yang, J., and Zhang, K.-Q. (2007). Bacteria used in the biological control of plant-parasitic nematodes: populations, mechanisms of action, and future prospects. *FEMS Microbiol. Ecol.* 61, 197–213. doi: 10.1111/j.1574-6941.2007.00349.x

Tohidfar, M., Mohammadi, M., and Ghareyazie, B. (2005). *Agrobacterium*-mediated transformation of cotton (*Gossypium hirsutum*) using a heterologous bean chitinase gene. *Plant Cell Tiss. Organ. Cult.* 83, 83–96. doi: 10.1007/s11240-004-6155-2

Vaghela, B., Vashi, R., Rajput, K., and Joshi, R. (2022). Plant chitinases and their role in plant defense: A comprehensive review. *Enzyme Microb. Tech.* 159, 110055. doi: 10.1016/j.enzmictec.2022.110055

van Loon, L. C., Rep, M., and Pieterse, C. M. J. (2006). Significance of inducible defense-related proteins in infected plants. *Annu. Rev. Phytopathol.* 44, 135–162. doi: 10.1146/annurev.phyto.44.070505.143425

Vellicce, G. R., Ricci, J. C. D., Hernández, L., and Castagnaro, A. P. (2006). Enhanced resistance to *Botrytis cinerea* mediated by the transgenic expression of the chitinase gene ch5B in strawberry. *Transgenic Res.* 15, 57–68. doi: 10.1007/s11248-005-2543-6

Vierheilig, H., Alt, M., Neuhaus, J. M., Boller, T., and Wiemken, A. (1993). Colonization of transgenic *Nicotiana sylvestris* plants, expressing different forms of *Nicotiana tabacum* chitinase, by the root pathogen *Rhizoctonia solani* and by the mycorrhizal symbiont *Glomus mosseae*. *MPMI.* 6, 261–264. doi: 10.1094/MPMI-6-261

Walters, D. R., Ratsep, J., and Havis, N. D. (2013). Controlling crop diseases using induced resistance: challenges for the future. *J. Exp. Bot.* 64, 1263–1280. doi: 10.1093/jxb/ert026

Wang, X., Chen, K., Zhou, M., Gao, Y., Huang, H., Liu, C., et al. (2022). GmNAC181 promotes symbiotic nodulation and salt tolerance of nodulation by directly regulating GmNINa expression in soybean. *New Phytol.* 236, 656–670. doi: 10.1111/nph.18343

Wang, Y., Liu, M., Wang, X., Zhong, L., Shi, G., Xu, Y., et al. (2021). A novel β-1,3-glucanase Gns6 from rice possesses antifungal activity against *Magnaporthe oryzae*. *J. Plant Physiol.* 265, 153493. doi: 10.1016/j.jplph.2021.153493

Wang, F., Yang, S., Wang, Y., Zhang, B., Zhang, F., Xue, H., et al. (2021). Overexpression of chitinase gene enhances resistance to *Colletotrichum gloeosporioides* and *Alternaria alternata* in apple (*Malus* × *domestica*). *Sci. Hortic.* 277, 109779. doi: 10.1016/j.scienta.2020.109779

Wen, Z., Bai, J., Wang, L., Yao, L., Ahmad, B., Hanif, M., et al. (2020). Over expression of a chitinase 2 gene from Chinese wild strawberry improves resistance to anthracnose disease in transgenic *Arabidopsis thaliana*. *Plant Biotechnol. Rep.* 14, 725–736. doi: 10.1007/s11816-020-00648-z

Xiao, Y.-H., Li, X.-B., Yang, X.-Y., Luo, M., Hou, L., Guo, S.-H., et al. (2007). Cloning and characterization of a balsam pear class I chitinase gene (Mcchit1) and its ectopic expression enhances fungal resistance in transgenic plants. *Biosci. Biotechnol. Biochem.* 71, 1211–1219. doi: 10.1271/bbb.60658

Xin, Y., Wang, D., Han, S., Li, S., Gong, N., Fan, Y., et al. (2022). Characterization of the chitinase gene family in mulberry (*Morus notabilis*) and MnChi18 involved in resistance to *Botrytis cinerea*. *Genes.* 13, 98. doi: 10.3390/genes13010098

Xu, J., Xu, X., Tian, L., Wang, G., Zhang, X., Wang, X., et al. (2016). Discovery and identification of candidate genes from the chitinase gene family for *Verticillium dahliae* resistance in cotton. *Sci. Rep.* 6, 29022. doi: 10.1038/srep29022

Yamamoto, T., Iketani, H., Ieki, H., Nishizawa, Y., Notsuka, K., Hibi, T., et al. (2000). Transgenic grapevine plants expressing a rice chitinase with enhanced resistance to fungal pathogens. *Plant Cell Rep.* 19, 639–646. doi: 10.1007/s002999900174

Yamazaki, S., Mardani-korrani, H., Kaida, R., Ochiai, K., Kobayashi, M., Nagano, A. J., et al. (2021). Field multi-omics analysis reveals a close association between bacterial communities and mineral properties in the soybean rhizosphere. *Sci. Rep.* 11, 8878. doi: 10.1038/s41598-021-87384-8

Yang, J., Gan, Z., Lou, Z., Tao, N., Mi, Q., Liang, L., et al. (2010). Crystal structure and mutagenesis analysis of chitinase CrChi1 from the nematophagous fungus *Clonostachys rosea* in complex with the inhibitor caffeine. *Microbiol.* 156, 3566–3574. doi: 10.1099/mic.0.043653-0

Zhang, X., Henriques, R., Lin, S.-S., Niu, Q.-W., and Chua, N.-H. (2006). *Agrobacterium*-mediated transformation of *Arabidopsis thaliana* using the floral dip method. *Nat. Protoc.* 1, 641–646. doi: 10.1038/nprot.2006.97

Zhong, Y., Yang, Y., Liu, P., Xu, R., Rensing, C., Fu, X., et al. (2019). Genotype and rhizobium inoculation modulate the assembly of soybean rhizobacterial communities. *Plant Cell Environment.* 42, 2028–2044. doi: 10.1111/pce.13519

Zhu, L., Huang, J., Lu, X., and Zhou, C. (2022). Development of plant systemic resistance by beneficial rhizobacteria: Recognition, initiation, elicitation and regulation. *Front. Plant Sci.* 13, 952397. doi: 10.3389/fpls.2022.952397

frontiers | Frontiers in Plant Science

TYPE Original Research
PUBLISHED 12 February 2024
DOI 10.3389/fpls.2024.1334189

OPEN ACCESS

EDITED BY
Choong-Min Ryu,
Korea Research Institute of Bioscience and Biotechnology (KRIBB), Republic of Korea

REVIEWED BY
Neelakantan Arumugam,
Pondicherry University, India
Tariq Mukhtar,
Pir Mehr Ali Shah Arid Agriculture University, Pakistan

*CORRESPONDENCE
Hongmei Miao
miaohongmeichina@163.com
Hongyan Liu
liuhy1219@163.com
Haiyang Zhang
zhanghaiyang@zzu.edu.cn

RECEIVED 06 November 2023
ACCEPTED 26 January 2024
PUBLISHED 12 February 2024

CITATION
Yan W, Ni Y, Zhao H, Liu X, Jia M, Zhao X, Li Y, Miao H, Liu H and Zhang H (2024) Comprehensive analysis of sesame LRR-RLKs: structure, evolution and dynamic expression profiles under *Macrophomina phaseolina* stress. *Front. Plant Sci.* 15:1334189. doi: 10.3389/fpls.2024.1334189

Comprehensive analysis of sesame LRR-RLKs: structure, evolution and dynamic expression profiles under *Macrophomina phaseolina* stress

Wenqing Yan[1,2], Yunxia Ni[1,2], Hui Zhao[1,2], Xintao Liu[2], Min Jia[2], Xinbei Zhao[2], Yongdong Li[2], Hongmei Miao[1,3]*, Hongyan Liu[1,2,3]* and Haiyang Zhang[1,3]*

[1]The Shennong Laboratory, Zhengzhou, Henan, China, [2]Institute of Plant Protection, Henan Academy of Agricultural Sciences, Key Laboratory of IPM of Pests on Crop (Southern North China), Ministry of Agriculture, Key Laboratory of Crop Pest Control of Henan, Zhengzhou, Henan, China, [3]Key Laboratory of Specific Oilseed Crops Genomics of Henan Province, Henan Sesame Research Center, Henan Academy of Agricultural Sciences, Zhengzhou, Henan, China

Leucine-rich repeat receptor-like kinases (LRR-RLKs) can participate in the regulation of plant growth and development, immunity and signal transduction. *Sesamum indicum*, one of the most important oil crops, has a significant role in promoting human health. In this study, 175 *SiLRR-RLK* genes were identified in *S. indicum*, and they were subdivided into 12 subfamilies by phylogenetic analysis. Gene duplication analysis showed that the expansion of the *SiLRR-RLK* family members in the sesame was mainly due to segmental duplication. Moreover, the gene expansion of subfamilies IV and III contributed to the perception of stimuli under *M. phaseolina* stress in the sesame. The collinearity analysis with other plant species revealed that the duplication of *SiLRR-RLK* genes occurred after the differentiation of dicotyledons and monocotyledons. The expression profile analysis and functional annotation of *SiLRR-RLK* genes indicated that they play a vital role in biotic stress. Furthermore, the protein–protein interaction and coexpression networks suggested that SiLRR-RLKs contributed to sesame resistance to *Macrophomina phaseolina* by acting alone or as a polymer with other SiLRR-RLKs. In conclusion, the comprehensive analysis of the *SiLRR-RLK* gene family provided a framework for further functional studies on *SiLRR-RLK* genes.

KEYWORDS

Sesamum indicum*, LRR-RLK, evolution, expression profiles, *Macrophomina phaseolina

1 Introduction

Receptor-like protein kinases (RLKs) represent numerous transmembrane kinases that sense stimulation at the cell surface and mediate cell signal transduction by phosphorylation in response to the environment (Trenker and Jura, 2020). Many duplication events of RLKs exist in terrestrial plants (Lehti-Shiu et al., 2009), in which RLKs involved in the stress response show duplications, while those involved in growth and development do not (Shiu et al., 2004), suggesting that duplication events of RLKs are important for terrestrial plants to respond to ever-changing environments (Lehti-Shiu et al., 2012). LRR-RLKs represent the largest family in RLKs, which consist of three protein domains: an LRR domain sensing signal outside the cell, a single-channel transmembrane domain anchoring proteins within the membrane, and a kinase domain involved in signal transduction by autophosphorylation and subsequent specific substrate phosphorylation (Liu et al., 2017).

LRR-RLKs can widely regulate plant development and stress responses by participating in brassinosteroid (BR) and abscisic acid (ABA) signaling pathways. BRI1 (BR insensitive 1), a key LRR-RLK in the BR pathway, could regulate stem elongation, vascular differentiation, seed size, fertility, flowering time and senescence by BR signaling in *Arabidopsis* by forming the BRI1/BAK1 (BRI1-associated receptor kinase 1) complex (Li et al., 2002; Nam and Li, 2002; Wang et al., 2005). In addition, barley *bri1* mutant have multiple effects on disease resistance and plant developmental regulation (Goddard et al., 2014). SERK2 (Somatic embryogenesis receptor kinase 2), another component of the BR pathway, can mediate salt tolerance in rice via BR signaling (Dong et al., 2020). Moreover, OsSERK2 confers rice immunity to *Xanthomonas oryzae* pv. *oryzae* by activating the resistance genes *XA21* and *XA3* (Chen et al., 2014). BAK1 plays an important role in ABA signaling in guard cells. The *bak1* mutants exhibited more water loss than the wild type and showed ABA insensitivity in stomatal closure. Additionally, ABA can facilitate the formation of the BAK1/OST1 (Open stomatal 1) complex that mediates ABA-induced stomatal closure in guard cells near the plasma membrane (Shang et al., 2016). Likewise, KIN7 (Kinase 7) is essential in ABA signaling in stomatal closure. Phosphorylation and activation of TPK1 (Tonoplast K^+ channel) by the KIN7 is indispensable for ABA- and CO_2-mediated stomatal closure (Isner et al., 2018). In addition, LRR-RLKs have been shown to be involved in plant immunity via other phytohormone pathways. PSKR1 (Phytosulfokine receptor 1), an antagonistic regulator between biotrophic and necrotrophic pathogens in plant defense, can mediate plant resistance to pathogens by suppressing salicylic acid-dependent defense while enhancing jasmonic acid-dependent defense (Mosher et al., 2013). However, OsPSKR1 is involved in rice resistance to *Pseudomonas syringae* DC3000 in rice by activating the expression of *PR* genes involved in the salicylic acid signaling pathway (Yang et al., 2019). Furthermore, PEPR1 (Pep1 receptor 1) and PEPR2 are involved in plant immunity due to ROS (Reactive oxygen species) production and ethylene signaling (Ma et al., 2016).

The interaction and regulation between LRR-RLK members is intricate during development and stress. For instance, the CLV1 (CLAVATA 1)-CLV2-CRN (CORYNE) trimer is essential in plant stem cell regulation (Bleckmann et al., 2010; Zhu et al., 2010), and the BAK1-TMM (TOO MANY MOUTHS) complex is involved in plant immunity (Jordá et al., 2016). The formation of some LRR-RLK complexes depends on ligand stimulation, for instance, flg22 and elf18 can stimulate FLS2 (Flagellin sensitive 2) and EFR (Elongation factor-Tu receptor) to form dimers with BAK1 and then plant defense is initiated (Roux et al., 2011). Similarly, ligands SCFE1 (Sclerotium culture filtrate ELICITOR1) or NLP20 (Peptide motif) stimulate the formation of the BAK1-SOBIR1 (Suppressor of BIR1-1)-RLP23 complex (Gao et al., 2009), which plays an important role in plant resistance to pathogens. Moreover, there have been fewer studies on the interactions of LRR-RLKs in other plants, with only a few having been confirmed in tomato (Peng and Kaloshian, 2014), tobacco (Franco-Orozco et al., 2017), rice (Chen et al., 2014), *Medicago truncatula* (Crook et al., 2016) and wheat (Singh et al., 2016).

The large number, the great diversity of structure and function and the intricate interaction networks of *LRR-RLKs* present a challenge in understanding the functions and mechanisms of *LRR-RLK* genes in complex signal transduction pathways in plants. Furthermore, the complementary functions between LRR-RLKs indicate the importance of systematic analysis using bioinformatics tools to understand the roles of LRR-RLKs in plants. Recently, the *LRR-RLK* gene family has been reported in *Arabidopsis* (Shiu and Bleecker, 2001), soybean (Zhou et al., 2016), wheat (Shumayla et al., 2016), cotton (Sun et al., 2018), rice (Sun and Wang, 2011) and maize (Song et al., 2015). Additionally, the potential roles of LRR-RLKs in response to stresses have been well-studied in *Thinopyrum elongatum* (Mishra et al., 2021). Sesame charcoal rot caused by *M. phaseolina* is one of the most serious fungal diseases in sesame production, and threatens the yield and quality of sesame. Although *LRR-RLKs* are crucial in plant immunity, there is still a lack of systematic studies of the *LRR-RLKs* in sesame. It is of great practical significance to study *LRR-RLK* gene family in sesame and their functions related to biotic stresses. In this study, the *LRR-RLK* gene family in sesame was comprehensively analyzed by phylogeny, structural evolution and expression profile analysis. The potential functions of the sesame LRR-RLK homologous to *Arabidopsis* were predicted by protein –protein interaction (PPI) and coexpression networks. Our studies tend to gain insight into the functions of the sesame *LRR-RLK* family and provide new insights into their roles in regulation under *M. phaseolina* stress at the transcriptome level.

2 Materials and methods

2.1 LRR-RLK gene discovery in *S. indicum*

Sesame genome and proteome sequences were provided by Henan Sesame Research Center, Henan Academy of Agricultural Sciences (Zhang et al., 2013; Miao et al., 2023). HMM (Hidden Markov Model) profiles of LRRs (PF00560, PF07723, PF07725, PF12799, PF13306, PF13516, PF13855, PF14580 and PF01816) and Pkinase/Pkinase_Tyr (PF00069 and PF07714) were used for

identification of putative *LRR-RLKs* in *S. indicum* through HMMER 3.1 (Finn et al., 2011) (E-value < 1×10^{-10}). LRR-RLKs identified from *Arabidopsis* (Shiu and Bleecker, 2001), soybean (Zhou et al., 2016), wheat (Shumayla et al., 2016), cotton (Sun et al., 2018), rice (Sun and Wang, 2011) and maize (Song et al., 2015) were used to run BLASTP with the sesame proteome (E-value < 1×10^{-5}). The sum putative LRR-RLKs of the HMMER search result and BLASTP result were used for subsequent analysis. The InterPro database (https://www.ebi.ac.uk/interpro/) was used to confirm the presence of the kinase domain, LRR domain and transmembrane domain in LRR-RLKs in sesame. Sequences that met the above conditions were regarded as *LRR-RLKs*.

2.2 Phylogenetic, structural and functional analysis of LRR-RLKs

The theoretical isoelectric points (*pI*) and molecular weights (MW) of SiLRR-RLKs were predicted with Expasy (https://www.expasy.org/). CELLO (http://cello.life.nctu.edu.tw/) was used to predict the subcellular localization while SignalP-5.0 (https://services.healthtech.dtu.dk/service.php?SignalP-5.0) was used for signal peptide prediction. A conserved domain analysis of the sesame SiLRR-RLK family members was performed using the InterPro database. The MEME online server (http://meme-suite.org/) was used to search for conserved motifs. The conserved domains and gene structure of SiLRR-RLKs were visualized by TBtools (Chen et al., 2020). GO annotation was performed on PANNZER 2 (http://ekhidna2.biocenter.helsinki.fi/sanspanz/).

A multiple sequence alignment was performed using ClustalW with the default parameters method based on the aa sequences of the SiLRR-RLK proteins. MEGA 7 software (Kumar et al., 2016) was used to construct a phylogenetic tree of LRR-RLK using the neighbor Joining (NJ) method, and the bootstrap value was set to 1,000. Then the phylogenetic tree was visualized and edited on the iTOL website (https://itol.embl.de/).

2.3 Chromosomal arrangement and gene duplication of LRR-RLK genes

The sesame genome file (In fna format) and the genome annotation file (In gff3 format) were used to visualize the chromosome localization with TBtools (Chen et al., 2020). The MCScanX (Wang et al., 2012) program was used to determine collinear orthologous gene duplications (Tandem and segmental duplications) among the sesame *LRR-RLK* gene family and syntenic *LRR-RLK* genes between sesame and other plant species. The genome files and annotation files of *Solanum tuberosum*, *Glycine max*, *Solanum lycopersicum*, *M. truncatula*, *A. thaliana*, *Vitis vinifera*, *Gossypium hirsutum*, *Hordeum vulgare*, *Zea mays*, *Triticum aestivum*, *Oryza sativa*, *Musa acuminata*, *Setaria italica* and *Sorghum bicolor* were downloaded from the Phytozome database (Goodstein et al., 2012).

2.4 *In silico* and *in vitro* expression analysis of LRR-RLK genes

RNA-seq data PRJNA892254 was used for *in silico* expression analysis of diverse sesame tissues. Flower tissues of variety *S. indicum* var. 'Zhengzhi No.13' that showed consistent growth were sampled, and the locations were marked. The capsules at the markers were sampled along with all other tissues (Roots, stems, leaves, capsules and seeds) two weeks later. For *in silico* expression analysis of sesame seed development, RNA-seq data of variety *S. indicum* var. 'Wanzhi No.2' during seed development comprising 7 days after flowering (7 DAF, S1), 14 DAF (S2), 21 DAF (S3) and full maturity (28 DAF, S4) were used (PRJNA739094) (Zhang et al., 2021). For *in silico* expression analysis, the RNA-seq data of the disease-resistant variety *S. indicum* var. 'Zhengzhi No.13' infected with *M. phaseolina* and root tissues were concomitantly collected at 0 h, 12 h, 24 h, 36 h and 48 h post inoculation (PRJNA706471). The data above were downloaded from the SRA database. The reads were filtered, and trimmed using fastp (Chen et al., 2018), then clean reads were mapped to the sesame genome with HISAT2 (version:2.0.4) (Pertea et al., 2015; Pertea et al., 2016). Finally, the FPKM value of each gene was calculated by trimmed mean of M values method (Robinson and Oshlack, 2010).

For *in vitro* expression analysis of sesame leaves under phytohormone treatment, variety *S. indicum* var. 'Zhengzhi No.13' sesame plants were treated by spraying with 1 mM ABA, SA and MeJA when they grew to 4 pairs of true leaves period. Leaf tissues before treatment and treated post 1h, 3h, 6h, 12h, 24h, 36h and 48h were taken for RNA extraction, reverse transcription and qPCR. The primers of selected 6 *SiLRR-RLK* genes are listed in Supplementary Table S1, UBQ5 gene was used as a reference gene. There were three replicates for each treatment. The samples were stored at -80°C.

2.5 Protein–protein interaction network of LRR-RLK proteins

The STRING database (https://string-db.org/) was used to analyze the interaction of sesame LRR-RLK proteins based on orthologs in *Arabidopsis* with a confidence parameter set at a 0.85 threshold.

3 Results

3.1 Phylogenetic analysis and physicochemical attributes of SiLRR-RLKs

Based on a comprehensive search of *LRR-RLK* genes by HMM profiles and BlastP, 175 LRR-RLK proteins were identified in the sesame genome. The identified *LRR-RLK* members were given names with the prefix 'Si' indicating *S. indicum*. Phylogenetic analysis of LRR-RLK protein sequences in *S. indicum* and *A. thaliana* was carried out (Figure 1). The LRR-RLK of *S. indicum*

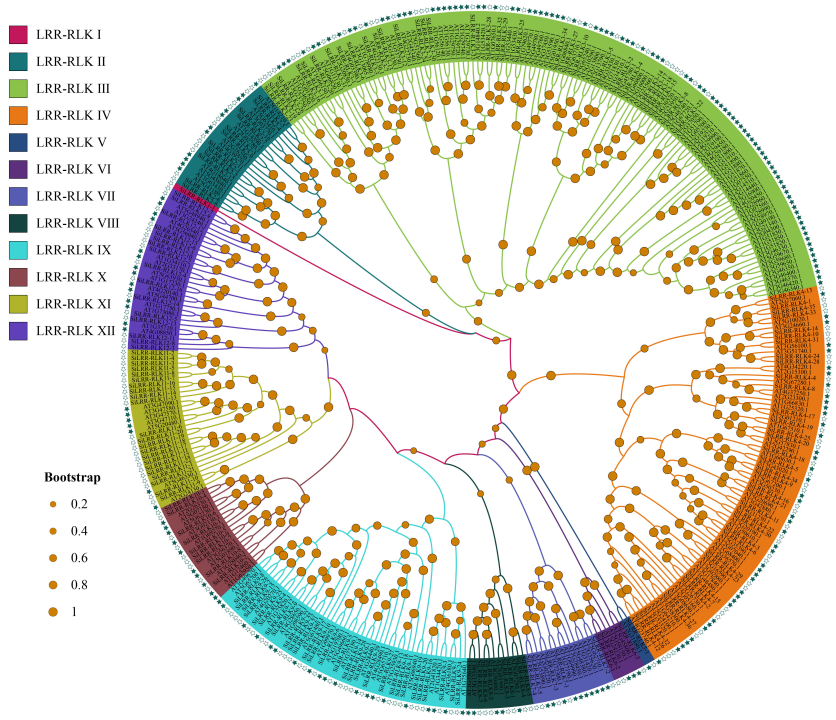

FIGURE 1
Phylogenetic analysis of the LRR-RLK proteins in *S. indicum* and *A. thaliana*. Green hollow pentacles represent LRR-RLKs in *S. indicum* while green solid pentacles represent those in *A. thaliana*.

was divided into 12 subfamilies together with those of *A. thaliana*. Group IV had the most members (36), followed by 34 members in group III and 29 members in group IX (Table 1). These three groups comprised 56.57% of SiLRR-RLKs (Figure 1). Group I and V comprising only one member were the smallest subfamily (Table 1). The details about the SiLRR-RLK family, including their accession numbers and characteristics, were given in Supplementary Table S2.

The physicochemical properties of SiLRR-RLKs enabled us to gain insight on their functions. The amino acid (aa) length of SiLRR-RLKs ranged from 466 to 1304 aa. Their isoelectric points (*pI*) were between 5.14 and 9.56, and their molecular weights ranged from 50.38 to 141.43 kDa (Supplementary Table S2). The summarized information regarding each subfamily was listed in Table 1.

3.2 Gene compositions, protein structure and functional annotation of SiLRR-RLKs

The conserved domains of proteins are closely related to their functions. Based on subfamily classification, conserved motif of *SiLRR-RLKs* were performed. Results showed that arrangement of motifs in same subfamily were similar (Figure 2). In addition, we identified the conserved domains of SiLRR-RLK proteins and found that they all contain both LRR and kinase domains (Figure 2), illustrating the accuracy of the *SiLRR-RLK* gene family. LRR-RLKs play a vital role in perceiving signals. Accordingly, a total of 78.29% of SiLRR-RLKs comprised signal peptides in our study (Supplementary Table S2). LRRNT_2 (PF08263) and LRR_8 (PF13855) constituted the major recognition domains in SiLRR-RLKs, which were found in 86.29% and 87.43% of SiLRR-RLKs, respectively. Furthermore, the brassinosteroid receptor island (PF20141) and Malectin (PF11721) domains were found in subfamilies III and VIII, implicating their additional roles in the recognition of BR and other plant hormones. Analysis of conversed motif and domain showed that kinase domains in LRR-RLKs C-terminal were more conserved, illustrating their potential roles in signal transduction. The structural compositions of the *SiLRR-RLK* genes were also further analyzed (Figure 2). The majority of *SiLRR-RLK* genes were composed of multiple exons, while only 16 *SiLRR-RLKs* were intron−less. *SiLRR-RLK10-3*, *SiLRR-RLK10-4* and *SiLRR-RLK10-6* have the most 27 exons. The exon−intron arrangement of *LRR-RLK* genes was conserved in same subfamilies while it varied in subfamilies III and X.

To further explore the potential functions of SiLRR-RLKs, GO (Gene Ontology) annotation was carried out. The results showed that SiLRR-RLKs were mainly involved in phosphorylation and defense response to fungus in terms of biological processes and functioned in kinase activity and ATP binding in molecular function (Figure 3A). All SiLRR-RLKs were predicted to localize to the membrane or plasma membrane. Consistently, all SiLRR-RLKs showed the characteristics of a high aliphatic index and low hydrophilicity (Supplementary Table S2), which further supported the idea that they were located on the plasma membrane. KEGG (Kyoto Encyclopedia of Genes and Genomes) enrichment of SiLRR-RLKs illustrated that SiLRR-RLKs were mainly enriched in

10.3389/fpls.2024.1334189

TABLE 1 Subfamily designation and physico-chemical properties of the identified SiLRR-RLKs.

Subfamily	Protein Number	Aa Length	MW (kDa)	pI	Aliphatic Index
LRR-RLK I	1	1107	123.73	5.66	90.97
LRR-RLK II	12	646-908	70.9-98.99	5.38-8.75	93.07-105.15
LRR-RLK III	34	579-1042	64.21-115.06	5.53-8.88	84.06-100.3
LRR-RLK IV	36	466-1107	50.38-119.62	5.56-9.42	90.04-104.32
LRR-RLK V	1	639	71.35478	9.09	97.81
LRR-RLK VI	3	687-855	76.65-94.15	5.7-9.56	90.54-96.25
LRR-RLK VII	5	605-1075	67.11-118.71	5.61-6.81	95.85-102.94
LRR-RLK VIII	7	1099-1304	120.92-141.43	5.14-6.16	96.87-109.68
LRR-RLK IX	29	619-1145	68.77-123.81	5.18- 8.8	96.24-108.76
LRR-RLK X	9	972-1135	104.44-122.7	5.47-8.92	99.44-106.51
LRR-RLK XI	22	522-1224	57.15-134.1	5.36-7.49	103.94-111.44
LRR-RLK XII	16	932-1222	102.53-134.7	5.18-6.97	102.63-112.15

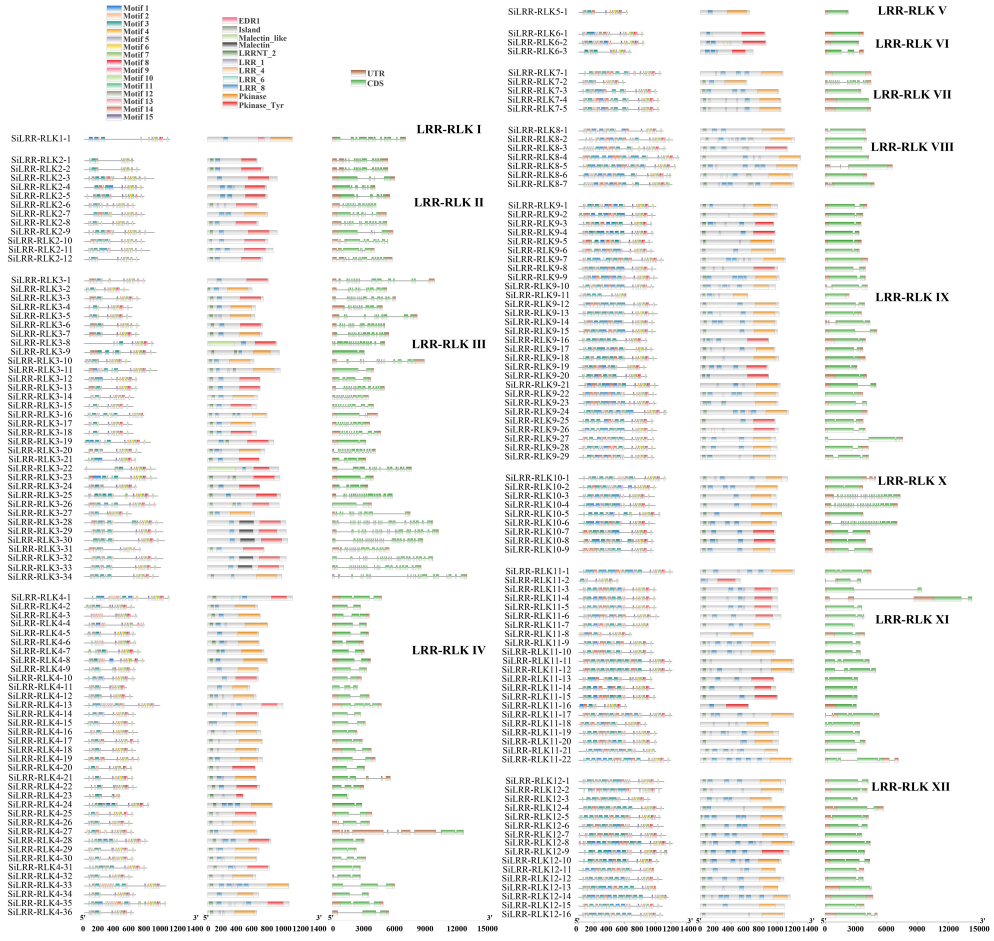

FIGURE 2
Conserved motifs, conserved domains and gene structures of 12 LRR-RLK subfamilies in *S. indicum*.

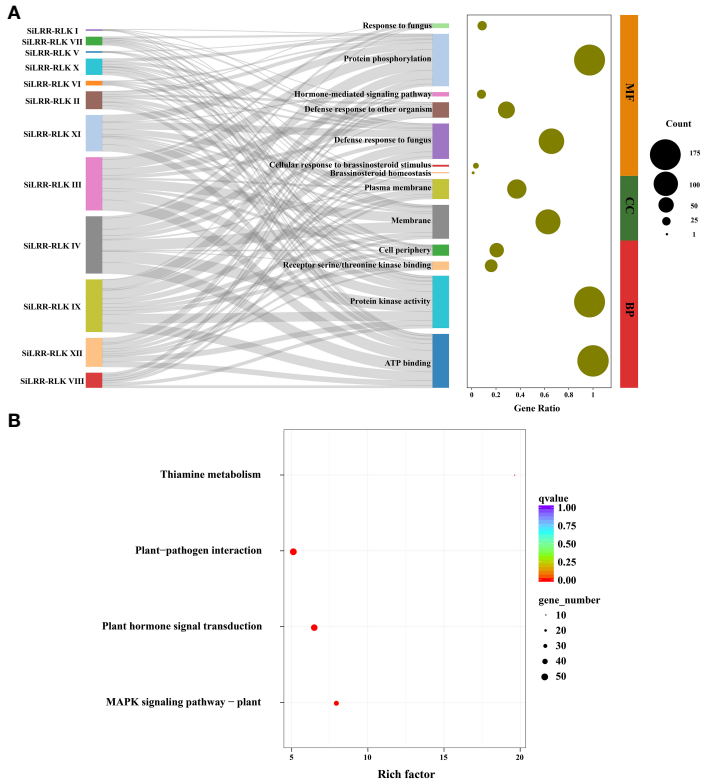

FIGURE 3
GO annotation and KEGG enrichment of SiLRR-RLK proteins. **(A)** GO annotation of 12 SiLRR-RLK protein subfamilies. MF, Molecular Function; CC, Cellular Component; BP, Biological Process. **(B)** KEGG enrichment of SiLRR-RLK proteins.

thiamine metabolism, MAPK signaling pathway, plant hormone signal transduction and plant–pathogen interaction (Figure 3B). All these results suggest that SiLRR-RLK proteins are essential for signaling recognition and transduction in the stress resistance, growth and development of sesame.

3.3 *Cis*-element analysis of SiLRR-RLK genes

Gene promoters in plants can regulate the expression of genes to respond to different biotic or abiotic stresses and different growing environments, hence, assessment of cis-elements and transcription factor binding sites in promoters is crucial for understanding transcriptional regulation and gene function (Biłas et al., 2016). The upstream sequences (~2000 bp) of the promoter were obtained to confirm the expression features of *SiLRR-RLKs*. The cis-elements of the *SiLRR-RLK* promoters were explored using the PlantCARE database (Lescot et al., 2002). The detailed effects of these motifs (cis-elements) are presented in Supplementary Table S3. *SiLRR-RLK* promoters contained many cis-elements in response to stresses, illustrating their potential roles in plant responses to adverse environments. *Cis*-elements of *SiLRR-RLK* promoters include light-responsive elements, phytohormone-responsive elements, stress-responsive elements and growth and development elements (Figure 4). The most abundant element in *SiLRR-RLK* promoters was the Box4 (Light) element, followed by the MYC (Drought) and STRE (Stress) elements (Figure 4; Supplementary Table S3), illustrating that *SiLRR-RLKs* not only had an important role in the light response but were also crucial in the response to both biotic and abiotic stresses. In addition, *SiLRR-RLKs* possessed the most AAGAA-motif (Seed specific expression) and ERE (Ethylene) elements in terms of growth development and hormone response.

Transcription factors (TFs) play key roles in many biological processes by regulating the expression of target genes. To investigate the possible regulatory relationship between TFs and *SiLRR-RLK* genes, the TF binding site prediction on PlantTFDB (Jin et al., 2017) was used. The results showed that the *SiLRR-RLK* genes could be regulated by 37 TF families (Supplementary Figure S1, Supplementary Table S4). C2H2, MIKC_MADS, MYB, AP2 and Dof were the TFs that can regulate most *SiLRR-RLK* genes. These TF families are involved in almost every aspect of plant development, hormone signaling, plant defense and stress response, suggesting that *SiLRR-RLKs* are extensively involved in the growth and stress defense of sesame.

3.4 Duplication and syntenic analysis of SiLRR-RLK genes

We found that 173 *SiLRR-RLKs* were unevenly distributed on 13 sesame chromosomes (Chr) while *SiLRR-RLK3-34* and *SiLRR-RLK4-36* were distributed on an unanchored scaffold (Figure 5A). Twenty-five *SiLRR-RLK* genes were mapped to Chr 2, followed by

10.3389/fpls.2024.1334189

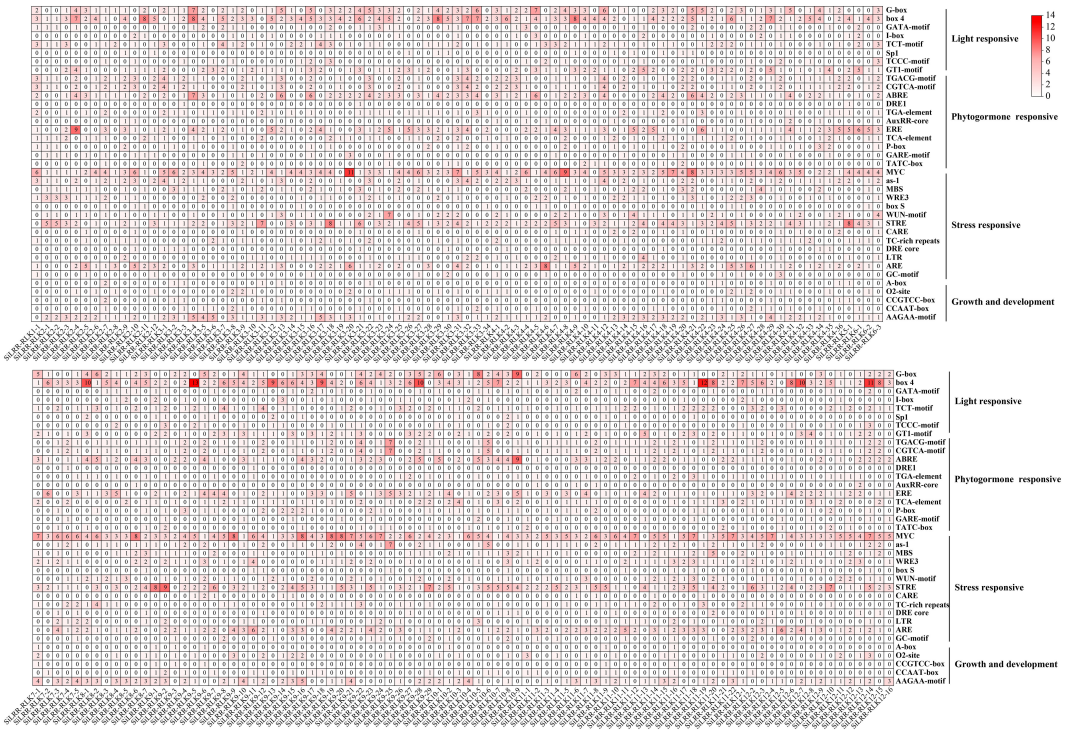

FIGURE 4
The distribution of *cis*-elements in *SiLRR-RLK* promoters. The gradient colors represent the number of cis-elements in *SiLRR-RLK* promoters.

15 *SiLRR-RLK* genes on Chr 4 and Chr 6. In contrast, minimum *SiLRR-RLK* genes (9) was found on Chr 5, Chr 7 and Chr 10 (Figure 5B). A total of 48 *SiLRR-RLK* genes formed 21 gene clusters. Chr 2 and Chr 4 both had maximum gene clusters with four. There are 2-4 *SiLRR-RLK* members within the gene clusters, most of them contain 2 *SiLRR-RLK* genes. The tandem duplication *SiLRR-RLK* genes were identified in each cluster with a threshold of 70% sequence similarity between two aa sequences of *SiLRR-RLKs*. Of the 21 gene clusters, 12 *SiLRR-RLK* genes from 7 clusters were considered to be tandem duplicated gene pairs (Figure 5A). In addition, segmental duplication of *SiLRR-RLK* genes was further analyzed within the sesame genome. 38 segmentally duplicated *SiLRR-RLK* pairs made by 70 *SiLRR-RLK* genes were predicted within the sesame genome (Figure 5C). A total of 46.29% of *LRR-RLK* genes underwent tandem or segmental duplication events, implying that gene duplication events were momentous in the expansion of the *SiLRR-RLK* gene family.

3.5 Evolution analysis of SiLRR-RLK genes in several plants

To infer the syntenic relationship of *LRR-RLK* genes in several plants, seven dicotyledons (*G. max*, *S. lycopersicum*, *S. tuberosum*, *G. hirsutum*, *V. vinifera*, *A. thaliana* and *M. truncatula*) (Figure 6A) and seven monocotyledons (*O. sativa*, *H. vulgare*, *Z. mays*, *T. aestivum*, *S. italica*, *M. acuminata* and *S. bicolor*) (Figure 6B) were used for evolution analysis with *S. indicum*. The *LRR-RLK* genes are homologous to genes in the dicotyledonous reference plants, and the number of homologous *LRR-RLK* genes is 120 (*G. max*), 132 (*S. lycopersicum*), 131 (*S. tuberosum*), 114 (*G. hirsutum*), 113 (*V. vinifera*), 98 (*A. thaliana*) and 114 (*M. truncatula*) (Supplementary Table S5). Nonetheless, only 36 (*O. sativa*), 16 (*H. vulgare*), 14 (*Z. mays*), 20 (*T. aestivum*), 38 (*S. italica*), 16 (*M. acuminata*) and 41 (*S. bicolor*) homologous *LRR-RLK* genes existed in monocotyledons (Supplementary Table S5). More homologous *LRR-RLK* genes were found in dicotyledons than in monocotyledons. In addition, *SiLRR-RLK4-27* and *SiLRR-RLK10-9* were homologous with all 14 species, suggesting that they are crucial in the evolution of the *LRR-RLK* gene family. Notably, *SiLRR-RLK10-9* also underwent segmental replication events in sesame (Figure 5C).

To further investigate the evolutionary relationship of LRR-RLK in dicotyledons, phylogenetic analysis of LRR-RLK proteins in dicotyledons was performed (Supplementary Figure S2). The results showed that SiLRR-RLK tended to gather with the LRR-RLKs of *A. thaliana* and *S. tuberosum*. We also used the MEME website to search for 10 conserved motifs of all LRR-RLK proteins. We found that the LRR-RLKs in *S. indicum* shared the most similar motif compositions with *A. thaliana* and *S. tuberosum* in the same branch, suggesting that SiLRR-RLKs were more closely related to those of *A. thaliana* and *S. tuberosum*.

3.6 *In silico* expression profiles of SiLRR-RLK genes in diverse tissues

To gain a broader understanding of the functions of *SiLRR-RLKs*, we analyzed the divergence in spatial expression among

10.3389/fpls.2024.1334189

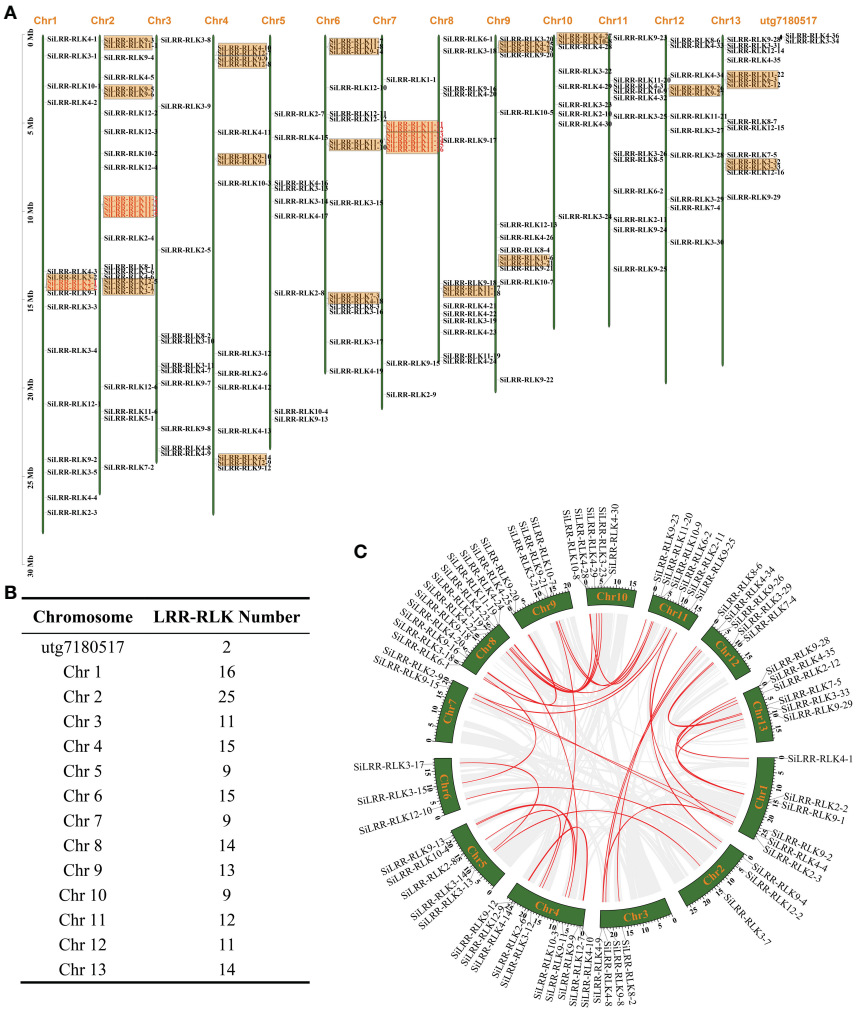

Chromosome	LRR-RLK Number
utg7180517	2
Chr 1	16
Chr 2	25
Chr 3	11
Chr 4	15
Chr 5	9
Chr 6	15
Chr 7	9
Chr 8	14
Chr 9	13
Chr 10	9
Chr 11	12
Chr 12	11
Chr 13	14

FIGURE 5
Chromosomal arrangement and gene duplication of *SiLRR-RLK* genes. **(A)** 173 *SiLRR-RLK* genes were mapped to 13 sesame chromosomes while 2 *SiLRR-RLK* genes mapped to unanchored scaffolds. The orange box indicates a gene cluster and the red names represent tandem duplication genes. **(B)** Number of *SiLRR-RLK* genes on each sesame chromosome. **(C)** The segmental duplication gene pairs of *SiLRR-RLK* genes. The gray lines indicate all the segmental duplicated gene pairs while red lines highlight the *SiLRR-RLK* pairs within the sesame genome.

SiLRR-RLK genes. Most *SiLRR-RLKs* exhibited different expression patterns in different tissues (Figure 7A). Some *SiLRR-RLK* genes were expressed tissue-characteristically. For instance, *SiLRR-RLK8-5* and *SiLRR-RLK12-9* were found to be expressed only in seeds, *SiLRR-RLK3-13* and *SiLRR-RLK4-6* were found to be expressed only in flowers, *SiLRR-RLK11-5* and *SiLRR-RLK11-18* were found to be expressed only in roots (*SiLRR-RLK* genes with FPKM values less than 0.1 were not considered expressed) (Supplementary Table S6). The gene expression patterns provided a preliminary clue to its function. 86, 73, 46, 40, 53 and 65 *LRR-RLK* genes were highly expressed (*SiLRR-RLK* genes with FPKM value more than 10 were considered as expressed highly) in roots, stems, leaves, flowers, capsules and seeds, respectively (Figure 7B). Of note, 14 *SiLRR-RLKs* (*SiLRR-RLK3-30*, *SiLRR-RLK3-16*, *SiLRR-RLK3-10*, *SiLRR-RLK3-5*, *SiLRR-RLK10-1*, *SiLRR-RLK3-22*, *SiLRR-RLK8-6*, *SiLRR-RLK6-3*, *SiLRR-RLK8-2*, *SiLRR-RLK3-26*, *SiLRR-RLK3-7*, *SiLRR-RLK9-8*, *SiLRR-RLK9-14* and *SiLRR-RLK3-1*) exhibited constitutively high expression across different tissues, indicating their important roles in the growth and development of sesame (Figure 7B). For example, AtTMK1 (Transmembrane kinase 1), a homolog of SiLRR-RLK3-16, can active GTPase in auxin sensing (Cao et al., 2019). TMK1-mediated auxin signaling regulates membrane-associated clathrin in *Arabidopsis* roots (Wang et al., 2022), suggesting the importance of SiLRR-RLK3-16 in sensing auxin.

The AAGAA motif (seed-specific expression) was found to be the most abundant cis-element in the promoter of *SiLRR-RLK* in terms of growth and development. Therefore, the expression pattern of *SiLRR-RLK* in seed development was determined based on PRJNA739094 (Zhang et al., 2021) (Supplementary Figure S3, Supplementary Table S7). The results showed that most *SiLRR-RLK* genes had a higher expression level in the early stage (S1 and S2) of seed development and then decreased in the later stage (S3 and S4), suggesting potential effects of *SiLRR-RLK* genes in early seed development. Notably, *SiLRR-RLK3-4*, *SiLRR-RLK3-6*, *SiLRR-RLK3-17* and *SiLRR-RLK9-16* possessed the most AAGAA motifs

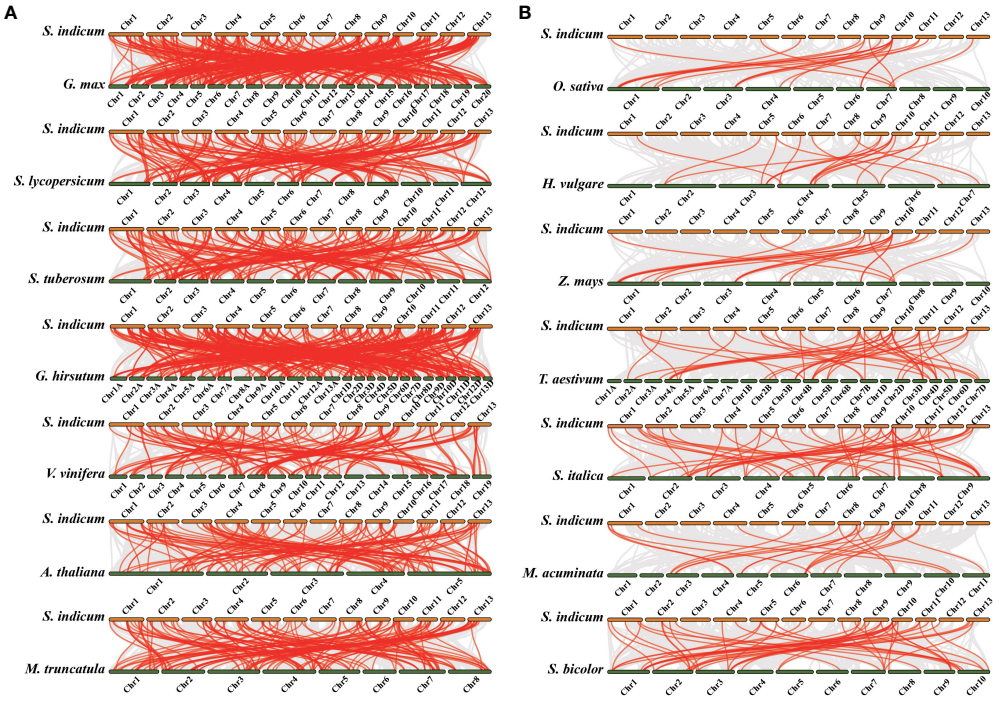

FIGURE 6
Synteny analysis of *LRR-RLK* genes between *S. indicum* and other plant species. The gray lines indicate all the syntenic gene pairs while red lines highlight the *SiLRR-RLK* pairs between *S. indicum* and other plant species. **(A)** Synteny analysis of *LRR-RLK* genes between *S. indicum* and dicotyledonous plants. **(B)** Synteny analysis of *LRR-RLK* genes between *S. indicum* and monocotyledonous plants.

with five (Figure 4). Among these, *SiLRR-RLK3-6* expressed at a low level in all stages. *SiLRR-RLK3-4* were induced at early stages S1, S2 and S3. Likewise, *SiLRR-RLK3-17* and *SiLRR-RLK9-16* were highly expressed during early seed development S1 and S2, implying that *SiLRR-RLK3-4*, *SiLRR-RLK3-17* and *SiLRR-RLK9-16* might contribute to sesame seed development. Furthermore, we found several *SiLRR-RLKs* (*SiLRR-RLK3-1*, *SiLRR-RLK3-7*, *SiLRR-RLK6-3* and *SiLRR-RLK10-4*) that were highly expressed during whole seed development (FPKM>10), which may also function in sesame seed development.

3.7 *In vitro* expression pattern of SiLRR-RLK genes in response to phytohormone treatment

LRR-RLK genes were functioned in plant hormone signaling pathways. Therefore, we selected *SiLRR-RLK5-1* (Homolog of SOBIR1), *SiLRR-RLK9-6* (Homolog of RLK7), *SiLRR-RLK3-5* (Homolog of BAK1), *SiLRR-RLK8-6* (Homolog of BRI1), *SiLRR-RLK12-13* (Homolog of PEPR1) and *SiLRR-RLK7-5* (Homolog of PSKR1) genes to investigate their expression patterns under SA, ABA and MeJA treatments (Figure 8).

The *SiLRR-RLK9-6*, *SiLRR-RLK3-5*, *SiLRR-RLK8-6*, *SiLRR-RLK12-13* and *SiLRR-RLK7-5* genes were down-regulated significantly at 1 h post SA treatment and remained suppressing within 48 h post SA treatment. However, *SiLRR-RLK5-1* was significantly down-regulated expression at 3 h post SA treatment. It is suggested that these genes play a negative role in the early stage (48 h) in SA signaling pathway. Under ABA treatment, *SiLRR-RLK5-1*, *SiLRR-RLK9-6*, *SiLRR-RLK3-5*, *SiLRR-RLK8-6*, *SiLRR-RLK12-13* and *SiLRR-RLK7-5* genes were significantly down-regulated at 1h and decreased to the lowest level at 6 h, followed by a significant up-regulation of expression at 48 h (*SiLRR-RLK3-5* restored its expression level at 48 h). Under MeJA treatment, *SiLRR-RLK5-1*, *SiLRR-RLK9-6*, *SiLRR-RLK3-5*, *SiLRR-RLK8-6*, *SiLRR-RLK12-13* and *SiLRR-RLK7-5* genes were significantly down-regulated, followed by partial restoration of their expression levels at 48 h. Notably, the expression trends of these six genes were similar under phytohormone treatment, suggesting that they may form dimers or polymers in phytohormone signaling pathway and synergistically regulate the downstream pathways.

3.8 *In silico* integrative expression analysis of SiLRR-RLKs during *M. phaseolina* stress

LRR-RLKs act as cell surface receptors and play a crucial role in signal sensing and transduction. To unravel the function of SiLRR-RLKs in response to pathogen *M. phaseolina*, the expression patterns of *SiLRR-RLK* genes under stress were investigated (Figure 9; Supplementary Table S8). Considering that there are many *LRR-RLK* genes in sesame, we divided them into six clusters based on their expression patterns (FPKM>0) (Supplementary Figure S4). The results showed that the *SiLRR-RLK* genes in Cluster 5 and Cluster 6 were decreased after inoculation with

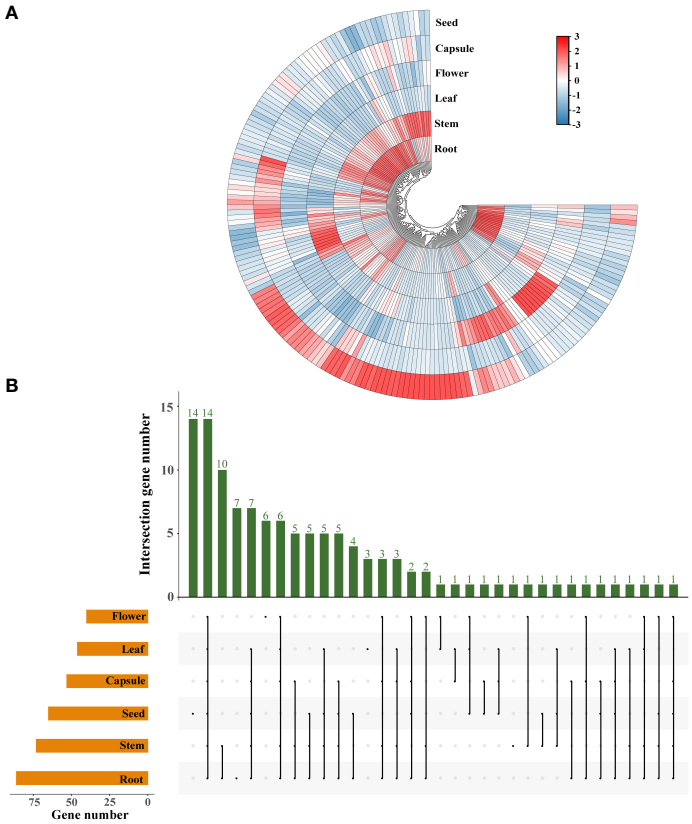

FIGURE 7
Expression profiles of *SiLRR-RLK* genes in different tissues. **(A)** Tissue-specific expression of *SiLRR-RLK* genes. The color scale shows the range of normalized FPKM values. **(B)** Number of *SiLRR-RLK* genes highly expressed in each tissue. Orange bars show the *SiLRR-RLK* genes highly expressed in each tissue while green bars indicate *SiLRR-RLK* genes highly expressed across diverse tissues.

M. phaseolina, they may mediate the susceptibility in plant immunity (Figure 9; Supplementary Figures S4E, S4F). However, most *SiLRR-RLKs* were induced at different times in Cluster 1, Cluster 2, Cluster 3 and Cluster 4 under *M. phaseolina* stress, which further confirmed the widely known disease resistance of *LRR-RLKs* (Figure 9; Supplementary Figures S4A-D). For instance, *SiLRR-RLK11-10* in Cluster 1 were upregulated 4.68-fold at 12 hours after infection while *SiLRR-RLK12-6* and *SiLRR-RLK9-22* in Cluster 2 were upregulated 4.89- and 10.48-fold at 48 hours after infection, respectively. *SiLRR-RLK* genes in Cluster 3 were upregulated 2-3 times overall during *M. phaseolina* treatment. Moreover, the expression of *SiLRR-RLK* genes in Cluster 4 were continuously induced by *M. phaseolina* (Supplementary Figures S4A-D, Supplementary Table S8).

The duplicated *SiLRR-RLK* genes identified were analyzed synchronously with their expression patterns to identify the genes designated for novel functions. The expression patterns of 7 pairs of tandemly duplicated *SiLRR-RLK* genes and 38 pairs of segmentally duplicated *SiLRR-RLK* genes during *M. phaseolina* stress were analyzed in a heatmap (Figure 10). We found that most tandemly and segmentally duplicated *SiLRR-RLK* genes exhibited antagonistic expression profiles under *M. phaseolina* stress, suggesting a function of redundancy between *SiLRR-RLK* genes during sesame disease resistance (Figure 10). There were only a few exceptions, the *LRR-RLK11-11*:*LRR-RLK11-12* gene pair showed a similar expression profile under *M. phaseolina* stress, that is, they were both induced at post infection.

3.9 Molecular protein–protein interaction network of SiLRR-RLKs

According to well-studied investigations, there are many complex interactions within the *LRR-RLK* gene family. To further gain insight into the functions of the SiLRR-RLK proteins, we constructed a PPI network by STRING database (https://STRING-db.org/) based on the well-studied LRR-RLKs in *Arabidopsis*. As shown in Figure 11, the SiLRR-RLK members showed interactions with some other members.

Obviously, SiLRR-RLK3-5, the homolog of AtBAK1, is the hub functional gene in the PPI network. Studies have showed that AtBAK1, acting as a coreceptor with other proteins, can form complexes (Dimer, trimer or tetramer) such as SOBIR1/BAK1, BAK1/BIR1, ER/BAK1/TMM, BIK1/BAK1/ERL1/ERL2, FLS2/BAK/BIK1 and FLS2/BIK1/RBOHD, and these complexes are all important in relaying signals to downstream components in plant immunity system (Gao et al., 2009; Lu et al., 2010; Wang et al., 2011; Li et al., 2014; Lin et al., 2014; Jordá et al., 2016). In addition, other

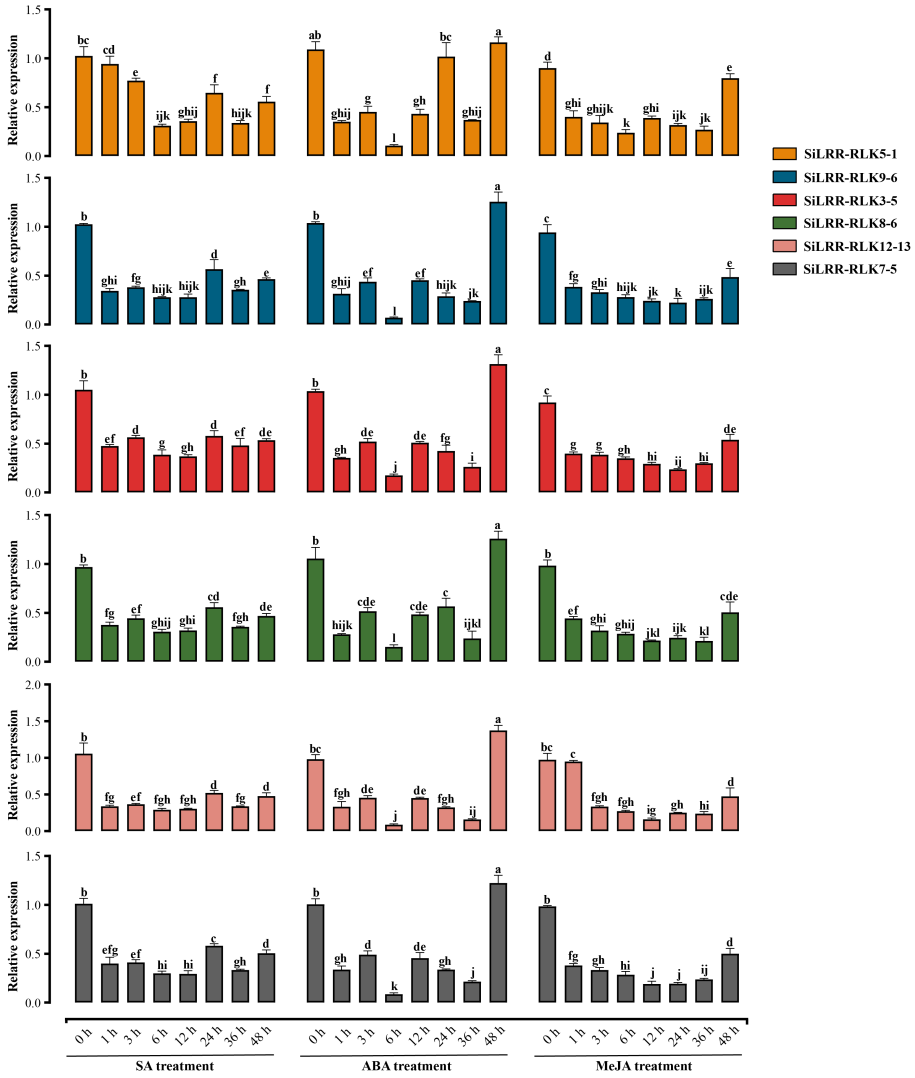

FIGURE 8
Relative expression level of *SiLRR-RLK5-1* (Homolog of SOBIR1), *SiLRR-RLK9-6* (Homolog of RLK7), *SiLRR-RLK3-5* (Homolog of BAK1), *SiLRR-RLK8-6* (Homolog of BRI1), *SiLRR-RLK12-13* (Homolog of PEPR1) and *SiLRR-RLK7-5* (Homolog of PSKR1) genes at 0 h, 1 h, 3 h, 6 h, 12 h, 24 h, 36 h and 48 h post treated by SA, ABA and MeJA.

AtLRR-RLK genes in the network have also been proven to be involved in plant biotic stress, such as SOBIR1, a homolog of SiLRR-RLK5-1, which was reported to form a complex with BAK1 for immunity against the fungi *Phytophthora infestans* and *Sclerotinia sclerotiorum* (Gao et al., 2009; Liu et al., 2016). SiLRR-RLK4-17 is homologous to ZAR1, which is a calcium-permeable channel triggering plant immune signaling (Bi et al., 2021). Notably, SiLRR-RLK8-6, a homolog of AtBRI1, was highly expressed in all tissues. BRI1 acts as a BR receptor and is extensively involved in plant growth, development and stresses (Wang et al., 2001). Recent studies have shown that BRI1 can form a heterodimer with SAUR15, which activates the plasma membrane H^+-ATPase to promote *Arabidopsis* organogenesis (Li et al., 2022). In addition, BRI1 is another LRR-RLK that can bind to BAK1, and the BRI1/BAK1 complex regulates stem elongation, vascular differentiation, seed size, fertility, flowering time and senescence by BR signaling in *A. thaliana* (Li et al., 2002; Nam and Li, 2002; Wang et al., 2005). Notably, BRI1 in cereals has been shown to contribute to disease resistance (Goddard et al., 2014) and drought tolerance (Feng et al., 2015) in plants, indicating that SiLRR-RLKs have complex biological functions by participating in the crosstalk between plant growth and development and stress.

3.10 Coexpression analysis of LRR-RLK genes in response to *M. phaseolina*

Based on the sequence structure, functional annotation, expression patterns and PPI prediction of SiLRR-RLKs, we can conclude that SiLRR-RLKs are crucial for plant immunity. In addition, previous studies have shown that SiLRR-RLKs are vital components in response to *M. phaseolina* stress (Yan et al.,

FIGURE 9
Expression patterns of *SiLRR-RLK* genes under *M. phaseolina* stress (0 - 48 h). The box plot on the left represents the expression trend of *SiLRR-RLK* genes in the same cluster, the heatmap in the middle indicates the expression patterns of *SiLRR-RLK* genes, and the annotation on the right explains the expression trend of *SiLRR-RLK* genes in each cluster.

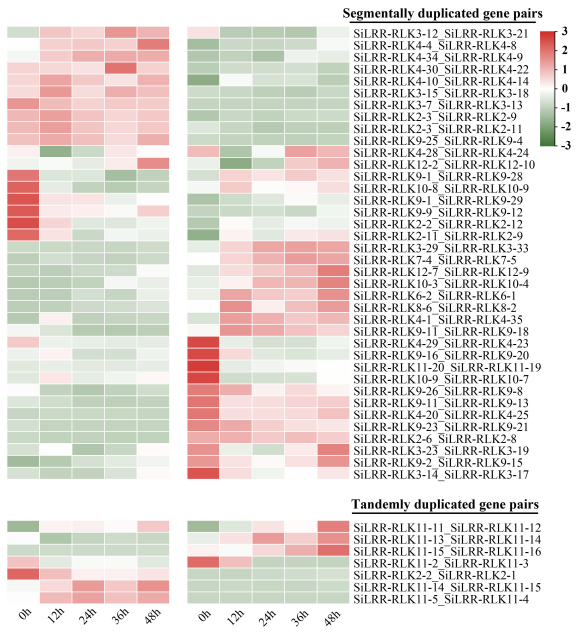

FIGURE 10
Expression patterns of tandemly and segmentally duplicated *SiLRR-RLK* gene pairs during *M. phaseolina* infection (0 - 48 h). "_" represents two *SiLRR-RLKs* are duplicated gene pairs.

2021). To further understand the relationship between *SiLRR-RLK* genes and sesame disease resistance, the expression patterns of *SiLRR-RLK* genes under *M. phaseolina* stress were used for correlation analysis. *SiLRR-RLK* gene pairs with a Pearson correlation coefficient greater than 0.95 or less than -0.95 suggested a correlation between the two *SiLRR-RLK* genes. The coexpression network of *SiLRR-RLK* genes was constructed according to the relationship between *SiLRR-RLK* genes (Figure 12). In a coexpression network, most genes interact with only a few other genes, while a few interact with a large number of other genes, which are the core genes in this gene network. Core *SiLRR-RLK* genes in the coexpression network might be vital in sesame resistance to *M. phaseolina*. Additionally, two core gene sets in the network attracted our attention (Figures 11, 12). One is the BAK1/PEPR1/RLK7/SOBIR1/MIK2 signaling pathway, whose function in plant immunity has been well elucidated in other plants. The other is the SRF8/PXC3/IRK signaling pathway. Notably, there exist a correlation between SiLRR-RLK10-8 and SiLRR-RLK9-20, as well as SiLRR-RLK12-3, SiLRR-RLK12-13, SiLRR-RLK12-8 and SiLRR-RLK9-6 (Figures 11, 12). Combined with coexpression analysis and the PPI network, the core genes, *SiLRR-RLK12-3/SiLRR-RLK12-13/SiLRR-RLK12-8/SiLRR-RLK9-6* and *SiLRR-RLK10-8/SiLRR-RLK9-20*, may be the core components of disease resistance to *M. phaseolina* in sesame.

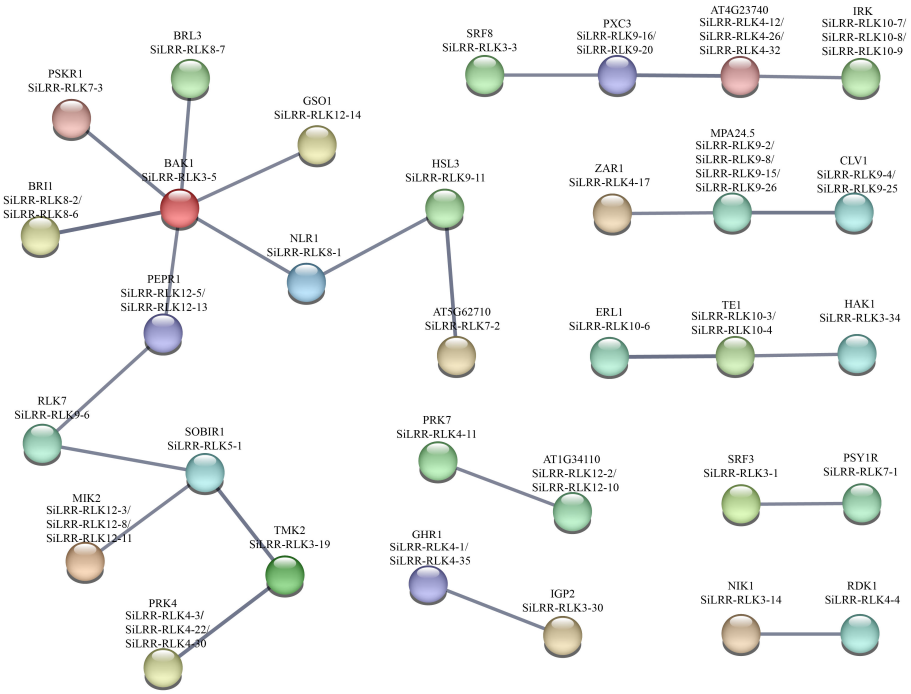

FIGURE 11
A protein–protein interaction network for SiLRR-RLKs based on their orthologs in *Arabidopsis*. SiLRR-RLK proteins are shown in brackets with *Arabidopsis* orthologs.

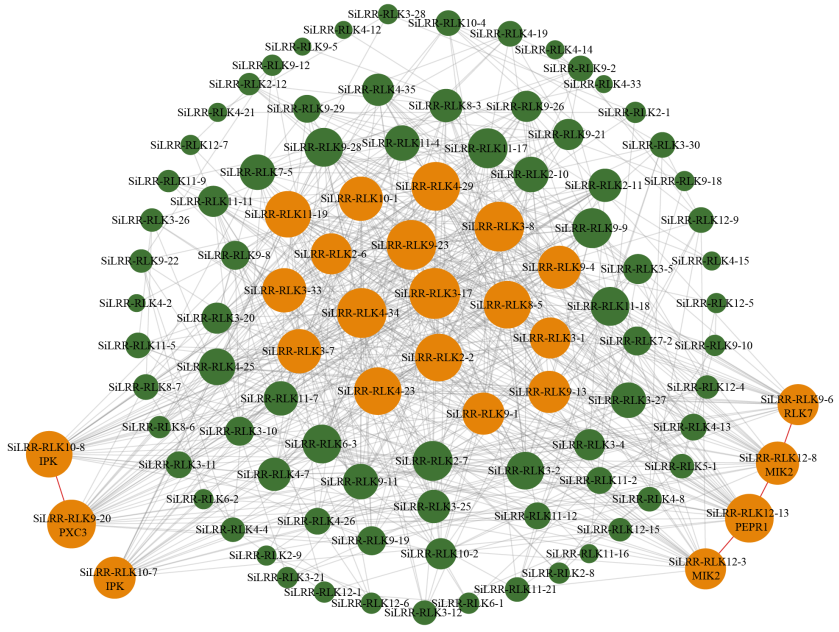

FIGURE 12
Coexpression network of *SiLRR-RLK* genes in response to *M. phaseolina*. The larger nodes represent core *SiLRR-RLKs* in the network, while the smaller nodes represent noncore *SiLRR-RLKs*. The size of the node circle is positively correlated with the number of *SiLRR-RLKs* it interacts. The orange nodes indicate core *SiLRR-RLKs* that may form multimers to defend against *M. phaseolina*.

4 Discussion

Recently, the *LRR-RLK* gene family has been identified in many plant species, and the number of *LRR-RLK* family members varies greatly. The proportion of *SiLRR-RLK* genes was consistent with Liu et al. (Liu et al., 2017), which showed a 0.67-1.39% proportion in angiosperm species. In higher plants, the number of identified *LRR-RLK* genes ranged from 180 (*C. sativus*) to 589 (*T. elongatum*) (Soltabayeva et al., 2022). A recent study has identified 14 classes resistance (R) genes, including *LRR-RLK* subclass, in the sesame genome (Miao et al., 2023). In this study, 175 *SiLRR-RLK* genes were identified from the sesame genome, accounting for 0.73% of the sesame genome and 14.61% of sesame R genes. Although there is a lack of information on the function of *LRR-RLK* genes in sesame, the evolutionary diversity and function of *SiLRR-RLK* genes can be inferred from phylogenetic analysis, protein structure, gene structure and expression profiles. The phylogenetic tree revealed that SiLRR-RLKs can be divided into 12 subfamilies. SiLRR-RLKs occurred in almost every major branch together with the *Arabidopsis* LRR-RLK subfamily (Figure 1), indicating that all *Arabidopsis* LRR-RLK subfamilies share a common ancestor with sesame. Additionally, the collinearity analysis showed that the homologous *LRR-RLK* genes existed much more in dicotyledons than monocotyledons (Figure 6). It is implied that the duplication of the *LRR-RLK* gene probably occurred after the differentiation of dicotyledons and monocotyledons, which has been consistent with a previous investigation(Miao et al., 2023).

Segmental and tandem replication are important drivers of the expansion of gene families, especially in the evolution of plant *LRR-RLK* gene families (Lehti-Shiu et al., 2009; Lehti-Shiu and Shiu, 2012). A total of 420 (71.31%) *LRR-RLK* genes with replication events were detected in *T. ponticum*, involving 191 segmentally duplicated *SiLRR-RLK* pairs and 145 tandemly duplicated *SiLRR-RLK* pairs (Mishra et al., 2021). It has been found that 73.3% and 20.3% of *LRR-RLK* genes in soybean were involve in segmental duplication and tandem duplication (Zhou et al., 2016). Similarly, in the present study, 81 (46.29%) *SiLRR-RLK* genes involved in 38 segmental pairs and 7 tandem pairs were perceived (Figure 5). Therefore, it is inferred that the expansion of the *LRR-RLK* gene family is mainly caused by gene segmental duplication. Interestingly, *SiLRR-RLK10-9* was found to have collinearity with other 14 species (Figure 6), and *SiLRR-RLK10-9* also underwent segmental replication events in sesame, suggesting its key contributions to the expansion of the *SiLRR-RLK* gene family.

The *SiLRR-RLK* IV and III subfamilies, representing the two largest subfamilies, exhibited duplication events. *SiLRR-RLKs* in the IV and III subfamilies were also syntenic with the *LRR-RLKs* in the other 14 species (Supplementary Table S5). 36 and 34 *LRR-RLK* members from sesame were found to form the *SiLRR-RLK* IV and III subfamilies, respectively, based on the phylogenetic tree (Figure 1). Furthermore, there were 16 genes and 12 genes underwent segmental duplication in IV and III subfamilies, respectively (Figures 1, 5C). Under *M. phaseolina* stress, 13 and 16 *SiLRR-RLK* genes in IV and III subfamilies were induced significantly (Figure 10, Supplementary Table S8). Notably, proteins from subfamilies IV and III were both assigned to the GO terms phosphorylation and kinase activity (Figure 3A). These results point to the idea that the duplicated events within the *SiLRR-RLK* IV and III subfamilies during evolution may contribute to the perception of *M. phaseolina* stress signals in sesame.

The *LRR-RLK* genes are crucial in recognition and signal transduction in biotic and abiotic stresses, as shown by the fact that their promoters possess many phytohormone and stress responsive cis-elements (Figure 4), hence, the ever-changing environment may also lead to the replication and expansion of the *SiLRR-RLK* gene family. On the other hand, evidence that there are the ubiquitous redundant functions of *SiLRR-RLK* genes has indicated that the diversity of *SiLRR-RLK* genes may also be the result of random genomic drift (Eyüboglu et al., 2007; Albrecht et al., 2008). After duplication, duplicated genes usually accumulate mutations and lead to a functional diversification of LRR-RLK proteins. *Arabidopsis* LRR-RLKs are primarily involved in regulating plant growth and development and stress responses (Biotic and abiotic stresses) or both (Li and Tax, 2013). In this investigation, KEGG enrichment of SiLRR-RLKs revealed the pathways involved in resistance to *M. phaseolina*, such as MAPK signaling pathway, plant hormone signal transduction and plant −pathogen interaction pathway (Figure 3B). SiLRR-RLKs may sense extracellular signals, act as early warning genes, and then regulate the early stress response in plants (Lin et al., 2017). In this study, SiLRR-RLKs were shown to play a role in plant−pathogen interactions by transmitting and amplifying signals downstream through protein phosphorylation and kinase activity (Figure 3).

In general, the expression patterns of genes represent their potential functions. Therefore, the expression profiles of *SiLRR-RLKs* under *M. phaseolina* stress may help us to gain insight on the function of *SiLRR-RLKs*. In our research, several genes in response to fungal infection were identified. Many *SiLRR-RLKs* act as pattern recognition receptors to initiate the PTI (Pathogen-associated molecular pattern-triggered immunity). SiLRR-RLK3-5, homologous to AtBAK1, can be continuously induced during *M. phaseolina* infection (Supplementary Table S8), implicating its positive function during plant immunity, which is supported by the central position of SiLRR-RLK3-5 in the PPI network (Figure 11). In *Arabidopsis*, the BAK1/BRI1 complex regulates the cell death process to participate in the immune response by the BR signaling pathway (Li et al., 2002). Likewise, in tobacco, NbBRI1 participates in brassinosteroid-regulated immune responses by regulating the concentrations of H_2O_2 and NO (Deng et al., 2016). In sesame, SiLRR-RLK8-6, which is homologous to BRI1, were induced during *M. phaseolina* stress (Supplementary Table S8). Their expression patterns were similar to those of SiLRR-RLK3-5, illustrating that SiLRR-RLK8-6 may form a complex with SiLRR-RLK3-5 and coregulate plant immunity through the BR pathway.

SiLRR-RLK3-14 is homologs of NIK1 (NSP-interacting kinase 1), and the abundance of their transcripts was downregulated at early stage (Supplementary Table S8), which coincides with the fact that NIK1 acts as a negative regulator in plant immunity (Li et al., 2019). BRL3 (BR insensitive1-like 3) in *Arabidopsis* not only senses FLG22 and regulates ROS homeostasis (Tunc-Ozdemir and Jones, 2017) but also increases permeating agents such as proline in plants,

which can improve plant drought tolerance without a penalty in growth (Fàbregas et al., 2018). In sesame, SiLRR-RLK8-7, as a homolog of BRL3, exhibited a upregulation trend during *M. phaseolina* infection, suggesting that SiLRR-RLK8-7 may play a crucial role in disease resistance (Supplementary Table S8).

The previous results of functional annotation, KEGG enrichment, promoter analysis, expression pattern and PPI network of SiLRR-RLKs all showed that SiLRR-RLKs are crucial in plant immunity. Thus, a coexpression network of SiLRR-RLKs under *M. phaseolina* stress was constructed. Interestingly, two coexpression immune modules were inferred in the core gene set based on PPI and coexpression network (Figures 11, 12). They are the *SiLRR-RLK12-3/SiLRR-RLK12-13/SiLRR-RLK12-8/SiLRR-RLK9-6* module, which is homologous to the *Arabidopsis* BAK1/PEPR1/RLK7/SOBIR1/MIK2 complex, and *SiLRR-RLK10-8/SiLRR-RLK9-20* module, which is homologous to the *Arabidopsis* SRF8/PXC3/IRK complex. In *Arabidopsis*, the function of the SOBIR1/BAK1 complex has been well studied, and exogenous NLP20 treatment stimulates the formation of the BAK1/SOBIR1/RLP23 complex and initiates immunity (Gao et al., 2009). Furthermore, the SOBIR1/BAK1 complex could enhance the resistance of *Arabidopsis* to the fungi *P. infestans* and *S. sculrotiorum* (Liu et al., 2016). In addition to BAK1, the function of SOBIR1 in other species has also been studied in detail. In tomato, the homolog of SOBIR1 interacts directly with the disease resistance genes CF-4 and VE1, which mediated the resistance to the fungi *Cladosporium fulvum* and *Verticillium dahliae* (Liebrand et al., 2013). SOBIR1 in cotton was reported to interact with bHLH171, phosphorylate bHLH171 and confer resistance to the fungus *V. dahliae* (Zhou et al., 2019). In tobacco, SOBIR1 can fine-tune ROS production involved in the immune response to the fungus *Cladosporium fulvum* (Huang et al., 2021). These results suggest that the *SiLRR-RLK12-3/SiLRR-RLK12-13/SiLRR-RLK12-8/SiLRR-RLK9-6* module might be important in resistance to the fungus *M. phaseolina* (Figures 11, 12). They might mediate resistance to the fungus *M. phaseolina* independently or form dimers or polymers with each other to mediate the immune response to *M. phaseolina* jointly, which needs further study. However, studies on the immune function of the SRF8/PXC3/IRK (Inflorescence and root apices receptor kinase) module are not clear. In *Arabidopsis*, PXC3 (Phloem intercalated with xylem-correlated 3) has been shown to interact with BAK1 to regulate vascular development (Xu et al., 2021), but whether it has a function in plant immunity is unknown. *Arabidopsis* SRF3 (Strubbelig receptor kinase 3) could coordinate immune responses, growth and development in plants (Platre et al., 2022), but the function of SRF8 is uncharted. Therefore, the role of the *SiLRR-RLK10-8/SiLRR-RLK9-20* module resistance to *M. phaseolina* in sesame is not clear, and further experiments are needed to solve this issue.

5 Conclusions

Whole genome identification and comprehensive analysis of the *SiLRR-RLK* gene family were carried out in this study. Phylogenetic, structural, evolutionary and expression profile analyses of *SiLRR-RLKs* revealed the complexity and diversity of the *LRR-RLK* gene family in sesame and its potential roles under *M. phaseolina* stress. Furthermore, we found several *SiLRR-RLK* genes that contributed to resistance to *M. phaseolina*. Altogether, the results provided a framework for further functional study of *SiLRR-RLK* genes.

Data availability statement

The datasets presented in this study can be found in online repositories. The names of the repository/repositories and accession number(s) can be found in the article/Supplementary Material.

Author contributions

WY: Data curation, Formal analysis, Investigation, Visualization, Writing – original draft. YN: Data curation, Resources, Writing – review & editing. HZ: Data curation, Resources, Writing – review & editing. XL: Data curation, Resources, Writing – review & editing. MJ: Data curation, Resources, Writing – review & editing. XZ: Resources, Writing – review & editing. YL: Resources, Writing – review & editing. HM: Conceptualization, Funding acquisition, Supervision, Writing – review & editing. HL: Conceptualization, Funding acquisition, Supervision, Writing – review & editing. HZ: Conceptualization, Funding acquisition, Supervision, Writing – review & editing.

Funding

The author(s) declare financial support was received for the research, authorship, and/or publication of this article. The work was supported by The Key Research Project of the Shennong Laboratory (SN01-2022-04), the Key Project of Science and Technology of Henan Province (201300110600), China Agriculture Research System of MOF and MARA (CARS-14), and Key Research and Development Project of Henan Province (221111520400).

Conflict of interest

The authors declare that the research was conducted in the absence of any commercial or financial relationships that could be construed as a potential conflict of interest.

Publisher's note

Supplementary material

The Supplementary Material for this article can be found online at: https://www.frontiersin.org/articles/10.3389/fpls.2024.1334189/full#supplementary-material

SUPPLEMENTARY FIGURE 1
Statistics of *SiLRR-RLK* genes regulated by TFs (Genes with TF binding sites were considered to be regulated by TFs).

SUPPLEMENTARY FIGURE 2
Phylogenetic analysis and motif compositions of LRR-RLK proteins in six dicotyledons. Green hollow pentacles highlight SiLRR-RLK proteins.

SUPPLEMENTARY FIGURE 3
Expression profiles of *SiLRR-RLKs* during seed development (S1, S2, S3 and S4).

SUPPLEMENTARY FIGURE 4
Expression profiles of *SiLRR-RLKs* of Cluster 1 **(A)**, Cluster 2 **(B)**, Cluster 3 **(C)**, Cluster 4 **(D)**, Cluster 5 **(E)** and Cluster 6 **(F)** during *M. phaseolina* infection (0 - 48 h).

References

Albrecht, C., Russinova, E., Kemmerling, B., Kwaaitaal, M., and De Vries, S. C. (2008). *Arabidopsis* SOMATIC EMBRYOGENESIS RECEPTOR KINASE proteins serve brassinosteroid-dependent and -independent signaling pathways. *Plant Physiol.* 148, 611–619. doi: 10.1104/pp.108.123216

Bi, G., Su, M., Li, N., Liang, Y., Dang, S., Xu, J., et al. (2021). The ZAR1 resistosome is a calcium-permeable channel triggering plant immune signaling. *Cell* 184, 3528–3541.e3512. doi: 10.1016/j.cell.2021.05.003

Biłas, R., Szafran, K., Hnatuszko-Konka, K., and Kononowicz, A. K. (2016). Cis-regulatory elements used to control gene expression in plants. *Plant Cell* 127, 269–287. doi: 10.1007/s11240-016-1057-7

Bleckmann, A., Weidtkamp-Peters, S., Seidel, C. A., and Simon, R. (2010). Stem cell signaling in *Arabidopsis* requires CRN to localize CLV2 to the plasma membrane. *Plant Physiol.* 152, 166–176. doi: 10.1104/pp.109.149930

Cao, M., Chen, R., Li, P., Yu, Y., Zheng, R., Ge, D., et al. (2019). TMK1-mediated auxin signalling regulates differential growth of the apical hook. *Nature* 568, 240–243. doi: 10.1038/s41586-019-1069-7

Chen, C., Chen, H., Zhang, Y., Thomas, H. R., Frank, M. H., He, Y., et al. (2020). TBtools: an integrative toolkit developed for interactive analyses of big biological data. *Mol. Plant* 13, 1194–1202. doi: 10.1016/j.molp.2020.06.009

Chen, S., Zhou, Y., Chen, Y., and Gu, J. (2018). fastp: an ultra-fast all-in-one FASTQ preprocessor. *Bioinformatics* 34, i884–i890. doi: 10.1093/bioinformatics/bty560

Chen, X., Zuo, S., Schwessinger, B., Chern, M., Canlas, P. E., Ruan, D., et al. (2014). An XA21-associated kinase (OsSERK2) regulates immunity mediated by the XA21 and XA3 immune receptors. *Mol. Plant* 7, 874–892. doi: 10.1093/mp/ssu003

Crook, A. D., Schnabel, E. L., and Frugoli, J. A. (2016). The systemic nodule number regulation kinase SUNN in Medicago truncatula interacts with MtCLV2 and MtCRN. *Plant J.* 88, 108–119. doi: 10.1111/tpj.13234

Deng, X. G., Zhu, T., Zou, L. J., Han, X. Y., Zhou, X., Xi, D. H., et al. (2016). Orchestration of hydrogen peroxide and nitric oxide in brassinosteroid-mediated systemic virus resistance in *Nicotiana benthamiana*. *Plant J.* 85, 478–493. doi: 10.1111/tpj.13120

Dong, N., Yin, W., Liu, D., Zhang, X., Yu, Z., Huang, W., et al. (2020). Regulation of brassinosteroid signaling and salt resistance by SERK2 and potential utilization for crop improvement in rice. *Front. Plant Sci.* 11, 621859. doi: 10.3389/fpls.2020.621859

Eyüboglu, B., Pfister, K., Haberer, G., Chevalier, D., Fuchs, A., Mayer, K. F., et al. (2007). Molecular characterisation of the STRUBBELIG-RECEPTOR FAMILY of genes encoding putative leucine-rich repeat receptor-like kinases in *Arabidopsis thaliana*. *BMC Plant Biol.* 7, 16. doi: 10.1186/1471-2229-7-16

Fàbregas, N., Lozano-Elena, F., Blasco-Escámez, D., Tohge, T., Martínez-Andújar, C., Albacete, A., et al. (2018). Overexpression of the vascular brassinosteroid receptor BRL3 confers drought resistance without penalizing plant growth. *Nat. Commun.* 9, 4680. doi: 10.1038/s41467-018-06861-3

Feng, Y., Yin, Y., and Fei, S. (2015). Down-regulation of BdBRI1, a putative brassinosteroid receptor gene produces a dwarf phenotype with enhanced drought tolerance in *Brachypodium distachyon*. *Plant Sci.* 234, 163–173. doi: 10.1016/j.plantsci.2015.02.015

Finn, R. D., Clements, J., and Eddy, S. R. (2011). HMMER web server: interactive sequence similarity searching. *Nucleic Acids Res.* 39, W29–W37. doi: 10.1093/nar/gkr367

Franco-Orozco, B., Berepiki, A., Ruiz, O., Gamble, L., Griffe, L. L., Wang, S., et al. (2017). A new proteinaceous pathogen-associated molecular pattern (PAMP) identified in *Ascomycete* fungi induces cell death in *Solanaceae*. *New Phytol.* 214, 1657–1672. doi: 10.1111/nph.14542

Gao, M., Wang, X., Wang, D., Xu, F., Ding, X., Zhang, Z., et al. (2009). Regulation of cell death and innate immunity by two receptor-like kinases in *Arabidopsis*. *Cell Host Microbe* 6, 34–44. doi: 10.1016/j.chom.2009.05.019

Goddard, R., Peraldi, A., Ridout, C., and Nicholson, P. (2014). Enhanced disease resistance caused by BRI1 mutation is conserved between *Brachypodium distachyon* and barley (*Hordeum vulgare*). *Mol. Plant Microbe Interact.* 27, 1095–1106. doi: 10.1094/MPMI-03-14-0069-R

Goodstein, D. M., Shu, S., Howson, R., Neupane, R., Hayes, R. D., Fazo, J., et al. (2012). Phytozome: a comparative platform for green plant genomics. *Nucleic Acids Res.* 40, D1178–D1186. doi: 10.1093/nar/gkr944

Huang, W. R. H., Schol, C., Villanueva, S. L., Heidstra, R., and Joosten, M. (2021). Knocking out SOBIR1 in *Nicotiana benthamiana* abolishes functionality of transgenic receptor-like protein Cf-4. *Plant Physiol.* 185, 290–294. doi: 10.1093/plphys/kiaa047

Isner, J. C., Begum, A., Nuehse, T., Hetherington, A. M., and Maathuis, F. J. M. (2018). KIN7 kinase regulates the vacuolar TPK1 K(+) channel during stomatal closure. *Curr. Biol.* 28, 466–472.e464. doi: 10.1016/j.cub.2017.12.046

Jin, J., Tian, F., Yang, D. C., Meng, Y. Q., Kong, L., Luo, J., et al. (2017). PlantTFDB 4.0: toward a central hub for transcription factors and regulatory interactions in plants. *Nucleic Acids Res.* 45, D1040–d1045. doi: 10.1093/nar/gkw982

Jordá, L., Sopeña-Torres, S., Escudero, V., Nuñez-Corcuera, B., Delgado-Cerezo, M., Torii, K. U., et al. (2016). ERECTA and BAK1 receptor like kinases interact to regulate immune responses in *Arabidopsis*. *Front. Plant Sci.* 7, 897. doi: 10.3389/fpls.2016.00897

Kumar, S., Stecher, G., and Tamura, K. (2016). MEGA7: molecular evolutionary genetics analysis version 7.0 for bigger datasets. *Mol. Biol. Evol.* 33, 1870–1874. doi: 10.1093/molbev/msw054

Lehti-Shiu, M. D., and Shiu, S. H. (2012). Diversity, classification and function of the plant protein kinase superfamily. *Philos. Trans. R. Soc. Lond. B. Biol. Sci.* 367, 2619–2639. doi: 10.1098/rstb.2012.0003

Lehti-Shiu, M. D., Zou, C., Hanada, K., and Shiu, S. H. (2009). Evolutionary history and stress regulation of plant receptor-like kinase/pelle genes. *Plant Physiol.* 150, 12–26. doi: 10.1104/pp.108.134353

Lehti-Shiu, M. D., Zou, C., and Shiu, S.-H. (2012). ""Origin, diversity, expansion history, and functional evolution of the plant receptor-like kinase/pelle family,"," in *Receptor-like Kinases in Plants: From Development to Defense*. Eds. F. Tax and B. Kemmerling (Berlin, Heidelberg: Springer Berlin Heidelberg), 1–22.

Lescot, M., Déhais, P., Thijs, G., Marchal, K., Moreau, Y., Van De Peer, Y., et al. (2002). PlantCARE, a database of plant cis-acting regulatory elements and a portal to tools for in *silico* analysis of promoter sequences. *Nucleic Acids Res.* 30, 325–327. doi: 10.1093/nar/30.1.325

Li, B., Ferreira, M. A., Huang, M., Camargos, L. F., Yu, X., Teixeira, R. M., et al. (2019). The receptor-like kinase NIK1 targets FLS2/BAK1 immune complex and inversely modulates antiviral and antibacterial immunity. *Nat. Commun.* 10, 4996. doi: 10.1038/s41467-019-12847-6

Li, L., Li, M., Yu, L., Zhou, Z., Liang, X., Liu, Z., et al. (2014). The FLS2-associated kinase BIK1 directly phosphorylates the NADPH oxidase RbohD to control plant immunity. *Cell Host Microbe* 15, 329–338. doi: 10.1016/j.chom.2014.02.009

Li, M., Liu, C., Hepworth, S. R., Ma, C., Li, H., Li, J., et al. (2022). SAUR15 interaction with BRI1 activates plasma membrane H+-ATPase to promote organ development of *Arabidopsis*. *Plant Physiol.* 189, 2454–2466. doi: 10.1093/plphys/kiac194

Li, J., and Tax, F. E. (2013). Receptor-like kinases: key regulators of plant development and defense. *J. Integr. Plant Biol.* 55, 1184–1187. doi: 10.1111/jipb.12129

Li, J., Wen, J., Lease, K. A., Doke, J. T., Tax, F. E., and Walker, J. C. (2002). BAK1, an Arabidopsis LRR receptor-like protein kinase, interacts with BRI1 and modulates brassinosteroid signaling. *Cell* 110, 213–222. doi: 10.1016/S0092-8674(02)00812-7

Liebrand, T. W., Van Den Berg, G. C., Zhang, Z., Smit, P., Cordewener, J. H., America, A. H., et al. (2013). Receptor-like kinase SOBIR1/EVR interacts with receptor-like proteins in plant immunity against fungal infection. *Proc. Natl. Acad. Sci. U.S.A.* 110, 10010–10015. doi: 10.1073/pnas.1220015110

Lin, C. W., Huang, L. Y., Huang, C. L., Wang, Y. C., Lai, P. H., Wang, H. V., et al. (2017). Common stress transcriptome analysis reveals functional and genomic architecture differences between early and delayed response genes. *Plant Cell Physiol.* 58, 546–559. doi: 10.1093/pcp/pcx002

Lin, W., Li, B., Lu, D., Chen, S., Zhu, N., He, P., et al. (2014). Tyrosine phosphorylation of protein kinase complex BAK1/BIK1 mediates *Arabidopsis* innate immunity. *Proc. Natl. Acad. Sci. U.S.A.* 111, 3632–3637. doi: 10.1073/pnas.1318817111

Liu, P. L., Du, L., Huang, Y., Gao, S. M., and Yu, M. (2017). Origin and diversification of leucine-rich repeat receptor-like protein kinase (LRR-RLK) genes in plants. *BMC Evol. Biol.* 17, 47. doi: 10.1186/s12862-017-0891-5

Liu, Y., Huang, X., Li, M., He, P., and Zhang, Y. (2016). Loss-of-function of Arabidopsis receptor-like kinase BIR1 activates cell death and defense responses mediated by BAK1 and SOBIR1. *New Phytol.* 212, 637–645. doi: 10.1111/nph.14072

Lu, D., Wu, S., Gao, X., Zhang, Y., Shan, L., and He, P. (2010). A receptor-like cytoplasmic kinase, BIK1, associates with a flagellin receptor complex to initiate plant innate immunity. *Proc. Natl. Acad. Sci. U.S.A.* 107, 496–501. doi: 10.1073/pnas.0909705107

Ma, X., Xu, G., He, P., and Shan, L. (2016). SERKing coreceptors for receptors. *Trends Plant Sci.* 21, 1017–1033. doi: 10.1016/j.tplants.2016.08.014

Miao, H., Wang, L., Qu, L., Liu, H., Sun, Y., Le, M., et al. (2023). Genomic evolution and insights into agronomic trait innovations of *Sesamum* Species. *Plant Commun.* 5, 100729. doi: 10.1016/j.xplc.2023.100729

Mishra, D., Suri, G. S., Kaur, G., and Tiwari, M. (2021). Comprehensive analysis of structural, functional, and evolutionary dynamics of Leucine Rich Repeats-RLKs in *Thinopyrum elongatum*. *Int. J. Biol. Macromol.* 183, 513–527. doi: 10.1016/j.ijbiomac.2021.04.137

Mosher, S., Seybold, H., Rodriguez, P., Stahl, M., Davies, K. A., Dayaratne, S., et al. (2013). The tyrosine-sulfated peptide receptors PSKR1 and PSY1R modify the immunity of Arabidopsis to biotrophic and necrotrophic pathogens in an antagonistic manner. *Plant J.* 73, 469–482. doi: 10.1111/tpj.12050

Nam, K. H., and Li, J. (2002). BRI1/BAK1, a receptor kinase pair mediating brassinosteroid signaling. *Cell* 110, 203–212. doi: 10.1016/S0092-8674(02)00814-0

Peng, H. C., and Kaloshian, I. (2014). The tomato leucine-rich repeat receptor-like kinases SlSERK3A and SlSERK3B have overlapping functions in bacterial and nematode innate immunity. *PloS One* 9, e93302. doi: 10.1371/journal.pone.0093302

Pertea, M., Kim, D., Pertea, G. M., Leek, J. T., and Salzberg, S. L. (2016). Transcript-level expression analysis of RNA-seq experiments with HISAT, StringTie and Ballgown. *Nat. Protoc.* 11, 1650–1667. doi: 10.1038/nprot.2016.095

Pertea, M., Pertea, G. M., Antonescu, C. M., Chang, T. C., Mendell, J. T., and Salzberg, S. L. (2015). StringTie enables improved reconstruction of a transcriptome from RNA-seq reads. *Nat. Biotechnol.* 33, 290–295. doi: 10.1038/nbt.3122

Platre, M. P., Satbhai, S. B., Brent, L., Gleason, M. F., Cao, M., Grison, M., et al. (2022). The receptor kinase SRF3 coordinates iron-level and flagellin dependent defense and growth responses in plants. *Nat. Commun.* 13, 4445. doi: 10.1038/s41467-022-32167-6

Robinson, M. D., and Oshlack, A. (2010). A scaling normalization method for differential expression analysis of RNA-seq data. *Genome Biol.* 11, R25. doi: 10.1186/gb-2010-11-3-r25

Roux, M., Schwessinger, B., Albrecht, C., Chinchilla, D., Jones, A., Holton, N., et al. (2011). The Arabidopsis leucine-rich repeat receptor-like kinases BAK1/SERK3 and BKK1/SERK4 are required for innate immunity to hemibiotrophic and biotrophic pathogens. *Plant Cell* 23, 2440–2455. doi: 10.1105/tpc.111.084301

Shang, Y., Dai, C., Lee, M. M., Kwak, J. M., and Nam, K. H. (2016). BRI1-associated receptor kinase 1 regulates guard cell ABA signaling mediated by open stomata 1 in *Arabidopsis*. *Mol. Plant* 9, 447–460. doi: 10.1016/j.molp.2015.12.014

Shiu, S. H., and Bleecker, A. B. (2001). Receptor-like kinases from Arabidopsis form a monophyletic gene family related to animal receptor kinases. *Proc. Natl. Acad. Sci. U.S.A.* 98, 10763–10768. doi: 10.1073/pnas.181141598

Shiu, S. H., Karlowski, W. M., Pan, R., Tzeng, Y. H., Mayer, K. F., and Li, W. H. (2004). Comparative analysis of the receptor-like kinase family in *Arabidopsis* and rice. *Plant Cell* 16, 1220–1234. doi: 10.1105/tpc.020834

Shumayla,, Sharma, S., Kumar, R., Mendu, V., Singh, K., and Upadhyay, S. K. (2016). Genomic dissection and expression profiling revealed functional divergence in *Triticum aestivum* leucine rich repeat receptor like kinases (TaLRRKs). *Front. Plant Sci.* 7, 1374. doi: 10.3389/fpls.2016.01374

Singh, A., Breja, P., Khurana, J. P., and Khurana, P. (2016). Wheat brassinosteroid-insensitive1 (TaBRI1) interacts with members of *TaSERK* gene family and cause early flowering and seed yield enhancement in *Arabidopsis*. *PloS One* 11, e0153273. doi: 10.1371/journal.pone.0153273

Soltabayeva, A., Dauletova, N., Serik, S., Sandybek, M., Omondi, J. O., Kurmanbayeva, A., et al. (2022). Receptor-like kinases (LRR-RLKs) in response of plants to biotic and abiotic stresses. *Plants (Basel)* 11, 2660. doi: 10.3390/plants11192660

Song, W., Wang, B., Li, X., Wei, J., Chen, L., Zhang, D., et al. (2015). Identification of immune related LRR-containing genes in maize (*Zea mays* L.) by genome-wide sequence analysis. *Int. J. Genomics* 2015, 231358. doi: 10.1155/2015/231358

Sun, X., and Wang, G. L. (2011). Genome-wide identification, characterization and phylogenetic analysis of the rice LRR-kinases. *PloS One* 6, e16079. doi: 10.1371/journal.pone.0016079

Sun, R., Wang, S., Ma, D., and Liu, C. (2018). Genome-wide analysis of *LRR-RLK* gene family in four *Gossypium* species and expression analysis during cotton development and stress responses. *Genes (Basel)* 9, 592. doi: 10.3390/genes9120592

Trenker, R., and Jura, N. (2020). Receptor tyrosine kinase activation: From the ligand perspective. *Curr. Opin. Cell Biol.* 63, 174–185. doi: 10.1016/j.ceb.2020.01.016

Tunc-Ozdemir, M., and Jones, A. M. (2017). BRL3 and AtRGS1 cooperate to fine tune growth inhibition and ROS activation. *PloS One* 12, e0177400. doi: 10.1371/journal.pone.0177400

Wang, X., Li, X., Meisenhelder, J., Hunter, T., Yoshida, S., Asami, T., et al. (2005). Autoregulation and homodimerization are involved in the activation of the plant steroid receptor BRI1. *Dev. Cell* 8, 855–865. doi: 10.1016/j.devcel.2005.05.001

Wang, Z., Meng, P., Zhang, X., Ren, D., and Yang, S. (2011). BON1 interacts with the protein kinases BIR1 and BAK1 in modulation of temperature-dependent plant growth and cell death in *Arabidopsis*. *Plant J.* 67, 1081–1093. doi: 10.1111/j.1365-313X.2011.04659.x

Wang, Z. Y., Seto, H., Fujioka, S., Yoshida, S., and Chory, J. (2001). BRI1 is a critical component of a plasma-membrane receptor for plant steroids. *Nature* 410, 380–383. doi: 10.1038/35066597

Wang, Y., Tang, H., Debarry, J. D., Tan, X., Li, J., Wang, X., et al. (2012). MCScanX: a toolkit for detection and evolutionary analysis of gene synteny and collinearity. *Nucleic Acids Res.* 40, e49. doi: 10.1093/nar/gkr1293

Wang, Y., Yan, X., Xu, M., Qi, W., Shi, C., Li, X., et al. (2022). TMK1-mediated auxin signal regulates membrane-associated clathrin in *Arabidopsis* roots. *J. Integr. Plant Biol.* 65, 82–99. doi: 10.1111/jipb.13366

Xu, K., Jourquin, J., Njo, M. F., Nguyen, L., Beeckman, T., and Fernandez, A. I. (2021). The phloem intercalated with xylem-correlated 3 receptor-like kinase constitutively interacts with brassinosteroid insensitive 1-associated receptor kinase 1 and is involved in vascular development in *Arabidopsis*. *Front. Plant Sci.* 12, 706633. doi: 10.3389/fpls.2021.706633

Yan, W., Ni, Y., Liu, X., Zhao, H., Chen, Y., Jia, M., et al. (2021). The mechanism of sesame resistance against *Macrophomina phaseolina* was revealed *via* a comparison of transcriptomes of resistant and susceptible sesame genotypes. *BMC Plant Biol.* 21, 159. doi: 10.1186/s12870-021-02927-5

Yang, W., Zhang, B., Qi, G., Shang, L., Liu, H., Ding, X., et al. (2019). Identification of the phytosulfokine receptor 1 (OsPSKR1) confers resistance to bacterial leaf streak in rice. *Planta* 250, 1603–1612. doi: 10.1007/s00425-019-03238-8

Zhang, H., Miao, H., Wang, L., Qu, L., Liu, H., Wang, Q., et al. (2013). Genome sequencing of the important oilseed crop *Sesamum indicum* L. *Genome Biol.* 14, 401. doi: 10.1186/gb-2013-14-1-401

Zhang, Y. P., Zhang, Y. Y., Thakur, K., Zhang, F., Hu, F., Zhang, J. G., et al. (2021). Integration of miRNAs, degradome, and transcriptome omics uncovers a complex regulatory network and provides insights into lipid and fatty acid synthesis during sesame seed development. *Front. Plant Sci.* 12, 709197. doi: 10.3389/fpls.2021.709197

Zhou, F., Guo, Y., and Qiu, L. J. (2016). Genome-wide identification and evolutionary analysis of leucine-rich repeat receptor-like protein kinase genes in soybean. *BMC Plant Biol.* 16, 58. doi: 10.1186/s12870-016-0744-1

Zhou, Y., Sun, L., Wassan, G. M., He, X., Shaban, M., Zhang, L., et al. (2019). GbSOBIR1 confers *Verticillium* wilt resistance by phosphorylating the transcriptional factor GbbHLH171 in *Gossypium barbadense*. *Plant Biotechnol. J.* 17, 152–163. doi: 10.1111/pbi.12954

Zhu, Y., Wang, Y., Li, R., Song, X., Wang, Q., Huang, S., et al. (2010). Analysis of interactions among the CLAVATA3 receptors reveals a direct interaction between CLAVATA2 and CORYNE in *Arabidopsis*. *Plant J.* 61, 223–233. doi: 10.1111/j.1365-313X.2009.04049.x

frontiers | Frontiers in Plant Science

TYPE Original Research
PUBLISHED 09 April 2024
DOI 10.3389/fpls.2024.1392637

OPEN ACCESS

EDITED BY
Choong-Min Ryu,
Korea Research Institute of Bioscience and Biotechnology (KRIBB), Republic of Korea

REVIEWED BY
Travis Robert Glare,
Lincoln University, New Zealand
Mohammad Sayyar Khan,
University of Agriculture, Peshawar, Pakistan

*CORRESPONDENCE
Yordan J. Romero-Contreras
jhroco@ccg.unam.mx
Mario Serrano
serrano@ccg.unam.mx

RECEIVED 27 February 2024
ACCEPTED 25 March 2024
PUBLISHED 09 April 2024

CITATION
Romero-Contreras YJ, Gonzalez-Serrano F, Formey D, Aragón W, Chacón FI, Torres M, Cevallos MÁ, Dib JR, Rebollar EA and Serrano M (2024) Amphibian skin bacteria display antifungal activity and induce plant defense mechanisms against *Botrytis cinerea*. *Front. Plant Sci.* 15:1392637.
doi: 10.3389/fpls.2024.1392637

Amphibian skin bacteria display antifungal activity and induce plant defense mechanisms against *Botrytis cinerea*

Yordan J. Romero-Contreras[1,2*], Francisco Gonzalez-Serrano[1,2], Damien Formey[1], Wendy Aragón[3], Florencia Isabel Chacón[4], Martha Torres[1], Miguel Ángel Cevallos[1], Julian Rafael Dib[4,5], Eria A. Rebollar[1] and Mario Serrano[1*]

[1]Centro de Ciencias Genómicas, Universidad Nacional Autónoma de México, Cuernavaca, Morelos, Mexico, [2]Programa de Doctorado en Ciencias Biomédicas, Centro de Ciencias Genómicas, Universidad Nacional Autónoma de México, Cuernavaca, Mexico, [3]Instituto de Biociencias, Universidad Autónoma de Chiapas, Tapachula, Chiapas, Mexico, [4]Planta Piloto de Procesos Industriales Microbiológicos (PROIM) - Consejo Nacional de Investigaciones Científicas y Técnicas (CONICET), Tucumán, Argentina, [5]Instituto de Microbiología, Universidad Nacional de Tucumán, Tucumán, Argentina

Botrytis cinerea is the causal agent of gray mold, which affects a wide variety of plant species. Chemical agents have been used to prevent the disease caused by this pathogenic fungus. However, their toxicity and reduced efficacy have encouraged the development of new biological control alternatives. Recent studies have shown that bacteria isolated from amphibian skin display antifungal activity against plant pathogens. However, the mechanisms by which these bacteria act to reduce the effects of *B. cinerea* are still unclear. From a diverse collection of amphibian skin bacteria, three proved effective in inhibiting the development of *B. cinerea* under *in vitro* conditions. Additionally, the individual application of each bacterium on the model plant *Arabidopsis thaliana, Solanum lycopersicum* and post-harvest blueberries significantly reduced the disease caused by *B. cinerea*. To understand the effect of bacteria on the host plant, we analyzed the transcriptomic profile of *A. thaliana* in the presence of the bacterium C32I and the fungus *B. cinerea*, revealing transcriptional regulation of defense-related hormonal pathways. Our study shows that bacteria from the amphibian skin can counteract the activity of *B. cinerea* by regulating the plant transcriptional responses.

KEYWORDS

frog skin microbiota, biological control, Botrytis cinerea, Arabidopsis thaliana, blueberries

Introduction

Botrytis cinerea is a necrotrophic fungal pathogen that causes gray mold disease, a devastating infection affecting a wide variety of economically important crops such as tomato, cucumber, pepper and strawberry (Dik & Wubben, 2007; Petrasch et al., 2019). Due to its broad distribution and ability to infect more than 250 plant species, it is considered the second most important agricultural pathogen (Haidar et al., 2016; Hua et al., 2018). This pathogen is characterized by its broad infectivity, causing damage to various tissues such as leaves, stems, flowers and fruits, particularly during the harvest, post-harvest and storage periods, resulting in significant losses in terms of quality and quantity of product (Roca-Couso et al., 2021; Bi et al., 2023). For decades, synthetic fungicides have been used to combat this pathogen, but their use has been restricted due to the adverse effects on the environment and human health and fungicide resistance acquired by several *B. cinerea* strains (Abbey et al., 2019; Fedele et al., 2020). In this context, there has been a growing interest in the development of new, more sustainable, ecological and environmentally safe alternatives for the control of this phytopathogenic fungus (Aladdin et al., 2018; Chacón et al., 2022).

Plants have developed several molecular strategies to counteract the effect of bacterial and fungal pathogens. Pathogen-Associated Molecular Patterns [PAMPs], such as chitin, are recognized by Plant Pattern-Recognition Receptors [PPRs], which activate plant immune signaling as a first line of defense. However, when the fungus crosses this barrier, the plant can counteract the effect of the pathogen through the activation of secondary responses, which involve the activation of hormones such as salicylic acid [SA], jasmonic acid [JA] and ethylene [ET], acting as key regulators of the defense against pathogens, such as *B. cinerea* (Mengiste et al., 2010; AbuQamar et al., 2017; El-Saadony et al., 2022). Finally, the induction of defense activation known as Systemic Acquired Resistance [SAR] and Induced Systemic Resistance [ISR] occurs (Choudhary et al., 2007). Despite these plant defense responses, *B. cinerea* can still infect a large number of crops, pointing out the suggesting the importance of identifying new ecofrendly alternatives. Plant disease biological control agents or BCAs refers to microorganisms, such as bacteria, fungi, and viruses [and/or their products], that suppress infections caused by a pathogen, through antagonism or induction of disease resistance, such as SAR and ISR (Babbal et al., 2017; O'Brien, 2017; Díaz et al., 2020; Pereyra et al., 2020). Besides preventing plant diseases, many BCAs also can promote plant growth, improve tolerance to abiotic stress and enhance nutrient acquisition (Babbal et al., 2017; El-Saadony et al., 2022).

Currently, it has been reported that many bacterial species can activate protective systems against plant pathogenic fungi (Aladdin et al., 2018). For example, *Bacillus* spp (Balthazar et al., 2022; Chacón et al., 2022), *Streptomyces* spp (Boukaew et al., 2017), *Pseudomonas* spp (Trotel-Aziz et al., 2008), *Acinetobacter* spp. (Zhang et al., 2019) and other bacteria are BCAs that help combat infections by *B. cinerea*. However, although some of these microorganisms are already used in the field, some concerns arise about their use, particularly due to the possible development of resistance to them by the pathogenic fungi (Di Francesco et al., 2018; Carmona-Hernandez et al., 2019). Moreover, there is still lack of information on the effect of BCAs on plant metabolism at the transcriptomic level (Ferreira-Saab et al., 2018). Recently, it was discovered that the use of amphibian skin bacteria have the potential to inhibit *Colletotrichum orbiculare*, the fungus causal of cucumber anthracnose (Susilawati et al., 2021). Additionally, we have recently described that bacteria isolated from neotropical frogs, belonging to the genus *Acinetobacter*, were able to inhibit the growth and development of *B. cinerea* (Cevallos et al., 2022).

In this work we investigate the mechanism used by three bacteria [C23F, C26G, and C32I], isolated from the frog *Craugastor fitzinger* to inhibit growth and development of *B. cinerea* and their involvement in the induction of the plant defense systems (Rebollar et al., 2016; Cevallos et al., 2022). We also determined that exogenous application of these bacteria and their filtrates protects the plants *Arabidopsis thaliana*, *Solanum lycopersicum* and blueberry fruits [*Vaccinium corymbosum*] against *B. cinerea* infection. Additionally, to understand the effect of the bacteria [*Acinetobacter* sp. C32I] we studied the transcriptional changes induced in *A. thaliana* and observed modifications in the expression levels of genes involved in plant defense. Based on these findings, we propose that the bacteria from amphibian skin have the potential to serve as promising biological control agents against plant pathogens.

Materials and methods

Antifungal activity assay for the selected bacteria against *B. cinerea*

Bacteria were previously identified by Rebollar et al. (2019). The bacteria C26G and C32I were recently described as new species of the *Acinetobacter* genus (Cevallos et al., 2022), while C23F was identified at the family level as *Enterobacteraceae* through 16S rRNA sequencing (Rebollar et al., 2018). All bacteria isolates were initially screened for their antifungal activity against the pathogen *B. cinerea* by the direct confrontation assay. For this, each bacteria was cultured on Luria-Bertani medium [LB] at 30°C for 24 h until an optical density of 0.6 [$O.D_{600nm}$]. The spore suspension of *B. cinerea* strain B05.10 [provided by Brigitte Mauch-Mani] was prepared as previously described (L'haridon et al., 2011). Dishes with potato dextrose agar [PDA, Sigma-Aldrich], were inoculated with 10 µl of each bacterial suspension at one end of the plate and 6 µl of the spore suspension of *B. cinerea* at the other end and incubated in the dark at 24°C for 7 days. The test was done in triplicate [n=3]. The fungal growth inhibition was evaluated by measuring the area of mycelium growth with ImageJ2 software [version 2].

Effect of bacterial filtrates on *B. cinerea* growth

Bacteria were cultivated in LB liquid medium, at 30 °C in the dark until an optical density of 0.6 [$O.D_{600nm}$]. Each bacterial liquid culture was centrifuged at 12,500 rpm for 15 min and the supernatant was filtered through a 0.22 µm Millipore membrane. For the inhibitory assay, Petri dishes [60 mm] containing PDA were supplemented with

50, 60, 70 and 80% [v/v] of bacterial filtrates [BFs]. As a control, dishes with PDA were supplemented with LB medium. A 5 mm sterile filter paper disk with 6 µl of suspension of *B. cinerea* [5×10^4 spores ml^{-1}] spores was placed at the center of the dish and incubated at 24°C for 7 days in the dark. The test was done in triplicate [n=3]. Inhibition was evaluated by measuring the diameter of the mycelium on the dish. Images of growing *B. cinerea* mycelium were analyzed using the ImageJ2 analysis software [version 2].

Effect of bacteria filtrates on the germination of *B. cinerea* spores

Three drops of a spore suspension of the fungus [5×10^4 spores ml^{-1}], including each bacteria filtrate at 80%, were placed on slides in a growth chamber at 24°C with >95% relative humidity for 24 h. Subsequently, the germinated spores were quantified in a Neubauer chamber. Staining of spores was performed (Romero-Contreras et al., 2019), and were observed under fluorescence microscope [Zeiss Axioskop 2, 40x].

Effect of bacterial volatile organic compounds [VOCs] over *B. cinerea* growth

To detect the inhibitory activity of bacterial volatile organic compounds [VOCs], 20 µl of a cell suspension of C23F, C26G, and C32I bacteria [0.6 $O.D_{600nm}$] was inoculated in the center of LB plates. Simultaneously, a suspension of *B. cinerea* spores [5×10^4 spores ml^{-1}) was inoculated on PDA medium plates. Subsequently, the bottom of each plate [fungus and bacteria] were placed face to face and immediately sealed with parafilm. The plates were then incubated at 26°C for 7 days, together with a control, which consisted of PDA plates inoculated with the pathogen and uninoculated LB plates. The experiment was conducted in duplicate [n=2]. Inhibition was assessed by measuring the diameter of the mycelium on the plates. The growth halo of *B. cinerea* was measured using the ImageJ2 software [version 2].

Pathogen infection assays on *Arabidopsis thaliana*

Seeds of the ecotype Columbia-0 [Col-0, Nottingham Arabidopsis Stock Centre, Nottingham, UK] as wild type and the mutants of *eds5-1* (Nawrath and Métraux, 1999), *jar1* (Chassot et al., 2007) and *ein3* (Roman et al., 1995), were germinated on 0.2X Murashige-Skoog [MS] medium supplemented with sucrose [0.5% w/v], and 1% [w/v] agar (Murashige and Skoog, 1962) for 7 days. The plants were then transplanted into germination trays containing a mixture of soil and vermiculite [3:1] and kept in a greenhouse at 22 ± 2°C and 60% humidity with 16 h/8 h light/dark cycles for one month with constant irrigation of non-sterile water. Then, 1 ml of each bacterial cell suspensions or bacterial filtrates was added [adjusted to 0.6 $O.D_{600}$] every five days for four weeks. For the pathogenicity assay, leaves of water-treated control or treated *A. thaliana* were infected with 6 µL of a suspension of *B. cinerea* spores [5×10^4 spores ml^{-1}]. The inoculated plants were covered with plastic lids to maintain >95% relative humidity and transferred to a growth chamber at 22 ± 2°C and a 24 h dark cycle. After 72 hours post-infection [hpi], symptoms were evaluated. To determine the percentage of plant survival, we quantified the number of infected plants [disease incidence]. The lesion sizes were quantified using the ImageJ2 software [version 2]. The experiment was performed with a randomized design with 45 plants [three leaves per plant] per treatment.

RNA extraction and transcriptomic analysis of *A. thaliana leaves*

Arabidopsis thaliana Col-0 plants were root-inoculated with *Acinetobacter* sp. *C32I* and foliar infected with the *B. cinerea* B05.10. After 6 hours post-infection [hpi], ten leaves per plant were collected and preserved in liquid nitrogen. Conditions were set for both dual and tripartite interactions of the plant with each microorganism. Total RNA extraction was performed from two independent experiments using Trizol, following the supplier instructions [Invitrogen]. RNA concentration and purity were measured with a NanoDrop spectrophotometer [Implen NP80, Thermo Fisher Scientific, USA]. Afterwards, 1 µg of total RNA was treated with DNAse [Thermo Scientific™, USA] to remove the genomic DNA, according to manufacturer of instructions. Library construction and sequencing were carried out by the Beijing Genomics Institute [BGI] Americas 2 using DNBSeq TM technology. The sequences are publicly available in the NCBI with number project PRJNA986187 and PRJNA1044848. To identify differentially expressed genes [DEGs], DESeq2 software in the Integrated Differential Expression Analysis MultiEXperiment [IDEAMEX] was used, with a FoldChange ≥ 2 or ≤ -2, and an adjusted p-value ≤ 0.05 (Jiménez-Jacinto et al., 2019). The DEG analysis was grouped through Gene Ontology [GO] analysis using PANTHER [v17.0]. GO term enrichment for the plant analysis was performed using the TAIR web tool [The Arabidopsis Information Resource [TAIR], https://www.arabidopsis.org/tools/go_term_enrichment.jsp, on www.arabidopsis.org, Feb 24, 2022], analyzed with the Fisher test and FDR correction. Non-redundant enriched terms were obtained by using REVIGO software (Supek et al., 2011). The graphs were created using the ggplot2 library with RStudio and heatmap libraries [v4.2.1].

qRT-PCR analysis

To analyze the expression of genes, a third independent biological replica was performed. Leaves from root-inoculated plants with *Acinetobacter* sp. C32I and foliar infected with the *B. cinerea* B05.10 were collected. RNA isolation using TRI Reagent® [Sigma-Aldrich, United States], were performed following the instructions of the manufacturer. RNA integrity was evaluated by using denaturing gel electrophoresis and measured using NanoDrop spectrophotometer [Implen NP80, Thermo Fisher Scientific, USA]. Afterwards, 1 µg of total RNA was treated with DNase I [Thermo

Fisher Scientific, Inc., Waltham, MA, USA]. For cDNA synthesis, we used 1 µg of the total RNA, and then processed with a RevertAid H Minus RevertAid First Strand cDNA Synthesis kit [Thermo Fisher Scientific, Inc., Waltham, MA, USA], according to manufacturer's instructions. Primers for the RT-qPCR gene expression analysis were: *AOS* [S_5'-ATCCAAAGATCTCCCGATCC-3', AS_5'-GTGGATTCTCGGCGATAAAA-3'], *ACS6* [S_5'-TGGTTGGTTAAAGGCCAAAG-3', AS_5'-TGGTCCATATTCGCAAAACA-3'], *PR1* [S_5'-TTCTTCCCTCGAAAGCTCAA-3', AS_5'-AAGGCCCACCAGAGTGTATG-3'] *and ZAT12* [S_5'-ATCAAGTCGACGGTGGATGT-3', AS_5'-ACAAAGCGTCGTTGTTAGGC-3']. To normalized transcript abundance two housekeeping genes were used. *ACTIN* [S_5'-TGCTTTGCCACATGCTATCC-3', AS_5'-GACTTCAGGGCATCGGAAAC-3'] and *CF150* [S_5'-CCGACAAGGAGAAGCTTAACAAGTT-3', AS_5'-CGGCAGATTTGGATGGACCAGCAAG-3']. The conditions of the reactions were performed according to Aragón et al. (2021).

In vivo biocontrol assay with blueberry fruits

For *in vivo* infection assays, blueberries at commercial maturity were harvested from organic fields that had not received any preharvest treatment with synthetic pesticides. Subsequently, the fruits were disinfected with a 2% NaClO solution for 2 minutes, followed by washing with tap water, and then left to dry at room temperature. Bacterial cultures [C23F, C26G, and C32I] were grown to a density of 0.6 [$O.D_{600nm}$]; subsequently, centrifuged at 12,500 rpm for 15 min. The supernatants were recovered and transferred through a 0.22 µm Millipore filter to obtain the bacterial filtrates [BF], which were then resuspended in physiological solution [NaCl 9 g/L], to achieve a concentration of 80% [v/v]. The cell pellets were dissolved in 3 ml of physiological solution. Blueberries were punctured to induce a lesion and were then independently sprayed with 3 ml of the bacterial solution and the BF. Subsequently, they were incubated at 25 ± 1°C and 95% relative humidity for 24 h. Three independent biological replicates, each one with 10 blueberries, were used for each treatment. Physiological solution served as the control. Following bacterial inoculation, blueberries were sprayed with a solution of *B. cinerea* ISIB-MMA/F-Bc01-S spores [$1x10^6$ conidia/mL] and kept at 25 ± 1°C for 7 dpi. Infection was assessed by counting healthy and infected fruits (Chacón et al., 2022).

Bacterial inoculations of *Solanum lycopersicum* plants

Solanum lycopersicum L. seeds were washed with a 3% solution of sodium hypochlorite [3 times] and absolute ethanol [1 time]. The seeds were germinated in hydrated vermiculite. After 7 days of growth, they were transferred to pots with a mixture of soil and vermiculite [3:1] and maintained in a greenhouse at 22 ± 2°C with 60% relative humidity under a 16 h/8 h light/dark cycle. Over five weeks, inoculations of the soil every three days were done with C32F, C26G, and C32I bacteria, grown in 0.2x MS liquid medium. Leaves were collected from plants pretreated with each of the bacteria and then infected with *B. cinerea* spores [5×10^4 spores ml^{-1}]. The plants were maintained under >95% relative humidity at 24°C for three days in a plant growth chamber with a 16 h/8 h light/dark cycle. Lesion evaluation was conducted with ImageJ2 software [version 2]. Three biological replicates were performed, each with 10 leaves per treatment.

Statistical analysis

The data obtained from each test are presented in the figures as mean values [± SEM]. Statistical analyses were conducted using a One-way ANOVA followed by Tukey *post-hoc* test [$p < 0.05$] to identify significant differences for each experiment. The graphs were generated using R [https://posit.co/]. These analyses were based on results from three independent experiments.

Results

Antifungal activity of amphibian skin bacteria against *B. cinerea*

Previously, we had demonstrated the inhibitory activity of bacteria isolated from amphibian skin against *B. cinerea* (Cevallos et al., 2022). Based on these results, two more promising strains belonging to the genus *Acinetobacter* C26G and C32I were selected, and the reproducibility and consistency of their antagonistic behavior was corroborated. In addition, a third bacterium, C23F, previously classified at the *Enterobacteraceae* family level, was included (Rebollar et al., 2018). The results revealed that all three bacteria exerted an antagonistic effect on the growth of *B. cinerea* (Figure 1A). In particular, the measurement of mycelial growth of the fungus showed that the three bacteria were able to significantly inhibit the growth of *B. cinerea*, compared to the uninoculated control, where the fungus invaded the entire plate (Figure 1B). These results indicated that bacteria from frog skin inhibited *B. cinerea* growth under *in vitro* assays.

The compounds released by frog skin bacteria inhibited the growth of *B. cinerea*

Several BCAs have been shown to have the ability to secrete various compounds with antifungal activity that contribute to counteract the effect of pathogenic fungi (Ferreira-Saab et al., 2018). To investigate whether C23F, C26G, and C32I bacteria secrete compounds that interfere in the germination and growth process of *B. cinerea*, we confronted the bacterial filtrates [BF] with the pathogen. Our results revealed that the BF of each bacteria inhibited the growth of *B. cinerea* in a dose-dependent manner (Figure 2A). We observed that when the pathogen was grown on PDA medium supplemented with 50% and 60% BF, approximately 10% inhibition occurred for the three bacterial strains. However, at concentrations of 70 and 80% BF, a direct correlation in the inhibition of *B. cinerea* growth was observed (Figure 2A). To determine the effect of BFs on spore germination, we co-cultured a suspension of *B. cinerea* spores, along with 80% of BFs

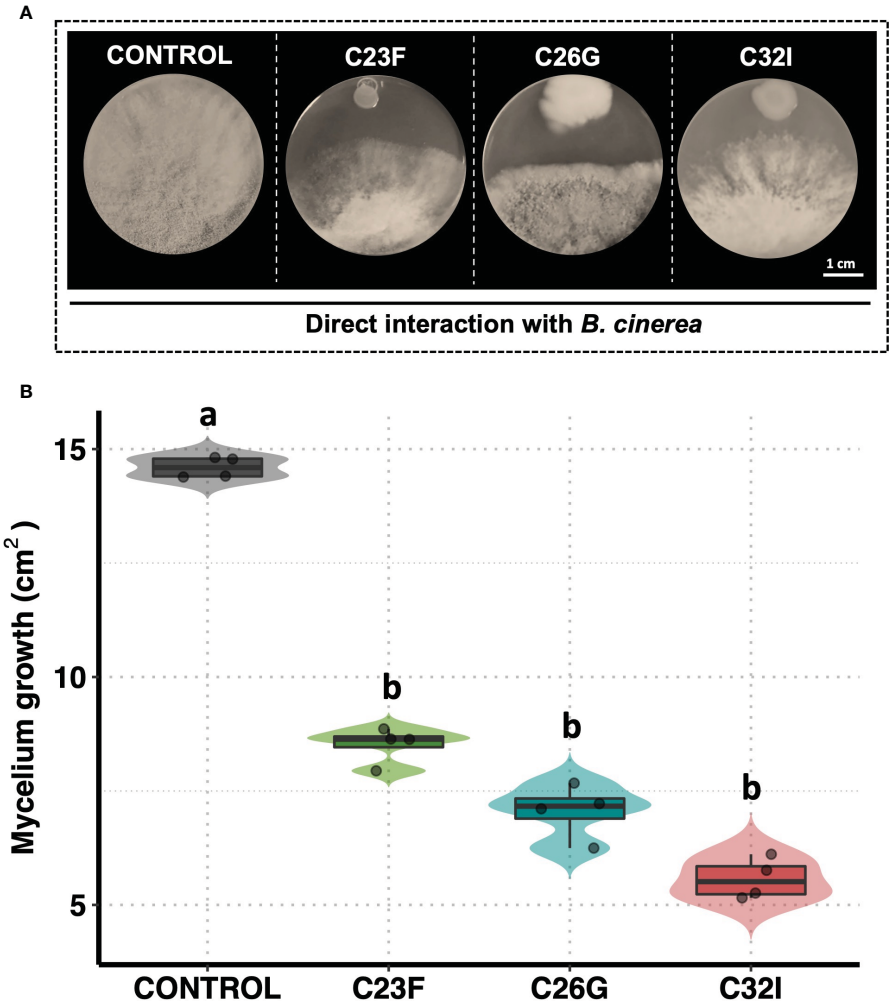

FIGURE 1
The C23F, C26G, and C32I bacterial inhibit the *B cinerea* growth in direct confrontation. The bacterial were inoculated in PDA medium with *B. cinerea* spore suspension [5x10^4 spores ml^{-1}] and incubated at 24°C for 72 (h) **(A)** Representative pictures of the inhibitory assay are included as a visual illustration. **(B)** The growth was evaluated by measuring the diameter of the mycelium on the dish compared with the control. Data represent the mean [± SD] of three independent experiments, each performed in duplicate, and presented relative to control. Letters indicate a statistically significant difference, according to one-way analysis of variance [ANOVA] [$p \leq 0.05$] followed the Tukey test.

for 24 h (Figure 2B). The data showed that strain C23F influenced the germination rate of spores of 8.5%, followed by C26G and C32I with 11.33% and 13.76%, respectively, compared to the unfiltered control, where 100% germination was observed (Figure 2C). Our results indicate that BFs significantly inhibits the development and growth of *B. cinerea*, which highlights their potential use as BCAs.

VOCs produced by bacteria can inhibit *B. cinerea* growth

To test the antagonistic activity of volatile organic compounds [VOCs] in inhibiting *B. cinerea*, a double-sided assay was performed. The data revealed an inhibitory effect of the VOCs produced by two frog-associated bacteria [C23F and C32I] on the growth of the pathogenic fungus, in contrast to the control without bacteria, where mycelial growth was observed throughout the entire surface of the plate (Figure 3A). A quantification of the growth area demonstrated that the bacteria C26G had the least inhibitory effect against *B. cinerea*, exhibiting similar growth as the untreated control and covering a total area of approximately 15 cm². In contrast, VOCs from bacteria C23F and C32I displayed inhibitory effects on the fungus, resulting in growth areas of 6.58 cm² and 3.17 cm², respectively (Figure 3B). Interestingly, our findings revealed that, in addition to the release of diffusible organic compounds, volatile organic compounds are also produced, which might play a role in restraining *B. cinerea*.

Frog skin microbiota contributed to the defense system in the plant against *B. cinerea*

Several biocontrol agents induce plant defense systems, which confer a protection system against pathogenic fungi (Wang et al., 2021). To analyze the effect of bacteria C23F, C26 and C32I directly on the plant, we inoculated the soil, in which *A. thaliana* plants were

10.3389/fpls.2024.1392637

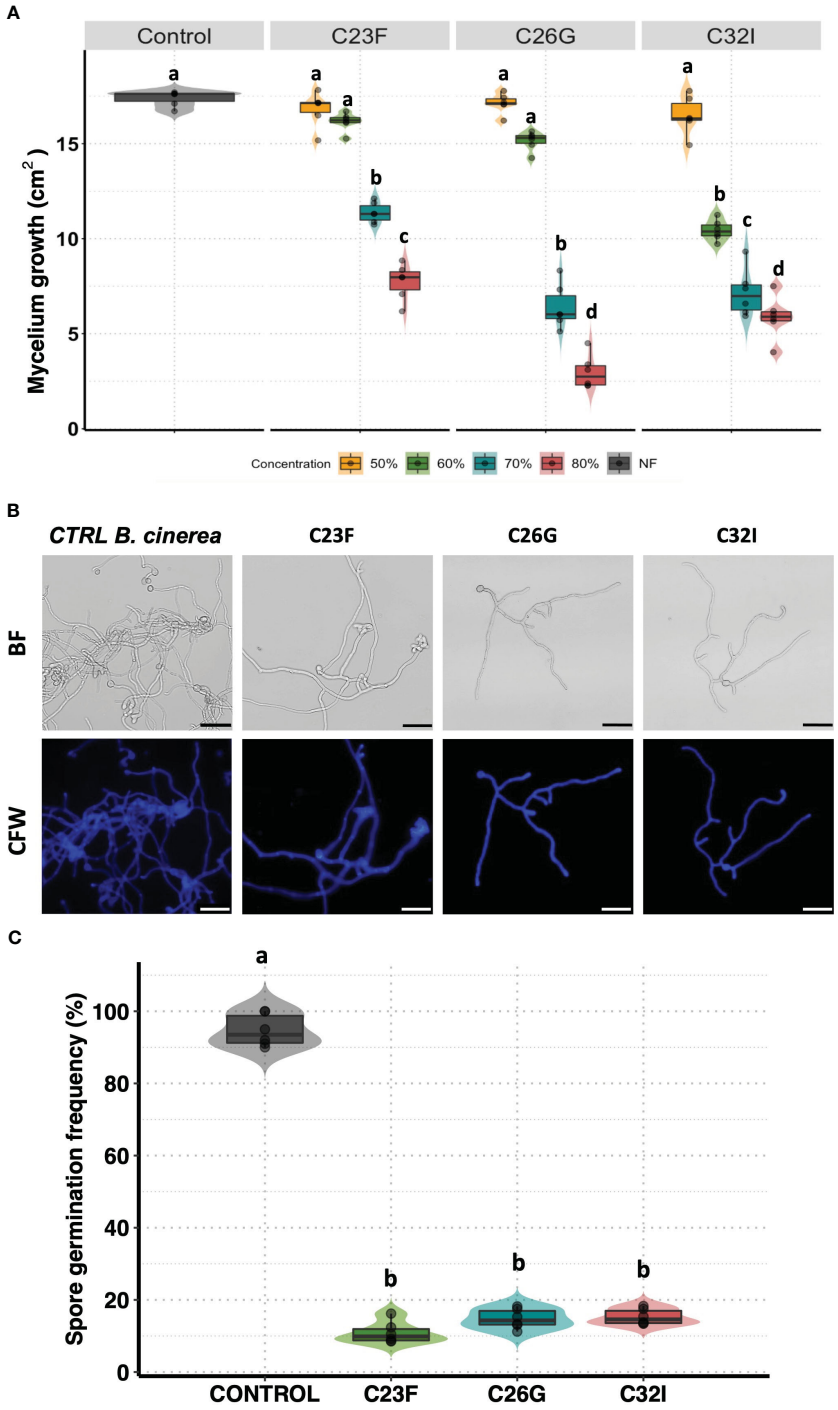

FIGURE 2
The filtrates of frog skin microbiota inhibit the growth *B cinerea*. Spore suspension of *B cinerea* [5 × 10^4 spores ml^{-1}] was placed on the center of the Petri dish containing PDA supplemented with different concentrations of BFs and incubated at 24°C to 72 (h) **(A)** The inhibition was measured calculated the area growth of *B cinerea* represented in percentage. The germination was observed co-cultured the *B. cinerea* spores with PDA supplemented with 80% BFs in the dark at 24°C for 24 (h) **(B)** The pictures represented the effect BFs in the germination de *B. cinerea*. Staining with Calcofluor-White [CFW], shows the integrity of the hyphae. **(C)** The development of the fungus was calculated by counting the number of spores germinated. Bars represent mean values [± SD] of three independent experiments. Letters indicate a statistically significant difference, according to a one-way analysis of variance [ANOVA] [$p \leq 0.05$] following to the Tukey test. Scale bars, 20 µm.

growing, with a suspension of cells or BFs and evaluated their effect against *B. cinerea* (Figure 4). Upon infecting *A. thaliana* leaves with *B. cinerea*, we observed that the lesions caused by the pathogen on the plants pre-treated with the bacterial cells or BFs were significantly smaller compared to the non-inoculated control after three days post-infection [3 dpi], (Figure 4A, B). Next, we measured the incidence of infection on the leaves and observed that plants inoculated with C23F cells and filtrates showed a disease incidence of

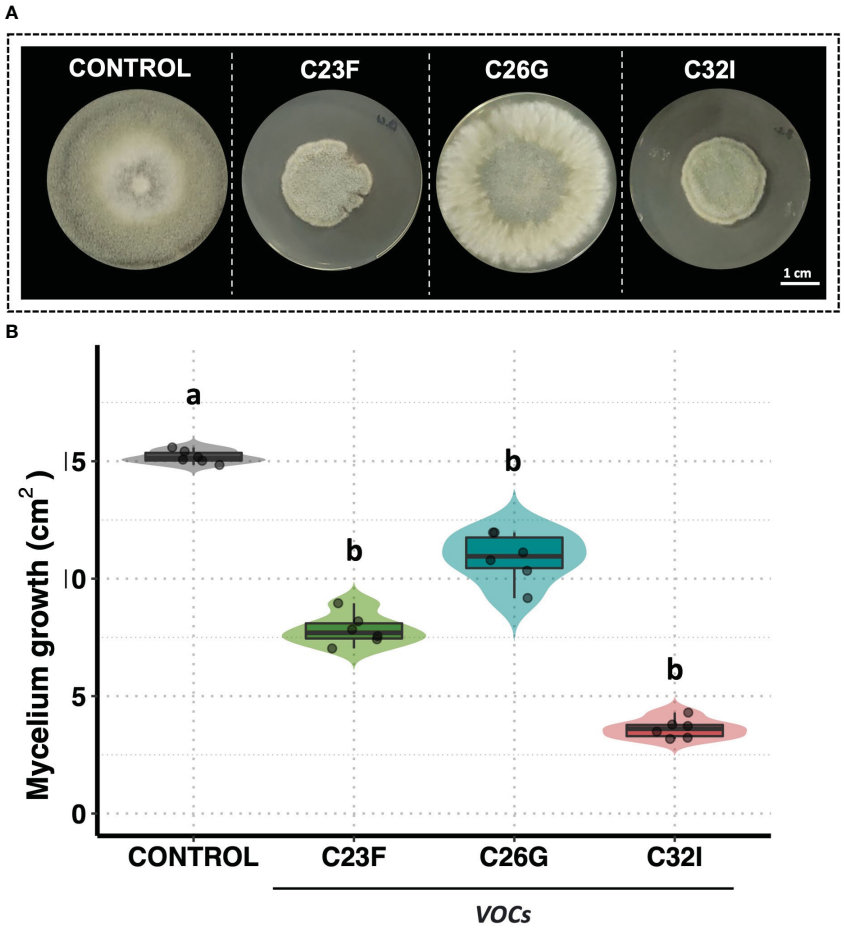

FIGURE 3
VOCs from bacteria C23F and C32I are involved in the inhibition of *B cinerea*. Double-sided experiments were performed, in which bacteria and fungi were grown in their respective culture medium. **(A)** Representative images of the inhibitory effect of the VOCs on the growth fungus mycelium. **(B)** The growth was evaluated by measuring the diameter of the mycelium on the dish compared with the control. Data represent the mean [± SD] of three independent experiments, each performed in duplicate, and presented relative to control. Letters indicate a statistically significant difference, according to one-way analysis of variance [ANOVA] [$p \leq 0.05$] followed the Tukey test.

46% and 71% respectively, and plants treated with C26G showed 48% and 66% incidence, followed of plant inoculated with C32I with 44% and 65%, disease incidence, compared with the controls that showed a 98% incidence (Figure 4C). These results indicate that both the bacteria and the BF induce defense responses in the plant when present in the soil, protecting leaves against *B. cinerea* infection.

Biocontrol activity of bacteria in blueberries against *B. cinerea* infection

To analyze the effect of bacteria to protect commercial crops such as blueberries during post-harvest, we performed an *in vivo* test using either cells or BFs of C23F, C26G and C32I, and inoculating with *B. cinerea* ISIB-MMA/F-Bc01-S (Chacón et al., 2022). We observed that blueberries fruits, treated with bacteria and infected with the fungus, showed a lower lesion grade compared to the non-inoculated control (Figure 5A). In untreated condition, 95% of the fruits developed the disease, while the fruits treated with cells bacteria, showed incidences of 58%, 49%, and 26% for bacteria C23F, C26G, and C32I, respectively (Figure 5B). For the treatment of blueberries inoculated with BF, the pathogen incidence was similar to the treatment with bacterial cells. The control treatment showed an incidence of 99%, while the BF treatments showed incidences of less than 80% (Figure 5C). Additionally, we analyzed the protective effects of each bacterium against *B. cinerea* using leaves from tomato plants inoculated with the respective bacterium. Our results showed a reduction in lesions in plants treated with each bacterium, compared to the control group where lesions were significantly higher (Supplementary Figure 1). Overall, the results indicate that C23F, C26G, and C32I and their filtrates [BF] protect plants and fruits against *B. cinerea*, suggesting a potential for biological control applications.

Transcriptional changes of *A. thaliana* in response to *Acinetobacter* sp. C32I and the pathogen *B. cinerea*

To investigate the transcriptional changes in the plant upon inoculation with the C32I bacterium and the pathogen *B. cinerea*,

10.3389/fpls.2024.1392637

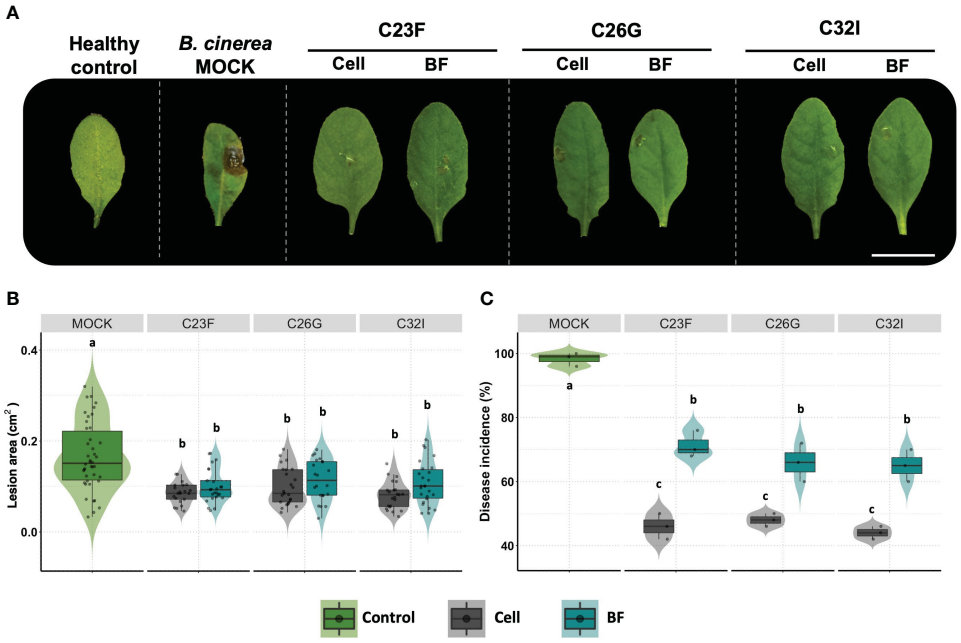

FIGURE 4
The cells and bacterial filtrates induced plant defense in presence of *B. cinerea*. Plants were inoculated with cells from the C23F, C26G and C32I strains, as well as their corresponding filtrates, and infected with pathogen. **(A)** The images show the impact of bacterial cells and filtrates on symptom development caused by *B. cinerea* after 3 days post-infection [dpi]. **(B)** Evaluation of lesion size in plants treated with bacteria. **(C)** Measuring of disease incidence in treated plants. The graphs represent two experiments were done [n=50, ± SD]. The letter indicate significance different, according to one-way analysis of variance [ANOVA] [$p \leq 0.05$] followed by Tukey test. Mock represent the plants with MS medium.

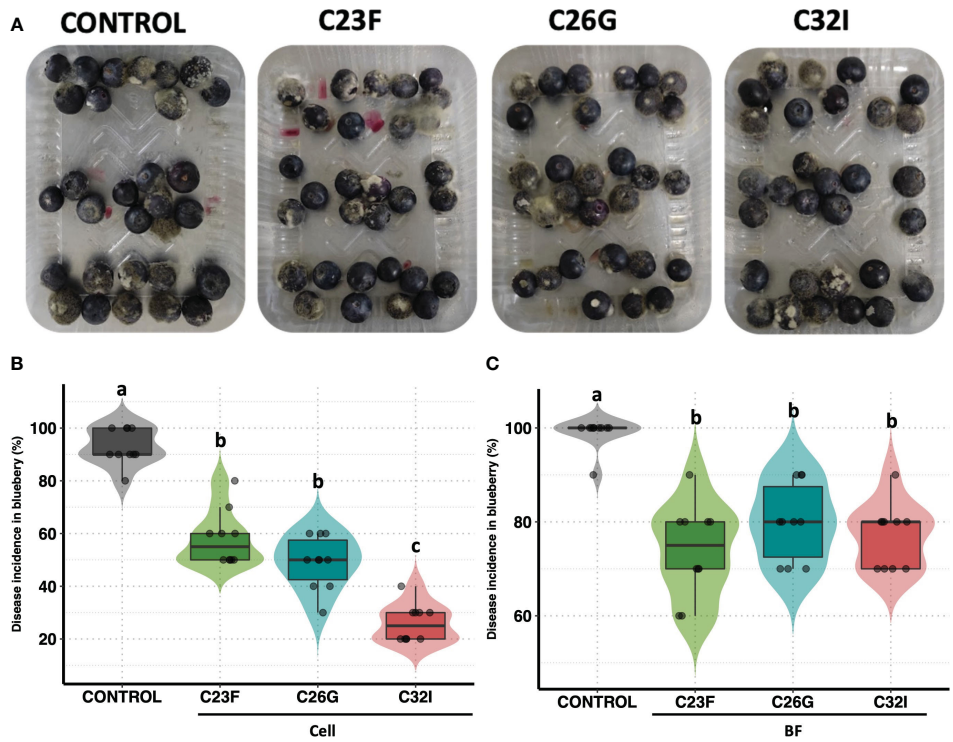

FIGURE 5
Biocontrol effect of bacterial cell and filtrates against *B. cinerea* on blueberries. Blueberries were treated with bacterial cells and filtrates [BF], and then infected with the *B. cinerea*. After 24 hours [hpi], photos were taken to evaluate the incidence. **(A)** Representative images of each treatment. **(B)** The graph represents the percentage incidence of the treatments with bacterial cells and filters. The analysis represents three independent experiments, each one with 10 blueberries. The letter indicate significance different, according to one-way analysis of variance [ANOVA] [$p \leq 0.05$] followed by Tukey test. Control represents the fruits with physiological solution.

we conducted both bipartite and tripartite interactions among the organisms under greenhouse conditions. We observed a difference in the number of up-regulated and down-regulated genes (Figure 6; Supplementary Data 1). We identified that 6,246 and 31 DEGs up-regulated, while 34,297, and 43 DEGs were down-regulated for each treatments, respectively (Figure 6A; Supplementary Data 2). Additionally, we explored whether these DEGs were shared among the treatments: we did not find shared DEGs for all the treatments and only few were shared when two treatments were compared (Figure 6B).

To assess the potential functions of the identified DEGs, these genes were assigned to significant annotations by Gene Ontology [GO] term enrichment analysis and were classified with respect to biological processes (Supplementary Data 3). All DEGs were classified into 22 biological processes, including the biological processes involved in interspecies interaction between organisms, response to biotic stimulus, response jasmonic acid, response to fungus, among others (Figure 6C). The results suggests that plants in the presence of C32I and *B. cinerea*, triggers the expression of various functional groups that differ with respect to dual interaction.

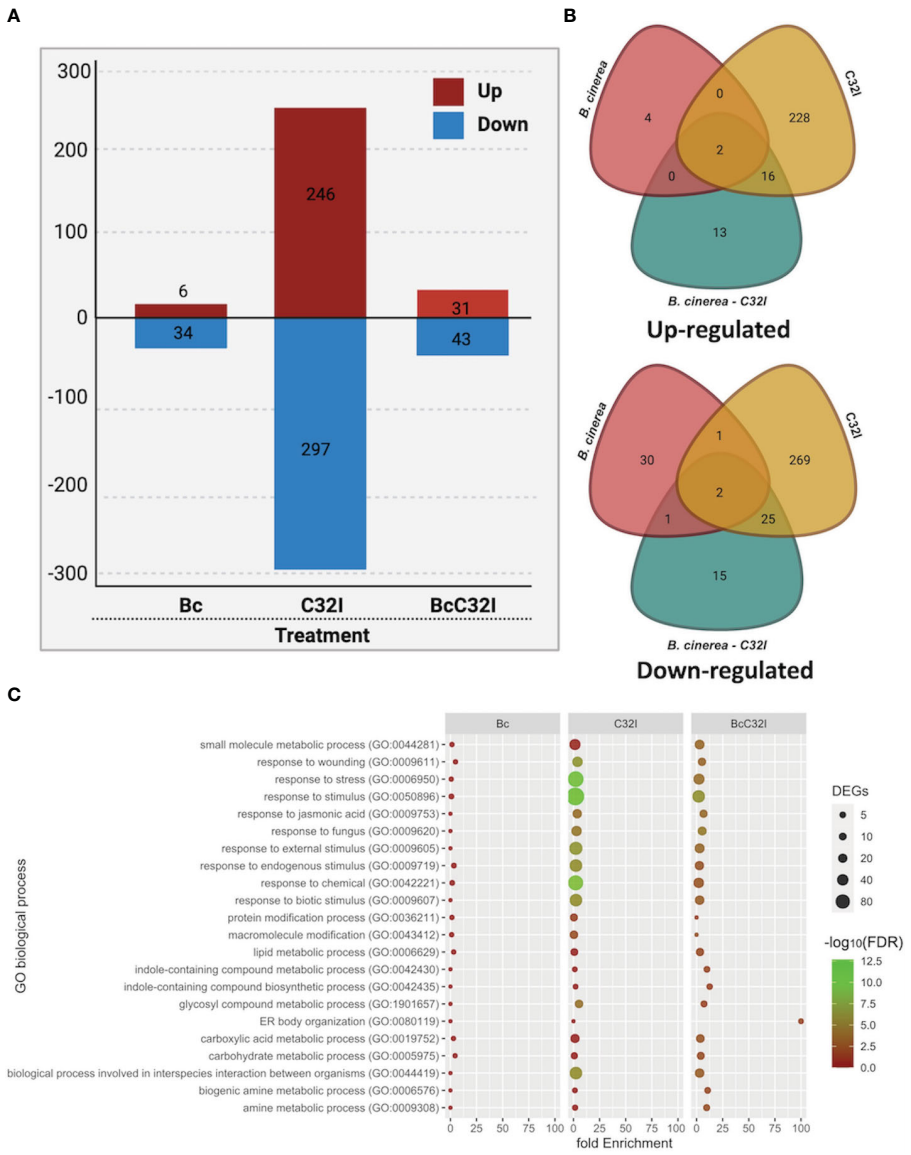

FIGURE 6
Transcriptome analysis of *A. thaliana* pathosystem with *Acinetobacter* sp. C32I and *B. cinerea* [6 hpi]. **(A)** Number of differentially expressed genes [DEGs] identified in the treatments, where red indicates up-regulated, and blue indicates down-regulated genes. **(B)** Venn diagrams show the number of up-regulated and down-regulated differentially expressed genes [DEGs] identified in the treatment compared to the control. **(C)** Distribution of the different biological functions of Gene Ontology [GO] for the up-regulated genes [$p<0.05$]. The graph represents the enrich "Biological process" GO-terms [FDR <0.01]. The color of the circles indicates the significance of the term [$-\log_{10}$ FDR], and the size of the dots represents the number of genes associated with that term. For the analysis of tripartite DEGs, we employed the Bc *vs* Bc-C32I comparison [Log2FC ≥ 2 or ≤ -2].

10.3389/fpls.2024.1392637

Genes related to plant defense responses are induced during the pathosystem in *Acinetobacter* sp. C32I and *B. cinerea*

To comprehend changes in the expression levels of genes associated with hormonal pathways, we performed a clustering of genes categorized into salicylic acid [SA]-, jasmonic acid [JA]-, ethylene [ET]-response to pathogen and others related to transcription factors. We analyzed the accumulation of transcripts in *A. thaliana* during the dual and tripartite interactions between the *Acinetobacter* sp. C32I and *B. cinerea* [6 hpi] (Figure 7). In the initial analysis, we compared the control condition [non-inoculated] with the plant exposed only to *B. cinerea*. In the ethylene [ET] pathway, we detected a down-regulation of genes, that participate in the resistance to *B. cinerea*. However, in the dual plant-bacteria interaction, we observed an induction of *ERF4, ACS6, CORI3* and *PR4* ET-related

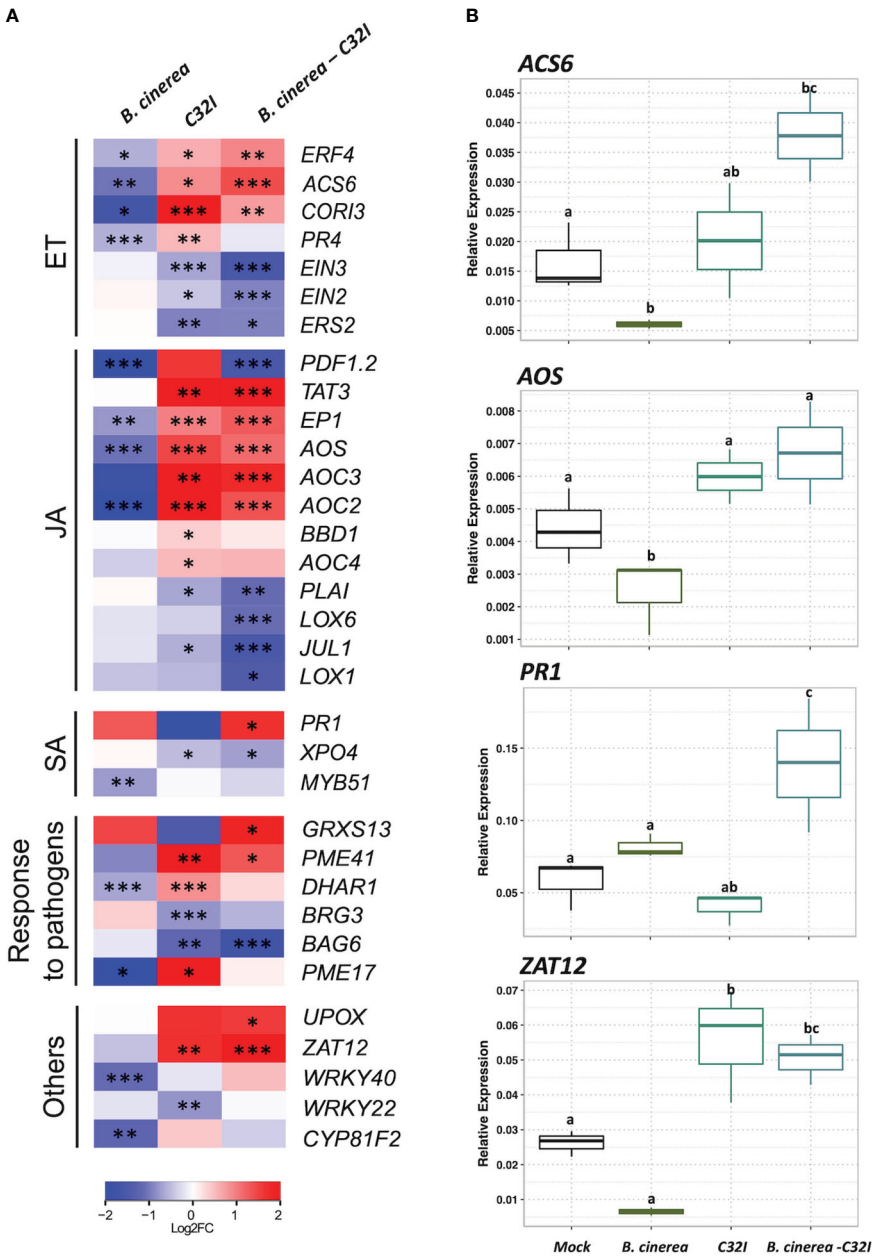

FIGURE 7
Expression analysis of jasmonic acid [JA]-, ethylene [ET]-, salicylic acid [SA]-response to pathogen and other genes in response to *B. cinerea* [6 hpi]. **(A)** Heatmap shows the expression levels of up-regulated genes. The colors represent the level of expression calculated between the control condition compared with each microorganism individually [dual interaction], and the tripartite interaction, ranging from blue [−2] to yellow [2]. **(B)** Expression analysis of genes *ACS6, AOS, PR1* and *ZAT12*, through RT-qPCR, based on Ct values, normalized with the expression of the two housekeeping genes. The data represent the means of three technical replicates. Error bars indicate ± SD. *p ≤ 0.05, **p ≤ 0.01, ***p ≤ 0.001.

genes and down-regulation of the receptors *EIN2* and *EIN3* (Wójcikowska and Gaj, 2017; Jiang et al., 2023; Shin et al., 2023; Tiwari et al., 2023). Regarding tripartite interaction, the genes showed the same up-regulation, except for *PR4* gene. Concerning jasmonic acid [JA] pathway, we observed a down-regulation of the responsive genes in presence of fungus. On the other hand, in the interaction of the plant with C32I, is observed up-regulation of the *PDF1.2, TAT3, EP1, AOS, AOC3, AOC2, BBD1*, and *OC4* genes (Stenzel et al., 2003; You et al., 2010; Omidvar et al., 2021; Mathan et al., 2022), and these expression levels were maintained in the tripartite interaction. Furthermore, in the salicylic acid [SA] pathway, *PR1* gene was induced during the infection with fungus and during the tripartite interaction.

Additionally, we analyzed a group of genes that have been described to respond to the defense against pathogens. Notably, during plant-bacteria interaction condition, there was an up-regulation of the genes *DHAR1* [DEHYDROASCORBATE REDUCTASE] and *PME17* and *PME41* [PECTIN METHYLESTERASE], the latter recently identified in defense against *B. cinerea* (Del Corpo et al., 2020; Aragón et al., 2021). The expression levels were similar during the tripartite interaction to genes, including *UPOX* [UPREGULATED BY OXIDATIVE*]* and *ZAT12* [ZINC FINGER OF ARABIDOPSIS] that participate in oxidative stress (Davletova et al., 2005; Vaahtera et al., 2014). Taken together, our results demonstrate that in the presence of the C32I bacterium, the transcriptional response of the plant is modified, indicating an early activation of the plant defense system, that is maintained in during the tripartite interaction, suggesting that the bacteria induce the plant immunity against *B. cinerea*. Finally, we confirmed the expression patterns found with RNA-seq with the expression of four genes selected from each hormone pathway: *ACS6*, *AOS*, *PR1*, and *ZAT12* through qRT-PCR (Figure 7B).

Resistance of *B. cinerea* is dependent on JA/ET

To elucidate the signal transduction pathways involved in the defense response induced by *Acinetobacter* sp. C32I against *B. cinerea*, the wild-type plant and mutants involved in the JA [*jar1*], ET [*ein3*], and SA [*eds5-1*] signaling pathways were inoculated with the bacterium C32I and infected with *B. cinerea*. The data demonstrated variation in the lesion size for each inoculated and non-inoculated treatment was detected (Figure 8A). An analysis of the lesion area in the Col-0 [WT] and *eds5-1* [SA] mutant showed a reduction in the lesion area caused by *B. cinerea* at 3dpi occurred when the plant was inoculated with the bacteria. However, the defense response in the *jar1* [JA] and *ein3* [ET] mutants showed the same lesion area, in both conditions (Figure 8B). Overall, the results suggested resistance of C32I-inoculated *A. thaliana* against *B. cinerea*, dependent on JA and ET signaling, rather than SA signaling.

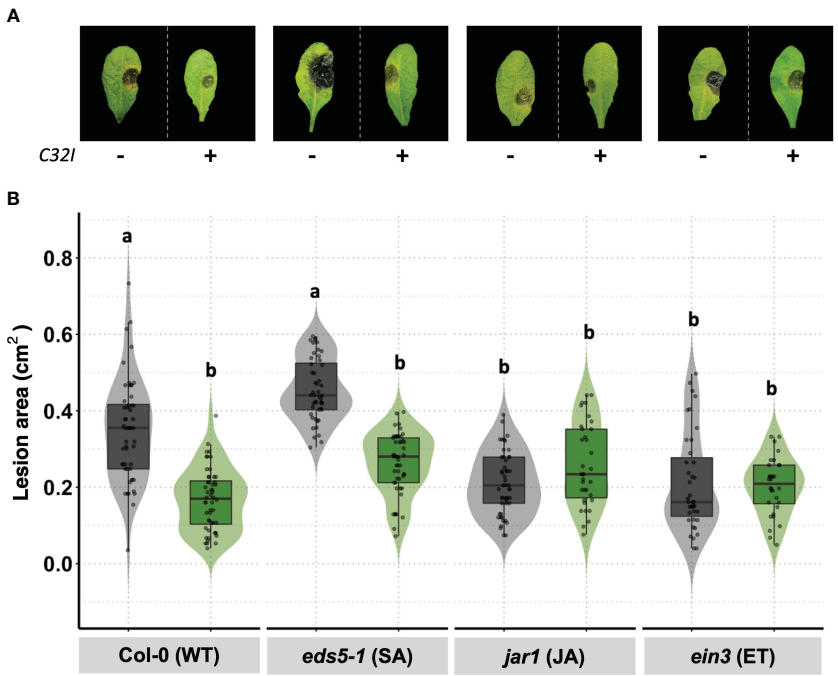

FIGURE 8
Acinetobacter sp. *C32I* treatment induces JA/ET-dependent resistance in *A. thaliana*. **(A)** Appearance of foliar symptoms in inoculated and non-inoculated plants. Representative leaves per genotype are shown. **(B)** Disease incidence of *B. cinerea* in wild-type *A. thaliana* [Col-0], and *eds5-1* [SA], *jar1* [jar1], and *ein3* [ET] mutants were tested. Experiments were repeated twice with similar results. The graphs represent the average of both experiments [n=50, ± SD]. Symptoms were determined at 3 days post-infection [dpi]. Letters indicate significant differences, according to one-way analysis of variance [ANOVA] [$p \leq 0.05$] followed by Tukey test. Control represents plants with MS medium.

The *Acinetobacter* sp. C32I produces transcriptional changes different from other biocontrol agents

We have observed that bacterium C32I induces transcriptional changes in the plant, manifesting differentially expressed genes [DEGs], both up-regulated and down-regulated, and some of the are related to defense systems. When comparing our results with other transcriptional reports of previously characterized biocontrol agents, we noticed a difference in the expressed genes in the presence of C32I, compared to *Bacillus valezensis FBZ42*, *Pseudomonas fluorescences SS01*, and *Burkholderia* sp. *SSG* (Figure 9) (van de Mortel et al., 2012; Tzipilevich et al., 2021; Kong et al., 2022). When we compared the transcriptional changes induced by C32I only few genes are shared with the other BCAs, suggesting that, even though all the analyzed BCAs have a biocontrol activity, transcriptional regulation by C32I triggers defense induction mechanisms distinct from other microorganisms.

Discussion

In nature, plants and animals interact with a plethora of microorganisms (Compant et al., 2010; Khare et al., 2018). Some bacteria can establish a beneficial association with plants, favoring plant growth, enhanced defense responses, and tolerance against biotic and abiotic stresses (Jones et al., 2019; Kang et al., 2019). Similarly, amphibians are known to possess a microbial community in their skin, which protects them against multiple factors, including the necrotrophic fungus *Batrachochytrium dendrobatidis* (Rebollar et al., 2018; Varga et al., 2019; Rebollar et al., 2020). It has been described that the amphibian skin and the phylosphere of the surrounding plants can share microbiomes, that can influence the tolerance to biotic and abiotic stresses in the amphibians (Fitzpatrick and Allison, 2014; Hernández-Gómez et al., 2020). In this study, we hypothesized that bacteria isolated from the skin of frogs may offer protective effect against the necrotrophic plant pathogen *Botrytis cinerea*.

To the best of our knowledge, only one study has reported the characterization of three bacteria isolated from Japanese frogs species as biocontrol agents against the fungus *C. orbiculare* (Susilawati et al., 2021). Similarly, in this work we analyzed the inhibitory effect of bacteria isolated from a tropical amphibian as biocontrol agents against *B. cinerea*, the causative agent of grey mold disease (Dean et al., 2012). Previously, we identified three different bacterial species that can inhibit the growth of *B. cinerea.* Our findings showed that compounds released by the bacteria modified the growth of the fungus at both early and late developmental stages. Numerous studies have demonstrated the potential of bacteria as biological control agents, including species of *Bacillus* spp., *Pseudomonas*, spp., and *Acinetobacter* spp., have been characterized for their effect in inhibiting *B. cinerea* (Trotel-Aziz et al., 2008; Kefi et al., 2015; Wang et al., 2020; Cevallos et al., 2022). *Bacillus* spp. it has been identified that their biocontrol activity is due to their secondary metabolism and the production of compounds, such as iturin, surfactin, and fengycin, bacteriocins, antimicrobial peptides, and lipopeptides, polyketides and siderophores, that participate in the inhibition of *B. cinerea* (Fira et al., 2018; Kiesewalter et al., 2021; Lu et al., 2021).

In addition to exerting antagonism mechanisms directly against pathogens, bacteria can also act indirectly through elicitors known as Microbial- or Pathogens-Associated Molecular Patterns [MAMPs or PAMPs], that are recognized through Pattern Recognition Receptors [PPRs] presents in the cell membrane plant, which activate the innate immunity (De Coninck et al., 2015; Wang et al., 2016). The MAMPs or PAMPs include the activation of hormonal pathways such as salicylic acid [SA], jasmonic acid [JA] and ethylene [ET], and consequently the induction of systemic defense responses (Robert-Seilaniantz et al., 2011). Studies have been conducted in recent years to demonstrate that the application of beneficial bacteria to plants activates their defense pathways, thereby protecting them against pathogenic

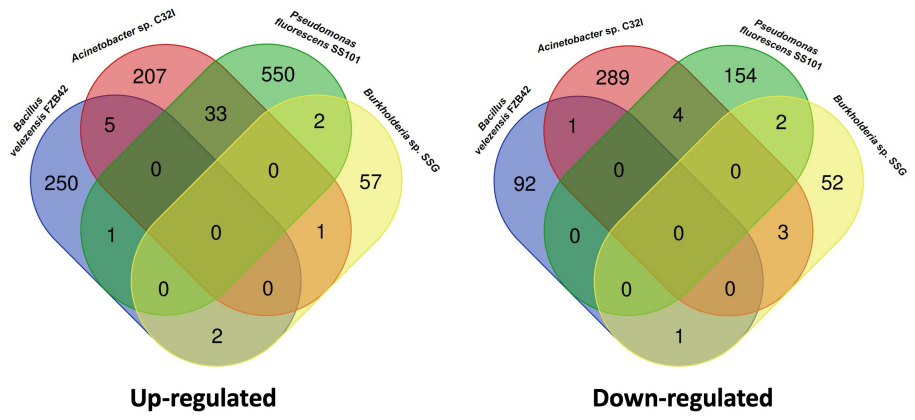

FIGURE 9
Comparative transcriptomic analysis with other biocontrol agents. Transcriptomic data of the bipartite interaction between *A. thaliana* with *Acinetobacter* sp. C32I, were compared with other biocontrols reported. Venn diagrams show the overlap of **(A)** up-regulated and **(B)** down-regulated genes.

fungi. Nie et al. (2017) demonstrated that the application of a *Bacillus cereus* AR156 strain to roots significantly reduced the incidence of *B. cinerea* disease by activating Induced Systemic Resistance [ISR]. Similarly, our results indicate that C23F, C26G, and C32I bacteria induce defense mechanisms in *A. thaliana* plants, leading to a decrease in *B. cinerea* disease. Since the bacteria was applied to the roots, while *B. cinerea* colonized the leaves, this suggests a possible activation of ISR, resulting in the observed resistance to infection by the pathogen.

Defense activity can trigger a series of events involving the transcriptional activation of hormone-related defense genes (AbuQamar et al., 2017; Lahlali et al., 2022). To determine changes in plant expression in response to the presence of C32I bacterium or/and *B. cinerea*, we analyzed the expression profiles between bipartite and tripartite interactions. Our analysis showed that DEGs are clustered into functional groups in response to biotic stimuli, jasmonic acid, and fungi (Figure 6C). During the plant-pathogen interaction, a decrease in the expression of genes related to the jasmonic acid pathway and the response to fungi was observed. Similarly, we observed an induction of genes related to pathogen recognition, which were triggered in the plant in response to *B. cinerea*. Previous studies report the induction of genes involved in the Induced Systemic Resistance [ISR], the jasmonic acid [JA], salicylic acid [SA], and ethylene [ET] hormone biosynthesis pathways, as well as other defense genes at 24 hpi (AbuQamar et al., 2006; Mulema and Denby, 2012; Sham et al., 2014; Xiong et al., 2018). In general, the authors report that gene expression initiates during the first hours of infection; however, a higher increase in the expression of these genes is observed at 24 hpi, which could explain under regulation of genes at 6 hpi in our study. Therefore, our results suggest a specific role of defense-related genes during the *A. thaliana* - *B. cinerea* interaction in the first hours of interaction.

In the case of the plant-bacteria interaction [*Acinetobacter* sp. *C32I*], we observed an increase in the number of up-regulated DEGs, which participate in the biosynthesis of growth hormones such as auxins [AUX], brassinosteroids [BR], and cytokinins [CK] [Romero et al., 2023, under review]. Additionally, we found that the bacteria can induce the expression of genes related to jasmonic acid, salicylic acid, and ethylene (Figure 7). Previous studies have reported the involvement of beneficial bacteria in the induction of the plant immune system, potentially facilitating the colonization processes of beneficial bacteria and enhancing defense against pathogens (Tzipilevich et al., 2021; Chakraborty, 2023). When analyzing the genes expressed during tripartite interactions, we observed an increased expression of genes related to defense hormones, response to pathogens, and other genes associated with oxidative stress [UPOX and ZAT12], which could be involved in the induction of defense through ISR (Davletova et al., 2005; Vaahtera et al., 2014). However, the increase in the expression observed in the plant-bacteria interaction, suggested that it could function as an ISR-priming, resulting in an accelerated activation of the defense response (Van der Ent et al., 2009; Zamioudis and Pieterse, 2012). The same effect has been observed with other biocontrols, where the inoculation of the fungus *Trichoderma hamatum T382* in *A. thaliana* induces early resistance against *B. cinerea*, which is subsequently moderated in response to the pathogen (Mathys et al., 2012). Similarly, was observed in the treatment of *A. thaliana* with the *Pseudomonas fluorescens bacterium PTA-CT2*, which induced the pre-infection plant defense against the pathogen *Pseudomonas syringae Pst DC3000* (Nguyen et al., 2020). Interestingly, a comparison of transcriptomic data from our results with other biocontrol agents, such as *Bacillus valezensis FBZ42, Pseudomonas fluorescences SS01*, and *Burkholderia* sp. *SSG*, shows transcriptomic differentiation, indicating that each strain elicits a plant-specific response and may be involved in ISR activation (van de Mortel et al., 2012; Tzipilevich et al., 2021; Kong et al., 2022). Based on this evidence, we can infer that the early activation of the plant defense system could contribute to an effective inhibition of *B. cinerea*.

It has been shown that ISR can be mediated by non-pathogenic bacteria that contribute to counteract the effects of pathogens, and this process is regulated by defense hormones (Pieterse et al., 1998; Van der Ent et al., 2009; van de Mortel et al., 2012). Interestingly, we observed using *A. thaliana* mutants that defense against *B. cinerea* is JA/ET-dependent and not SA-dependent. These results agree with previous reports suggesting that mutants with blocked ethylene [*ein2*] and jasmonic [*jar1*] signaling show increased susceptibility to *B. cinerea*. On the other hand, in the salicylic acid mutant [*eds5-1*], no significant impact on lesion size was observed (Ferrari et al., 2003). In other systems, it has been observed that JA [*jar1*] and ET [*ein2*] mutant plants treated with *Penicillium* sp. *GP16-2* did not reduce symptoms caused by *Pseudomonas syringae pv. tomato DC3000* (Hossain et al., 2008). Although there is no clear correlation between the expression levels of any of the genes and the degree of susceptibility to *B. cinerea*, the use of mutants inoculated with the C32I can provide information on the mechanisms used by the plant to defend itself against *B. cinerea* attack.

Studies have shown that the application of bacteria on agronomically important crops can serve as a biocontrol agent against *B. cinerea* to prolong fruit life during postharvest (Donmez et al., 2011; Lu et al., 2021; Chacón et al., 2022). To test the suppression of gray mold disease in fruits during postharvest and serve as inducers to elicit defense responses, we found that cells and bacterial filtrates of C23F, C26G, and C32I protect blueberry fruits against *B. cinerea* infection. Susilawati et al. (2021) showed HjD57, HjD92 and B341 from Japanese frogs-skin could reduce disease of the pathogen *Colletotrichum orbiculare* on cucumber plants. Similarly, tomato leaf assays that were inoculated with frog skin bacteria showed increased resistance to the pathogen. These results correlate with previous studies where the application of beneficial bacteria has been observed to reduce leaf disease severity (Kefi et al., 2015; Toral et al., 2020). Overall, the latter assay showed inhibitory activity of frog skin bacteria in the control of gray mold on plants of agronomic interest, therefore, an effective and feasible method to prevent postharvest fruit diseases is proposed.

Conclusion

Bacteria as biocontrol agents present antagonistic mechanisms that inhibit the development of pathogens. However, little has been

explored on bacteria from animals as potential fungicides. In this work, we demonstrate the inhibitory effects of three bacteria isolated from amphibian skin identified as *Acinetobacter* sp. C26G and C32I, and one *Enterobacteraceae* C23F on the growth and development of the plant pathogen *B. cinerea*. Additionally, we observed a reduction in the degree of infection upon the application of bacterial cells and filtrates. Moreover, the inoculation of the C32I bacteria to *A. thaliana* plants induced defense mechanisms by activating various defense genes associated with hormones such as salicylic acid [SA], jasmonic acid [JA], and ethylene [ET]. These activated defense pathways effectively protected the plant against *B. cinerea*. Based on these findings, we propose these bacterial strains as potential candidates for biological control agents, presenting an efficient and feasible method to prevent fruit diseases by inhibiting pathogen development and contributing to plant defense through immune system induction.

Data availability statement

The datasets presented in this study can be found in online repositories. The names of the repository/repositories and accession number(s) can be found in the article/Supplementary Material.

Author contributions

YR-C: Conceptualization, Formal analysis, Investigation, Validation, Writing – original draft, Writing – review & editing. FG: Data curation, Formal analysis, Writing – review & editing. DF: Conceptualization, Data curation, Formal analysis, Investigation, Writing – review & editing. WA: Data curation, Formal analysis, Writing – review & editing. FC: Conceptualization, Investigation, Methodology, Writing – review & editing. MT: Investigation, Methodology, Writing – review & editing. MC: Conceptualization, Supervision, Writing – review & editing. JD: Conceptualization, Formal analysis, Methodology, Supervision, Writing – review & editing. EAR: Conceptualization, Formal analysis, Funding acquisition, Investigation, Resources, Writing – original draft, Writing – review & editing. MS: Conceptualization, Funding acquisition, Investigation, Project administration, Supervision, Writing – original draft, Writing – review & editing.

Funding

The author(s) declare that financial support was received for the research, authorship, and/or publication of this article. This study was supported by funds from Programa de Apoyo a Proyectos de Investigación e Innovación Tecnológica [PAPIIT]-UNAM grants IN203023 and IG200224 [to MS and EAR], respectively and CONAHCyT grant 319266 to MS, YR-C and FG-S are doctoral students from Programa de Doctorado en Ciencias Biomédicas, Universidad Nacional Autónoma de México, and they received the fellowship No. 745733 and 856429, respectively, from Consejo Nacional de Humanidades Ciencias y Tecnologías [CONAHCYT]. The bacterial collection from which the study strains were obtained was supported by grants DEB-1136602 to Reid N. Harris and DEB-1136640 to Lisa K. Belden of the National Science Foundation. FC and YR-C thanks the support from United Nations University Programme for Biotechnology in Latin America and the Caribbean [UNU-BIOLAC].

Acknowledgments

We thank Paul Goodwing for the constructive comments to the work.

Conflict of interest

The authors declare that the research was conducted in the absence of any commercial or financial relationships that could be construed as a potential conflict of interest.

The author(s) declared that they were an editorial board member of Frontiers, at the time of submission. This had no impact on the peer review process and the final decision.

Publisher's note

Supplementary material

The Supplementary Material for this article can be found online at: https://www.frontiersin.org/articles/10.3389/fpls.2024.1392637/full#supplementary-material

SUPPLEMENTARY FIGURE 1
Biocontrol activity of frog skin bacteria against *B. cinerea* by the detached leaf test. Five-week-old tomato leaves treated with each bacterium were collected were infected with spore suspension of *B. cinerea*, after three days of incubation the lesion was evaluated. **(A)** Representative images of each treatment are shown. **(B)** Infection was assessed by measuring the lesion area. The graphs represent three biological replicates [n=30 ± SD]. Letters indicate a statistically significant difference, according to a one-way analysis of variance [ANOVA] [$p \leq 0.05$] followed the Tukey test. Mock represents the plants with MS medium. Scale bar 1 cm.

SUPPLEMENTARY DATA SHEET 1
List of differentially expressed genes for each condition, associated to .

SUPPLEMENTARY DATA SHEET 2
List of differentially expressed genes [DEGs] in the bipartite and tripartite interactions [up-regulated and down-regulated], associated to .

SUPPLEMENTARY DATA SHEET 3
Gene Ontology [GO] term enrichment list of differentially expressed genes associated to .

References

Abbey, J. A., Percival, D., Abbey, L., Asiedu, S. K., Prithiviraj, B., and Schilder, A. (2019). Biofungicides as alternative to synthetic fungicide control of grey mould (Botrytis cinerea) – prospects and challenges. *Biocontrol Sci. Technol.* 29, 207–228. doi: 10.1080/09583157.2018.1548574

AbuQamar, S., Chen, X., Dhawan, R., Bluhm, B., Salmeron, J., Lam, S., et al. (2006). Expression profiling and mutant analysis reveals complex regulatory networks involved in Arabidopsis response to Botrytis infection. *Plant J.* 48, 28–44. doi: 10.1111/j.1365-313X.2006.02849.x

AbuQamar, S., Moustafa, K., and Tran, L. S. (2017). Mechanisms and strategies of plant defense against Botrytis cinerea. *Crit. Rev. Biotechnol.* 37, 262–274. doi: 10.1080/07388551.2016.1271767

Aladdin, A., Dib, J. R., Malek, R. A., and El Enshasy, H. A. (2018). "Killer Yeast, a Novel Biological Control of Soilborne Diseases for Good Agriculture Practice," in *Sustainable Technologies for the Management of Agricultural Wastes*. Ed. Z. A. Zakaria (Springer, Singapore), 71–86. doi: 10.1007/978-981-10-5062-6_6

Aragón, W., Formey, D., Aviles-Baltazar, N. Y., Torres, M., and Serrano, M. (2021). Arabidopsis thaliana cuticle composition contributes to differential defense response to Botrytis cinerea. *Front. Plant Sci.* 12, 738949. doi: 10.3389/fpls.2021.738949

Babbal,, Adivitiya,, and Khasa, Y. P. (2017). "Microbes as Biocontrol Agents," in *Probiotics and Plant Health*. Eds. V. Kumar, M. Kumar, S. Sharma and &R. Prasad (Springer, Singapore), 507–552. doi: 10.1007/978-981-10-3473-2_24

Balthazar, C., Novinscak, A., Cantin, G., Joly, D. L., and Filion, M. (2022). Biocontrol activity of Bacillus spp. and Pseudomonas spp. against Botrytis cinerea and other cannabis fungal pathogens. *Phytopathology®* 112, 549–560. doi: 10.1094/PHYTO-03-21-0128-R

Bi, K., Liang, Y., Mengiste, T., and Sharon, A. (2023). Killing softly: A roadmap of Botrytis cinerea pathogenicity. *Trends Plant Sci.* 28, 211–222. doi: 10.1016/j.tplants.2022.08.024

Boukaew, S., Prasertsan, P., Troulet, C., and Bardin, M. (2017). Biological control of tomato gray mold caused by Botrytis cinerea by using Streptomyces spp. *BioControl* 62, 793–803. doi: 10.1007/s10526-017-9825-9

Carmona-Hernandez, S., Reyes-Pérez, J. J., Chiquito-Contreras, R. G., Rincon-Enriquez, G., Cerdan-Cabrera, C. R., and Hernandez-Montiel, L. G. (2019). Biocontrol of postharvest fruit fungal diseases by bacterial antagonists: a review. *Agronomy* 9, 121. doi: 10.3390/agronomy9030121

Cevallos, M. A., Basanta, M. D., Bello-López, E., Escobedo-Muñoz, A. S., González-Serrano, F. M., Nemec, A., et al. (2022). Genomic characterization of antifungal Acinetobacter bacteria isolated from the skin of the frogs Agalychnis callidryas and Craugastor fitzingeri. *FEMS Microbiol. Ecol.* 98. doi: 10.1093/femsec/fiac126

Chacón, F. I., Sineli, P. E., Mansilla, F. I., Pereyra, M. M., Diaz, M. A., Volentini, S. I., et al. (2022). Native cultivable bacteria from the blueberry microbiome as novel potential biocontrol agents. *Microorganisms* 10, 969. doi: 10.3390/microorganisms10050969

Chakraborty, J. (2023). Microbiota and the plant immune system work together to defend against pathogens. *Arch. Microbiol.* 205, 347. doi: 10.1007/s00203-023-03684-9

Chassot, C., Nawrath, C., and Métraux, J. P. (2007). Cuticular defects lead to full immunity to a major plant pathogen. *Plant J.* 49, 972–980. doi: 10.1111/j.1365-313X.2006.03017.x

Choudhary, D. K., Prakash, A., and Johri, B. N. (2007). Induced systemic resistance (ISR) in plants: mechanism of action. *Indian J. Microbiol.* 47, 289–297. doi: 10.1007/s12088-007-0054-2

Compant, S., van der Heijden, M. G., and Sessitsch, A. (2010). Climate change effects on beneficial plant–microorganism interactions. *FEMS Microbiol. Ecol.* 73, 197–214. doi: 10.1111/j.1574-6941.2010.00900.x

Davletova, S., Schlauch, K., Coutu, J., and Mittler, R. (2005). The zinc-finger protein Zat12 plays a central role in reactive oxygen and abiotic stress signaling in Arabidopsis. *Plant Physiol.* 139, 847–856. doi: 10.1104/pp.105.068254

Dean, R., Van Kan, J., Pretorius, Z., Hammond-Kosack, K., Di Pietro, A., Spanu, P., et al. (2012). Rothamsted repository download. *Pathology* 13, 414–430. doi: 10.1111/j.1364-3703.2011.00783.x

De Coninck, B., Timmermans, P., Vos, C., Cammue, B. P. A., and Kazan, K. (2015). What lies beneath: belowground defense strategies in plants. *Trends Plant Sci.* 20, 91–101. doi: 10.1016/j.tplants.2014.09.007

Del Corpo, D., Fullone, M. R., Miele, R., Lafond, M., Pontiggia, D., Grisel, S., et al. (2020). AtPME17 is a functional Arabidopsis thaliana pectin methylesterase regulated by its PRO region that triggers PME activity in the resistance to Botrytis cinerea. *Mol. Plant Pathol.* 21, 1620–1633. doi: 10.1111/mpp.13002

Díaz, M. A., Pereyra, M. M., Picón-Montenegro, E., Meinhardt, F., and Dib, J. R. (2020). Killer yeasts for the biological control of postharvest fungal crop diseases. *Microorganisms* 8, 1680. doi: 10.3390/microorganisms8111680

Di Francesco, A., Mari, M., Ugolini, L., and Baraldi, E. (2018). Effect of Aureobasidium pullulans strains against Botrytis cinerea on kiwifruit during storage and on fruit nutritional composition. *Food Microbiol.* 72, 67–72. doi: 10.1016/j.fm.2017.11.010

Dik, A. J., and Wubben, J. P. (2007). "Epidemiology of Botrytis cinerea diseases in greenhouses," in *Botrytis: biology, pathology and control* (Dordrecht: Springer Netherlands), 319–333.

Donmez, M., Esitken, A., Yildiz, H., and Ercisli, S. (2011). Biocontrol of Botrytis cinerea on strawberry fruit by plant growth promoting bacteria. *J. Anim. Plant Sci.* 21.

El-Saadony, M. T., Saad, A. M., Soliman, S. M., Salem, H. M., Ahmed, A. I., Mahmood, M., et al. (2022). Plant growth-promoting microorganisms as biocontrol agents of plant diseases: Mechanisms, challenges and future perspectives. *Front. Plant Sci.* 13. doi: 10.3389/fpls.2022.923880

Fedele, G., González-Domínguez, E., and Rossi, V. (2020). "Influence of environment on the biocontrol of Botrytis cinerea: A systematic literature review," in De Cal, A., Melgarejo, P., and Magan, N. (eds) *How research can stimulate the development of commercial biological control against plant diseases*, 61–82. (Springer, Cham). doi: 10.1007/978-3-030-53238-3_5

Ferrari, S., Plotnikova, J. M., De Lorenzo, G., and Ausubel, F. M. (2003). Arabidopsis local resistance to Botrytis cinerea involves salicylic acid and camalexin and requires EDS4 and PAD2, but not SID2, EDS5 or PAD4. *Plant J.* 35, 193–205. doi: 10.1046/j.1365-313X.2003.01794.x

Ferreira-Saab, M., Formey, D., Torres, M., Aragón, W., Padilla, E. A., Tromas, A., et al. (2018). Compounds Released by the Biocontrol Yeast Hanseniaspora opuntiae Protect Plants Against Corynespora cassiicola and Botrytis cinerea. *Front. Microbiol.* 9. doi: 10.3389/fmicb.2018.01596

Fira, D., Dimkić, I., Berić, T., Lozo, J., and Stanković, S. (2018). Biological control of plant pathogens by Bacillus species. *J. Biotechnol.* 285, 44–55. doi: 10.1016/j.jbiotec.2018.07.044

Fitzpatrick, B. M., and Allison, A. L. (2014). Similarity and differentiation between bacteria associated with skin of salamanders (Plethodon Jordani) and free-living assemblages. *FEMS Microbiol. Ecol.* 88, 482–494. doi: 10.1111/fem.2014.88.issue-3

Haidar, R., Fermaud, M., Calvo-Garrido, C., Roudet, J., and Deschamps, A. (2016). Modes of action for biological control of Botrytis cinerea by antagonistic bacteria. *Phytopathol. Mediterr.* 55, 301–322. doi: 10.14601/Phytopathol_Mediterr-18079

Hernández-Gómez, O., Byrne, A. Q., Gunderson, A. R., Jenkinson, T. S., Noss, C. F., Rothstein, A. P., et al. (2020). Invasive vegetation affects amphibian skin microbiota and body condition. *PeerJ* 8, e8549. doi: 10.7717/peerj.8549

Hossain, M. M., Sultana, F., Kubota, M., and Hyakumachi, M. (2008). Differential inducible defense mechanisms against bacterial speck pathogen in Arabidopsis thaliana by plant-growth-promoting-fungus Penicillium sp. GP16-2 and its cell free filtrate. *Plant Soil* 304, 227–239. doi: 10.1007/s11104-008-9542-3

Hua, L., Yong, C., Zhanquan, Z., Boqiang, L., Guozheng, Q., and Shiping, T. (2018). Pathogenic mechanisms and control strategies of Botrytis cinerea causing post-harvest decay in fruits and vegetables. *Food Qual. Saf.* 2, 111–119. doi: 10.1093/fqsafe/fyy016

Jiang, Y., Zhang, S., Chen, K., Xia, X., Tao, B., and Kong, W. (2023). Impacts of DNA methylases and demethylases on the methylation and expression of Arabidopsis ethylene signal pathway genes. *Funct. Integr. Genomics* 23, 1–15. doi: 10.1007/s10142-023-01069-1

Jiménez-Jacinto, V., Sanchez-Flores, A., and Vega-Alvarado, L. (2019). Integrative differential expression analysis for multiple experiments (IDEAMEX): a web server tool for integrated rna-seq data analysis. *Front. Genet.* 10, 279. doi: 10.3389/fgene.2019.00279

Jones, P., Garcia, B. J., Furches, A., Tuskan, G. A., and Jacobson, D. (2019). Plant host-associated mechanisms for microbial selection. *Front. Plant Sci.* 862. doi: 10.3389/fpls.2019.00862

Kang, S.-M., Hamayun, M., Khan, M. A., Iqbal, A., and Lee, I.-J. (2019). Bacillus subtilis JW1 enhances plant growth and nutrient uptake of Chinese cabbage through gibberellins secretion. *J. Appl. Bot. Food Qual* 92, 172–178. doi: 10.5073/JABFQ.2019.092.023

Kefi, A., Slimene, I. B., Karkouch, I., Rihouey, C., Azaeiz, S., Bejaoui, M., et al. (2015). Characterization of endophytic Bacillus strains from tomato plants (Lycopersicon esculentum) displaying antifungal activity against Botrytis cinerea Pers. *World J. Microbiol. Biotechnol.* 31, 1967–1976. doi: 10.1007/s11274-015-1943-x

Khare, E., Mishra, J., and Arora, N. K. (2018). Multifaceted interactions between endophytes and plant: developments and prospects. *Front. Microbiol.* 9, 2732. doi: 10.3389/fmicb.2018.02732

Kiesewalter, H. T., Lozano-Andrade, C. N., Wibowo, M., Strube, M. L., Maróti, G., Snyder, D., et al. (2021). Genomic and chemical diversity of Bacillus subtilis secondary metabolites against plant pathogenic fungi. *Msystems* 6, e00770–e00720. doi: 10.1128/mSystems.00770-20

Kong, P., Li, X., Gouker, F., and Hong, C. (2022). cDNA transcriptome of Arabidopsis reveals various defense priming induced by a broad-spectrum biocontrol agent Burkholderia sp. SSG. *Int. J. Mol. Sci.* 23, 3151. doi: 10.3390/ijms23063151

Lahlali, R., Ezrari, S., Radouane, N., Kenfaoui, J., Esmaeel, Q., El Hamss, H., et al. (2022). Biological control of plant pathogens: A global perspective. *Microorganisms* 10, 596. doi: 10.3390/microorganisms10030596

L'haridon, F., Besson-Bard, A., Binda, M., Serrano, M., Abou-Mansour, E., Balet, F., et al. (2011). A permeable cuticle is associated with the release of reactive oxygen species and induction of innate immunity. *PloS Pathog.* 7, e1002148. doi: 10.1371/journal.ppat.1002148

Lu, Y., Ma, D., He, X., Wang, F., Wu, J., Liu, Y., et al. (2021). Bacillus subtilis KLBC BS6 induces resistance and defence-related response against Botrytis cinerea in

blueberry fruit. *Physiol. Mol. Plant Pathol.* 114, 101599. doi: 10.1016/j.pmpp.2020.101599

Mathan, L., Dubey, N., Verma, S., and Singh, K. (2022). "Transcription Factors Associated with Defense Response Against Fungal Necrotrophs," in *Transcription Factors for Biotic Stress Tolerance in Plants* (Cham: Springer International Publishing), 61–78.

Mathys, J., De Cremer, K., Timmermans, P., Van Kerckhove, S., Lievens, B., Vanhaecke, M., et al. (2012). Genome-wide characterization of ISR induced in Arabidopsis thaliana by Trichoderma hamatum T382 against Botrytis cinerea infection. *Front. Plant Sci.* 3, 108. doi: 10.3389/fpls.2012.00108

Mengiste, T., Laluk, K., and AbuQamar, S. (2010). "Mechanisms of Induced Resistance Against B. cinerea," in *Postharvest Pathology*. Eds. D. Prusky and M. L. Gullino (Springer, Netherlands), 13–30. doi: 10.1007/978-1-4020-8930-5_2

Mulema, J. M. K., and Denby, K. J. (2012). Spatial and temporal transcriptomic analysis of the Arabidopsis thaliana–Botrytis cinerea interaction. *Mol. Biol. Rep.* 39, 4039–4049. doi: 10.1007/s11033-011-1185-4

Murashige, T., and Skoog, F. (1962). A revised medium for rapid growth and bio assays with tobacco tissue cultures. *Physiologia plantarum* 15, 473–497. doi: 10.1111/j.1399-3054.1962.tb08052.x

Nawrath, C., and Métraux, J.-P. (1999). Salicylic acid induction–deficient mutants of Arabidopsis express PR-2 and PR-5 and accumulate high levels of camalexin after pathogen inoculation. *Plant Cell* 11, 1393–1404. doi: 10.1105/tpc.11.8.1393

Nguyen, N. H., Trotel-Aziz, P., Villaume, S., Rabenoelina, F., Schwarzenberg, A., Nguema-Ona, E., et al. (2020). Bacillus subtilis and Pseudomonas fluorescens trigger common and distinct systemic immune responses in Arabidopsis thaliana depending on the pathogen lifestyle. *Vaccines* 8, 503. doi: 10.3390/vaccines8030503

Nie, P., Li, X., Wang, S., Guo, J., Zhao, H., and Niu, D. (2017). Induced systemic resistance against Botrytis cinerea by Bacillus cereus AR156 through a JA/ET-and NPR1-dependent signaling pathway and activates PAMP-triggered immunity in Arabidopsis. *Front. Plant Sci.* 8, 238. doi: 10.3389/fpls.2017.00238

O'Brien, P. A. (2017). Biological control of plant diseases. *Australas. Plant Pathol.* 46, 293–304. doi: 10.1007/s13313-017-0481-4

Omidvar, R., Vosseler, N., Abbas, A., Gutmann, B., Grünwald-Gruber, C., Altmann, F., et al. (2021). Analysis of a gene family for PDF-like peptides from Arabidopsis. *Sci. Rep.* 11, 18948. doi: 10.1038/s41598-021-98175-6

Pereyra, M. M., Andrea Diaz, M., Meinhardt, F., and Rafael Dib, J. (2020). Effect of stress factors associated with postharvest citrus conditions on the viability and biocontrol activity of Clavispora lusitaniaestrain 146. *PloS One* 15. doi: 10.1371/journal.pone.0239432

Petrasch, S., Knapp, S. J., van Kan, J. A. L., and Blanco-Ulate, B. (2019). Grey mould of strawberry, a devastating disease caused by the ubiquitous necrotrophic fungal pathogen Botrytis cinerea. *Mol. Plant Pathol.* 20, 877–892. doi: 10.1111/mpp.12794

Pieterse, C. M. J., van Wees, S. C. M., van Pelt, J. A., Knoester, M., Laan, R., Gerrits, H., et al. (1998). A novel signaling pathway controlling induced systemic resistance in arabidopsis. *Plant Cell* 10, 1571–1580. doi: 10.1105/tpc.10.9.1571

Rebollar, E. A., Bridges, T., Hughey, M. C., Medina, D., Belden, L. K., and Harris, R. N. (2019). Integrating the role of antifungal bacteria into skin symbiotic communities of three Neotropical frog species. *ISME J.* 13, 1763–1775. doi: 10.1038/s41396-019-0388-x

Rebollar, E. A., Gutiérrez-Preciado, A., Noecker, C., Eng, A., Hughey, M. C., Medina, D., et al. (2018). The skin microbiome of the neotropical frog craugastor fitzingeri: inferring potential bacterial-host-pathogen interactions from metagenomic data. *Front. Microbiol.* 9. doi: 10.3389/fmicb.2018.00466

Rebollar, E. A., Hughey, M. C., Medina, D., Harris, R. N., Ibáñez, R., and Belden, L. K. (2016). Skin bacterial diversity of Panamanian frogs is associated with host susceptibility and presence of Batrachochytrium dendrobatidis. *ISME J.* 10, 1682–1695. doi: 10.1038/ismej.2015.234

Rebollar, E. A., Martínez-Ugalde, E., and Orta, A. H. (2020). The amphibian skin microbiome and its protective role against chytridiomycosis. *Herpetologica* 76, 167–177. doi: 10.1655/0018-0831-76.2.167

Robert-Seilaniantz, A., Grant, M., and Jones, J. D. (2011). Hormone crosstalk in plant disease and defense: more than just jasmonate-salicylate antagonism. *Annu. Rev. Phytopathol.* 49, 317–343. doi: 10.1146/annurev-phyto-073009-114447

Roca-Couso, R., Flores-Félix, J. D., and Rivas, R. (2021). Mechanisms of Action of Microbial Biocontrol Agents against Botrytis cinerea. *J. Fungi* 7. doi: 10.3390/jof7121045

Roman, G., Lubarsky, B., Kieber, J. J., Rothenberg, M., and Ecker, J. R. (1995). Genetic analysis of ethylene signal transduction in Arabidopsis thaliana: five novel mutant loci integrated into a stress response pathway. *Genetics* 139, 1393–1409. doi: 10.1093/genetics/139.3.1393

Romero-Contreras, Y. J., Ramírez-Valdespino, C. A., Guzmán-Guzmán, P., Macías-Segoviano, J. I., Villagómez-Castro, J. C., and Olmedo-Monfil, V. (2019). Tal6 from Trichoderma atroviride is a LysM effector involved in mycoparasitism and plant association. *Front. Microbiol.*, 2231. doi: 10.3389/fmicb.2019.02231

Sham, A., Al-Azzawi, A., Al-Ameri, S., Al-Mahmoud, B., Awwad, F., Al-Rawashdeh, A., et al. (2014). Transcriptome analysis reveals genes commonly induced by Botrytis cinerea infection, cold, drought and oxidative stresses in Arabidopsis. *PloS One* 9, e113718. doi: 10.1371/journal.pone.0113718

Shin, S. Y., Lee, C.-M., Kim, H.-S., Kim, C., Jeon, J.-H., and Lee, H.-J. (2023). Ethylene signals modulate the survival of Arabidopsis leaf explants. *BMC Plant Biol.* 23, 1–11. doi: 10.1186/s12870-023-04299-4

Stenzel, I., Hause, B., Miersch, O., Kurz, T., Maucher, H., Weichert, H., et al. (2003). Jasmonate biosynthesis and the allene oxide cyclase family of Arabidopsis thaliana. *Plant Mol. Biol.* 51, 895–911. doi: 10.1023/A:1023049319723

Supek, F., Bošnjak, M., Škunca, N., and Šmuc, T. (2011). REVIGO summarizes and visualizes long lists of gene ontology terms. *PloS One* 6, e21800. doi: 10.1371/journal.pone.0021800

Susilawati, L., Iwai, N., Komatsu, K., and Arie, T. (2021). Antifungal activity of bacteria isolated from Japanese frog skin against plant pathogenic fungi. *Biol. Control* 153, 104498. doi: 10.1016/j.biocontrol.2020.104498

Tiwari, R., Garg, K., Senthil-Kumar, M., and Bisht, N. C. (2023). XLG2 and CORI3 function additively to regulate plant defense against the necrotrophic pathogen Sclerotinia sclerotiorum. *Plant J.* 117 (2), 616–631. doi: 10.1111/tpj.16518

Toral, L., Rodríguez, M., Béjar, V., and Sampedro, I. (2020). Crop Protection against Botrytis cinerea by Rhizhosphere Biological Control Agent Bacillus velezensis XT1. *Microorganisms* 8, 992. doi: 10.3390/microorganisms8070992

Trotel-Aziz, P., Couderchet, M., Biagianti, S., and Aziz, A. (2008). Characterization of new bacterial biocontrol agents Acinetobacter, Bacillus, Pantoea and Pseudomonas spp. mediating grapevine resistance against Botrytis cinerea. *Environ. Exp. Bot.* 64, 21–32. doi: 10.1016/j.envexpbot.2007.12.009

Tzipilevich, E., Russ, D., Dangl, J. L., and Benfey, P. N. (2021). Plant immune system activation is necessary for efficient root colonization by auxin-secreting beneficial bacteria. *Cell Host Microbe* 29, 1507–1520. e1504. doi: 10.1016/j.chom.2021.09.005

Vaahtera, L., Brosché, M., Wrzaczek, M., and Kangasjärvi, J. (2014). Specificity in ROS signaling and transcript signatures. *Antioxidants Redox Signaling* 21, 1422–1441. doi: 10.1089/ars.2013.5662

van de Mortel, J. E., de Vos, R. C., Dekkers, E., Pineda, A., Guillod, L., Bouwmeester, K., et al. (2012). Metabolic and transcriptomic changes induced in Arabidopsis by the rhizobacterium Pseudomonas fluorescens SS101. *Plant Physiol.* 160, 2173–2188. doi: 10.1104/pp.112.207324

Van der Ent, S., Van Wees, S. C. M., and Pieterse, C. M. J. (2009). Jasmonate signaling in plant interactions with resistance-inducing beneficial microbes. *Phytochemistry* 70, 1581–1588. doi: 10.1016/j.phytochem.2009.06.009

Varga, J. F., Bui-Marinos, M. P., and Katzenback, B. A. (2019). Frog skin innate immune defences: sensing and surviving pathogens. *Front. Immunol.*, 3128. doi: 10.3389/fimmu.2018.03128

Wang, H., Liu, R., You, M. P., Barbetti, M. J., and Chen, Y. (2021). Pathogen biocontrol using plant growth-promoting bacteria (PGPR): Role of bacterial diversity. *Microorganisms* 9, 1988. doi: 10.3390/microorganisms9091988

Wang, K., Sipilä, T. P., and Overmyer, K. (2016). The isolation and characterization of resident yeasts from the phylloplane of Arabidopsis thaliana. *Sci. Rep.* 6, 1–13. doi: 10.1038/srep39403

Wang, X., Zhou, X., Cai, Z., Guo, L., Chen, X., Chen, X., et al. (2020). A biocontrol strain of Pseudomonas aeruginosa CQ-40 promote growth and control Botrytis cinerea in tomato. *Pathogens* 10, 22. doi: 10.3390/pathogens10010022

Wójcikowska, B., and Gaj, M. D. (2017). Expression profiling of AUXIN RESPONSE FACTOR genes during somatic embryogenesis induction in Arabidopsis. *Plant Cell Reports 36*, 843–858. doi: 10.1007/s00299-017-2114-3

Xiong, J.-S., Zhu, H.-Y., Bai, Y.-B., Liu, H., and Cheng, Z.-M. (2018). RNA sequencing-based transcriptome analysis of mature strawberry fruit infected by necrotrophic fungal pathogen Botrytis cinerea. *Physiol. Mol. Plant Pathol.* 104, 77–85. doi: 10.1016/j.pmpp.2018.08.005

You, M. K., Shin, H. Y., Kim, Y. J., Ok, S. H., Cho, S. K., Jeung, J. U., et al. (2010). Novel bifunctional nucleases, OmBBD and AtBBD1, are involved in abscisic acid-mediated callose deposition in Arabidopsis. *Plant Physiol.* 152, 1015–1029. doi: 10.1104/pp.109.147645

Zamioudis, C., and Pieterse, C. M. (2012). Modulation of host immunity by beneficial microbes. *Mol. Plant-Microbe Interact.* 25, 139–150. doi: 10.1094/MPMI-06-11-0179

Zhang, Y., Liu, S., Wang, C., and Liao, X. (2019). Biocontrol potential of Acinetobacter johnsonii ZY86 against gray mold by Botrytis cinerea. *Int. J. Agric. Biol.* 22, 1467–1475. doi: 10.17957/IJAB/15.1223

frontiers | Frontiers in Plant Science

TYPE Original Research
PUBLISHED 23 April 2024
DOI 10.3389/fpls.2024.1394821

OPEN ACCESS

EDITED BY
Brigitte Mauch-Mani,
Université de Neuchâtel, Switzerland

REVIEWED BY
Alessandra Ferrandino,
University of Turin, Italy
Luca Nerva,
Council for Agricultural and Economics Research (CREA), Italy

*CORRESPONDENCE
Sophie Trouvelot
sophie.trouvelot@u-bourgogne.fr

†These authors have contributed equally to this work and share first authorship

RECEIVED 02 March 2024
ACCEPTED 02 April 2024
PUBLISHED 23 April 2024

CITATION
Moret F, Jacquens L, Larignon P, Clément G, Coppin C, Noirot E, Courty P-E, Fontaine F, Adrian M and Trouvelot S (2024) Physiological and developmental disturbances caused by Botryosphaeria dieback in the annual stems of grapevine.
Front. Plant Sci. 15:1394821.
doi: 10.3389/fpls.2024.1394821

Physiological and developmental disturbances caused by Botryosphaeria dieback in the annual stems of grapevine

Florian Moret[1†], Lucile Jacquens[1†], Philippe Larignon[2], Gilles Clément[3], Cindy Coppin[4], Elodie Noirot[1], Pierre-Emmanuel Courty[1], Florence Fontaine[4], Marielle Adrian[1] and Sophie Trouvelot[1*]

[1]Agroécologie, INRAE, Institut Agro, Univ. Bourgogne, Dijon, France, [2]IFV, Pôle Rhône-Méditerranée, Rodilhan, France, [3]Institut Jean-Pierre Bourgin, INRAE, AgroParisTech, CNRS, Université Paris-Saclay, Versailles, France, [4]Université de Reims Champagne-Ardenne, Unité Résistance Induite et Bioprotection des Plantes RIBP USC INRAE 1488, Reims, France

Botryosphaeria dieback is a grapevine trunk disease caused by fungi of the Botryosphaeriaceae family, which attacks more specifically the woody tissues. The infection leads to different symptoms including a severe form with a leaf drop as well as premature plant death. Botryosphaeria dieback causes major economic losses, since no effective treatment is yet available. A better understanding is necessary to find solutions to fight this disease. In this study, our objective was to characterize the "leaf drop" form by (1) looking for the presence of pathogens in the basal internodes of stems, (2) quantifying blocked vessels by tylosis and/or gummosis, and (3) describing the impact of the disease on vine physiology (gene expression and metabolome) and development (establishment and functioning of the cambium and phellogen) at the level of xylem and phloem of basal stem internodes. Our study has shown that Botryosphaeriaceae were present in both phloem and xylem of the basal internodes of the annual stem, with xylem vessels obturated. We have also clearly demonstrated that gene expression and metabolite profiles were strongly modified in both xylem and phloem of diseased plants. Differences in stems between healthy (control, C) and diseased (D) plants were low at flowering (vines not yet symptomatic), higher at the onset of symptom expression and still present, although less marked, at full disease expression. qRT-PCR analysis showed in both phloem and xylem an overexpression of genes involved in plant defense, and a repression of genes related to meristematic activity (i.e. vascular cambium and phellogen). Metabolomic analysis showed specific fingerprints in stems of healthy and diseased plants from the onset of symptom expression, with an increase of the level of phytoalexins and mannitol, and a decrease of 1-kestose one. At the structural level, many alterations were observed in internodes, even before the onset of symptoms: a classical obstruction of xylem vessels and, for the first time, a disorganization of the secondary phloem with an obstruction of the sieve plates by callose. The

disease modifies the development of both secondary phloem (liber) and phellogen. Altogether, this study combining different approaches allowed to highlight deep vine dysfunction in the internodes at the base of stems, that may explain vine decline due to Botryosphaeria dieback.

KEYWORDS

Vitis vinifera, grapevine trunk diseases, targeted genes, metabolomic, cytology

Introduction

Cultivated grapevine (*Vitis vinifera* L.) is an economically very important crop, covering 7.2 mha worldwide, with a grape and wine production of 79.4 mt and 262 mhl respectively, and an international wine trade (export) of about 37.6 billion euros (OIV (International Organisation of Vine and Wine), 2022). However, one major problem for winegrowers is the vine susceptibility to a wide range of fungal pathogens responsible for cryptogamic diseases. Some of them are specific of the plant aerial organs such as leaves and berries (i.e. mildews, bunch rots), others are localized into the roots (Armillaria) and, finally, some are able to attack the perennial parts of the wood. These latter correspond to a complex of xylem-inhabiting fungi responsible for grapevine trunk diseases (GTDs). GTDs are a group of various and complex diseases, which thus attack woody organs and often lead to plant death (Bertsch et al., 2013; Fontaine et al., 2016 for reviews). Although these diseases are not recent, they are considered as emerging since their incidence has increased significantly over the past decades (Bertsch et al., 2013). In this context, controlling GTDs is a significant challenge for the grape industry since they impact production, longevity of vines and more generally the economy of the production system. In Europe, some GTDs were traditionally controlled by sodium arsenite applications (Larignon, 2004; Bisson et al., 2006; Spinosi and Févotte, 2008), but its use was banned in France in 2001 regarding its carcinogenic activity (IARC (International Agency for Research on Cancer), 1987). To date, there are no effective and available control methods against GTDs and the lack of alternative strategies to fight them could exacerbate the situation.

Among GTDs, Botryosphaeria dieback, previously called black dead arm (Lehoczky, 1974) causes considerable damage in vineyards (Larignon, 2016; Guérin-Dubrana et al., 2019). Disease symptoms are characterized by stunted growth, cankers, wood necrosis, as well as cordon and cane dieback (Phillips, 1998; Van Niekerk et al., 2006; Savocchia et al., 2007; Mondello et al., 2018). In some cases, reduced bud burst has been reported (Castillo-Pando et al., 2001; Qiu et al., 2011; Wunderlich et al., 2011a). A severe form is characterized by a leaf drop associated to a poor cane maturation, a shriveling and drying of inflorescences or fruit clusters and a chronic form with leaf discoloration from the margin to the blade (Larignon et al., 2001). Typical foliar symptoms of the chronic form vary between white and red cultivars. White cultivars show yellowish-orange discolored spots on the margins of the leaves and the blade, whereas red cultivars present wine-red spots. Moreover, a cross-section in the trunk shows a yellowish-orange area at the edge of a characteristic brown stripe, limited at few millimeters in depth, where xylem vessels are clogged. The infection by the pathogens blocks xylem vessels by the formation of tylosis or gummosis, as well as by their physical presence (Bertsch et al., 2013). Finally, grey sectorial necrosis can be also observed in woody tissue (Larignon, 2012).

Botryosphaeria dieback is due to ascomycete fungi belonging to the family of Botryosphaeriaceae and capable of developing in the wood by producing necrosis or cankers (Wunderlich et al., 2011b; Dissanayake et al., 2016). They are well-known pathogens causing dieback in a wide range of plant hosts such as apples, pine trees and grapevines (Liu et al., 2012; Mehl et al., 2013). The importance and wide distribution of these fungi in different vineyards has been largely reported (Larignon et al., 2009; Bertsch et al., 2013; Yan et al., 2013). To date, more than 25 species of Botryosphaeriaceae have been associated with Botryosphaeria dieback in grapevine (Urbez-Torres, 2011; Berraf-Tebbal et al., 2014; Carlucci et al., 2015; Linaldeddu et al., 2015). Among them, two major species are found systematically, notably in France: *Diplodia seriata* (teleomorph *Botryosphaeria obtusa*; Shoemaker, 1964; Lehoczky, 1974; Cristinzio, 1978) and *Neofusicoccum parvum* (Pennycook and Samuels, 1985; teleomorph *Botryosphaeria parva*, Crous et al., 2006), as reported by Larignon et al. (2015). In diseased vines, those fungi have always been isolated from wood and could occasionally be isolated from other tissues such as diseased berries (Steel et al., 2007; Taylor and Wood, 2007; Wunderlich et al., 2011a).

Botryosphaeriaceae species are characterized by a latent phase, when they are present inside the plant as endophytes (Slippers et al., 2007) and by a pathogenic one, when they become virulent and actively colonize the wood (Leal et al., 2024). Due to high enzymatic activity (cell wall-degrading enzymes, especially cellulolytic ones) and toxin production, affected tissues die and local or entire vine drying can occur (Andolfi et al., 2011; Esteves et al., 2014; Claverie et al., 2020; Belair et al., 2023). Given that pathogens are always found in the wood but never in the leaves of infected plants, where typical symptoms occur, it has been also hypothesized that the leaf symptoms may result from extracellular compounds such as exopolysaccharides and proteins

(Martos et al., 2008; Bénard-Gellon et al., 2015) produced by fungi in the colonized woody tissues of the trunk. Those compounds, suggested as phytotoxic, would then be translocated to the leaves through the transpiration stream (Mugnai et al., 1999). Besides, some of the Botryosphaeriaceae toxins have been isolated and characterized (Andolfi et al., 2011 for review; Reveglia et al., 2019; Trotel-Aziz et al., 2022).

Infection of vines occurs mainly through pruning wounds, but also at the grafting point in nurseries (Chamberlain et al., 1964; Lehoczky, 1974; Hewitt, 1988; Lehoczky, 1988; Leavitt, 1990), through wounds caused during cultural practices such as disbudding (Molot et al., 2006; Epstein et al., 2008; Makatini, 2014) or from buds (Phillips, 1998; Epstein et al., 2008; Amponsah et al., 2012). However, it was recently shown that artificial infections of annual canes in greenhouse (Reis et al., 2016) and in field (Reis et al., 2019) by Botryosphaeria species lead to the development of necrosis and in some cases, the expression of foliar symptoms. An annual contamination of annual stems by some Botryosphaeriaceae species was hypothesized, resulting from foliar symptoms expression related to vessels obstruction or cambium dysfunction. In our study, our objectives were to better understand the triggering and expression of grapevine severe form of Botryosphaeria dieback in vineyard. Three biological questions were thus asked (1) is the expression of leaf symptoms (leaf drop) conditioned by the presence of pathogens in the annual stems; (2) is there a link between the quantity of blocked vessels (tylosis/gummosis) and the expression of leaf symptoms, and (3) what are the repercussions of such dieback on vine physiology (gene expression and metabolome) and development (establishment and functioning of the cambium and phellogen) at the stem internode level. A transdisciplinary study was thus conducted in a naturally infected vineyard and with different approaches, especially at molecular, cellular and anatomical levels.

Materials and methods

Experimental plot

The experiments were performed on grapevine shoots collected in a plot of the EPLEFPA Nîmes-Rodilhan located at Rodilhan (France, GPS coords: latitude 43.829685, longitude 4.450104), in the Costières de Nîmes vineyard. It was planted in 2005 with *Vitis vinifera* cv. Cabernet Franc grafted onto R110 rootstock at a density of 4444 vines/ha, the vines are trained to in bilateral cordon. The soil is clay-limestone type with rolled stones and vines were not irrigated. Climatic data (temperatures and rainfall) collected between 2010 and 2021 are given in Supplementary File 1.

Evaluation of the Botryosphaeria dieback severity in the studied plot

Monitoring and mapping of the expression of the Botryosphaeria dieback have been carried out for each grapevine of the plot since august 2016, and weekly, from flowering to the end of symptom appearance in 2017, 2018 and 2019.

Sampling for Botryosphaeria isolation by Pasteurian method

In 2018, stems of asymptomatic (control, C) and symptomatic (severe form, D) vines of Botryosphaeriaceae dieback were collected at six different stages: inflorescences visible, flowering, cluster closure, veraison, maturity, leaf fall (Supplementary Figure 1). For each stage, new vines (C and D) were sampled. Thirty stems of 30 to 40 cm length were collected per stage, randomly from the plot, and 40 fragments per stem were cut from the three first basal internodes to be analyzed. In this approach, 20 fragments became from internodes 1 and 2 (in mix) and 20 others became from the 3rd internode.

Sampling for cytological and molecular analysis

In 2018, stems of asymptomatic (control, C) and symptomatic (severe form, D) vines of Botryosphaeriaceae dieback were collected at three different stages: flowering (T1: pre-symptomatic stage), cluster closure (T2: early expression of symptoms) and late veraison (T3: severe symptomatic stage with leaf drop; Supplementary Figure 1). At flowering stage, no symptoms were observed leading to sample D stems on vines expressing disease in 2017. For each stage, 5 new vines (C and D) were sampled. For each of the five vines selected for both modalities C and D, two stems were sampled: one for the anatomical characterization (type A) and the second (type B) for molecular analyses (Supplementary Figure 1).

Sampling for macroscopic and microscopic analyzes

Stems of type A, without inflorescences, clusters and leaves were stored at 4°C. Then, samples were taken from the first three basal internodes for macroscopic and microscopic observations of vascular tissues.

Sampling for gene and metabolomic analyzes

Pieces of internodes 1, 2 and 3 (number 1 being closest to the base) were sectioned from stems of type B. The xylem area was detached from the phloem/bark (thereafter called “Xylem” or “X” and “Phloem”, “P” or “bark”, respectively) part, individually snap-frozen and then stored at -80°C. As small quantities of tissues were sampled by internode, we mixed tissues from the same internode of the five sampled vines. Each sample was ground in liquid nitrogen using a ball mill (Retsch MM400) and divided in two sub-samples: one for molecular analyzes (PCR and qRT-PCR), and one for metabolic analysis (GC-MS).

Detection of Botryosphaeria pathogens

Pasteurian analysis: pathogen isolation and colony discrimination

Stems of three first internodes from the five asymptomatic and symptomatic plants were sampled at 6 stages. Four pieces of

approximately 3x1x1 mm in size from each internode were placed in Petri dishes containing malt agar medium (15 gL^{-1} cristomalt, 20 gL^{-1} agar, 200 mgL^{-1} of chloramphenicol) and incubated in the dark at room temperature (Larignon and Dubos, 1997). Xylem and bark were weekly observed and pictures were acquired (Canon Power Shot G7) for 4 weeks for visual examination. The color, the hyphal and pycnidiospore morphology, and the aerial mycelium of the colony were examined under light microscope (Larignon et al., 2001).

Molecular identification: DNA extraction and PCR tests

The genomic DNA was extracted from molecular analyses sample powder of X and P tissues, by following the extraction protocol of Mundy et al. (2018). The genomic DNA of X and P samples was extracted using the DNeasy Plant Mini kit (Qiagen, Hilden, Germany). The quality of DNA was checked by agarose gel electrophoresis and the quantity was determined by measuring the absorbance at 260 nm.

Amplicons were generated by PCR using the Phusion High-Fidelity DNA polymerase, 20 ng of DNA, and the primers ITS1-F and ITS4, as described by White et al. (1990) and Udayanga et al. (2012) (Supplementary Table 1). A nested PCR was performed taking 5 µL of the 1:100 diluted PCR1 template and using primers BOT100F and BOT472R, as described by Ridgway et al. (2011) (Supplementary Table 1).

Macroscopic observation and image analysis obstruction of xylem vessels

Macroscopic observation and image acquisition

From the collected internodes 1, 2 and 3, cross sections were performed and observed under a macroscope (ZEISS, AXIOZoom.V16). Two images were acquired using the "SNAP" command (ZEN2.3 system software); one with samples exposed to white light (RGB experiment settings), and one with samples exposed to blue light only (DAPI experiment settings, excitation 365 nm, emission 445-450 nm).

Image analysis to estimate the percentage of xylem vessels obstructed

A semi-automatic analysis was performed to establish the proportion of obstructed vessels among the total number of vessels. First, the total number of vessels (both obstructed or not obstructed) was counted automatically with an ImageJ macro. The image acquired with DAPI settings was processed with ImageJ 1.52 software with the Fiji package. Images were contrasted manually, then an automatic threshold was created (Auto Local Threshold parameter: method Phansalkar), thus converting the picture in either black or white pixels, without grey shades. Then using the "Analyze particles" setting, the total number of vessels was assessed (parameters: size: 35-1000; circularity: 0.35-1.00). The number of obstructed vessels was assessed manually on the RGB image using the multi-point count tool from the Fiji package.

The ratio of obstruction was calculated as follows:

$$(Number\ of\ obstructed\ vessels / Total\ number\ of\ vessels) * 100$$

RNA extraction and real-time qRT-PCR analysis

RNA extraction

Total RNA was isolated from 3 x 100 mg of X and P powder using the PureLink Plant RNA Purification Reagent (Invitrogen, Cergy Pontoise, France). The manufacter's protocol was followed until the phase of separation with the chloroform: isoamylic alcohol (24:1). Then, one volume of ethanol 70% was added to the aqueous solution, before purification using the NucleoSpin RNA kit (Macherey-Nagel, Düren, Germany). The quality of RNA was checked by agarose gel electrophoresis and the quantity was determined by measuring the absorbance at 260 nm for each sample and adjusted to 100 ng µL-1. First-strand cDNA was synthetized from 150 ng of total RNA using the Verso cDNA Synthesis kit (Thermo Fisher Scientific, Inc., Waltham, MA, United States).

Real-time qRT-PCR

Real-time polymerase reaction (PCR) was performed using Absolute Blue qPCR SYBR Green (Thermo Fisher Scientific, Waltham, MA, USA), in a CFX96 real-time PCR detection system (Bio-Rad, Hercules, CA, USA). The thermal profile was 10 s at 95°C (denaturation) and 45 s at 60°C (annealing/extension) for 40 cycles. The specificity of PCR amplification was checked using a heat dissociation curve from 65 to 95°C following the final cycle. For each experiment, PCR reactions were performed in duplicate. Expression of two reference genes (*EF1-α* and *60SRP*) and of genes encoding enzymes involved in the sucrose metabolism and signalization (*αAMY*, *βAMY*, *CWINV* and *SUC27*), the plant defense responses (*Cal-S7*, *GLU*, *GST5*, *PAL*, *POX4*, *PR6*, *STS*, *TL* and *WAT1*), detoxification and stress tolerance (*epoxH2* and *SOD*), vascular cambium (*CDKB2*, *ERF5*, *MOL* and *WOX4*) and cork cambium (*APL*, *EBP1*, *HA3*, *SHR*, *PSKR1* and *PSKR2*) was tracked by quantitative reverse transcription-PCR (qRT-PCR) using the primers listed in Supplementary Table 2.

Metabolic analysis (GC-MS)

GC-MS analyses were performed from 50 mg of X and P powder (Moret et al., 2019). Briefly, samples were extracted for 10 min at 4°C with shaking in 1 mL of water:acetonitrile:isopropanol (2:3:3) and ribitol 4 µg/mL. After centrifugation (20,000 g, 5 min), 100 µl supernatant were collected and dried for 5 h in a SpeedVac vacuum centrifuge. Samples were derivatized as described in Krzyżaniak et al. (2018) and analyzed using an Agilent 7890A gas chromatograph coupled to an Agilent 5975C mass spectrometer. A Quality Control (QC) made of all samples merged together was injected 3 times and was used as a standard to evaluate the quality of the analysis.

Microscopic observation of bark and xylem tissues

Segments (2 by 5 mm) were randomly excised from the same C and D stems used for macroscopic analyses.

After inclusion in paraffin and aniline blue staining

The samples were fixed into a fresh mixture of 4% paraformaldehyde in potassium phosphate buffer (PBS 10mM, pH 7.4, with addition of tween 20 1‰ only in the first 1 h bath) and then embedded in paraffin (Colas et al., 2010). Wax sections at 10 µm thickness were obtained using a microtome and deposited on silanized slides. The samples were then dewaxed by 2 Q Path® Safesolv baths (20 min each at room temperature), gently rinsed with a pipette in ethanol 90° (1 min at room temperature) and then gradually rehydrated; deposits of drops of ethanol 70°, 50° and 25° were gradually made and each was left for 1 min in contact with the sections. Finally, ultra-pure water was put in contact on the slide during 2 min in order to completely rehydrate the sample.

Aniline blue staining (1% in 3% acetic acid) was carried out by leaving the drop of dye 30 s on the samples, then rinsing once 10 s with 3% acetic acid and then twice 10 s with ultra-pure water in order to remove excess dye. Finally, the samples were observed under a bright-field light microscope (Leitz DM RB, Leica), and images were acquired using a camera (Nikon Digital Sight), with respect of the same shooting parameters for each observed sample.

After inclusion in Epon resin and toluidine blue staining

The samples were fixed immediately in 2.5% glutaraldehyde (in 0.1 M sodium- phosphate buffer, pH 7.2, 1% sucrose, 1 ‰ Tween 20) for 20 to 25 min under vacuum, then overnight at 4°C with gentle rotation (without Tween 20). Samples were washed twice (10 min) in the same buffer and postfixed in 1% osmium tetroxide (OsO_4) in the same buffer for 1 h at 4°C. Then, samples were washed in phosphate buffer, dehydrated in a graded ethanol series, and treated with propylene oxide. Dehydrated samples were subsequently embedded in Epon (Merck, Darmstadt, Germany) and sectioned using a Reichert Ultracut E microtome (Leica, Reuil-Malmaison, France) with glass or diamond knives (Diatome, Bienne, Switzerland). Semithin (0.5 µm) sections from the tissue blocks were stained with 1% aqueous toluidine blue (in 1% sodium tetraborate) and examined under a bright-field light microscope (Leitz DM RB, Leica) in order to observe anatomical characteristics of both bark and xylem.

Data processing and statistical analysis

Anatomical studies

Data analysis were carried out using Past 4.08 software. A Chi-square (X^2) test of homogeneity was used to compare the distribution of obstructed to non-obstructed vessels in shoot of asymptomatic and symptomatic stems. Moreover, a Kruskal Wallis test ($p<0.05$) was used to analyze and compare the proportions of obstructed vessels between internodes and sampling period.

Expression of genes

For each gene and for each modality, a mean Cq value was obtained. Relative gene expression (RE) was determined with the 2-ΔΔCq method using CFX Manager 3.0 software. For every sample, ΔΔCq was the ΔCq difference between 2 samples (diseased *vs* control). These values were used to generate a gene expression heat map through Past 4.08 software. Hierarchical clustering (ward's method, Euclidian distance) was applied to group samples with similar expression level.

Metabolomic studies

GC-MS data were processed as described in Moret et al. (2020). Briefly, Data files in NetCDF format were analyzed with AMDIS software. A home retention indices/mass spectra library and standard compounds were used for metabolite identification. Peak areas were determined with the Targetlynx software (Waters). AMDIS, Target Lynx in splitless and split 30 mode data were compiled into a single Excel file for comparison and peak areas were normalized to ribitol and fresh weight. GC-MS data were then pre-processed and filtered RSD (relative standard deviation) on QC samples was calculated for each compound. Only features with RSD > 30% and non-aberrant QC were conserved for further analysis. Missing values were replaced by half the lowest value, corresponding to limit detection of the method. PCA (Principal Component Analysis) and PLS (Partial Least Square) analyses were made on the processed data. Mean, fold change and two-sided Student's T-test p-value ($p<0.05$) were calculated and compiled into a data frame that was used for the Volcano plots (Goodacre et al., 2007; Vinaixa et al., 2012; Worley and Powers, 2013; Schiffman et al., 2019). Significant compounds highlighted by Volcano plots (T-test $p<0.05$) were verified and compounds with aberrant concentrations across samples were removed.

Results

Health status of vines

The results of the monitoring of diseased vines within the plot are displayed in Table 1. During the 4 years of monitoring, the dead/absent/complant vines number increased significantly from 4% to 18%. From 2017 (7.65%) to 2018 (10.84%) it was 1.4-fold that is lower compared to other years (2016-2017: 1.87-fold; 2018-2019: 1.72-fold).

TABLE 1 Sanitary situation of the plot during the different vintages.

% vines	2016	2017	2018	2019
Dead/absent/complant	4,08	7,65	10,84	18,27
Eutypa dieback	nd	1,17	1,79	2,63
Apoplexy	0,61	0,39	0,61	0,39
Botryosphaeria dieback	6,37	14,36	9,33	4,64
Unproductive vines	11,06	23,58	22,57	25,92

Eutypa dieback occurrence increased from 1.17 to 2.63% from 2017 to 2019. Apoplexy occurrence was low, of about 0.5% from 2016 to 2019. Botryosphaeria dieback occurrence increased from 6.37% in 2016 to 14.36% in 2017, and then decreases from 9.33% in 2018 to 4.64% in 2019. Therefore, the foliar expression in 2018 was considered as moderate when comparing with 2016, 2017 and 2019.

Botryosphaeriaceae fungi could be detected in the three basal internodes in both bark (phloem) and xylem tissues

Botryosphaeriaceae fungi are isolated both in the bark and the xylem

Table 2 summarizes the analysis of 1200 fragments of either bark or xylem. In 2018, Botryosphaeriaceae were isolated whatever the sampling time, with a maximum detection at maturity in both phloem (bark) and xylem. Botryosphaeriaceae isolates were more abundant from bark samples than from xylem samples (i.e., 14 times more at the "inflorescences visible" stage). The number of isolates was similar in both tissues at flowering stage, but two times more abundant in the bark than in the xylem at maturity stage.

Botryosphaeriaceae fungi are detected by PCR in phloem and xylem tissues of internodes of control and diseased vines

Botryosphaeriaceae were present in both control (C) and diseased (D) vines, in both phloem (P) and xylem (X), whatever the internode (1, 2 and 3) and the sampling period (Table 3). The detection of Botryosphaeriaceae is less frequent at T3 (late veraison stage; 6 out of 12 samples) than at T1 (flowering; 10 out of 12 samples) and T2 (cluster closure; 11 samples out of 12).

The quantity of blocked vessels and the foliar disease expression are not related to the grouped or localized repartition of the obstructed vessels

In diseased vines, a higher obstruction ratio was observed in the three internodes (Figures 1A–C) for the three sampling periods (Figures 1D–F) in comparison to control plants. For a same internode, the obstruction percentages were significantly higher at the late symptomatic stage (Figures 1A–C, T3_D samples) than at the pre-symptomatic one (Figures 1A–C, T1_D samples) for diseased vines only. For each sampling time, there was no significant difference among internodes (Figures 1D,E), except for the internodes 2 and 3 that were significantly less obstructed than the internode 1 at the late symptomatic stage (Figure 1F, D_2 and D_3 *vs* D_1 samples).

The image analysis of the spatial distribution of obstructed vessels in the circumference of the internode revealed a random distribution in each cane whatever the stage (pre-symptomatic or symptomatic stage; Figure 2 and Supplementary Figure 2).

TABLE 2 Percentage of vine fragments in which Botryosphaeria were isolated in 2018 from the bark and xylem tissues" of stems.

	Bark (phloem)	Xylem
Inflorescences visible	1.17	0.08
Flowering	0.41	0.5
Cluster closure	1	1.25
Veraison	5.41	0.67
Harvest Maturity	6.42	2.58
Leaf fall	4.92	1.33

Botryosphaeria dieback impacts grapevine stems before the onset of leaf symptoms

Modification of gene expression is enhanced by the appearance of foliar symptoms

In xylem (X) and phloem (P), targeted genes on sucrose metabolism and signalization, plant defense response and detoxification process, and secondary meristems were studied on the 3 internodes before and during the expression of foliar symptoms. A hierarchical clustering (heatmap) was made in order to group samples, in P or X tissues, with similar expression levels (Figure 3). Regardless of the tissue observed (P or X), the samples from times T1, T2 and T3 were clearly separated. Overall and regardless of the plant tissue, defense genes such as *TL*, *PR6*, *GLU* and *STS* were among the most up-regulated, followed by genes related to detoxification (*GST5*) and to the degradation of storage or transit sugars (*αAMY* and *CWINV*).

Even if the most regulations (up and down) were observed for the time T2 (start of appearance of symptoms), it is interestingly to note that regulations (up and down) were also detected before the expression of leaf symptoms (T1; Figure 3, light grey). At this stage, genes related to carbohydrate metabolism (*aAMY* and *CWINV*) and defense responses (*GLU, PR6, GTS5, POX4, STS* and *TL*) were up-regulated in both X and P tissues. Moreover, the *Cal-S7* gene was up-regulated in P tissues (Figure 3A) and down-regulated in X tissues (Figure 3B). At T1, no gene modifications related to the formation of the secondary meristem were detected except for *APL*, repressed in X tissues. At the early symptomatic stage (emergence of symptoms at T2), the expression of the majority of targeted genes was modified in X and P tissues of D vines (Figure 3). A down-regulation of genes associated to the cambium (*WOX4, CDKB2* and *MOL*), the phellogen (*APL* and *SHR*) and sucrose signalization (*SUC27*), and an up-regulation of genes associated to carbohydrates (*aAMY, βAMY* and *CWINV*), plant defense (*GLU, PR6, GTS5, STS, PAL* and *TL*) and phellogen (*HA3*, and *PSKR2*) were observed (Figure 3, medium grey). Changes at the late symptomatic stage (T3) were similar to changes at T2, except for genes involved in the formation of secondary meristems and showing less changes (Figure 3, dark grey).

Changes of the grapevine metabolome is tissue- and time-specific with Botryosphaeria dieback

Hierarchical Cluster Analysis (HCA) analysis performed on the whole sample set allows to clearly separate the phloem (P) and

10.3389/fpls.2024.1394821

TABLE 3 PCR detection of fungi and Botryosphaeriaceae ("Botryo") according to internode and tissue (P: phloem; X: xylem) levels and sampling times (T1, from pre-symptomatic stems; T2 and T3 from symptomatic ones).

			T1		T2		T3	
	tissue	internode	Fungi	Botryo	Fungi	Botryo	Fungi	Botryo
C	P	1	✓	✓	✓	✓	✓	✓
		2	✓	✓	✓	✓	✓	✓
		3	✓	✓	✓	✓	✓	✓
	X	1	✓	✓	✓	✓	✓	✓
		2	✓	✓	✓	✓	✓	–
		3	✓	✓	✓	✓	✓	–
D	P	1	✓	–	✓	✓	✓	–
		2	✓	✓	✓	✓	✓	–
		3	✓	✓	✓	✓	✓	–
	X	1	✓	✓	✓	✓	✓	✓
		2	✓	✓	✓	✓	✓	–
		3	✓	–	✓	–	✓	✓

Minus indicates that fungi were not detected, whereas the symbol "✓" indicates that a PCR amplicon was obtained at the expected size.

xylem (X) samples in two clusters (Supplementary Figure 3). PCA analyses were therefore performed on GC-MS data of each tissue (Figure 4). Samples were separated depending on time (PC1, 32.2%), and to a lesser extent depending on health state (PC2, 25.7%). For both tissues, at time T1 (before symptom expression), there is no separation of C and D samples (red and green ellipses, respectively), suggesting a similar metabolic profile. At T2 and T3, all groups are different and different from T1, indicating that their metabolic profile evolves over time with disease expression. For both tissues, variability is low whatever the modality and the sampling time.

Volcano plants represent the distribution of compounds for which the concentration is significantly different in X and P tissues between C and D samples (Figure 5, Supplementary Tables 3, 4). The number of compounds differentially accumulated in P and X tissues is of 1 and 0 for P and X, respectively at T1, of 42 and 39 for P and X, respectively, at T2, and of 22 and 27 for P and X, respectively, at T3. At T1, glycosylsalicylate was less than two-times more accumulated in P tissues of D plants than in P tissues of C plants. At T2, there was two-times more compounds accumulated in samples from D plants than in samples from C plants. In P tissues, 1-kestose, digalactosylglycerol and threonate were more accumulated in tissues from C plants than from D plants, and mannitol, *trans*- and *cis*-resveratrol and leucine were more accumulated in tissues from D plants than from C plants (Supplementary Table 3). In X tissues, 1-kestose and galactinol were more accumulated in tissues from C plants than from D plants, and *trans*- and *cis*-resveratrol, mannitol and piceid were more accumulated in tissues from D plants than from C plants (Supplementary Table 4). At T3, there was more compounds accumulated in tissues from D plants than from C plants. In P tissues, 1-kestose, threonate and phenylalanine were more accumulated in tissues from C plants than from D plants, and glutamine and isoleucine were more accumulated in tissues from D plants than from C plants (Supplementary Table 3). In X tissues, raffinose, digalactosylglycerol and 1-kestose were more accumulated in tissues from C plants than from D plants, and *trans*- and *cis*-resveratrol, and piceid were more accumulated in tissues from D plants than from C plants (Supplementary Table 4). The concentration of 1-kestose was determined in all samples as significantly accumulated in tissues from C samples (Figure 6). At T1, the concentration of 1-kestose was similar in X and P tissues from C and D samples (C/D ratio from 0.8 to 1, and from 1 and 1.9 in P and X tissues, respectively). At T2, the concentration sharply decreased in X and P tissues from D plants (not detected in internode 1 of P). At T3, the concentration increased (except in X of internode 3: not detected) in X and P tissues, without reaching T1 values (C/D ratio from 4.6 to 7.5, and from 4.1 to 5.1 in P and X tissues, respectively).

Botryosphaeria dieback strongly affects the anatomy of bark and xylem tissues

A similar pattern was observed in all internodes from D samples, revealing deep tissue disorganization from pre-symptomatic vines to the full expression phase.

Annual stems present deep alterations in phloem, xylem and secondary meristems establishment and/or functioning

At T1, the herbaceous stems were collected before the onset of leaf symptom expression (Figure 7).

Regarding its anatomy, the overall view of the C sample (Figure 7A) has a characteristic structure of the Euvitis section of Vitis genus (Metcalfe and Chalk, 1950; Esau, 1965). The secondary

10.3389/fpls.2024.1394821

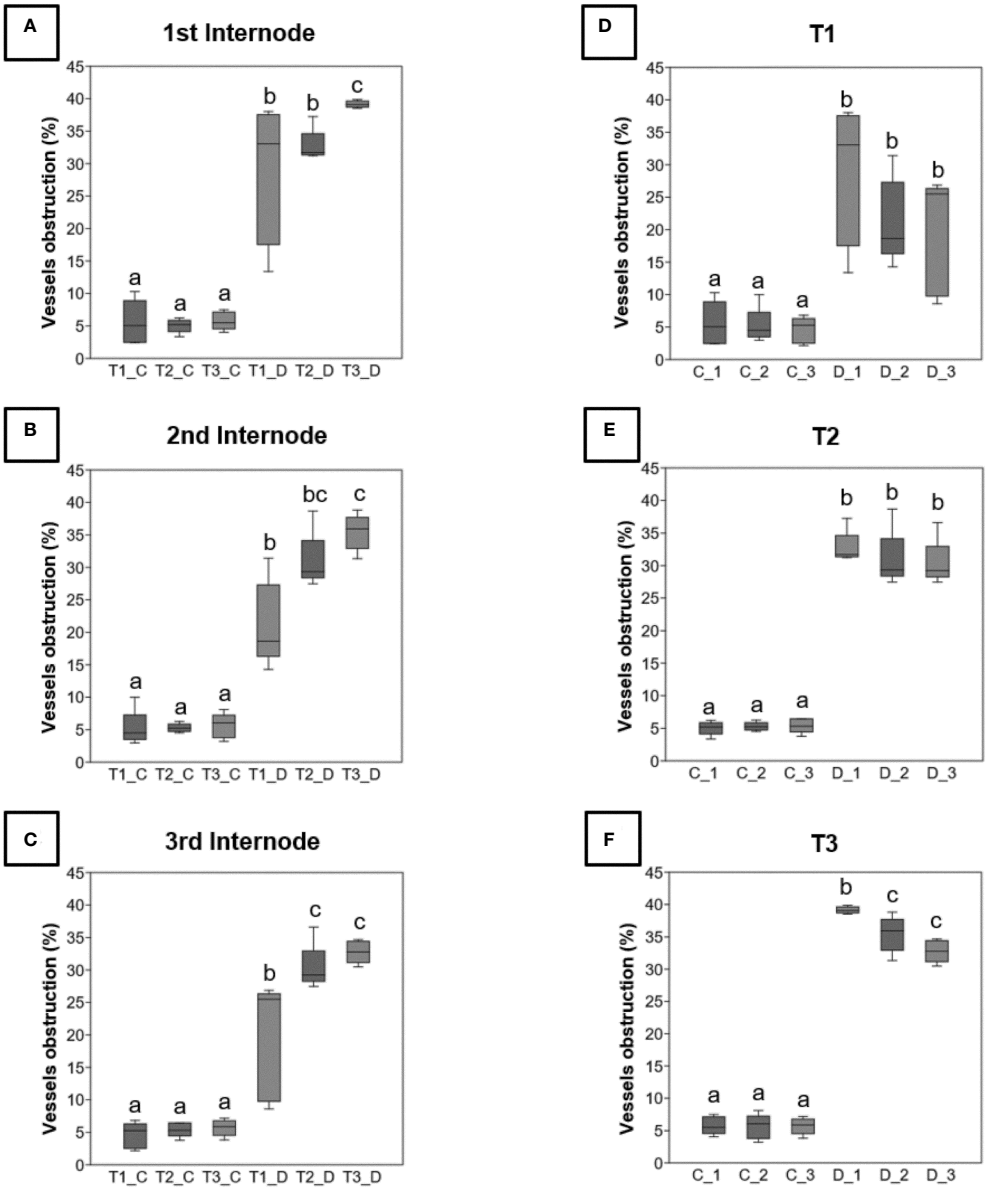

FIGURE 1
Rate of obstruction of xylem vessels detected by analysis of images acquired from sections of 3 internodes (_1, _2 and _3) taken from control **(C)** or diseased **(D)** stems for the three times of sampling (T1, T2 and T3). These rates are expressed as a percentage and were evaluated on the three levels of internodes **(A-C)**, and at the three sampling times **(D-F)**. Differences between control and diseased for each time were statistically significant ($p<10^{-6}$, chi square test) and differences between internodes were noted in figure by letters ($p<0.05$, Kruskal-Wallis test).

phloem appears in blocks separated from another one by wide rays (Figure 7A, r). Within the blocks, tangential strata of sieve elements (Figure 7A, s) with associated companion cells alternate with tangential bands of fibers (Figure 7A, fi). Separating the secondary P from the secondary X, the presence of the vascular cambium is clearly observed (Figure 7A, ca). At the level of the secondary P (Figure 7B), the sieve tubes and their companion cells are distinguished, indicating that this tissue is functional in the transport of the elaborate sap. Moreover, functional sieve plates can also be observed (Figure 7C, arrow). The secondary X presents functional, unobstructed vessels (Figures 7A, D), and many amyloplasts could be observed in parenchyma rays (Figure 7D, arrow).

In the stems sampled on declining vines (pre-symptomatic), clear anatomical alterations were observed in both secondary P and X (Figure 7E). In the secondary P, even if the layers of fibers appear conform to what is observed in C samples, vascular cells are disorganized. Indeed, in some areas the sieve plates appeared blocked by a material more or less intensely stained with toluidine blue (Figures 7F, G, arrows). In the meantime, the P vascular cells appeared collapsed in some layers, crushed and therefore non-functional (Figure 7G). Finally, in the secondary X some vessels were obstructed by the presence of tylosis (Figures 7E, H). It clearly also appeared that, unlike C samples, the parenchyma rays were empty of any amyloplast (Figure 7H, arrow).

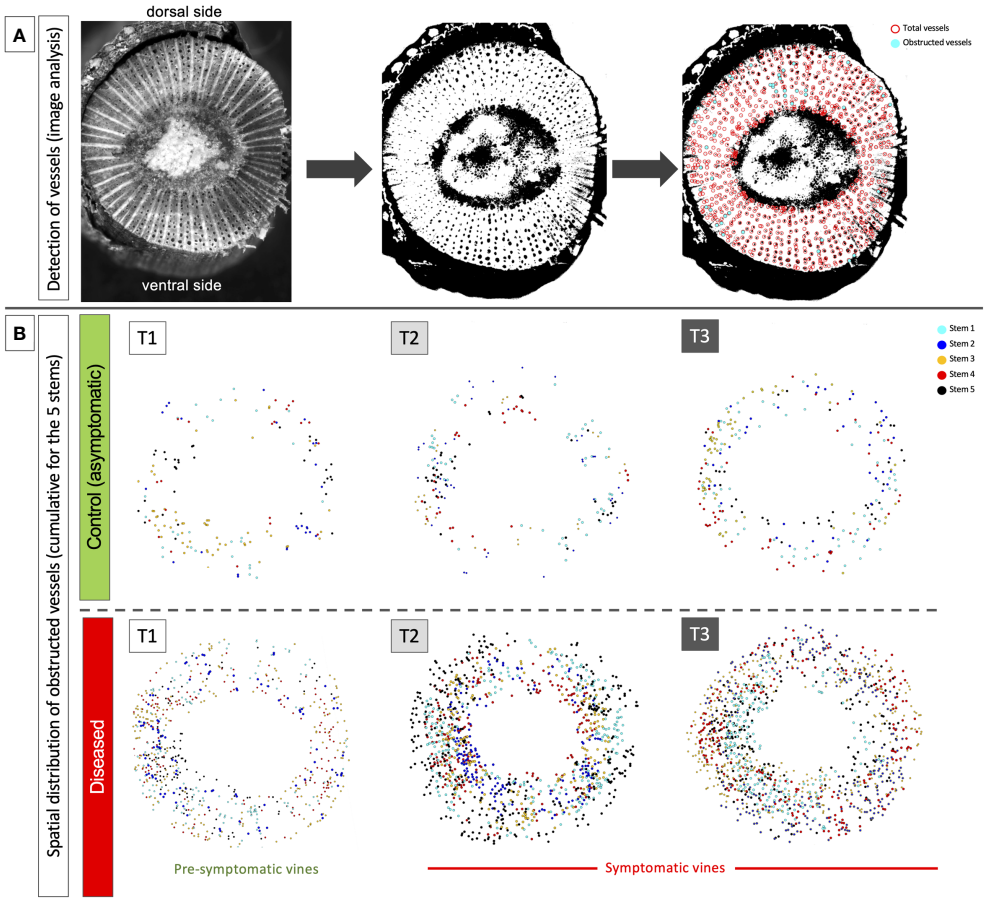

FIGURE 2
Example of results acquired by image analysis in the second internode of the stems. **(A)** illustration of the process carried out from image acquisition, contrast/thresholding and semi-automatic detection of total (in red) and obstructed vessels (in cyan). **(B)** illustration of the temporal and spatial cumulative distribution (stems 1 to 5) of obstructed vessels at the circumference of the stems and along the dorsal/ventral and lateral axes. The results were presented for the three sampling times: T1 (pre-symptomatic), T2 (appearance of the first symptoms) and T3 (leaf drop). Each layer obtained for each stem taken in a same modality **(C** or **D)** presents a different color: cyan for stem 1, blue for stem 2, orange for stem 3, red for stem 4 and black for stem 5.

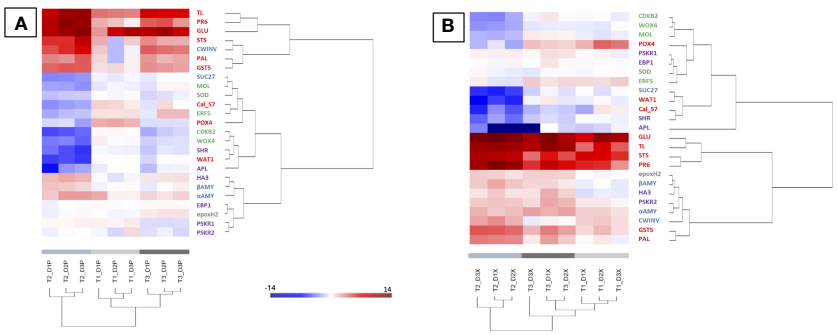

FIGURE 3
Heatmap generated from qPCR gene expression analysis in diseased vine stems compared to control one. Expression of 25 genes related to plant defense (in red), detoxification and stress tolerance (in grey), sucrose metabolism and signalization (in blue), or cambial (in green) and phellogen (in purple) activity was assessed in phloem **(A)** and xylem **(B)** tissues. Hierarchical clustering (ward's method, Euclidean distance) was applied to group samples with similar expression levels, emphasizing the overall changed expression during pre-symptomatic (T1, light grey) and symptomatic (T2, medium grey and T3, dark grey) stages. The color intensity indicates expression levels; red: up-regulation, blue: down-regulation.

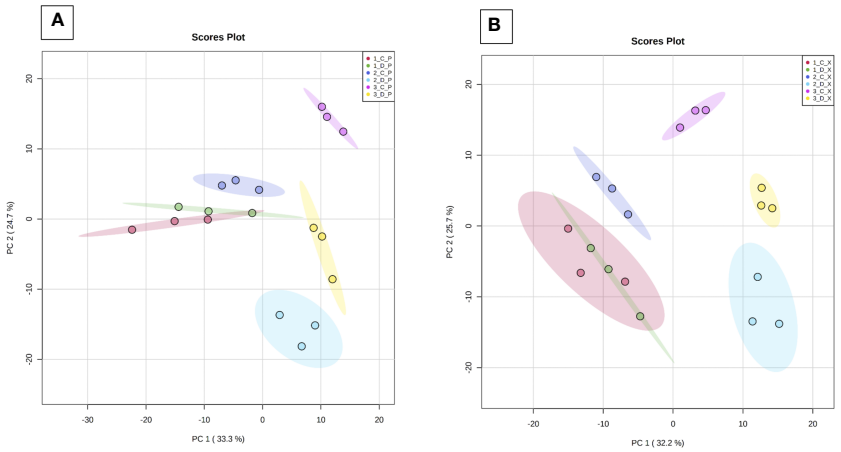

FIGURE 4
Principal component analysis (PCA) of GC-MS data. Analyses were performed from phloem (Panel **A**) and xylem (Panel **B**) extracts of the three basal internodes of control and diseased stems. Samples were collected at T1 (before symptom expression), T2 (onset of symptom expression) and T3 (full symptom expression). 1 to 3: sampling time (T1, T2, T3), C/D (control/diseased), P: phloem and X: xylem. PC1: Time of sample collection; PC2: health state.

At T2 and in normal development (C plants, Figure 8.1), the stem will transform from an immature state with a green cortex (herbaceous stage), to a stem with collapsed and brownish epidermis created by the developing periderm from an active phellogen (the cork cambium, a lateral meristem that creates the periderm). Indeed, on the 5 C stems taken, all had a periderm (data not shown). Structural observations of C stem (Figure 8A) revealed that the initial periderm is formed, normally, within the secondary phloem (Figure 8A). Periderm is the secondary protective tissue that replaced the epidermis. It consisted of phellem (cork), phellogen (cork cambium) and only few layers of phelloderm (Esau, 1948). Under the periderm, we observed the same tissues as those described previously with the secondary phloem, separated from the secondary X by the vascular cambium (Figure 8A, ca). As

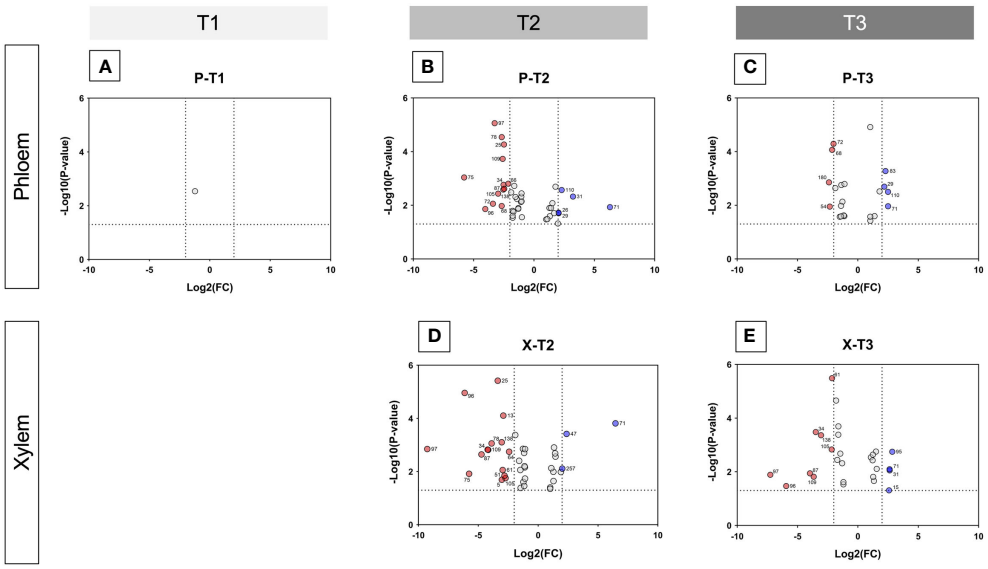

FIGURE 5
Volcano plots showing metabolite variations in internodes. For each metabolite, fold change (C/D) and Student's T test p-value were calculated between C and D samples (C control, D diseased) for both xylem and phloem tissues of the three internodes of the base of stems, and for T1 (before symptom expression), T2 (onset of symptom expression) and T3 (full symptom expression) sampling times. The results are displayed on a Volcano plot, with p< 0,05 and FC > 2 thresholds. Each metabolite is displayed by a point and corresponds to (i) p-value< 0.05 and FC > 2 (in red and blue), (ii) p-value< 0.05 and FC< 2 (in grey). Metabolites that were significant and validated the fold change threshold are annotated on the plot with their ID number. In red: metabolites in higher concentration in D than in C tissues; in blue: metabolites in higher concentration in C than in D tissues. **(A, B)**: Volcano plots for xylem samples collected at T2 (onset of symptom expression) and T3 (full symptom expression), respectively. **(C-E)** Volcano plots for phloem samples collected at T1 (before symptom expression), T2 (onset of symptom expression) and T3 (full symptom expression), respectively.

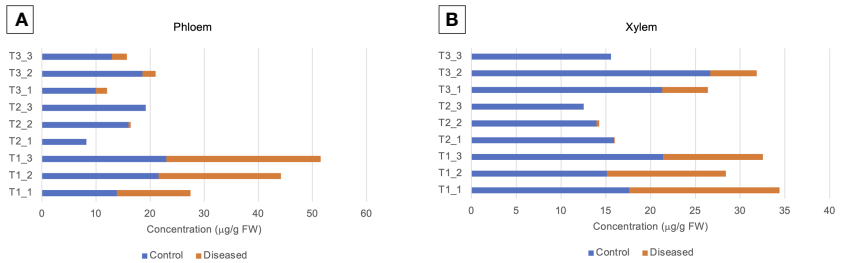

FIGURE 6
Level of 1-kestose (µg/g FW) in **(A)** phloem and **(B)** xylem samples.1-kestose was analyzed by GC-MS. Phloem (P) and xylem (X) tissues were obtained from samples collected before symptom expression ("1"), at the onset of symptom expression ("2") and at full symptom expression ("3"). Samples were obtained from control (C) and diseased (D) internodes 1, 2, 3 located at the base of stems.

for the previous sampling time, the secondary phloem appears functional (Figure 8B), with the presence of sieve tubes and unobstructed sieve plates separating neighboring vascular elements (Figure 8C, arrow). In addition, the xylem also appears to be functional (Figure 8D), with the presence of empty, unobstructed vessels and a large number of amyloplasts in the parenchymal rays (Figure 8E, arrow), suggesting an efficient starch storage.

In D vines, periderm development was complete for two canes, incomplete for one and not differentiated for two (data not shown). As example, green islands found on the stem of a D cane (Figure 8.2) consist on an incomplete periderm formation and subsequent uneven cane maturation. At the structural level, we therefore observed a defect in the placement of the phellogen, reflected by the absence of this meristem at the level of the outermost secondary phloem layers (Figure 8F). Moreover, as at

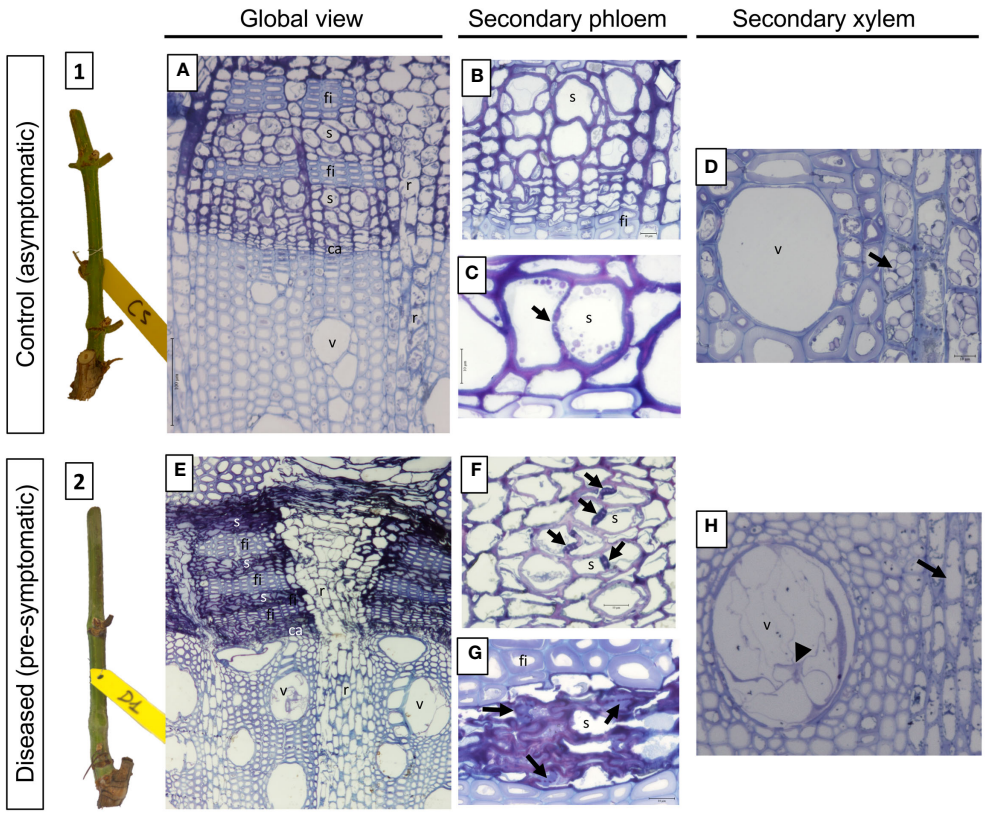

FIGURE 7
Phenotypic and structural observations of grapevine stems harvested at T1 (pre-symptomatic stage) from control (1, **A-D**) or diseased (2, **E-H**) plants. A representative picture of the phenotype of the stems sampled is given in illustrations 1 (control) and 2 (pre-symptomatic). The observation of semi-thin sections stained with toluidine blue also allows the comparison of the anatomical structure of the stems. Thus, a global view is given in A (control) and B (diseased), while focuses are made on the secondary vascular tissues that are the phloem (B and C: control; F and G: diseased) and the xylem (D: control; H: diseased), respectively. The photographs produced are representative of a minimum of 15 blocks observed per internode level (5 stems with 3 blocks per cane and per internode). ca, vascular cambium; fi, phloem fibers; r, vascular rays; s, sieve plate; v, xylem vessel.

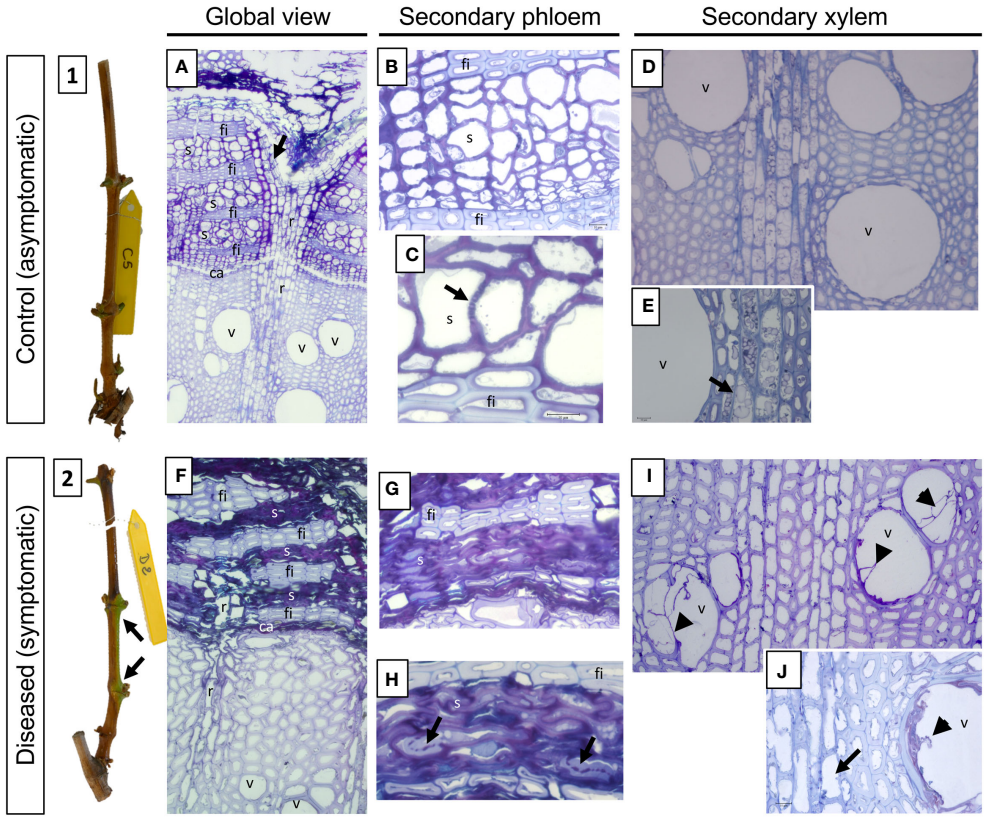

FIGURE 8
Phenotypic and structural observations of grapevine stems harvested, at T2 (symptomatic stage), from control (1, **A-E**) or diseased (2, **F-J**) plants. A representative picture of the phenotype of the stems sampled is given in illustrations 1 (control) and 2 (leaf drop). The observation of semi-thin sections stained with toluidine blue also allows the comparison of the anatomical structure of the stems. Thus, a global view is given in **A** (control) and **B** (diseased), while focuses are made on the secondary vascular tissues that are the phloem (**B**, **C**: control; **G**, **H**: diseased) and the xylem (**D**, **E**: control; **I**, **J**: diseased), respectively. The photographs produced are representative of a minimum of 15 blocks observed per internode level (5 stems with 3 blocks per cane and per internode). ca: vascular cambium; fi: phloem fibers; r: vascular rays; s: sieve plate; v: xylem vessel.

the previous sampling time, and whatever the inter-node, the secondary phloem appears non-functional from a vascular point of view (Figures 8F–H). Indeed, the vascular cells are totally collapsed and it even becomes almost impossible to distinguish them individually (Figures 8G, H). Occasionally, the presence of sieve plates is still observed which appears obstructed by a component weakly stained with toluidine blue (Figure 8H, arrows). In the secondary xylem we also observed the presence of vessels obstructed by tylosis (Figures 8I, J) and the lack of amyloplast in the parenchymal rays (Figure 8J, arrow), indicating a defective storage in D vines. Finally, in the internodes at the base of the canes (internode 1), we were able to demonstrate the presence of fungal hyphae in the secondary phloem (Supplementary Figures 4C-E, arrows). In all cases, the presence of these hyphae was found in the tissue layers closest to the vascular cambium and not in the most peripheral or internal layers.

Callose deposition on sieve plates affects the sap conduction and phloem functioning in diseased pre-symptomatic and symptomatic vines

The potential alterations in the secondary P were observed and identified after aniline blue staining from samples of C and D plants included in paraffin. In samples from C plants, the sieve tubes appear functional (Supplementary Figures 5A, B), the sieve plates are visible (Supplementary Figure 5B, arrows) and a simple pale blue staining (ie. background staining) is detected. At T1, in samples of D plants, an intense blue staining is observed at the level of the cell walls of the sieve tubes whatever the internode, suggesting the presence of callose (Supplementary Figures 5C, D) and a potential alteration of the transversal elaborate sap conduction.

Discussion

Studies on Botryosphaeria dieback were already performed at multiple levels using i) *in vitro* grapevine models to better characterize phytotoxic activity of fungal metabolites (Ramírez-Suero et al., 2014; Bénard-Gellon et al., 2015; Trotel-Aziz et al., 2022); ii) greenhouse cuttings and artificial inoculation to understand in-depth grapevine-pathogens interactions (Amponsah et al., 2012; Czemmel et al., 2015; Labois et al., 2020; Obrador-Sanchez and Hernandez-Martinez, 2020) and defense reactions (Urbez-Torres et al., 2010; Lambert et al., 2012; Guan et al., 2016); and iii) in naturally infected vineyards to better characterize the pathogenic

species, the response of different cultivars (Larignon et al., 2001; Spagnolo et al., 2014a) and studying the impact of environmental factors on symptom expression (Van Niekerk et al., 2011). If it is now obvious that Botryosphaeriaceae species impact the plant physiology in both wood (Labois et al., 2020) and leaves (Czemmel et al., 2015), but, the stem has so far been less studied (Spagnolo et al., 2014b). Therefore, the main objective of this work was to better characterize the triggering and expression of Botryosphaeria dieback in the stem of plants from vineyard during three stages: the pre-symptomatic (at flowering), the early expression of symptoms (at cluster closure) and the severe symptomatic stage with leaf drop (at late veraison).

Botryosphaeriaceae infection and vascular obstruction in the vine stem during the expression of leaf symptoms

Our results were suggesting that stems were contaminated annually by Botryosphaeriaceae through the bark from the visible inflorescence stage, possibly by lenticels or buds. We have observed that the expression of leaf symptoms was related to the number of vessels obstructed (by tylosis or gummosis). This number significantly increased from T1 (asymptomatic phase) to T3 (leaf drop), suggesting a potential threshold of obstruction to exceed (25 to 30%) that leads to the expression of symptoms (leaf drop). This observation is therefore different for Esca disease, where the disease severity was not significantly related to the non-functional vessels due to tyloses and gels in leaves (Bortolami et al., 2019). We also observed that the distribution of obstructed vessels in the circumference of internodes seemed relatively random at pre-symptomatic and symptomatic stages. The obstruction affected both the unilateral (in lateral position) and bilateral (in ventral and dorsal positions) vessels of the shoot orthostics (Fournioux and Bessis, 1979) could reduce water supply to leaves, and then lead to the leaf drop process.

Molecular changes in the vine stem during the expression of leaf symptoms

Genes related to carbohydrate metabolism, defense responses, and secondary meristems activity (vascular cambium and phellogen) were strongly regulated in stems from D plants than from control plants. Of interest, genes associated with the activity of secondary meristems were often down-regulated during symptomatic phase, suggesting physiological and structural responses of the grapevine to the fungal colonization. Gene modulation was less intense at the pre-symptomatic stage than at symptomatic phase, but always different between samples from C and D plants. At T1, defense-related genes were up-regulated in both P and X tissues, suggesting that vines responded to the fungal infection. Moreover, we also reported that *Cal-S7* gene, known to be specific for callose deposition in P (Xie et al., 2011), was induced only in P tissues, as already reported in other woody plants in response to P-vascular agents (Granato et al., 2019).

Similar patterns between P and X samples were observed at symptomatic phase for genes related to carbohydrate metabolism and defense. Targeted defense responses (PR-proteins, superoxide dismutase) were shown to be altered in canes after artificial infections by Botryosphaeriaceae (Spagnolo et al., 2014a; Reis et al., 2016). Interestingly, the down-regulation of *SUC27* at T2 was described as related to embolism formation in X (Chitarra et al., 2014) and water stress (Perrone et al., 2012). Moreover, Chitarra et al. (2014) suggested that, upon X embolism, the main provision of sugars to vessel-associated cells derived from starch breakdown and not from P unloading. This is consistent with our anatomical study where an embolism of the vessels (tylosis) and a strong reduction in amyloplasts were observed. Furthermore, at T2, the expression of genes related to secondary meristems was strongly reduced in P and X samples. The down-regulation of the *APL* gene, required for P differentiation (Furuta et al., 2014; Kalmbach and Helariutta, 2019), could be related with the alteration/disorganization of conductive P observed in diseased canes. The down-regulation of *CDKB2* (meristem regulator; Andersen et al., 2008), *MOL* (required for the formation of secondary vascular tissue in fascicular and interfascicular region; Agusti et al., 2011) and *WOX* (required for auxin-dependent stimulation of cambium activity; Suer et al., 2011) genes could be related with the weakening of the cambium in diseased canes. Finally, the down-regulation of the *SHR* gene (required for phellogen activity; Miguel et al., 2016) was consistent with the lack or the alteration of cane maturation (i.e. “aoûtement”) observed in diseased vines.

Metabolic changes in the vine stem during the expression of leaf symptoms

The metabolite fingerprints of C and D tissues were similar at the pre-symptomatic stage. Interestingly, glycosylsalicylate was already accumulated in P of declining vines. Ratzinger et al. (2009) also reported an accumulation of SA-glucoside, but in the X sap of shoots, after infection with *Verticillium longisporum*. During symptom occurrence, the stilbenes *cis-* and *trans-*resveratrol and piceid were more accumulated in the X tissues of D samples than of C samples. This result was consistent with the overexpression of *PAL* and *STS* genes in our targeted gene expression analysis. The presence of grapevine phytoalexins (Chong et al., 2009; Loupit et al., 2023) was previously reported in various parts of vines infected by Botryosphaeria dieback (Labois et al., 2020), but also in the green stems of Tempranillo cuttings infected by *N. parvum* and *D. seriata* (Reis et al., 2016), in the wood of Cabernet Sauvignon cuttings infected by *N. parvum* (Massonnet et al., 2018), in Merlot cuttings inoculated by *D. seriata* and *N. parvum* (Lambert et al., 2012), and in the brown stripe area of trunks (Spagnolo et al., 2014a; Lemaître-Guillier et al., 2020). Stilbene production can be induced by proteins secreted by fungi associated to Botryosphaeria dieback (Stempien et al., 2017). Using *in vitro* agar plate assays, Lambert et al. (2012) have shown that Botryosphaeriaceae are very susceptible to stilbenes, but with resveratrol and piceid slightly active.

For both P and X tissues, 1-kestose, a fructan constituted by 3 frutosylfructose units, was similarly accumulated in C and D plants at T1. But, its concentration in D plants was null or weak at T2 and T3, suggesting its concentration was related to disease symptom

expression. 1-kestose is known to be produced by several plants such as Banana (Agopian et al., 2008), Asparagus (Forsythe et al., 1990), and grapevine (Dos Santos Lima et al., 2019), and was also described in human to make the resident bifidobacterial more vigorous in the intestinal flora (Hidaka et al., 1986). Mannitol is a polyol commonly found in plants and fungi. In plants, mannitol is as carbon stockpiling compound, an osmolyte, a store of reducing power, and an oxygen radical quencher (for review, see Meena et al., 2015). It is also translocated to source organs when the sucrose pool is drained (Davis and Loescher, 1990), suggesting it can be found in P tissue. In fungi, mannitol has important biological functions under stress conditions, such as the regulation of osmotic pressure and removal of reactive oxygen species (ROS) (Meena et al., 2015). In Arabidopsis/*Alternaria alternata* interaction, the fungus secretes mannitol to quench the plant defense-related ROS production whereas the plant produces mannitol dehydrogenase to catabolize mannitol and preserve this defense event (Jennings et al., 1998). The concentration of mannitol was higher in P and X tissues of D plants than of C plants at T2, suggesting a production by both the grapevine (caused by the fungal infection) and the pathogenic fungus (to quench plant ROS).

A structural and functional shift in P and X tissues already during the pre-symptomatic stage

We have described structural changes and a dysfunction in both P and X tissues in the stem of internodes of D plants before the shift from the pre-symptomatic to the symptomatic phase.

For the first time, we have shown many alterations in stems before the onset of symptoms, including the obstruction of X vessels (by tylosis and gums) and starch depletion, two processes already mentioned for a trunk dieback (Czemmel et al., 2015). In the pre-symptomatic stage, we have also revealed the simultaneous presence of Botryosphaeriaceae with the secondary P that is disorganized, and appeared collapsed and non-functional regarding callose deposits that could obstruct sieve plates. Callose, a β-1,3-glucan, plugs P sieve tubes during winter and protects vines from cold temperatures (Esau, 1948). Callose is also a defense barrier against pathogens, prevents disease development, and accumulates in wound tissues, becoming a boundary between damaged zone and healing tissue (Taiz and Zeiger, 2002). Callose deposition in the secondary P of woody grape tissue has been studied in relation to seasonal vine development (Aloni and Peterson, 1991; Aloni et al., 1991), but rarely in response to pathogen invasion. Close alterations, with sieve tubes appearing not collapsed, have been described in response to wounding and crown gall in grapevine (Creasap et al., 2005).

Our study also revealed the alteration in the functioning and the establishment of secondary meristems. In diseased vines, the vascular cambium has been able to generate both secondary P and X. However, the vascular meristem appeared collapsed and therefore weakened, in vines suffering from dieback. In addition, we observed that the formation of the periderm is random in diseased vines. In half the cases, the phellogen was not differentiated in a peripheral layer of secondary P in stems. This disorganization is classically reported in other declines of the vine, particularly Pierce's disease (Stevenson et al., 2005). In the meantime, the defect in the establishment of the periderm and the lack of amyloplasts in the decline vine stems reflected a defect in stem maturation, similarly to the grapevine Pierce's disease (Stevenson et al., 2005).

Conclusion

In our study, we combined different approaches to evaluate anatomical, developmental and functional changes related to the presence of Botryosphaeriaceae, both in symptomatic and asymptomatic vine. We have reported structural and molecular modulations from the pre-symptomatic phase T1 (Figure 9), with a probable annual contamination of stems through the bark. We have highlighted anatomical and functional disorders in X and P tissues from internodes of the base of stems that may explain symptoms (leaf drop) observed for the severe form of this dieback. At the pre-symptomatic stage (T1), targeted gene expression related to plant defense, sugar metabolism and callose synthesis was consistent to microscopic observations, and highlighted for the first-time P

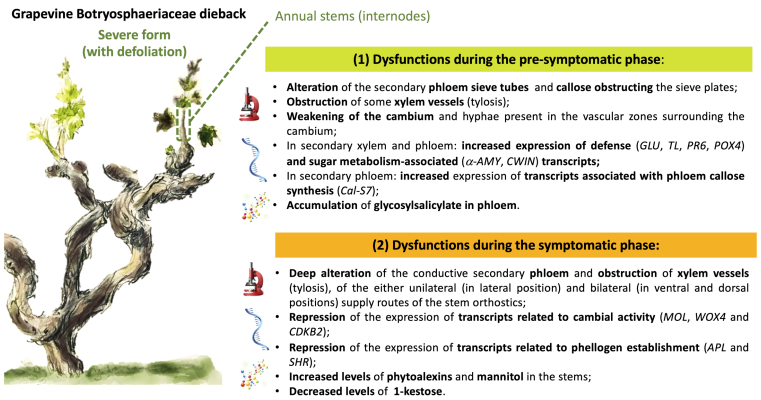

FIGURE 9
Graphical summary of the main results acquired, reporting the dysfunctions observed during the pre-symptomatic and symptomatic phases of the severe form (leaf drop) of Botryosphaeria dieback in grapevine.

dysfunctions in response to Botryosphaeriaceae. During the symptomatic stage, from early (T2) to leaf drop (T3), a failure to establish the cane maturation (i.e., "aoûtement") was observed for declining vines and was consistent with (i) the down-regulation of genes related to sucrose signalization, cambial activity and establishment of phellogen, and with (ii) differential accumulation of some metabolites. These plant descriptors of the vine holobiont, involved in plant immunity or wood quality, could be considered as bioindicators of the dysfunctions associated with the severe form of this dieback. Among metabolites, the role of 1-kestose as other ones (i.e., glycosylsalicylate and fructan) in the microbial equilibrium and immunity of vine now deserves to be investigated. In addition, there is a growing interest in understanding the interactions between plants and their microbiome (Pinto et al., 2014; ZarraonaIndia and Gilbert, 2015; Belda et al., 2017; Bettenfeld et al., 2020), especially when related to plant health (Bettenfeld et al., 2022). Thus, in order to have a global view of the vine holobiont dysfunction it would be interesting to evaluate the modulation of the microbial component (i.e., bacteria, fungi and viruses) of the stems associated with the foliar expression of this dieback.

Data availability statement

The raw data supporting the conclusions of this article will be made available by the authors, without undue reservation.

Author contributions

FM: Conceptualization, Formal analysis, Investigation, Methodology, Software, Writing – review & editing. LJ: Conceptualization, Formal analysis, Investigation, Methodology, Visualization, Writing – review & editing. PL: Conceptualization, Investigation, Methodology, Writing – review & editing. GC: Data curation, Formal analysis, Investigation, Methodology, Writing – review & editing. CC: Investigation, Methodology, Writing – review & editing. EN: Investigation, Methodology, Software, Writing – review & editing. P-EC: Data curation, Funding acquisition, Project administration, Resources, Validation, Writing – review & editing. FF: Conceptualization, Funding acquisition, Resources, Supervision, Writing – review & editing. MA: Conceptualization, Formal analysis, Funding acquisition, Investigation, Resources, Supervision, Writing – review & editing. ST: Writing – original draft, Writing – review & editing, Conceptualization, Data curation, Formal analysis, Funding acquisition, Investigation, Methodology, Project administration, Resources, Supervision, Validation.

Funding

The author(s) declare financial support was received for the research, authorship, and/or publication of this article. This research was financed by the national program on grapevine decline (Plan National du Dépérissement de la Vigne): HOLOVITI. Moreover, FM was supported by « Comité Interprofessionnel de la Vigne et du vin de Champagne », « Bureau Interprofessionel des Vins de Bourgogne », and Conseil Régional de Bourgogne Franche-Comté.

Acknowledgments

The authors thank, Coline Chevalier, Aline Sauvage and Véronique Aubert for providing technical assistance in stems sample, Botryosphaeriaceae isolation and cytological preparation respectively. The authors thanks also Nicolas Richet for his help in making one qPCR plate and Tania Marzari for contribution to Volcano plot production.

Conflict of interest

The authors declare that the research was conducted in the absence of any commercial or financial relationships that could be construed as a potential conflict of interest.

The author(s) declared that they were an editorial board member of Frontiers, at the time of submission. This had no impact on the peer review process and the final decision.

Publisher's note

Supplementary material

The Supplementary Material for this article can be found online at: https://www.frontiersin.org/articles/10.3389/fpls.2024.1394821/full#supplementary-material

SUPPLEMENTARY FIGURE 1
Presentation of the sequence of samples and samplings carried out during this study. For Botryosphaeria detection by Pasteurian method, six sampling times were analyzed (top of the figure, in orange). For other analyses, the vines sampled on the plot showed 2 distinct health conditions: C (control), D (diseased, severe form). Note that samples "D" of time sample 1 provide from vines that were noted expressive in 2017 (sample collected before symptoms expression). **(A)** For each of the 5 vines identified by modality **(C, D)**, 2 shoots were taken. One was reserved for anatomical characterization and the other one was used for transcriptomic and metabolomic analyzes. **(B)** the samples used for anatomical characterization were sectioned from the base at the 5th or 6th internode and then stored at 4°C until use. **(C)** for the samples planned for the transcriptomic and metabolomic analyzes, fragments of the 3 basal internodes were sectioned, the woody (xylem) and "Phloem/bark" parts were then immediately separated and frozen in liquid nitrogen. The samples were then stored at -80°C until use.

SUPPLEMENTARY FIGURE 2
Example of illustration of the spatial distribution (canes 1 to 5) of obstructed vessels at the circumference of the stems and along the dorsal/ventral and lateral axes. The data reflect observations made in the second internode. Each layer obtained for each stem taken in a same modality (C or D) presents a different color: cyan for stem 1, blue for stem 2, orange for stem 3, red for stem 4 and black for stem 5. In the case of vines affected by Botryosphaeria dieback (diseased), the T1 (pre-symptomatic) and T3 (symptomatic) times are compared.

SUPPLEMENTARY FIGURE 3
Hierarchical Cluster Analysis (HCA) analysis of the whole GC-MS data set. "Tissue" corresponds to phloem (P) or xylem (X); "Time" corresponds to sampling time, "1": before symptom expression (T1), "2": onset of symptom expression (T2) and "3": full symptom expression (T3); "Expression" corresponds to Control (C) and Diseased (D) samples; class corresponds to the internode position (1, 2 and 3 from the base of the stem).

SUPPLEMENTARY FIGURE 4
Focus on structural observations and hyphae localization in grapevine stems harvested at T2 (symptomatic stage) from diseased plants. Observations were made in the internode of the base of the stems (internode 1), both at the level of the secondary phloem **(A, B)** and of the secondary xylem **(C, E)**. The presence of hyphae is indicated by arrows.

SUPPLEMENTARY FIGURE 5
Evaluation of the presence of callose in the vascular secondary liber of control **(A, B)** and diseased **(C, D)** plants, detected after aniline blue staining. The staining is specific for β-1,3-glucan and stains the callose in intense blue.

SUPPLEMENTARY FILE 1
Climatic data (temperatures and rainfall) collected between 2010 and 2021.

SUPPLEMENTARY TABLE 1
Primer sets used to detect Botryosphaeriaceae in grapevine stems.

SUPPLEMENTARY TABLE 2
Sequences of the primers derived from *Vitis vinifera* and used for RT-q-PCR.

SUPPLEMENTARY TABLE 3
List of the metabolites differently accumulated in the internode phloem of control and diseased grapevines. GC-analysis was performed on phloem tissues collected at different times (T1, from pre-symptomatic stems; T2 and T3 from symptomatic ones). "Pvalue": p value corresponding to the T-test, "FC": fold change C/D, "id": identification number indicated on Volcano plots, "C > D": metabolites more accumulated in control samples than in diseased ones. "D > C": metabolites more accumulated in diseased samples than in control ones.

SUPPLEMENTARY TABLE 4
List of the metabolites differently accumulated in the internode xylem of control and diseased grapevines. GC-analysis was performed on samples collected at different times (T1, from pre-symptomatic stems; T2 and T3 from symptomatic ones). "Pvalue": p value corresponding to the T-test, "FC": fold change C/D, "id": identification number indicated on Volcano plots, "C > D": metabolite more accumulated in control samples than in D ones. "D > C": metabolite more accumulated in diseased samples than in control ones.

References

Agopian, R. G. D., Soares, C. A., Purgatto, E., Cordenunsi, B. R., and Lajolo, F. M. (2008). Identification of fructooligosaccharides in different banana cultivars. *J. Agric. Food Chem.* 56, 3305–3310. doi: 10.1021/jf073011l

Agusti, J., Lichtenberger, R., Schwarz, M., Nehlin, L., and Greb, T. (2011). Characterization of transcriptome remodeling during cambium formation identifies MOL1 and RUL1 as opposing regulators of secondary growth. *PloS Genet.* 7, e1001312. doi: 10.1371/journal.pgen.1001312

Aloni, R., and Peterson, C. A. (1991). Seasonal changes in callose levels and fluorescein translocation in the phloem of *Vitis vinifera* L. *IAWA. J.* 12, 223–234. doi: 10.1163/22941932-90001247

Aloni, R., Raviv, A., and Peterson, C. A. (1991). The role of auxin in the removal of dormancy callose and resumption of phloem activity in *Vitis vinifera*. *Can. J. Bot.* 69, 1825–1832. doi: 10.1139/b91-232

Amponsah, N. T., Jones, E., Ridgway, H. J., and Jaspers, M. V. (2012). Evaluation of fungicides for the management of Botryosphaeria dieback diseases of grapevines. *Pest Manage. Sci.* 68, 676–683. doi: 10.1002/ps.2309

Andersen, S. U., Buechel, S., Zhao, Z., Ljung, K., Novak, O., Busch, W., et al. (2008). Requirement of B2-type cyclin-dependent kinases for meristem integrity in Arabidopsis thaliana. *Plant Cell* 20, 88–100. doi: 10.1105/tpc.107.054676

Andolfi, A., Mugnai, L., Luque, J., Surico, G., Cimmino, A., and Evidente, A. (2011). Phytotoxins produced by fungi associated with grapevine trunk diseases. *Toxins* 3, 1569–1605. doi: 10.3390/toxins3121569

Belair, M., Restrepo-Leal, J. D., Praz, C., Fontaine, F., Rémond, C., Fernandez, O., et al. (2023). *Botryosphaeriaceae* gene machinery: Correlation between diversity and virulence. *Fungal Biol.* 127, 1010–1031. doi: 10.1016/j.funbio.2023.03.004

Belda, I., ZarraonaIndia, I., Perisin, M., Palacios, A., and Acedo, A. (2017). From vineyard soil to wine fermentation: microbiome approximations to explain the "terroir" concept. *Front. Microbiol.* 8. doi: 10.3389/fmicb.2017.00821

Bénard-Gellon, M., Farine, S., Goddard, M. L., Schmitt, M., Stempien, E., Pensec, F., et al. (2015). Toxicity of extracellular proteins from *Diplodia seriata* and *Neofusicoccum parvum* involved in grapevine Botryosphaeria dieback. *Protoplasma* 252, 679–687. doi: 10.1007/s00709-014-0716-y

Berraf-Tebbal, A., Guereiro, M. A., Phillips, A. J., and Von Arx, J. A. (2014). Phylogeny of Neofusicoccum species associated with grapevine trunk diseases in Algeria, with description of Neofusicoccum algeriense sp. nov. *Phytopathol. Mediterr.* 53, 416–427. doi: 10.14601/Phytopathol_Mediterr-14385

Bertsch, C., Ramirez-Suero, M., Magnin-Robert, M., Larignon, P., Chong, J., Abou-Mansour, E., et al. (2013). Grapevine trunk diseases, complex and still poorly understood. *Plant Pathol.* 62, 243–265. doi: 10.1111/j.1365-3059.2012.02674.x

Bettenfeld, P., Cadena I Canals, J., Jacquens, L., Fernandez, O., Fontaine, F., van Schaik, E., et al. (2022). The microbiota of the grapevine holobiont: A key component of plant health. *Int. J. Adv. Res.* 40, 1–15. doi: 10.1016/j.jare.2021.12.008

Bettenfeld, P., Fontaine, F., Trouvelot, S., Fernandez, O., and Courty, P. E. (2020). Woody plant declines. What's wrong with the microbiome? *Trends Plant Sci.* 25, 381–394. doi: 10.1016/j.jare.2021.12.008

Bisson, M., Houeix, N., Hulot, C., Lacroix, G., Lefevre, J. P., Leveque, S., et al. (2006) Arsenic et ses dérivés inorganiques. INERIS, fiches de données toxicologiques et environnementales des substances chimiques. Available at: https://substances.ineris.fr/fr/substance/getDocument/2715.

Bortolami, G., Gambetta, G. A., Delzon, S., Lamarque, L. J., Pouzoulet, J., Badel, E., et al. (2019). Exploring the hydraulic failure hypothesis of esca leaf symptom formation. *Plant Physiol.* 181, 1163–1174. doi: 10.1104/pp.19.00591

Carlucci, A., Cibelli, F., Lops, F., and Raimondo, M. L. (2015). Characterization of Botryosphaeriaceae species as causal agents of trunk diseases on grapevines. *Plant Dis.* 99, 1678–1688. doi: 10.1094/PDIS-03-15-0286-RE

Castillo-Pando, M., Somers, A., Green, C. D., Priest, M., and Sriskanthades, M. (2001). Fungi associated with dieback of Semillon grapevines in the Hunter Valley of New South Wales. *Australas. Plant Pathol.* 30, 59–63. doi: 10.1071/AP00068

Chamberlain, G. C., Willison, R. S., Townshend, J. L., and Ronde, J. D. (1964). Two fungi associated with the dead-arm disease of grapes. *Can. J. Bot.* 42, 351–355. doi: 10.1139/b64-034

Chitarra, W., Balestrini, R., Vitali, M., Pagliarani, C., Perrone, I., Schubert, A., et al. (2014). Gene expression in vessel-associated cells upon xylem embolism repair in *Vitis vinifera* L. *Petioles. Planta.* 239, 887–899. doi: 10.1007/s00425-013-2017-7

Chong, J., Poutaraud, A., and Hugueney, P. (2009). Metabolism and roles of stilbenes in plants. *Plant Sci.* 177, 143–155. doi: 10.1016/j.plantsci.2009.05.012

Claverie, M., Notaro, M., Fontaine, F., and Wery, J. (2020). Current knowledge on Grapevine Trunk Diseases with complex etiology: a systemic approach. *Phytopathol. Mediterr.* 59, 29–53. doi: 10.14601/Phyto-11150

Colas, S., Jacquens, L., Manteau, S., Devy, J., Coneíjeíro, G., Cleíment, C., et al. (2010). Expression analysis in grapevine by in *situ* hybridization and immunohistochemistry. *Methodol. Results. Grapevine. Res.* 361–374. doi: 10.1007/978-90-481-9283-0_26

Creasap, J. E., Reid, C. L., Goffinet, M. C., Aloni, R., Ullrich, C., and Burr, T. J. (2005). Effect of wound position, auxin, and *Agrobacterium vitis* strain F2/5 on wound healing and crown gall in grapevine. *Phytopathology* 95, 362–367. doi: 10.1094/PHYTO-95-0362

Cristinzio, G. (1978). Gravi attacchi di Botryosphaeria obtusa su vite in provincia di Isernia. *Inf. Tore. Fitopatol.* 6, 21–23.

Crous, P. W., Slippers, B., Wingfield, M. J., Rheeder, J., Marasas, W. F., Philips, A. J., et al. (2006). Phylogenetic lineages in the botryosphaeriaceae. *Stud. Mycol* 55, 235–253. doi: 10.3114/sim.55.1.235

Czemmel, S., Galarneau, E. R., Travadon, R., McElrone, A. J., Cramer, G. R., and Baumgartner, K. (2015). Genes expressed in grapevine leaves reveal latent wood infection by the fungal pathogen *Neofusicoccum parvum*. *Plos one* 10 (3), e0121828. doi: 10.1371/journal.pone.0121828

Davis, J. M., and Loescher, W. H. (1990). ^{14}C-Assimilate translocation in the light and dark in celery (Apium graveolens) leaves of different ages. *Physiol. Plant* 79, 656–662. doi: 10.1111/j.1399-3054.1990.tb00040.x

Dissanayake, A. J., Phillips, A. J. L., Li, X. H., and Hyde, K. D. (2016). Botryosphaeriaceae: Current status of genera and species. *Mycosphere* 7, 1001–1073. doi: 10.5943/mycosphere/si/1b/13

Dos Santos Lima, M., Nunes, P. C., de Lourdes de Arauújo Silva, B., da Silva Padilha, C. V., do Bonfim, T. H. F., Stamford, T. L. M., et al. (2019). Determining 1-kestose, nystose and raffinose oligosaccharides in grape juices and wines using HPLC, method validation and characterization of products from Northeast Brazil. *J. Food Sci. Technol.* 56, 4575–4584. doi: 10.1007/s13197-019-03936-x

Epstein, L., Sukhwinder, K., and Vander Gheynst, J. S. (2008). Botryosphaeria-related dieback and control investigated in noncoastal California grapevines. *California. Agric.* 62, 161–166. doi: 10.3733/ca.v062n04p161

Esau, K. (1948). Phloem structure in the grapevine, and its seasonal changes. *Hilgardia* 18, 217–296. doi: 10.3733/hilg.v18n05p217

Esau, K. (1965). *Vascular differentiation in plants* (New York: Holt, Rinehart and Winston), 160.

Esteves, A. C., Saraiva, M., Correia, A., and Alves, A. (2014). Botryosphaeriales fungi produce extracellular enzymes with biotechnological potential. *Can. J. Microbiol.* 60, 332–342. doi: 10.1139/cjm-2014-0134

Fontaine, F., Pinto, C., Vallet, J., Clément, C., Gomes, A. C., and Spagnolo, A. (2016). The effects of grapevine trunk diseases (GTDs) on vine physiology. *Eur. J. Plant Pathol.* 144, 707–721. doi: 10.1007/s10658-015-0770-0

Forsythe, K. L., Feather, M. S., Gracz, H., and Wong, T. C. (1990). Detection of kestoses and kestose-related oligosaccharides in extracts of Festuca arundinacea, Dactylis glomerata L, and Asparagus officinalis L. root cultures and invertase by 13C and 1H nuclear magnetic resonance spectroscopy. *Plant Physiol.* 92, 1014–1020. doi: 10.1104/pp.92.4.1014

Fournioux, J. C., and Bessis, R. (1979). Etude des relations criblo-vasculaires entre les différents organes de la tige de la vigne (*Vitis vinifera* L.). *Oeno. One* 13, 91–114. doi: 10.20870/oeno-one.1979.13.2.1398

Furuta, K. M., Yadav, S. R., Lehesranta, S., Belevich, I., Miyashima, S., Heo, J. O., et al. (2014). *Arabidopsis* NAC45/86 direct sieve element morphogenesis culminating in enucleation. *Science* 345, 933–937. doi: 10.1126/science.1253736

Goodacre, R., Broadhurst, D., Smilde, A. K., Kristal, B. S., Baker, J. D., Beger, R., et al. (2007). Proposed minimum reporting standards for data analysis in metabolomics. *Metabolomics* 3), 231–241. doi: 10.1007/s11306-007-0081-3

Granato, L. M., Galdeano, D. M., D'Alessandre, N. D. R., Breton, M. C., and MaChado, M. A. (2019). Callose synthase family genes plays an important role in the Citrus defense response to Candidatus Liberibacter asiaticus. *Eur. J. Plant Pathol.* 155, 25–38. doi: 10.1007/s10658-019-01747-6

Guan, X., Essakhi, S., Laloue, H., Nick, P., Bertsch, C., and Chong, J. (2016). Mining new resources for grape resistance against Botryosphaeriaceae, a focus on *Vitis vinifera* subsp. *sylvestris*. *Plant Pathol.* 65, 273–284. doi: 10.1111/ppa.12405

Guérin-Dubrana, L., Fontaine, F., and Mugnai, L. (2019). Grapevine trunk disease in European and Mediterranean vineyards, occurrence, distribution and associated disease-affecting cultural factors. *Phytopathol. Mediterr.* 58, 49–71. doi: 10.14601/Phytopathol_Mediterr-25153

Hewitt, R. W. B. (1988). *Diplodia cane dieback and bunch rot. Compendium of grape diseases*. St Paul, MN: Am. Phytopathol. Soc. Press, 25–26

Hidaka, H., Eida, T., Takizawa, T., Tokunaga, T., and Tashiro, Y. (1986). Effects of fructooligosaccharides on intestinal flora and human health. *Bifidobacteria. Microflora.* 5, 37–50. doi: 10.12938/bifidus1982.5.1_37

IARC (International Agency for Research on Cancer) (1987). Arsenic and arsenic compounds (group1*). IARC Monographs on the evaluation of the carcinogenic risks to humans, Overall evaluations of carcinogenicity: An updating of IARC monographs 1-42, S7, 100–106.

Jennings, D. B., Ehrenshaft, M., Pharr, D. M., and Williamson, J. D. (1998). Roles for mannitol and mannitol dehydrogenase inactive oxygen-mediated plant defense. *Proc. Natl. Acad. Sci.* 95, 1512915133. doi: 10.1073/pnas.95.25.15129

Kalmbach, L., and Helariutta, Y. (2019). Sieve plate pores in the phloem and the unknowns of their formation. *Plants* 8, 25. doi: 10.3390/plants8020025

Krzyżaniak, Y., Negrel, J., Lemaitre-Guillier, C., Clément, G., Mouille, G., Klinguer, A., et al. (2018). Combined enzymatic and metabolic analysis of grapevine cell responses to elicitors. *Plant Physiol. Biochem.* 123, 141–148. doi: 10.1016/j.plaphy.2017.12.013

Labois, C., Wilhelm, K., Laloue, H., Tarnus, C., Bertsch, C., Goddard, M. L., et al. (2020). Wood metabolomic responses of wild and cultivated grapevine to infection with *neofusicoccum parvum*, a trunk disease pathogen. *Metabolites* 10, 232. doi: 10.3390/metabo10060232

Lambert, C., Bisson, J., Waffo-Téguo, P., Papastamoulis, Y., Richard, T., Corio-Costet, M. F., et al. (2012). Phenolics and their antifungal role in grapevine wood decay, focus on the Botryosphaeriaceae family. *J. Agric. Food Chem.* 60, 11859–11868. doi: 10.1021/jf303290g

Larignon, P. (2004). Réflexions sur l'esca. *Phytoma* 576, 28–31.

Larignon, P. (2012). *Maladies cryptogamiques du bois de la vigne, symptomatologie et agents pathogeènes* (Grau du Roi dans le Gard: Institut Français de la Vigne et du Vin).

Larignon, P. (2016). *Maladies cryptogamiques du bois de la vigne, symptomatologie et agents pathogens*, Vol. 165. Available at: https://www.vignevin.com.

Larignon, P., and Dubos, B. (1997). Fungi associated with esca disease in grapevine. *Eur. J. Plant Pathol.* 103, 147–157. doi: 10.1023/A:1008638409410

Larignon, P. F. F., Farine, S., Cleíment, C., and Bertsch, C. (2009). Esca et black dead arm, deux acteurs majeurs des maladies du bois chez la vigne. *Comptes. Rendus. l'Acadeimie. Des. Sci. III-Vie.* 333, 765–783. doi: 10.1016/j.crvi.2009.05.005

Larignon, P., Fulchic, R., Laurent, C., and Dubos, B. (2001). Observation on black dead arm in French vineyards. *Phytopathol. Mediterr.* 40, 336–342. doi: 10.14601/Phytopathol_Mediterr-1629

Larignon, P., Spagnolo, A., Bertsch, C., and Fontaine, F. (2015). First report of young grapevine decline caused by *Neofusicoccum parvum* in France. *Plant Dis.* 99, 1859. doi: 10.1094/PDIS-03-15-0280-PDN

Leal, L., Trotel-Aziz, P., Gramaje, D., Armengol, J., and Fontaine, F. (2024). Exploring factors conditioning the expression of Botryosphaeria dieback in grapevine for integrated management of the disease. *Phytopathology* 114, 21–34. doi: 10.1094/PHYTO-04-23-0136-RVW

Leavitt, G. M. (1990). *The occurrence, distribution, effects and control of Botryodiplodia theobromae on Vitis vinifera in California, Arizona and northern Mexico* (Riverside, CA, USA: University of California), 120.

Lehoczky, J. (1974). Black dead arm disease of grapevine caused by *Botryosphaeria stevensii* infection. *Acta Phytopathol. Academiae. Sci. Hungaricae.* 9, 319–327.

Lehoczky, J. (1988). "Black dead Arm," in *Compendium of Grape Diseases*. Eds. R. C. Pearson and A. C. Goheen (APSPress, MN, USA), 35.

Lemaître-Guillier, C., Fontaine, F., Roullier-Gall, C., Harir, M., Magnin-Robert, M., Clément, C., et al. (2020). Cultivar-and wood area-dependent metabolomic fingerprints of grapevine infected by Botryosphaeria dieback. *Phytopathology* 110, 1821–1837. doi: 10.1094/PHYTO-02-20-0055-R

Linaldeddu, B. T., Deidda, A., Scanu, B., Franceschini, A., Serra, S., Berraf-Tebbal, A., et al. (2015). Diversity of Botryosphaeriaceae species associated with grapevine and other woody hosts in Italy, Algeria and Tunisia, with descriptions of *Lasiodiplodia exigua* and Lasiodiplodia mediterranea sp. *nov*. *Fungal Diversity* 71, 201–214. doi: 10.1007/s13225-014-0301-x

Liu, J. K., Phookamsak, R., Doilom, M., Wikee, S., Li, Y. M., Ariyawansha, H., et al. (2012). Towards a natural classification of Botryosphaeriales. *Fungal Diversity* 57, 149–210. doi: 10.1007/s13225-012-0207-4

Loupit, G., Fonayet, J. V., Lorensen, M. D., Franc, C., De Revel, G., Janfelt, C., et al. (2023). Tissue-specific stilbene accumulation is an early response to wounding/grafting as revealed by using spatial and temporal metabolomics. *Plant. Cell Environ.* 46, 3871–3886. doi: 10.1111/pce.14693

Makatini, G. J. (2014). *The role of sucker wounds as portals for grapevine trunk pathogen infections* (Stellenbosch: Stellenbosch University), 121.

Martos, S., Andolfi, A., Luque, J., Mugnai, L., Surico, G., and Evidente, A. (2008). Production of phytotoxic metabolites by five species of Botryosphaeriaceae causing decline on grapevines, with special interest in the species *Neofusicoccum luteum* and N. parvum. *Eur. J. Plant Pathol.* 121, 451–461. doi: 10.1007/s10658-007-9263-0

Massonnet, M., Morales-Cruz, A., Figueroa-Balderas, R., Lawrence, D. P., Baumgartner, K., and Cantu, D. (2018). Condition-dependent co-regulation of genomic clusters of virulence factors in the grapevine trunk pathogen *Neofusicoccum parvum*. *Mol. Plant Pathol.* 19, 21–34. doi: 10.1111/mpp.12491

Meena, M., Prasad, V., Zehra, A., Gupta, V. K., and Upadhyay, R. S. (2015). Mannitol metabolism during pathogenic fungal-host interactions under stressed conditions. *Front. Microbiol.* 24. doi: 10.3389/fmicb.2015.01019

Mehl, J. W., Slippers, B., Roux, J., and Wingfield, M. J. (2013). 14 cankers and other diseases caused by the botryosphaeriaceae. *Infect. For. Dis.*, 298–317. doi: 10.1079/9781780640402.0298

Metcalfe, C. R., and Chalk, L. (1950). *Anatomy of the Dicotyledons, leaves, stem, and wood, in relation to taxonomy, with notes on economic uses*.

Miguel, A., Milhinhos, A., Novák, O., Jones, B., and Miguel, C. M. (2016). The SHORT-ROOT-like gene PtSHR2B is involved in Populus phellogen activity. *J. Exp. Bot.* 67, 1545–1555. doi: 10.1093/jxb/erv547

Molot, B., Larignon, P., and Coarer, M. (2006). *Black dead arm. De nouvelles pistes* (Bordeaux: Colloque Mondiaviti), 15–17.

Mondello, V., Songy, A., Battiston, E., Pinto, C., Coppin, C., Trotel-Aziz, P., et al. (2018). Grapevine trunk diseases, a review of fifteen years of trials for their control with chemicals and biocontrol agents. *Plant Dis.* 102, 1189–1217. doi: 10.1094/PDIS-08-17-1181-FE

Moret, F., Cleíment, G., Grosjean, C., Lemaître-Guillier, C., Morvan, G., Trouvelot, S., et al. (2020). Metabolic fingerprint of Chardonnay leaves affected by esca disease is

both clone and year dependent. *Physiopathol. Mediterr.* 59, 153–161. doi: 10.14601/Phyto-11170

Moret, F., Lemaître-Guillier, C., Grosjean, C., Cleíment, G., Coelho, C., Negrel, J., et al. (2019). Clone-dependent expression of esca disease Revealed by leaf metabolite analysis. *Front. Plant Sci.* 9. doi: 10.3389/fpls.2018.01960

Mugnai, L., Graniti, A., and Surico, G. (1999). Esca (black measles) and brown wood streaking, two old and elusive diseases of grapevines. *Plant Dis.* 83, 404–417. doi: 10.1094/pdis.1999.83.5.404

Mundy, D. C., Vanga, B. R., Thompson, S., and Bulman, S. (2018). Assessment of sampling and DNA extraction methods for identification of grapevine trunk microorganisms using metabarcoding. *New Z. Plant Prot.* 71, 10–18. doi: 10.30843/nzpp.2018.71.159

Obrador-Sanchez, J. A., and Hernandez-Martinez, R. (2020). Microscope observations of Botryosphaeriaceae spp. in the presence of grapevine wood. *Phytopathol. Mediterr.* 59, 119–129. doi: 10.14601/Phyto-11040

OIV (International Organisation of Vine and Wine) (2022). Annual Assessment of World Vine and Wine Sector. 30. Available at: https://www.oiv.int/sites/default/files/documents/OIV_Annual_Assessment-2023.pdf.

Pennycook, S. R., and Samuels, G. J. (1985). Botryosphaeria and Fusicoccum species associated with ripe fruit rot of *Actinidia deliciosa* (kiwifruit) in New Zealand. *Mycotaxon* 24, 445–458.

Perrone, I., Pagliarani, C., Lovisolo, C., Chitarra, W., Roman, F., and Schubert, A. (2012). Recovery from water stress affects grape leaf petiole transcriptome. *Planta* 235, 1383–1396. doi: 10.1007/s00425-011-1581-y

Phillips, A. J. L. (1998). *Botryosphaeria dothidea* and other fungi associated with excoriose and dieback of grapevines in Portugal. *J. Phytopathol.* 146, 327–332. doi: 10.1111/j.1439-0434.1998.tb04700.x

Pinto, C., Pinho, D., Sousa, S., Pinheiro, M., Egas, C., and Gomes, A. C. (2014). Unravelling the diversity of grapevine microbiome. *PloS One* 9, e85622. doi: 10.1371/journal.pone.0085622

Qiu, Y., Steel, C. C., Ash, G. J., and Savocchia, S. (2011). Survey of Botryosphaeriaceae associated with grapevine decline in the Hunter Valley and Mudgee grape growing regions of New South Wales. *Australas. Plant Pathol.* 40, 1–11. doi: 10.1007/s13313-010-0007-9

Ramírez-Suero, M., Bénard-Gellon, M., Chong, J., Laloue, H., Stempien, E., Abou-Mansour, E., et al. (2014). Extracellular compounds produced by fungi associated with Botryosphaeria dieback induce differential defence gene expression patterns and necrosis in *Vitis vinifera* cv. Chardonnay cells. *Protoplasma* 251, 1417–1426. doi: 10.1007/s00709-014-0643-y

Ratzinger, A., Riediger, N., Von Tiedemann, A., and Karlovsky, P. (2009). Salicylic acid and salicylic acid glucoside in xylem sap of Brassica napus infected with Verticillium longisporum. *J. Plant Res.* 122, 571–579. doi: 10.1007/s10265-009-0237-5

Reis, P., Magnin-Robert, M., Nascimento, T., Spagnolo, A., Abou-Mansour, E., Fioretti, C., et al. (2016). Reproducing Botryosphaeria dieback foliar symptoms in a simple model system. *Plant Dis.* 100, 1071–1079. doi: 10.1094/PDIS-10-15-1194-RE

Reis, P., Pierron, R., Larignon, P., Lecomte, P., Abou-Mansour, E., Farine, S., et al. (2019). Vitis methods to understand and develop strategies for diagnosis and sustainable control of grapevine trunk diseases. *Phytopathology* 109, 916–931. doi: 10.1094/PHYTO-09-18-0349-RVW

Reveglia, P., Savocchia, S., Billones-Baaijens., R., Masi, M., Cimmino, A., and Evidente, A. (2019). Phytotoxic metabolites by nine species of Botryosphaeriaceae involved in grapevine dieback in Australia and identification of those produced by *Diplodia mutila, Diplodia seriata, Neofusicoccum australe* and *Neofusicoccum luteum*. *Natural Product. Res.* 33, 2223–2229. doi: 10.1080/14786419.2018.1497631

Ridgway, H. J., Amponsah, N. T., Dalin, D., Baskarathevan, J., Jones., E. E., and Jaspers, M. V. (2011). Detection of botryosphaeriaceous species in environmental samples using a multi-species primer pair. *Plant Pathol.* 60, 1118–1127. doi: 10.1111/j.1365-3059.2011.02474.x

Savocchia, S., Steel, C. C., Stodart, B. J., and Somers, A. (2007). Pathogenicity of Botryosphaeria species isolated from declining grapevines in subtropical regions of Eastern Australia. *Vitis-geilweilerhof* 46, 27–32. doi: 10.5073/vitis.2007.46.27-32

Schiffman, C., Petrick, L., Perttula, K., Yano, Y., Carlsson, H., Whitehead, T., et al. (2019). Filtering procedures for untargeted LC-MS metabolomics data. *BMC Bioinf.* 20, 1–10. doi: 10.1186/s12859-019-2871-9

Shoemaker, R. A. (1964). Conidial states of some Botryosphaeria species on Vitis and Quercus. *Can. J. Bot.* 42, 1297–1301. doi: 10.1139/b64-122

Slippers, B., Smit, W. A., Crous, P. W., Coutinho., T. A., Wingfield, B. D., and Wingfield, M. J. (2007). Taxonomy, phylogeny and identification of Botryosphaeriaceae associated with pome and stone fruit trees in South Africa and other regions of the world. *Plant Pathol.* 56, 128–139. doi: 10.1111/j.1365-3059.2006.01486.x

Spagnolo, A., Larignon, P., Magnin-Robert, M., Hovasse, A., Cilindre, C., van Dorsselaer, A., et al. (2014b). Flowering as the most highly sensitive period of grapevine (*Vitis vinifera* L. cv Mourvèdre) to the Botryosphaeria dieback agents *Neofusicoccum parvum* and *Diplodia seriata* infection. *Int. J. Mol. Sci.* 15, 9644–9669. doi: 10.3390/ijms15069644

Spagnolo, A., Magnin-Robert, M., Alayi, T. D., Cilindre, C., Schaeffer-Reiss, C., van Dorsselaer, A., et al. (2014a). Differential responses of three grapevine cultivars to Botryosphaeria dieback. *Phytopathology* 104, 1021–1035. doi: 10.1094/PHYTO-01-14-0007-R

Spinosi, J., and Févotte, J. (2008). *Le Programme MATPHYTO. Matrice Cultures-Expositions aux Pesticides Arsenicaux* (Saint- Maurice, France: InVS).

Steel, C. C., Greer, L. A., and Savocchia, S. (2007). Studies on *Colletotrichum acutatum* and *Greeneria uvicola*, two fungi associated with bunch rot of grapes in sub-tropical Australia. *Aust. J. Grape Wine Res.* 13, 23–29. doi: 10.1111/j.1755-0238.2007.tb00068.x

Stempien, E., Goddard, M. L., Wilhelm, K., Tarnus, C., Bertsch, C., and Chong, J. (2017). Grapevine Botryosphaeria dieback fungi have specific aggressiveness factor repertory involved in wood decay and stilbene metabolization. *PloS One* 12, e0188766. doi: 10.1371/journal.pone.0188766

Stevenson, J. F., Matthews, M. A., and Rost, T. L. (2005). The developmental anatomy of Pierce's disease symptoms in grapevines: green islands and matchsticks. *Plant Dis.* 89, 543–548. doi: 10.1094/PD-89-0543

Suer, S., Agusti, J., Sanchez, P., Schwarz, M., and Greb, T. (2011). WOX4 imparts auxin responsiveness to cambium cells in arabidopsis. *Plant Cell* 23, 3247–3259. doi: 10.1105/tpc.111.087874

Taiz, L., and Zeiger, E. (2002). *Plant Physiology. 3rd* Vol. 196-197 (England: Sinauer Associates), 283–308. doi: 10.1093/aob/mcg079

Taylor, A., and Wood, S. (2007). "Non-Botrytis bunch rots occuring in Western Australian vineyards," in *16th Biennial Aust. Plant Path. Soc. Conf*, Adelaide, SA.

Trotel-Aziz, P., Robert-Siegwald, G., Fernandez, O., Leal, C., Villaume., S., Guise, J. F., et al. (2022). Diversity of *neofusicoccum parvum* for the production of the phytotoxic metabolites (-)-terremutin and (*R*)-mellein. *J. Fungi. (Basel).* 8, 319. doi: 10.3390/jof8030319

Udayanga, D., Liu, X., Crous, P. W., McKenzie, E. H., Chukeatirote, E., and Hyde, K. D. (2012). A multi-locus phylogenetic evaluation of *Diaporthe (Phomopsis)*. *Fungal Diversity* 56, 157–171. doi: 10.1007/s13225-012-0190-9

Urbez-Torres, J. R. (2011). The status of Botryosphaeriaceae species infecting grapevines. *Phytopathol. Mediterr.* 50, S5–S45. doi: 10.14601/Phytopathol_Mediterr-9316

Urbez-Torres, J. R., Peduto, F., and Gubler, W. D. (2010). First report of grapevine cankers caused by Lasiodiplodia crassispora and *Neofusicoccum mediterraneum* in California. *Plant Dis.* 94, 785–785. doi: 10.1094/PDIS-94-6-0785B

Van Niekerk, J. M., Crous, P., Halleen, F., and Fourie, P. H. (2006). Botryosphaeria spp. as grapevine trunk disease pathogens. *Phytopathol. Mediterr.* 45, S43–S54. doi: 10.1400/52260

Van Niekerk, J. M., Bester, W., Halleen, F., Crous, P. W., and Fourie, P. W. (2011). The distribution and symptomatology of grapevine trunk disease pathogens are influenced by climate. *Phytopathol. Mediterr.* 50, 98–111. doi: 10.14601/Phytopathol_Mediterr-8645

Vinaixa, M., Samino, S., Saez, I., Duran, J., Guinovart, J. J., and Yanes, O. (2012). A guideline to univariate statistical analysis for LC/MS-based untargeted metabolomics-derived data. *Metabolites* 2, 775–795. doi: 10.3390/metabo2040775

White, T. J., Bruns, T., Lee, S., and Taylor, J. (1990). "Amplification and direct sequencing of fungal ribosomal RNA genes for phylogenetics," in *PCR Protocols, a Guide to Methods and Applications*. Eds. M. A. Innis, D. H. Gelfand, J. J. Sninsky and T. J. White (Academic Press, New York), 315–322. doi: 10.1016/B978-0-12-372180-8.50042-1

Worley, B., and Powers, R. (2013). Multivariate analysis in metabolomics. *Curr. Metabolomics.* 1, 92–107. doi: 10.2174/2213235X11301010092

Wunderlich, N., Ash, G. J., Steel, C. C., Raman, H., Cowling, A., and Savocchia, S. (2011b). Refining the biological factors affecting virulence of Botryosphaeriaceae on grapevines. *Ann. Appl. Biol.* 159, 467–477. doi: 10.1111/j.1744-7348.2011.00508.x

Wunderlich, N., Ash, G. J., Steel, C. C., Raman, H., and Savocchia, S. (2011a). Association of Botryosphaeriaceae grapevine trunk disease fungi with the reproductive structures of *Vitis vinifera*. *Vitis* 50, 89–96. doi: 10.5073/vitis.2011.50.89-96

Xie, B., Wang, X., Zhu, M., Zhang, Z., and Hong, Z. (2011). CalS7 encodes a callose synthase responsible for callose deposition in the phloem. *Plant J.* 65, 1–14. doi: 10.1111/j.1365-313X.2010.04399.x

Yan, J. Y., Xie, Y., Zhang, W., Wang, Y., Liu, J. K., Hyde, K. D., et al. (2013). Species of *Botryosphaeriaceae* involved in grapevine dieback in China. *Fungal Diversity* 61, 221–236. doi: 10.1007/s13225-013-0251-8

ZarraonaIndia, I., and Gilbert, J. A. (2015). Understanding grapevine-microbiome interactions, implications for viticulture industry. *Microbial. Cell* 2, 171. doi: 10.15698/mic2015.05.204

frontiers | Frontiers in Plant Science

TYPE Original Research
PUBLISHED 02 May 2024
DOI 10.3389/fpls.2024.1339559

OPEN ACCESS

EDITED BY
Choong-Min Ryu,
Korea Research Institute of Bioscience and Biotechnology (KRIBB), Republic of Korea

REVIEWED BY
Nicolás M. Cecchini,
National University of Cordoba (CIQUIBIC), Argentina
Takaki Maekawa,
University of Cologne, Germany

*CORRESPONDENCE
Nam-Soo Jwa
nsjwa@sejong.ac.kr

†These authors have contributed equally to this work

RECEIVED 16 November 2023
ACCEPTED 17 April 2024
PUBLISHED 02 May 2024

CITATION
Wang J, Choi W-G, Nguyen NK, Liu D, Kim S-H, Lim D, Hwang BK and Jwa N-S (2024) Cytoplasmic Ca^{2+} influx mediates iron- and reactive oxygen species-dependent ferroptotic cell death in rice immunity. *Front. Plant Sci.* 15:1339559. doi: 10.3389/fpls.2024.1339559

Cytoplasmic Ca^{2+} influx mediates iron- and reactive oxygen species-dependent ferroptotic cell death in rice immunity

Juan Wang[1†], Won-Gyu Choi[2†], Nam Khoa Nguyen[1], Dongping Liu[1], Su-Hwa Kim[2], Dongyeol Lim[3], Byung Kook Hwang[4] and Nam-Soo Jwa[1*]

[1]Division of Integrative Bioscience and Biotechnology, College of Life Sciences, Sejong University, Seoul, Republic of Korea, [2]Department of Biochemistry and Molecular Biology, University of Nevada, Reno, NV, United States, [3]Department of Chemistry, College of Natural Sciences, Sejong University, Seoul, Republic of Korea, [4]Division of Biotechnology, College of Life Sciences and Biotechnology, Korea University, Seoul, Republic of Korea

Iron- and reactive oxygen species (ROS)-dependent ferroptosis occurs in plant cells. Ca^{2+} acts as a conserved key mediator to control plant immune responses. Here, we report a novel role of cytoplasmic Ca^{2+} influx regulating ferroptotic cell death in rice immunity using pharmacological approaches. High Ca^{2+} influx triggered iron-dependent ROS accumulation, lipid peroxidation, and subsequent hypersensitive response (HR) cell death in rice (*Oryza sativa*). During *Magnaporthe oryzae* infection, 14 different Ca^{2+} influx regulators altered Ca^{2+}, ROS and Fe^{2+} accumulation, *glutathione reductase* (*GR*) expression, glutathione (GSH) depletion and lipid peroxidation, leading to ferroptotic cell death in rice. High Ca^{2+} levels inhibited the reduction of glutathione isulphide (GSSG) to GSH *in vitro*. Ca^{2+} chelation by ethylene glycol-bis (2-aminoethylether)-*N, N, N′, N′*-tetra-acetic acid (EGTA) suppressed apoplastic Ca^{2+} influx in rice leaf sheaths during infection. Blocking apoplastic Ca^{2+} influx into the cytoplasm by Ca^{2+} chelation effectively suppressed Ca^{2+}-mediated iron-dependent ROS accumulation and ferroptotic cell death. By contrast, acibenzolar-*S*-methyl (ASM), a plant defense activator, significantly enhanced Ca^{2+} influx, as well as ROS and iron accumulation to trigger ferroptotic cell death in rice. The cytoplasmic Ca^{2+} influx through calcium-permeable cation channels, including the putative resistosomes, could mediate iron- and ROS-dependent ferroptotic cell death under reduced *GR* expression levels in rice immune responses.

KEYWORDS

iron, ROS, Ca^{2+} influx, *GR* expression, ferroptotic cell death, rice, *Magnaporthe oryzae*

Introduction

Plant cell death is an effective immune response to defend against microbial pathogens (Heath, 2000; Greenberg and Yao, 2004). Plant-pathogen interactions induce both pathogen-associated molecular patterns (PAMP)-triggered immunity (PTI) and effector-triggered immunity (ETI) in plant cells, depending on the mode of pathogen recognition (Jones and Dangl, 2006; Dangl et al., 2013; Ngou et al., 2021). Reactive oxygen species (ROS), such as superoxide, H_2O_2, and hydroxyl radical (•OH) are required to signal and execute plant cell death (Levine et al., 1994; Van Breusegem and Dat, 2006). ROS act as cellular signaling molecules that trigger PTI and ETI in plant cells after plants recognize pathogen infection (Jwa and Hwang, 2017). Robust ROS bursts are common signaling events that occur in hypersensitive response (HR) cell death (Van Breusegem and Dat, 2006; Jwa and Hwang, 2017). Virulent plant pathogens induce transient PTI with low levels of ROS. However, avirulent pathogens induce ETI with strong ROS bursts, leading to HR cell death (Grant and Loake, 2000). ETI is more potent in plant immunity than PTI and greatly limits the entry of microbial pathogens into plant cells via HR induced by intracellular nucleotide-binding leucine-rich repeat (NLR) receptors which can recognize pathogen effectors (Jones and Dangl, 2006). Plant pathogens have evolved to acquire a variety of effectors to suppress ROS bursts, which are key components of the plant immune response (Jwa and Hwang, 2017).

Ferroptosis is a nonapoptotic form of iron-dependent cell death first discovered in animal cells (Dixon et al., 2012; Stockwell et al., 2017) and then in plants, fungi, and bacteria (Distéfano et al., 2017; Dangol et al., 2019; Shen et al., 2020; Aguilera et al., 2022). Iron, ROS, and lipid hydroperoxides are directly involved in ferroptotic cell death (Stockwell et al., 2017; Dangol et al., 2019). The Fenton reaction (Fenton, 1894; Pierre and Fontecave, 1999) by iron ions (Fe^{2+}) and ROS (H_2O_2) induces glutathione (GSH) depletion and iron- and ROS-dependent ferroptosis in the rice immune response (Dangol et al., 2019). Ca^{2+} is a conserved second messenger and a major mediator in plant immune responses (Köster et al., 2022). However, whether an abnormally high concentration of Ca^{2+} influx is directly associated with HR cell death is not fully understood, except for its role as a signal transducer in plant immunity (Moeder et al., 2019). Moreover, the role of Ca^{2+} in ferroptosis remains unclear.

Recently, it has been proposed that plant nucleotide-binding leucine-rich repeat receptors (NLRs) (Jones and Dangl, 2006; Dangl et al., 2013; Ngou et al., 2021) recognize pathogen effectors to form resistosome complexes as calcium-permeable cation channels in the plasma membrane (Bi et al., 2021). The ZAR1 (HOPZ-ACTIVATED RESISTANCE 1) resistosome (Lewis et al., 2020) is a membrane-localized Ca^{2+}-permeable channel which can trigger immune signaling and cell death in *Arabidopsis* (Bi et al., 2021). The monocot wheat protein Sr35, which belongs to the CC-NLR class, has been demonstrated to assemble into a resistosome with a structure similar to ZAR1 (Förderer et al., 2022). *Arabidopsis* 'helper' immune NLRs form Ca^{2+}-permeable cation channels, leading to cytoplasmic Ca^{2+} influx and subsequent cell death (Jacob et al., 2021). Ca^{2+}-permeable cation channels of NLR-mediated resistosomes may induce a sustained high cytoplasmic Ca^{2+} influx during plant ETI (Jacob et al., 2021). Thus, the discovery of resistosomes that exhibit Ca^{2+} channel activity in plants provided a crucial clue to elucidate the common mechanism of plant cell death and immunity (Bi et al., 2021; Jacob et al., 2021).

The Ca^{2+} concentration in the apoplast (~1 mM) is approximately 10,000-fold higher than that in the cytoplasm (~100 nM) (Stael et al., 2012). The significant Ca^{2+} concentration gradient in the cell may be maintained by both passive impermeability of the plasma membrane to calcium ions and their active transport from the cytoplasm to the apoplast. Schanne et al. (1979) first demonstrated that perturbation of calcium homeostasis triggers toxic cell death in rat hepatocytes through cytoplasmic Ca^{2+} influx due to impaired membrane integrity, highlighting the pivotal role of Ca^{2+} in toxic cell death. During toxic cell death, disruption of Ca^{2+} homeostasis coincides with a decrease in glutathione peroxidase (GPX) and glutathione reductase (GR) activity, resulting in cellular damage due to the acute oxidative stress by glutathione depletion (Bellomo et al., 1982; Jewell et al., 1982). The other alternative hypothesis was that the cell death is not only due to ROS themselves, but also due to the generation of the hydroxyl radical, a more potent oxidizing species, through its reaction with iron (Starke and Farber, 1985; Farber, 1994). Reduced glutathione (GSH) plays a crucial role in controlling ROS in cells. ROS function as intracellular and extracellular signaling molecules. Complex crosstalks between ROS, oxidized glutathione (GSSG) and reduced glutathione (GSH), and the antioxidant enzyme glutathione reductase (GR) control the redox state inside the cell to be suitable for activation of programmed cell death (Couto et al., 2016). However, the roles of GPX and GR in plant HR cell death are largely unknown.

Rice (*Oryza sativa*)-*Magnaporthe oryzae* interaction is a good experimental system to analyze if Ca^{2+} mediates iron- and ROS-dependent ferroptotic cell death in plant immunity (Valent, 2021). In this study, Ca^{2+} sensor (*35S::GCaMP6mC*) transgenic rice lines, the Ca^{2+} indicator Fluo-5F AM, and the *o*-cresolphthalein complexone (*o*-CPC) method were used to visualize and quantify intracellular and apoplastic Ca^{2+} levels in rice leaf sheaths treated with multiple Ca^{2+} influx enhancers and/or inhibitors during *M. oryzae* infection. Taken together, our results suggest that Ca^{2+} influx from apoplast via calcium-permeable cation channels, triggers iron-dependent lipid-based reactive oxygen species (lipid ROS) accumulation by reduced *Glutathione Reductase* (*GR*) expression and glutathione depletion in rice cells, which acts as a critical redox switch for iron- and lipid ROS-dependent ferroptotic cell death.

Materials and methods

Plant material and growth conditions

Rice (*Oryza sativa L.*) cultivar Kitaake was used as the wild type (WT) in this study. Seeds of Kitaake were obtained from the National Institute of Crop Science, Jeonju, Korea (http://

www.nics.go.kr). Plants were raised in a growth chamber at 30°C under 60% humidity and 16 h light/8 h dark photoperiod.

Magnaporthe oryzae strains and culture conditions

M. oryzae strains RO1-1 and 007 were obtained from the Center for Fungal Genetic Resources, Seoul National University, Korea (http://genebank.snu.ac.kr). *M. oryzae* RO1-1 is virulent to rice cultivar Kitaake, whereas *M. oryzae* 007 is avirulent. Both *M. oryzae* strains were stored at −20°C and cultured on rice bran agar medium (20 g of rice bran, 20 g of sucrose, and 20 g of agar in 1 L of water) at 25°C in the dark for 10–14 days (Singh et al., 2016). Sporulation of *M. oryzae* cultures was induced by incubating the culture plates under continuous light for 3–4 days. *M. oryzae* conidia were harvested from the sporulated culture plates using 0.025% Tween20 (Sigma-Aldrich) in sterile water (Kankanala et al., 2007). A conidial suspension of *M. oryzae* in 0.025% (v/v) Tween 20 was adjusted to appropriate conidial concentrations using a hemacytometer.

Plasmid construction and rice transformation

GCaMP6f was cloned into the plant expression vector pGWB554 using standard molecular techniques, as described previously (Choi et al., 2014; Weigand et al., 2021). The resultant construct was transformed into rice cultivar Kitaake using *Agrobacterium tumefaciens* strain LBA4404. Briefly, *35S::GCaMP6f-mCherry* (*GCaMP6fmC*) was delivered into rice calli using *Agrobacterium*-mediated transformation (Hiei et al., 1994). Transformed calli were selected on the half-strength Murashige and Skoog (1/2 MS; Sigma-Aldrich) medium (2.15 g of MS salts, 15 g of sucrose, and 3.5 g of Gelrite [Duchefa Biochemie] in 1 L of water) supplemented with 20 $\mu g \cdot mL^{-1}$ hygromycin B (Duchefa Biochemie). After root and shoot formation, rice seedlings were transferred to water and acclimated for 2 days. Rice seedlings were then transferred into pots containing Baroker soil (Seoul Bio) and raised in a growth chamber.

Construction and cloning of the crystal structure of GCaMP6-mCherry

The crystal structures of Ca^{2+}-free GCaMP6 (ID: 3wlc), Ca^{2+}-bound GCaMP6 (ID: 3wld), and mCherry (ID: 2h5q) were obtained from the RCSB Protein Data Bank (https://www.rcsb.org) (Shu et al., 2006; Ding et al., 2014). These three crystal structures were then used to construct crystal images of GCaMP6-mCherry using the PyMOL software (https://pymol.org) (Ding et al., 2014). The Ca^{2+} sensor construct GCaMP6f-mCherry (GCaMP6fmC) was cloned into the vector pGWB554 under the control of the Cauliflower mosaic virus (CaMV) 35S promoter (Supplementary Figure 1A).

Generation of Ca^{2+} sensor (*35S:: GCaMP6fmC)* transgenic rice lines

The seeds of rice cultivar Kitaake and Ca^{2+} sensor (*35S::GCaMP6fmC*) transgenic rice lines were hulled, sterilized first with 100% ethanol for 1 min and then with 50% Clorox for 30 min, and washed three times with 3DW. The surface-sterilized seeds were then cultured on 1/2 MS medium (Sigma-Aldrich, St. Louis, MO) at 25°C under continuous light for 2 weeks. Leaves were collected from rice plants and subjected to genomic DNA extraction using the cetyltrimethylammonium bromide (CTAB) method. Plants were genotyped by PCR as described previously (Kim et al., 2011), and Ca^{2+} sensor (GCaMP6fmC) transgenic lines were identified using the hygromycin gene-specific and GCaMP6f-specific primers (Supplementary Table 1). Ca^{2+} sensor (GCaMP6fmC) expression was verified in the transgenic lines by PCR using hygromycin resistance (HygR) and GCaMP6fmC primers (Supplementary Figure 1B). Without Ca^{2+} binding, the GCaMP6fmC has low intrinsic fluorescence. However, the green fluorescence of GCaMP6fmC increases after binding of Ca^{2+} to the calmodulin domain (Figures 1A, B).

RNA extraction and gene expression analysis

Total RNA was extracted from rice plants using the TRIzol Reagent (Invitrogen) and used for cDNA synthesis. Transcript levels of rice *Glutathione Reductase 1* (*OsGR1*), *OsGR2*, *OsGR3*, and *Ubiquitin* (*OsUbi*) genes were analyzed by reverse transcription polymerase chain reaction (RT-PCR) and real-time quantitative RT-PCR (real-time qRT-PCR) using gene-specific primers (Supplementary Table 1). Transcript levels of *OsGR1–3* were normalized relative to that of *OsUbi* and presented as mean ± standard deviation (SD) of three biological replicates. The experiments were repeated three times.

M. oryzae inoculation and Ca^{2+} influx inhibitor and enhancer treatment of rice

To investigate Ca^{2+}-mediated iron- and ROS-dependent ferroptotic cell death in rice during *M. oryzae* infection, Ca^{2+} influx inhibitors, including ethylene glycol-bis(2-aminoethylether)-*N, N, N′, N′*-tetra-acetic acid (EGTA; Sigma-Aldrich) (Atkinson et al., 1990; Cessna and Low, 2001), verapamil hydrochloride (verapamil; Sigma-Aldrich) (Beneloujaephajri et al., 2013), N-acetyl-cysteine (NAC; Sigma-Aldrich) (Sun et al., 2012), neomycin sulfate (neomycin; ChemCruz) (Franklin-Tong et al., 1996), LiCl (Tokyo Chemical Industry) (Moyen et al., 1998), $AlCl_3$ (Sigma-Aldrich) (Kadota et al., 2005), and ruthenium red (RR; ChemCruz) (Bae et al., 2003), and Ca^{2+} influx enhancers, including acibenzolar-*S*-methyl (ASM; Sigma-Aldrich) (Brisset et al., 2000; Buonaurio et al., 2002), diamide (Sigma-Aldrich) (Kosower et al., 1969; Gilge et al., 2008), trifluoperazine hydrochloride (TFP; Sigma-

10.3389/fpls.2024.1339559

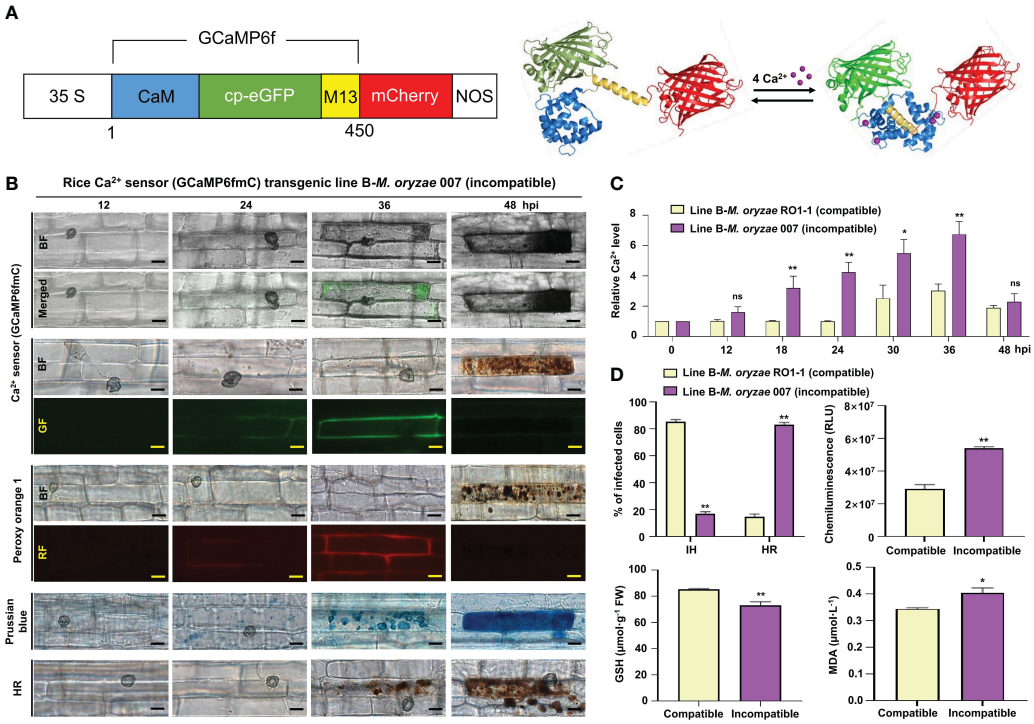

FIGURE 1
Ca^{2+} influx mediates ROS- and iron-dependent HR cell death in rice immune responses. **(A)** Schematic diagram of the Ca^{2+} sensor construct. When Ca^{2+} is free, the calmodulin (CaM) domain is dissociated from M13; however, the binding of Ca^{2+} to CaM promotes CaM-M13 binding, leading to increased eGFP fluorescence. mCherry (red fluorescence) serves as an internal fluorescence reference. **(B)** Time-course images of Ca^{2+} influx, ROS and Fe^{3+} accumulation, and HR cell death in the leaf sheaths of rice (Kitaake) Ca^{2+} sensor (GCaMP6fmC) transgenic line B during avirulent *M. oryzae* infection. Bars = 10 μm. **(C)** Time-course quantification of Ca^{2+} influx during virulent and avirulent *M. oryzae* infection. At least three regions of interest (ROIs) were selected to quantify Ca^{2+} changes by calculating the GCaMP6f/mCherry ratio at different time points (hpi) using the software ImageJ. The ratio values of GCaMP6f/mCherry were compared with those of the controls (0 hpi). **(D)** Quantification of disease phenotypes (HR/IH) (48 hpi) and ROS (36 hpi), GSH (48 hpi), and lipid (MDA) peroxidation (48 hpi) levels during virulent and avirulent *M. oryzae* infection. Data are represented as the mean ± SD (n = 4 leaf sheaths from different plants). Asterisks indicate statistically significant differences (*P< 0.05, **P< 0.01; Student's *t*-test). hpi, hours post-inoculation; ns, non-significant; IH, invasive hyphae; HR, hypersensitive response; RLU, relative luminescent units; MDA, malondialdehyde.

Aldrich) (Kang et al., 2017), $CaCl_2$/calcimycin (C/C; Sigma-Aldrich) (Verma et al., 2011), $CaCl_2/H_2O_2$ (C/H; Sigma-Aldrich) (Rentel and Knight, 2004), rotenone (Sigma-Aldrich) (Li et al., 2003), and butylmalonic acid (BMA; Sigma-Aldrich) (Kamga et al., 2010), were applied onto rice leaf sheaths. All Ca^{2+} influx inhibitors and enhancers used in this study were treated on rice leaf sheaths with appropriate concentrations that never inhibited *M. oryzae* spore germination, appressorium formation and growth that are important for *M. oryzae* infection in rice. Among the Ca^{2+} influx enhancers, diamide and BMA were used to induce the depletion of reduced glutathione (GSH) (Gilge et al., 2008; Kamga et al., 2010), and rotenone was used to inhibit ROS burst by mitochondrial complex I (Li et al., 2003). Each Ca^{2+} influx inhibitor was applied onto a 5–7 cm long section of rice leaf sheath, together with avirulent *M. oryzae* 007 (5×10^5 conidia·mL^{-1}) inoculation. Similarly, each Ca^{2+} influx enhancer (except TFP and rotenone) was applied onto a 5–7 cm long section of rice leaf sheath, together with virulent *M. oryzae* RO1-1 (5×10^5 conidia·mL^{-1}) inoculation; TFP or rotenone was applied to rice sheath (5–7 cm long section) at 23 h post-inoculation (hpi) with virulent *M. oryzae* RO1-1. The Ca^{2+} influx inhibitor/enhancer treated and pathogen-inoculated rice leaf sheaths were incubated at 25°C under moist conditions. Rice leaf sheath samples were collected at different time points after inoculation with *M. oryzae*.

Determination of infection types

The epidermal cell layers excised from the inoculated rice leaf sheaths were observed under a microscope (Zeiss equipped with Axioplan 2; Campbell, CA), as described previously (Kankanala et al., 2007). The infected epidermal cells were counted and categorized into two types: cells with invasive hyphae (IH) and cells with hypersensitive response (HR) cell death. Infected cells of each infection type were quantified. The experiment was repeated three times.

Ca^{2+} influx detection and quantification

Images of Ca^{2+} influx in rice sheath cells were taken using a microscope (Zeiss equipped with Axioplan2) with bright field filter, green fluorescence filter (excitation [Ex]/emission [Em] wavelengths: 450–490/515–565 nm), and red fluorescence filter

(Ex/Em: 546/590 nm). At least three regions of interest (ROIs) were selected to quantify changes in Ca^{2+} levels by calculating the GCaMP6f/mCherry ratio at different time points or at 36 hpi using the ImageJ software. Green and red fluorescence signal intensities were measured using ImageJ installed with the Macro (Weigand et al., 2021). Data were exported into an Excel file, and the ratio of green to red fluorescence signal intensities was calculated. The values were compared with those of the mock control and expressed as relative fluorescence intensities (RFI). Images were taken using Leica TCS SP5 confocal microscope (Leica, Mannheim, Germany), with bright field, EGFP (Ex/Em: 488/500–540 nm), and mCherry (Ex/Em: 587/600–680 nm) filters, and merged.

Visualization and fluorescence quantification of cellular Ca^{2+} levels using Ca^{2+} indicator Fluo-5F AM

Fluo-5F AM (Invitrogen) is a low affinity intracellular Ca^{2+} indicator suitable for detecting high intracellular Ca^{2+} levels ranging from 1 μM to 1 mM. Binding of Ca^{2+} to Fluo-5F is catalyzed by cellular esterases that break the ester bonds of Fluo-5F AM (Figure 2B). Intracellular Ca^{2+} dynamics in *M. oryzae*-infected rice sheaths were determined by the Ca^{2+} indicator Fluo-5F AM (Invitrogen) (Eaddy and Schnellmann, 2011). Fluo-5F AM was used to visualize intracellular Ca^{2+} ions during *M. oryzae* infection. Briefly, the epidermal layer recovered from the rice leaf sheaths was immersed in 0.5 M sucrose for 10 min for rapid plasmolysis. The leaf sheath epidermis was then incubated in a solution of Fluo-5F AM at a final concentration of 50 μM at 37°C for 1 h, followed by a rapid washing using 3DW. The epidermis was kept at room temperature for another 30 min to allow the reaction to occur. To visualize both Ca^{2+} and ROS simultaneously inside the same rice cell, a mixture of 50 μM Fluo-5F AM and 5 μM PO1 was used as described above. The above steps were performed under light-blocking conditions. Samples were observed under a fluorescence microscope (Zeiss equipped with an Axioplan 2; Campbell, CA) with a bright field (BF) filter and/or a green fluorescence (GF) filter. Fluorescence intensities of at least three regions of interest (ROIs) were selected to quantify changes in Ca^{2+} levels by measuring green fluorescence intensities at different time points using ImageJ software (Grossi et al., 2016). Corrected total cell fluorescence (CTCF) values were calculated as previously described (Jakic

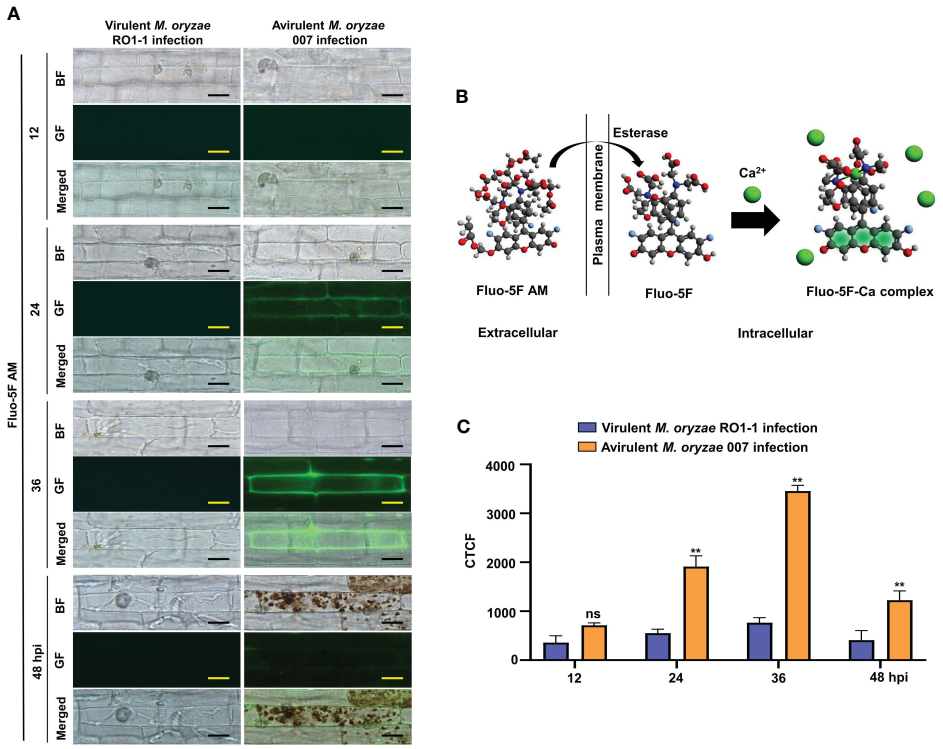

FIGURE 2
Dynamics of Ca^{2+} influx in the leaf sheaths of rice Kitaake during *Magnaprthe oryzae* 007 (avirulent) and RO1-1 (virulent) infection. **(A)** Time-course images of Ca^{2+} influx in the rice leaf sheaths during *M. oryzae* infection. The rice leaf sheaths were inoculated with *M. oryzae* RO1-1 (virulent) and 007 (avirulent), and the Ca^{2+} dynamics were detected at 12, 24, 36, and 48 hpi. Rice leaf sheath cells were stained with Fluo-5F AM and were observed under a microscope (Zeiss equipped with Axioplan 2) using a bright field filter and/or the green fluorescence filter. Bars = 10 μm. WT, wild type; BF, bright field; GF, green fluorescence. hpi, hours post-inoculation. **(B)** Schematic diagram of Ca^{2+} detection by Fluo-5F AM. When Fluo-5F AM enters the cytoplasm from the apoplast, the AM is cut off by cellular esterases. When free Ca^{2+} binds to Fluo-5F, the Fluo-5F-Ca complex becomes fluorescent. **(C)** Time-course quantification of Ca^{2+} influx during *M. oryzae* infection. At least three regions of interest (ROIs) were selected to quantify Ca^{2+} changes by calculating the corrected total cell fluorescence (CTCF) at different time points (hpi) using the software ImageJ. Data are represented as the mean ± SD (n = 4 leaf sheaths from different plants). Asterisks above bars indicate significantly different means (**P< 0.01; Student's *t*-test). hpi, hours post-inoculation; ns, non-significant.

et al., 2017; Bora et al., 2021): CTCF = integrated fluorescence density – (ROI area × mean fluorescence of background readings).

Detection of apoplastic (intercellular) Ca^{2+} concentration

Rice leaf sheaths were inoculated with avirulent *M. oryzae* 007 (4×10^5 conidia·mL^{-1}) in 10 mM EGTA, and apoplastic washing fluid was prepared at 12, 24, 36, and 48 hpi as described previously (Rohringer et al., 1983), with some modifications. The *M. oryzae*-inoculated and/or EGTA-treated rice leaf sheaths were vacuum-infiltrated with 3DW (distilled water) and then centrifuged at 4,000× *g*. The supernatants were completely evaporated to dryness using an evaporator, and the residue was resuspended in a certain amount of 3DW. Apoplastic Ca^{2+} concentration in rice leaf sheaths was measured using the *o*-CPC method (Corns and Ludman, 1987), which is based on the reaction of Ca^{2+} with *o*-cresolphthalein complexone (*o*-CPC), resulting in the formation of an intense violet-colored complex. Briefly, 100 µL of intercellular fluid prepared from rice leaf sheath was added to a reaction solution containing 375 µL of 1 M ethanolamine (pH 10.6; Sigma-Aldrich), 71.6 µL of 100 mM 8-hydroxyquinoline (Sigma-Aldrich), 8.2 µL of 10 mM *o*-CPC (Sigma-Aldrich), 2.32 µL of 37% HCl (Samchun), and 3DW (up to a total volume of 1 mL). The absorbance of the Ca^{2+}-*o*-CPC complex was measured at 575 nm using SP-2000 UV spectrophotometer (SmartPlus) (Corns and Ludman, 1987). Apoplastic Ca^{2+} concentration in rice leaf sheaths was calculated based on a standard curve obtained using 0–25 µM standard $CaCl_2$ (Sigma-Aldrich).

ROS detection and quantification

ROS (H_2O_2) localization in *M. oryzae*-infected rice sheath cells was determined by Peroxy Orange 1 (PO1; Sigma-Aldrich) staining. The red fluorescent ROS indicator PO1 simultaneously visualizes Ca^{2+} (green fluorescence) and ROS accumulation inside the same infected rice cell through its distinct red fluorescence emission. Briefly, the epidermal cell layer peeled off from rice leaf sheaths was soaked in 5 µM PO1 for 40 min in the dark at room temperature (Muhlemann et al., 2018; Samuel et al., 2022). The samples were washed three times with 1× phosphate-buffered saline (PBS) and observed under a fluorescence microscope (Zeiss equipped with Axioplan 2; Campbell, CA) (Ex/Em: 546/590 nm).

A chemiluminescence assay (Singh et al., 2016; Chen et al., 2022) was performed to measure ROS levels in *M. oryzae*-infected rice leaf sheath cells. Briefly, small sections of epidermal cell layer (0.5 cm × 0.2 cm) were transferred into individual wells of a 96-well plate, with each well containing 100 µL of chemiluminescent solution (30 µL of luminol [Bio-Rad, Hercules, CA], 1 µL of 1 mg·mL^{-1} horseradish peroxidase [HRP; Jackson Immunoresearch, West Grove, PA], and 69 µL of Milli-Q water), and incubated in the dark for 5 min at room temperature. ROS chemiluminescence was detected using GloMax 96 Microplate Luminometer (Promega, Madison, WI) and expressed as relative luminescence units (RLU). Experiments were independently repeated three times.

Ferric ion detection

Fe^{3+} accumulation in rice leaf sheath cells was detected and visualized by Prussian blue staining (Liu et al., 2007). Briefly, the epidermal layer of rice leaf sheath cells was isolated and then stained with a Prussian blue solution (7% potassium ferrocyanide [Sigma-Aldrich] and 2% HCl [Samchun], v:v = 1:1) for 15 h at room temperature and washed three times with 3DW. The stained epidermal cells were observed under a microscope (Zeiss equipped with Axioplan 2, Campbell, CA). Fe^{3+} were detected as a bright blue signal in sheath epidermal cells, because of their binding to ferric ferrocyanide in cells.

Lipid peroxidation (MDA) assay

Lipid peroxidation in rice leaf sheath samples was determined by measuring the level of malondialdehyde (MDA), a product of unsaturated fatty acid peroxidation, using thiobarbituric acid (TBA). Rice leaf sheath tissue was ground in liquid nitrogen, and the powdered tissue was mixed with an equal amount of reaction solution (0.5% [w/v] TBA [Sigma-Aldrich], 20% [v/v] trichloroacetic acid [TCA; Sigma-Aldrich], and 0.25 mL of 175 mM NaCl in a total of 2 mL of 50 mM Tris-Cl [pH 8.0]). Samples were incubated in boiling water for 5 min and then centrifuged at 14,000 × *g* for 5 min at 4°C. The absorbance (optical density [OD]) of each supernatant was measured at 450, 532, and 600 nm with the SP-2000UV spectrophotometer (Woongki Science, Seoul), as previously described (Zhang et al., 2009). MDA concentration was calculated using the following equation (Dangol et al., 2019).

$$C_{MDA} = [6.45 \times (OD_{532} - OD_{600})] - (0.56 \times OD_{450})$$

where C_{MDA} is the concentration of MDA, and OD_{450}, OD_{532}, and OD_{600} represent the OD of the supernatant at 450, 532, and 600 nm, respectively.

Measurement of GSH levels

The content of reduced glutathione (GSH) in rice leaf sheaths was measured spectrophotometrically. Freshly harvested conidial suspensions (4×10^5 conidia·mL^{-1}) of *M. oryzae* strains, with or without Ca^{2+} influx inhibitor or enhancer, were used to inoculate rice leaf sheaths. The inoculated leaf sheaths were incubated for 48 h in the dark in a moistened box at 25°C and then ground in liquid nitrogen. Equal amounts of the powdered sample and 5% (w/v) metaphosphoric acid (Sigma-Aldrich) were mixed, and the homogenates were centrifuged at 21,000 × *g* for 20 min at 4°C. The supernatants were collected, and each supernatant was passed through a 0.45 µm nylon filter (Sigma-Aldrich). GSH quantification was performed as described previously (Griffith, 1980; Airaki et al., 2011).

Briefly, 100 µL of the filtered supernatant was added to 600 µL of reaction buffer (100 mM sodium phosphate buffer [pH 7.5] and 1 mM EDTA [Sigma-Aldrich]). Then, 40 µL of 0.4% (w/v) 5,5'-dithiobis (2-nitrobenzoic acid) (DTNB, Sigma-Aldrich) and 350 µL of Milli-Q water were added to each sample, and the mixtures were incubated at room temperature for 5 min. To detect GSH, the absorbance of each mixture was measured at a wavelength of 412 nm using a spectrophotometer. The GSH content of each rice leaf sheath sample was quantified by constructing a calibration curve using a wide range of concentrations (0–25 µM) of standard GSH (Sigma-Aldrich).

Analysis of the inhibitory effect of Ca^{2+} on glutathione reductase activity *in vitro*

To investigate the effect of Ca^{2+} influx on the conversion of glutathione disulfide (GSSG; oxidized glutathione) into GSH (reduced glutathione) by GR, 30 µL of 1 mM GSSG (Sigma-Aldrich) and 20 µL of 4.8 mM NADPH (nicotinamide adenine dinucleotide phosphate, reduced form; Sigma-Aldrich) were added to 50 mM Tris-Cl (pH 7.5). Then, 10 µL (0.06 U) of rice GR (Koma Biotech) and yeast GR (Sigma-Aldrich) each was added to the mixture to initiate the reduction of GSSG, and the total volume of the reaction mixture was increased to 1 mL. According to the Beer-Lambert Law, 0.1 mM NADPH has an optical density which is equal to 0.622 through a 1 cm light path. Therefore, because of the consumption of NADPH during the reduction of GSSG, the OD_{340} of the sample was expected to decrease with a molar extinction coefficient of 6.22 $mmol^{-1} \cdot cm^{-1}$ at 340 nm. The decrease in the absorbance of each sample was measured at 340 nm using SP-2000 UV spectrophotometer (SmartPlus). The reactions were monitored for 5 min at room temperature.

To perform the inhibition assay, different volumes of 100 mM $CaCl_2$ were added to the reaction system so that the final concentrations of $CaCl_2$ were 0, 10, 20, 30, and 50 mM. To investigate the inhibitory effect of different cations on GSSG reduction *in vitro*, 20 mM $CaCl_2$ (Sigma-Aldrich), $MgCl_2$ (Sigma-Aldrich), NaCl (Samchun), and KCl (Duksan) were added to the reaction system. The reaction was then monitored for 5 min by detecting the decrease in OD at 340 nm.

Data analysis

All the results are expressed as the mean ± standard deviation (SD). Statistical comparisons were performed by the least significant difference (LSD) test and Student's *t*-test using GraphPad Prism 8 software (GraphPad Software, Inc., San Diego, CA, USA).

Results

Ca^{2+} influx mediates ROS- and iron-dependent HR cell death in rice-*M. oryzae* interactions

We first examined time-course images and levels of Ca^{2+} influx in the leaf sheaths of rice Kitaake during *M. oryzae* RO1-1 (virulent) and 007 (avirulent) infection (Figure 2). During virulent (compatible) *M. oryzae* RO1-1 infection, primary hyphae grew from the appressorium, differentiated into thicker, bulbous invasive hyphae (IH) in the invaded rice cell to spread into neighboring cells (Figure 2A). However, avirulent (incompatible) *M. oryzae* 007 infection induced severe HR death response with dark brown cellular aggregates at 48 h post-inoculation (hpi) in rice leaf sheath cells. We have used the Ca^{2+} indicator Fluo-5F AM to monitor time-course changes in cytoplasmic Ca^{2+} influx by visualizing and quantifying Ca^{2+} fluorophores in living rice cells (Eaddy and Schnellmann, 2011). Fluo-5F is initially non-fluorescent. However, it becomes fluorescent when it binds to free Ca^{2+} in cells. During avirulent *M. oryzae* 007 infection, cytoplasmic Ca^{2+} influx began to appear at 12 hpi, increased markedly at 24 hpi, and peaked at 36 hpi (Figures 2A, C). At 48 hpi, extensive HR cell death occurred with dark brown cellular aggregates; however, Ca^{2+} influx levels decreased rapidly. By contrast, cytoplasmic Ca^{2+} levels were rarely or not detected in rice cells during virulent *M. oryzae* RO1-1 infection. We also stained rice leaf sheaths with a mixture of Fluo-5F AM and Peroxy Orange 1 (PO1) to visualize localization of Ca^{2+} and ROS (H_2O_2) accumulation (36 hpi) during infection, respectively (Figure 3A). The interplay of Ca^{2+} and ROS during plant immunity is a well-known phenomenon, but its mechanisms are not fully understood. Interestingly, we observed a marked co-localization of Ca^{2+} and ROS accumulation around invasive hyphae (IH) as well as inside the invaded and neighboring cells of rice leaf sheaths at 36 hpi with avirulent *M. oryzae* 007 (Figure 3A). To determine the role of ferric ions (Fe^{3+}) in HR cell death during *M. oryzae* infection, we further stained rice leaf sheath tissues with Prussian blue solution to detect Fe^{3+}, as described previously (Dangol et al., 2019). Unlike Ca^{2+} or ROS accumulation, Fe^{3+} was observed (blue color) at hyphal invasion sites in the HR cell death response of rice leaf sheath cells at 48 hpi with avirulent *M. oryzae* 007 (Figure 3A). By contrast, Ca^{2+}, ROS and iron (Fe^{3+}) accumulation was not detected in the rice sheath cells infected by virulent *M. oryzae* RO1-1 (Figure 3A). Avirulent *M. oryzae* 007 infection, but not virulent *M. oryzae* RO1-1 infection, significantly induced Ca^{2+} and ROS accumulation (36 hpi), iron accumulation (48 hpi), HR cell death (48 hpi), reduced glutathione (GSH, γ-L-glutamyl-L-cysteinylglycine) depletion (48 hpi), and lipid peroxidation (48 hpi) in rice leaf sheath cells (Figures 3A, D).

The Ca^{2+} sensor was designed as the mCherry fused to the N-terminus of GCaMP6f and consisted of two tandem fluorescent proteins (Weigand et al., 2021). The protein-based Ca^{2+} sensor (GCaMP6fmC) was used as an alternative tool to compare two separate cytoplasmic Ca^{2+} influxes in the wild type and Ca^{2+} sensor transgenic rice lines. To investigate if Ca^{2+} mediates ferroptotic cell death in rice immunity, we next generated Ca^{2+} sensor rice (cultivar Kitaake) transgenic lines as an alternative Ca^{2+} visualization tool, in which GCaMP6f-mCherry fusion Ca^{2+} reporter (GCaMP6fmC) can be expressed to emit strong green fluorescence by binding of Ca^{2+} to the calmodulin domain (Figure 1A; Supplementary Figure 1). The Ca^{2+} sensor (GCaMP6fmC) made it possible to specifically detect and visualize intracellular Ca^{2+} changes inside living rice cells without any additional calcium indicator staining. Avirulent (incompatible) *M. oryzae* 007 grew poorly, with only a few

10.3389/fpls.2024.1339559

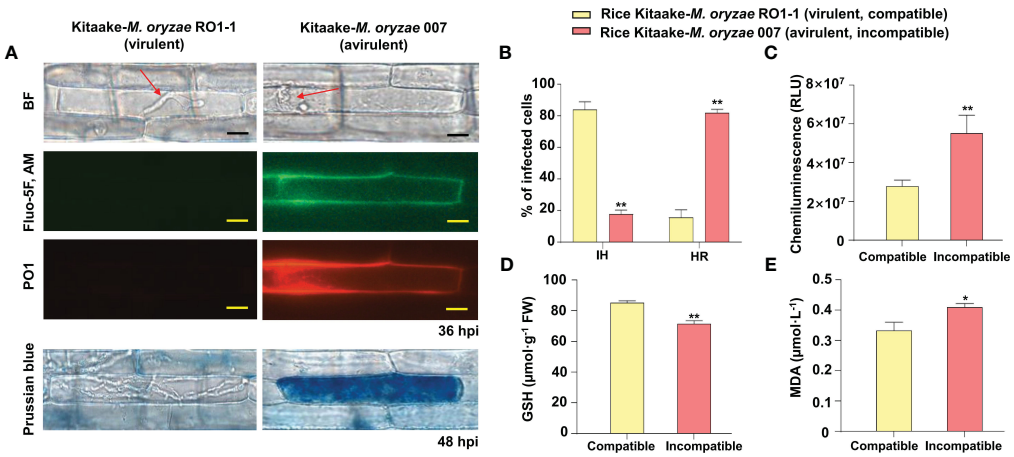

FIGURE 3
Images and quantification of Ca^{2+} influx, ROS and iron accumulation, hypersensitive response (HR) cell death, reduced glutathione (GSH) depletion, and lipid peroxidation in rice leaf sheaths during *Magnaporthe oryzae* infection. **(A)** Images of Ca^{2+} influx and ROS and iron accumulation in rice leaf sheaths during *M. oryzae* infection. The leaf sheaths of Kitaake (WT) were inoculated with *M. oryzae* RO1-1 (virulent) and 007 (avirulent). Rice leaf sheath cells were stained with a mixture of Fluo-5F AM and Peroxy Orange 1 (PO1) to visualize Ca^{2+} influx and H_2O_2 accumulation in the rice cell during infection. Fe^{3+} accumulation was detected by Prussian blue staining. Images of Ca^{2+} influx, H_2O_2 accumulation, and Fe^{3+} accumulation in rice leaf sheaths were observed under a microscope (Zeiss equipped with Axioplan 2) using a bright field filter and/or fluorescence filters. Bars = 10 μm. Red arrows indicate invasive hyphae (IH). WT, wild type; BF, bright field. **(B)** Quantification of infection phenotypes, classified as cells showing invasive hyphal (IH) growth and HR cell death, in the leaf sheaths (48 hpi). **(C)** ROS quantification (36 hpi) in rice cells via a chemiluminescence assay using GloMax 96 Microplate Luminometer (Promega, Madison, WI). Values are mean ± standard deviation (SD; n = 10) of the total relative luminescence units (RLU) of different rice sheath discs. **(D)** Quantification of GSH levels in rice leaf sheaths (48 hpi). Values represent mean ± SD (n = 4) of GSH concentrations in the leaf sheaths of different plants. GSH reacts with 5,5′-dithiobis (2-nitrobenzoic acid) to generate 2-nitro-5-thiobenzoic acid, which was measured using the SP-2000UV spectrophotometer (Woongki Science, Seoul) at a wavelength of 412 nm. **(E)** Quantification of lipid peroxidation in rice leaf sheaths (48 hpi) by measuring malondialdehyde (MDA) levels. Values are mean ± SD (n = 4) of MDA concentrations in the leaf sheaths of different plants. Asterisks above bars indicate significantly different means (*P< 0.05, **P< 0.01; Student's t-test). Experiments were repeated three times with similar results. hpi, hours post-inoculation.

invasive hyphae (IH) leading to HR cell death in rice leaf sheaths (Figures 2A, 1B, D). Ca^{2+} influx levels in the rice leaf sheaths were measured by confocal and fluorescence microscopy (Figure 2A, green fluorescence in the GF images; Figure 1B; Supplementary Figures 1C, 2). Peroxy Orange 1 and Prussian blue staining showed the accumulation of ROS (H_2O_2) and Fe^{3+}, respectively, in leaf sheath cells (Figure 1B, red fluorescence in the RF images for ROS and blue-colored deposits for Fe^{3+}). Ca^{2+} and ROS accumulation was significantly induced around the IH and within the invaded rice cells at 36-48 hpi with avirulent *M. oryzae* 007 (Figures 1B, D). By contrast, ROS accumulation was not detected in rice cells infected with virulent *M. oryzae* RO1-1. Avirulent *M. oryzae* 007, but not virulent *M. oryzae* RO1-1, significantly induced Fe^{3+} accumulation inside and around the IH in rice sheath cells at 36-48 hpi (Figure 1B). Fe^{3+} was observed as a blue color inside the IH and at the hyphal invasion sites in the HR cell death response where ROS accumulated. HR cell death was detected as vesicle-containing dark brown cellular aggregates inside the infected rice cells at 48 hpi (Figure 1B). During avirulent *M. oryzae* infection, abundant ROS bursts and HR cell death at 48 hpi were accompanied by significant depletion of reduced glutathione (GSH, γ-L-glutamyl-L-cysteinylglycine) and significant increase in lipid peroxidation [malondialdehyde (MDA) levels] (Figures 1B, D). GSH is one of the major water-soluble small molecule antioxidants that protect plant cells from oxidative damage (Airaki et al., 2011).

Ca^{2+} influx into the leaf sheath cells of Ca^{2+} sensor (GCaMP6fmC) transgenic line B was quantified over time during *M. oryzae* RO1-1 (virulent) and 007 (avirulent) infection (Figure 1C). During avirulent *M. oryzae* 007 infection, we observed *M. oryzae* appressorium formation at 12 hpi, hyphal invasion initiation at 24 hpi, strong Ca^{2+} influx at 18-36 hpi, abundant HR cell death at 48 hpi, along with ROS and iron accumulation, GSH depletion, and lipid peroxidation (Figures 1B, D). Overall, our data suggest that avirulent *M. oryzae* 007 infection induces higher levels of Ca^{2+} influx to mediate ROS- and iron-dependent ferroptotic cell death compared with virulent *M. oryzae* RO1-1 infection (Figures 2-1; Supplementary Figure 2).

The calcium chelator EGTA effectively blocks Ca^{2+}-mediated ROS- and iron-dependent HR cell death

During avirulent *M. oryzae* 007 infection, Ca^{2+}-mediated ROS and iron accumulation in cells induced ferroptotic HR cell death (Figure 4). Avirulent *M. oryzae* infection induced high levels of Ca^{2+} influx and ROS and iron accumulation in rice leaf sheath cells, as visualized by confocal and fluorescence microscopy (Figure 4A). We applied the membrane-nonpermeable calcium chelator ethylene glycol-bis(2-aminoethylether)-*N, N, N′, N′*-tetra-acetic

acid (EGTA) (Ellis-Davies and Kaplan, 1994) onto rice leaf sheaths to investigate whether EGTA blocks Ca^{2+} influx from the apoplast to the cytoplasm during rice HR cell death. EGTA (10 mM) treatment inhibited the accumulation of Ca^{2+}, ROS and iron, and the induction of HR cell death by avirulent *M. oryzae* infection, which ultimately allowed the fungal hyphae to grow normally inside the leaf sheath cells (Figure 4A). We also quantified the infection phenotypes (IH and HR), Ca^{2+} influx, ROS production, and GSH and MDA levels in mock (water)- and EGTA-treated rice Kitaake and Ca^{2+} sensor (GCaMP6fmC) transgenic line B at different times after inoculation with avirulent *M. oryzae* 007 (Figures 4B, C). EGTA-treated leaf sheaths contained more pathogen-infected cells but fewer HR cells, compared to the mock (water)-treated leaf sheaths during avirulent *M. oryzae* 007 infection (Figure 4B). EGTA treatment significantly inhibited Ca^{2+} influx and ROS production, correlated with strong GSH production and reduced lipid peroxidation in avirulent *M. oryzae* 007-infected rice cells (Figure 4C).

Binding of Ca^{2+} to EGTA forms the EGTA-Ca complex (Figure 5A). To investigate if EGTA causes chelation of apoplastic Ca^{2+} in rice cells, we prepared apoplastic washing fluid from *M. oryzae*-inoculated and/or EGTA-treated rice leaf sheaths (Figure 5; Supplementary Figure 3). Ca^{2+} in the intercellular (apoplastic) fluid of rice leaf sheaths was detected using the calcium-*o*-cresolphthalein complexone (*o*-CPC) method (Supplementary Figure 3A). EGTA treatment markedly lowered apoplastic Ca^{2+} levels to block Ca^{2+} influx into the cytoplasm of rice leaf sheaths throughout avirulent *M. oryzae* 007 infection, ultimately suppressing ferroptotic HR cell death, but leading to normal fungal growth and susceptible disease (Figures 5B, C; Supplementary Figure 3B). Avirulent *M. oryzae* 007 infection resulted in 83.93% of HR cell death in rice sheaths. However, EGTA treatment significantly reduced HR cell death to 16.60%, which is comparable to virulent *M. oryzae* RO1-1 infection (Figure 5C). Together, our data suggest that the membrane-nonpermeable calcium chelator EGTA effectively blocks apoplastic Ca^{2+} influx into the cytoplasm to inhibit Ca^{2+}-mediated iron-dependent ROS accumulation leading to the formation of normal *M. oryzae* hyphal structure and susceptible blast disease.

The Ca^{2+} influx enhancer ASM effectively induces Ca^{2+}-mediated ROS- and iron-dependent HR cell death

Acibenzolar-*S*-methyl (ASM) is one of the most effective plant activators that can induce systemic acquired resistance (SAR) against a broad range of plant pathogens (Matsuo et al., 2019). During virulent *M. oryzae* RO1-1 infection, fungal hyphae grew well inside the rice leaf sheath epidermal cells (Figure 6A). However,

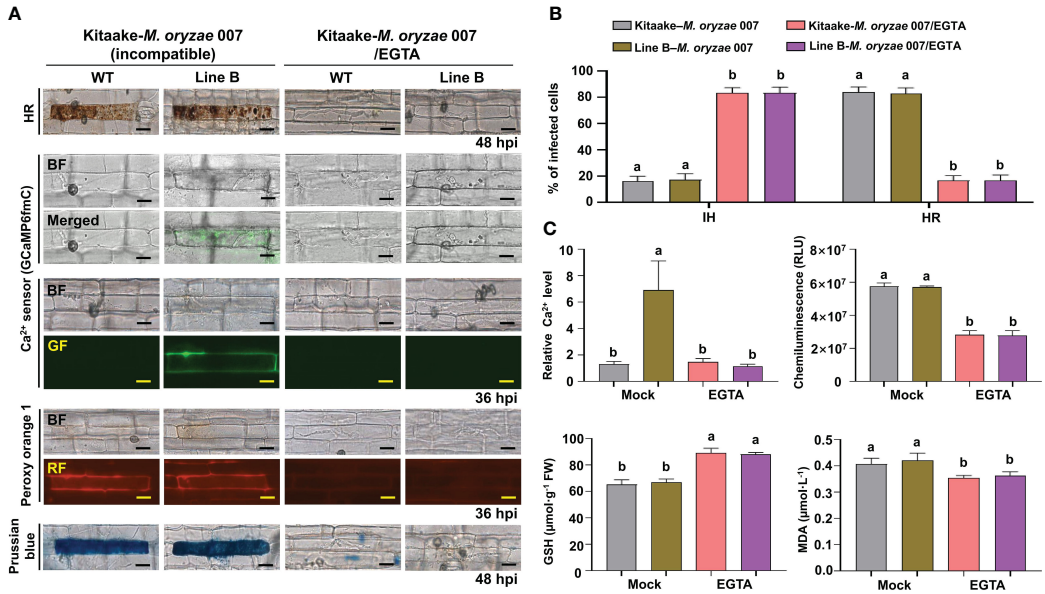

FIGURE 4
EGTA suppresses Ca^{2+}-mediated ROS- and iron-dependent HR cell death in rice immune responses. **(A)** Images of HR cell death (48 hpi), Ca^{2+} influx (36 hpi), ROS accumulation (36 hpi), and Fe^{3+} accumulation (48 hpi) in the leaf sheaths of rice Kitaake (WT) and Ca^{2+} sensor (GCaMP6fmC) transgenic line B during avirulent *M. oryzae* 007 infection after 10 mM EGTA treatment. Bars = 10 μm. **(B)** Quantification of IH/HR infection phenotypes (48 hpi). **(C)** Quantification of Ca^{2+} influx (36 hpi), ROS accumulation (36 hpi), reduced glutathione (GSH) levels (48 hpi), and lipid peroxidation (MDA) levels (48 hpi). For Ca^{2+} quantification, at least three ROIs were selected to calculate the GCaMP6f/mCherry ratio at 36 hpi using the software ImageJ. The ratio values of GCaMP6f/mCherry were compared with that of the control (Mock, Kitaake-*M. oryzae* 007). Data are represented as the mean ± SD (n = 4 leaf sheaths from different plants). Different letters above the bars indicate significantly different means, as determined by the least significant difference (LSD) test ($P < 0.05$). WT, wild type (Kitaake); EGTA, ethylene glycol-bis(2-aminoethylether)-*N, N, N′, N′*-tetra-acetic acid; hpi, hours post-inoculation; IH, invasive hyphae; HR, hypersensitive response; RLU, relative luminescent units; MDA, malondialdehyde.

10.3389/fpls.2024.1339559

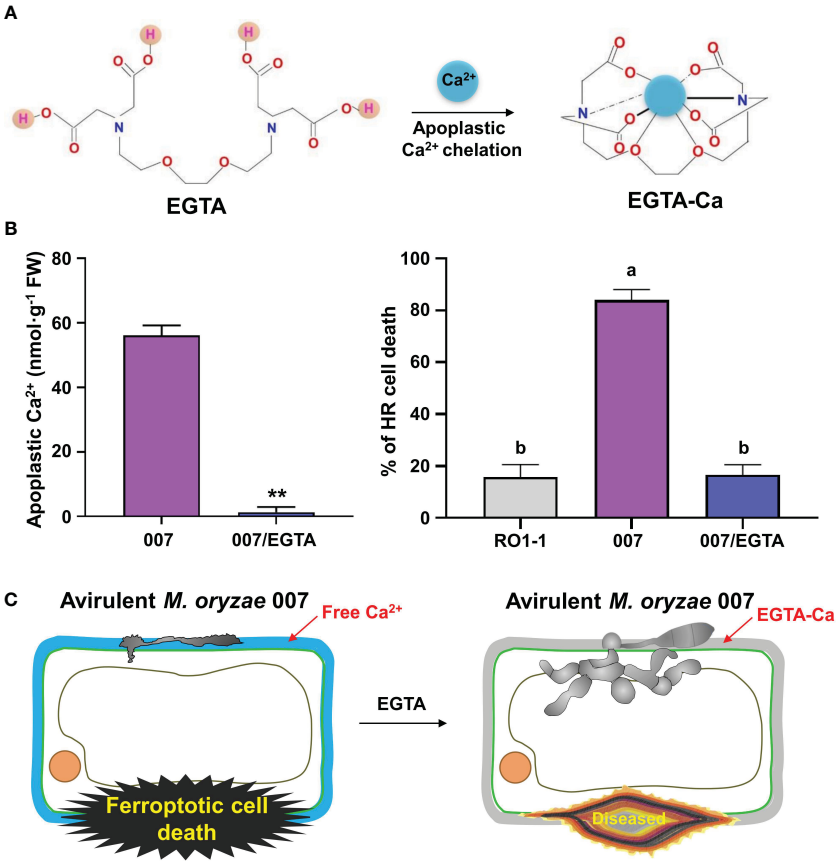

FIGURE 5
Ca^{2+} chelation by EGTA suppresses ferroptotic cell death in rice leaf sheaths during avirulent *Magnaporthe oryzae* 007 infection. **(A)** Schematic diagram of apoplastic Ca^{2+} chelation by EGTA. The binding of Ca^{2+} to EGTA forms the EGTA-Ca complex. **(B)** Quantification of apoplastic Ca^{2+} concentrations and HR cell death in rice (Kitaake) leaf sheaths treated with 10 mM EGTA during *M. oryzae* RO1-1 (virulent) and 007 (avirulent) infection. Data are represented as the mean ± SD (n = 4 leaf sheaths from different plants). Asterisks indicate significantly different means (**P< 0.01; Student's t-test). Different letters above the bars indicate significantly different means, as determined by the least significant difference (LSD) test (P< 0.05). Experiments were repeated three times with similar results. **(C)** Schematic diagram of inhibition of ferroptotic cell death by apoplastic Ca^{2+} chelation using EGTA. During avirulent *M. oryzae* 007 infection, EGTA treatment effectively inhibits apoplastic Ca^{2+} influx into the cytoplasm to completely attenuate ferroptotic HR cell death in rice sheaths, which ultimately leads to the formation of normal hyphal structures and susceptible disease.

compared with the mock (water) treatment, ASM treatment effectively induced HR cell death and ROS and iron accumulation in virulent *M. oryzae*-infected rice cells (Figures 6A, B). ASM treatment reduced the number of cells with IH, but increased the number of cells with HR, in susceptible rice leaf sheaths infected (Figure 6B). ROS and iron accumulation in rice cells was detected by Peroxy Orange 1 and Prussian blue staining, respectively (Figure 6A). We also visualized Ca^{2+} influx under confocal and fluorescence microscopy (Figure 6A). The quantification of Ca^{2+} influx revealed that ASM treatment induced Ca^{2+} influx compared with the mock treatment (Figure 6C). A chemiluminescent assay showed that ASM treatment significantly induced the accumulation of ROS in rice leaf sheath cells at 36 hpi (Figure 6C). However, ASM treatment inhibited GSH accumulation, but enhanced lipid peroxidation (MDA levels), in rice leaf sheath cells at 48 h after inoculation with virulent *M. oryzae* RO1-1 (Figure 6C). Collectively, these results suggest that ROS and iron accumulation, GSH depletion and lipid peroxidation are required for ASM-induced Ca^{2+}-mediated ferroptotic cell death during rice-*M. oryzae* interactions.

Different Ca^{2+} influx inhibitors effectively limit Ca^{2+}-mediated iron- and ROS-dependent ferroptotic cell death

Based on the knowledge of pharmacological Ca^{2+} channel modulation identified in animal systems, we selected some cytoplasmic Ca^{2+} influx regulators to investigate whether exogenous chemicals control Ca^{2+}-mediated iron- and ROS-dependent ferroptotic cell death in the rice immune response. Different Ca^{2+} influx inhibitors, including EGTA (Atkinson et al., 1990; Cessna and Low, 2001), verapamil hydrochloride (verapamil) (Beneloujaephajri et al., 2013), N-acetyl-cysteine (NAC) (Sun et al., 2012), neomycin sulfate (neomycin) (Franklin-Tong et al., 1996), lithium chloride (LiCl) (Moyen et al., 1998), aluminum chloride

10.3389/fpls.2024.1339559

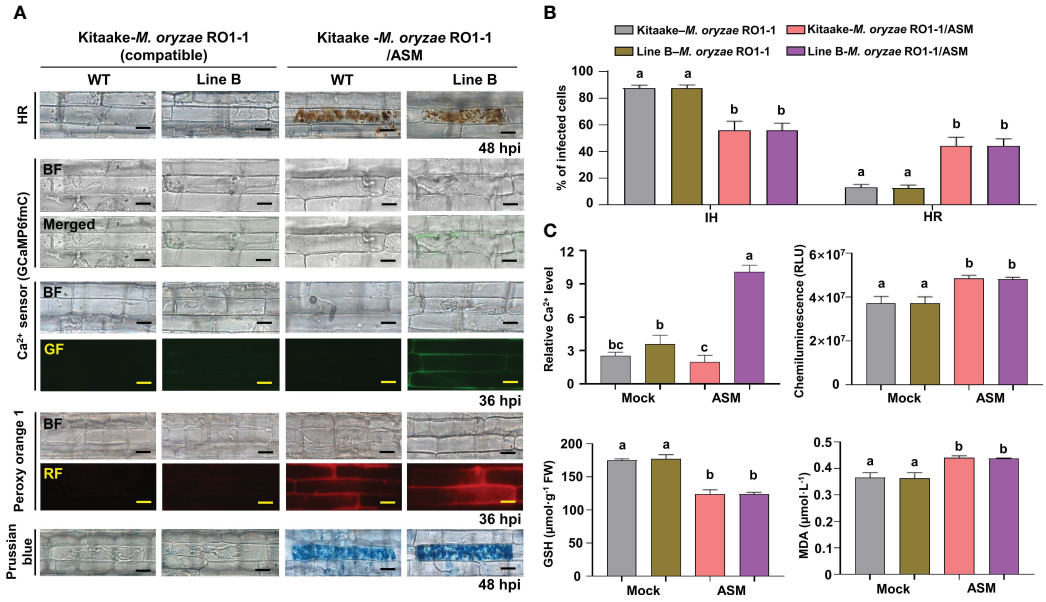

FIGURE 6
ASM induces Ca^{2+}-mediated ROS- and iron-dependent HR cell death in rice immune responses. **(A)** Images of HR cell death (48 hpi), Ca^{2+} influx (36 hpi), ROS accumulation (36 hpi), and ferric ion accumulation (48 hpi) in the leaf sheaths of rice Kitaake (WT) and Ca^{2+} sensor (GCaMP6fmC) transgenic line B during virulent *M. oryzae* RO1-1 infection after 125 μM acibenzolar-*S*-methyl (ASM) treatment. Bars = 10 μm. **(B)** Quantification of IH/HR infection phenotypes (48 hpi). **(C)** Quantification of Ca^{2+} influx (36 hpi), ROS accumulation (36 hpi), reduced glutathione (GSH) levels (48 hpi), and lipid peroxidation (MDA) levels (48 hpi). For Ca^{2+} quantification, at least three ROIs were selected to calculate the GCaMP6f/mCherry ratio at 36 hpi using the software ImageJ. The ratio values of GCaMP6f/mCherry were compared with that of the control (Mock, Kitaake-*M. oryzae* RO1-1). Data are represented as the mean ± SD (n = 4 leaf sheaths from different plants). Different letters above the bars indicate significantly different means, as determined by the least significant difference (LSD) test (P< 0.05). WT, wild type; hpi, hours post-inoculation; IH, invasive hyphae; HR, hypersensitive response; RLU, relative luminescent units; MDA, malondialdehyde.

($AlCl_3$) (Kadota et al., 2005), and ruthenium red (RR) (Bae et al., 2003) were applied onto the rice leaf sheaths infected with avirulent *M. oryzae* 007 to compare their effects on Ca^{2+} influx, ROS accumulation, lipid peroxidation, and HR cell death (Figures 4, 7A; Supplementary Figure 4).

Treatment with the calcium chelator EGTA dramatically inhibited Ca^{2+} influx, ROS and iron accumulation and HR cell death in rice cells compared with the other tested Ca^{2+} influx inhibitors during avirulent *M. oryzae* infection (Figures 4, 7A). However, other Ca^{2+} influx inhibitors showed variation in the suppression of Ca^{2+} influx, ROS accumulation, lipid peroxidation (MDA level) and HR cell death (Figure 7A; Supplementary Figure 4). Verapamil treatment is known to reduce cytoplasmic Ca^{2+} levels with attenuated ROS bursts in plant cells (Beneloujaephajri et al., 2013). Inhibition of Ca^{2+} influx by verapamil reduced cytoplasmic Ca^{2+} and ROS accumulation, lipid peroxidation and HR ferroptotic cell death, as detected by Prussian blue staining (Figure 7A; Supplementary Figure 4). NAC treatment increased GSH concentration and consequently reduced ROS accumulation, lipid peroxidation, and HR cell death, accompanied by decreased Ca^{2+} levels and increased *M. oryzae* infection (Figures 7A, 8D; Supplementary Figure 4). LiCl inhibits the release of intracellular Ca^{2+} from vacuoles (Moyen et al., 1998). The two-pore channel 1 (TPC1) channel family is a ROS-responsive Ca^{2+} channel, and aluminum is a specific blocker for TPC1, a voltage-dependent Ca^{2+} permeable channel (Kawano et al., 2004). TPC1 plays an important role in inducing ROS-dependent cytoplasmic Ca^{2+} influx during oxidative stress (Kadota et al., 2005). Neomycin, LiCl, $AlCl_3$, and RR significantly inhibited Ca^{2+} influx during avirulent *M. oryzae* 007 infection (Figure 7A; Supplementary Figure 4). They also significantly reduced the ROS accumulation during avirulent *M. oryzae* 007 infection (Figure 7A; Supplementary Figure 4). They were relatively effective in limiting lipid peroxidation (MDA level) and HR cell death (Figure 7A; Supplementary Figure 4). The Ca^{2+} influx inhibitors also suppressed Fe^{3+} accumulation and HR cell death induced by avirulent *M. oryzae* 007 infection, which led to the successful colonization of IH as detected by Prussian blue staining (Supplementary Figure 4). These data indicate that different Ca^{2+} influx inhibitors significantly limit Ca^{2+}-mediated ROS and iron accumulation, and lipid peroxidation, allowing the formation of normal hyphal structures of avirulent *M. oryzae* 007 in rice leaf sheaths and leading to blast disease (Figures 4, 7A; Supplementary Figure 4).

Different Ca^{2+} influx enhancers effectively trigger Ca^{2+}-mediated iron- and ROS-dependent ferroptotic cell death

Different Ca^{2+} influx enhancers, including ASM (Brisset et al., 2000; Buonaurio et al., 2002), diamide (Kosower et al., 1969; Gilge et al., 2008), trifluoperazine dihydrochloride (TFP) (Kang et al., 2017), $CaCl_2$/calcimycin (C/C) (Verma et al., 2011), $CaCl_2/H_2O_2$

10.3389/fpls.2024.1339559

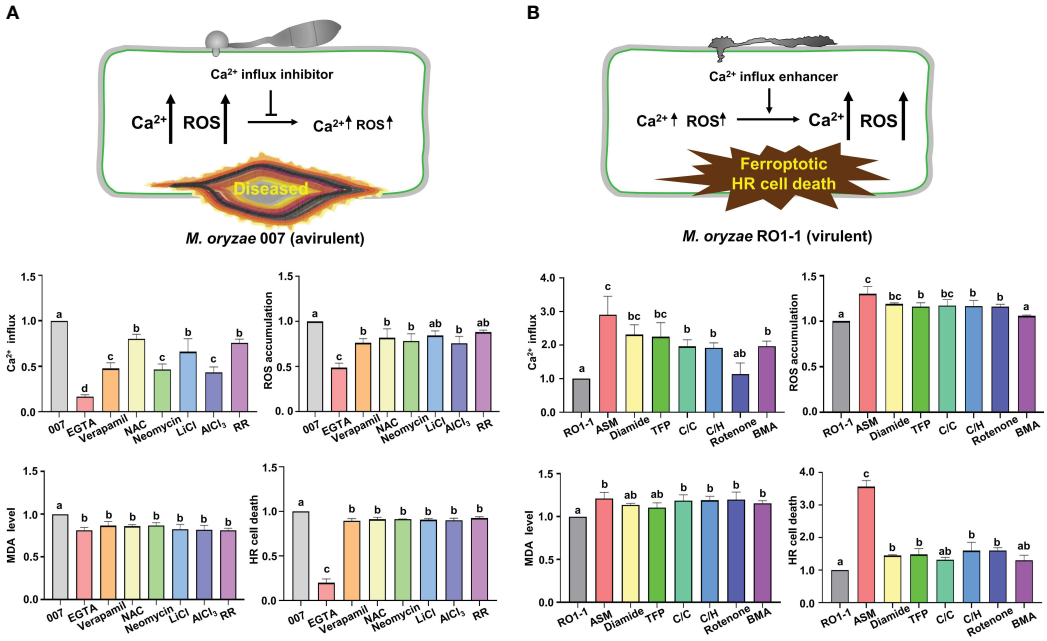

FIGURE 7
Ca^{2+} influx regulators differentially control Ca^{2+}-mediated iron-and ROS-dependent ferroptotic cell death in rice immune responses. **(A, B)** Quantifications of Ca^{2+} influx (36 hpi), ROS accumulation (36 hpi), lipid peroxidation (MDA levels) (48 hpi), and HR cell death (48 hpi) in the leaf sheath cells of rice (Kitaake) Ca^{2+} sensor (GCaMP6fmC) transgenic line B infected with *M. oryzae* 007 (avirulent) and *M. oryzae* RO1-1 (virulent) and treated with Ca^{2+} influx inhibitors. **(A)** Ca^{2+} influx inhibitors included ethylene glycol-bis(2-aminoethylether)-*N, N, N′, N′*-tetra-acetic acid (EGTA), verapamil hydrochloride (verapamil), N-acetyl-cysteine (NAC), neomycin sulfate (neomycin), lithium chloride (LiCl), aluminum chloride ($AlCl_3$) and ruthenium red (RR). **(B)** Ca^{2+} influx enhancers included acibenzolar-*S*-methyl (ASM), diamide, trifluoperazine dihydrochloride (TFP), $CaCl_2$/calcimycin (C/C), $CaCl_2/H_2O_2$ (C/H), rotenone and butylmalonic acid (BMA). For Ca^{2+} quantification, at least three ROIs were selected to calculate the GCaMP6f/mCherry ratio at 36 hpi using the software ImageJ. The ratio values of Ca^{2+} influx regulators were compared with those of the controls (*M. oryzae* 007 or *M. oryzae* RO1-1). Data are represented as the mean ± SD (n=4 leaf sheaths from different plants). Different letters above the bars indicate significantly different means, as determined by the LSD test (P< 0.05). hpi, hours post- inoculation; MDA, malondialdehyde.

(C/H) (Rentel and Knight, 2004), rotenone (Li et al., 2003), and butylmalonic acid (BMA) (Kamga et al., 2010) were applied onto rice leaf sheaths infected with virulent *M. oryzae* RO1-1 to compare their effects on Ca^{2+} influx, ROS accumulation, lipid peroxidation, and HR cell death (Figures 6, 7B; Supplementary Figure 5). ASM treatment significantly enhanced Ca^{2+} influx, ROS and iron accumulation and HR cell death in rice leaf sheath cells during virulent *M. oryzae* infection compared with the other tested Ca^{2+} influx enhancers (Figures 6, 7B).

Other Ca^{2+} influx enhancers differentially induced Ca^{2+} influx, ROS accumulation, lipid peroxidation (MDA level) and HR cell death during virulent *M. oryzae* infection (Figure 7B; Supplementary Figure 5). Diamide, TFP, C/C, C/H, and BMA differentially induced Ca^{2+} influx; however, the induction of Ca^{2+} influx by rotenone was not significant. Diamide, TFP, C/C, C/H, and rotenone increased ROS levels by at least 15.98%. However, BMA did not affect ROS levels during infection. These Ca^{2+} influx enhancers also increased only slightly MDA levels in rice leaf sheath cells. However, diamide, TFP, C/C, C/H, rotenone, and BMA increased HR cell death up to 22.06-26.23% (Figure 7B). Prussian blue staining showed that Ca^{2+} influx enhancers effectively stimulated Fe^{3+} accumulation inside and around IH in rice cells during virulent *M. oryzae* infection (Supplementary Figure 5). These data indicate that Ca^{2+} influx enhancers trigger robust Ca^{2+} influx to varying degrees in compatible (susceptible) rice cells due to their different mode of actions, leading to iron- and ROS-dependent ferroptotic HR cell death in response to virulent *M. oryzae* infection (Figures 6, 7B; Supplementary Figure 5).

Ca^{2+} influx triggers reduced *OsGR* expression and GSH depletion in rice immune responses

Glutathione reductase (GR) reduces glutathione disulfide (GSSG; oxidized glutathione) to produce reduced glutathione (GSH) in the presence of NADPH which can be converted to $NADP^+$ in plant cells (Figure 8A). *In vitro*, increasing Ca^{2+} concentration from 10 mM to 50 mM gradually inhibited the activity of rice GR or yeast GR (Figure 8B; Supplementary Figures 6A, D), indicating that higher Ca^{2+} concentration more effectively inhibits the reduction of GSSG to GSH by GR. Lineweaver-Burt plot showed non-competitive inhibition of GSSG reduction to GSH through rice GR or yeast GR by increasing Ca^{2+} concentration from 10 mM to 50 mM (Supplementary Figures 6B, E). Several metal ions, including Ca^{2+}, Mg^{2+}, K^+, and Na^+, which are abundant intracellular cations in plant cells, exhibited different inhibitory effects on the reduction of GSSG to GSH by rice GR or yeast GR *in vitro* (Tandoğan and Ulusu, 2007); however, Ca^{2+} was the most effective in inhibiting the reduction of GSSG to GSH

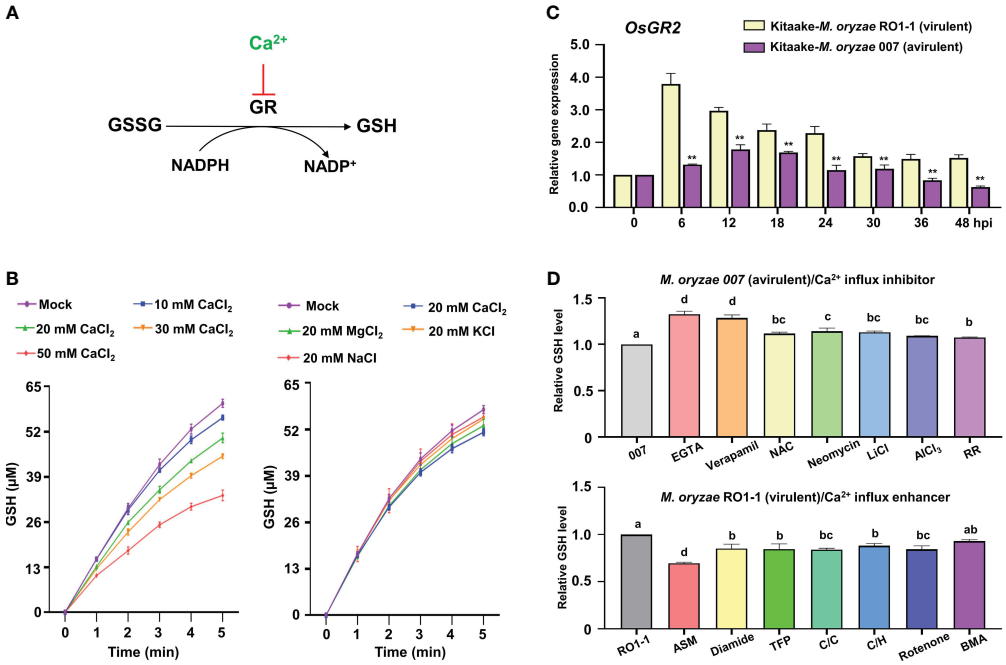

FIGURE 8
Ca^{2+} influx triggers reduced *OsGR* expression and GSH depletion during *Magnaporthe oryzae* infection. **(A)** Ca^{2+} inhibits GSSG reduction to GSH by glutathione reductase (GR). **(B)** Effects of $CaCl_2$, $MgCl_2$, KCl, and NaCl on the conversion of GSSG to GSH by rice GR. **(C)** Relative expression of rice *Glutathione Reductase 2* (*OsGR2*) in the leaf sheaths of rice (Kitaake) during *M. oryzae* RO1-1 (virulent) and *M. oryzae* 007 (avirulent) infection. **(D)** Comparison of GSH levels in rice leaf sheaths treated with different Ca^{2+} influx regulators during *M. oryzae* infection. The ratio values of Ca^{2+} influx regulators were compared with those of the controls (*M. oryzae* 007 or *M. oryzae* RO1-1). Data are represented as the mean ± SD (n = 4 leaf sheaths from different plants). Asterisks indicate significantly different means (**P< 0.01; Student's t-test). Different letters above the bars indicate significantly different means, as determined by the LSD test (P< 0.05). hpi, hours post-inoculation; GSSG, glutathione disulfide; GSH, reduced glutathione.

(Figure 8B; Supplementary Figures 6C, F). This suggests that Ca^{2+} may more specifically inhibit *OsGR* activity and deplete GSH production than the other ions Mg^{2+}, K^+, and Na^+ in rice cells.

The antioxidant enzyme glutathione reductase (GR) is responsible for maintaining the supply of reduced glutathione (GSH) for the cellular control of ROS inside cells (Couto et al., 2016). GR plays an important role in scavenging ROS to regulate the redox state of glutathione in plants (Wang et al., 2018). During avirulent *M. oryzae* infection, the expression of rice cytoplasmic *OsGR2* was effectively reduced relative to chloroplast *OsGR1* and *OsGR3* in leaf sheath cells compared with virulent *M. oryzae* infection (Figure 8C; Supplementary Figure 7). This indicates that avirulent *M. oryzae* infection significantly downregulates cytoplasmic *OsGR* expression to inhibit the reduction of GSSG to GSH. GSH depletion and lipid peroxidation are essential signaling events leading to iron- and lipid ROS-dependent ferroptotic cell death during avirulent *M. oryzae* infection (Dangol et al., 2019). During avirulent *M. oryzae* infection, treatment with the Ca^{2+} influx inhibitors EGTA and verapamil effectively rescued GSH depletion, increasing GSH content by 32.2%, and 28.3%, respectively (Figure 8D). The other Ca^{2+} influx inhibitors also more significantly increased GSH content compared with that of the control *M. oryzae* infection alone. However, during virulent *M. oryzae* infection, the Ca^{2+} influx enhancer ASM significantly decreased GSH production by 30.2% (Figure 8D). The other Ca^{2+} influx enhancers also more significantly reduced GSH production compared with that of the control *M. oryzae* infection alone.

Discussion

Iron- and ROS-dependent ferroptotosis occurs not only in animals (Dixon et al., 2012), but also in plants (Dangol et al., 2019; Nguyen et al., 2022). Fe^{2+} present in the cell is highly reactive with ROS (H_2O_2), which subsequently produces Fe^{3+} and hydroxyl radicals (·OH) (Fenton, 1894; Pierre and Fontecave, 1999). Ferric ions (Fe^{3+}) and ROS accumulated in rice tissues undergoing HR cell death during avirulent *M. oryzae* infection (Dangol et al., 2019). Iron- and ROS-dependent signaling is required for the ferroptotic cell death pathway in rice to disrupt *M. oryzae* infection. Rice iron storage protein ferritin 2 (OsFER2) could positively regulate rice ferroptosis and immune responses against *M. oryzae* infection (Nguyen et al., 2022). Mitogen-activated protein kinase (MAPK) signaling cascades are involved in plant immunity and HR cell death responses to pathogen infection (Meng and Zhang, 2013; Thulasi Devendrakumar et al., 2018). Rice MAP kinase (*OsMEK2* and *OsMPK1*) expression triggered iron- and ROS-dependent ferroptotic cell death (Dangol et al., 2021).

Calcium (Ca^{2+}) is a secondary messenger that mediates diverse signaling pathways in eukaryotic cells (Zhao et al., 2021). In plants,

Ca^{2+} influx is required for HR cell death in immune responses (Atkinson et al., 1990; Grant and Loake, 2000; Moeder et al., 2019). The ZAR1 resistosome is a calcium-permeable channel triggering plant immune signaling (Bi et al., 2021). Given the key role of calcium in plant immune responses and the emerging role of resistosomes as novel Ca^{2+} channels in plants, we hypothesized that Ca^{2+} acts as a key trigger of iron- and ROS-dependent ferroptotic cell death in rice immunity. In this study, we suggest that cytoplasmic Ca^{2+} influx through calcium-permeable cation channels, including the putative resistosomes, mediates iron- and lipid ROS-dependent ferroptotic cell death under reduced *OsGR* expression levels in rice immune responses.

Reliable detection of Ca^{2+} influx in rice cells

To study the role of cytoplasmic Ca^{2+} influx in plant cells, it is absolutely necessary to accurately monitor fine spatial and temporal changes in intracellular Ca^{2+} concentration (Choi et al., 2012). The discovery and application of the Ca^{2+}-sensitive bioluminescent photoprotein aequorin, made it possible to detect changes in cytoplasmic Ca^{2+} in the submicromolar range (Shimomura et al., 1963). However, despite advances in the Ca^{2+} detection techniques, the difficult detection and imaging of the weak luminescence signal of aequorin have been a limiting factor for its use in Ca^{2+} research (Hepler, 2005). Ca^{2+} indicators used for intracellular Ca^{2+} monitoring are mainly small molecules or proteins with highly specific sensitivity and responsiveness to intracellular Ca^{2+} (Kanchiswamy et al., 2014). The emerging role of resistosomes as Ca^{2+}-permeable channels has stimulated the study of intracellular Ca^{2+} in plant immunity (Bi et al., 2021; Jacob et al., 2021). Accurate spatial and temporal Ca^{2+} imaging approaches are required to monitor resistsome-mediated Ca^{2+} influx into living rice cells during *M. oryzae* infection. Genetically encoded Ca^{2+} sensors that can be expressed inside the transgenic plant cells are preferably used because they do not require a staining step for Ca^{2+} detection.

In this study, we used fluorescence-based chemical Ca^{2+} indicator (Fluo-5F AM) and protein Ca^{2+} sensor (GCaMP6fmC), which are relatively more reliable compared to luminescence, to detect Ca^{2+} changes in living cells during cell death in rice immunity. The non-ratiometric Fluo Ca^{2+} indicator was first introduced to monitor Ca^{2+} influx in Lima bean leaf cells in response to herbivore attack (Maffei et al., 2004). Here, we selected Fluo-5F AM as a low-affinity intracellular Ca^{2+} indicator suitable for detecting high intracellular Ca^{2+} levels in the range of 1 µM to 1 mM in rice cells. We next used a genetically encoded ratiometric Ca^{2+} sensor (GCaMP6fmC) (Weigand et al., 2021) to investigate cytoplasmic Ca^{2+} influx in rice sheath cell during *M. oryzae* infection. The two different fluorescence-based Ca^{2+} detection tools were first shown to be highly reliable for detecting and quantifying changes in cytoplasmic Ca^{2+} levels in living rice cells during *M. oryzae* infection. In parallel with Ca^{2+} imaging, staining with Peroxy Orange 1 (PO1), a red fluorescent ROS indicator, revealed that the ROS burst occurs in the same region of the rice cell where Ca^{2+} influx occurs during avirulent *M. oryzae* infection. The red fluorescent ROS indicator PO1 could simultaneously visualize Ca^{2+} (green fluorescence) and ROS accumulation inside the same rice cell through its distinct red fluorescence emission.

Ca^{2+} influx mediates ROS- and iron-dependent cell death in rice immunity

In the current study, we found that avirulent *M. oryzae* infection triggers a robust Ca^{2+} influx, which mediates iron- and ROS-dependent ferroptotic cell death in rice. The strong ROS burst is a cellular signaling event that occurs in HR cell death in plant immunity (Van Breusegem and Dat, 2006; Jwa and Hwang, 2017). Pathogen effectors can interact with NLR receptors of host plants, leading to ROS burst and HR cell death in plant immune responses (Jones and Dangl, 2006; Dangl et al., 2013; Han and Hwang, 2017). The ZAR1 resistosome has recently been proposed to be a calcium-permeable channel triggering plant immunity and cell death (Bi et al., 2021). Ca^{2+} influx from the apoplast to the cytoplasm may mediate iron- and ROS-dependent ferroptotic HR cell death in rice immunity. Plant cells maintain a steady state Ca^{2+} concentration of 100-200 nM in contrast to the Ca^{2+} concentration in the extracellular space at 1-10 mM (Martins et al., 2013). The steep Ca^{2+} concentration gradient between the cytoplasm (~100 nM) and apoplast (~1 mM) (Stael et al., 2012) may rapidly increase cytoplasmic Ca^{2+} influx through the resistosome, a membrane-localized Ca^{2+}-permeable channel, which triggers calcium signaling of ROS- and iron-dependent ferroptotic cell death in rice immunity. Avirulent *M. oryzae* infection sustained high iron and ROS accumulation in ferroptotic HR cell death, with a layer of high Ca^{2+} concentration near the cell membrane, GSH depletion, and lipid peroxidation. The maintenance of a persistently high Ca^{2+} concentration gradient near the cell membrane is an ionic stress, which can have a significant impact on ambient ROS burst, iron accumulation, and antioxidant defense machineries. Ferroptotic HR cell death may only be caused by prolonged Ca^{2+}/ROS bursts during ETI, but not transient Ca^{2+}/ROS bursts during PTI (Grant and Loake, 2000). It is thus likely that continuous Ca^{2+} influx into the cytoplasm through the calcium-permeable cation channels, including the putative NLR resistosomes, mediates iron- and ROS-dependent ferroptotic HR cell death in the rice immune response.

Ca^{2+} influx inhibitors block Ca^{2+}-mediated iron- and ROS-dependent cell death

Different Ca^{2+} influx inhibitors such as EGTA, verapamil, NAC, neomycin, LiCl, AlCl3, and RR significantly suppressed cytoplasmic Ca^{2+} influx, ROS accumulation, glutathione (GSH) depletion, and lipid peroxidation, leading to reduced iron- and ROS-dependent ferroptotic HR cell death during avirulent *M. oryzae* infection. Notably, the membrane-impermeable Ca^{2+} chelator EGTA (Ellis-Davies and Kaplan, 1994; Cessna and Low, 2001) and the Ca^{2+} channel blocker verapamil (Beneloujaephajri et al., 2013) more

effectively suppressed GSH depletion in rice sheaths than other Ca^{2+} influx inhibitors during avirulent *M. oryzae* infection. Ca^{2+} chelation by EGTA blocked Ca^{2+} influx from the apoplastic environment into the cytosol of rice cells during infection. EGTA can deplete extracellular free Ca^{2+} sources through high-affinity Ca^{2+} chelation, which essentially blocks Ca^{2+} influx from the apoplast. Resistosomes are thought to act as Ca^{2+}-permeable channels that connect the cytoplasm to a high-level extracellular Ca^{2+} pool (Bi et al., 2021). The binding of Ca^{2+} to EGTA may prevent Ca^{2+} from freely diffusing across the cell membrane and consequently lower cytoplasmic Ca^{2+} levels.

Verapamil limits the transport of extracellular Ca^{2+} across the plasma membrane into the cytosol (Bergson et al., 2011). However, the inhibitory effect of verapamil on ferroptotic cell death was significantly lower than that of Ca^{2+} chelation with EGTA. NAC is a precursor of the antioxidant glutathione, which inhibits ROS levels and the oxidation of cellular glutathione (Sun et al., 2012). Neomycin acts as an inhibitor of polyphosphoinositide hydrolysis in animals and also inhibits Ca^{2+}-dependent polyphosphoinositide-specific phospholipase C (PLC) activity in plants (Franklin-Tong et al., 1996). RR, a non-competitive inhibitor of the mitochondrial uniporter, is responsible for Ca^{2+} uptake into mitochondria in animal cells (Bae et al., 2003), and it also inhibits plant cell cation channels in a voltage-independent manner (White, 1996). Taken together, the seven different Ca^{2+} influx inhibitors tested in this study significantly inhibit Ca^{2+}-mediated ROS, iron accumulation, GSH depletion, and lipid peroxidation, which ultimately increase the growth of invasive hyphae (IH) inside rice cells during avirulent *M. oryzae* infection leading to blast disease.

Ca^{2+} influx enhancers promote Ca^{2+}-mediated iron- and ROS-dependent cell death

Plant cells have high Ca^{2+} levels in both the apoplast and internal stores, and the cytoplasmic Ca^{2+} influx can increase intracellular Ca^{2+} concentration (Stael et al., 2012). Different Ca^{2+} influx enhancers ASM, diamide, TFP, $CaCl_2$/calcimycin (C/C), $CaCl_2/H_2O_2$ (C/H), rotenone, and BMA differentially induced Ca^{2+} influx, ROS accumulation, GSH depletion, lipid peroxidation (MDA level) leading to iron- and ROS-dependent ferroptotic HR cell death during virulent *M. oryzae* infection. The plant defense activator ASM, a salicylic acid (SA) analogue, induces systemic acquired resistance (SAR) against a broad spectrum of plant pathogens and is widely used for crop protection (Buonaurio et al., 2002; Matsuo et al., 2019). ASM significantly enhanced Ca^{2+} influx, as well as iron and ROS accumulation leading to ferroptotic cell death in rice even during virulent *M. oryzae* infection. ASM induced the highest increase in cytoplasmic Ca^{2+} level among the seven Ca^{2+} enhancers tested and effectively inhibited virulent *M. oryzae* infection. These results suggest that the enhancement of Ca^{2+} influx by ASM may activate SAR via resistosomes in plants, thereby contributing to disease control.

Diamide is a cell-permeable chemical oxidant that can specifically target thiols of GSH and free SH groups in proteins (Kosower et al., 1969; Gilge et al., 2008). Diamide treatment reduced intracellular GSH concentration as expected. The increase in Ca^{2+} levels induced a decrease in GSH, which increased ROS accumulation, lipid peroxidation, and HR cell death, resulting in a decrease in *M. oryzae* growth. These results suggest that reduced cytoplasmic GSH levels play a crucial role in iron- and lipid ROS-dependent HR cell death in rice immunity. TFP directly dissociates calmodulin (CaM) from IP_3R [IP_3 (inositol 1,4,5-trisphosphate) receptor] by interacting at the TFP-binding site of CaM and opens IP_3R to release large amounts of Ca^{2+} from intracellular stores such as the endoplasmic reticulum (ER) in animals (Kang et al., 2017). Calcium ionophore A23187 (calcimycin), a hydrophobic molecule, can selectively bind to Ca^{2+} and permeate the hydrophobic interior of lipid bilayers, increasing cell permeability to Ca^{2+} (Verma et al., 2011). H_2O_2 is known to induce a biphasic cytoplasmic Ca^{2+} response in *Arabidopsis* seedling plants (Rentel and Knight, 2004). The recent discovery of a novel plant receptor that covalently regulates Ca^{2+} channel activity by H_2O_2 is a good example of direct activation of Ca^{2+} influx by H_2O_2 (Wu et al., 2020). Rotenone specifically targets mitochondrial complex 1 of the electron transport chain and causes impaired ATP production and oxidative stress, leading to cellular dysfunction and ultimately cell death (Li et al., 2003). BMA inhibits the dicarboxylate transporter (DIC), which transports glutathione into mitochondria in animal cells (Kamga et al., 2010). Taken together, Ca^{2+} influx enhancers could effectively promote cytoplasmic Ca^{2+} influx to trigger iron- and ROS-dependent ferroptotic cell death in rice plants during virulent *M. oryzae* infection.

Ca^{2+} influx reduced GR expression that causes GSH depletion, and iron- and lipid ROS-dependent cell death

Ca^{2+} may operate more like an essential switch to signal plant cell death and immunity (Scrase-Field and Knight, 2003). Glutathione reductase (GR) catalyzes the NADPH-dependent reduction of oxidized glutathione (GSSG) to reduced glutathione (GSH) (Tandoğan and Ulusu, 2007). Robust Ca^{2+} influx into the cytoplasm triggered reduced *OsGR* expression and GSH depletion during avirulent *M. oryzae* infection. Inhibition of cytoplasmic *OsGR2* expression by avirulent *M. oryzae* infection may cause GSH depletion, leading to rice ferroptotic cell death. The intracellular concentration of glutathione can indicate the condition of oxidative stress in cells (Pastore et al., 2001). Within the cell, glutathione exists in a reduced state (GSH) and an oxidized state (GSSG). Glutathione, an important cellular antioxidant, plays a crucial role in disease resistance in plants by helping to regulate intracellular ROS homeostasis (Hwang et al., 1992; Parisy et al., 2007). GSH depletion disrupts intracellular ROS homeostasis and leads to iron- and ROS-dependent ferroptotic cell death (Dangol et al., 2019). GSH depletion is a common phenomenon observed during both plant and animal ferroptosis (Stockwell et al., 2017; Dangol et al., 2019).

An increase in free Ca^{2+} levels in apoplasts during avirulent *M. oryzae* infection may cause Ca^{2+} influx into the cytoplasm via

calcium-permeable cation channels, including the putative NLR-activated resistosomes. High cytoplasmic Ca^{2+} influx can inhibit the reduction of oxidized glutathione (GSSG) to GSH by GR, leading to GSH depletion *in vitro*. Cytoplasmic Ca^{2+} influx from the apoplast through the putative resistosomes induces GSH depletion, which leads to the production of lipid ROS, thus promoting iron-dependent ferroptotic cell death in rice. Robust Ca^{2+}, ROS and iron accumulation occurred together in the vicinity of the plasma membrane, where resistosomes are likely localized, during avirulent *M. oryzae* infection. This highlights the importance of GSH depletion for the initiation of Ca^{2+}-mediated ferroptotic cell death in rice during *M. oryzae* infection. Strong Ca^{2+} influx into the cytoplasm leading to GSH depletion may be due primarily to the irreversible influx of apoplastic Ca^{2+} through the putative resistosomes, Ca^{2+}-permeable selective channels (Bi et al., 2021), in the plasma membrane. It is thus likely that the irreversible Ca^{2+} influx acts as a driving force for lipid ROS production that induces ferroptotic cell death.

Our data collectively support a model of Ca^{2+}-mediated iron- and lipid ROS-dependent ferroptotic cell death by calcium-permeable cation channels, including the putative NLR-activated resistosomes and consequent GSH depletion during *M. oryzae* infection in rice (Figure 9). Recently, multiple major NLR genes, including *PigmR*, which confer broad-spectrum resistance to *M. oryzae* have been identified in the rice genome (Deng et al., 2017; Wang L. et al., 2019; Zhai et al., 2019). Plant NLRs form resistosomes upon the recognition of pathogen effectors (Bi et al., 2021); however, there is still no experimental evidence that rice NLRs such as *PigmR* form resistosomes that recognize *M. oryzae* effectors. The NLR resistosomes (Wang J. et al., 2019) act as irreversible Ca^{2+}-permeable channels in the plasma membrane to trigger HR cell death in plant immunity (Bi et al., 2021). Cytoplasmic Ca^{2+} influx by calcium-permeable cation channels, including the putative resistosome induces GSH depletion and eventually triggers a ROS burst at the same site where Ca^{2+} accumulation occurs. During virulent *M. oryzae* infection, NLR-activated resistosome formation and GSH depletion do not occur due to increased expression of rice *glutathione reductase* (*OsGR*), and *M. oryzae* hyphae grow invasively inside rice cells, causing disease without ferroptotic cell death. Blast disease (susceptibility)-related cell death is ROS-dependent but iron-independent in the compatible rice–*M. oryzae* interaction (Dangol et al., 2021). However, during avirulent *M. oryzae* infection, strong cytoplasmic Ca^{2+} influx through calcium-permeable cation channels, including the putative NLR-activated resistosomes triggers iron- and ROS-dependent ferroptotic cell death owing to the increase in Fe^{2+}, ROS and lipid ROS levels as well as GSH depletion by repressed *OsGR2* expression. Overall, our results suggest that cytoplasmic Ca^{2+} influx from the

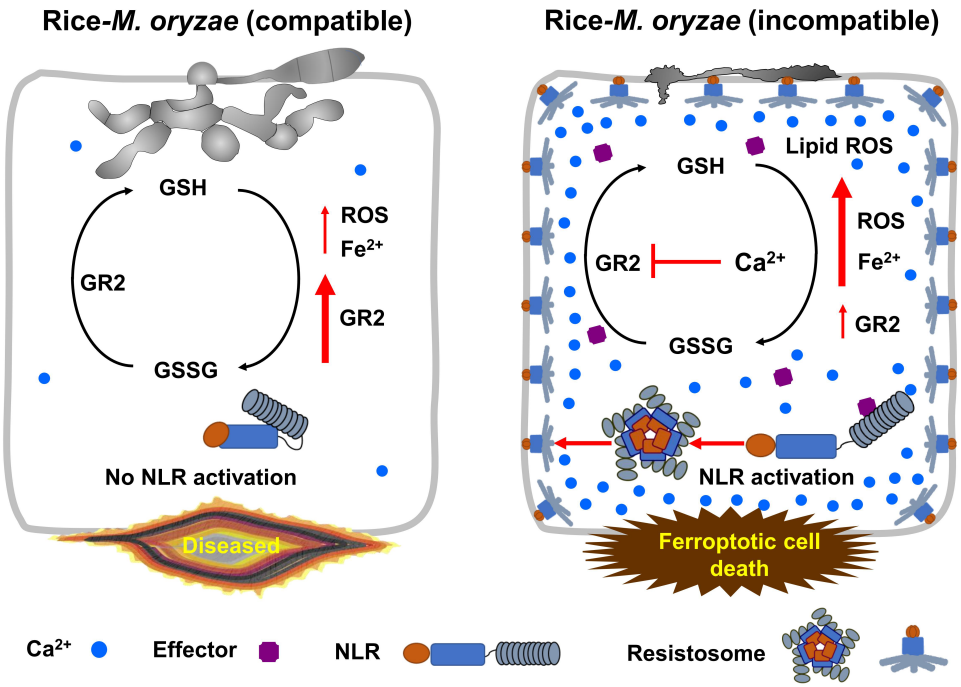

FIGURE 9
Model of Ca^{2+}-mediated iron- and lipid ROS-dependent ferroptotic cell death by the putative NLR-activated resistosomes in rice immune responses. Glutathione is an important and potent antioxidant that regulates intracellular ROS homeostasis through the continuous redox. In compatible rice-*M. oryzae* (virulent) interactions, massive cytoplasmic Ca^{2+}-influx does not occur due to inactivation of NLR, ROS homeostasis is well maintained by redox of glutathione due to increased expression of *glutathione reductase* (*GR*), and *M. oryzae* hyphae grow normally and successfully infect rice. By contrast, during incompatible rice-*M. oryzae* (avirulent) interactions, plant NLR-pathogen effector recognition leads to resistosome formation, and resistosome-mediated massive influx of cytoplasmic Ca^{2+} from the apoplast sharply represses *GR* expression in rice cells during the early infection stage. Consequently, reduced GR activity exacerbates glutathione depletion, leading to iron- and lipid ROS-dependent ferroptotic cell death in the rice immune response. GR, glutathione reductase; GSSG, glutathione disulfide; GSH, reduced glutathione; NLR, nucleotide-binding leucine-rich repeat receptor.

apoplast through calcium-permeable cation channels, including the putative NLR resistosomes (Wang J. et al., 2019) inhibits the reduction of GSSG to GSH under reduced *OsGR* expression levels, leading to iron- and lipid ROS-dependent ferroptotic cell death in the rice immune response.

Data availability statement

The original contributions presented in the study are included in the article/Supplementary Materials, further inquiries can be directed to the corresponding author/s.

Author contributions

JW: Conceptualization, Data curation, Formal analysis, Investigation, Methodology, Visualization, Writing – original draft, Writing – review & editing. W-GC: Formal analysis, Funding acquisition, Investigation, Methodology, Software, Validation, Visualization, Writing – review & editing. NKN: Data curation, Formal analysis, Investigation, Methodology, Validation, Visualization, Writing – review & editing. DPL: Data curation, Formal analysis, Investigation, Methodology, Validation, Visualization, Writing – review & editing. S-HK: Formal analysis, Investigation, Methodology, Validation, Writing – review & editing. DYL: Formal analysis, Methodology, Validation, Writing – review & editing. BKH: Conceptualization, Formal analysis, Methodology, Supervision, Validation, Visualization, Writing – original draft, Writing – review & editing. N-SJ: Conceptualization, Data curation, Formal analysis, Funding acquisition, Investigation, Methodology, Project administration, Resources, Software, Supervision, Validation, Visualization, Writing – original draft, Writing – review & editing.

Funding

The author(s) declare financial support was received for the research, authorship, and/or publication of this article. This work was supported by the National Research Foundation (NRF) of Korea (grant no. 2023R1A2C1003099 to N-SJ) and the National Science Foundation of United States (MCB grant no. 2016143 to W-GC).

Acknowledgments

We thank B. R. Stockwell (Columbia University), S. Gilroy (University of Wisconsin, Madison), and J. F. Harper (University of Nevada, Reno) for critical reading and commenting on the manuscript. We also thank the Sejong University Research Facility Center Confocal Microscopy Team for technical support and J-S Ha for fluorescence microscopy imaging.

Conflict of interest

The authors declare that the research was conducted in the absence of any commercial or financial relationships that could be construed as a potential conflict of interest.

The author(s) declared that they were an editorial board member of Frontiers, at the time of submission. This had no impact on the peer review process and the final decision.

Publisher's note

Supplementary material

The Supplementary Material for this article can be found online at: https://www.frontiersin.org/articles/10.3389/fpls.2024.1339559/full#supplementary-material

SUPPLEMENTARY FIGURE 1
Analysis of the effect of Ca^{2+} influx on the immunity of avirulent *Magnaprthe oryzae* 007-inoculated rice using the transgenic approach. **(A)** Schematic diagram of the Ca^{2+} sensor construct. The Ca^{2+} sensor GCaMP6fmC is composed of the calmodulin (CaM)-binding site M13, a circularly permutated enhanced green fluorescent protein (cp-eGFP), and mCherry-fused CaM. The Ca^{2+} sensor construct *GCaMP6f-mCherry* (*GCaMP6fmC*) was cloned into the vector pGWB554 under the control of the Cauliflower mosaic virus (CaMV) *35S* promoter. LB, left border; RB, right border. **(B)** PCR confirmation of Ca^{2+} sensor (GCaMP6fmC) transgenic lines of the rice cultivar Kitaake using hygromycin resistance (HygR) and GCaMP6fmC primers. **(C)** Detection of Ca^{2+} influx in rice leaf sheaths during avirulent *M. oryzae* 007 infection. The leaf sheaths of wild-type (WT) plants and Ca^{2+} sensor (GCaMP6fmC) transgenic lines A, B, and C were inoculated with avirulent *M. oryzae* 007, and Ca^{2+} influx in leaf sheath cells was visualized by fluorescence microscopy at 36 h post-inoculation (hpi). Images were taken using a microscope (Zeiss equipped with Axioplan 2) with bright field filter, green fluorescence filter (Ex/Em: 450–490/515–565 nm), and red fluorescence filter (Ex/Em: 546/590 nm). Bars = 10 μm. BF, bright field; GF, green fluorescence; RF, red fluorescence.

SUPPLEMENTARY FIGURE 2
Images of Ca^{2+} influx and ROS and iron accumulation in the leaf sheaths of rice Kitaake (WT) and *35S::GCamP6fmC* line B plants during *Magnaporthe oryzae* infection. The leaf sheaths of WT and Ca^{2+} sensor (GCaMP6fmC) transgenic line B plants were inoculated with *M. oryzae* RO1-1 (virulent) and 007 (avirulent), and the influx of Ca^{2+}, accumulation of ROS (H_2O_2), and accumulation of ferric ions (Fe^{3+}) were measured at 36, 40, and 48 hpi, respectively. Rice leaf sheath cells were stained with Peroxy Orange 1 (PO1) to visualize H_2O_2 accumulation around the site of infection. Fe^{3+} accumulation was detected by Prussian blue staining. Ca^{2+} influx, H_2O_2 accumulation, and Fe^{3+} accumulation in rice leaf sheaths were observed under a microscope (Zeiss equipped with Axioplan 2) using a bright field filter and/or fluorescence filters. Bars = 10 μm. Red arrows indicate invasive hyphae. WT, wild type; BF, bright field; GF, green fluorescence; RF, red fluorescence. hpi, hours post-inoculation.

SUPPLEMENTARY FIGURE 3

Ca^{2+} chelation by EGTA suppresses apoplastic Ca^{2+} influx in rice leaf sheaths during avirulent *Magnaporthe oryzae* 007 infection. **(A)** Schematic diagram of apoplastic Ca^{2+} detection using the calcium-*o*-cresolphthalein complexone (*o*-CPC) method. The binding of Ca^{2+} to *o*-CPC results in the formation of an intense violet-colored complex, which can be quantified by measuring the absorbance of the intercellular fluid of the rice leaf sheath at 575 nm using the SP-2000UV spectrophotometer. **(B)** Quantitative determination of apoplastic Ca^{2+} concentrations in rice leaf sheaths treated with 10 mM EGTA during avirulent *M. oryzae* 007 infection. The leaf sheaths of rice (Kitaake) plants were inoculated with avirulent *M. oryzae* 007 (4×10^5 conidia·mL^{-1}) supplemented with 10 mM EGTA. Ca^{2+} in the intercellular fluid of rice leaf sheath was detected using the *o*-CPC method, and Ca^{2+} concentration was measured at 575 nm using the SP-2000UV spectrophotometer. Data are represented as the mean ± SD (n = 4 leaf sheaths from different plants). Asterisks above bars indicate significantly different means (*P< 0.05, **P< 0.01; Student's t-test). Experiments were repeated three times with similar results.

SUPPLEMENTARY FIGURE 4

Different Ca^{2+} influx inhibitors significantly limit Ca^{2+}-mediated iron- and ROS-dependent ferroptotic cell death in rice immune responses. Images show HR cell death (48 hpi), Ca^{2+} influx (36 hpi), ROS accumulation (36 hpi), and Fe^{3+} accumulation (48 hpi) in the leaf sheath cells of rice (Kitaake) Ca^{2+} sensor (GCaMP6fmC) transgenic line B infected with *M. oryzae* 007 (avirulent), supplemented with Ca^{2+} influx inhibitors, including verapamil hydrochloride (verapamil), N-acetyl-cysteine (NAC), neomycin sulfate (neomycin), lithium chloride (LiCl), aluminum chloride ($AlCl_3$), and ruthenium red (RR). HR, hypersensitive response; BF, bright field; GF, green fluorescence; RF, red fluorescence; hpi, hours post-inoculation. Bars = 10 μm. Different Ca^{2+} influx inhibitors significantly limit Ca^{2+}-mediated iron- and ROS-dependent ferroptotic cell death in rice immune responses. Images show HR cell death (48 hpi), Ca^{2+} influx (36 hpi), ROS accumulation (36 hpi), and Fe^{3+} accumulation (48 hpi) in the leaf sheath cells of rice (Kitaake) Ca^{2+} sensor (GCaMP6fmC) transgenic line B infected with *M. oryzae* 007 (avirulent), supplemented with Ca^{2+} influx inhibitors, including verapamil hydrochloride (verapamil), N-acetyl-cysteine (NAC), neomycin sulfate (neomycin), lithium chloride (LiCl), aluminum chloride ($AlCl_3$), and ruthenium red (RR). HR, hypersensitive response; BF, bright field; GF, green fluorescence; RF, red fluorescence; hpi, hours post-inoculation. Bars = 10 μm.

SUPPLEMENTARY FIGURE 5

Different Ca^{2+} influx enhancers significantly trigger Ca^{2+}-mediated iron- and ROS-dependent ferroptotic cell death in rice immune responses. Images show HR cell death (48 hpi), Ca^{2+} influx (36 hpi), ROS accumulation (36 hpi), and Fe^{3+} accumulation (48 hpi) in the leaf sheath cells of rice (Kitaake) Ca^{2+} sensor (GCaMP6fmC) transgenic line B infected with *M. oryzae* RO1-1 (virulent), supplemented with Ca^{2+} influx enhancers, including diamide, trifluoperazine dihydrochloride (TFP), $CaCl_2$/calcimycin (C/C), $CaCl_2/H_2O_2$ (C/H), rotenone and butylmalonic acid (BMA). HR, hypersensitive response; BF, bright field; GF, green fluorescence; RF, red fluorescence; hpi, hours post inoculation. Bars = 10 μm.

SUPPLEMENTARY FIGURE 6

High concentrations of $CaCl_2$ inhibit the reduction of GSSG to GSH. GSSG can be reduced to GSH by glutathione reductase (GR) using NADPH as a cofactor, which is converted to $NADP^+$ during the reaction. The decrease in the absorbance of NADPH at 340 nm was measured spectrophotometrically for 5 min at room temperature. **(A, D)** Effect of the increase in $CaCl_2$ concentration on the inhibition of GSSG reduction to GSH by rice GR **(A)** or yeast GR **(D)**. Values represent mean ± SD of OD_{340} at different time points. **(B, E)** Linerweaver-Burt plot showing non-competitive inhibition of the GSSG reduction reaction by rice GR **(B)** or yeast GR **(E)**. The x-axis represents the inverse of the substrate concentration (1/S), and the y-axis represents the inverse of the initial reaction velocity ($1/V_0$). **(C, F)** Inhibitory effects of $CaCl_2$, $MgCl_2$, KCl, and NaCl on GSSG reduction to GSH by rice GR (**C**) or yeast GR **(F)**. Values represent mean ± SD of OD_{340} values at different time points.

SUPPLEMENTARY FIGURE 7

RT-PCR and q-RT-PCR analyses of the expression levels of rice glutathione reductase (*OsGR*) genes in the leaf sheaths of rice (Kitaake) plants during *Magnaporthe oryzae* infection. **(A)** Reverse transcription PCR (RT-PCR) analysis of the expression levels of *OsGR1*, *OsGR2*, *OsGR3*, and *Ubiquitin* (*OsUbiquitin*) in rice leaf sheaths at different time points after inoculation with *M. oryzae* RO1-1 (virulent) and 007 (avirulent). **(B)** Real-time quantitative RT-PCR (qRT-PCR) analysis of the expression levels of *OsGR1*, *OsGR3*, and *OsUbiquitin* in rice leaf sheaths at different time points after inoculation with *M. oryzae* RO1-1 (virulent) and 007 (avirulent). Transcription levels of *OsGR* genes were normalized relative to that of the internal reference gene *OsUbiquitin*. hpi, hours post-inoculation.

References

Aguilera, A., Berdun, F., Bartoli, C., Steelheart, C., Alegre, M., Bayir, H., et al. (2022). C-ferroptosis is an iron-dependent form of regulated cell death in cyanobacteria. *J. Cell Biol.* 221, e201911005. doi: 10.1083/jcb.201911005

Airaki, M., Sánchez-Moreno, L., Leterrier, M., Barroso, J. B., Palma, J. M., and Corpas, F. J. (2011). Detection and quantification of S-nitrosoglutathione (GSNO) in pepper (*Capsicum annuum L.*) plant organs by LC-ES/MS. *Plant Cell Physiol.* 52, 2006–2015. doi: 10.1093/pcp/pcr133

Atkinson, M. M., Keppler, L. D., Orlandi, E. W., Baker, C. J., and Mischke, C. F. (1990). Involvement of plasma membrane calcium influx in bacterial induction of the k/h and hypersensitive responses in tobacco. *Plant Physiol.* 92, 215–221. doi: 10.1104/pp.92.1.215

Bae, J. H., Park, J. W., and Kwon, T. K. (2003). Ruthenium red, inhibitor of mitochondrial Ca^{2+} uniporter, inhibits curcumin-induced apoptosis via the prevention of intracellular Ca^{2+} depletion and cytochrome c release. *Biochem. Biophys. Res. Commun.* 303, 1073–1079. doi: 10.1016/s0006-291x(03)00479-0

Bellomo, G., Jewell, S. A., Thor, H., and Orrenius, S. (1982). Regulation of intracellular calcium compartmentation: studies with isolated hepatocytes and t-butyl hydroperoxide. *Proc. Natl. Acad. Sci. U. S. A.* 79, 6842–6846. doi: 10.1073/pnas.79.22.6842

Beneloujaephajri, E., Costa, A., L'Haridon, F., Métraux, J. P., and Binda, M. (2013). Production of reactive oxygen species and wound-induced resistance in *Arabidopsis thaliana* against *Botrytis cinerea* are preceded and depend on a burst of calcium. *BMC Plant Biol.* 13, 160. doi: 10.1186/1471-2229-13-160

Bergson, P., Lipkind, G., Lee, S. P., Duban, M. E., and Hanck, D. A. (2011). Verapamil block of T-type calcium channels. *Mol. Pharmacol.* 79, 411–419. doi: 10.1124/mol.110.069492

Bi, G., Su, M., Li, N., Liang, Y., Dang, S., Xu, J., et al. (2021). The ZAR1 resistosome is a calcium-permeable channel triggering plant immune signaling. *Cell* 184, 3528–3541.e12. doi: 10.1016/j.cell.2021.05.003

Bora, P., Gahurova, L., Mašek, T., Hauserova, A., Potěšil, D., Jansova, D., et al. (2021). p38-MAPK-mediated translation regulation during early blastocyst development is required for primitive endoderm differentiation in mice. *Commun. Biol.* 4, 788. doi: 10.1038/s42003-021-02290-z

Brisset, M. N., Cesbron, S., Thomson, S. V., and Paulin, J. P. (2000). Acibenzolar-*S*-methyl induces the accumulation of defense-related enzymes in apple and protects from fire blight. *Eur. J. Plant Pathol.* 106, 529–536. doi: 10.1023/A:1008728119087

Buonaurio, R., Scarponi, L., Ferrara, M., Sidoti, P., and Bertona, A. (2002). Induction of systemic acquired resistance in pepper plants by acibenzolar-*S*-methyl against bacterial spot disease. *Eur. J. Plant Pathol.* 108, 41–49. doi: 10.1023/A:1013984511233

Cessna, S. G., and Low, P. S. (2001). Activation of the oxidative burst in aequorin-transformed *Nicotiana tabacum* cells is mediated by protein kinase- and anion channel-dependent release of Ca^{2+} from internal stores. *Planta* 214, 126–134. doi: 10.1007/s004250100596

Chen, Y., Wang, J., Nguyen, N. K., Hwang, B. K., and Jwa, N. S. (2022). The NIN-like protein OsNLP2 negatively regulates ferroptotic cell death and immune responses to *Magnaporthe oryzae* in rice. *Antioxidants* 11, 1795. doi: 10.3390/antiox11091795

Choi, W. G., Swanson, S. J., and Gilroy, S. (2012). High-resolution imaging of Ca^{2+}, redox status, ROS and pH using GFP biosensors. *Plant J.* 70, 118–128. doi: 10.1111/j.1365-313X.2012.04917.x

Choi, W. G., Toyota, M., Kim, S. H., Hilleary, R., and Gilroy, S. (2014). Salt stress-induced Ca^{2+} waves are associated with rapid, long-distance root-to-shoot signaling in plants. *Proc. Natl. Acad. Sci. U. S. A.* 111, 6497–6502. doi: 10.1073/pnas.1319955111

Corns, C. M., and Ludman, C. J. (1987). Some observations on the nature of the calcium-cresolphthalein complexone reaction and its relevance to the clinical laboratory. *Ann. Clin. Biochem.* 24, 345–351. doi: 10.1177/000456328702400403

Couto, N., Wood, J., and Barber, J. (2016). The role of glutathione reductase and related enzymes on cellular redox homoeostasis network. *Free Radic. Biol. Med.* 95, 27–42. doi: 10.1016/j.freeradbiomed.2016.02.028

Dangl, J. L., Horvath, D. M., and Staskawicz, B. J. (2013). Pivoting the plant immune system from dissection to deployment. *Science* 341, 746–751. doi: 10.1126/science.1236011

Dangol, S., Chen, Y., Hwang, B. K., and Jwa, N. S. (2019). Iron- and reactive oxygen species-dependent ferroptotic cell death in rice-*Magnaporthe oryzae* interactions. *Plant Cell.* 31, 189–209. doi: 10.1105/tpc.18.00535

Dangol, S., Nguyen, N. K., Singh, R., Chen, Y., Wang, J., Lee, H. G., et al. (2021). Mitogen-activated protein kinase OsMEK2 and OsMPK1 signaling is required for ferroptotic cell death in rice-*Magnaporthe oryzae* interactions. *Front. Plant Sci.* 12. doi: 10.3389/fpls.2021.710794

Deng, Y., Zhai, K., Xie, Z., Yang, D., Zhu, X., Liu, J., et al. (2017). Epigenetic regulation of antagonistic receptors confers rice blast resistance with yield balance. *Science* 355, 962–965. doi: 10.1126/science.aai8898

Ding, J., Luo, A. F., Hu, L., Wang, D., and Shao, F. (2014). Structural basis of the ultrasensitive calcium indicator GCaMP6. *Sci. China Life Sci.* 57, 269–274. doi: 10.1007/s11427-013-4599-5

Distéfano, A. M., Martin, M. V., Córdoba, J. P., Bellido, A. M., D'Ippólito, S., Colman, S. L., et al. (2017). Heat stress induces ferroptosis-like cell death in plants. *J. Cell Biol.* 216, 463–476. doi: 10.1083/jcb.201605110

Dixon, S. J., Lemberg, K. M., Lamprecht, M. R., Skouta, R., Zaitsev, E. M., Gleason, C. E., et al. (2012). Ferroptosis: an iron-dependent form of nonapoptotic cell death. *Cell* 149, 1060–1072. doi: 10.1093/jxb/eraa42510.1016/j.cell.2012.03.042

Eaddy, A. C., and Schnellmann, R. G. (2011). Visualization and quantification of endoplasmic reticulum Ca^{2+} in renal cells using confocal microscopy and Fluo5F. *Biochem. Biophys. Res. Commun.* 404, 424–427. doi: 10.1093/jxb/eraa42510.1016/j.bbrc.2010.11.137

Ellis-Davies, G. C., and Kaplan, J. H. (1994). Nitrophenyl-EGTA, a photolabile chelator that selectively binds Ca^{2+} with high affinity and releases it rapidly upon photolysis. *Proc. Natl. Acad. Sci. U. S. A.* 91, 187–191. doi: 10.1093/jxb/eraa42510.1073/pnas.91.1.187

Farber, J. L. (1994). Mechanisms of cell injury by activated oxygen species. *Environ. Health Perspect.* 102, 17–24. doi: 10.1289/ehp.94102s1017

Fenton, H. J. H. (1894). Oxidation of tartaric acid in presence of iron. *J. Chem. Soc. Trans.* 65, 899–910. doi: 10.1039/CT8946500899

Förderer, A., Li, E., Lawson, A. W., Deng, Y. N., Sun, Y., Logemann, E., et al. (2022). A wheat resistosome defines common principles of immune receptor channels. *Nature* 610, 532–539. doi: 10.1038/s41586-022-05231-w

Franklin-Tong, V. E., Drobak, B. K., Allan, A. C., Watkins, P., and Trewavas, A. J. (1996). Growth of pollen tubes of *Papaver rhoeas* is regulated by a slow-moving calcium wave propagated by inositol 1,4,5-trisphosphate. *Plant Cell.* 8, 1305–1321. doi: 10.1105/tpc.8.8.1305

Gilge, J. L., Fisher, M., and Chai, Y. C. (2008). The effect of oxidant and the non-oxidant alteration of cellular thiol concentration on the formation of protein mixed-disulfides in HEK 293 cells. *PloS One* 3, e4015. doi: 10.1371/journal.pone.0004015

Grant, J. J., and Loake, G. J. (2000). Role of reactive oxygen intermediates and cognate redox signaling in disease resistance. *Plant Physiol.* 124, 21–29. doi: 10.1104/pp.124.1.21

Greenberg, J. T., and Yao, N. (2004). The role and regulation of programmed cell death in plant-pathogen interactions. *Cell Microbiol.* 6, 201–211. doi: 10.1111/j.1462-5822.2004.00361.x

Griffith, O. W. (1980). Determination of glutathione and glutathione disulfide using glutathione reductase and 2-vinylpyridine. *Anal. Biochem.* 106, 207–212. doi: 10.1016/0003-2697(80)90139-6

Grossi, M., Morgunova, M., Cheung, S., Scholz, D., Conroy, E., Terrile, M., et al. (2016). Lysosome triggered near-infrared fluorescence imaging of cellular trafficking processes in real time. *Nat. Commun.* 7, 10855. doi: 10.1038/ncomms10855

Han, S. W., and Hwang, B. K. (2017). Molecular functions of *Xanthomonas type* III effector AvrBsT and its plant interactors in cell death and defense signaling. *Planta* 245, 237–253. doi: 10.1007/s00425-016-2628-x

Heath, M. C. (2000). Hypersensitive response-related death. *Plant Mol. Biol.* 44, 321–334. doi: 10.1023/a:1026592509060

Hepler, P. K. (2005). Calcium: a central regulator of plant growth and development. *Plant Cell.* 17, 2142–2155. doi: 10.1105/tpc.105.032508

Hiei, Y., Ohta, S., Komari, T., and Kumashiro, T. (1994). Efficient transformation of rice (*Oryza sativa L.*) mediated by *Agrobacterium* and sequence analysis of the boundaries of the T-DNA. *Plant J.* 6, 271–282. doi: 10.1046/j.1365-313x.1994.6020271.x

Hwang, C., Sinskey, A. J., and Lodish, H. F. (1992). Oxidized redox state of glutathione in the endoplasmic reticulum. *Science* 257, 1496–1502. doi: 10.1126/science.1523409

Jacob, P., Kim, N. H., Wu, F., El-Kasmi, F., Chi, Y., Walton, W. G., et al. (2021). Plant "helper" immune receptors are Ca^{2+}-permeable nonselective cation channels. *Science* 373, 420–425. doi: 10.1126/science.abg7917

Jakic, B., Buszko, M., Cappellano, G., and Wick, G. (2017). Elevated sodium leads to the increased expression of HSP60 and induces apoptosis in HUVECs. *PloS One* 12, e0179383. doi: 10.1371/journal.pone.0179383

Jewell, S. A., Bellomo, G., Thor, H., Orrenius, S., and Smith, M. (1982). Bleb formation in hepatocytes during drug metabolism is caused by disturbances in thiol and calcium ion homeostasis. *Science* 217, 1257–1259. doi: 10.1126/science.7112127

Jones, J. D., and Dangl, J. L. (2006). The plant immune system. *Nature* 444, 323–329. doi: 10.1038/nature05286

Jwa, N. S., and Hwang, B. K. (2017). Convergent evolution of pathogen effectors toward reactive oxygen species signaling networks in plants. *Front. Plant Sci.* 8. doi: 10.3389/fpls.2017.01687

Kadota, Y., Furuichi, T., Sano, T., Kaya, H., Gunji, W., Murakami, Y., et al. (2005). Cell-cycle-dependent regulation of oxidative stress responses and Ca^{2+} permeable channels NtTPC1A/B in tobacco BY-2 cells. *Biochem. Biophys. Res. Commun.* 336, 1259–1267. doi: 10.1016/j.bbrc.2005.09.004

Kamga, C. K., Zhang, S. X., and Wang, Y. (2010). Dicarboxylate carrier-mediated glutathione transport is essential for reactive oxygen species homeostasis and normal respiration in rat brain mitochondria. *Am. J. Physiol. Cell Physiol.* 299, 497–505. doi: 10.1152/ajpcell.00058.2010

Kanchiswamy, C. N., Malnoy, M., Occhipinti, A., and Maffei, M. E. (2014). Calcium imaging perspectives in plants. *Int. J. Mol. Sci.* 15, 3842–3859. doi: 10.3390/ijms15033842

Kang, S., Hong, J., Lee, J. M., Moon, H. E., Jeon, B., Choi, J., et al. (2017). Trifluoperazine, a well-known antipsychotic, inhibits glioblastoma invasion by binding to calmodulin and disinhibiting calcium release channel IP_3R. *Mol. Cancer Ther.* 16, 217–227. doi: 10.1158/1535-7163.MCT-16-0169-T

Kankanala, P., Czymmek, K., and Valent, B. (2007). Roles for rice membrane dynamics and plasmodesmata during biotrophic invasion by the blast fungus. *Plant Cell.* 19, 706–724. doi: 10.1105/tpc.106.046300

Kawano, T., Kadono, T., Fumoto, K., Lapeyrie, F., Kuse, M., Isobe, M., et al. (2004). Aluminum as a specific inhibitor of plant TPC1 Ca^{2+} channels. *Biochem. Biophys. Res. Commun.* 324, 40–45. doi: 10.1016/j.bbrc.2004.09.015

Kim, S. R., Jeon, J. S., and An, G. (2011). Development of an efficient inverse PCR method for isolating gene tags from T-DNA insertional mutants in rice. *Methods Mol. Biol.* 678, 139–146. doi: 10.1007/978-1-60761-682-5_11

Kosower, N. S., Kosower, E. M., Wertheim, B., and Correa, W. S. (1969). Diamide, a new reagent for the intracellular oxidation of glutathione to the disulfide. *Biochem. Biophys. Res. Commun.* 37, 593–596. doi: 10.1016/0006-291x(69)90850-x

Köster, P., DeFalco, T. A., and Zipfel, C. (2022). Ca^{2+} signals in plant immunity. *EMBO J.* 41, e110741. doi: 10.15252/embj.2022110741

Levine, A., Tenhaken, R., Dixon, R., and Lamb, C. (1994). H_2O_2 from the oxidative burst orchestrates the plant hypersensitive disease resistance response. *Cell* 79, 583–593. doi: 10.1016/0092-8674(94)90544-4

Lewis, J. D., Wu, R., Guttman, D. S., and Desveaux, D. (2010). Allele-specific virulence attenuation of the *Pseudomonas syringae* HopZ1a type III effector via the *Arabidopsis* ZAR1 resistance protein. *PloS Genet.* 6, e1000894. doi: 10.1371/journal.pgen.1000894

Li, N., Ragheb, K., Lawler, G., Sturgis, J., Rajwa, B., Melendez, J. A., et al. (2003). Mitochondrial complex I inhibitor rotenone induces apoptosis through enhancing mitochondrial reactive oxygen species production. *J. Biol. Chem.* 278, 8516–8525. doi: 10.1074/jbc.M210432200

Liu, G., Greenshields, D. L., Sammynaiken, R., Hirji, R. N., Selvaraj, G., and Wei, Y. (2007). Targeted alterations in iron homeostasis underlie plant defense responses. *J. Cell Sci.* 120, 596–605. doi: 10.1242/jcs.001362

Maffei, M., Bossi, S., Spiteller, D., Mithöfer, A., and Boland, W. (2004). Effects of feeding *Spodoptera littoralis* on lima bean leaves. I. Membrane potentials, intracellular calcium variations, oral secretions, and regurgitate components. *Plant Physiol.* 134, 1752–1762. doi: 10.1104/pp.103.034165

Martins, T. V., Evans, M. J., Woolfenden, H. C., and Morris, R. J. (2013). Towards the physics of calcium signalling in plants. *Plants* 2, 541–588. doi: 10.3390/plants2040541

Matsuo, Y., Novianti, F., Takehara, M., Fukuhara, T., Arie, T., and Komatsu, K. (2019). Acibenzolar-*S*-methyl restricts infection of *Nicotiana benthamiana* by plantago asiatica mosaic virus at two distinct stages. *Mol. Plant Microbe Interact.* 32, 1475–1486. doi: 10.1094/MPMI-03-19-0087-R

Meng, X., and Zhang, S. (2013). MAPK cascades in plant disease resistance signaling. *Annu. Rev. Phytopathol.* 51, 245–266. doi: 10.1146/annurev-phyto-082712-102314

Moeder, W., Phan, V., and Yoshioka, K. (2019). Ca^{2+} to the rescue - Ca^{2+} channels and signaling in plant immunity. *Plant Sci.* 279, 19–26. doi: 10.1016/j.plantsci.2018.04.012

Moyen, C., Hammond-Kosack, K. E., Jones, J., Knight, M. R., and Johannes, E. (1998). Systemin triggers an increase of cytoplasmic calcium in tomato mesophyll cells: Ca^{2+} mobilization from intra- and extracellular compartments. *Plant Cell Environ.* 21, 1101–1111. doi: 10.1046/j.1365-3040.1998.00378.x

Muhlemann, J. K., Younts, T. L. B., and Muday, G. K. (2018). Flavonols control pollen tube growth and integrity by regulating ROS homeostasis during high-temperature stress. *Proc. Natl. Acad. Sci. U. S. A.* 115, E11188–E11197. doi: 10.1073/pnas.1811492115

Ngou, B. P. M., Ding, P., and Jones, J. D. G. (2021). Channeling plant immunity. *Cell* 184, 3358–3360. doi: 10.1016/j.cell.2021.05.035

Nguyen, N. K., Wang, J., Liu, D., Hwang, B. K., and Jwa, N. S. (2022). Rice iron storage protein ferritin 2 (OsFER2) positively regulates ferroptotic cell death and

defense responses against *Magnaporthe oryzae*. *Front. Plant Sci.* 13. doi: 10.3389/fpls.2022.1019669

Parisy, V., Poinssot, B., Owsianowski, L., Buchala, A., Glazebrook, J., and Mauch, F. (2007). Identification of PAD2 as a γ-glutamylcysteine synthetase highlights the importance of glutathione in disease resistance of *Arabidopsis*. *Plant J.* 49, 159–172. doi: 10.1111/j.1365-313X.2006.02938.x

Pastore, A., Piemonte, F., Locatelli, M., Russo, A. L., Gaeta, L. ,. M., Tozzi, G., et al. (2001). Determination of blood total, reduced, and oxidized glutathione in pediatric subjects. *Clin. Chem.* 47, 1467–1469. doi: 10.1093/clinchem/47.8.1467

Pierre, J. L., and Fontecave, M. (1999). Iron and activated oxygen species in biology: the basic chemistry. *Biometals* 12, 195–199. doi: 10.1023/a:1009252919854

Rentel, M. C., and Knight, M. R. (2004). Oxidative stress-induced calcium signaling in *Arabidopsis*. *Plant Physiol.* 135, 1471–1479. doi: 10.1104/pp.104.042663

Rohringer, R., Ebrahim-Nesbat, F., and Wolf, G. (1983). Proteins in intercellular washing fluids from leaves of barley (*Hordeum vulgare* L.). *J. Exp. Bot.* 34, 1589–1605. doi: 10.1093/jxb/34.12.1589

Samuel, A. M., Mather, A. K., Arun, G., Norma, A. C., Ricarda, H., Jiamei, L., et al. (2022). Cadmium interference with iron sensing reveals transcriptional programs sensitive and insensitive to reactive oxygen species. *J. Exp. Bot.* 73, 324–338. doi: 10.1093/jxb/erab393

Schanne, F. A., Kane, A. B., Young, E. E., and Farber, J. L. (1979). Calcium dependence of toxic cell death: a final common pathway. *Science* 206, 700–702. doi: 10.1126/science.386513

Scrase-Field, S. A., and Knight, M. R. (2003). Calcium: just a chemical switch? *Curr. Opin. Plant Biol.* 6, 500–506. doi: 10.1016/s1369-5266(03)00091-8

Shen, Q., Liang, M., Yang, F., Deng, Y. Z., and Naqvi, N. I. (2020). Ferroptosis contributes to developmental cell death in rice blast. *New Phytol.* 227, 1831–1846. doi: 10.1111/nph.16636

Shimomura, O., Johnson, F. H., and Saiga, Y. (1963). Further data on the bioluminescent protein, aequorin. *J. Cell Comp. Physiol.* 62, 1–8. doi: 10.1002/jcp.1030620102

Shu, X., Shaner, N. C., Yarbrough, C. A., Tsien, R. Y., and Remington, S. J. (2006). Novel chromophores and buried charges control color in mFruits. *Biochemistry* 45, 9639–9647. doi: 10.1021/bi060773l

Singh, R., Dangol, S., Chen, Y., Choi, J., Cho, Y. S., Lee, J. E., et al. (2016). *Magnaporthe oryzae* effector AVR-Pii helps to establish compatibility by inhibition of the rice NADP-malic enzyme resulting in disruption of oxidative burst and host innate immunity. *Mol. Cells* 39, 426–438. doi: 10.14348/molcells.2016.0094

Stael, S., Wurzinger, B., Mair, A., Mehlmer, N., Vothknecht, U. C., and Teige, M. (2012). Plant organellar calcium signalling: an emerging field. *J. Exp. Bot.* 63, 1525–1542. doi: 10.1093/jxb/err394

Starke, P. E., and Farber, J. L. (1985). Ferric iron and superoxide ions are required for the killing of cultured hepatocytes by hydrogen peroxide. Evidence for the participation of hydroxyl radicals formed by an iron-catalyzed Haber-Weiss reaction. *J. Biol. Chem.* 260, 10099–10104. doi: 10.1016/S0021-9258(17)39218-9

Stockwell, B. R., Friedmann Angeli, J. P., Bayir, H., Bush, A. I., Conrad, M., Dixon, S. J., et al. (2017). Ferroptosis: A regulated cell death nexus linking metabolism, redox biology, and disease. *Cell* 171, 273–285. doi: 10.1016/j.cell.2017.09.021

Sun, L., Gu, L., Wang, S., Yuan, J., Yang, H., Zhu, J., et al. (2012). N-acetylcysteine protects against apoptosis through modulation of group I metabotropic glutamate receptor activity. *PloS One* 7, e32503. doi: 10.1371/journal.pone.0032503

Tandoğan, B., and Ulusu, N. N. (2007). The inhibition kinetics of yeast glutathione reductase by some metal ions. *J. Enzyme Inhib. Med. Chem.* 22, 489–495. doi: 10.1080/14756360601162147

Thulasi Devendrakumar, K., Li, X., and Zhang, Y. (2018). MAP kinase signalling: interplays between plant PAMP- and effector-triggered immunity. *Cell Mol. Life Sci.* 75, 2981–2989. doi: 10.1007/s00018-018-2839-3

Valent, B. (2021). The impact of blast disease: past, present, and future. *Methods Mol. Biol.* 2356, 1–18. doi: 10.1007/978-1-0716-1613-0_1

Van Breusegem, F., and Dat, J. F. (2006). Reactive oxygen species in plant cell death. *Plant Physiol.* 141, 384–390. doi: 10.1104/pp.106.078295

Verma, A., Bhatt, A. N., Farooque, A., Khanna, S., Singh, S., and Dwarakanath, B. S. (2011). Calcium ionophore A23187 reveals calcium related cellular stress as "I-Bodies": an old actor in a new role. *Cell Calcium.* 50, 510–522. doi: 10.1016/j.ceca.2011.08.007

Wang, J., Hu, M., Wang, J., Qi, J., Han, Z., Wang, G., et al. (2019). Reconstitution and structure of a plant NLR resistosome conferring immunity. *Science* 364, eaav5870. doi: 10.1126/science.aav5870

Wang, Q., Pu, Y., Yang, D., Yin, X., He, Z., Yang, Y., et al. (2018). Molecular cloning and characterization of the glutathione reductase gene from *Stipa purpurea*. *Biochem. Biophys. Res. Commun.* 495, 1851–1857. doi: 10.1016/j.bbrc.2017.12.054

Wang, L., Zhao, L., Zhang, X., Zhang, Q., Jia, Y., Wang, G., et al. (2019). Large-scale identification and functional analysis of NLR genes in blast resistance in the Tetep rice genome sequence. *Proc. Natl. Acad. Sci. U. S. A.* 116, 18479–18487. doi: 10.1073/pnas.1910229116

Weigand, C., Kim, S. H., Brown, E., Medina, E., Mares, M., Miller, G., et al. (2021). A ratiometric calcium reporter CGf reveals calcium dynamics both in the single cell and whole plant levels under heat stress. *Front. Plant Sci.* 12. doi: 10.3389/fpls.2021.777975

White, P. J. (1996). Specificity of ion channel inhibitors for the maxi cation channel in rye root plasma membranes. *J. Exp. Bot.* 47, 713–716. doi: 10.1093/jxb/47.5.713

Wu, F., Chi, Y., Jiang, Z., Xu, Y., Xie, L., Huang, F., et al. (2020). Hydrogen peroxide sensor HPCA1 is an LRR receptor kinase in *Arabidopsis*. *Nature* 578, 577–581. doi: 10.1038/s41586-020-2032-3

Zhai, K., Deng, Y., Liang, D., Tang, J., Liu, J., Yan, B., et al. (2019). RRM transcription factors interact with NLRs and regulate broad-spectrum blast resistance in rice. *Mol. Cell.* 74, 996–1009.e7. doi: 10.1016/j.molcel.2019.03.013

Zhang, W., Zhou, R. G., Gao, Y. J., Zheng, S. Z., Xu, P., Zhang, S. Q., et al. (2009). Molecular and genetic evidence for the key role of AtCaM3 in heat-shock signal transduction in *Arabidopsis*. *Plant Physiol.* 149, 1773–1784. doi: 10.1104/pp.108.133744

Zhao, C., Tang, Y., Wang, J., Zeng, Y., Sun, H., Zheng, Z., et al. (2021). A mis-regulated cyclic nucleotide-gated channel mediates cytosolic calcium elevation and activates immunity in *Arabidopsis*. *New Phytol.* 230, 1078–1094. doi: 10.1111/nph.17218

frontiers | Frontiers in Plant Science

TYPE Mini Review
PUBLISHED 10 May 2024
DOI 10.3389/fpls.2024.1400659

OPEN ACCESS

EDITED BY
Choong-Min Ryu,
Korea Research Institute of Bioscience and Biotechnology (KRIBB), Republic of Korea

REVIEWED BY
Hee-Kyung Ahn,
The Sainsbury Laboratory, United Kingdom
Takaki Maekawa,
University of Cologne, Germany
Jennifer D. Lewis,
Agricultural Research Service (USDA), United States

*CORRESPONDENCE
Walter Gassmann
gassmannw@missouri.edu

RECEIVED 14 March 2024
ACCEPTED 26 April 2024
PUBLISHED 10 May 2024

CITATION
Horton KN and Gassmann W (2024) Greater than the sum of their parts: an overview of the AvrRps4 effector family. *Front. Plant Sci.* 15:1400659. doi: 10.3389/fpls.2024.1400659

Greater than the sum of their parts: an overview of the AvrRps4 effector family

Katie N. Horton and Walter Gassmann*

Division of Plant Science and Technology, Bond Life Sciences Center, and Interdisciplinary Plant Group, University of Missouri, Columbia, MO, United States

Phytopathogenic microbes use secreted effector proteins to increase their virulence *in planta*. If these effectors or the results of their activity are detected by the plant cell, the plant will mount an immune response which applies evolutionary pressure by reducing growth and success of the pathogen. Bacterial effector proteins in the AvrRps4 family (AvrRps4, HopK1, and XopO) have commonly been used as tools to investigate plant immune components. At the same time, the *in planta* functions of this family of effectors have yet to be fully characterized. In this minireview we summarize current knowledge about the AvrRps4 effector family with emphasis on properties of the proteins themselves. We hypothesize that the HopK1 C-terminus and the AvrRps4 C-terminus, though unrelated in sequence and structure, are broadly related in functions that counteract plant defense responses.

KEYWORDS

effector, pathogen, Pseudomonas, Xanthomonas, virulence, HopK1, XopO, XopAK

Introduction

Plants constantly interact with new challenges presented by their surroundings, and perhaps one of the most relevant interactions for humanity is that between a plant and a pest or pathogen attempting to benefit from the unique position of plants as primary nutrient sources. In the case of microbial biotrophic pathogens, the association between host and co-evolved pathogen is accompanied by intricate manipulation of the plant for the pathogen's benefit (Jones and Dangl, 2006; Ebert and Fields, 2020). Usually manipulation involves secretion by the attacking pathogen of proteins called effectors into the plant cell which, broadly, attempt to improve the attacker's virulence and ultimate ecological success by blocking plant recognition and resistance and/or by increasing availability of resources the attacker needs (McCann and Guttman, 2008; Feng and Zhou, 2012; Kazan and Lyons, 2014; Wang et al., 2022). Successful pathogens cause diseased crops, reduced yield and, in extreme cases, total crop loss. Identifying the *in planta* virulence targets, or the functions, of these effectors is the first step along a pathway that leads to developing crops with greater resistance to disease and eventually to greater food security. In this review, we take this first

step by examining the well-known AvrRps4 effector family and reviewing published information that may provide insight into the *in planta* functions of each effector domain.

As the first isolated bacterial effector known to trigger resistance through a Toll/Interleukin-1 Receptor - Nucleotide Binding - Leucine Rich Repeat (TNL) resistance protein, AvrRps4 was used widely among plant-microbe researchers as a tool for the discovery and investigation of plant resistance components (Gassmann et al., 1999). Though AvrRps4 has been invaluable to the field of molecular plant-pathogen interactions, many facets of the effector's virulence and avirulence targets *in planta* remain unknown.

The three members of the AvrRps4 effector family (AvrRps4, HopK1, and XopO) are characterized by high N-terminal homology to each other followed by a GGGKRVY motif. After secretion into a plant cell via the type III secretion system (T3SS), all members of the family are processed by an unknown protease(s) that cleaves the N-terminus from the C-terminus between GG and GKRVY. This occurs between G133 and G134 (G123 and 124 in XopO) and for unknown reasons requires an arginine at position 112 (R112) (R111 in XopO) (Figure 1) (Roden et al., 2004; Sohn et al., 2009; Li et al., 2014; Halane et al., 2018; Su et al., 2021; Nguyen et al., 2022). AvrRps4 and XopO possess homologous AvrRps4-type N- and C-termini (AvrRps4^{N} and AvrRps4^{C}), but HopK1 only shares N-terminal homology with AvrRps4. HopK1 C-terminus (HopK1^{C}) instead shares homology with XopAK (Figure 1) and RipBQ, a *Ralstonia* effector not discussed in this minireview due to limited space and literature (Sabbagh et al., 2019). Although XopAK is not a proper member of the AvrRps4 effector family due to lack of a GGGKRVY motif or any homology to AvrRps4^{N}, it is present in multiple important bacterial crop pathogens, including those that cause banana Xanthomonas wilt, maize bacterial leaf streak, bacterial leaf streak of rice, and all currently known citrus canker strains (Moreira et al., 2010; Studholme et al., 2010; Jalan et al., 2011, 2013; Bart et al., 2012; Darrasse et al., 2013; Wichmann et al., 2013; Gagnevin et al., 2014; Aritua et al., 2015). We believe its inclusion will provide useful insights into the *in planta* function(s) of HopK1^{C}.

This summary is intended to be used as a collection of knowledge on the topic and to be viewed as a description of possibilities to be explored further. We strive to consider the preponderance of evidence available rather than focusing on any singular result when we discuss these effectors below.

AvrRps4

The founding member of the family, the *avrRps4* avirulence gene from *Pseudomonas syringae* pv. *pisi* (Psp) str. 151, was described in 1996 and was one of the first avirulence genes shown to be present in all tested strains of a pathovar (Hinsch and Staskawicz, 1996). In both Psp 151 and *P. syringae* pv.

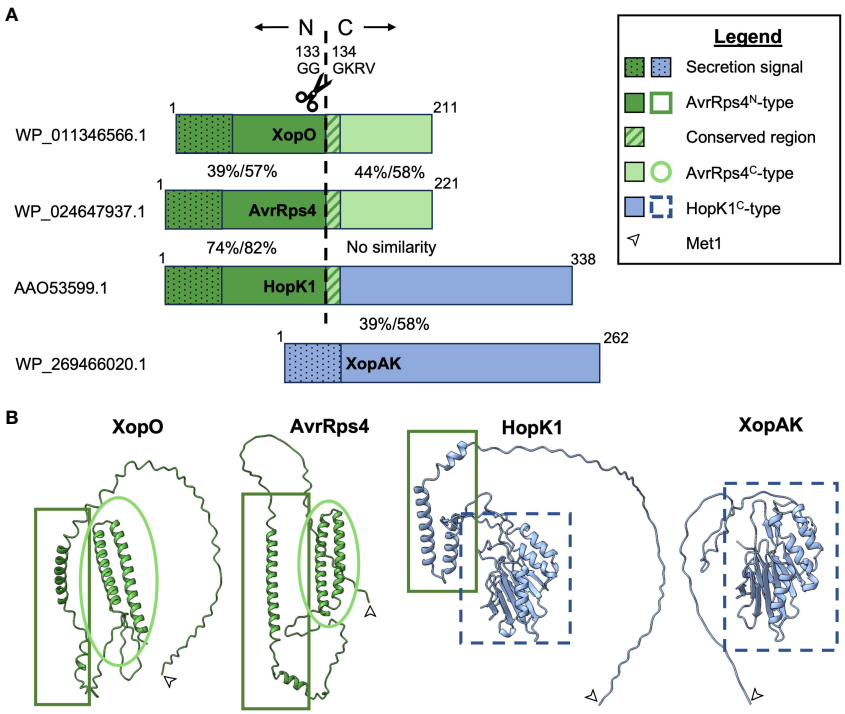

FIGURE 1
Visual representations of AvrRps4 effector family homology. **(A)** Proportional amino acid sequence homology indicated by color and pattern. AvrRps4^{N}-type sequences are indicated in dark green, AvrRps4^{C}-type sequences are indicated in light green, and HopK1^{C}-type sequences are indicated in light blue. NCBI accession numbers for proteins used in this comparison are listed on the left. Percentages between the termini indicate % identity/% positives for each pair as predicted by NCBI's blastp (Altschul et al., 1990). The ~50AA secretion signals (represented by dots) are included in this comparison but the 12AA central homologous regions (represented by stripes) are not. **(B)** Protein structural homology with Met1 indicated by an arrow. Structural predictions were made with ColabFold and visualized using ChimeraX (Pettersen et al., 2021; Mirdita et al., 2022).

phaseolicola str. 1448A, *avrRps4* is located on a plasmid (Kim et al., 1998; Joardar et al., 2005).

After secretion and subsequent processing inside the plant cell, both AvrRps4 termini are largely nucleo-cytoplasmically localized (Bhattacharjee et al., 2011; Heidrich et al., 2011; Sohn et al., 2012; Li et al., 2014; Park et al., 2017; Halane et al., 2018). Interestingly, Li et al., 2014 also reported N-terminus-dependent localization of transgenically expressed AvrRps4 and HopK1 to the chloroplast. Independently, *in vitro* import assays showed localization of HopK1 in chloroplasts (De Torres Zabala et al., 2015). More recent work has shown that deliberate AvrRps4 mislocalization to the plasma membrane by replacing the N-terminus does not prevent processing, accumulation of the C-terminus in the nucleus, or contribution to resistance (Halane et al., 2018). AvrRps4^{N} (aa 1-136) in particular has been used with varied success in the past as part of the effector detector vector system (pEDV) for identification of candidate effectors from other bacteria (Kim et al., 2023), oomycetes (Sohn et al., 2007; Fabro et al., 2011; Kemen et al., 2011; Badel et al., 2013; Upadhyaya et al., 2014), fungi (Sharma et al., 2013; Zhang et al., 2020), insects (Navarro-Escalante et al., 2020; Peng et al., 2023), and nematodes (Shi et al., 2018b, 2018a). This, alongside the apparent similarities between N-terminal secretion signals of type III secreted effector proteins and chloroplast/mitochondrial transit peptides (Guttman et al., 2002) indicate that while a portion of the cellular pool of AvrRps4 may be targeted to the chloroplast for its virulence function, presence of AvrRps4^{N} is likely not the only factor leading to the observed chloroplast localization.

Further, the AvrRps4 N-terminus appears to have a greater role in virulence than exclusively as a signal peptide. Transgenic expression of AvrRps4^{N} alone in *Arabidopsis thaliana* (Arabidopsis) Col-0 increased virulence of *P. syringae* pv. *tomato* (Pto) strain DC3000 *hopk1*$^{-}$ (Halane et al., 2018). Furthermore, AvrRps4^{N} was necessary and sufficient to trigger a strong hypersensitive response (HR) in resistant lettuce cultivars (Halane et al., 2018; Su et al., 2021). When co-expressed in resistant lettuce with AvrRps4^{C}, this AvrRps4^{N}-triggered HR phenotype was reduced. In contrast, full avirulence in Arabidopsis Col-0 requires the presence of both AvrRps4^{N} and AvrRps4^{C} (Halane et al., 2018). These dual roles of AvrRps4^{N} are the hallmarks of an effector: benefiting the pathogen while being detrimental enough to some plants that they have evolved to detect it. As for a virulence function, reports directly examining the N-terminus suggest AvrRps4^{N} interacts with EDS1 (Bhattacharjee et al., 2011; Halane et al., 2018), an important immune regulator for TNL proteins and basal resistance (Dongus and Parker, 2021). Interaction with EDS1 has also been reported for the unrelated *P. syringae* pv. *glycinea* effector AvrA1 when transiently expressed in *N. benthamiana* (Wang et al., 2014). For both AvrRps4^{N} and AvrA1 the immediate functional effects of their interactions with EDS1 in terms of virulence or avirulence have not been determined. Taken together, these works highlight a need for greater understanding of AvrRps4^{N} functions.

Contrastingly, AvrRps4^{C} functions are well understood. An electronegative patch (Sohn et al., 2012) interacts with defense-related WRKY transcription factors (Kim et al., 2024) and with the C-terminal integrated WRKY decoy domain of resistance protein RRS1 (Sarris et al., 2015; Mukhi et al., 2021; Kim et al., 2024), providing a mechanism for earlier observations of AvrRps4-dependent suppression of HR in tobacco (Fujikawa et al., 2006; Cvetkovska and Vanlerberghe, 2012), pattern-triggered immunity (PTI) in Arabidopsis, and enhancement of pathogen growth within *N. benthamiana* (Sohn et al., 2009). Processing of AvrRps4 is not necessary for AvrRps4^{C}-specific triggering of HR in cultivars of *Brassica rapa* (turnip) nor for resistance to be triggered in Arabidopsis, but is necessary for its virulence function (Sohn et al., 2009). Other work has shown that AvrRps4^{C} directly interacts with BRUTUS (BTS), an iron-sensing protein in the nucleus, causing interference with the degradation of bHLH115 and ILR3 and, when not recognized, leading to increased levels of apoplastic iron (Xing et al., 2021).

XopO

XopO was first described in 2004 from *Xanthomonas euvesicatoria* pv. *vesicatoria* (Xev) str. 85-10 and is only known to exist in this strain (formerly: *Xanthomonas axonopodis* pv. *vesicatoria* and *Xanthomonas campestris* pv. *vesicatoria*) and *Xanthomonas oryzae* pv. *oryzicola* (Xoc), neither of which appear to be greatly affected by its deletion (Roden et al., 2004; Hajri et al., 2009, 2012; Liao et al., 2020). Indeed, in multiple strains XopO was found to be mutationally inactivated or to possess insertions or deletions within the first 100 amino acids of the protein, suggesting an evolutionary advantage in removing the effector from the secretion repertoire (Wang et al., 2011, p. 20; Barak et al., 2016).

It is not known whether XopO^{C} interacts with WRKY proteins in the same manner as AvrRps4^{C}, but we do know that XopO^{C} does not trigger HR in turnip as AvrRps4^{C} does and likewise does not appear to weaken the recognition of XopO^{N} in lettuce to the same degree that AvrRps4^{C} does for AvrRps4^{N} (Sohn et al., 2009; Nguyen et al., 2022). These amino acid polymorphisms and the differential recognition between AvrRps4^{C} and XopO^{C} may be related to functionality within specific plant hosts, and future functional analyses of these effectors should take this into consideration.

HopK1

HopK1 (previously HopPtoK) was identified in 2002 from Pto DC3000 (Petnicki-Ocwieja et al., 2002). HopK1 in its full length is found almost exclusively within pathovars of *P. syringae*, although not every pathovar or strain carries it. After AvrRps4, HopK1 is the most well-researched bacterial effector protein in the AvrRps4 family.

In Pto DC3000, the *hopK1* gene is located on the chromosome and is encoded in a 24 kb Tn*6022*-like element, but in other strains *hopK1* may occur on a plasmid (Li et al., 2014; Peters et al., 2014). In the case of Pto DAPP-PG 215, *hopK1* is borne on p107, a small plasmid which possesses two prophage regions and some precursors for coronatine production in addition to the effector (Orfei et al., 2023).

Pto DC3000 *hopk1*$^{-}$ strains are significantly reduced in their ability to grow and cause disease within plants. The full wild-type growth of

the mutant in Arabidopsis Col-0 was not restored by simultaneous transgenic expression of HopK1^{C} but was restored by expression in the same manner of the full-length protein. The N-terminus was also necessary for reduction in reactive oxygen species (ROS) and callose deposition, both indicators of PTI, indicating that HopK1^{N} is indispensable for effector virulence activities (Li et al., 2014). Presence of HopK1 in an otherwise effectorless Pto DC3000 strain did not contribute to nor inhibit growth compared to Pto DC3000 with no effectors at all, nor did it reduce production of ROS in *N. benthamiana.* Nevertheless, authors reported a moderate reduction in "non-avirulence-related" cell death caused by other effectors when HopK1 was present (Wei et al., 2018). Finally, expression of HopK1 did not suppress flg22-mediated activation of FRK1-LUC, another PTI indicator, in Arabidopsis protoplasts (He et al., 2006). Together, these findings may indicate that HopK1^{N} works synergistically with an unknown Pto DC3000 effector(s) in order to counteract early PTI events. This synergistic interaction resulting in reduced ROS and callose may also be required for maximum effectiveness of HopK1, as HopK1^{C} has been shown to travel intercellularly up to one cell layer away by using plasmodesmata as long as movement is not restricted by excess callose deposition (Li et al., 2021; Iswanto et al., 2022).

When infiltrated into Arabidopsis Col-0 alongside AvrRps4^{C}, HopK1^{N} fully complements the resistance response seen when AvrRps4^{N} and AvrRps4^{C} are infiltrated together. The central conserved portion of the N-terminus containing the positively charged R112 is required for recognition in lettuce (Halane et al., 2018; Su et al., 2021; Nguyen et al., 2022). However, processing is not required for full pathogenicity (Li et al., 2014).

As mentioned above with AvrRps4, HopK1 was bioinformatically predicted to localize to the chloroplast and was shown to localize to the chloroplast stroma when inducibly expressed by transgenic Arabidopsis, yet nucleo-cytoplasmically when expressed by *A. tumefaciens* in a constitutive transient manner in *N. benthamiana* (Li et al., 2014; De Torres Zabala et al., 2015).

XopAK

Perhaps representative of its presence in many *Xanthomonas* species with different life histories, *xopAK* is variable in length and number of accumulated mutations. For example, the gene showed very few polymorphic sites among strains of *X. axonopodis manihotis* (Bart et al., 2012; Trujillo et al., 2014) but is believed to be inactivated in *X. phaseoli* pv. *dieffenbachiae* due to a frameshift (Constantin et al., 2017) and is in some cases missing a significant coding region that nearly halves the length of the protein (Fan et al., 2022). Machine learning predicted the presence of a deaminase catalytic domain at the C-terminus of XopAK and at least one potential myristoylation or palmitoylation motif which could target the effector to the plasma membrane (Teper et al., 2015; Barak et al., 2016). This putative deaminase domain is well within the region of homology with HopK1^{C} and may therefore contribute to a more thorough picture of the AvrRps4 family's *in planta* functions.

Like HopK1, XopAK had no significant effect on flg22-triggered activation of FRK1 in Arabidopsis protoplasts (He et al., 2006; Popov et al., 2016). Unlike *hopK1*, deletion of *xopAK* from Xoc caused no visible changes in disease symptoms on its host (rice) (Liao et al., 2020).

Discussion

The AvrRps4-type N-terminus is a metaphorical black box for researchers of this family. Its proposed functional region is very small, only about 37 aa long (Su et al., 2021), yet it provokes a strong HR from lettuce (Halane et al., 2018; Su et al., 2021), interacts with a major TNL resistance hub (EDS1) (Bhattacharjee et al., 2011; Halane et al., 2018), and appears more important for the growth of Pto DC3000 than HopK1^{C} alone (Li et al., 2014; Halane et al., 2018), but we still know almost nothing about its function. Intriguingly, using AvrRps4^{N} similarly to pEDV for delivery of the full-length unrelated effector XopQ into *N. benthamiana* cells resulted in a weaker response by the plant than when XopQ was delivered by the AvrRpt2 signal peptide (Gantner et al., 2018). Authors did not test further but hypothesized that this weakness could be the result of differences in stability or translocated amount of protein. While this may be the case, it is also possible that AvrRps4^{N} interaction with EDS1 interferes with the EDS1-mediated recognition of XopQ (Adlung et al., 2016), but more study is needed.

We also do not yet know how detrimental simply possessing an endogenous *avrRps4*^{N} might be for bacteria themselves. *xopO* and *xopAK* both naturally occur within the genome of Xev 85-10, but the same is not true for *avrRps4* and *hopK1*, which to date have never been found to naturally co-occur. There are no examples of a strain possessing multiple members of the AvrRps4 effector family (*sensu stricto*), multiple copies of a single member, the *avrRps4*-type C-terminus without an attached N-terminus, or even a single copy of the *avrRps4*-type N-terminus without an attached C-terminus of any type. It is tempting to conclude from this that AvrRps4^{N} may be detrimental to the bacterium over evolutionary time, and we look forward to any future work examining AvrRps4^{N} more thoroughly.

Neither HopK1^{C} nor XopAK cause any significant effect on flg22-triggered FRK1 activation (He et al., 2006; Popov et al., 2016), an early PTI response, yet HopK1 has still been shown to block or reduce HR and PTI (Jamir et al., 2004; Li et al., 2014; Gimenez-Ibanez et al., 2018; Wei et al., 2018). This reduction appears to be related to the action of HopK1^{N} and to be essential for the full virulence of HopK1^{C}, yet its homologue XopAK occurs in many more species of *Xanthomonas* without the N-terminus-bearing XopO than it does with it. In fact, their co-occurrence is limited to the only two known pathovars possessing XopO: Xev and Xoc. This raises the question whether XopAK benefits from another effector with redundant function when XopO is not present, or if polymorphisms between the homologues render them dissimilar enough that a 'helper' effector is not necessary for XopAK. In the latter case, addition of XopO may have presented an opportunity for range expansion by the effector and the pathogen alike.

As summarized in this review, the presence of *xopO* and *xopAK* within the same strains of *Xanthomonas*, *hopK1* association with transposable elements (Peters et al., 2014; Orfei et al., 2023), and *avrRps4* and *hopK1*'s occasional location on plasmids (Kim et al.,

1998; Chang et al., 2005; Orfei et al., 2023) seem to indicate that our modern chimeric effectors may have been formed in a *Xanthomonas* melting pot and then shared with bacteria inhabiting a similar niche, such as *Pseudomonas*, via horizontal gene transfer (HGT). HGT has been implicated in the evolution of *Pseudomonas* (Kim et al., 1998; Rohmer et al., 2004; Dillon et al., 2019) and *Xanthomonas* (Merda et al., 2017; Ruh et al., 2017; Chen et al., 2018) pathogenicity in the past, though not specifically for the AvrRps4 effector family. The rapidity and therefore the agricultural implications of these transfers could be uncovered with examination of the evolutionary history of the family.

As the 30th anniversary of the discovery and cloning of *avrRps4* approaches, we hope investigators will revisit the last 3 decades of AvrRps4 research and open questions with renewed interest, paving the way for (at least)! 3 more decades of insightful molecular plant-pathogen interactions research.

Author contributions

KH: Conceptualization, Data curation, Writing – original draft, Writing – review & editing. WG: Conceptualization, Funding acquisition, Supervision, Writing – review & editing.

Funding

The author(s) declare financial support was received for the research, authorship, and/or publication of this article. This work was supported by a University of Missouri Life Sciences Graduate Fellowship (KNH) and grants from NSF (IOS-1456181) and USDA-NIFA (PBI 2022-11933) (WG).

Acknowledgments

We apologize to colleagues whose work we were unable to include. We thank members of the Gassmann lab and Michael Pisias for discussions.

Conflict of interest

The authors declare that the research was conducted in the absence of any commercial or financial relationships that could be construed as a potential conflict of interest.

The author(s) declared that they were an editorial board member of Frontiers, at the time of submission. This had no impact on the peer review process and the final decision.

Publisher's note

References

Adlung, N., Prochaska, H., Thieme, S., Banik, A., Blüher, D., John, P., et al. (2016). Non-host resistance induced by the *Xanthomonas* effector XopQ is widespread within the genus *Nicotiana* and functionally depends on EDS1. *Front. Plant Sci.* 7. doi: 10.3389/fpls.2016.01796

Altschul, S. F., Gish, W., Miller, W., Myers, E. W., and Lipman, D. J. (1990). Basic local alignment search tool. *J. Mol. Biol.* 215, 403–410. doi: 10.1016/S0022-2836(05)80360-2

Aritua, V., Harrison, J., Sapp, M., Buruchara, R., Smith, J., and Studholme, D. J. (2015). Genome sequencing reveals a new lineage associated with lablab bean and genetic exchange between *Xanthomonas axonopodis* pv. *phaseoli* and *Xanthomonas fuscans* subsp. *fuscans*. *Front. Microbiol.* 6. doi: 10.3389/fmicb.2015.01080

Badel, J. L., Piquerez, S. J. M., Greenshields, D., Rallapalli, G., Fabro, G., Ishaque, N., et al. (2013). *In planta* effector competition assays detect *Hyaloperonospora arabidopsidis* effectors that contribute to virulence and localize to different plant subcellular compartments. *Mol. Plant Microbe Interact.* 26, 745–757. doi: 10.1094/MPMI-06-12-0154-R

Barak, J. D., Vancheva, T., Lefeuvre, P., Jones, J. B., Timilsina, S., Minsavage, G. V., et al. (2016). Whole-genome sequences of *Xanthomonas euvesicatoria* strains clarify taxonomy and reveal a stepwise erosion of type 3 effectors. *Front. Plant Sci.* 7. doi: 10.3389/fpls.2016.01805

Bart, R., Cohn, M., Kassen, A., McCallum, E. J., Shybut, M., Petriello, A., et al. (2012). High-throughput genomic sequencing of cassava bacterial blight strains identifies conserved effectors to target for durable resistance. *Proc. Natl. Acad. Sci.* 109, E1972–E1979. doi: 10.1073/pnas.1208003109

Bhattacharjee, S., Halane, M. K., Kim, S. H., and Gassmann, W. (2011). Pathogen effectors target *Arabidopsis* EDS1 and alter its interactions with immune regulators. *Science* 334, 1405–1408. doi: 10.1126/science.1211592

Chang, J. H., Urbach, J. M., Law, T. F., Arnold, L. W., Hu, A., Gombar, S., et al. (2005). A high-throughput, near-saturating screen for type III effector genes from *Pseudomonas syringae*. *Proc. Natl. Acad. Sci.* 102, 2549–2554. doi: 10.1073/pnas.0409660102

Chen, N. W. G., Serres-Giardi, L., Ruh, M., Briand, M., Bonneau, S., Darrasse, A., et al. (2018). Horizontal gene transfer plays a major role in the pathological convergence of *Xanthomonas* lineages on common bean. *BMC Genomics* 19, 606. doi: 10.1186/s12864-018-4975-4

Constantin, E. C., Haegeman, A., Van Vaerenbergh, J., Baeyen, S., Van Malderghem, C., Maes, M., et al. (2017). Pathogenicity and virulence gene content of *Xanthomonas* strains infecting Araceae, formerly known as *Xanthomonas axonopodis* pv. *dieffenbachiae*. *Plant Pathol.* 66, 1539–1554. doi: 10.1111/ppa.12694

Cvetkovska, M., and Vanlerberghe, G. C. (2012). Coordination of a mitochondrial superoxide burst during the hypersensitive response to bacterial pathogen in *Nicotiana tabacum*. *Plant Cell Environ.* 35, 1121–1136. doi: 10.1111/j.1365-3040.2011.02477.x

Darrasse, A., Carrère, S., Barbe, V., Boureau, T., Arrieta-Ortiz, M. L., Bonneau, S., et al. (2013). Genome sequence of *Xanthomonas fuscans* subsp. *fuscans* strain 4834-R reveals that flagellar motility is not a general feature of xanthomonads. *BMC Genomics* 14, 761. doi: 10.1186/1471-2164-14-761

De Torres Zabala, M., Littlejohn, G., Jayaraman, S., Studholme, D., Bailey, T., Lawson, T., et al. (2015). Chloroplasts play a central role in plant defence and are targeted by pathogen effectors. *Nat. Plants* 1, 15074. doi: 10.1038/nplants.2015.74

Dillon, M. M., Almeida, R. N. D., Laflamme, B., Martel, A., Weir, B. S., Desveaux, D., et al. (2019). Molecular evolution of *Pseudomonas syringae* type III secreted effector proteins. *Front. Plant Sci.* 10. doi: 10.3389/fpls.2019.00418

Dongus, J. A., and Parker, J. E. (2021). EDS1 signalling: At the nexus of intracellular and surface receptor immunity. *Curr. Opin. Plant Biol.* 62, 102039. doi: 10.1016/j.pbi.2021.102039

Ebert, D., and Fields, P. D. (2020). Host–parasite co-evolution and its genomic signature. *Nat. Rev. Genet.* 21, 754–768. doi: 10.1038/s41576-020-0269-1

Fabro, G., Steinbrenner, J., Coates, M., Ishaque, N., Baxter, L., Studholme, D. J., et al. (2011). Multiple candidate effectors from the Oomycete pathogen *Hyaloperonospora arabidopsidis* suppress host plant immunity. *PloS Pathog.* 7, e1002348. doi: 10.1371/journal.ppat.1002348

Fan, Q., Bibi, S., Vallad, G. E., Goss, E. M., Hurlbert, J. C., Paret, M. L., et al. (2022). Identification of genes in *Xanthomonas euvesicatoria* pv. *rosa* that are host limiting in tomato. *Plants* 11, 796. doi: 10.3390/plants11060796

Feng, F., and Zhou, J.-M. (2012). Plant–bacterial pathogen interactions mediated by type III effectors. *Biot. Interact.* 15, 469–476. doi: 10.1016/j.pbi.2012.03.004

Fujikawa, T., Yamashita, T., and Tsuyumu, S. (2006). Hypersensitive response suppression by type III effectors of plant pathogenic bacteria. *J. Gen. Plant Pathol.* 72, 176–179. doi: 10.1007/s10327-005-0268-2

Gagnevin, L., Bolot, S., Gordon, J. L., Pruvost, O., Vernière, C., Robène, I., et al. (2014). Draft genome sequence of *Xanthomonas axonopodis* pv. *allii* strain CFBP 6369. *Genome Announc* 2, e00727-14. doi: 10.1128/genomea.00727-14

Gantner, J., Ordon, J., Ilse, T., Kretschmer, C., Gruetzner, R., Löfke, C., et al. (2018). Peripheral infrastructure vectors and an extended set of plant parts for the Modular Cloning system. *PloS One* 13, e0197185. doi: 10.1371/journal.pone.0197185

Gassmann, W., Hinsch, M. E., and Staskawicz, B. J. (1999). The *Arabidopsis* RPS4 bacterial-resistance gene is a member of the TIR-NBS-LRR family of disease-resistance genes. *Plant J.* 20, 265–277. doi: 10.1046/j.1365-313X.1999.t01-1-00600.x

Gimenez-Ibanez, S., Hann, D. R., Chang, J. H., Segonzac, C., Boller, T., and Rathjen, J. P. (2018). Differential suppression of *Nicotiana benthamiana* innate immune responses by transiently expressed *Pseudomonas syringae* type III effectors. *Front. Plant Sci.* 9. doi: 10.3389/fpls.2018.00688

Guttman, D. S., Vinatzer, B. A., Sarkar, S. F., Ranall, M. V., Kettler, G., and Greenberg, J. T. (2002). A functional screen for the type III (Hrp) secretome of the plant pathogen *Pseudomonas syringae*. *Science* 295, 1722–1726. doi: 10.1126/science.295.5560.1722

Hajri, A., Brin, C., Hunault, G., Lardeux, F., Lemaire, C., Manceau, C., et al. (2009). A «repertoire for repertoire» hypothesis: repertoires of type three effectors are candidate determinants of host specificity in *Xanthomonas*. *PloS One* 4, e6632. doi: 10.1371/annotation/92d243d0-22b2-44da-9618-83b4aa252724

Hajri, A., Brin, C., Zhao, S., David, P., Feng, J.-X., Koebnik, R., et al. (2012). Multilocus sequence analysis and type III effector repertoire mining provide new insights into the evolutionary history and virulence of *Xanthomonas oryzae*. *Mol. Plant Pathol.* 13, 288–302. doi: 10.1111/j.1364-3703.2011.00745.x

Halane, M. K., Kim, S. H., Spears, B. J., Garner, C. M., Rogan, C. J., Okafor, E. C., et al. (2018). The bacterial type III-secreted protein AvrRps4 is a bipartite effector. *PloS Pathog.* 14, e1006984. doi: 10.1371/journal.ppat.1006984

He, P., Shan, L., Lin, N.-C., Martin, G. B., Kemmerling, B., Nürnberger, T., et al. (2006). Specific bacterial suppressors of MAMP signaling upstream of MAPKKK in *Arabidopsis* innate immunity. *Cell* 125, 563–575. doi: 10.1016/j.cell.2006.02.047

Heidrich, K., Wirthmueller, L., Tasset, C., Pouzet, C., Deslandes, L., and Parker, J. E. (2011). *Arabidopsis* EDS1 connects pathogen effector recognition to cell compartment–specific immune responses. *Science* 334, 1401–1404. doi: 10.1126/science.1211641

Hinsch, M., and Staskawicz, B. (1996). Identification of a new *Arabidopsis* disease resistance locus, RPs4, and cloning of the corresponding avirulence gene, avrRps4, from *Pseudomonas syringae* pv. *pisi*. *Mol. Plant Microbe Interact.* 9, 55–61. doi: 10.1094/MPMI-9-0055

Iswanto, A. B. B., Vu, M. H., Pike, S., Lee, J., Kang, H., Son, G. H., et al. (2022). Pathogen effectors: what do they do at plasmodesmata? *Mol. Plant Pathol.* 23, 795–804. doi: 10.1111/mpp.13142

Jalan, N., Aritua, V., Kumar, D., Yu, F., Jones, J. B., Graham, J. H., et al. (2011). Comparative genomic analysis of *Xanthomonas axonopodis* pv. *citrumelo* F1, which causes citrus bacterial spot disease, and related strains provides insights into virulence and host specificity. *J. Bacteriol* 193, 6342–6357. doi: 10.1128/JB.05777-11

Jalan, N., Kumar, D., Andrade, M. O., Yu, F., Jones, J. B., Graham, J. H., et al. (2013). Comparative genomic and transcriptome analyses of pathotypes of *Xanthomonas citri* subsp. *citri* provide insights into mechanisms of bacterial virulence and host range. *BMC Genomics* 14, 551. doi: 10.1186/1471-2164-14-551

Jamir, Y., Guo, M., Oh, H.-S., Petnicki-Ocwieja, T., Chen, S., Tang, X., et al. (2004). Identification of *Pseudomonas syringae* type III effectors that can suppress programmed cell death in plants and yeast. *Plant J.* 37, 554–565. doi: 10.1046/j.1365-313X.2003.01982.x

Joardar, V., Lindeberg, M., Jackson, R. W., Selengut, J., Dodson, R., Brinkac, L. M., et al. (2005). Whole-genome sequence analysis of *Pseudomonas syringae* pv. *phaseolicola* 1448A reveals divergence among pathovars in genes involved in virulence and transposition. *J. Bacteriol* 187, 6488–6498. doi: 10.1128/JB.187.18.6488-6498.2005

Jones, J. D. G., and Dangl, J. L. (2006). The plant immune system. *Nature* 444, 323–329. doi: 10.1038/nature05286

Kazan, K., and Lyons, R. (2014). Intervention of phytohormone pathways by pathogen effectors. *Plant Cell* 26, 2285–2309. doi: 10.1105/tpc.114.125419

Kemen, E., Gardiner, A., Schultz-Larsen, T., Kemen, A. C., Balmuth, A. L., Robert-Seilaniantz, A., et al. (2011). Gene gain and loss during evolution of obligate parasitism in the white rust pathogen of *Arabidopsis thaliana*. *PloS Biol.* 9, e1001094. doi: 10.1371/journal.pbio.1001094

Kim, B., Yu, W., Kim, H., Dong, Q., Choi, S., Prokchorchick, M., et al. (2023). A plasma membrane nucleotide-binding leucine-rich repeat receptor mediates the recognition of the *Ralstonia pseudosolanacearum* effector RipY in *Nicotiana benthamiana*. *Plant Commun.* 4, 100640. doi: 10.1016/j.xplc.2023.100640

Kim, H., Kim, J., Choi, D. S., Kim, M.-S., Deslandes, L., Jayaraman, J., et al. (2024). Molecular basis for the interference of the *Arabidopsis* WRKY54-mediated immune response by two sequence-unrelated bacterial effectors. *Plant J.* 118, 839-855. doi: 10.1111/tpj.16639

Kim, J. F., Charkowski, A. O., Alfano, J. R., Collmer, A., and Beer, S. V. (1998). Sequences related to transposable elements and bacteriophages flank avirulence genes of *Pseudomonas syringae*. *Mol. Plant Microbe Interact.* 11, 1247–1252. doi: 10.1094/MPMI.1998.11.12.1247

Li, G., Froehlich, J. E., Elowsky, C., Msanne, J., Ostosh, A. C., Zhang, C., et al. (2014). Distinct *Pseudomonas* type-III effectors use a cleavable transit peptide to target chloroplasts. *Plant J.* 77, 310–321. doi: 10.1111/tpj.12396

Li, Z., Variz, H., Chen, Y., Liu, S.-L., and Aung, K. (2021). Plasmodesmata-dependent intercellular movement of bacterial effectors. *Front. Plant Sci.* 12. doi: 10.3389/fpls.2021.640277

Liao, Z.-X., Li, J.-Y., Mo, X.-Y., Ni, Z., Jiang, W., He, Y.-Q., et al. (2020). Type III effectors *xopN* and *avrBS2* contribute to the virulence of *Xanthomonas oryzae* pv. *oryzicola* strain GX01. *Res. Microbiol.* 171, 102–106. doi: 10.1016/j.resmic.2019.10.002

McCann, H. C., and Guttman, D. S. (2008). Evolution of the type III secretion system and its effectors in plant–microbe interactions. *New Phytol.* 177, 33–47. doi: 10.1111/j.1469-8137.2007.02293.x

Merda, D., Briand, M., Bosis, E., Rousseau, C., Portier, P., Barret, M., et al. (2017). Ancestral acquisitions, gene flow and multiple evolutionary trajectories of the type three secretion system and effectors in *Xanthomonas* plant pathogens. *Mol. Ecol.* 26, 5939–5952. doi: 10.1111/mec.14343

Mirdita, M., Schütze, K., Moriwaki, Y., Heo, L., Ovchinnikov, S., and Steinegger, M. (2022). ColabFold: making protein folding accessible to all. *Nat. Methods* 19, 679–682. doi: 10.1038/s41592-022-01488-1

Moreira, L. M., Almeida, N. F., Potnis, N., Digiampietri, L. A., Adi, S. S., Bortolossi, J. C., et al. (2010). Novel insights into the genomic basis of citrus canker based on the genome sequences of two strains of *Xanthomonas fuscans* subsp. *aurantifolii*. *BMC Genomics* 11, 238. doi: 10.1186/1471-2164-11-238

Mukhi, N., Brown, H., Gorenkin, D., Ding, P., Bentham, A. R., Stevenson, C. E. M., et al. (2021). Perception of structurally distinct effectors by the integrated WRKY domain of a plant immune receptor. *Proc. Natl. Acad. Sci. U. S. A* 118, e2113996118. doi: 10.1073/pnas.2113996118

Navarro-Escalante, L., Zhao, C., Shukle, R., and Stuart, J. (2020). BSA-seq discovery and functional analysis of candidate Hessian Fly (*Mayetiola destructor*) avirulence genes. *Front. Plant Sci.* 11. doi: 10.3389/fpls.2020.00956

Nguyen, Q.-M., Iswanto, A. B. B., Son, G. H., Vuong, U. T., Lee, J., Kang, J.-H., et al. (2022). AvrRps4 effector family processing and recognition in lettuce. *Mol. Plant Pathol.* 23, 1390–1398. doi: 10.1111/mpp.13233

Orfei, B., Pothier, J. F., Fenske, L., Blom, J., Moretti, C., Buonaurio, R., et al. (2023). Race-specific genotypes of *Pseudomonas syringae* pv. *tomato* are defined by the presence of mobile DNA elements within the genome. *Front. Plant Sci.* 14. doi: 10.3389/fpls.2023.1197706

Park, E., Lee, H.-Y., Woo, J., Choi, D., and Dinesh-Kumar, S. P. (2017). Spatiotemporal monitoring of *Pseudomonas syringae* effectors via type III secretion using split fluorescent protein fragments. *Plant Cell* 29, 1571–1584. doi: 10.1105/tpc.17.00047

Peng, Z., Su, Q., Ren, J., Tian, L., Zeng, Y., Yang, Y., et al. (2023). A novel salivary effector, BtE3, is essential for whitefly performance on host plants. *J. Exp. Bot.* 74, 2146–2159. doi: 10.1093/jxb/erad024

Peters, J. E., Fricker, A. D., Kapili, B. J., and Petassi, M. T. (2014). Heteromeric transposase elements: generators of genomic islands across diverse bacteria. *Mol. Microbiol.* 93, 1084–1092. doi: 10.1111/mmi.12740

Petnicki-Ocwieja, T., Schneider, D. J., Tam, V. C., Chancey, S. T., Shan, L., Jamir, Y., et al. (2002). Genomewide identification of proteins secreted by the Hrp type III protein secretion system of *Pseudomonas syringae* pv. *tomato* DC3000. *Proc. Natl. Acad. Sci.* 99, 7652–7657. doi: 10.1073/pnas.112183899

Pettersen, E. F., Goddard, T. D., Huang, C. C., Meng, E. C., Couch, G. S., Croll, T. I., et al. (2021). UCSF ChimeraX: structure visualization for researchers, educators, and developers. *Protein Sci. Publ. Protein Soc.* 30, 70–82. doi: 10.1002/pro.3943

Popov, G., Fraiture, M., Brunner, F., and Sessa, G. (2016). Multiple *Xanthomonas euvesicatoria* type III effectors inhibit flg22-triggered immunity. *Mol. Plant Microbe Interact.* 29, 651–660. doi: 10.1094/MPMI-07-16-0137-R

Roden, J. A., Belt, B., Ross, J. B., Tachibana, T., Vargas, J., Mudgett, MB, et al. (2004). A genetic screen to isolate type III effectors translocated into pepper cells during *Xanthomonas* infection. *Proc. Natl. Acad. Sci.* 101, 16624–16629. doi: 10.1073/pnas.0407383101

Rohmer, L., Guttman, D. S., and Dangl, J. L. (2004). Diverse evolutionary mechanisms shape the type III effector virulence factor repertoire in the plant pathogen *Pseudomonas syringae*. *Genetics* 167, 1341–1360. doi: 10.1534/genetics.103.019638

Ruh, M., Briand, M., Bonneau, S., Jacques, M.-A., and Chen, N. W. G. (2017). *Xanthomonas* adaptation to common bean is associated with horizontal transfers of genes encoding TAL effectors. *BMC Genomics* 18, 670. doi: 10.1186/s12864-017-4087-6

Sabbagh, C. R. R., Carrere, S., Lonjon, F., Vailleau, F., Macho, A. P., Genin, S., et al. (2019). Pangenomic type III effector database of the plant pathogenic Ralstonia spp. *PeerJ* 7, e7346. doi: 10.7717/peerj.7346

Sarris, P. F., Duxbury, Z., Huh, S. U., Ma, Y., Segonzac, C., Sklenar, J., et al. (2015). A Plant immune receptor detects pathogen effectors that target WRKY transcription factors. *Cell* 161, 1089–1100. doi: 10.1016/j.cell.2015.04.024

Sharma, S., Sharma, S., Hirabuchi, A., Yoshida, K., Fujisaki, K., Ito, A., et al. (2013). Deployment of the *Burkholderia glumae* type III secretion system as an efficient tool for translocating pathogen effectors to monocot cells. *Plant J.* 74, 701–712. doi: 10.1111/tpj.12148

Shi, Q., Mao, Z., Zhang, X., Ling, J., Lin, R., Zhang, X., et al. (2018a). The novel secreted *Meloidogyne incognita* effector MiISE6 targets the host nucleus and facilitates parasitism in *Arabidopsis*. *Front. Plant Sci.* 9. doi: 10.3389/fpls.2018.00252

Shi, Q., Mao, Z., Zhang, X., Zhang, X., Wang, Y., Ling, J., et al. (2018b). A *Meloidogyne incognita* effector MiISE5 suppresses programmed cell death to promote parasitism in host plant. *Sci. Rep.* 8, 7256. doi: 10.1038/s41598-018-24999-4

Sohn, K. H., Hughes, R. K., Piquerez, S. J., Jones, J. D. G., and Banfield, M. J. (2012). Distinct regions of the *Pseudomonas syringae* coiled-coil effector AvrRps4 are required for activation of immunity. *Proc. Natl. Acad. Sci.* 109, 16371–16376. doi: 10.1073/pnas.1212332109

Sohn, K. H., Lei, R., Nemri, A., and Jones, J. D. G. (2007). The downy mildew effector proteins ATR1 and ATR13 promote disease susceptibility in *Arabidopsis thaliana*. *Plant Cell* 19, 4077–4090. doi: 10.1105/tpc.107.054262

Sohn, K. H., Zhang, Y., and Jones, J. D. G. (2009). The *Pseudomonas syringae* effector protein, AvrRPS4, requires in planta processing and the KRVY domain to function. *Plant J.* 57, 1079–1091. doi: 10.1111/j.1365-313X.2008.03751.x

Studholme, D. J., Kemen, E., MacLean, D., Schornack, S., Aritua, V., Thwaites, R., et al. (2010). Genome-wide sequencing data reveals virulence factors implicated in banana *Xanthomonas* wilt. *FEMS Microbiol. Lett.* 310, 182–192. doi: 10.1111/j.1574-6968.2010.02065.x

Su, J., Nguyen, Q.-M., Kimble, A., Pike, S. M., Kim, S. H., and Gassmann, W. (2021). The conserved arginine required for AvrRps4 processing is also required for recognition of its N-terminal fragment in lettuce. *Mol. Plant Microbe Interact.* 34, 270–278. doi: 10.1094/MPMI-10-20-0285-R

Teper, D., Burstein, D., Salomon, D., Gershovitz, M., Pupko, T., and Sessa, G. (2015). Identification of novel *Xanthomonas euvesicatoria* type III effector proteins by a machine-learning approach. *Mol. Plant Pathol.* 17, 398–411. doi: 10.1111/mpp.12288

Trujillo, C. A., Ochoa, J. C., Mideros, M. F., Restrepo, S., López, C., and Bernal, A. (2014). A complex population structure of the cassava pathogen *Xanthomonas axonopodis* pv. *manihotis* in recent years in the Caribbean region of Colombia. *Microb. Ecol.* 68, 155–167. doi: 10.1007/s00248-014-0411-8

Upadhyaya, N. M., Mago, R., Staskawicz, B. J., Ayliffe, M. A., Ellis, J. G., and Dodds, P. N. (2014). A bacterial type III secretion assay for delivery of fungal effector proteins into wheat. *Mol. Plant Microbe Interact.* 27, 255–264. doi: 10.1094/MPMI-07-13-0187-FI

Wang, Y., Pruitt, R. N., Nürnberger, T., and Wang, Y. (2022). Evasion of plant immunity by microbial pathogens. *Nat. Rev. Microbiol.* 20, 449–464. doi: 10.1038/s41579-022-00710-3

Wang, J., Shine, M. B., Gao, Q.-M., Navarre, D., Jiang, W., Liu, C., et al. (2014). Enhanced Disease Susceptibility1 mediates pathogen resistance and virulence function of a bacterial effector in soybean. *Plant Physiol.* 165, 1269–1284. doi: 10.1104/pp.114.242495

Wang, Y., Zhang, Q., Sun, M., and Guo, D. (2011). High-accuracy prediction of bacterial type III secreted effectors based on position-specific amino acid composition profiles. *Bioinformatics* 27, 777–784. doi: 10.1093/bioinformatics/btr021

Wei, H.-L., Zhang, W., and Collmer, A. (2018). Modular study of the type III effector repertoire in *Pseudomonas syringae* pv. *tomato* DC3000 reveals a matrix of effector interplay in pathogenesis. *Cell Rep.* 23, 1630–1638. doi: 10.1016/j.celrep.2018.04.037

Wichmann, F., Vorhölter, F.-J., Hersemann, L., Widmer, F., Blom, J., Niehaus, K., et al. (2013). The noncanonical type III secretion system of *Xanthomonas translucens* pv. *graminis* is essential for forage grass infection. *Mol. Plant Pathol.* 14, 576–588. doi: 10.1111/mpp.12030

Xing, Y., Xu, N., Bhandari, D. D., Lapin, D., Sun, X., Luo, X., et al. (2021). Bacterial effector targeting of a plant iron sensor facilitates iron acquisition and pathogen colonization. *Plant Cell* 33, 2015–2031. doi: 10.1093/plcell/koab075

Zhang, N., Yang, J., Fang, A., Wang, J., Li, D., Li, Y., et al. (2020). The essential effector SCRE1 in *Ustilaginoidea virens* suppresses rice immunity via a small peptide region. *Mol. Plant Pathol.* 21, 445–459. doi: 10.1111/mpp.12894

frontiers | Frontiers in Plant Science

TYPE Original Research
PUBLISHED 16 May 2024
DOI 10.3389/fpls.2024.1387153

OPEN ACCESS

EDITED BY
Brigitte Mauch-Mani,
Université de Neuchâtel, Switzerland

REVIEWED BY
Maria Helena S. Goldman,
University of São Paulo, Brazil
Mario Serrano,
National Autonomous University of Mexico, Mexico

*CORRESPONDENCE
Carlos Priminho Pirovani
pirovani@uesc.br

RECEIVED 16 February 2024
ACCEPTED 23 April 2024
PUBLISHED 16 May 2024

CITATION
De Oliveira IB, Alves SdS, Ferreira MM, Santos AS, Farias KS, Assis ETCdM, Mora-Ocampo IY, Muñoz JJM, Costa EA, Gramacho KP and Pirovani CP (2024) Apoplastomes of contrasting cacao genotypes to witches' broom disease reveals differential accumulation of PR proteins. *Front. Plant Sci.* 15:1387153. doi: 10.3389/fpls.2024.1387153

Apoplastomes of contrasting cacao genotypes to witches' broom disease reveals differential accumulation of PR proteins

Ivina Barbosa De Oliveira[1], Saline dos Santos Alves[1], Monaliza Macêdo Ferreira[1], Ariana Silva Santos[1], Keilane Silva Farias[1], Elza Thaynara Cardoso de Menezes Assis[1], Irma Yuliana Mora-Ocampo[1], Jonathan Javier Mucherino Muñoz[1], Eduardo Almeida Costa[1], Karina Peres Gramacho[2] and Carlos Priminho Pirovani[1]*

[1]Departamento de Ciências Biológicas (DCB), Centro de Biotecnologia e Genética (CBG), Universidade Estadual de Santa Cruz (UESC), Ilhéus, Bahia, Brazil, [2]Molecular Plant Pathology Laboratory, Centro de Pesquisa do Cacau (CEPEC/CEPLAC), Ilhéus, Bahia, Brazil

Witches' broom disease (WBD) affects cocoa trees (*Theobroma cacao* L.) and is caused by the fungus *Moniliophthora perniciosa* that grows in the apoplast in its biotrophic phase and later progresses into the tissues, causing serious losses in the production of cocoa beans. Therefore, the apoplast of *T. cacao* can provide important defense responses during the interaction with *M. perniciosa*. In this work, the protein profile of the apoplast of the *T. cacao* genotypes Catongo, susceptible to WBD, and CCN-51, resistant one, was evaluated. The leaves of *T. cacao* were collected from asymptomatic plants grown in a greenhouse (GH) and from green witches' brooms grown under field (FD) conditions for extraction of apoplastic washing fluid (AWF). AWF was used in proteomic and enzymatic analysis. A total of 14 proteins were identified in Catongo GH and six in Catongo FD, with two proteins being common, one up-accumulated, and one down-accumulated. In CCN-51, 19 proteins were identified in the GH condition and 13 in FD, with seven proteins being common, one up-accumulated, and six down-accumulated. Most proteins are related to defense and stress in both genotypes, with emphasis on pathogenesis-related proteins (PR): PR-2 (β-1,3-glucanases), PR-3 and PR-4 (chitinases), PR-5 (thaumatine), PR-9 (peroxidases), and PR-14 (lipid transfer proteins). Furthermore, proteins from microorganisms were detected in the AWF. The enzymatic activities of PR-3 showed a significant increase ($p < 0.05$) in Catongo GH and PR-2 activity ($p < 0.01$) in CCN-51 FD. The protein profile of the *T. cacao* apoplastome offers insight into the defense dynamics that occur in the interaction with the fungus *M. perniciosa* and offers new insights in exploring future WBD control strategies.

KEYWORDS

apoplast, defense proteins, apoplastic washing fluid, *Theobroma cacao*, *Moniliophthora perniciosa*

1 Introduction

The species *Theobroma cacao* originated in South America (Motamayor et al., 2013). This species produces cocoa, which plays a very important role in the global economy, especially in the chocolate industry, because its beans are the main raw material for chocolate and its derivatives (Beg et al., 2017). According to reports from the International Cocoa Organization (ICCO, 2022), global cocoa bean production was approximately 5.2 million tons in 2021. The African continent stood out by contributing the largest share, 77% of the total production. In this scenario, Brazil is one of the main producers in the Americas, totaling almost 300 thousand tons in 2023 (IBGE, 2024).

Cocoa farming is threatened by one of the most serious agricultural diseases, witches' broom disease (WBD), caused by the hemibiotrophic fungus *Moniliophthora perniciosa* (Aime and Phillips-Mora, 2005; Meinhardt et al., 2008; Evans, 2016; Santos et al., 2023). WBD can cause substantial losses to cocoa farming, with particular impact on plantations in Brazil, specifically in the state of Bahia, which has been facing challenges since the arrival of the fungus in 1989 (Santos et al., 2023). During the biotrophic phase, the fungus *M. perniciosa* grows in the apoplast of *T. cacao*, which represents a key environment in the interaction between plant molecules and molecules released by *M. perniciosa* (Ceita et al., 2007; Meinhardt et al., 2008; Santos et al., 2023).

The apoplast is an essential compartment in various physiological processes and in the plant communication with the environment. Its relevance is evident because it influences important responses to environmental stresses and plays a crucial role in plant defense against pathogens (Sakurai, 1998; Agrawal et al., 2010). Communication between apoplast with the environment is fundamental for the activation of defense mechanisms, contributing to the plant ability to quickly recognize and respond to pathogenic threats, thus strengthening resistance against invasive molecules (Agrawal et al., 2010; Doehlemann and Hemetsberger, 2013).

The apoplastic protein content of the plant is modified during plant–pathogen interaction (Martínez-González et al., 2018). Many studies have aimed to understand this modulation in order to gain better knowledge of the behavior of both the pathogen, by interfering in the plant's defense, and of the plant whose normal development is impaired (Martínez-González et al., 2018; Wang and Wang, 2018; Hassett et al., 2020). The advent of omics technologies, particularly proteomics, has helped to elucidate cellular responses involved in different biological conditions (Mares et al., 2016, Mares et al., 2017, Mares et al., 2020; de Almeida et al., 2023; de Oliveira et al., 2024; Zugaib et al., 2023).

Understanding the molecular processes involved in the apoplast during a plant–pathogen interaction remains a challenge. Apoplastic proteomic studies, even with their challenges, have contributed to the understanding of molecular processes in pathogen–host interactions. Many defense proteins, such as pathogenesis-related proteins (PR proteins), have been identified in the apoplast (Floerl et al., 2008; Guerra-Guimarães et al., 2015; Li et al., 2016). Recently, the first apoplastic proteomic profile of contrasting genotypes regarding *Theobroma cacao* resistance to the WBD was reported (de Oliveira et al., 2024).

The term apoplastome described by de Oliveira et al. (2024) refers to the set of proteins identified in the apoplast of contrasting *T. cacao* genotypes regarding resistance to WBD. The proteins identified in this study are mainly involved in defensive processes of *T. cacao*, such as peroxidases, chitinases, and osmotin. Furthermore, the efficiency of the apoplastic washing fluid (AWF) from *T. cacao* genotypes in inhibiting the germination of *M. perniciosa* spores was demonstrated. The inhibition reached almost 90% for the resistant genotype (CCN-51) and 82% for the susceptible one (Catongo), as well as inducing morphological alterations in basidiospores (de Oliveira et al., 2024). These results reveal that the *T. cacao* apoplast represents a fundamental compartment in the complex defense network of plants.

Considering this, the present work aims to characterize the protein profile of the AWF obtained from asymptomatic plants grown in a greenhouse (GH) and from broom branches collected from field (FD)–grown plants with WBD, in two contrasting genotypes for WBD resistance (Catongo-susceptible and CCN-51–resistant). Our intention is to deepen the understanding of *T. cacao* defense responses, thus comprehending the role of the apoplast in the *T. cacao–M. perniciosa* interaction, to contribute to disease control efforts in the future.

2 Materials and methods

2.1 Collection of biological material and extraction of apoplastic fluid

Fully expanded mature leaves of adult *T.cacao* plants of the genotypes Catongo (susceptible to *M. perniciosa*) and CCN-51 (resistant to *M. perniciosa*) (Gramacho et al., 1992) cultivated under FD and GH conditions were collected and used to extract AWF. The collection of mature leaves on branches infected by *M. perniciosa* (green witches' broom) were carried out randomly at the Active Germplasm Bank (BAG) of CEPLAC/CEPEC in Ilhéus, Bahia, Brazil (14°45′40.2″S, 39°14′03.9″W) on plants under FD conditions. Leaves from asymptomatic plants, grown in a GH at CEPLAC/CEPEC, were also used. AWF extraction was performed by vacuum infiltration followed by centrifugation, as previously described (Pirovani et al., 2008; de Oliveira et al., 2024). A total of approximately 200 µL/g fresh weight of *T. cacao* leaf was collected. For proteomic analysis, approximately 1,200 g of leaves of the Catongo GH genotype, 715 g of Catongo FD leaves, 800 g of CCN-51 GH leaves, and 750 g of CCN-51 FD leaves were collected. For the analysis of chitinase, β-1,3-glucanase, and protease activity, three biological replicates were performed for each sample using a total of five leaves in each AWF extraction.

2.2 Protein extraction from apoplastic fluid and SDS-PAGE

The collected AWF was lyophilized in aliquots with a volume of 15 mL and used in protein extraction according to Wang et al. (2003), with modifications according to Pirovani et al. (2008). After protein recovery, the precipitate was resuspended in urea (8 mol L^{-1}) and

quantified using the 2-D Quant Kit (Cytiva), according to the manufacturer's recommendations, using BSA (bovine serum albumin) as standard.

After quantification, the proteins were resolved in SDS-PAGE (sodium dodecyl sulfate–polyacrylamide gel electrophoresis) in mini vats electrophoresis (Hoefer), with 8 cm × 10 cm gels at 12.5% acrylamide (Laemmli, 1970). A total of 30 µg of AWF protein from *T. cacao* genotypes was applied onto gels, along with 30 µg of total leaf protein extract (TE) from CCN-51 FD extracted according to Pirovani et al. (2008), to verify the protein band profiles of each sample (AWF and TE) and their differences.

2.3 Mass spectrometry and database analysis

A mass of 100 µg of AWF proteins from *T. cacao* genotype samples was treated and subjected to tryptic digestion according to Villén and Gygi (2008) with modifications described by de Almeida et al. (2023). The peptides were then analyzed in technical triplicates on a liquid chromatography system (Agilent 1290 Infinity II HPLC) coupled to a quadrupole/Time-of-Flight mass spectrometer (Agilent 6545 LC/QTOF) with C18 columns (100 mm × 100 mm) (de Almeida et al., 2023).

To analyze the spectral data generated for the identification of peptides, we used the software Spectrum Mill from the Broad Institute (Rev BI.07.08.214). Raw data files were converted to a peak list format (mgf) without summing the scans by the Mascot Distiller software v.2.6.2.0, 2009 (Matrix Science Ldt.). After extracting the mass spectrometry (MS)/MS spectra, a database search of *T. cacao* and fungi was performed. All databases were downloaded from UniProt (https://www.uniprot.org). A database of the theoretical *T. cacao* apoplastome (de Oliveira et al., 2024) was also used to identify predicted proteins for the apoplast. The research was carried out according to the following configurations: carbamidomethylation with fixed modifications, methionine oxidation with variable modification, trypsin for cleavage, and 0.1-Da tolerance for precursor and fragment ions. Statistical analyses were performed using the Mass Profiler Professional 15.1 software (MPP; Agilent), determined through analyses in which the inclusion criteria were defined as $p \leq 0.05$ and a fold change ≥ 1.5.

The identified proteins were submitted for functional annotation and categorization according to function and cellular processes using the BLAST2GO software (Conesa et al., 2005) available at the OmicsBox platform (https://www.biobam.com/blast2go/).

2.4 Comparison of methods for characterizing the *T. cacao* apoplastome

The extraction efficiency of AWF from *T. cacao* leaves for recovery of apoplastic proteins was compared and evaluated with the efficiency of total extract (TE) of *T. cacao* leaves for identification of apoplastic proteins.

Initially, proteins were recovered from the AWF of *T. cacao* leaves carried out in the present study obtained as described in the section "Protein extraction from apoplastic fluid and SDS-PAGE." Then, files containing raw peptide data from TE samples from *T. cacao* leaves carried out in previous work (de Almeida et al., 2023) were used for comparison. In terms of methodology comparison, only the CCN-51 variety was used. The raw peptide data were analyzed against the *T. cacao* database and the database of predicted proteins for the apoplast (de Oliveira et al., 2024) as per the previous section ("Mass spectrometry and database analysis"). For this analysis, differences in accumulation among the identified proteins were not taken into account. The data obtained did not need to pass statistical inclusion criteria ($p \leq 0.05$ and fold change ≥ 1.5). Verification was based on the number of proteins obtained in each sample rather than on protein abundance.

2.5 Transcript profile of predicted apoplast proteins

The transcript pattern for the predicted apoplast proteins was verified from reference files containing transcripts from *Theobroma* cacao cv. 'Comum' (Forastero). The files in FASTA format (GCA_000208745.2_Criollo_cocoa_genome_V2/and GCA_000403535.1_Theobroma_cacaoMatina) were obtained from the GenBank database (https://ftp.ncbi.nlm.nih.gov/genomes/genbank/plant/Theobroma_cacao/latest_assembly_versions/). Relative quantification was performed for the six transcripts exclusive to the Catongo genotype and 19 exclusive to CCN-51, with 14 being common, totaling 39 transcripts, which correspond to the diversity of proteins identified in the apoplast of *T. cacao* in this study. Therefore, proteins that appeared repeatedly in the samples of both Catongo and CCN-51, regardless of the growth condition, were excluded to prevent duplication. Public data were used from10 *T. Cacao* RNA-Seq libraries (Teixeira et al., 2014), available at NCBI's Sequence Read Archive (SRA) (https://www.ncbi.nlm.nih.gov/sra) under accession number SRA066232, with five libraries of the control condition and five of the *M. perniciosa*–infected condition. The relative quantification of *T. cacao* transcripts and ranking in descending order of expression was performed with the Galaxy platform (https://rna.usegalaxy.eu), using the Salmon extension (Patro et al., 2017). The corresponding proteins of each analyzed transcript were found with the BlastX search tool (https://blast.ncbi.nlm.nih.gov/).

To visualize the expression profile of the transcripts, a heatmap was plotted using the Complex Heatmap packages in the statistical software R (R Core Team, 2022).

2.6 System biology analysis

The protein–protein interaction network was created with the proteins identified in the apoplast of the Catongo and CCN-51 genotypes of *T. cacao* using the homologous sequences of *Arabidopsis thaliana* as reference. The network was built according to the STRING 11.5 database (https://string-db.org/) based on the following parameters: high level of confidence (0.7), no more than 50 interactions, and addition of nodes until network saturation.

The results obtained were analyzed using the Cytoscape software version 3.9.1 (https://cytoscape.org/) (Shannon et al., 2003). The Igraph package of the statistical tool R Studio was used to group the proteins and calculate the centrality (betweenness) and nodes (degree) parameters. To enrich genetic ontology terms and categories, the Biological Networks Gene Ontology v.3.0.3 (BiNGO) tool was used (Maere et al., 2005) with a Cytoscape plugin (https://apps.cytoscape.org/apps/bingo).

2.7 Western blot

A mass of 30 µg of AWF protein from cacao genotypes and 7 µL of molecular weight marker (Kaleidoscope, pre-stained, 0.45 µm pore, Bio-Rad, USA) were applied to SDS-PAGE in electrophoresis minivats (Hoefer), with 8 cm × 10 cm gels containing 12.5% acrylamide and run at a constant amperage of 30 mA as described by Oliveira et al. (2020). The membranes were incubated with PR-3 primary antibodies (8:20,000) for 1 h. Subsequently, the membrane was washed three times, for 15 min each wash, with 1× Tris-buffered saline (TBS-T) buffer followed by incubation with the secondary antibody (anti-rabbit Immunoglobulin G (IgG)) conjugated to alkaline phosphatase (7.5 µ:2000 of 1× TBS-T) for 2 h. After incubation, the membrane was washed again three times and finally incubated for 15 min with development buffer [$MgCl_2$, 5 mmol L^{-1}; NaCl, 100 mmol L^{-1}; Tris-HCl (pH 9.8), 100 mmol L^{-1}; and H_2O]. The development was carried out in the absence of light with Nitroblue tetrazolium/5-bromo-4-chloro-3-indolyl phosphate (NBT/BCIP) substrates for approximately 5 min. Finally, the apparent accumulation was determined from images of the nitrocellulose membrane, using the Gel Quant Net 1.8.2 program (http://biochemlabsolutions.com/GelQuantNET.html).

2.8 Enzyme activities

For enzyme activity analysis, AWF from Catongo and CCN-51 GH and FD genotypes was collected by infiltration in ice-cold distilled water as described by de Oliveira et al. (2024). A 30-µL aliquot of each sample was separated for quantification by the Bradford method (Bradford, 1976) using BSA as standard.

2.8.1 Chitinase activity

For the analysis of chitinase activity, the Chitinase Assay Kit, Fluorimetric (SIGMA-ALDRICH), was used according to the manufacturer's recommendations. The assay was based on the enzymatic hydrolysis of chitinase substrates that releases 4-methylumbelliferone (4MU). The fluorescence released in basic medium was measured at an excitation wavelength of 360 nm and an emission wavelength of 450 nm. Samples were pipetted in duplicates into 96-well microplates and analyzed on a SpectraMax Paradigm (Molecular Devices). Two substrates were used in each test: the substrate 4-methylumbelliferyl beta-D-N,N′,N″-triacetylchitotriose (for detection of endochitinase activity) and methylumbelliferyl beta-D-N,N′-dediacetylchitobioside hydrate (for detection of exochitinase activity). In each assay, chitinase from *Trichoderma viride* was used as positive control and the blank (only the substrate) as negative control. The calculation of chitinase activity was performed according to the standard curve. One unit of chitinase activity was defined as the amount of enzyme to release 1 µmol of 4-metilumbeliferona per minute.

2.8.2 β-1,3-glucanase activity

The enzymatic activity of glucanase was determined in accordance with the 3,5-dinitrosalicylic acid (DNS) method for measuring the released reducing sugar, as reported by Miller (1959). A reaction solution containing laminarin as substrate (2 mg mL^{-1}) and crude AWF samples from *T. cacao* genotypes, in a 1:1 ratio, was incubated at 40°C under shaking for 18 h. The samples were then centrifuged at 1,792 g for 5 min and the supernatant was collected. Next, 200 µL of the reaction solution and 100 µL of the DNS solution were added to new microtubes, which were vortexed and incubated in a water bath at 100°C for 5 min. Then, the reaction was stopped by cooling on ice for about 2 min. The final volume was adjusted to 1,000 µL by adding water, and, finally, the samples were pipetted in quadruplicate into 96-well microplates and analyzed in a SpectraMax Paradigm multi-mode microplate reader (Molecular Devices), with absorbance read at a wavelength of 550 nm. Controls of each sample containing laminarin, AWF sample, and DNS were also read. A glucose standard curve was plotted as a reference. One unit (U) of enzyme activity was defined as the amount of enzyme required to release 1 µmol of glucose per minute.

2.8.3 Protease activity

The AWF of *T. cacao* genotypes was suspended in non-reducing loading buffer [50% glycerol, Tris-HCl (pH 6.8), and 1% bromophenol blue], and the samples were applied to 10% SDS-PAGE (Michaud et al., 1996; Pirovani et al., 2010). After the run, the qualitative analysis of the proteases present in the samples was carried out using 0.1% gelatin gel and stained in colloidal Coomassie G-250 (0.08%) according to Neuhoff et al. (1988).

3 Results

3.1 Identification of AWF proteins from *T. cacao* genotypes

The AWF proteins were resolved on SDS-PAGE for qualitative analysis alongside the total leaf protein extract (TE) samples to confirm differential bands between AWF and TE protein samples (Supplementary Figure 1). The full identification of *T. cacao* AWF peptides was initially carried out using the general *T. cacao* database (Supplementary Figure 2). Next, the AWF peptides were also identified against the library of proteins predicted for the apoplast proposed by de Oliveira et al. (2024) considering differentially abundant proteins ($p \leq 0.05$ and a fold change ≥ 1.5) and identified exclusively in both genotypes (Figures 1, 2). For the Catongo genotype, 14 proteins were identified in the GH condition and six in the FD condition. Catongo presented 12 exclusive proteins in the GH condition and four exclusive ones in the FD condition, with two proteins in common, one up-

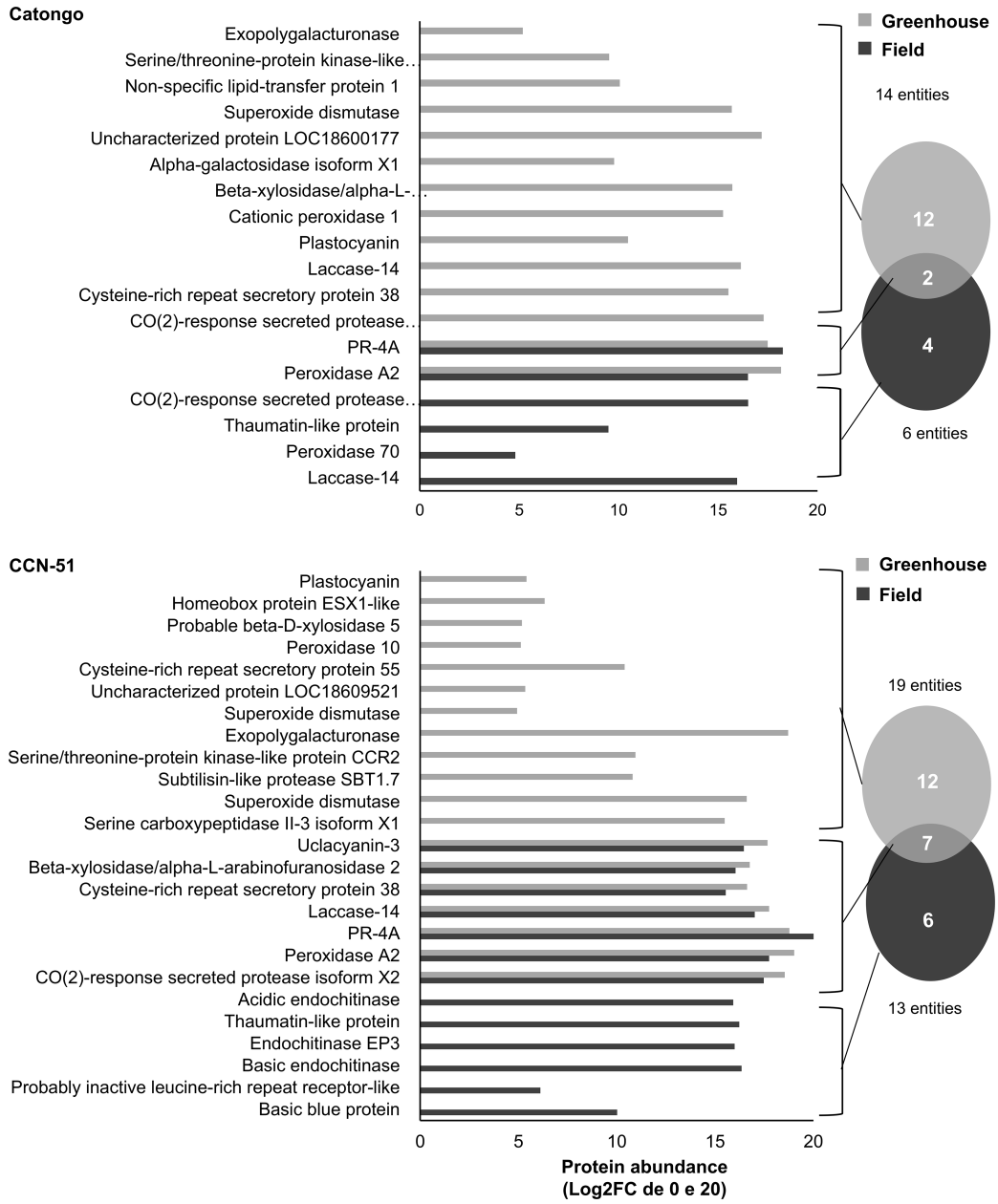

FIGURE 1
Proteins identified in the apoplastic washing fluid within *T. cacao* genotypes under different growth conditions. Unique and differentially abundant proteins ($p < 0.05$ and fold change ≥ 1.5) identified in the apoplastic fluid of the *T. cacao* Catongo (susceptible) and CCN-51 (resistant) genotypes of asymptomatic plants grown in a greenhouse and plants at the stage of green witch's broom grown in field conditions.

accumulated (PR-4), and the other down-accumulated (Peroxidase A2) (Figure 1). For the CCN-51 genotype, 19 proteins were identified in the GH condition and 13 in FD. CCN-51 GH presented 12 unique proteins and six in the FD condition. There were seven proteins in common for both conditions, with one up-accumulated (PR-4) and six down-accumulated [Peroxidase A2, CO(2)-response secreted protease isoform X2, Laccase-14, Cysteine-rich repeat secretory protein, Beta-xylosidase/alpha-L-arabinofuranosidase 2, and Uclacyanin-3] (Figure 1).

In the comparison between the two genotypes in the GH condition, 22 proteins were identified in the resistant genotype (CCN-51) and 12 proteins in the susceptible genotype (Catongo), presenting 13 exclusive proteins in CCN-51 and three exclusive in Catongo. Nine proteins were in common, all being up-accumulated for the CCN-51 genotype [CO(2)-response secreted protease isoform X2, Peroxidase A2, Cysteine-rich repeat secretory protein, Subtilisin-like protease SBT1.9, PR-4, Cationic peroxidase, Beta-xylosidase/alpha-L-arabinofuranosidase 2, Uclacyanin-3, and Superoxide dismutase (SOD)] (Figure 2). In the FD condition, 17 proteins were identified in CCN-51 and five proteins in Catongo, with 14 exclusive to the CC51 genotype and two to the Catongo genotype. Three proteins were found in common to be up-

10.3389/fpls.2024.1387153

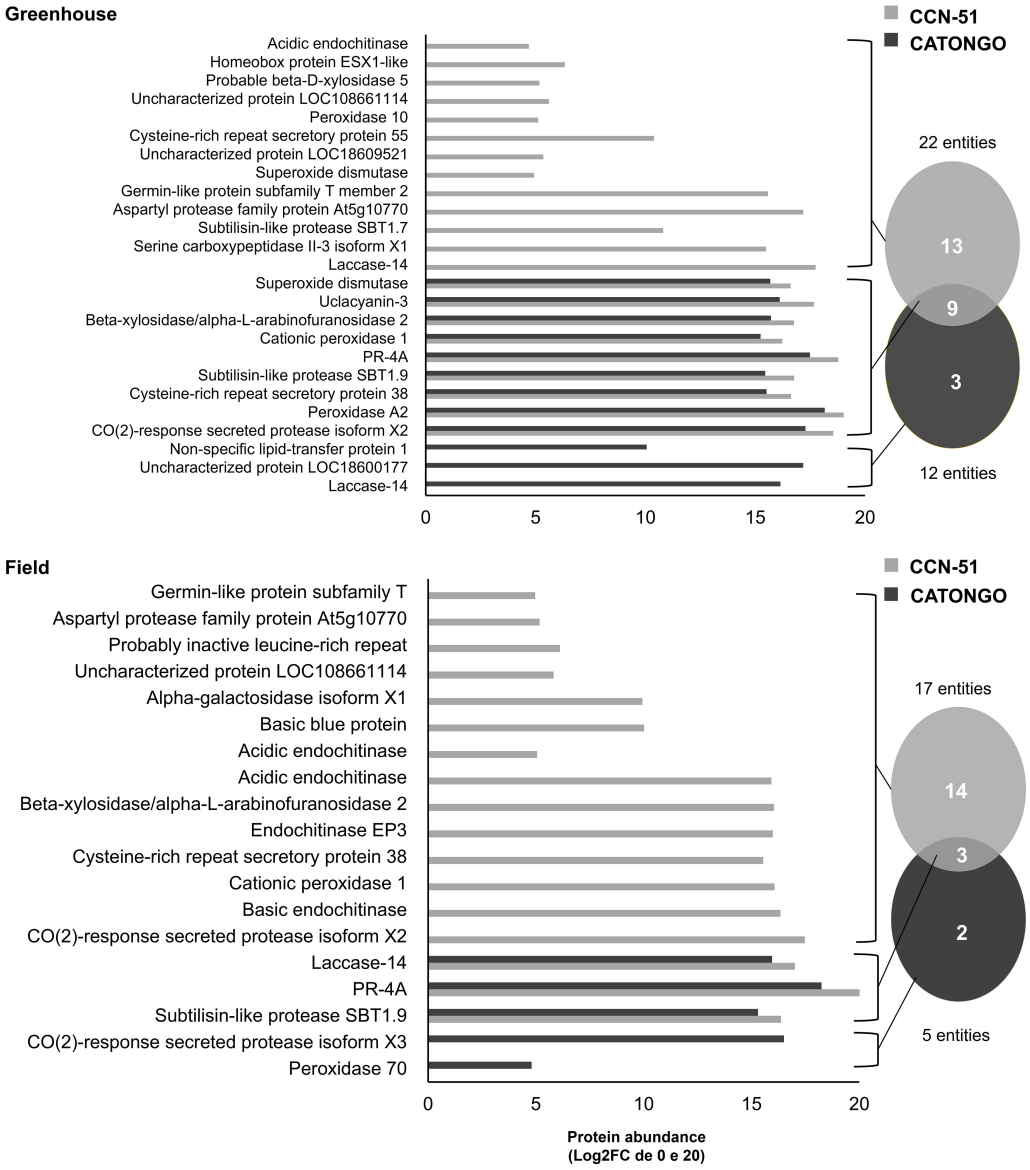

FIGURE 2
Proteins identified in the apoplastic washing fluid between *T. cacao* genotypes under different growth conditions. Unique and differentially abundant proteins ($p < 0.05$ and fold change ≥ 1.5) identified in the apoplastic fluid of the *T. cacao* Catongo (susceptible) and CCN-51 (resistant) genotypes of asymptomatic plants grown in a greenhouse and plants at the stage of green witch's broom grown in field conditions.

accumulated in the resistant genotype (Subtilisin-like protease SBT1.9, PR-4, and Laccase-14) (Figure 2).

3.2 Efficiency of AWF extraction for apoplastome characterization

Raw peptide data from AWF samples (performed in the present study) and TE samples performed in previous work (de Almeida et al., 2023) of the CCN-51 genotype were initially analyzed against the *T. cacao* database to evaluate the efficiency of the methods used in the identification of apoplastic proteins. A total of 62 proteins were identified from AWF extraction and 151 proteins from TE (Figure 3). Next, the raw peptide data were analyzed against the database of predicted proteins for the *T. cacao* apoplast (de Oliveira et al., 2024). A total of 27 proteins (44%) predicted for the apoplast through AWF extraction and 19 proteins (13%) through leaf TE sampling (Figure 3).

3.3 Transcriptional profile of proteins predicted for the apoplast of *T. cacao* genotypes

The majority transcripts were up-accumulated, such as the transcripts of the 70 peroxidase proteins identified in Catongo FD (lcl_NC_030853.1_mrna_XM_007033525.2_15125 with 89% coverage and 100% identity) and acidic proteins endochitinase and endochitinase EP3 identified in CCN-51 FD (lcl_NC

10.3389/fpls.2024.1387153

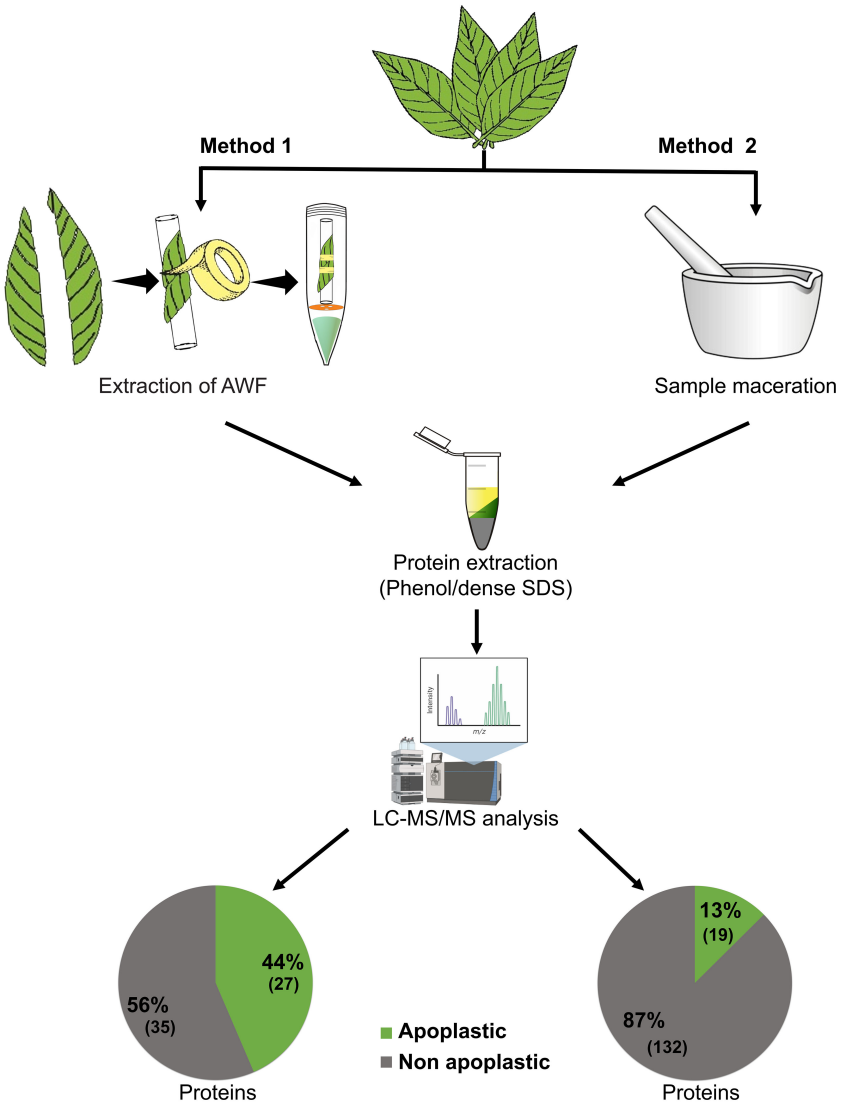

FIGURE 3
Efficiency of extracting apoplastic washing fluid from *T. cacao* leaves for characterization of the apoplastome compared to the total extract of *T. cacao* leaves. Method 1: Recovery of apoplastic proteins from the extraction of apoplastic washing fluid from leaves of the CCN-51 genotype (resistant), carried out in the present study. Method 2: Recovery of apoplastic proteins from the extraction of total extract from leaves of the CCN-51 genotype (resistant), carried out in a previous work (de Almeida et al., 2023). The raw peptide data were analyzed against the database of predicted proteins for the *T. cacao* apoplast (de Oliveira et al., 2024).

_030850.1_mrna_XM_007051131.2_3841, with 74% coverage and 100% identity and lcl_NC_030853.1_mrna_XM_007033739.2_15288 with 78% coverage and 100% identity, respectively). A protein transcript common in both genotypes, thaumatin-like protein, also showed increased accumulation (lcl_NC_030852.1_mrna_XM_007040102.2_12731 with 69% coverage and 100% identity). On the other hand, transcripts referring to SOD proteins (lcl_NC_030854.1_mrna_XM_018122149.1_19942 with 54% coverage and 100% identity) identified in CCN-51 and CO(2)-response secreted protease isoform X2 identified in both genotypes (lcl_NC_030857.1_mrna_XM_007017808.2_26401 with 82% coverage and 100% identity) had reduced accumulation (Figure 4). All proteins showed coverage above 40% and 100% identity (Supplementary Table 1).

3.4 Functional classification of *T. cacao* apoplastome proteins

According to the functional classification, most of the proteins identified from both genotypes, regardless of the plant's condition, were related to the defense and stress response and metabolic processes. For the Catongo genotype, 10 proteins (53%) were related to defense and 11 proteins (42%) were related to the CCN-51 genotype (Figure 5). A total of five proteins (26%) were involved in metabolic processes in Catongo and 10 proteins (39%) in CCN-51. Other categories were assigned in the functional classification, where one protein (4%) in the CCN-51 genotype was involved in redox processes and two (11%) proteins in the Catongo genotype.

10.3389/fpls.2024.1387153

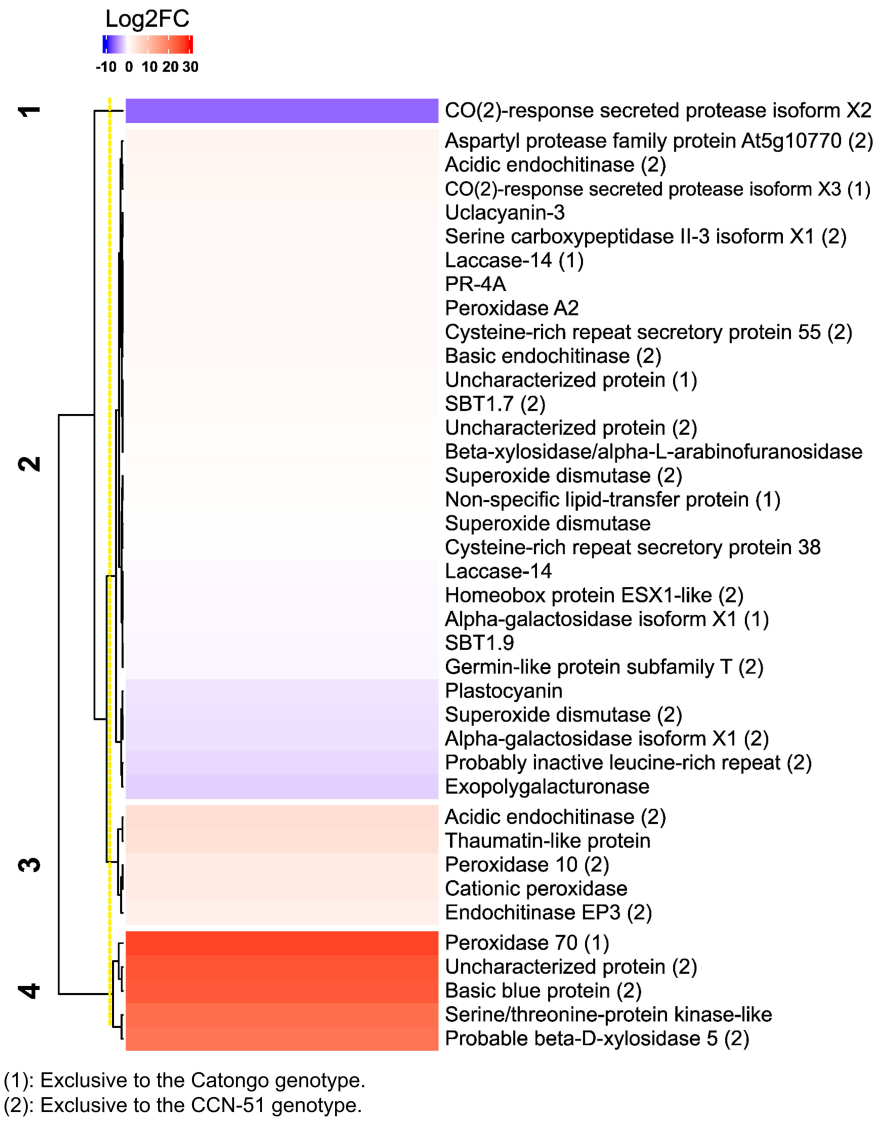

FIGURE 4
Transcriptional profile of apoplastic washing fluid proteins from *T. cacao* genotypes. Heatmap based on Pearson's correlation coefficient, representing the differential accumulation of transcripts corresponding to apoplastic proteins of *T. cacao* genotypes in the database of Teixeira et al. (2014) (SRA066232). In blue, transcripts with reduced accumulation; in red, transcripts with relative increase in accumulation, related to the Log2FC scales of –10 and 30, respectively. The full name of the protein is described in Supplementary Table 1.

3.5 Interaction network of *T. cacao* apoplastome proteins

The protein interaction network of the Catongo genotype samples (GH and FD) showed 722 nodes, which corresponded to each specific protein, and 5,718 connectors, which corresponded to physical or functional interactions between proteins. The CCN-51 genotype (GH and FD) resulted in 941 nodes and 7,251 connectors. The larger nodes correspond to proteins found within the network (Figure 6). Of the total of 20 orthologous protein sequences in the Catongo sample, 14 were found in the network. In CCN-51, out of 35 sequences, 23 were located within the network.

Based on the gene ontology for biological processes, 16 functional clusters for the Catongo genotype and 12 for the CCN-51 genotype were predicted. (Figure 6). According to the network analysis of the Catongo samples, the proteins predicted for cluster 1 stood out for being involved in the carbohydrate metabolic process. In cluster 1, there were 200 proteins, five of which were orthologous: Hevein-like preproprotein (PR4) and Osmotin-like (OSM34) that were up-accumulated and Alpha-galactosidase 2 (AGAL2) and Beta-D-xylosidase 4 (XYL4) down-accumulated. In cluster 2, the predicted proteins were involved in the steroid biosynthetic process, containing 117 proteins, two of which were orthologous, one peroxidase and one kinase (PRX52, up-accumulated, and AT3G22060, down-accumulated, respectively). Cluster 3 contained 119 proteins that may be involved in the generation of precursor metabolites and energy, with emphasis on the superoxide dismutase (CSD1) protein. In addition, cluster 4 contained 71 proteins possibly involved in ribosome biogenesis, with the only up-accumulated laccase (LAC14) orthologous protein (Figure 6).

10.3389/fpls.2024.1387153

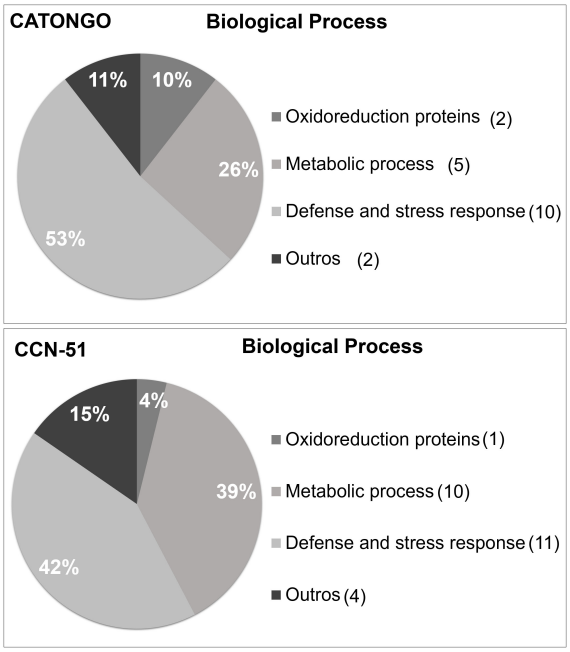

FIGURE 5
Functional annotation of proteins identified in apoplastic washing fluid from *T. cacao* genotypes. Characterization by biological processes of proteins identified in the apoplastic washing fluid of the *T. cacao* Catongo (susceptible) and CCN-51 (resistant) genotypes of asymptomatic plants grown in a greenhouse and plants at the stage of green witch's broom grown in field conditions.

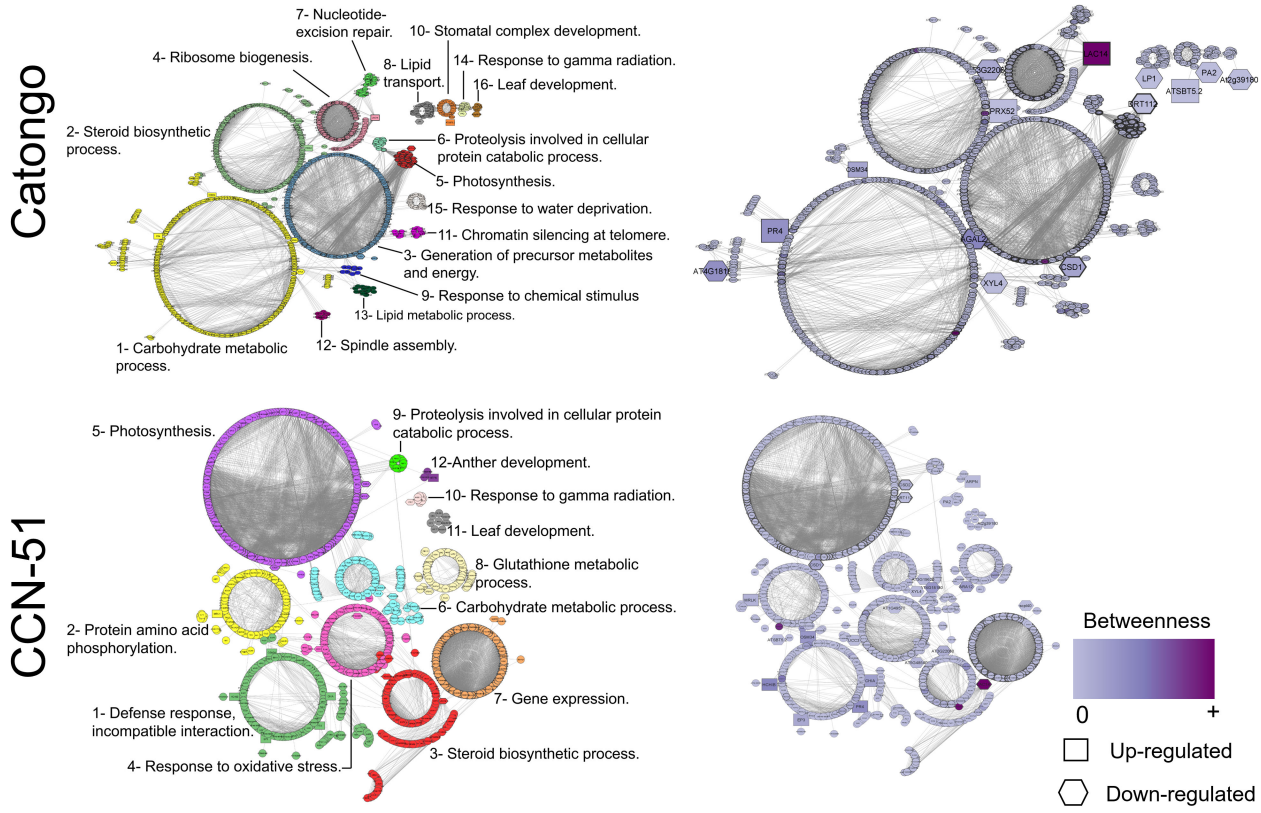

FIGURE 6
Protein–protein interaction network. Interaction network of apoplastic washing fluid proteins of the *T. cacao* Catongo (susceptible) and CCN-51 (resistant) genotypes according to homology with *Arabidopsis thaliana*. Each cluster is represented by a different color. The purple color scale represents the betweenness of a node and the thickness of each node represents the degree centrality. Interactions were generated and visualized in software STRING 10.5 and reconstructed by Cytoscape software.

The main clusters resulting from proteins of the CCN-51 genotype were cluster 1, where the proteins were involved in the incompatible interaction defense response. With 141 proteins, five of which were orthologous and were up-accumulated, the proteins basic endochitinase (HCHIB), osmotin (OSM34), chitinases (EP3 and CHIA), and hevein-like preproprotein (PR4). Cluster 3 with 130 proteins involved in the steroid biosynthetic process, having three orthologous proteins with reduced accumulation, the laccase proteins (LAC14) and two kinases (AT3G22060 and AT5G48540). Cluster 4 proteins may be involved in the response to oxidative stress, where it contains 89 proteins, two of which are up-accumulated orthologs, the uclacyanin protein (UCC3), and peroxidase (AT1G49570) (Figure 6).

The Laccase protein (LAC14), identified in both genotypes, presented a higher betweenness value (Figure 6), indicating a high interaction with other proteins (Nithya et al., 2023). The superoxide dismutase protein (CSD1) identified in both genotypes in the GH condition presented degree values above the average (Figure 6), being considered a protein that has an important regulatory role within the network (Nithya et al., 2023).

3.6 Chitinase immunodetection

The accumulation of chitinase (PR-3) identified in the apoplast of *T. cacao* genotypes was visualized by Western blot (Supplementary Figure 3; Figure 7). The presence of PR-3 was mainly detected in samples from plants of both genotypes under FD conditions (green witches' broom stage) in both genotypes, with an increase of approximately 15 times in relation to samples in GH condition (asymptomatic grown in a GH) (Figure 7).

3.7 Enzymatic activity of chitinase, β-1,3-glucanase, and proteases in AWF of *T. cacao*

Chitinase activity maintained similar behavior for both substrates in all samples, with higher activity detected in Catongo GH and lower activity in Catongo FD. A statistically significant difference ($p < 0.05$) was observed between these samples when evaluated with the substrate for endochitinase detection. Catongo GH showed activity approximately two times greater than Catongo FD (Figure 8).

The activity of the enzyme β-1,3-glucanase was higher in CCN-51 FD compared to the other samples. Activity was significantly ($p < 0.01$) higher in CCN-51 FD, both compared to the GH condition and the Catongo FD sample (Figure 9).

To evaluate protease activity in the crude AWF extract of *T. cacao* genotypes, zymography was performed on a polyacrylamide gel. The gel image (Figure 10) shows clear regions (highlighted with white outlines) where the proteases present in AWF have degraded the substrates used in the packaging gel, confirming their activity and location in the gel. The clear and continuous regions throughout the gel can be noted mainly above 30 kDa.

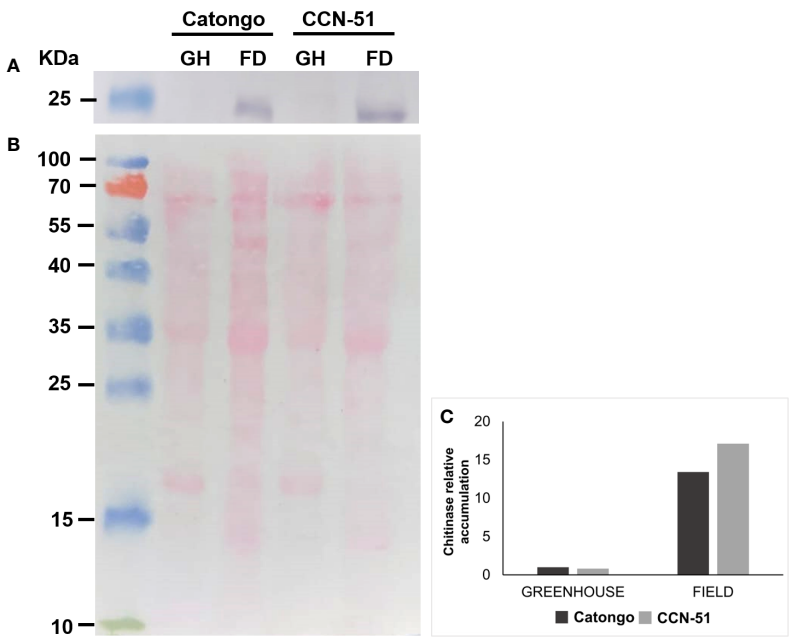

FIGURE 7
Immunodetection of PR-3 in apoplastic washing fluid from T. cacao genotypes. Western blot using an antibody against PR-3 in a protein sample from apoplastic washing fluid of T. cacao genotypes Catongo (susceptible) and CCN-51 (resistant) from asymptomatic plants grown in a greenhouse (GH) and of green witches' broom stage plants grown under field (FD) conditions. **(A)** Protein accumulation in samples of apoplastic washing fluid from T. cacao genotypes. **(B)** Mirror gel. **(C)** Protein accumulation in T. cacao genotypes estimated by the Gel Quant Net 1.7.8 program. kDa, molecular weight.

10.3389/fpls.2024.1387153

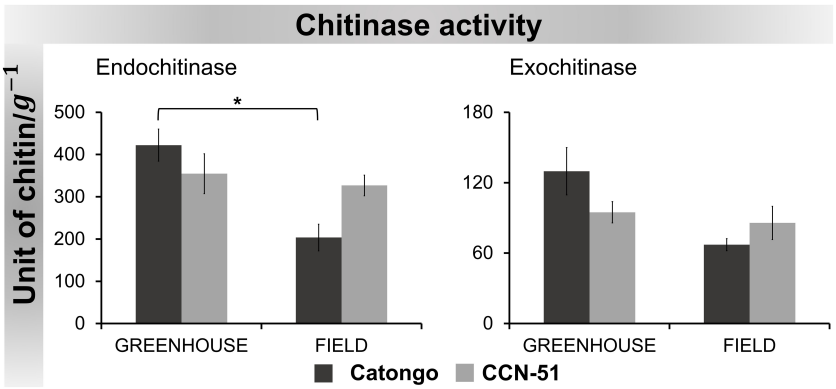

FIGURE 8
Chitinase activity in apoplastic washing fluid from *T. cacao* genotypes. The points represent the means of the triplicates of the analyses of each variety. * Significance of $p < 0.05$ by ANOVA followed by comparison using the Tukey test ($p < 0.01$ and $p < 0.05$). Bars correspond to standard errors of the means.

3.8 Microorganism proteins in the AWF of *T. cacao*

Microorganism proteins were identified in the AWF of the Catongo and CCN-51 genotypes of *T. cacao*. Most of the proteins belong to the fungus *M. perniciosa*. Twenty-three proteins were identified in the Catongo and CCN-51 FD genotypes, with eight proteins being exclusive to the susceptible genotype (Catongo) and 10 being exclusive to the resistant genotype (CCN-51). Five *M. perniciosa* proteins were common to both genotypes (Tables 1, 2).

Interestingly, in Catongo GH, proteins from the filamentous fungus *M. perniciosa* were found, as well as from the fungi *Lasiodiplodia theobromae* and *Ashbya gossypi* and the yeast *Schizosaccharomyces pombe*. In the CCN-51 GH genotype, a protein from *M. perniciosa* was also found, in addition to proteins from *Candida glabrata*, *Yarrowia lipolytica*, *A. gossypi* and *Saccharomyces cerevisiae*. In Catongo FD, proteins from *M. perniciosa*, *L. theobromae*, *A. gossypi*, *S. pombe*, and *Debaryomyces hansenii* were found. Proteins from *M. perniciosa*, *L. theobromae*, *A. gossypi*, *S. pombe*, as well as *Aspergillus nidulans* and *S. cerevisiae* were also found in CCN-51 FD (Tables 1, 2).

4 Discussion

4.1 The AWF extraction step improves the identification of proteins secreted in *T. cacao* leaves

Obtaining a good yield of apoplast proteins, which can be soluble in AWF or linked to the cell wall, is still a challenge, due to the difficulties of avoiding disruption of the cell wall and membrane. As a result, they are still poorly characterized (Delaunois et al., 2014).

The technique for obtaining apoplastic proteins, which initially involves the extraction of AWF, demonstrated a high protein yield in samples of *T. cacao* leaves, despite presenting cytoplasmic contamination of 56% (Figure 3). The number of apoplastic proteins identified (27) was greater from AWF extraction compared to obtaining apoplastic proteins from TE (19). For the recovery of apoplastic proteins from the TE of *T. cacao* leaves (Figure 3), cytoplasmic contamination of 87% was observed, corresponding to 132 proteins out of a total of 151, due to the leaf maceration process.

The total number of proteins recovered is reduced using the optimized AWF extraction technique from *T. cacao* leaves (62 proteins), compared to the number of proteins in the TE sample (151 proteins). However, it is important to highlight that the concentration of proteins in the apoplast is lower compared to those present in the internal space of the cells (Delaunois et al., 2014), additionally obtaining AWF also reduces cytoplasmic contamination compared to TE samples. The centrifugal force used in AWF extraction is essential to reduce this contamination, and the centrifugation-infiltration method that was used in this

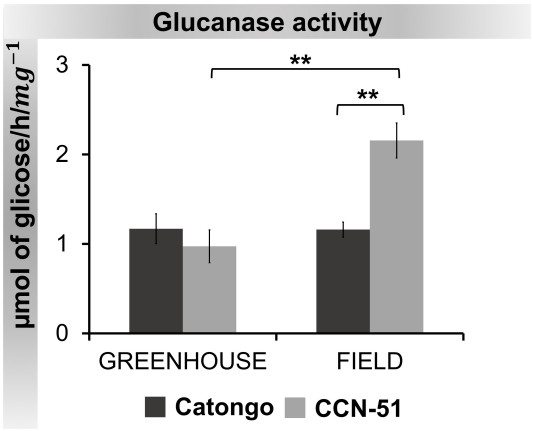

FIGURE 9
β-1,3-Glucanase activity in apoplastic washing fluid from *T. cacao* genotypes. The points represent the means of the triplicates of the analyzes of each variety. ** Significance of $p < 0,01$ by ANOVA followed by comparison using the Tukey test ($p < 0.01$ and $p < 0.05$). Bars correspond to standard errors of the means.

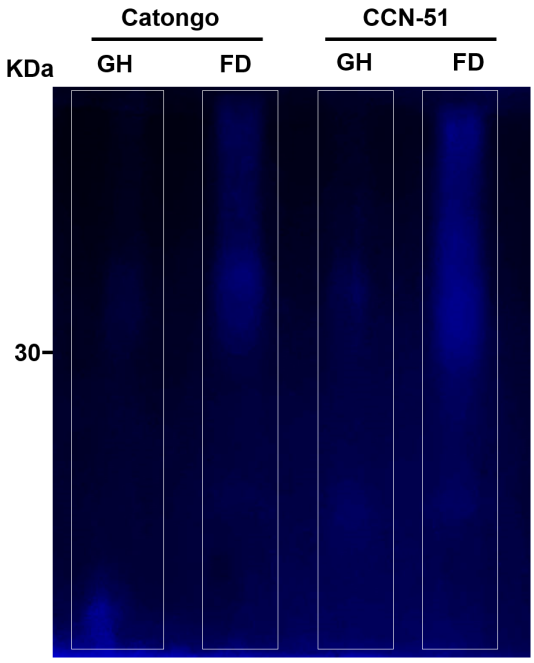

FIGURE 10
Proteases activity in apoplastic washing fluid from *T. cacao* genotypes. Zymogram with protease activity in apoplastic washing fluid of *T. cacao* of the Catongo (susceptible) and CCN-51 (resistant) genotypes of asymptomatic plants grown in a greenhouse (GH) and plants at the green witch's broom stage grown under conditions of field (FD). kDa, Molecular weight.

work has already been adopted in several works (Soares et al., 2007; Delannoy et al., 2008; Pirovani et al., 2008; Pechanova et al., 2010; de Oliveira et al., 2024), being adapted for each species and enabling better investigation within the area of subcellular proteomics.

4.2 The apoplast is rich in defense and stress proteins

Most of the proteins identified in the AWF of *T. cacao* genotypes are related to defense and stress, with emphasis on pathogenesis-related proteins (PR-proteins).

PR-proteins make up an important class of proteins that play a crucial role in the plant defense response against pathogens. The production of these proteins is increased when the plant is under stress, and they perform several functions, ranging from directly inhibiting the growth of pathogens to strengthening the plant's defenses (Sels et al., 2008; Sudisha et al., 2012; dos Santos and Franco, 2023).

Currently, 19 families of PRs have been described (dos Santos and Franco, 2023), among which we identified representatives of the families PR-3, PR-4, PR-5, PR-9, and PR-14. Based on the analysis of cacao transcripts using public data carried out in a previous work (Teixeira et al., 2014), some transcripts belonging to apoplastic PR-proteins were up-accumulated in infected plants compared to healthy *T. cacao* (Forastero) plants used by Teixeira et al. (2014), as members of PR-3, PR-4, PR-5, PR-9, and PR-14

TABLE 1 Proteins from microorganisms identified in apoplastic washing fluid of the Catongo GH and FD genotype.

	Accession	Species	Protein ID	Protein_MW (Da)	Protein_pI
Catongo GH					
1	A0A5N5CX20	*Lasiodiplodia theobromae*	Elongation factor 1-alpha	50,346	9.39
2	E2LT56	*Moniliophthora perniciosa*	Ribose-phosphate diphosphokinase	25,506.1	6.08
3	E2LP61	*Moniliophthora perniciosa*	ArgoN domain-containing protein (fragment)	17,483.8	8.8
4	Q756G2.2	*Ashbya gossypii*	RecName: Full=Probable E3 ubiquitin-protein ligase TOM1	374,219.9	4.99
5	Q9UT10.1	*Schizosaccharomyces pombe*	RecName: Full=Uncharacterized GTP-binding protein P8A3.05	78,337	9.19
Catongo FD					
1	E2LZF6	*Moniliophthora perniciosa*	Rhizoctonia solani AG1-IB WGS project CAOJ00000000 data, isolate 7/3/14, contig (fragment)	31,159.7	8.8
2	E2L970	*Moniliophthora perniciosa*	Protein kinase domain-containing protein (fragment)	26,816.9	5.82
3	E2LKI3	*Moniliophthora perniciosa*	Peroxisomal membrane protein 11B	23,070.2	10.08
4	E2LMQ4	*Moniliophthora perniciosa*	CAC1F_C domain-containing protein (fragment)	30,372.4	6.17

(Continued)

10.3389/fpls.2024.1387153

TABLE 1 Continued

	Accession	Species	Protein ID	Protein_MW (Da)	Protein_pI
Catongo FD					
5	E2LWM7	*Moniliophthora perniciosa*	Gluconate transport inducer 1/Pac2 (fragment)	32,475.9	9.28
6	E2LLF1	*Moniliophthora perniciosa*	NAD(P)-binding protein (fragment)	15,120.1	5.12
7	E2L833	*Moniliophthora perniciosa*	DUF2428 domain-containing protein (fragment)	17,704.9	7.04
8	E2M402	*Moniliophthora perniciosa*	Btz domain-containing protein (fragment)	19,962.6	3.88
9	E2LQ59	*Moniliophthora perniciosa*	DUF4238 domain-containing protein (fragment)	39,094.1	6.11
10	E2LGU4	*Moniliophthora perniciosa*	PFK domain-containing protein (fragment)	20,282.8	8.23
11	E2LD68	*Moniliophthora perniciosa*	fn3_5 domain-containing protein	37,933.7	4.43
12	E2L3A9	*Moniliophthora perniciosa*	Peptidase A2 domain-containing protein (fragment)	21,452.5	9.36
13	E2LQ59	*Moniliophthora perniciosa*	DUF4238 domain-containing protein (fragment)	39,094.1	6.11
14	A0A5N5DBM4	*Lasiodiplodia theobromae*	Protein transport protein SEC13	33,030.2	5.86
15	Q756G2.2	*Ashbya gossypii*	RecName: Full=Probable E3 ubiquitin-protein ligase TOM1	374,219.9	4.99
16	O74465.2	*Schizosaccharomyces pombe*	RecName: Full=Helicase required for RNAi-mediated heterochromatin assembly 1	115,136.9	6.12
17	O74762.1	*Schizosaccharomyces pombe*	RecName: Full=26S proteasome regulatory subunit rpn2	107,730.9	4.93
18	A0A0S6XHH0.1	*Fungal* sp	RecName: Full=FR901469 synthetase	1,721,677.5	5.3
19	Q6BKW6.2	*Debaryomyces hansenii*	RecName: Full=Protoheme IX farnesyltransferase, mitochondrial	51,651.1	9.91

TABLE 2 Proteins from microorganisms identified in apoplastic washing fluid of the CCN-51 GH and FD genotypes.

	Accession	Species	Protein ID	Protein_MW (Da)	Protein_pI
CCN-51 GH					
1	Q6FPW3.1	*Candida glabrata*	RecName: Full=Glyceraldehyde-3-phosphate dehydrogenase 1	36,089.3	5.25
2	E2LT56	*Moniliophthora perniciosa*	Ribose-phosphate diphosphokinase	25,506.1	6.08
3	Q6FM42.1	*Candida glabrata*	RecName: Full=Peroxisomal targeting signal receptor	66,872.2	4.88
4	Q6CG48.1	*Yarrowia lipolytica*	RecName: Full=Nuclear distribution protein PAC1	48,693.1	7.37
5	Q756G2.2	*Ashbya gossypii*	RecName: Full=Probable E3 ubiquitin-protein ligase TOM1	374,219.9	4.99
6	P15442.3	*Saccharomyces cerevisiae*	RecName: Full=eIF-2-alpha kinase GCN2	190,589.3	5.98
CCN-51 FD					
1	E2LVC0	*Moniliophthora perniciosa*	Aminotran_1_2 domain-containing protein (fragment)	44,596.5	4.89

(Continued)

10.3389/fpls.2024.1387153

TABLE 2 Continued

	Accession	Species	Protein ID	Protein_MW (Da)	Protein_pI
CCN-51 FD					
2	E2L970	*Moniliophthora perniciosa*	Protein kinase domain-containing protein (fragment)	26,816.9	5.82
3	E2LZF6	*Moniliophthora perniciosa*	Rhizoctonia solani AG1-IB WGS project CAOJ00000000 data, isolate 7/3/14, contig (fragment)	31,159.7	8.8
4	E2L603	*Moniliophthora perniciosa*	G_PROTEIN_RECEP_F1_2 domain-containing protein (fragment)	20,709	9.66
5	E2LMQ4	*Moniliophthora perniciosa*	CAC1F_C domain-containing protein (fragment)	30,372.4	6.17
6	E2LXQ7	*Moniliophthora perniciosa*	Cytochrome P450	35,812.5	9.77
7	E2LWM7	*Moniliophthora perniciosa*	Gluconate transport inducer 1/Pac2 (fragment)	32,475.9	9.28
8	E2LEU9	*Moniliophthora perniciosa*	40S ribosomal protein S17 (fragment)	23,822.1	9.83
9	E2LMX7	*Moniliophthora perniciosa*	Translation elongation factor 1-alpha	33,561.9	9.32
10	E2LCF0	*Moniliophthora perniciosa*	Kinase	13,470.3	6.83
11	E2LFU0	*Moniliophthora perniciosa*	FYR N-terminal domain-containing protein	22,653.3	7.94
12	E2LD68	*Moniliophthora perniciosa*	fn3_5 domain-containing protein	37,933.7	4.43
13	E2LGJ7	*Moniliophthora perniciosa*	FGGY_C domain-containing protein	28,311.4	6.19
14	E2L9L1	*Moniliophthora perniciosa*	Cyclin-domain-containing protein	12,219.8	8.08
15	E2LEA8	*Moniliophthora perniciosa*	DUF3475 domain-containing protein	18,919.1	5.49
16	A0A5N5DN88	*Lasiodiplodia theobromae*	Uncharacterized protein	52,449.6	5.56
17	Q756G2.2	*Ashbya gossypii*	RecName: Full=Probable E3 ubiquitin-protein ligase TOM1	374,219.9	4.99
18	P47155.1	*Saccharomyces cerevisiae*	RecName: Full=Protein ILM1	23,758.4	4.35
19	P07754.1	*Aspergillus nidulans*	RecName: Full=Alcohol dehydrogenase 3	37,524.8	6.62
20	Q9USW2.1	*Schizosaccharomyces pombe*	RecName: Full=Inheritance of peroxisomes protein 2	55,425.6	8.39

(Figure 4). This corroborates findings in the present work, due to the importance that PR-proteins have in host defense.

Proteins from the PR-3 family (chitinases) were detected only in the resistant genotype (CCN-51), with most representatives showing a greater accumulation in green brooms (FD) (Figure 1). Recently, chitinases (EC 3.2.1.14) were identified in the AWF of *T. cacao* only in the FD-grown CCN-51 genotype (de Oliveira et al., 2024). This corroborates the data revealed on PR-3 accumulation in CCN-51 FD (Figure 7). Although not identified by proteomic analysis, the protein was also accumulated in the Catongo GH and FD genotypes (susceptible) and verified by Western blot (Figure 7). A previous study demonstrated that the Catongo genotype contained a greater amount of upregulated defense and stress-related proteins, such as an acid chitinase isoform, at 45 days after inoculation with *M. perniciosa*, compared to the downregulated proteins (dos Santos et al., 2020). The genotype of *T. cacao* resistant to WBD (TSH1188) showed upregulated chitinase isoforms 42 h after inoculation and 45 days after inoculation with *M. perniciosa* (dos Santos et al., 2020).

Chitinases play an effective role in breaking down chitin, an essential component in the constitution of the fungal cell wall. One of the main functions of chitinases in plants is associated with the defense response against pathogenic fungi, but they can also have

antibacterial and antiviral actions (dos Santos and Franco, 2023). In the *T. cacao* apoplast of the CCN-51 genotype (resistant), chitinases were identified, represented in cluster 1 and are involved in the defense response (Figure 6). According to the network of interactions, these proteins have a high betweenness value and can be considered bottleneck proteins. Bottleneck proteins play an important role in the regulation and control of metabolic pathways and/or cell signaling and are, therefore, essential in the communication and integration of different parts of the network (Nithya et al., 2023).

Chitinases are important in cell signaling, due to their chitinolytic activity and the formation of oligosaccharides, which act as elicitor molecules that are recognized by the host plant, favoring a cascade of signals (Kaur et al., 2022; dos Santos and Franco, 2023). Extracellular chitinases can have direct antimicrobial action by the degradation of invading hyphae (Stangarlin and Pascholati, 2000) and can be acidic or basic (Vaghela et al., 2022).

PR-4 was identified in both *T. cacao* genotypes, being up-accumulated in the FD condition (green witch's broom stage) (Figure 1). When comparing protein accumulation between genotypes under the same condition, PR-4 was up-accumulated in the CCN-51 FD (resistant) genotype and down-accumulated in Catongo FD (susceptible) (Figure 2). PR-4 can act directly on the pathogen's cell wall due to its ability to bind to chitin and may present chitinolytic activity (Ali et al., 2018; Butassi et al., 2022). Recently, this protein showed increased abundance in the apoplast of peach plants inoculated with the fungus *Taphrina deformans* (Butassi et al., 2022). The antifungal activity of PR-4 was proven in wheat against fungi of the genus *Fusarium* (Caruso et al., 1996), in transgenic grapevines in response to powdery mildew disease (Dai et al., 2016) and in response to abiotic stress in rice (Wang et al., 2011).

The PR-4 protein identified in Catongo is represented in cluster 1, involved in the carbohydrate metabolic process. In the CCN-51 genotype, it is represented in cluster 1 and has a high betweenness value and can be considered a bottleneck protein (Figure 6).

Thaumatin-like protein (PR-5) was detected in the Catongo (susceptible) and CCN-51 (resistant) genotypes exclusively in the FD condition (Figure 1). The PR-5 protein is recognized for its role in plants' defense response against a variety of pathogens. It can accumulate in the apoplast or vacuole and act directly as an antifungal agent, inhibiting the growth and spread of invasive fungi (Stintzi et al., 1993; de Jesús-Pires et al., 2020; Manghwar and Hussain, 2021). Previous studies have demonstrated that the PR-5 protein delayed the disease caused by *Phytophthora infestans* in potato (Liu et al., 1994). In garlic, PR-5 genes are involved in defense against *Fusarium* infection (Anisimova et al., 2021). Silencing of a *PR-5* gene in the wheat apoplast leads to compromised resistance against the pathogen *Puccinia triticina* (Zhang et al., 2018). Recently, an osmotin (PR-5) was identified in the apoplast of the WBD-resistant genotype of *T. cacao* (de Oliveira et al., 2024). The Catongo thaumatin-like protein is represented in cluster 1, being involved in the carbohydrate metabolic process (Figure 6). In CCN-51, it is involved in the defense response (cluster 1) representing a bottleneck protein within the network (Figure 6). Accordingly, it is suggested that this protein plays a crucial role in immune responses in *T. cacao*, contributing to the reinforcement and tentative resistance of *T. cacao* to pathogenic threats.

Peroxidases (PR-9) were detected in both genotypes under both growth conditions. Peroxidase 70 was exclusively detected in Catongo FD, peroxidase A2 was up-accumulated in Catongo and CCN-51 GH, and peroxidase 10 was exclusively detected in CCN-51 GH. The expression of two peroxidases was increased in the apoplast of barley infected by the pathogen *Pyrenophora teres* f. *teres* (Hassett et al., 2020). This protein plays an important role against pathogens in the initial stages of infection, acting as an antioxidant enzyme, and also actively participates in cell wall synthesis and remodeling (Hiraga et al., 2001; dos Santos and Franco, 2023). In CCN-51, peroxidase 10 is represented in cluster 4 (Figure 6), related to the response to oxidative stress. According to the findings in the present work, the production of peroxidases may be induced in infected FD genotypes. Because some PR-proteins can be produced constitutively (van Loon et al., 2006), it is likely that this is occurring in GH genotypes. Therefore, in normal situations, plants may express peroxidases to manage natural ROS production.

The PR-14 protein (nsLTPs) was detected exclusively in the Catongo GH genotype. PR-14 facilitates the transfer of lipids and has antifungal and antibacterial activity, by acting on the permeability of the fungal/bacterial membrane (Van Loon and Van Strien, 1999; Hoffmann-Sommergruber, 2002; Gorjanović et al., 2005; Patkar and Chattoo, 2006). This protein was represented in cluster 8, involved in lipid transport (Figure 6), but the exact biological role remains to be determined.

4.3 Down-accumulated proteins in the apoplastome in *T. cacao* genotypes suggest sequestration of defense pathways in FD genotypes by *M. perniciosa*

Asymptomatic *T. cacao* plants grown in the GH had a greater number of proteins identified in the apoplastome, both in comparison within and between genotypes in relation to green witches' broom plants grown in the FD. This may be related to the modulation of the defense system (Nishad et al., 2020). It can be inferred that the defense system of FD plants was previously turned off due to more dynamic interactions with the environment and that *M. perniciosa* infection favors the reduction of prolonged defense.

In a previous work, it was proven that 45 days after inoculation with *M. perniciosa* in the Catongo (susceptible) and TSH1188 (resistant to WBD) genotypes, the accumulation of proteins related to stress and defense is reduced in Catongo, whereas, in TSH1188, it was significantly increased (dos Santos et al., 2020). The period of onset and development of WBD in the FD plants used in the present work is unknown. However, presumably more than 45 days had already passed since the onset of the disease, which may explain the reduction in protein accumulation in the genotypes of infected plants (FD).

A cysteine-rich secretory protein showed increased accumulation in the Catongo (susceptible) and CCN-51 (resistant) GH genotypes but decreased in CCN-51 FD and was not detected in Catongo FD. The cysteine-rich repeat protein is apoplastic and plays a fundamental role in plant defense against phytopathogens. A

cysteine-rich repeat protein from wheat was proven to be effective against the phytopathogens *Rhizoctonia cerealis* and *Bipolaris sorokiniana*, through its proven antifungal activity in inhibiting mycelium growth, as well as regulating the expression of pathogenesis-related genes such as of β-1,3-glucanase and chitinases (Guo et al., 2020). A cotton cysteine-rich repeat protein acted on the stability of a chitinase, protecting it from cleavage by *Verticillium dahliae* protease. Overexpression of the protein increased resistance against the cotton fungal phytopathogen (Han et al., 2019). The Catongo cysteine-rich secretory protein is represented in cluster 2 and in CCN-51 in cluster 3, being involved in the steroid biosynthetic process in both genotypes (Figure 6). It is likely that this protein acts in the production of important compounds in the stress response of *T. cacao*. The reduced accumulation of cysteine-rich repeat protein in *T. cacao* FD (green witch broom stage) genotypes may have been mediated by the strong inhibitory activity of the fungus *M. perniciosa*, unlike what occurred in *T. cacao* GH (asymptomatic grown in a GH) genotypes.

The protein SOD was detected in both genotypes only in the GH condition. SOD plays a fundamental role in antioxidant defense in plants due to the increase in reactive oxygen species (ROS) (Mase and Tsukagoshi, 2021). SOD acts as the first line of defense against oxygen free radicals in less toxic forms, such as hydrogen peroxide (H_2O_2) and oxygen (O_2), reducing oxidative damage (Qi et al., 2017; Wang et al., 2018). The main type of SOD found in the apoplast is copper-zinc (Cu-Zn SOD) (Alscher et al., 2002). The SOD protein identified in Catongo (susceptible) GH is represented in cluster 3 and may be involved in the generation of precursor metabolites and energy (Figure 6). This protein is classified according to the biological network as a "hub" protein, where it plays an important role in the transmission of signals, the integration of metabolic pathways, and the regulation of biological processes (Nithya et al., 2023).

Increased SOD accumulation may be associated with increased ROS, especially in response to biotic stress (Jwa and Hwang, 2017; Wang et al., 2018). The decrease in SOD in FD genotypes (green witch broom stage) in the present work may be an effect of the plant's response to infection, where manipulation of antioxidant defenses may be a strategy used by the pathogen *M. perniciosa* to facilitate disease progression. Therefore, the fungus possibly interferes with the defense mechanisms of *T. cacao*, reducing the effectiveness of antioxidant enzymes such as SOD, which could result in greater oxidative damage and benefit the pathogen in the plant.

4.4 The activity of enzymes occurring in the *T. cacao* apoplast

Some PR-proteins that have enzymatic action, such as PR-3 and PR-2, were evaluated in the present study.

The chitinases evaluated, although they demonstrated a similar pattern of activity in all samples, exhibited higher endochitinase activity compared to the exochitinase activity (Figure 8). Plant chitinases are generally endochitinases with a molecular weight of 25 kDa to 36 kDa (Hoffmann-Sommergruber, 2002; Hamid et al., 2013; Vaghela et al., 2022) and are active in plant self-defense in response to phytopathogen attack (Vaghela et al., 2022).

For endochitinase (EC 3.2.1.14) activity, a statistically significant difference was observed between samples of the susceptible genotype (Catongo GH and FD) (Figure 8). The activity in the Catongo GH genotype was significantly higher than in the FD sample. Although proteomic data did not reveal the accumulation of chitinase in Catongo GH, it was possible to measure its ability to catalyze reactions in this genotype. The use of crude AWF extract with proteins in the native state may have favored its dosage in GH samples (asymptomatic plants grown in a GH).

When evaluating PR-2 activity, we observed statistically significant increases between CCN-51 FD and GH and between CCN-51 FD and Catongo FD, approximately twice as high (Figure 9). Increased PR-2 activity after infection was reported in rice infected by *Magnaporthe oryzae* (Wang et al., 2021), in chickpea AWF infected by *Ascochyta rabiei* (Hanselle and Barz, 2001), and in resistant cultivars of wheat infected by *Diuraphis noxia* (Van Der Westhuizen et al., 1998).

PR-2 (EC 3.2.1.39) has beta-1,3-glucanase activity, an enzyme that breaks beta-1,3-glucan bonds, an important component in the cell wall of many fungi (Hoffmann-Sommergruber, 2002). Therefore, beta-1,3-glucanases play a crucial role in the defense response of plants against fungal pathogens, because the breakdown of beta-1,3-glucan compromises the integrity of the fungal cell wall (Balasubramanian et al., 2012; dos Santos and Franco, 2023). This can lead to the death of the fungus or at least weaken its ability to invade and colonize plant tissue.

The apoplastic AWF of *T. cacao* genotypes also revealed a high protease activity through the zymogram gel (Figure 10), confirming the activity of proteases, such as the subtilases identified in the present work: protease secreted by CO_2 response and similar proteases to subtilisin (XP_017981649.1, XP_007017870.2, XP_007018543.2 and XP_007017195.2). Subtilases are very numerous in plants and can be directed to the cell wall and contribute to wall modification, cell signaling, and response to biotic and abiotic stress (Figueiredo et al., 2014; Schaller et al., 2018). A subtilase gene in cotton is involved in the plant's defense against the pathogen *Verticillium dahliae* (Duan et al., 2016). The identification of subtilases in AWF has already been reported in coffee leaves (Guerra-Guimarães et al., 2015), *Arabidopsis thaliana* leaves (Jiang et al., 2023) and leaves of the Catongo and CCN-51 genotypes of *T. cacao* (de Oliveira et al., 2024). The transcript belonging to two protein isoforms were up-accumulated (lcl_NC_030857.1_mrna_XM_018126160.1_26400 and lcl_NC_030857.1_mrna_XM_007018481.2_26945) (Figure 4). The activity of these proteases in the *T. cacao* apoplast, together with others identified and shown in Figures 1, 2, may be important in the infection process by modulating the plant's defense responses.

4.5 Peptides from microorganisms are detected in the apoplast of *T. cacao* genotypes

A total of 40 proteins from microorganisms were identified in the AWF of *T. cacao* genotypes, 23 of which belonged to the fungus *M. perniciosa* present in the FD genotype samples (plants in the green

witch's broom stage) (Tables 1, 2). Some functions of these proteins are associated with biosynthetic processes, protein transport, and proteolysis. The FD genotypes were under a high level of stress, evident with the branches at the green witch's broom stage used in AWF extraction, and, in this context, it was predicted that the fungus *M. perniciosa* would secrete molecules in the *T. cacao* apoplast in order to interfere with the plant defense (Fiorin et al., 2018).

It is known that the microbial community can exert a symbiotic relationship with plants, resulting from coevolution between species (Pathak et al., 2022). This relationship is possible because their genomes were shaped to survive together, so they stand out for having characteristics that prevent the recognition of microorganisms by the plants' immune systems (Khare et al., 2018; Pathak et al., 2022).

A protein belonging to an unidentified fungal species (ID: A0A0S6XHH0.1) was found in the Catongo GH sample (Table 1). This protein's beta-1,3-glucan inhibitory activity has already been established by *in vitro* and *in vivo* studies, showing antifungal activity against the fungi *Candida albicans* and *Aspergillus fumigatus* (Fujie et al., 2000a, Fujie et al., 2000b). We suggest that the fungus has a beneficial relationship in Catongo against possible invaders. Additional studies are essential for a more thorough understanding of its action.

In a previous work, the diversity of endophytic fungi in *T. cacao* (Rubini et al., 2005) was proven, including the fungus *Lasiodiplodia theobromae*. This corroborates our data from this study, where peptides from *L. theobromae* were identified. Interestingly, *L. theobromae* peptides were detected in both GH and FD plants. *L. theobromae* is a pathogenic necrotrophic fungus important to several crops, including *T. cacao* (Pereira et al., 2006; de Oliveira et al., 2013). Under controlled conditions, the first symptoms can be visible within 2 weeks after inoculation, such as wilting and death within 10 days (Moreira-Morrillo et al., 2021). Because the GH genotypes (asymptomatic plants grown in a GH) had no visible symptoms of any of the fungi mentioned, it is necessary to perform more comprehensive investigations, using other methods, in order to more precisely elucidate the identification of these peptides and/or functions in the plant, such as metagenome sequencing.

Yeast peptides were also found in both genotypes. Endophytic yeasts have been associated with several plant species: *Saccharomyces cerevisiae*, considered endophytic of *Ficus carica* (Ling et al., 2020); and *Debaryomyces hansenii*, endophytic of wheat (Wachowska et al., 2018) and rice (Tantirungkij et al., 2015), all identified in the apoplast of *T. cacao*. Although endophytes may play a role in increasing growth, acquiring nutrients and strengthening tolerance to stress in plants (Ling et al., 2020), additional studies are needed. Such studies would offer a more comprehensive understanding of the possible symbiotic relationship between these microorganisms and *T. cacao*, clarifying the benefits for the host plant.

5 Conclusion

In this study, we report the dynamics and differences of the apoplast proteome between Catongo (WBD-susceptible) and CCN-51 (WBD-resistant) *T. cacao* genotypes, asymptomatic, and infected by the destructive *pathogen M. perniciosa*. Proteins detected in the apoplast are related to the plant's defense response; in addition to the enzymatic profile of chitinases, β-1,3-glucanases, and proteases present in AWF, we demonstrate the great importance of the *T. cacao* apoplast during the plant–pathogen interaction. A possible modulation and suppression of the *T. cacao* defense system promoted by *M. perniciosa* can be suggested, based on the protein profile of the FD genotypes with a significant number of down-accumulated defense proteins. A symbiotic relationship between microorganisms and *T. cacao* has been proposed; however, more in-depth studies should be carried out with the addition of different methodologies to confirm endophytes and their possible benefits for *T. cacao*. The *T. cacao* apoplast reveals important responses in the molecular battle *against M. perniciosa* and the crucial phase of the infection, biotrophic, can be understood in the light of the apoplastome. Target proteins identified here can be functionally explored in future studies with biotechnological applications in order to control WBD.

Data availability statement

The datasets presented in this study can be found in online repositories. The names of the repository/repositories and accession number(s) can be found in the article/Supplementary Material.

Author contributions

IdO: Data curation, Formal analysis, Investigation, Methodology, Writing – original draft. SA: Investigation, Methodology, Writing – original draft. MF: Conceptualization, Investigation, Methodology, Software, Writing – original draft. AS: Data curation, Software, Writing – original draft. KF: Investigation, Methodology, Writing – original draft. EA: Formal analysis, Investigation, Methodology, Writing – original draft. IM-O: Conceptualization, Methodology, Software, Writing – original draft. JM: Software, Writing – original draft. EC: Software, Writing – original draft. KG: Investigation, Methodology, Supervision, Writing – original draft. CP: Conceptualization, Funding acquisition, Project administration, Resources, Supervision, Visualization, Writing – original draft.

Funding

The author(s) declare financial support was received for the research, authorship, and/or publication of this article. This work was supported by Coordenação de Aperfeiçoamento de Pessoal de Nıível Superior (CAPES) (0001), Conselho Nacional de Desenvolvimento Cientıífico e Tecnoloígico (CNPq—Processes 303765/2019-4 and 421787/2021-0), and Financier of Studies and Projects (Process 01.18.0087.00/2018).

Acknowledgments

We are grateful for the financial support granted by Coordenação de Aperfeiçoamento de Pessoal de Nível Superior (CAPES) and Financiadora de Estudos e Projetos (FINEP).

Conflict of interest

The authors declare that the research was conducted in the absence of any commercial or financial relationships that could be construed as a potential conflict of interest.

Publisher's note

Supplementary material

The Supplementary Material for this article can be found online at: https://www.frontiersin.org/articles/10.3389/fpls.2024.1387153/full#supplementary-material

References

Agrawal, G. K., Jwa, N.-S., Lebrun, M.-H., Job, D., and Rakwal, R. (2010). Plant secretome: Unlocking secrets of the secreted proteins. *Proteomics* 10, 799–827. doi: 10.1002/pmic.200900514

Aime, M. C., and Phillips-Mora, W. (2005). The causal agents of witches' broom and frosty pod rot of cacao (chocolate, Theobroma cacao) form a new lineage of Marasmiaceae. *Mycologia* 97, 1012–1022. doi: 10.3852/mycologia.97.5.1012

Ali, S., Ganai, B. A., Kamili, A. N., Bhat, A. A., Mir, Z. A., Bhat, J. A., et al. (2018). Pathogenesis-related proteins and peptides as promising tools for engineering plants with multiple stress tolerance. *Microbiol. Res.* 212–213, 29–37. doi: 10.1016/j.micres.2018.04.008

Alscher, R. G., Erturk, N., and Heath, L. S. (2002). Role of superoxide dismutases (SODs) in controlling oxidative stress in plants. *J. Exp. Bot.* 53, 1331–1341. doi: 10.1093/jexbot/53.372.1331

Anisimova, O. K., Shchennikova, A. V., Kochieva, E. Z., and Filyushin, M. A. (2021). Pathogenesis-related genes of PR1, PR2, PR4, and PR5 families are involved in the response to fusarium infection in garlic (Allium sativum L.). *Int. J. Mol. Sci.* 22, 6688. doi: 10.3390/ijms22136688

Balasubramanian, V., Vashisht, D., Cletus, J., and Sakthivel, N. (2012). Plant β-1,3-glucanases: their biological functions and transgenic expression against phytopathogenic fungi. *Biotechnol. Lett.* 34, 1983–1990. doi: 10.1007/s10529-012-1012-6

Beg, M. S., Ahmad, S., Jan, K., and Bashir, K. (2017). Status, supply chain and processing of cocoa - A review. *Trends Food Sci. Technol.* 66, 108–116. doi: 10.1016/j.tifs.2017.06.007

Bradford, M. M. (1976). A rapid and sensitive method for the quantitation of microgram quantities of protein utilizing the principle of protein-dye binding. *Anal. Biochem.* 72, 248–254. doi: 10.1016/0003-2697(76)90527-3

Butassi, E., Novello, M. A., and Lara, M. V. (2022). Prunus persica apoplastic proteome analysis reveals candidate proteins involved in the resistance and defense against Taphrina deformans. *J. Plant Physiol.* 276, 153780. doi: 10.1016/j.jplph.2022.153780

Caruso, C., Caporale, C., Chilosi, G., Vacca, F., Bertini, L., Magro, P., et al. (1996). Structural and antifungal properties of a pathogenesis-related protein from wheat kernel. *J. Protein Chem.* 15, 35–44. doi: 10.1007/BF01886809

Ceita, G., de, O., Macêdo, J. N. A., Santos, T. B., Alemanno, L., da Silva Gesteira, A., et al. (2007). Involvement of calcium oxalate degradation during programmed cell death in Theobroma cacao tissues triggered by the hemibiotrophic fungus Moniliophthora perniciosa. *Plant Sci.* 173, 106–117. doi: 10.1016/j.plantsci.2007.04.006

Conesa, A., Götz, S., García-Gómez, J. M., Terol, J., Talón, M., and Robles, M. (2005). Blast2GO: a universal tool for annotation, visualization and analysis in functional genomics research. *Bioinformatics* 21, 3674–3676. doi: 10.1093/bioinformatics/bti610

Dai, L., Wang, D., Xie, X., Zhang, C., Wang, X., Xu, Y., et al. (2016). The Novel Gene VpPR4-1 from Vitis pseudoreticulata Increases Powdery Mildew Resistance in Transgenic Vitis vinifera L. *Front. Plant Sci.* 7. doi: 10.3389/fpls.2016.00695

de Almeida, N. M., de Almeida, A.-A. F., de Almeida Santos, N., Mora-Ocampo, I. Y., and Pirovani, C. P. (2023). Leaf proteomic profiles in cacao scion-rootstock combinations tolerant and intolerant to cadmium toxicity. *Plant Physiol. Biochem.* 203, 107987. doi: 10.1016/j.plaphy.2023.107987

de Jesús-Pires, C., Ferreira-Neto, J. R. C., Pacifico Bezerra-Neto, J., Kido, E. A., de Oliveira Silva, R. L., Pandolfi, V., et al. (2020). Plant thaumatin-like proteins: Function, evolution and biotechnological applications. *Curr. Protein Pept. Sci.* 21, 36–51. doi: 10.2174/1389203720666190318164905

Delannoy, M., Alves, G., Vertommen, D., Ma, J., Boutry, M., and Navarre, C. (2008). Identification of peptidases in Nicotiana tabacum leaf intercellular fluid. *Proteomics* 8, 2285–2298. doi: 10.1002/pmic.200700507

Delaunois, B., Jeandet, P., Clément, C., Baillieul, F., Dorey, S., and Cordelier, S. (2014). Uncovering plant-pathogen crosstalk through apoplastic proteomic studies. *Front. Plant Sci.* 5. doi: 10.3389/fpls.2014.00249

de Oliveira, M. Z. A., Júnior, P. P., de Barbosa, C. J., and Assmar, C. C. (2013) *Fungo Lasiodiplodia theobromae: um problema para agricultura baiana*. Available online at: https://www.embrapa.br/busca-de-publicacoes/-/publicacao/962191/fungo-lasiodiplodia-theobromae-um-problema-para-agricultura-baiana (Accessed January 13, 2024).

de Oliveira, I. B., Moura, I. M., Santana, J. O., Gramacho, K. P., Alves, S., dos, S., et al. (2024). Cocoa apoplastome contains defense proteins against pathogens. *Phytopathology®* 114 (2), 427–440. doi: 10.1094/PHYTO-03-23-0101-R

Doehlemann, G., and Hemetsberger, C. (2013). Apoplastic immunity and its suppression by filamentous plant pathogens. *New Phytol.* 198, 1001–1016. doi: 10.1111/nph.12277

dos Santos, C., and Franco, O. L. (2023). Pathogenesis-related proteins (PRs) with enzyme activity activating plant defense responses. *Plants* 12, 2226. doi: 10.3390/plants12112226

dos Santos, E. C., Pirovani, C. P., Correa, S. C., Micheli, F., and Gramacho, K. P. (2020). The pathogen Moniliophthora perniciosa promotes differential proteomic modulation of cacao genotypes with contrasting resistance to witches´ broom disease. *BMC Plant Biol.* 20, 1. doi: 10.1186/s12870-019-2170-7

Duan, X., Zhang, Z., Wang, J., and Zuo, K. (2016). Characterization of a novel cotton subtilase gene gbSBT1 in response to extracellular stimulations and its role in verticillium resistance. *PLoS One* 11, e0153988. doi: 10.1371/journal.pone.0153988

Evans, H. C. (2016). "Witches' Broom disease (Moniliophthora perniciosa): history and biology," in *Cacao Diseases*. Eds. B. A. Bailey and L. W. Meinhardt (Springer International Publishing, Cham), 137–177. doi: 10.1007/978-3-319-24789-2_5

Figueiredo, A., Monteiro, F., and Sebastiana, M. (2014). Subtilisin-like proteases in plant–pathogen recognition and immune priming: a perspective. *Front. Plant Sci.* 5. doi: 10.3389/fpls.2014.00739

Fiorin, G. L., Sanchéz-Vallet, A., Thomazella, D. P., de, T., do Prado, P. F. V., do Nascimento, L. C., et al. (2018). Suppression of plant immunity by fungal chitinase-like effectors. *Curr. Biol.* 28, 3023–3030.e5. doi: 10.1016/j.cub.2018.07.055

Floerl, S., Druebert, C., Majcherczyk, A., Karlovsky, P., Kües, U., and Polle, A. (2008). Defence reactions in the apoplastic proteome of oilseed rape (Brassica napus var. napus) attenuate Verticillium longisporum growth but not disease symptoms. *BMC Plant Biol.* 8, 129. doi: 10.1186/1471-2229-8-129

Fujie, A., Iwamoto, T., Muramatsu, H., Okudaira, T., Nitta, K., Nakanishi, T., et al. (2000a). FR901469, a novel antifungal antibiotic from an unidentified fungus No.11243. I. Taxonomy, fermentation, isolation, physico-chemical properties and biological properties. *J. Antibiot (Tokyo)* 53, 912–919. doi: 10.7164/antibiotics.53.912

Fujie, A., Iwamoto, T., Muramatsu, H., Okudaira, T., Sato, I., Furuta, T., et al. (2000b). FR901469, a novel antifungal antibiotic from an unidentified fungus No.11243. II. *In vitro* and *in vivo* activities. *J. Antibiot (Tokyo)* 53, 920–927. doi: 10.7164/antibiotics.53.920

Gorjanović, S., Spillner, E., Beljanski, M. V., Gorjanović, R., Pavlović, M., and Gojgić-Cvijanović, G. (2005). Malting barley grain non-specific lipid-transfer protein (ns-LTP): Importance for grain protection. *J. Institute Brewing* 111, 99–104. doi: 10.1002/jib.2005.111.issue-2

Gramacho, I. C. P., Magno, A. E. S., Mandarino, E. P., and Matos, A. (1992). *Cultivo e Beneficiamento do Cacau na Bahia.* (Ilhéus: CEPLAC/CEDEX).

Guerra-Guimarães, L., Tenente, R., Pinheiro, C., Chaves, I., Silva, M., do, C., et al. (2015). Proteomic analysis of apoplastic fluid of Coffea arabica leaves highlights novel biomarkers for resistance against Hemileia vastatrix. *Front. Plant Sci.* 6. doi: 10.3389/fpls.2015.00478

Guo, F., Shan, Z., Yu, J., Xu, G., and Zhang, Z. (2020). The Cysteine-Rich Repeat Protein TaCRR1 Participates in Defense against Both Rhizoctonia cerealis and Bipolaris sorokiniana in Wheat. *Int. J. Mol. Sci.* 21, 5698. doi: 10.3390/ijms21165698

Hamid, R., Khan, M. A., Ahmad, M., Ahmad, M. M., Abdin, M. Z., Musarrat, J., et al. (2013). Chitinases: an update. *J. Pharm. Bioallied Sci.* 5, 21–29. doi: 10.4103/0975-7406.106559

Han, L.-B., Li, Y.-B., Wang, F.-X., Wang, W.-Y., Liu, J., Wu, J.-H., et al. (2019). The Cotton Apoplastic Protein CRR1 Stabilizes Chitinase 28 to Facilitate Defense against the Fungal Pathogen Verticillium dahliae. *Plant Cell* 31, 520–536. doi: 10.1105/tpc.18.00390

Hanselle, T., and Barz, W. (2001). Purification and characterisation of the extracellular PR-2b β-1,3-glucanase accumulating in different Ascochyta rabiei-infected chickpea (Cicer arietinum L.) cultivars. *Plant Sci.* 161, 773–781. doi: 10.1016/S0168-9452(01)00468-X

Hassett, K., Ellwood, S. R., Zulak, K. G., and Muria-Gonzalez, M. J. (2020). Analysis of apoplastic proteins expressed during net form net blotch of barley. *J. Plant Dis. Prot* 127, 683–694. doi: 10.1007/s41348-020-00318-w

Hiraga, S., Sasaki, K., Ito, H., Ohashi, Y., and Matsui, H. (2001). A large family of class III plant peroxidases. *Plant Cell Physiol.* 42, 462–468. doi: 10.1093/pcp/pce061

Hoffmann-Sommergruber, K. (2002). Pathogenesis-related (PR)-proteins identified as allergens. *Biochem. Soc. Trans.* 30, 930–935. doi: 10.1042/bst0300930

IBGE. (2024). *Instituto Brasileiro de Geografia e Estatística*. Available at: https://sidra.ibge.gov.br/tabela/1618 (Accessed February 14, 2024).

ICCO (2022) *International Cocoa Organization - Statistics* (International Cocoa Organization). Available online at: https://www.icco.org/statistics/ (Accessed January 23, 2023).

Jiang, S., Pan, L., Zhou, Q., Xu, W., He, F., Zhang, L., et al. (2023). Analysis of the apoplast fluid proteome during the induction of systemic acquired resistance in Arabidopsis thaliana. *PeerJ* 11, e16324. doi: 10.7717/peerj.16324

Jwa, N.-S., and Hwang, B. K. (2017). Convergent evolution of pathogen effectors toward reactive oxygen species signaling networks in plants. *Front. Plant Sci.* 8. doi: 10.3389/fpls.2017.01687

Kaur, S., Samota, M. K., Choudhary, M., Choudhary, M., Pandey, A. K., Sharma, A., et al. (2022). How do plants defend themselves against pathogens-Biochemical mechanisms and genetic interventions. *Physiol. Mol. Biol. Plants* 28, 485–504. doi: 10.1007/s12298-022-01146-y

Khare, E., Mishra, J., and Arora, N. K. (2018). Multifaceted interactions between endophytes and plant: Developments and prospects. *Front. Microbiol.* 9. doi: 10.3389/fmicb.2018.02732

Laemmli, U. K. (1970). Cleavage of structural proteins during the assembly of the head of bacteriophage T4. *Nature* 227, 680–685. doi: 10.1038/227680a0

Li, Y.-B., Han, L.-B., Wang, H.-Y., Zhang, J., Sun, S.-T., Feng, D.-Q., et al. (2016). The thioredoxin gbNRX1 plays a crucial role in homeostasis of apoplastic reactive oxygen species in response to verticillium dahliae infection in cotton. *Plant Physiol.* 170, 2392–2406. doi: 10.1104/pp.15.01930

Ling, L., Tu, Y., Ma, W., Feng, S., Yang, C., Zhao, Y., et al. (2020). A potentially important resource: endophytic yeasts. *World J. Microbiol. Biotechnol.* 36, 110. doi: 10.1007/s11274-020-02889-0

Liu, D., Raghothama, K. G., Hasegawa, P. M., and Bressan, R. A. (1994). Osmotin overexpression in potato delays development of disease symptoms. *Proc. Natl. Acad. Sci. U.S.A.* 91, 1888–1892. doi: 10.1073/pnas.91.5.1888

Maere, S., Heymans, K., and Kuiper, M. (2005). BiNGO: a Cytoscape plugin to assess overrepresentation of gene ontology categories in biological networks. *Bioinformatics* 21, 3448–3449. doi: 10.1093/bioinformatics/bti551

Manghwar, H., and Hussain, A. (2021). Mechanism of tobacco osmotin gene in plant responses to biotic and abiotic stress tolerance: A brief history. *biocell* 46, 623–632. doi: 10.32604/biocell.2022.017316

Mares, J. H., Gramacho, K. P., dos Santos, E. C., da Silva Santiago, A., de Andrade Silva, E. M., Alvim, F. C., et al. (2016). Protein profile and protein interaction network of Moniliophthora perniciosa basidiospores. *BMC Microbiol.* 16, 120. doi: 10.1186/s12866-016-0753-0

Mares, J. H., Gramacho, K. P., Santana, J. O., Oliveira de Souza, A., Alvim, F. C., and Pirovani, C. P. (2020). Hydrosoluble phylloplane components of Theobroma cacao modulate the metabolism of Moniliophthora perniciosa spores during germination. *Fungal Biol.* 124, 73–81. doi: 10.1016/j.funbio.2019.11.008

Mares, J. H., Gramacho, K. P., Santos, E. C., da Silva Santiago, A., Santana, J. O., de Sousa, A. O., et al. (2017). Proteomic analysis during of spore germination of Moniliophthora perniciosa, the causal agent of witches' broom disease in cacao. *BMC Microbiol.* 17, 176. doi: 10.1186/s12866-017-1085-4

Martínez-González, A. P., Ardila, H. D., Martínez-Peralta, S. T., Melgarejo-Muñoz, L. M., Castillejo-Sánchez, M. A., and Jorrín-Novo, J. V. (2018). What proteomic analysis of the apoplast tells us about plant–pathogen interactions. *Plant Pathol.* 67, 1647–1668. doi: 10.1111/ppa.12893

Mase, K., and Tsukagoshi, H. (2021). Reactive oxygen species link gene regulatory networks during arabidopsis root development. *Front. Plant Sci.* 12. doi: 10.3389/fpls.2021.660274

Meinhardt, L. W., Rincones, J., Bailey, B. A., Aime, M. C., Griffith, G. W., Zhang, D., et al. (2008). Moniliophthora perniciosa, the causal agent of witches' broom disease of cacao: what's new from this old foe? *Mol. Plant Pathol.* 9, 577–588. doi: 10.1111/j.1364-3703.2008.00496.x

Michaud, D., Cantin, L., Raworth, D. A., and Vrain, T. C. (1996). Assessing the stability of cystatin/cysteine proteinase complexes using mildly-denaturing gelatin-polyacrylamide gel electrophoresis. *Electrophoresis* 17, 74–79. doi: 10.1002/elps.1150170113

Miller, G. L. (1959). Use of dinitrosalicylic acid reagent for determination of reducing sugar. *Anal. Chem.* 31, 426–428. doi: 10.1021/ac60147a030

Moreira-Morrillo, A. A., Cedeño-Moreira, Á.V., Canchignia-Martínez, F., Garcés-Fiallos, F. R., Moreira-Morrillo, A. A., Cedeño-Moreira, Á.V., et al. (2021). Lasiodiplodia theobromae (Pat.) Griffon & Maul [(sin.) Botryodiplodia theobromae Pat] en el cultivo de cacao: síntomas, ciclo biológico y estrategias de manejo. *Scientia Agropecuaria* 12, 653–662. doi: 10.17268/sci.agropecu.2021.068

Motamayor, J. C., Mockaitis, K., Schmutz, J., Haiminen, N., Livingstone, D., Cornejo, O., et al. (2013). The genome sequence of the most widely cultivated cacao type and its use to identify candidate genes regulating pod color. *Genome Biol.* 14, r53. doi: 10.1186/gb-2013-14-6-r53

Neuhoff, V., Arold, N., Taube, D., and Ehrhardt, W. (1988). Improved staining of proteins in polyacrylamide gels including isoelectric focusing gels with clear background at nanogram sensitivity using Coomassie Brilliant Blue G-250 and R-250. *Electrophoresis* 9, 255–262. doi: 10.1002/elps.1150090603

Nishad, R., Ahmed, T., Rahman, V. J., and Kareem, A. (2020). Modulation of plant defense system in response to microbial interactions. *Front. Microbiol.* 11. doi: 10.3389/fmicb.2020.01298

Nithya, C., Kiran, M., and Nagarajaram, H. A. (2023). Dissection of hubs and bottlenecks in a protein-protein interaction network. *Comput. Biol. Chem.* 102, 107802. doi: 10.1016/j.compbiolchem.2022.107802

Oliveira, B. R. M., de Almeida, A.-A. F., Pirovani, C. P., Barroso, J. P., de C Neto, C. H., Santos, N. A., et al. (2020). Mitigation of Cd toxicity by Mn in young plants of cacao, evaluated by the proteomic profiles of leaves and roots. *Ecotoxicology* 29, 340–358. doi: 10.1007/s10646-020-02178-4

Pathak, P., Rai, V. K., Can, H., Singh, S. K., Kumar, D., Bhardwaj, N., et al. (2022). Plant-endophyte interaction during biotic stress management. *Plants* 11, 2203. doi: 10.3390/plants11172203

Patkar, R. N., and Chattoo, B. B. (2006). Transgenic indica Rice Expressing ns-LTP-Like Protein Shows Enhanced Resistance to Both Fungal and Bacterial Pathogens. *Mol. Breed.* 17, 159–171. doi: 10.1007/s11032-005-4736-3

Patro, R., Duggal, G., Love, M. I., Irizarry, R. A., and Kingsford, C. (2017). Salmon provides fast and bias-aware quantification of transcript expression. *Nat. Methods* 14, 417–419. doi: 10.1038/nmeth.4197

Pechanova, O., Hsu, C.-Y., Adams, J. P., Pechan, T., Vandervelde, L., Drnevich, J., et al. (2010). Apoplast proteome reveals that extracellular matrix contributes to multistress response in poplar. *BMC Genomics* 11, 674. doi: 10.1186/1471-2164-11-674

Pereira, A. L., Silva, G. S., and Ribeiro, V. Q. (2006). Caracterização fisiológica, cultural e patogênica de diferentes isolados de Lasiodiplodia theobromae. *Fitopatol. Bras.* 31, 572–578. doi: 10.1590/S0100-41582006000600006

Pirovani, C. P., Carvalho, H. A. S., MaChado, R. C. R., Gomes, D. S., Alvim, F. C., Pomella, A. W. V., et al. (2008). Protein extraction for proteome analysis from cacao leaves and meristems, organs infected by Moniliophthora perniciosa, the causal agent of the witches' broom disease. *Electrophoresis* 29, 2391–2401. doi: 10.1002/elps.200700743

Pirovani, C. P., da Silva Santiago, A., dos Santos, L. S., Micheli, F., Margis, R., da Silva Gesteira, A., et al. (2010). Theobroma cacao cystatins impair Moniliophthora perniciosa mycelial growth and are involved in postponing cell death symptoms. *Planta* 232, 1485–1497. doi: 10.1007/s00425-010-1272-0

Qi, J., Wang, J., Gong, Z., and Zhou, J.-M. (2017). Apoplastic ROS signaling in plant immunity. *Curr. Opin. Plant Biol.* 38, 92–100. doi: 10.1016/j.pbi.2017.04.022

R Core Team. (2022). R: A language and environment for statistical computing. Vienna, Austria: R Foundation for Statistical Computing. Available at: https://www.r-project.org/ (Accessed December 20, 2023).

Rubini, M. R., Silva-Ribeiro, R. T., Pomella, A. W. V., Maki, C. S., Araújo, W. L., dos Santos, D. R., et al. (2005). Diversity of endophytic fungal community of cacao (Theobroma cacao L.) and biological control of Crinipellis perniciosa, causal agent of Witches' Broom Disease. *Int. J. Biol. Sci.* 1, 24–33. doi: 10.7150/ijbs.1.24

Sakurai, N. (1998). Dynamic function and regulation of apoplast in the plant body. *J. Plant Res.* 111, 133–148. doi: 10.1007/BF02507160

Santos, A. S., Mora-Ocampo, I. Y., de Novais, D. P. S., Aguiar, E. R. G. R., and Pirovani, C. P. (2023). State of the art of the molecular biology of the interaction between cocoa and witches' Broom disease: A systematic review. *Int. J. Mol. Sci.* 24, 5684. doi: 10.3390/ijms24065684

Schaller, A., Stintzi, A., Rivas, S., Serrano, I., Chichkova, N. V., Vartapetian, A. B., et al. (2018). From structure to function – a family portrait of plant subtilases. *New Phytol.* 218, 901–915. doi: 10.1111/nph.14582

Sels, J., Mathys, J., De Coninck, B. M. A., Cammue, B. P. A., and De Bolle, M. F. C. (2008). Plant pathogenesis-related (PR) proteins: A focus on PR peptides. *Plant Physiol. Biochem.* 46, 941–950. doi: 10.1016/j.plaphy.2008.06.011

Shannon, P., Markiel, A., Ozier, O., Baliga, N. S., Wang, J. T., Ramage, D., et al. (2003). Cytoscape: a software environment for integrated models of biomolecular interaction networks. *Genome Res.* 13, 2498–2504. doi: 10.1101/gr.1239303

Soares, N. C., Francisco, R., Ricardo, C. P., and Jackson, P. A. (2007). Proteomics of ionically bound and soluble extracellular proteins in Medicago truncatula leaves. *Proteomics* 7, 2070–2082. doi: 10.1002/pmic.200600953

Stangarlin, J. R., and Pascholati, S. F. (2000). Activities of ribulose-1,5-bisphosphate carboxylase-oxygenase (rubisco), chlorophyllase, β-1,3 glucanase and chitinase and chlorophyll content in bean cultivars (Phaseolus vulgaris) infected with Uromyces appendiculatus. *Summa Phytopathologica* 26, 34–42.

Stintzi, A., Heitz, T., Prasad, V., Wiedemann-Merdinoglu, S., Kauffmann, S., Geoffroy, P., et al. (1993). Plant 'pathogenesis-related' proteins and their role in defense against pathogens. *Biochimie* 75, 687–706. doi: 10.1016/0300-9084(93)90100-7

Sudisha, J., Sharathchandra, R. G., Amruthesh, K. N., Kumar, A., and Shetty, H. S. (2012). ""Pathogenesis related proteins in plant defense response,"," in *Plant Defence: Biological Control*. Eds. J. M. Mérillon and K. G. Ramawat (Springer Netherlands, Dordrecht), 379–403. doi: 10.1007/978-94-007-1933-0_17

Tantirungkij, M., Nasanit, R., and Limtong, S. (2015). Assessment of endophytic yeast diversity in rice leaves by a culture-independent approach. *Antonie van Leeuwenhoek* 108, 633–647. doi: 10.1007/s10482-015-0519-y

Teixeira, P. J. P. L., Thomazella, D. P., de, T., Reis, O., do Prado, P. F. V., do Rio, M. C. S., et al. (2014). High-resolution transcript profiling of the atypical biotrophic interaction between Theobroma cacao and the fungal pathogen Moniliophthora perniciosa. *Plant Cell* 26, 4245–4269. doi: 10.1105/tpc.114.130807

Vaghela, B., Vashi, R., Rajput, K., and Joshi, R. (2022). Plant chitinases and their role in plant defense: A comprehensive review. *Enzyme Microbial Technol.* 159, 110055. doi: 10.1016/j.enzmictec.2022.110055

Van Der Westhuizen, A. J., Qian, X.-M., and Botha, A.-M. (1998). β-1,3-Glucanases in wheat and resistance to the Russian wheat aphid. *Physiologia Plantarum* 103, 125–131. doi: 10.1034/j.1399-3054.1998.1030115.x

van Loon, L. C., Rep, M., and Pieterse, C. M. J. (2006). Significance of inducible defense-related proteins in infected plants. *Annu. Rev. Phytopathol.* 44, 135–162. doi: 10.1146/annurev.phyto.44.070505.143425

Van Loon, L. C., and Van Strien, E. A. (1999). The families of pathogenesis-related proteins, their activities, and comparative analysis of PR-1 type proteins. *Physiol. Mol. Plant Pathol.* 55, 85–97. doi: 10.1006/pmpp.1999.0213

Villén, J., and Gygi, S. P. (2008). The SCX/IMAC enrichment approach for global phosphorylation analysis by mass spectrometry. *Nat. Protoc.* 3, 1630–1638. doi: 10.1038/nprot.2008.150

Wachowska, U., Irzykowski, W., and Jędryczka, M. (2018). Agrochemicals: Effect on genetic resistance in yeasts colonizing winter wheat kernels. *Ecotoxicol. Environ. Saf.* 162, 77–84. doi: 10.1016/j.ecoenv.2018.06.042

Wang, Y., Branicky, R., Noë, A., and Hekimi, S. (2018). Superoxide dismutases: Dual roles in controlling ROS damage and regulating ROS signaling. *J. Cell Biol.* 217, 1915–1928. doi: 10.1083/jcb.201708007

Wang, Y., Liu, M., Wang, X., Zhong, L., Shi, G., Xu, Y., et al. (2021). A novel β-1,3-glucanase Gns6 from rice possesses antifungal activity against Magnaporthe oryzae. *J. Plant Physiol.* 265, 153493. doi: 10.1016/j.jplph.2021.153493

Wang, W., Scali, M., Vignani, R., Spadafora, A., Sensi, E., Mazzuca, S., et al. (2003). Protein extraction for two-dimensional electrophoresis from olive leaf, a plant tissue containing high levels of interfering compounds. *Electrophoresis* 24, 2369–2375. doi: 10.1002/elps.200305500

Wang, Y., and Wang, Y. (2018). Trick or treat: Microbial pathogens evolved apoplastic effectors modulating plant susceptibility to infection. *Mol. Plant Microbe Interact.* 31, 6–12. doi: 10.1094/MPMI-07-17-0177-FI

Wang, N., Xiao, B., and Xiong, L. (2011). Identification of a cluster of PR4-like genes involved in stress responses in rice. *J. Plant Physiol.* 168, 2212–2224. doi: 10.1016/j.jplph.2011.07.013

Zhang, J., Wang, F., Liang, F., Zhang, Y., Ma, L., Wang, H., et al. (2018). Functional analysis of a pathogenesis-related thaumatin-like protein gene TaLr35PR5 from wheat induced by leaf rust fungus. *BMC Plant Biol.* 18, 76. doi: 10.1186/s12870-018-1297-2

Zugaib, M., Gramacho, K. P., Mares, J. H., Camillo, L. R., Ocampo, I. Y. M., Arevalo-Gardini, E., et al. (2023). Comparative proteome profile of ungerminated spores and mycelium of the fungus Moniliophthora roreri, causal agent of frosty pod rot disease in cacao. *J. Phytopathol.* 171, 242–257. doi: 10.1111/jph.13177

frontiers | Frontiers in Plant Science

TYPE Original Research
PUBLISHED 29 July 2024
DOI 10.3389/fpls.2024.1398770

OPEN ACCESS

EDITED BY
Brigitte Mauch-Mani,
Université de Neuchâtel, Switzerland

REVIEWED BY
Patricia Manosalva,
University of California, Riverside, United States
Iris F. Kappers,
Wageningen University and Research, Netherlands

*CORRESPONDENCE
Brian Kvitko
bkvitko@uga.edu
Li Yang
li.yang1@uga.edu

†PRESENT ADDRESS
Lanxi Hu,
Weill Institute for Cell and Molecular Biology and School of Integrative Plant Science, Section of Plant Biology, Cornell University, Ithaca, NY, United States
Jovana Mijatovic,
Botany and Plant Pathology Department, Oregon State University, Corvallis, OR, United States

‡These authors have contributed equally to this work

RECEIVED 10 March 2024
ACCEPTED 24 June 2024
PUBLISHED 29 July 2024

CITATION
Hu L, Mijatovic J, Kong F, Kvitko B and Yang L (2024) Ontogenic stage-associated SA response contributes to leaf age-dependent resistance in *Arabidopsis* and cotton. *Front. Plant Sci.* 15:1398770. doi: 10.3389/fpls.2024.1398770

Ontogenic stage-associated SA response contributes to leaf age-dependent resistance in *Arabidopsis* and cotton

Lanxi Hu†‡, Jovana Mijatovic†‡, Feng Kong, Brian Kvitko* and Li Yang*

Department of Plant Pathology, College of Agricultural and Environmental Sciences, University of Georgia, Athens, GA, United States

Introduction: As leaves grow, they transition from a low-microbe environment embedded in shoot apex to a more complex one exposed to phyllosphere microbiomes. Such change requires a coordinated reprogramming of cellular responses to biotic stresses. It remains unclear how plants shift from fast growth to robust resistance during organ development.

Results: Here, we reported that salicylic acid (SA) accumulation and response were temporarily increased during leaf maturation in herbaceous annual *Arabidopsis*. Leaf primordia undergoing active cell division were insensitive to the elicitor-induced SA response. This age-dependent increase in SA response was not due to prolonged exposure to environmental microbes. Autoimmune mutants with elevated SA levels did not alter the temporal pattern dependent on ontogenic stage. Young *Arabidopsis* leaves were more susceptible than mature leaves to *Pseudomonas syringae* pv. *tomato* (*Pto*) DC3000 *cor*– infection. Finally, we showed a broadly similar pattern in cotton, a woody perennial, where young leaves with reduced SA signaling were preferentially invaded by a *Xanthomonas* pathogen after leaf surface infection.

Discussion: Through this work, we provided insights in the SA-mediated ontogenic resistance in Arabidopsis and tomato.

KEYWORDS

temporal resistance, salicylic acid, ontogenic resistance, cotton, leaf maturation

Introduction

Plant lateral organs start as small clusters of cells in the shoot apex and eventually grow into complex structures that are exposed to a diverse range of environmental microbes, including beneficial, commensal, and pathogenic microbes (Sinha, 1999; Bar and Ori, 2014). Young tissues are generally protected by surrounding pre-existing organs and

therefore have limited exposure to microbes in their environment. During their development, these organs may shift from being susceptible to resistant to certain pathogens, which is referred to as ontogenic resistance or age-related resistance (ARR) (Develey-Riviere and Galiana, 2007; Berens et al., 2019; Hu and Yang, 2019). This phenomenon has been observed in various pathosystems (Bowling et al., 1994; Gusberti et al., 2013; Asalf et al., 2014; Twomey et al., 2015; Mansfeld et al., 2017). For instance, susceptibility of hop cones to powdery mildew gradually decreases after the transition from bloom to cone development (Twomey et al., 2015). Fruits of several cucurbit crops, including melon, butternut squash, watermelon, zucchini, squash, and pumpkin, also enhanced resistance to the oomycete pathogen *Phytophthora capsica*, as they increase in fruit size (Ando et al., 2009). Young cucumber (*Cucumis sativus*) fruits from some cultivars are highly susceptible to infection to the oomycete pathogen, *P. capsica*. However, they become resistant once they complete their exponential growth (Ando et al., 2009). Genes involved in multiple defense pathways, including physical barriers (e.g., cuticle thickness), penetration defense, flavonoid biosynthesis, oxidative stress, and microbe-associated molecular pattern (MAMP)- or effector-triggered immune responses, are enhanced in mature fruits (Ando et al., 2015). Comparing peel transcriptomes and metabolomes from mature "ARR-capable" and "ARR-defective" cucumber lines have linked an upregulation in terpenoid glycoside production during development to the ARR against *P. capsica* (Mansfeld et al., 2017). The regulatory mechanisms upstream of those age-related metabolisms and whether there are any signaling pathways conserved in operating ontogenic resistance are less clear.

Salicylic acid (SA) is a plant hormone vital in promoting resistance against biotrophic and hemibiotrophic pathogens (Huot et al., 2014; Berens et al., 2019; van Butselaar and Van den Ackerveken, 2020; Chan, 2022). The isochorismate synthase (ICS) pathway contributes to the pathogen-induced SA accumulation in *Arabidopsis* (Nawrath and Metraux, 1999). The AVRPPHB SUSCEPTIBLE 3 (PBS3) enzyme converts IC to SA by catalyzing the conjugation of IC and glutamate to produce isochorismate-9-glutamate (Rekhter et al., 2019). Then, the multidrug and toxin extrusion (MATE) transporter ENHANCED DISEASE SUSCEPTIBILITY 5 (EDS5) is responsible for transporting SA from chloroplast to cytosol. Mutations in EDS5, also known as *sid1*, lead to lower levels of SA upon pathogen infection (Nawrath and Metraux, 1999; Nawrath et al., 2002; Rekhter et al., 2019). In *Arabidopsis*, NONEXPRESSER OF PR GENES (NPR) family members act as major SA receptors in conducting SA-mediated defense signaling (Zhou et al., 2023). NPR1 and NPR3/4 can bind to SA with varying affinities, and a key conserved arginine residue in NPR1 ($NPR1^{R432}$) and NPR3/4 ($NPR3^{R428}$ and $NPR4^{R419}$) is indispensable for SA binding (Fu et al., 2012; Ding et al., 2018; Liu et al., 2020). When associated with transcription factors, such as TGACG-binding (TGA) family members, NPR proteins act as either transcriptional co-activators (NPR1) or co-repressors (NPR3/4) to play opposing roles in regulating the transcription of downstream genes, including CAM-BINDING PROTEIN 60-LIKE G (CBP60g, AT5G26920) and SAR DEFICIENT 1 (SARD1, AT1G73805) (Fan and Dong, 2002; Despres et al., 2003; Ding et al., 2018). On the other hand, SA plays a pivotal role in plant development (Rivas-San Vicente and Plasencia, 2011; Li et al., 2022). SA modulates cell cycle transition in both positive and negative manners (Vanacker et al., 2001; Xia et al., 2009; Xu et al., 2017). SA also regulates specific developmental processes such as apical hook formation (Huang et al., 2020), flowering time (Martínez et al., 2004), root patterning (Pasternak et al., 2019), and leaf senescence (Morris et al., 2000).

Organ maturation has been associated with changes in disease resistance in several pathosystems, with varying hormone and metabolic pathways modulating these processes in coordination with ontogenic stages (Gusberti et al., 2013; Asalf et al., 2014; Twomey et al., 2015; Mansfeld et al., 2017). In *Arabidopsis*, a priority was given to either ABA-mediated abiotic or SA-mediated biotic stress responses at different leaf ages, enabling plants to balance abiotic and biotic stresses during growth (Berens et al., 2019). This suggests a temporal signaling coordination between fast growth and potent resistance during organ development. Still, much remains unknown about the amplitude and regulation of innate immunity during distinct developmental stages of an organ and if they are conserved across species. Our study revealed an ontogenic increase in SA accumulation and response during the maturation of *Arabidopsis* leaves. At the stage and the location of active cell division, leaves were compromised in activating SA responses and were associated with high susceptibility to pathogen. This age-dependent increase in SA response is not a result of prolonged exposure to environmental microbes. Furthermore, we found that auto-immune mutants with elevated SA did not alter the temporal pattern of SA response. Similar to the observations in *Arabidopsis*, we found that *Xanthomonas citri* pv. *malvacearum* displayed enhanced colonization in young cotton leaves. Likewise, SA signaling was reduced in young cotton leaves relative to expanded leaves. This implies a potential shared mechanism of ontogenic ARR between Brassicales and Malvales sister taxa.

Results

Arabidopsis mature leaves showed higher SA response than young leaves

PATHOGENESIS-RELATED 1 and *2* (*PR1* and *PR2*) are canonical markers for SA-induced response (Cao et al., 1997; Nawrath and Metraux, 1999; Vogel and Somerville, 2000). In soil grown plants, we observed that the activity of β-glucuronidase (GUS) driven by the promoters of *PR1* and *PR2* were preferentially activated in mature leaves after treatment with benzothiadiazole (BTH), an SA analogue (Figures 1A–C), which is consistent with previously reported age-dependent accumulation of *PR1* transcripts (Berens et al., 2019). To better understand the cellular status of leaves at different ages, we examined the expression of *proCyclinB1::GUS*, a marker for actively dividing cells, in successive leaves and defined young, expanding, and mature leaves based on their staining pattern (Figure 1C). Leaves first mature at the distal end,

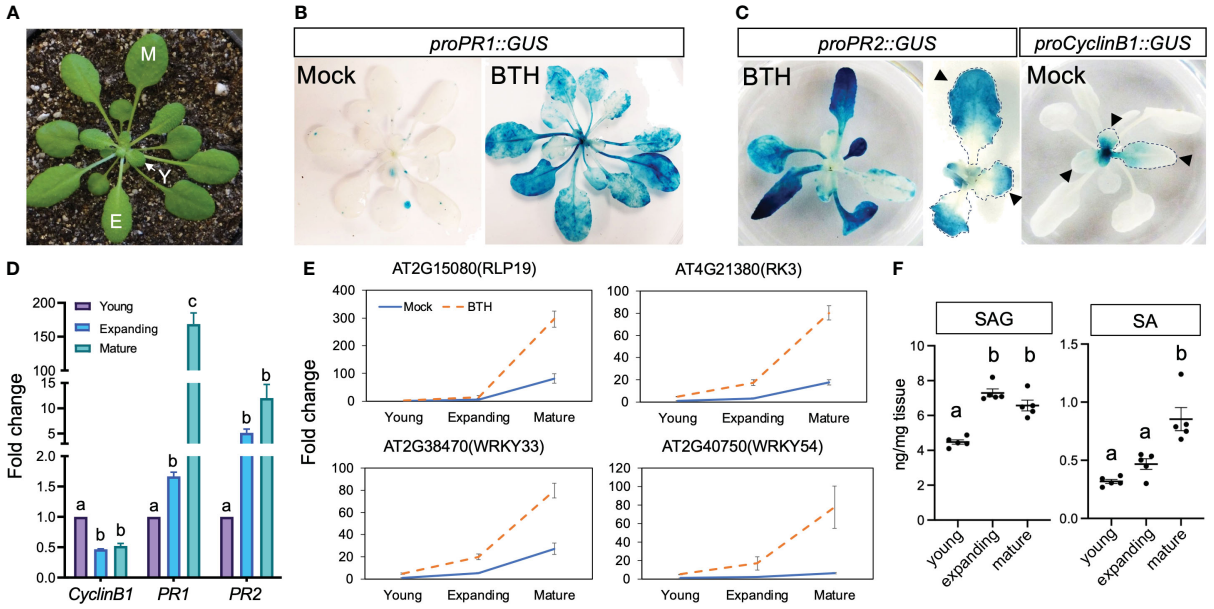

FIGURE 1
Mature leaves showed elevated SA accumulation and response. **(A)** A 5-week-old *Arabidopsis* plant grown in short-day condition. Y, young leaves; E, expanding leaves; M, mature leaves. Plants used in Figure 1 were grown in soil. **(B)** The expression of *proPR1::GUS* at 24 h after mock or BTH treatment. Note the lack of induction in the center of BTH-treated plant where young (newly emerging) leaves were located (n>12 plants grown in soil were used for each treatment). **(C)** Complementary staining pattern between *proPR2::GUS* and *proCyclinB1::GUS*. The middle panel shows enlarged view of *proPR2::GUS* staining in young leaves. Note the staining first appeared at tip of leaves, which is complementary to the staining pattern of *proCyclinB1::GUS*. The lack of *proCyclinB1*::GUS and appearance of *proPR2::GUS* at the leaf tip is indicated by arrowheads (n>10 plants grown in soil were used for each treatment). **(D)** Expression patterns of *CyclinB1*, *PR1*, and *PR2* in young, expanding, and mature leaves. The fold change is relative to the expression of each gene in young leaves. Different letters above each date set indicate significant difference based on one-way ANOVA. Similar results were seen in two biological replicates. **(E)** Expression patterns of SA-responsive genes in young, expanding, and mature leaves. Leaves were harvested from 5-week-old plants grown in SD conditions. Error bars: standard error of three technical repeats. Similar results were observed in three independent biological replicates. Each biological replicate contained at least six leaves. Fold change is relative to the expression of each gene in mock-treated young leaves. **(F)** Accumulation of SA and SAG in young, expanding, and mature leaves. Young, expanding, and mature leaves were harvested from 5–7-week-old plants grown in SD conditions. Same plants were used to harvest young, expanding, and mature leaves. Different letters above each data set indicate significant difference based on one-way ANOVA.

indicated as the lack of *proCyclinB1*::GUS at leaf tip (arrowhead in Figure 1C), while *proPR2*::GUS often first appeared at the distal end of leaves (arrowhead in Figure 1C). We defined young leaves as those showing active cell division in the whole or a part of a leaf (>50% leaf area); expanding leaves have not reached their full size but with limited cell division; mature leaves reach full size without signs of senescence (Figure 1A). We noticed that *proPR2*::GUS was mostly evident in the tips of premature leaves, complementary to the staining pattern of *proCyclinB1*::GUS, indicating a suppression of SA response in actively dividing cells (Figure 1C). The ontogenic expression pattern was confirmed with qPCR-based quantification for transcript levels of these marker genes (Figure 1D). To further validate the observation, we tested the ontogenic stage expression of four additional SA-activated genes (*AT2G15080*, *AT4G21380*, *AT2G38470*, and *AT2G40750*) during leaf maturation (Yang et al., 2017) (Supplementary Table S1). Like *PR1* and *PR2*, these genes also showed high expressions in mature leaves after the BTH treatment (Figure 1D, E). Interestingly, despite the relatively low expression in mock-treated samples, the ontogenic increasing pattern remained, suggesting that endogenous SA accumulation or response was enhanced in mature leaves (Figure 1E). Indeed, mature leaves accumulated high level of free SA and SA metabolites, salicylic acid beta-glucoside (SAG), compared to young leaves or expanding leaves (Figure 1F). Taken together, our analysis suggested that both the SA accumulation and signaling pathway were temporally derepressed during leaf expansion.

The ontogenic increase in SA response was not due to prolonged exposure to the phyllosphere microbiome

To test if the ontogenic increase in SA response in mature leaves was due to prolonged exposure to the phyllosphere microbiome, we grew *Arabidopsis* seedlings under axenic short-day conditions and measured the basal expression levels of the forementioned four SA-responsive genes in young, expanding, and mature leaves harvested 4 weeks after planting (Figure 2A). All four genes showed higher expression in mature leaves, suggesting that ontogenic maturation of SA responses can occur independently of phyllosphere microbes. Nevertheless, we cannot exclude the possibility that prolonged exposure to environmental microbes may also contribute to the age-dependent enhancement of SA signaling. To obtain a global view of SA response during leaf expansion, we re-analyzed published transcriptomes of young, expanding, and mature leaves from plants grown in axenic conditions (Pan et al., 2019). A total of

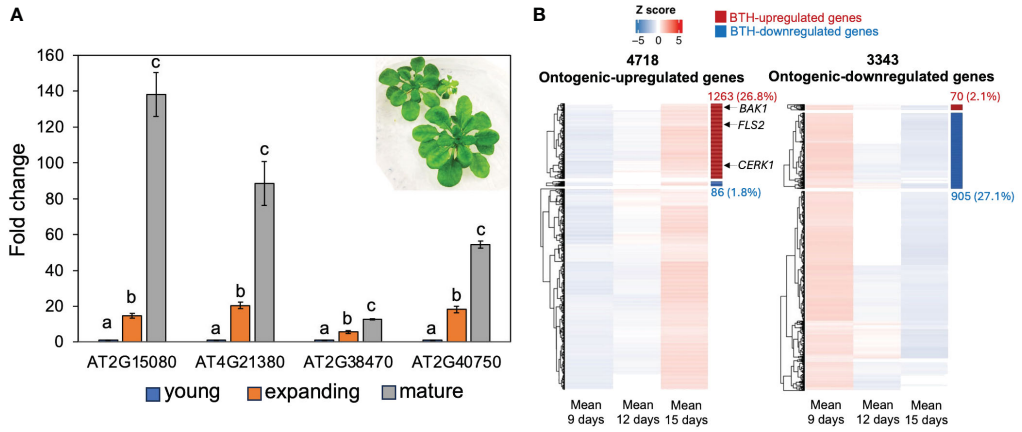

FIGURE 2
SA-responsive genes were upregulated during leaf expansion in sterile conditions. **(A)** The expression of SA-responsive genes in young, expanding, and mature leaves. Plants were grown in deep Petri dish (15 mm depth) and kept in an SD condition (see the image insert) for 3 weeks. The fold change is relative to the expression of each gene in young leaves. Error bars: standard error of three technical repeats. Different letters above each data set indicate significant difference based on one-way ANOVA. Similar results were observed from two independent experiments, each with 8–10 leaves at their respective ages. **(B)** Gene clusters show ontogenic stage expression pattern during leaf expansion. The left panel shows the increasing expression trajectory of 4,718 genes during leaf maturation; right panel shows the expression trajectory of 3,343 genes with decreasing patterns. These genes were detected in Pan et al. (2019) and combined in this work (see *Materials and methods*). SA-responsive genes were defined by Yang et al. (2017). Red and blue bars on the right side of the heatmap indicate BTH-activated and repressed genes, respectively. The heatmap position of *FLS2*, *BAK1*, and *CERK1* was indicated by arrows (see Supplementary Table S2).

4,718 and 3,343 genes showed ontogenic increases and decreases during leaf growth, respectively (Pan et al., 2019). Using SA-responsive genes defined by Yang et al. (2017), we found that 26.8% of ontogenic-increased genes were upregulated by SA (Figure 2B, Supplementary Table S2), including *CBP60g* and *SARD1*. Similarly, 27.1% of the temporally decreased genes were suppressed by SA (Figure 2B, Supplementary Table S2). In summary, SA-responsive genes counted for at least a quarter of genes that were temporally expressed during leaf maturation, suggesting an age-dependent tradeoff between growth and defense.

Arabidopsis auto-immune mutants did not alter the temporal pattern of SA response

Auto-immune mutants have enhanced disease resistance due to hyperactivation of a branch of plant innate immunity, including the SA signaling (van Wersch et al., 2016). To investigate if the temporal pattern of SA response could be maintained in auto-immune mutants, we measured the activity of the *PR2* promoter in gain of function *SUPPRESSOR OF NPR1–1, CONSTITUTIVE 1* (*snc1*), and loss-of-function *CONSTITUTIVE EXPRESSER OF PR GENES 1* (*cpr1*) mutants (Bowling et al., 1994; Li et al., 2001). Both mutants accumulate a higher level of SA than Col-0 wild type and are more resistant to biotrophic pathogens (Bowling et al., 1994; Li et al., 2001). As previously reported, *cpr1* mutant was smaller than Col-0 (Figure 3A). Notably, we found that although these mutants exhibited intense *proPR2::GUS* staining, their young leaves were still compromised in *PR2* promoter activity, indicating that the SA response was constrained in auto-immune young leaves (Figures 3B, C). Consistent with the staining pattern of *proPR2::GUS*, expressions of SA-responsive genes showed temporal increases from young to mature leaves in the *snc1* mutant background (Figure 3D). Thus, the hyperactivation of SA response in autoimmune mutants was not due to a precocious activation in young leaves.

Premature *Arabidopsis* leaves were more susceptible to *Pseudomonas syringae* pv. tomato DC3000 coronatine–

Next, we tested whether young and mature leaves differentially activate SA response during pathogen infection. We challenged young and mature *Arabidopsis* leaves with *Pseudomonas syringae* pv. *tomato* (*Pto*) DC3000, a hemibiotrophic bacterial pathogen. As their responses to BTH, mature leaves showed a strong response to *Pto* DC3000 infection indicated by a high activation of *proPR1::GUS* (Figure 4A). In contrast, the amplitude of activation was compromised in young leaves (Figure 4A). This suggests that the pathogen-triggered SA signaling was temporally elevated during leaf ontogenesis.

We further assessed whether the ontogenic maturation of SA response contributes to disease resistance by challenging premature and mature leaves with *Pto* DC3000 and *Pto* DC3000 *cor–* (coronatine defective) strains. Coronatine, a phytotoxin produced by *Pto* DC3000, dampens *Arabidopsis* SA-mediated immunity by activating jasmonic acid responses (Zheng et al., 2012). Consistent with the previous report, *Pto* DC3000 multiplication was not affected by leaf age (Figure 4B) (Berens et al., 2019). We reasoned that the presence of coronatine in wild-type *Pto* DC3000 may help it counteract the enhancement of the SA pathway from young to

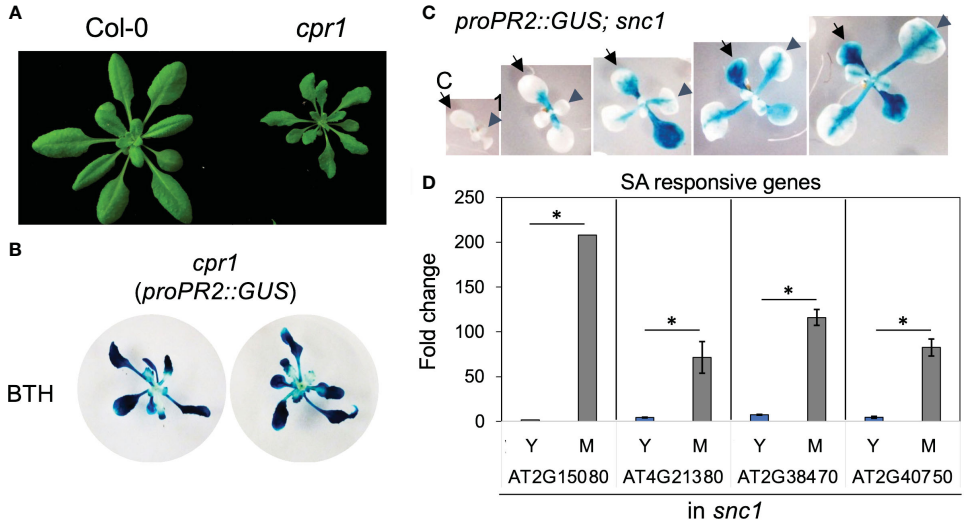

FIGURE 3
Young leaves had compromised SA response in autoimmune mutants cpr1 and snc1. **(A)** cpr1 mutant showing dwarf phenotype. **(B)** Staining of *proPR2::GUS* in *cpr1*. Note the reduced staining in the center of plants where young leaves were located (n>20 plants grown in soil for each genotype). **(C)** Staining of *proPR2::GUS* in *snc1* gain-of-function mutant. Note the gradual increase in staining during leaf (arrowhead) and cotyledon (arrow) expansion. C, cotyledon; 1, first leaf (n>20 plants grown in soil for each genotype). **(D)** The expression of SA-responsive genes in young and mature leaves from *snc1* mutant. Error bars: standard error of three technical repeats. Similar results were observed in two independent biological replicates. *Significant difference between young and mature leaves using Student's t-test. Y, young leaves; M, mature leaves. Similar results were obtained from two independent experiments. Fold change is relative to the expression of each gene in young leaves.

mature leaves (Zheng et al., 2012). In line with this, we found that mature leaves were more resistant than young leaves to the *Pto* DC3000 *cor*– strain, implying that the ontogenic resistance in mature leaves can be linked to the enhanced SA-mediated defense (Figure 4C). Surprisingly, blocking SA signaling in *npr1* mutant did not abolish the difference of bacterial multiplication between young and mature leaves (Figure 4D), suggesting NPR1-independent pathways contribute to ontogenic resistance. In support of this, the expressions of pattern-triggered immunity (PTI) components including *FLAGELLIN SENSING2* (*FLS2*, *AT5G46330*), *BRI1 ASSOCIATED RECEPTOR KINASE 1* (*BAK1*, *AT4G33430*), and *CHITIN ELICITOR RECEPTOR KINASE 1* (*CERK1*, *AT3G21630*) were higher in mature leaves than in young leaves (Figure 2B, Supplementary Table S2), with the expression pattern of *FLS2* being consistent with what was reported previously (Zou et al., 2018).

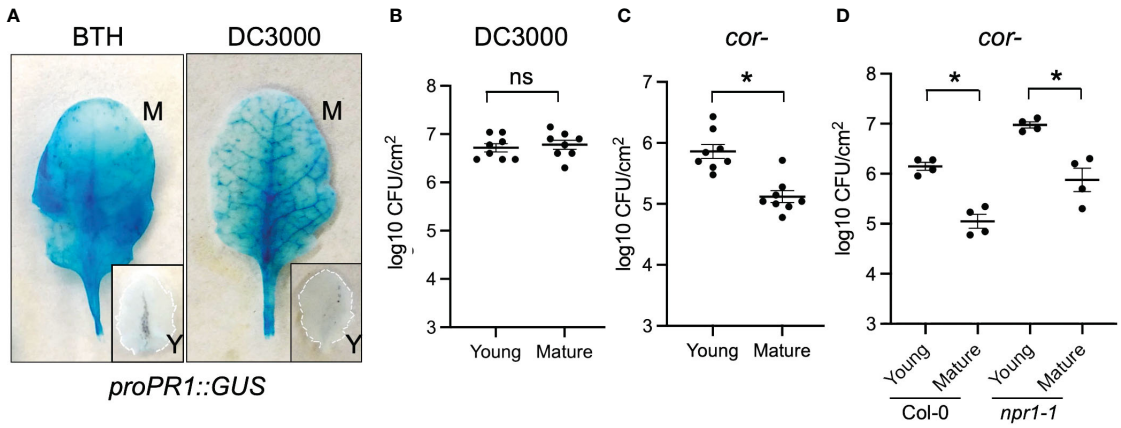

FIGURE 4
Young *Arabidopsis* leaves were compromised in defense against *Pto* DC3000 *cor*– stain. **(A)** *Pto* DC3000 and BTH triggered *proPR1::GUS* expressions in mature (M) but not young (Y) leaves. Leaves were sampled 24 h after BTH or *Pto* DC3000 infiltration. **(B)** Mature and young leaves showed the same level of susceptibility to *Pto* DC3000. Samples were collected at 48 h after *Pto* DC3000 infiltration (n=8). **(C)** Young leaves were more susceptible to *Pto* DC3000 *cor*– than mature leaves. Samples were collected at 48 h after *Pto* DC3000 *cor*– infiltration (n=8). **(D)** The difference in susceptibility between young and mature leaves were maintained in *npr1–1* mutant. Samples were collected at 48 h after *Pto* DC3000 infiltration. From panels **(B–D)** ns, no significance. *Significant difference between young and mature leaves using Student's t-test. Similar results were obtained from at least three independent experiments.

10.3389/fpls.2024.1398770

Young cotton leaves were more susceptible to *Xanthomonas citri* pv. *malvacearum* infection than mature leaves

To test whether the findings in herbaceous *Arabidopsis* could be generalized in distantly related species such as cotton, we dip inoculated 2-week-old cotton seedlings with at least one fully expanded true leaves with *Xcm* 4.02 wild-type Tn*7*LUX or *Xcm* 4.02 Δ*hrcV* Tn*7*LUX (T3SS-, defective in Type III secretion systems) (Mijatović et al., 2021). To track the pattern of *Xcm* colonization, we recorded bacterial auto-bioluminescence and examined bacterial population in leaves at different levels of maturity (Figure 5). As it takes up to 3 weeks for disease development in cotton, we marked the youngest actively expanding leaf (leaf "0") at the time of inoculation to monitor relative leaf age (Figure 5A). Image overlay of auto-bioluminescence patterns revealed variable colonization dependent on leaf age at the time of inoculation (Figure 5B). As observed in our previous work (Mijatović et al., 2021), both *Xcm* 4.02 WT Tn*7*LUX (Figures 5C, D) and *Xcm* 4.02 Δ*hrcV* Tn*7*LUX (Figure 5E) can colonize cotton tissue, but at different bacterial loads. The youngest actively developing leaves (leaf "0") at the time of inoculation consistently showed increased Xcm auto-bioluminescence when compared to leaves developed pre-noculation (leaf "−1") and post-inoculation (leaf "+1") (Figure 5B). It is worth noting that auto-bioluminescence observed from overlayed images corresponds with the location of water-soaking disease symptoms in *Xcm* 4.02 WT Tn*7*LUX inoculated seedlings (Figure 5C). Comparison of *Xcm* loads in tested leaf samples revealed differences in bacterial population of both the WT and *hrcV* mutant between leaves of different age (Figures 5D, E), consistent with the ontogenic enhancement in basal resistance observed in *Arabidopsis*. Both pathogens consistently displayed higher colonization in the youngest actively developing leaves (leaf 0) at the time of inoculation (Figures 5C, D). Lower bacterial populations in leaves developed pre-inoculation (leaf "−1") indicate that more mature cotton leaves have enhanced defense responses to *Xcm* infection. This is in line with the compromised basal defense response observed in young leaves of *Arabidopsis*.

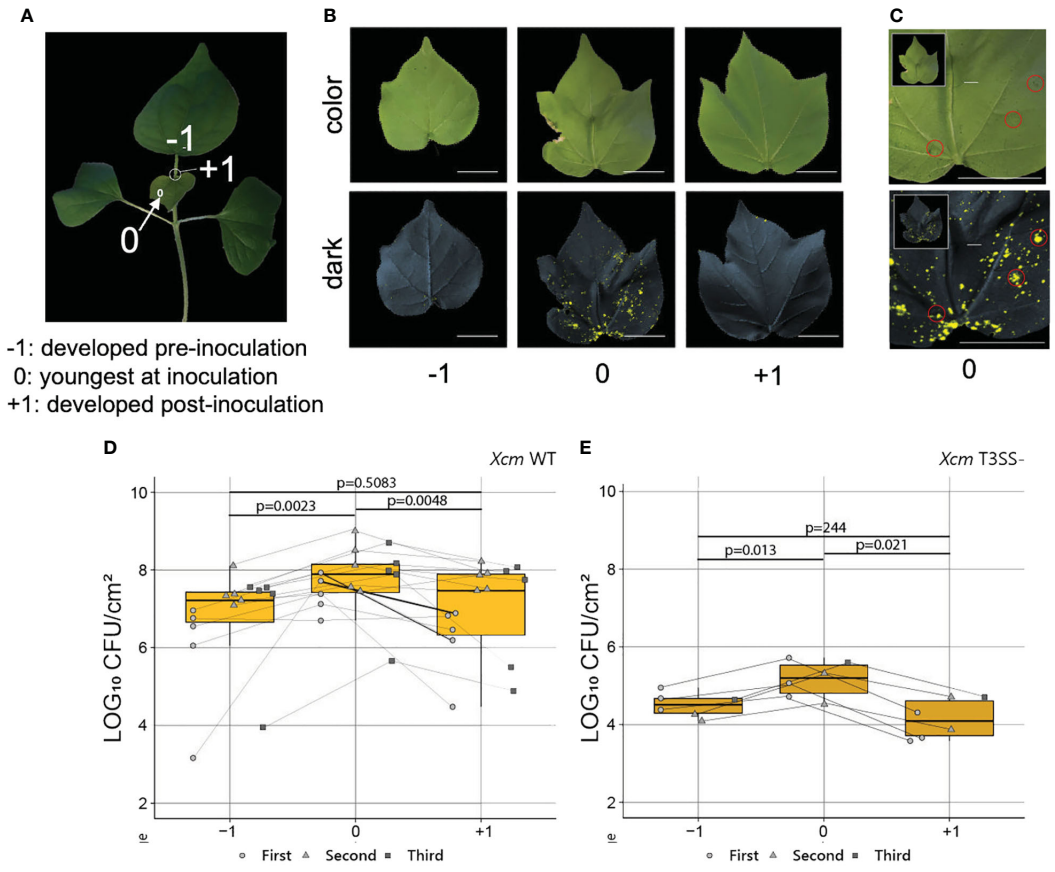

FIGURE 5
Young cotton leaves were preferentially colonized by *Xcm*. **(A)** A 2-week-old cotton plant. "−1", mature leaves developed pre inoculation; "0", young leaves actively developing at the time of inoculation; "+1", young leaves actively developing post-inoculation. **(B)** Representative color and 2-min exposure auto-bioluminescence overlay images of infected cotton true leaves developed pre and post *Xcm* 4.02 WT Tn7LUX dip inoculation. **(C)** Correlation of symptoms developed 2 weeks post-Xcm 4.02 WT Tn7LUX dip inoculation and the zones of auto-bioluminescence. **(D, E)** Bacterial populations in log10 CFU/cm^2 value post-*Xcm* 4.02 WT Tn7LUX **(D)** and Xcm 4.02 ΔhrcV Tn7LUX **(E)** infection, combined from three experimental replicates. Boxplots show mean ± SD. p-values were calculated using Student's t-test.

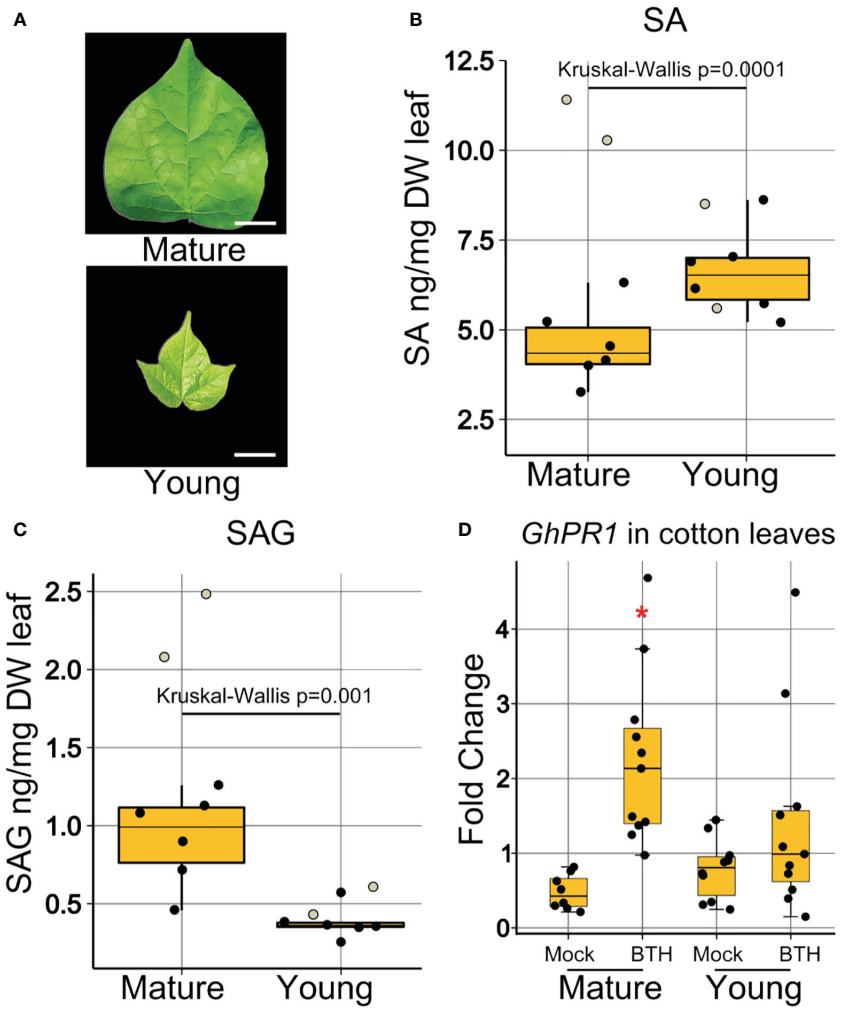

FIGURE 6
Young cotton leaves were compromised in SA signaling. **(A)** Visual representation of the morphology of collected mature and young leaf samples. Bars represent 1 cm length. **(B)** Concentration of free SA in ng/mg of dry leaf weight. **(C)** Concentration of SAG in ng/mg of dry leaf weight. Boxplots show mean ± SD. Eight samples of five pooled biological replicates each represented as jitter dots on boxplots. Two dots representing two samples (white filled) were not used in statistical analysis, as they were found to be outliers outside of the first and third quartile. Data were analyzed by Kruskal–Wallis test because the results met non-parametric requirements. **(D)** Expression of SA-responsive genes in mature and young cotton leaves at 24-h post-BTH treatment. Points represent biological replicates from three experimental replicates. Boxplots show mean ± SD. Differences in gene expression from 3 experimental replicates were pooled and analyzed using ANOVA. *Significant difference between *Gh*PR1 expression in young and mature leaves.

SA and SAG accumulation varied in young and mature cotton leaves

Having determined that young leaves at the time of inoculation are more heavily colonized, we hypothesized that, similar to *Arabidopsis*, ontogenic differences in SA accumulation or SA signaling might mediate age-related susceptibility to *Xcm* in cotton. Samples representing mature and young cotton leaves (Figure 6A) were collected, lyophilized, macerated, and examined by quadrupole time-of-flight mass spectrometry (QTOF-MS). Analysis of accumulation of free SA revealed higher concentration in young leaves than in mature leaves (Figure 6B). Conversely, the inactive vacuole stored SAG was at a higher concentration in mature leaves compared to young leaves (Figure 6C). These results indicate that the cause of young leaf age-related immunodeficiency in cotton is likely not linked to the free SA level but may be correlated with accumulations of SAG or impaired SA signaling.

GhPR1 induction by BTH differs between young and mature cotton leaves

To further elucidate the contribution of SA to the immunodeficiency in young cotton leaves, we investigated the accumulation of *GhPR1*, an SA-responsive gene in cotton and an orthologue of *Arabidopsis PR1*. We dip inoculated cotton leaves with BTH and recorded expression of *GhPR1* at 24 h after treatment in mature and young (Figure 6D) leaves. *GhPR1* was induced by BTH treatment in mature leaves at 24 h post-inoculation, but

induction in young leaves was not statistically significant (Figure 6D). Thus, the SA signaling response was elevated in mature leaves in cotton, which correlated with the enhanced disease resistance against *Xcm* 4.02 strains (Figures 5D, E).

Discussion

Leaf development involves two types of cell divisions. In the first type, cells undergo rapid proliferation with a high incidence in the initial primordium. When these cells exit the mitotic cycle, they continuously expand in volume and increase further in size. Endoreduplication is a variant of the cell cycle in which cells undergo DNA replication without subsequent mitosis. During plant organ ontogenesis, cell division often first occurs densely at the distal half of an organ and then progresses toward the base over time. This common spatial pattern is known as the basipetal gradient (Nath et al., 2003; Ori et al., 2007; Nelissen et al., 2012; Du et al., 2018). Resemble to this gradient of cell proliferation, in our work, we observed that SA response indicated by *PR1* and *PR2* promoter activities first appeared in the distal part of an expanding leaf where cells mature earlier than those in the proximal end of a leaf (Figure 1), suggesting that the elevated SA response is associated with cellular maturation status in a leaf. On the other hand, genes involved in regulating endoreduplication could play dual roles in plant immunity. For example, SIAMESE (SIM) and SIAMESE RELATED 1 (SMR1) act synergistically to promote endoreplication (Churchman et al., 2006; Hamdoun et al., 2016). Cells in a *sim smr1* double mutant showed a low endoreduplication index. Interestingly, *smr1* mutant also partially suppressed the dwarfism and cell death phenotypes caused by high SA levels in *acd6–1*, indicating that SMR1 may be a positive regulator of plant defense (Hamdoun et al., 2016). These studies indicate that SMR1 may coordinate the increase in ploidy level and SA response during leaf maturation. On the other side, overexpressing a D-type CYCLIN 3;1 (CYCD3;1) restrains endoreduplication (Menges et al., 2006). *Cycd3;1,2,3* mutants showed a higher ploidy level than wild type and were more susceptible to a virulent strain *Pseudomonas syringae* pv. *maculicola ES4326*, which could be rescued by BTH (Hamdoun et al., 2016). In another case, OMISSION OF SECOND DIVISION (OSD1) and UV-B-INSENSITIVE 4 (UVI4) inhibited endoreduplication because their loss-of-function mutants showed high endoreduplication indices (Bao and Hua, 2014). However, overexpressing OSD1 and UVI4 can enhance immunity to a bacterial pathogen (Bao and Hua, 2014). Thus, the level of endoreduplication is not always positively correlated with high SA response or elevated defense, indicating a more complex crosstalk.

Despite cell division, other developmental constraints may contribute to SA-mediated ontogenic resistance. Key steps of SA biosynthesis include the synthesis of isochorismate that are processed in chloroplasts and then transported to cytoplasm by EDS5, a MATE family transporter (Serrano et al., 2013; Rekhter et al., 2019; Lefevere et al., 2020). Chloroplast differentiation is tightly associated with leaf maturation, from proplastids in cells of primordia to chloroplasts in mature leaves. During chloroplast biogenesis, thylakoids are formed, and proteins required for photosynthesis are arranged within the thylakoid (Jarvis and López-Juez, 2013; Gugel and Soll, 2017; Cackett et al., 2022). Premature leaves contain a reduced number of thylakoids per chloroplast (Gugel and Soll, 2017). The transition from plastids to mature chloroplasts during leaf development is shared between monocots and dicots seedlings (Pogson et al., 2015), although it is not clear if fully differentiated chloroplasts are more potent in producing SA precursors. Still, reduced SA biogenesis alone is not sufficient to explain the diminished SA response because young leaves were also compromised in SA signaling transduction upon SA treatment or pathogen infection (Figures 2, 3, 6).

In our research, both SA biogenesis and signaling were developmentally regulated. In *Arabidopsis*, SA is glucosylated to SAG or SA glucose ester (SGE) (George Thompson et al., 2017). SAG is mostly accumulated in the vacuole, and the majority of SGE is located in the cytosol (Vaca et al., 2017). It is proposed that in *Arabidopsis*, SAG acts as a long-term storage form of SA, while SGE, due to its ease of modification for active SA release, acts as a mobile SA factor (Vaca et al., 2017). Our results indicate that, unlike *Arabidopsis*, free SA is more abundant in young cotton leaves than that in mature leaves (Figure 6B), while the SAG concentration was consistently higher in mature than in young leaves (Figures 1E, 6C). It is possible that free SA and SAG played distinct roles in ontogenic resistance of *Arabidopsis* and cotton leaves, which remain to be investigated. We also observed a significant induction of *GhPR1* in mature but not young cotton leaves at 24 h post-BTH treatment. These data were further supported by the disease resistance output.

Like many *Xanthomonas* pathogens, *Xcm* infection of cotton takes place over the course of weeks rather than over the course days as seen for the *Pto* DC3000-*Arabidopsis* interaction. However, a similar pattern of ontogenic resistance was observed in both pathosystems. We observed increased *Xcm* colonization of young cotton leaves actively developing at the time of inoculation based on both bacterial load and auto-bioluminescence localization pattern. Similar age-dependent reductions in bacterial loads were observed for both the WT and disarmed *Xcm hrcV* T3SS mutant, which is consistent with decreased basal immunity in young cotton leaves. Although cotton is grown as an annual crop, it is a perennial plant that develops a woody stem. These observations suggest an SA-dependent ontogenic resistance pathway exists in both herbaceous annual and woody perennial plants, despite the differences in infection strategies and disease progression.

It is interesting that the mutation in *NPR1* did not fully abolish the ontogenic resistance as we observed in *Arabidopsis*. Other genetic factors in charge of ontogenic resistance may be tied to genes involved in the downstream function of different NPR proteins, such as key transcription factors in SA signaling: TGAs and WRKYs. In addition to genes involved in SA pathway, we also noticed that key components of the PTI signaling in *Arabidopsis* were upregulated during leaf maturation (Figure 2B, Supplementary Table S2). The activation of either SA or PTI responses can result in stunted growth, spontaneous cell death, and other developmental defects. These negative impacts on plant growth could be more detrimental in young tissues than in old tissues. Thus, the age-

dependent activating of PTI or SA responses may have evolved to protect young tissues from strong immune damages.

Overall, we showed that age-dependent SA signaling, and part of the SA accumulation, are positively associated with the enhanced disease resistance in both mature *Arabidopsis* and cotton leaves. This positions SA as a potentially conserved pathway regulating ontogenic resistance across woody and herbaceous species. As cotton displays both apical and axillary growth throughout the growing season, young cotton leaves are continuously available as a potential entry point for pathogen invasion. Given the diversity of SA biogenesis and signaling mechanisms (Ullah et al., 2023), further investigations of SA molecular components in cotton and other plants could shed lights on the conservation and divergence of SA-mediated ontogenic resistances.

Materials and methods

Plant material, growth conditions, and bacterial strains

For *Arabidopsis*, wild type, transgenic lines, and mutants utilized in this study were in a Columbia-0 (Col-0) genetic background. The plants were sown on Fafard #3 Mix propagation soil, and the planted seeds were placed under 4°C for 2 days before transferring to a growth room with a temperature of 22°C and 45% humidity. A short-day condition with a photoperiod of 9 h light and 15 h dark and 180 µmol m^{-2} s^{-1} was employed, and the lighting was provided by a 5:3 combination of white (USHIO F32T8/741) and red-enriched (interlectric F32/T8/WS Gro-Lite) fluorescent lights. Plant age was counted from the day when seeds were transferred to the growth room. Young, expanding, and mature leaves were collected from 5–7-week-old plants, using the same plants for each leaf age. These leaves were in adult stage beyond leaf 10. Under axenic conditions, plants grown on autoclaved 1/2 MS media had leaves harvested from 3-week-old plants in the same manner as those grown in soil.

For cotton, seeds of an Xcm-susceptible cotton cultivar Deltapine 1747NR B2XF (DP 1747NR B2XF) were sown (one to two seeds/pot) directly in SunGrow Professional growing potting mix (Farfard 3B, Sungro; Agawam, MA) in 9-cm pots. Pots were incubated in a growth chamber (Conviron A1000) with a 12-h day at 26°C and a 12-h night at 23°C.

P. syringae DC3000 wild type and DC3000 *cor*– mutant strains were described in (Yang et al., 2017). *Xanthomonas* 4.02 WT and Δ*hrcV* mutant creation and Lux Tn7 tagging were described previously (Mijatović et al., 2021).

Bacterial infection

Arabidopsis infection with *P. syringae.* Bacteria strains were cultivated on King's B solid medium [10 g/L peptone, 10 g/L glycerol, 15 g/L agar, 10 g/L Tryptone, 10 mL 10% K_2HPO_4 (10 g K_2HPO_4/100 mL), and 10 mL 10% $MgSO_4$ (10 g $MgSO_4$ anhydrous/100 mL)] at 28°C. The medium was supplemented with rifamycin for selection, and cycloheximide was added to prevent fungal growth. Before inoculation, bacterial stocks were streaked on a plate and allowed to grow for 2 days before being re-streaked one day prior to hand inoculation. To initiate infiltration, bacteria were collected from the plate and suspended in a 10-mM $MgCl_2$ solution. Bacteria were inoculated into *Arabidopsis* leaves using a needless syringe. The initial inoculum was at OD = 0.1 and with 500 times dilution. After inoculation, plants were covered with transparent lids for 1 h. Each sample was composed of four-leaf disks obtained from four individual leaves using a corer. Two days after infiltration, leaf samples were collected and homogenized using an OMNI International homogenizer, diluted serially, and plated on KB plates with 10 µL of bacterial suspension per sample. The plates were incubated in a 28°C incubator for 2 days, and colony forming units were counted manually and normalized based on the inside area of the corer.

Cotton infection with *Xanthomonas citri* pv. *malvacearum*. Two-week-old cotton seedlings of the Xcm-susceptible (DP 1747NR B2XF) cotton cultivar, with the first two true leaves developed, were dip inoculated by submerging in 400 mL of bacterial cell suspension for 30 s. Inoculum (~5×10^8 CFU/mL) was made by suspending plate-cultured cells cultured 48 h on LB agar augmented with 50 µg/mL Kanamycin of *Xcm* 4.02 WT Tn*7*LUX or *Xcm* 4.02 Δ*hrcV* Tn*7*LUX in Milli-Q H_2O with 0.02% Silwet adjuvant (Silwet L-77 Ag, PhytoTech). The youngest actively developing leaf at the time of inoculation was marked with plastic flagging for future analysis. This experiment was repeated three times. The Student's t-test was conducted to analyze *Xcm* load using R studio.

Leaves that developed from inoculated cotton seeds were collected and imaged at 2 weeks after transplanting into soil. For each sample, three images were taken with the following conditions: color (Samsung galaxy s10+), grayscale (70% aperture) (Analytic Jena UVP ChemStudio, Upland, CA), and no light with 2 min of exposure time (100% aperture) (Analytic Jena UVP ChemStudio, Upland, CA). Grayscale and 2-min exposure images were overlayed in Adobe Photoshop CC 2020. Details regarding image processing using Adobe Photoshop (2022) are as previously described (Mijatović et al., 2021).

Bacterial load quantification (CFU/cm^2) was done by collecting 4×4 mm^2 leaf disks with a biopsy punch, suspending it in 200 µL water in 2 mL, screw-cap with o-ring plastic tubes (Fisher Scientific) with three high-density 3 mm zirconium beads (Glen Mills). Maceration was done twice for 1 min each at 1,750 Hz, using a GenoGrinder (SPEX SamplePrep, Metuchen, NJ). The macerate was then 10-fold serially diluted and plated on LB agar media supplemented with 50 µg/mL of kanamycin and 80 µg/mL cephalexin. Bacterial populations were determined after incubation for 2 days at 28°C.

HPLC-QTOF-MS

For *Arabidopsis*, adult Col-0 leaves harvested from 5-, 6-, or 7-week-old plants grown in soil constituted one biological replicate for young (eight leaves per replicate), expanding (eight leaves per

replicate), and fully mature leaves (three leaves per replicate). Five biological replicates were prepared for each developmental stage. Each biological replicate was flash frozen in a 50-mL falcon tube. The leaves were lyophilized and proceed for the high-performance liquid chromatography coupled with quadrupole time-of-flight mass spectrometry (HPLC-QTOF-MS) following the method described in Hu et al (Hu et al., 2023). The amount of salicylic acid beta-glucoside (SAG) and salicylic acid (SA) were quantified in the unit of nanogram metabolite per milligram of tissue (ng/mg tissue).

For cotton, eight samples, each consisting of five pooled biological replicates were flash frozen in 50-mL conical tubes and lyophilized for 24 h at 0.008 mbar and −84°C in a freeze dryer (Labconco). Following lyophilization, samples were macerated in 50 mL conical tubes with three 3-mm steel beads, two times for 2 min at 1,750 Hz, using a GenoGrinder (SPEX SamplePrep, Metuchen, NJ). Samples were then sent for metabolite extraction and QTOF analysis at Warnell School of Forestry and Natural Resources, UGA. The amount of SAG and SA were measured and calculated in the unit of nanogram metabolite per milligram of dry weight (ng/mg DW).

qRT-PCR

For *Arabidopsis*, RNA extraction was conducted using an Omega biotek EZNA plant RNA kit (Omega Biotek) or a RNeasy Plant Mini Kit (Qiagen), and quantitative PCR (qPCR) was performed on an Applied Biosystems QuantStudio 1 Real-Time PCR system with SYBR Green master mix (Applied Biosystems). The following PCR conditions were used: 95°C for 5 min, followed by 40 cycles of 95°C for 15 s, 56°C for 30 s, and 72°C for 20–30 s. Reference gene *SAND* (*AT2G28390*) was utilized. *SAND* expression was not affected by leaf age (Klepikova et al., 2016) (Pan et al., 2019) or infection (Yang et al., 2017). Relative expression was determined using the relative standard curve method, while delta–delta CT was used when the PCR efficiency for the primers was previously established to be at least 95%. The oligonucleotides used in this study are listed in Supplementary Table S1.

For cotton, RNA was extracted following the woody plant protocol from Gambino et al. (2008). Briefly, 900 µl of extraction buffer (2% CTAB, 2.5% PVP-40, 2M NaCl, 100 mM Tris–HCl pH 8.0 and 2% β-mercaptoethanol added just before use) preheated at 65°C were added to ~150 mg of cotton tissue sampled previously, ground in liquid nitrogen with three 3-mm zirconium beads (Glen Mills) and one metal bead, macerated two times for 1 min at 1,750 Hz, using a GenoGrinder (SPEX SamplePrep, Metuchen, NJ). The tubes were then vortexed and incubated at 65°C for 10 min. An equal volume of chloroform:isoamyl alcohol (24:1 v/v) was added. Tubes were then inverted vigorously and centrifuged in a pre-cooled centrifuge for 10 min at 4°C, 11,000 RCF. Following centrifugation, the supernatant was extracted into clean 1.5-mL tubes and a second chloroform:isoamyl alcohol extraction was done. The supernatant was then transferred into a new microcentrifuge tube with 400 µL 3M LiCl. The mixture was then incubated on ice for 30 min and incubated at −20°C overnight. The next day, the RNA was pelleted by centrifugation at 21,000 RCF for 20 min at 4°C. The supernatant was decanted, and the pellet was resuspended in 500 µL of SSTE buffer consisting of 10 mM Tris–HCl pH 8.0, 1 mM EDTA pH 8.0, 1% SDS, and 1M NaCl preheated at 65°C. An equal volume of chloroform:isoamyl alcohol was added, and the mixture was centrifuged for 10 min at 4°C, 11,000 RCF. The supernatant was then precipitated with 0.7 volumes of cold isopropanol and centrifuged for 15 min at 4°C, 21,000 RCF. The RNA pellet was subsequently washed with 70% EtOH in nuclease-free water, dried, and resuspended in nuclease-fee water.

Cotton RNA samples were subjected to an off-column DNase treatment using a TURBO DNA-free kit (Thermo Fisher Scientific) following the manufacturer's recommendations. Following DNase treatment, the samples were cleaned using New England Biolabs (NEB) Monarch RNA Clean and Concentrate kit, following manufacturer's instructions. The cDNA library was then created using qScript cDNA supermix (Quantabio) according to manufacturer's instructions. All RNA and cDNA samples were tested for genomic DNA (gDNA) contamination before qPCR analysis using cotton *GhGAPDH* (*glyceraldehyde 3-phosphate dehydrogenase*) gene primers (Supplementary Table S1). For the qPCR reaction, 1–5 ng of cDNA template was used (standardized to the same concentration per experimental replicate). Conditions of the qPCR were kept identical throughout all runs within experimental replicates following the protocol of Smith et al. (2018). Amplification of cDNA was done in 10 µl reactions using Luna Universal qPCR Master Mix (NEB), 0.25 µM primers, and 2 µL of standardized cDNA. Master mixes and primers were pre-aliquoted for single use and stored at −20°C. All PCR reactions were run in triplicate wells, and sample-well organization was kept identical between plates within experimental replicates. We followed the default thermal cycling protocol in the StepOne software v2.3 (Thermo Fisher Scientific) with real-time capture of SYBR green and ROX (passive reference) fluorescence as follows: 10 min at 90°C, followed by 40 cycles of 95°C for 15 s and 60°C for 1 min, with camera capture at the end of each cycle. A melt curve was generated after the 40th cycle, using the following parameters: 95°C for 15 s, 60°C for 1 min, then a slow ramp (0.3°C/s) to 95°C, with camera capture. All runs were conducted on the Step One Plus real-time PCR system (Thermo Fisher Scientific). For housekeeping gene controls, we used previously published *GhUBQ1* (Cox et al., 2017) and *GhGAPDH* (McGarry et al., 2016) primers (Supplementary Table S1). Relative quantification of *GhPR1* was calculated as described by Smith et al. (2018) following the modified Pfaffl method (Hellemans et al., 2007; Pfaffl, 2007). Three biological and three technical replicates were included in each run. Differences in gene expression were determined by comparing all 24-h data to 6-h mock-treated sample set. Relative expression was calculated using average Cqs and PCR efficiencies. The E^ΔCq values from reference genes (*GhGAPDH*, *GhUBQ1*) (Supplementary Table S1) were geometrically averaged to make the Normalizing Factor (NF). NF is divided into the E^ΔCq of *GhPR1* to give Fold Change (FC). The FC of all three experimental replicates was analyzed using Rstudio to determine significant difference based on one-way ANOVA.

GUS staining assay

Plants containing *proPR2::GUS*, *proPR1::GUS*, or *proCyclinB1::GUS* were harvested at the specified time after planting. To prepare the GUS solution, a mixture of 0.1 M $NaPO_4$ (pH 7.0), 10 mM EDTA, 0.1% Triton X-100, 1 mM $K_3Fe(CN)_6$, and 2 mM X-Gluc (dissolved in N,N-DMF and freshly made) was vacuum infiltrated into the plants. Samples were incubated at 37°C for various time from 1 h to 24 h. The staining solution was then substituted with 70% ethanol. The tissues were washed multiple times with 70% ethanol until the chlorophyll in the leaves was removed. The GUS-stained leaves were then observed under a dissecting microscope (VWR).

Re-analysis of published RNA-seq datasets

We reanalyzed cluster 1 (3,918 genes), cluster 2 (800 genes), cluster 3 (1,512 genes), and cluster 4 (1,831 genes) derived from Pan et al. (2019). Clusters 1 and 2 were combined as 4,718 upregulated genes during leaf development. Clusters 3 and 4 were combined as 3,343 downregulated genes during leaf development. In Excel, we calculated the arithmetic mean and standard deviation of transcripts per million (TPM) for each gene using three replicates derived from 9 days, 12 days, and 15 days, respectively. The Z-score for each gene, replicate, and day was calculated with the following formula: (observed TPM – arithmetic mean)/standard deviation. The mean Z-score per gene per day was generated by averaging the Z-score of the three replicates. Next, we overlapped the BTH-responsive genes identified by Yang et al. (2017) with these ontogenic genes and marked the BTH-triggered genes as visualized in the heatmaps (R package ComplexHeatmap v.2.15.4) (Gu et al., 2016; Gu, 2022).

BTH treatment

For *Arabidopsis*, BTH (Actigard 50WG, Syngenta) at a concentration of 50 μM was sprayed onto seedlings. Water was used as a mock control. Samples were collected at 24 h post-treatment.

For cotton, 2-week old plants with one fully expanded true leaf (mature) and one actively expanding (young) true leaf were dipped into the 3-mM suspension of BTH with 0.02% Silwet. Samples were collected in liquid nitrogen at 6 h and 24 h post-dip inoculation, for RNA extraction. This experiment was repeated three times with similar results.

Data availability statement

The original contributions presented in the study are included in the article/Supplementary Material. Further inquiries can be directed to the corresponding authors.

Author contributions

LH: Writing – original draft, Writing – review & editing, Conceptualization, Data curation, Formal analysis, Investigation, Methodology, Visualization. JM: Writing – original draft, Writing – review & editing, Conceptualization, Data curation, Formal analysis, Investigation, Methodology, Visualization. FK: Data curation, formal analysis, Investigation, Methodology, Visualization, Writing – review & editing. BK: Writing – original draft, Writing – review & editing. LY: Writing – original draft, Writing – review & editing.

Funding

The author(s) declare financial support was received for the research, authorship, and/or publication of this article. This project is supported by NIH R35GM143067 to LY and Cotton Incorporated and The Georgia Cotton Commission to BK. Funding for the Agilent UPLC-QTOF was provided by the US Department of Agriculture, National Institute of Food and Agriculture, Equipment Grant Program award no. 2021–70410-35297.

Acknowledgments

We thank Scott Harding and Khadijeh Mozaffari for analytical assistance. The *cpr1* and *snc1* with *proPR2::GUS* reporter lines were kindly provided by Yuelin Zhang, University of British Columbia. We thank all the members of Yang lab for helpful discussions and critical reading and reviews of this manuscript, Stephanie Chen for sample collection and preparation in HPLC-QTOF-MS, and an undergraduate researcher, Jaimie Seymour, for accumulating preliminary data.

Conflict of interest

The authors declare that the research was conducted in the absence of any commercial or financial relationships that could be construed as a potential conflict of interest.

The author(s) declared that they were an editorial board member of Frontiers, at the time of submission. This had no impact on the peer review process and the final decision.

Publisher's note

Supplementary material

The Supplementary Material for this article can be found online at: https://www.frontiersin.org/articles/10.3389/fpls.2024.1398770/full#supplementary-material

SUPPLEMENTARY TABLE 1
Primers used in this study.

SUPPLEMENTARY TABLE 2
Ontogenic stage preferred gene lists in Figure 2B.

References

Ando, K., Carr, K. M., Colle, M., Mansfeld, B. N., and Grumet, R. (2015). Exocarp Properties and Transcriptomic Analysis of Cucumber (Cucumis sativus) Fruit Expressing Age-Related Resistance to Phytophthora capsici. *PloS One* 10, e0142133. doi: 10.1371/journal.pone.0142133

Ando, K., Hammar, S., and Grumet, R. (2009). Age-related resistance of diverse cucurbit fruit to infection by Phytophthora capsici. *J. Am. Soc. Hortic. Sci.* 134, 176–182. doi: 10.21273/JASHS.134.2.176

Asalf, B., Gadoury, D. M., Tronsmo, A. M., Seem, R. C., Dobson, A., Peres, N. A., et al. (2014). Ontogenic resistance of leaves and fruit, and how leaf folding influences the distribution of powdery mildew on strawberry plants colonized by Podosphaera aphanis. *Phytopathology* 104, 954–963. doi: 10.1094/PHYTO-12-13-0345-R

Bao, Z., and Hua, J. (2014). Interaction of CPR5 with cell cycle regulators UVI4 and OSD1 in Arabidopsis. *PloS One* 9, e100347. doi: 10.1371/journal.pone.0100347

Bar, M., and Ori, N. (2014). Leaf development and morphogenesis. *Development* 141, 4219–4230. doi: 10.1242/dev.106195

Berens, M. L., Wolinska, K. W., Spaepen, S., Ziegler, J., Nobori, T., Nair, A., et al. (2019). Balancing trade-offs between biotic and abiotic stress responses through leaf age-dependent variation in stress hormone cross-talk. *Proc. Natl. Acad. Sci. U.S.A.* 116, 2364–2373. doi: 10.1073/pnas.1817233116

Bowling, S. A., Guo, A., Cao, H., Gordon, A. S., Klessig, D. F., and Dong, X. (1994). A mutation in Arabidopsis that leads to constitutive expression of systemic acquired resistance. *Plant Cell* 6, 1845–1857. doi: 10.1105/tpc.6.12.1845

Cackett, L., Luginbuehl, L. H., Schreier, T. B., Lopez-Juez, E., and Hibberd, J. M. (2022). Chloroplast development in green plant tissues: the interplay between light, hormone, and transcriptional regulation. *New Phytol.* 233, 2000–2016. doi: 10.1111/nph.17839

Cao, H., Glazebrook, J., Clarke, J. D., Volko, S., and Dong, X. (1997). The Arabidopsis NPR1 gene that controls systemic acquired resistance encodes a novel protein containing ankyrin repeats. *Cell* 88, 57–63. doi: 10.1016/S0092-8674(00)81858-9

Chan, C. (2022). Progress in salicylic acid-dependent signaling for growth-defense trade-off. *Cells* 11, 2985. doi: 10.3390/cells11192985

Churchman, M. L., Brown, M. L., Kato, N., Kirik, V., Hulskamp, M., Inze, D., et al. (2006). SIAMESE, a plant-specific cell cycle regulator, controls endoreplication onset in Arabidopsis thaliana. *Plant Cell* 18, 3145–3157. doi: 10.1105/tpc.106.044834

Cox, K. L., Meng, F., Wilkins, K. E., Li, F., Wang, P., Booher, N. J., et al. (2017). TAL effector driven induction of a SWEET gene confers susceptibility to bacterial blight of cotton. *Nat. Commun.* 8, 15588. doi: 10.1038/ncomms15588

Despres, C., Chubak, C., Rochon, A., Clark, R., Bethune, T., Desveaux, D., et al. (2003). The Arabidopsis NPR1 disease resistance protein is a novel cofactor that confers redox regulation of DNA binding activity to the basic domain/leucine zipper transcription factor TGA1. *Plant Cell* 15, 2181–2191. doi: 10.1105/tpc.012849

Develey-Riviere, M. P., and Galiana, E. (2007). Resistance to pathogens and host developmental stage: a multifaceted relationship within the plant kingdom. *New Phytol.* 175, 405–416. doi: 10.1111/j.1469-8137.2007.02130.x

Ding, Y., Sun, T., Ao, K., Peng, Y., Zhang, Y., Li, X., et al. (2018). Opposite roles of salicylic acid receptors NPR1 and NPR3/NPR4 in transcriptional regulation of plant immunity. *Cell* 173, 1454–1467.e1415. doi: 10.1016/j.cell.2018.03.044

Du, F., Guan, C., and Jiao, Y. (2018). Molecular mechanisms of leaf morphogenesis. *Mol. Plant* 11, 1117–1134. doi: 10.1016/j.molp.2018.06.006

Fan, W., and Dong, X. (2002). *In vivo* interaction between NPR1 and transcription factor TGA2 leads to salicylic acid-mediated gene activation in Arabidopsis. *Plant Cell* 14, 1377–1389. doi: 10.1105/tpc.001628

Fu, Z. Q., Yan, S., Saleh, A., Wang, W., Ruble, J., Oka, N., et al. (2012). NPR3 and NPR4 are receptors for the immune signal salicylic acid in plants. *Nature* 486, 228–232. doi: 10.1038/nature11162

Gambino, G., Perrone, I., and Gribaudo, I. (2008). A rapid and effective method for RNA extraction from different tissues of grapevine and other woody plants. *Phytochem. Anal.* 19, 520–525. doi: 10.1002/pca.1078

George Thompson, A. M., Iancu, C. V., Neet, K. E., Dean, J. V., and Choe, J.-Y. (2017). Differences in salicylic acid glucose conjugations by UGT74F1 and UGT74F2 from Arabidopsis thaliana. *Sci. Rep.* 7, 46629. doi: 10.1038/srep46629

Gu, Z. (2022). Complex heatmap visualization. *Imeta* 1, e43. doi: 10.1002/imt2.43

Gu, Z., Eils, R., and Schlesner, M. (2016). Complex heatmaps reveal patterns and correlations in multidimensional genomic data. *Bioinformatics* 32, 2847–2849. doi: 10.1093/bioinformatics/btw313

Gugel, I. L., and Soll, J. (2017). Chloroplast differentiation in the growing leaves of Arabidopsis thaliana. *Protoplasma* 254, 1857–1866. doi: 10.1007/s00709-016-1057-9

Gusberti, M., Gessler, C., and Broggini, G. A. (2013). RNA-Seq analysis reveals candidate genes for ontogenic resistance in Malus-Venturia pathosystem. *PloS One* 8, e78457. doi: 10.1371/journal.pone.0078457

Hamdoun, S., Zhang, C., Gill, M., Kumar, N., Churchman, M., Larkin, J. C., et al. (2016). Differential roles of two homologous cyclin-dependent kinase inhibitor genes in regulating cell cycle and innate immunity in Arabidopsis. *Plant Physiol.* 170, 515–527. doi: 10.1104/pp.15.01466

Hellemans, J., Mortier, G., De Paepe, A., Speleman, F., and Vandesompele, J. (2007). qBase relative quantification framework and software for management and automated analysis of real-time quantitative PCR data. *Genome Biol.* 8, 1–14. doi: 10.1186/gb-2007-8-2-r19

Hu, L., Qi, P., Peper, A., Kong, F., Yao, Y., and Yang, L. (2023). Distinct function of SPL genes in age-related resistance in Arabidopsis. *PloS Pathog.* 19, e1011218. doi: 10.1371/journal.ppat.1011218

Hu, L., and Yang, L. (2019). Time to fight: Molecular mechanisms of age-related resistance. *Phytopathology* 109, 1500–1508. doi: 10.1094/PHYTO-11-18-0443-RVW

Huang, P., Dong, Z., Guo, P., Zhang, X., Qiu, Y., Li, B., et al. (2020). Salicylic acid suppresses apical hook formation via NPR1-mediated repression of EIN3 and EIL1 in Arabidopsis. *Plant Cell* 32, 612–629. doi: 10.1105/tpc.19.00658

Huot, B., Yao, J., Montgomery, B. L., and He, S. Y. (2014). Growth-defense tradeoffs in plants: a balancing act to optimize fitness. *Mol. Plant* 7, 1267–1287. doi: 10.1093/mp/ssu049

Jarvis, P., and López-Juez, E. (2013). Biogenesis and homeostasis of chloroplasts and other plastids. *Nat. Rev. Mol. Cell Biol.* 14, 787–802. doi: 10.1038/nrm3702

Klepikova, A. V., Kasianov, A. S., Gerasimov, E. S., Logacheva, M. D., and Penin, A. A. (2016). A high resolution map of the Arabidopsis thaliana developmental transcriptome based on RNA-seq profiling. *Plant J.* 88, 1058–1070. doi: 10.1111/tpj.13312

Lefevere, H., Bauters, L., and Gheysen, G. (2020). Salicylic acid biosynthesis in plants. *Front. Plant Sci.* 11, 338. doi: 10.3389/fpls.2020.00338

Li, A., Sun, X., and Liu, L. (2022). Action of salicylic acid on plant growth. *Front. Plant Sci.* 13, 878076. doi: 10.3389/fpls.2022.878076

Li, X., Clarke, J. D., Zhang, Y., and Dong, X. (2001). Activation of an EDS1-mediated R-gene pathway in the snc1 mutant leads to constitutive, NPR1-independent pathogen resistance. *Mol. Plant Microbe Interact.* 14, 1131–1139. doi: 10.1094/MPMI.2001.14.10.1131

Liu, Y., Sun, T., Sun, Y., Zhang, Y., Radojicic, A., Ding, Y., et al. (2020). Diverse roles of the salicylic acid receptors NPR1 and NPR3/NPR4 in plant immunity. *Plant Cell* 32, 4002–4016. doi: 10.1105/tpc.20.00499

Mansfeld, B. N., Colle, M., Kang, Y., Jones, A. D., and Grumet, R. (2017). Transcriptomic and metabolomic analyses of cucumber fruit peels reveal a developmental increase in terpenoid glycosides associated with age-related resistance to Phytophthora capsici. *Hortic. Res.* 4, 17022. doi: 10.1038/hortres.2017.22

Martínez, C., Pons, E., Prats, G., and León, J. (2004). Salicylic acid regulates flowering time and links defence responses and reproductive development. *Plant J.* 37, 209–217. doi: 10.1046/j.1365-313X.2003.01954.x

McGarry, R. C., Prewitt, S. F., Culpepper, S., Eshed, Y., Lifschitz, E., Ayre, B. G., et al. (2016). Monopodial and sympodial branching architecture in cotton is differentially regulated by the Gossypium hirsutum SINGLE FLOWER TRUSS and SELF-PRUNING orthologs. *New Phytologist* 212, 244–258.

Menges, M., Samland, A. K., Planchais, S., and Murray, J. A. (2006). The D-type cyclin CYCD3; 1 is limiting for the G1-to-S-phase transition in Arabidopsis. *Plant Cell* 18, 893–906. doi: 10.1105/tpc.105.039636

Mijatović, J., Severns, P. M., Kemerait, R. C., Walcott, R. R., and Kvitko, B. H. (2021). Patterns of seed-to-seedling transmission of Xanthomonas citri pv. malvacearum, the causal agent of cotton bacterial blight. *Phytopathology®* 111, 2176–2184. doi: 10.1094/PHYTO-02-21-0057-R

Morris, K., Mackerness, S. A. H., Page, T., John, C. F., Murphy, A. M., Carr, J. P., et al. (2000). Salicylic acid has a role in regulating gene expression during leaf senescence. *Plant J.* 23, 677–685. doi: 10.1046/j.1365-313x.2000.00836.x

Nath, U., Crawford, B. C., Carpenter, R., and Coen, E. (2003). Genetic control of surface curvature. *Science* 299, 1404–1407. doi: 10.1126/science.1079354

Nawrath, C., Heck, S., Parinthawong, N., and Métraux, J.-P. (2002). EDS5, an essential component of salicylic acid–dependent signaling for disease resistance in Arabidopsis, is a member of the MATE transporter family. *Plant Cell* 14, 275–286. doi: 10.1105/tpc.010376

Nawrath, C., and Metraux, J. P. (1999). Salicylic acid induction-deficient mutants of Arabidopsis express PR-2 and PR-5 and accumulate high levels of camalexin after pathogen inoculation. *Plant Cell* 11, 1393–1404. doi: 10.1105/tpc.11.8.1393

Nelissen, H., Rymen, B., Jikumaru, Y., Demuynck, K., Van Lijsebettens, M., Kamiya, Y., et al. (2012). A local maximum in gibberellin levels regulates maize leaf growth by spatial control of cell division. *Curr. Biol.* 22, 1183–1187. doi: 10.1016/j.cub.2012.04.065

Ori, N., Cohen, A. R., Etzioni, A., Brand, A., Yanai, O., Shleizer, S., et al. (2007). Regulation of LANCEOLATE by miR319 is required for compound-leaf development in tomato. *Nat. Genet.* 39, 787–791. doi: 10.1038/ng2036

Pan, J., Zhao, F., Zhang, G., Pan, Y., Sun, L., Bao, N., et al. (2019). Control of *de novo* root regeneration efficiency by developmental status of Arabidopsis leaf explants. *J. Genet. Genomics* 46, 133–140. doi: 10.1016/j.jgg.2019.03.001

Pasternak, T., Groot, E. P., Kazantsev, F. V., Teale, W., Omelyanchuk, N., Kovrizhnykh, V., et al. (2019). Salicylic acid affects root meristem patterning via auxin distribution in a concentration-dependent manner. *Plant Physiol.* 180, 1725–1739. doi: 10.1104/pp.19.00130

Pfaffl, M. W. (2007). "Relative quantification". in *Real-time PCR* (Milton Park, in Oxfordshire: Taylor & Francis), 89–108.

Pogson, B. J., Ganguly, D., and Albrecht-Borth, V. (2015). Insights into chloroplast biogenesis and development. *Biochim. Biophys. Acta* 1847, 1017–1024. doi: 10.1016/j.bbabio.2015.02.003

Rekhter, D., Ludke, D., Ding, Y., Feussner, K., Zienkiewicz, K., Lipka, V., et al. (2019). Isochorismate-derived biosynthesis of the plant stress hormone salicylic acid. *Science* 365, 498–502. doi: 10.1126/science.aaw1720

Rivas-San Vicente, M., and Plasencia, J. (2011). Salicylic acid beyond defence: its role in plant growth and development. *J. Exp. Bot.* 62, 3321–3338. doi: 10.1093/jxb/err031

Serrano, M., Wang, B., Aryal, B., Garcion, C., Abou-Mansour, E., Heck, S., et al. (2013). Export of salicylic acid from the chloroplast requires the multidrug and toxin extrusion-like transporter EDS5. *Plant Physiol.* 162, 1815–1821. doi: 10.1104/pp.113.218156

Sinha, N. (1999). Leaf development in angiosperms. *Annu. Rev. Plant Physiol. Plant Mol. Biol.* 50, 419–446. doi: 10.1146/annurev.arplant.50.1.419

Smith, A., Lovelace, A. H., and Kvitko, B. H. (2018). Validation of RT-qPCR approaches to monitor Pseudomonas syringae gene expression during infection and exposure to pattern-triggered immunity. *Mol. Plant-Microbe Interact.* 31, 410–419. doi: 10.1094/MPMI-11-17-0270-TA

Twomey, M. C., Wolfenbarger, S. N., Woods, J. L., and Gent, D. H. (2015). Development of partial ontogenic resistance to powdery mildew in hop cones and its management implications. *PloS One* 10, e0120987. doi: 10.1371/journal.pone.0120987

Ullah, C., Chen, Y.-H., Ortega, M. A., and Tsai, C.-J. (2023). The diversity of salicylic acid biosynthesis and defense signaling in plants: Knowledge gaps and future opportunities. *Curr. Opin. Plant Biol.* 72, 102349. doi: 10.1016/j.pbi.2023.102349

Vaca, E., Behrens, C., Theccanat, T., Choe, J. Y., and Dean, J. V. (2017). Mechanistic differences in the uptake of salicylic acid glucose conjugates by vacuolar membrane-enriched vesicles isolated from Arabidopsis thaliana. *Physiol. Plant.* 161, 322–338. doi: 10.1111/ppl.12602

Vanacker, H., Lu, H., Rate, D. N., and Greenberg, J. T. (2001). A role for salicylic acid and NPR1 in regulating cell growth in Arabidopsis. *Plant J.* 28, 209–216. doi: 10.1046/j.1365-313X.2001.01158.x

van Butselaar, T., and Van den Ackerveken, G. (2020). Salicylic acid steers the growth-immunity tradeoff. *Trends Plant Sci.* 25, 566–576. doi: 10.1016/j.tplants.2020.02.002

van Wersch, R., Li, X., and Zhang, Y. (2016). Mighty dwarfs: Arabidopsis autoimmune mutants and their usages in genetic dissection of plant immunity. *Front. Plant Sci.* 7, 1717. doi: 10.3389/fpls.2016.01717

Vogel, J., and Somerville, S. (2000). Isolation and characterization of powdery mildew-resistant Arabidopsis mutants. *Proc. Natl. Acad. Sci. U.S.A.* 97, 1897–1902. doi: 10.1073/pnas.030531997

Xia, J., Zhao, H., Liu, W., Li, L., and He, Y. (2009). Role of cytokinin and salicylic acid in plant growth at low temperatures. *Plant Growth Regul.* 57, 211–221. doi: 10.1007/s10725-008-9338-8

Xu, L., Zhao, H., Ruan, W., Deng, M., Wang, F., Peng, J., et al. (2017). ABNORMAL INFLORESCENCE MERISTEM1 functions in salicylic acid biosynthesis to maintain proper reactive oxygen species levels for root meristem activity in rice. *Plant Cell* 29, 560–574. doi: 10.1105/tpc.16.00665

Yang, L., Teixeira, P. J. P. L., Biswas, S., Finkel, O. M., He, Y., Salas-Gonzalez, I., et al. (2017). Pseudomonas syringae type III effector hopBB1 promotes host transcriptional repressor degradation to regulate phytohormone responses and virulence. *Cell Host Microbe* 21, 156–168. doi: 10.1016/j.chom.2017.01.003

Zheng, X. Y., Spivey, N. W., Zeng, W., Liu, P. P., Fu, Z. Q., Klessig, D. F., et al. (2012). Coronatine promotes Pseudomonas syringae virulence in plants by activating a signaling cascade that inhibits salicylic acid accumulation. *Cell Host Microbe* 11, 587–596. doi: 10.1016/j.chom.2012.04.014

Zhou, P., Zavaliev, R., Xiang, Y., and Dong, X. (2023). Seeing is believing: Understanding functions of NPR1 and its paralogs in plant immunity through cellular and structural analyses. *Curr. Opin. Plant Biol.* 73, 102352. doi: 10.1016/j.pbi.2023.102352

Zou, Y., Wang, S., Zhou, Y., Bai, J., Huang, G., Liu, X., et al. (2018). Transcriptional regulation of the immune receptor FLS2 controls the ontogeny of plant innate immunity. *Plant Cell* 30, 2779–2794. doi: 10.1105/tpc.18.00297

frontiers | Frontiers in Plant Science

TYPE Original Research
PUBLISHED 02 August 2024
DOI 10.3389/fpls.2024.1401526

OPEN ACCESS

EDITED BY
Brigitte Mauch-Mani,
Université de Neuchâtel, Switzerland

REVIEWED BY
Ho-jong Ju,
Jeonbuk National University,
Republic of Korea
Rafael F. Rivera-Bustamante,
Center for Research and Advanced Studies, Mexico

*CORRESPONDENCE
Selvaraju Kanagarajan
selvaraju.kanagarajan@slu.se
Raveendran Muthurajan
raveendrantnau@gmail.com
Sudha Manickam
sudhatamil@gmail.com

†These authors have contributed equally to this work

RECEIVED 15 March 2024
ACCEPTED 17 June 2024
PUBLISHED 02 August 2024

CITATION
Balasubramaniam M, Thangavel T, Aiyanathan KEA, Rathnasamy SA, Rajagopalan VR, Subbarayalu M, Natesan S, Kanagarajan S, Muthurajan R and Manickam S (2024) Unveiling mungbean yellow mosaic virus: molecular insights and infectivity validation in mung bean (*Vigna radiata*) via infectious clones. *Front. Plant Sci.* 15:1401526. doi: 10.3389/fpls.2024.1401526

Unveiling mungbean yellow mosaic virus: molecular insights and infectivity validation in mung bean (*Vigna radiata*) via infectious clones

Madhumitha Balasubramaniam[1,2†], Tamilnayagan Thangavel[3], Karupiah Eraivan Arutkani Aiyanathan[1], Sakthi Ambothi Rathnasamy[4], Veera Ranjani Rajagopalan[4], Mohankumar Subbarayalu[4], Senthil Natesan[4], Selvaraju Kanagarajan[5,6*], Raveendran Muthurajan[4*] and Sudha Manickam[4*†]

[1]Department of Plant Pathology, Agricultural College and Research Institute, Tamil Nadu Agricultural University, Madurai, Tamil Nadu, India, [2]School of Agricultural Sciences, Karunya Institute of Technology and Sciences, Coimbatore, Tamil Nadu, India, [3]Department of Agricultural Entomology, Tamil Nadu Agricultural University, Coimbatore, Tamil Nadu, India, [4]Department of Biotechnology, Center for Plant Molecular Biology and Biotechnology, Tamil Nadu Agricultural University, Coimbatore, Tamil Nadu, India, [5]Department of Plant Breeding, Swedish University of Agricultural Sciences, Lomma, Sweden, [6]School of Science and Technology, The Life Science Centre, Örebro University, Örebro, Sweden

Yellow mosaic disease (YMD) with typical symptoms of alternating bright yellow to green patches associated with stunting, downward cupping, and wrinkling has been observed in mung bean on agricultural farms in Coimbatore, Tamil Nadu, India. PCR using gene-specific primers indicated the presence of the yellow mosaic virus in symptomatic plants. Rolling circle amplification (RCA) followed by restriction digestion detected ~2.7 kb of DNA-A and DNA-B, allowing the identification of a bipartite genome. The full-length genome sequences were deposited in NCBI GenBank with the accession numbers MK317961 (DNA-A) and MK317962 (DNA-B). Sequence analysis of DNA-A showed the highest sequence identity of 98.39% to the DNA-A of mungbean yellow mosaic virus (MYMV)-Vigna radiata (MW736047), while DNA-B exhibited the highest level of identity (98.21%) to the MYMV-Vigna aconitifolia isolate (DQ865203) reported from Tamil Nadu. Recombinant analysis revealed distinct evidence of recombinant breakpoints of DNA-A within the region encoding the open reading frame (ORF) AC2 (transcription activation protein), with the major parent identified as MYMV-PA1 (KC9111717) and the potential minor parent as MYMV-Namakkal (DQ86520.1). Interestingly, a recombination event in the common region (CR) of DNA-B, which encodes the nuclear shuttle protein and the movement protein, was detected. MYMIV-M120 (FM202447) and MYMV-Vigna (AJ132574) were identified as the event's major and minor parents, respectively. This large variation in DNA-B led us to suspect a recombination in DNA-B. Dimeric MYMV infectious clones were

constructed, and the infectivity was confirmed through agroinoculation. In future prospects, unless relying on screening using whiteflies, breeders and plant pathologists can readily use this agroinoculation procedure to identify resistant and susceptible cultivars to YMD.

KEYWORDS

mungbean yellow mosaic virus, cloning, yellow mosaic disease, agroinoculation, phylogeny, recombinant analysis

1 Introduction

Yellow mosaic disease (YMD) in legumes is one of the important constraints for pulse production in India (Varma and Malathi, 2003). Significant pulse crops such as black gram (*Vigna mungo*), moth bean (*Vigna aconitifolia*), lima bean (*Phaseolus lunatus*), pigeon pea (*Cajanus cajan*), French bean (*Phaseolus vulgaris*), cowpea (*Vigna unguiculata*), dolichos (*Lablab purpureus*), horse gram (*Macrotyloma uniflorum*), and soybean (*Glycine max*) are widely impacted by YMD infection (Ramesh et al., 2017). YMD-infected plants generally exhibit symptoms in the form of alternating green and yellow mosaic patterns on the leaves, followed by necrosis, internode shortening, and severe stunting of plants with malformed pods that contain tiny, immature, and shriveled seeds, with yield losses ranging from 5% to 100% (Rathi, 2002; Habib et al., 2007). In parts of South and Southeast Asia, four separate bipartite begomoviruses (yellow mosaic viruses, YMVs) have been reported as the cause of YMD in legumes, i.e., mungbean yellow mosaic virus (MYMV), mungbean yellow mosaic India virus (MYMIV), horse gram yellow mosaic virus (HgYMV), and *Dolichos* yellow mosaic virus (DoYMV) (Padidam et al., 1999). In India, MYMV and MYMIV are the most important YMVs, infecting many legumes. Interestingly, MYMV is most prevalent in the southern and western regions (Karthikeyan et al., 2004; Girish and Usha, 2005; Fauquet et al., 2008), whereas MYMIV is predominant in the northern, central, and eastern regions (Usharani et al., 2004). However, recently, MYMIV has been reported in South India, while MYMV has been reported in North India (Reddy et al., 2015). YMV belongs to the genus *Begomovirus*, under the family Geminiviridae, with twin geminate particles having rolling circle replication. Whiteflies (*Bemisia tabaci*) transmit the deadly begomoviruses that infect both leguminous and non-leguminous crops (Agnihotri et al., 2019; Ansar et al., 2021). The MYMV genome is characterized by a small, circular single-strand DNA with a bipartite (DNA-A and DNA-B) genome of ~2.7 kb in size with several open reading frames (ORFs). These two components share a 200-bp-long highly conserved common region (CR), which has an origin of replication (ori) and a highly conserved stem–loop or hairpin structure with the replication-assisting invariant non-nucleotide motif (TAATATTAC). Seven ORFs or genes in DNA-A (two in the virion sense and five in the complementary sense) encode the proteins needed for transcription, replication, and encapsidation. On the other hand, the DNA-B component has two ORFs in each virion sense and a complementary sense that encodes the proteins necessary for the inter- and intracellular movement of the virus (Briddon and Stanley, 2006). The development of mung bean cultivars resistant to YMD has long been considered an effective and economical method of managing MYMV (Karthikeyan et al., 2011). Previous reports have indicated that the development of resistant cultivars is substantial due to the rapid evolution of novel MYMV isolates and the complexity of the control mechanism (Akhtar et al., 2011). Therefore, an accurate description of the virus is necessary for a successful resistance breeding approach, with virus resistance screened out in the available germplasm. Field-level screening to identify resistant germplasm often fails due to the inefficacy of whitefly transmission (Sudha et al., 2013). Hence, the "agroinoculation" technique, a different approach that uses the Ti plasmid of the *Agrobacterium* for viral infection, has become superior to other phenotyping techniques in terms of infection pattern accuracy and the speed of identification of both resistant and susceptible cultivars (Sudha et al., 2013; Madhumitha et al., 2022). The present study aimed to characterize the complete genome of the MYMV isolates from mung bean in southern India. Nucleotide identity, phylogenetic relationship, and recombination analyses were assessed with those of previously reported Old World and New World begomoviruses, particularly legumoviruses, in order to identify the distinctiveness of the genome. In addition, cloning of MYMV in tandem orientation and infectivity screening using agroinoculation were performed, which could be used as additional tools for the screening of resistant lines against YMD.

2 Materials and methods

2.1 Viral source

Mung bean (*Vigna radiata* L. Wilczek) plants showing characteristic yellow mosaic, downward cupping, wrinkling,

necrosis, and stunted-like YMD symptoms were collected from fields located in southern India (11°00′21.00′′ N, 76°49′24.59′′ E), Thondamuthur, Coimbatore District, Tamil Nadu, India.

2.2 DNA extraction from virally infected samples

The total genomic DNA was extracted using a modified CTAB method (Sudha, 2009). The preliminary virus detection methods were carried out using MYMV-specific primers, i.e., coat protein (CP) and movement protein (MP) primers (Maheshwari et al., 2014).

2.3 Rolling circle amplification and cloning of the full-length viral genome

The DNA samples that were PCR-positive with the MYMV gene-specific primers were subjected to rolling circle amplification (RCA) using *phi*29 DNA polymerase (TempliPhi™ 100 Amplification Kit; Merck, Darmstadt, Germany) as per the manufacturer's protocol. The replicative DNA concatemers obtained using RCA were subjected to restriction digestion with different endonucleases, i.e., *Bam*HI, *Hind*III, *Pst*I, *Xba*I, *Eco*RI, and *Kpn*I (Thermo Scientific FastDigest, Waltham, MA, USA) for the full-length viral genomic DNA components (~2.7 kb). The linearized restricted products (~2.7 kb) were further purified, and the fragments were cloned into the cloning vector pUC18 and transformed into competent cells of the DH5α strain of *Escherichia coli*. Recombinant plasmids holding full-length genomic fragments were identified. Initially, partial sequencing was performed, and the selected clones were then sequenced through a commercial facility using the primer walking strategy at Bioserve Biotechnologies, Pvt. Ltd., Hyderabad, India.

2.4 Sequencing and sequence analysis

Database searches were carried out with NCBI BLAST (https://www.ncbi.nlm.nih.gov/) to align our viral genome sequences with those of previously reported viruses. The complete genome sequences of both DNA-A and DNA-B were analyzed using BioEdit version 7.0.9 (Hall, 1999). The ORFs were predicted using GENERUNNER (http://www.generunner.net/). The isolate in the present study was compared with the Old World and New World begomovirus sequences retrieved from the NCBI database. The complete nucleotide sequences of the full-length genomes were aligned using MUSCLE (Edgar, 2004), and the percentage pairwise nucleotide identity plot was generated using the SDTV 1.12 program (http://web.cbio.uct.ac.za/~brejnev/) (Muhire et al., 2014). A phylogenetic tree was constructed by aligning the selected full-length sequences of DNA-A and DNA-B through ClustalW (Thompson et al., 1994), and the tree was prepared using MEGA7 version 7.0.26 (Kumar et al., 2016). Bootstrap analysis with 1,000 replications was performed using the neighbor-joining method. Identification of the recombination events of MYMV DNA-A and DNA-B was analyzed using the Recombination Detection Program (RDP 4.97), which utilizes seven different algorithms: RDP, BOOTSCAN, GENECONV, MAXCHI, CHIMAERA, SISCAN, and 3SEQURE (Smith, 1992; Salminen et al., 1995; Padidam et al., 1999; Gibbs et al., 2000; Posada and Crandall, 2001; Boni et al., 2007; Martin et al., 2015). A cutoff of 0.05 was used as the *p*-value with default settings.

2.5 Construction of agroinfectious partial tandem repeat constructs and their infectivity

For the construction of infectious clones, partial tandem repeat constructs of DNA-A and DNA-B were prepared by directional cloning of a bitmer (a part of the genome with the ori), followed by further cloning of the fullmer (~2.7 kb full-length genome) of DNA-A or DNA-B. For bitmer release into DNA-A, the pUC18 plasmid (harboring the full-length 2.7-kb fragment of DNA-A) was restricted with the restriction endonucleases *Hind*III and *Pst*I. Approximately 2.4 kb, consisting of the ori, was eluted from the agarose gel and ligated into the binary vector pCAMBIA2300, restricted with the same restriction endonucleases. Recombinant colonies were screened and designated as pCamA~0.8 mer. Subsequently, one selected positive clone in the pUC18 plasmid was carried for incorporation of the full-length DNA-A genome, which was restricted with the restriction endonucleases *Hind*III/*Bgl*I and was ligated into the pCamA~0.8 mer by linearizing them through *Hind*III. Similarly, the bitmer release in DNA-B from the full-length clone in the pUC18 vector was prepared using the restriction endonucleases *Hind*III and *Sma*I. The fragment was eluted and ligated into the *Hind*III/*Sma*I-restricted pCAMBIA2300 (binary vector). The recombinant plasmid was designated as pCamB~0.4 mer. Incorporation of the full length (2.7 kb) of DNA-B from the PUC18 plasmid restriction was performed with the *Hind*III/*Pvu*II enzymes. The pCamB~0.4 mer was linearized with *Hind*III, and the full-length (2.7 kb) genome was incorporated into it. The transformation was carried out for both the DNA-A and DNA-B components with antibiotic selection. The orientation of the construct was determined through restriction analysis for both pCamA~0.8 mer, pCamB~0.4 mer, and their respective fullmer using the enzymes *Hind*III, *Pvu*II, *Sma*I, *Bgl*I, and *Pst*I.

The tandem repeat constructs of the viruses were mobilized from the *E. coli* strain XL1-Blue into the *Agrobacterium tumefaciens* strain LBA 4404 (Hood et al., 1993) using pRK 2013 as a helper plasmid in a triparental mating system (Ditta et al., 1980). The distinct colonies that appeared were confirmed transconjugants through colony PCR using internal primers specific to the DNA-A and DNA-B genomes. *Agrobacterium* harboring the viral DNA components was grown in Luria–Bertani (LB) broth at 28°C with shaking at 200 rpm. The overnight-grown lawn of bacterial growth was collected and resuspended in *Agrobacterium* (AB) minimal medium (OD_{600} = 0.8) and used for agroinoculation. The *Agrobacterium* cultures containing the constructs of DNA-A and DNA-B were mixed in equal proportion, and 30 µl of the culture

was inoculated on 2-day-old sprouted seeds of 20 cultivars of mung bean [i.e., VGGRU2, VGGRU3, VGGRU4, CO8, CO7, CO980, PUSA-118, PUSA-9871, VBN (Gg)2, PLS-316, LM469, Bapatla, VGGRU1, NDM 5–3, AVT/RMI-6/1, Maduramoong, SML119, PUSA-0672, PUSA-101, and VRM (Gg)1] after puncturing the hypocotyl region with a 30-G needle using the seed-sprout method (Mandal et al., 1997). Infection was carried out at 25°C for 12 h in the dark. Subsequently, the seedlings were washed with sterile single-distilled water and sown in soil/compost (1:1) in a controlled growth chamber at 25°C with a proper relative humidity of 60%–70% and a photoperiod of 16/18 h. Hoagland's solution was sprayed twice a week for the proper growth and development of plants. The uninoculated plants without agroinoculation were maintained as controls. The observation of symptoms in the trifoliate leaves was recorded after the 15th day of inoculation. The plants were identified as susceptible or resistant based on the presence or absence of yellow mosaic symptoms at a given time across replications. Scaling was conducted based on the rating (Singh et al., 1992). Leaves with typical YMD symptoms were collected 15–17 days after inoculation for DNA analysis and were confirmed through PCR using the CP primers.

3 Results

The digested RCA products revealed a single band of size ~2.7 kb on restriction with *Hind*III and *Pst*I. In comparison, *Hind*III was found to be a unique cutter in the viral genome for both DNA-A and DNA-B (Figure 1A) and was further utilized for the construction of infectious clones. The ~2.7-kb band of digested products was cloned. Five transformed clones (~2.7 kb) were identified and partially sequenced for DNA-A and DNA-B. The sequence analysis for obtaining potential ORFs using ORF Finder (http://www.ncbi.nlm.nih.gov/gorf/gorf.html) revealed three clones that had an arrangement of genes typical of DNA-A components.

In contrast, two clones had an arrangement typical of DNA-B components of bipartite begomoviruses, and no satellite DNA was observed. The complete nucleotide sequence for one of each clone of DNA-A and DNA-B was determined in both orientations through primer walking. The nucleotide sequences of the DNA-A and DNA-B components were determined to be 2,726 and 2,739 bp, respectively. The sequence data obtained from the two clones were submitted to the GenBank database with accession numbers MK317961 (DNA-A) and MK317962 (DNA-B). The DNA

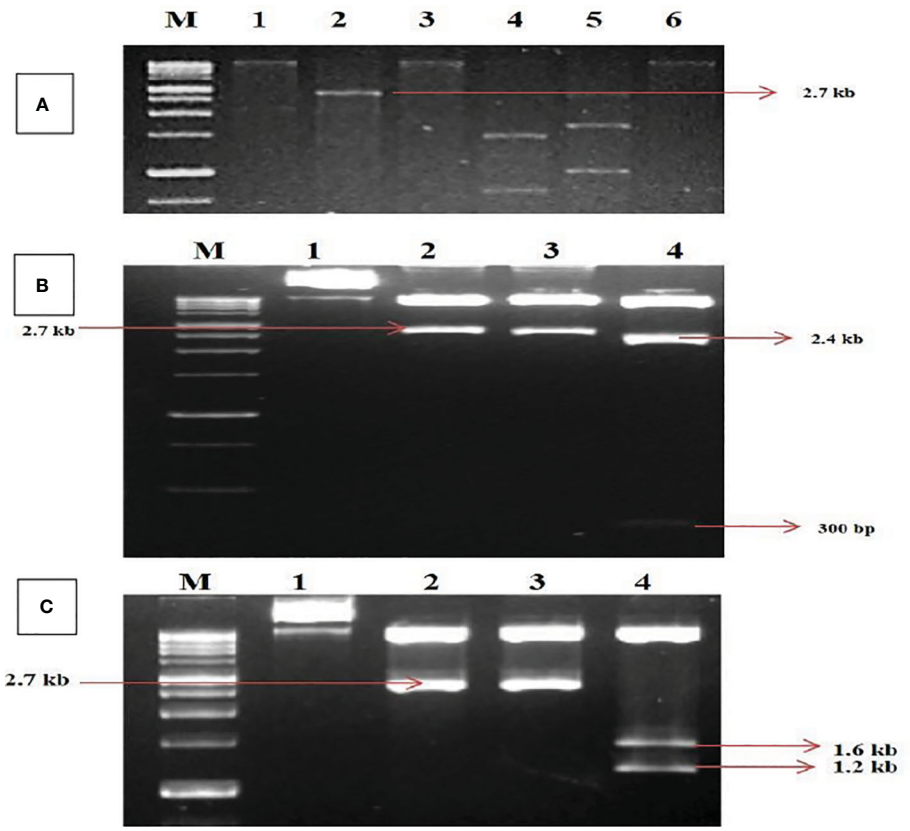

FIGURE 1
Identification and cloning of MYMV genome on tandem orientation. **(A)** Rolling circle amplification followed by restriction digestion. Lanes M (1Kb Marker),1, 2, 3, 4, 5, 6 represent digestion with *Bam*HI, *Hind*III, *Pst*I, *Xba*I, *EcoR*I and *Kpn*I respectively. **(B)** Confirmation of tandem orientation of PcamA~ 0.8 mer and full length using two different restriction endonucleases with *Hind*III and *Pst*I, Lane M - 1Kb Marker,1,2,3,4 represent Uncut plasmid DNA, a restricted product of plasmid with *Hind*III, a restricted product of plasmid with *Pst*I, a restricted product of plasmid with *Hind*III and *Pst*I. **(C)** Confirmation of tandem orientation of PcamB~ 0.4 and full length using two different restriction endonucleases with *Hind*III and *Sma*I, Lane M - 1Kb Marker,1, 2, 3, 4 represent Uncut plasmid DNA, restricted product of plasmid with *Hind*III, *Sma*I restricted product, *Hind*III and *Sma*I restricted product.

sequence studied was typical of the Old World begomoviruses, with two ORFs on the viral sense strand and four ORFs on the complementary sense strand. The viral strand consists of the ORF AV1 (~28 kDa)–CP, which overlaps with the small ORF AV2–pre-coat protein (~13 kDa), while the complementary sense strand consists of the ORF AC1–replication initiator protein (~40 kDa), ORF AC2–transcription activation protein (~15 kDa), ORF AC3–replication enhancer protein (~15 kDa), and ORF AC4–symptom determinant (~11 kDa). The DNA-B components were determined to have a genome length of 2,739 bp that encodes two ORFs: BV1–nuclear shuttle protein (~28 kDa) on the viral sense strand and BC1–MP (~33 kDa) on the complementary sense strand (Supplementary Tables S1, S2). For further characterization, the clones were designated as MK317961-MYMV-ThC03 and MK317962-MYMV-ThC15. For infectious clone construction, the full-length clones were subjected to tandem orientation cloning, and the orientation of the construct was determined through restriction analysis (Figures 1B, C).

3.1 Genome characterization of DNA-A

In the BLASTn search, the complete nucleotide sequence of DNA-A showed the highest sequence identity of 98.39% to the DNA-A of the MYMV-Vigna radiata (MYMV : MW736047) reported from Namakkal District, Tamil Nadu, India. Pairwise sequence identity of the isolate in the present study, DNA-A MK317961-MYMV-ThC03, with other selected Old World and New World begomoviruses, particularly legumoviruses in the BLASTn search, was also determined using the Sequence Demarcation Tool (SDT v1.2), which exhibited that the DNA-A of the Old World begomoviruses shared 98.2% - 98.3% identity with the MYMV reported from Tamil Nadu, India (MW736047, MW736048, MW736045, and DQ865201), followed by 84.2%–84.7% identity with HgYMV (AJ627904, OP784475, and OP777488), 80%–83.5% with MYMIV (MN885468, MN698289, and EU523045), 74%–74.6% with the *Rhynchosia* yellow mosaic virus (RhYMV) (AM999981, FM208847, and KP752090), 68.6%–69.3% with Kudzu mosaic virus (KuMV) (DQ641690, ON181435, and MW805421), 61.6%–62.3% with DoYMV (MH795972, AM157412, and KJ481204), 61.9% with the soybean mild mottle virus (SbMMoV) (GQ472984), and 58.3%–58.8% identity with the soybean chlorotic blotch virus (SbCBV) (GQ472985, GQ472987, and KC508643) (Figure 2A). Similarly, the New World begomovirus shared the highest identity of 58.3% with the common bean severe mosaic virus (CBSMV) (KX011477) from Cuba and the lowest identity of 52.9% with the beet chlorosis virus (BChV) range from the USA. The amino acid sequence of an Old World begomovirus, MYMV-DQ865201-Na06-moth bean-Indian isolate, showed 98.3%, 94.8%, 90.2%, 96.9%, and 100% sequence identity in the AC1, AC2, AC3, AC4, AV1, and AV2 ORFs, respectively. AV1 was found to be highly conserved among the six ORF proteins, with a mean value of 85% in Old World begomoviruses, followed by the AC1 protein with a mean value of 78% in amino acid levels (Supplementary Tables S3, S4). Based on the complete nucleotide sequence alignment of the MYMV DNA-A isolate of MYMV-MK31791-ThCo3 and 48 other published nucleotide sequences of the New World and Old World begomoviruses, infected host plant sequences were retrieved from the NCBI database. An outgroup of maize streak virus (MSV) was used for phylogenetic analysis. The phylogenetic analysis exhibited two main groups that were separated and diverged in the tree analysis. The separation of the New World begomoviruses from the Old World viruses was very well evident in

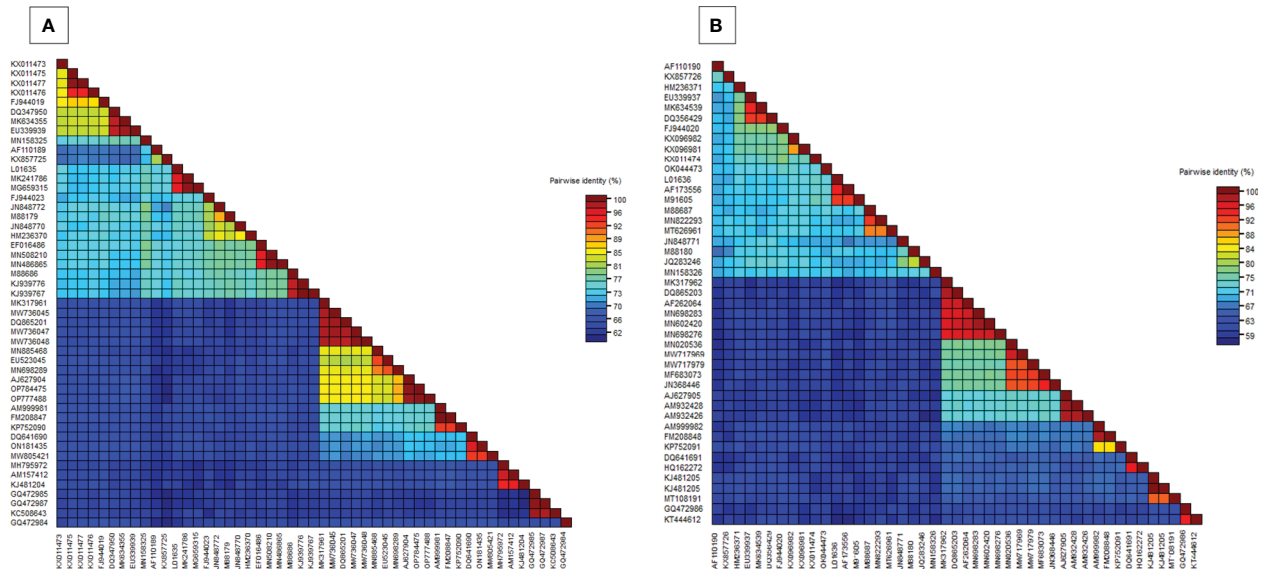

FIGURE 2
(A) Pairwise nucleotide identity matrices of DNA-A (MK317961) with previously worldwide reported begomovirus nucleotide sequences, **(B)** Pairwise nucleotide identity matrices of DNA-B (MK317962) with previously worldwide reported begomovirus nucleotide sequences.

this analysis. The first major group included all the New World begomoviruses that were diverged, closely related to each other, and placed in the first major branch (i.e., BGYMV, BChV, BLCrV, BGMV, SbBMV, BYMMxV, BWCMV, BDMV, BChMV, RhRGMV, BLV, RhGMV, CBMoV, RhMMV, and CBSMV), except for the Old World begomovirus. The isolate in the present study, DNA-A MYMV-MK31791-ThCo3, was placed in the second major group of Old World begomoviruses in clade F. They are closely related to the MYMV-Namakkal isolates, with the following accession numbers: DQ865201, MW736045, MW736047, and MW736048 (Figure 3A). The non-coding intergenic region between the ORFs AV1 and AC1 of DNA-A was found to be ~414 bp in length. Pairwise alignment of the non-coding region between ORFs AC1/AV2 in DNA-A was carried out to identify the highly conserved CR between DNA-As. The length of the deduced CR was approximately 142 nt between the cognate DNA-A and DNA-B. The CR encompasses the predicted stem and loop structure with the conserved nonanucleotide sequence TAATATTAC, which represents the origin of replication. The putative Rep-binding iteron sequence, which consists of eight nucleotide repeats, was identified to be ATCGGTGT, which occurs as one copy in the 5′ of the CR and as two tandem repeats upstream of the TATA box in DNA-A.

3.2 Genome characterization of DNA-B

BLASTn search analysis of the DNA-B nucleotide sequence revealed the highest sequence identity (98.21%) to the other MYMV-Vigna aconitifolia (DQ865203) reported from Namakkal District, Tamil Nadu, India. The pairwise sequence identity of the isolate in the present study, DNA-B MK317962-MYMV-ThC15, to the other Old World begomovirus isolates published in NCBI and the New World begomovirus isolates that appeared in the BLASTn search was determined using the Sequence Demarcation Tool (SDT v1.2). Analysis of the pairwise sequence identity of DNA-B exhibited 95.4%–98.1% identity to the MYMV isolates (DQ865203 and AF262064) from Tamil Nadu, India, followed by 70.2%–70.5% identity to DNA-B of MYMIV, 65.70% - 66.50% to HgYMV (AJ627905, AM932428, and AM932426), 55.9%–57.2% to

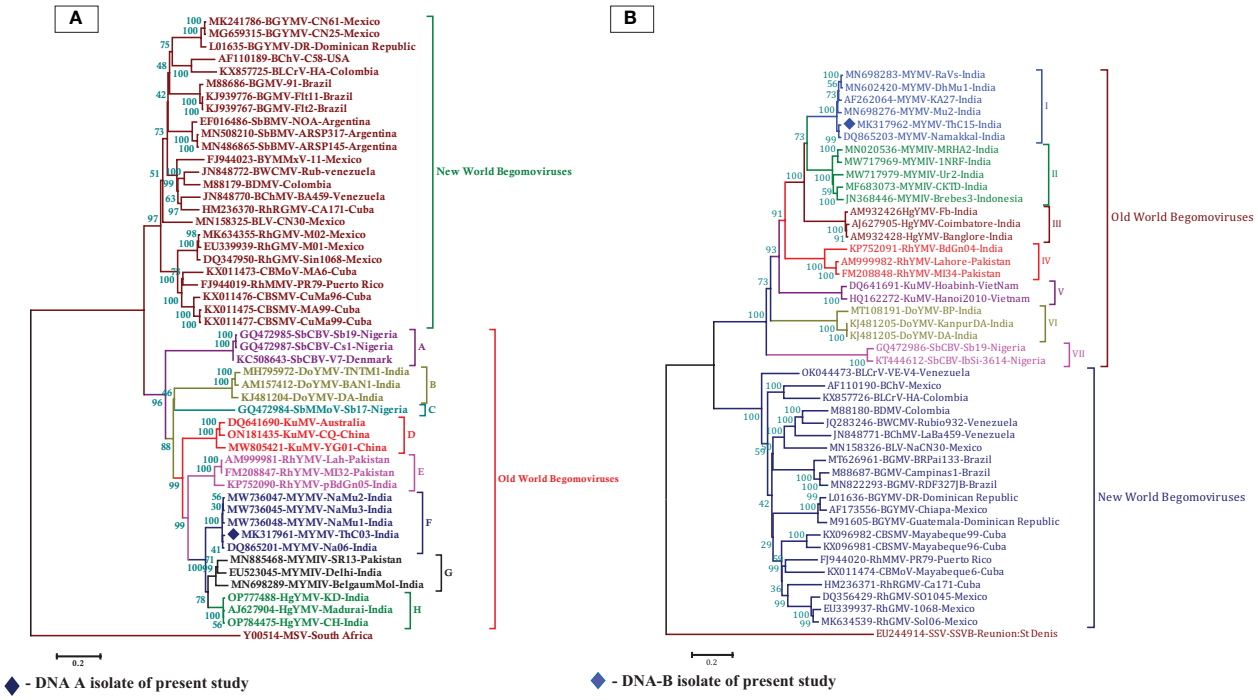

FIGURE 3
(A) Phylogenetic relationship between MYMV isolate with other Old World and New World begomoviruses generated from aligned full-length genome sequences of DNA-A, blue-filled diamond representing MK317961 (DNA-A) investigated in the present study, **(B)** The phylogenetic relationship between MYMV isolate with other Old World and New World begomoviruses generated from aligned full-length genome sequences of DNA-B, the blue filled diamond representing MK317962 (DNA-B) investigated in the present study. The tree was generated by the neighbor-joining method by aligning the sequences in MEGA 7 using CLUSTAL W. Vertical branches are arbitrary; horizontal branches are proportional to calculated mutation distance values at nodes indicated percentage bootstraps values (1000 replicates). mungbean yellow mosaic virus (MYMV), mungbean yellow mosaic India virus (MYMIV), dolichos yellow mosaic virus (DoYMV), kudzu mosaic virus (KuMV), horsegram yellow mosaic virus (HgYMV), rhynchosia yellow mosaic virus (RhYMV), soybean chlorotic blotch virus (SbCBV), rhynchosia rugose golden mosaic virus (RhRGMV), rhynchosia mild mosaic virus (RhMMV), rhynchosia golden mosaic virus (RhGMV), bean calico mosaic virus (BChV), common bean severe mosaic virus (CBSMV), common bean mottle virus (CBMoV), bean golden mosaic virus (BGMV), bean chlorosis virus (BChMV), bean dwarf mosaic virus (BDMV), bean white chlorotic mosaic virus (BWCMV), bean leaf crumple virus (BLCrV), bean latent virus (BLV), bean golden yellow mosaic virus (BGYMV), bean yellow mosaic Mexico virus (BYMMxV), maize streak virus (MSV), soybean mild mottle virus (SbMMoV), soybean blistering mosaic virus (SbBMV), sugarcane streak virus (SSV).

RhYMV (AM999982, FM208848, and KP752091), 53.90%–54.70% identity to KuMV (DQ641691 and HQ162272), 48.40%–49.80% identity to DoYMV (MT108191 and KJ481205), and 45%–45.3% identity to SbCBV (KT444612 and GQ472986) (Figure 2B). The amino acid sequences showed the highest sequence identity of 100% to both nuclear shuttle and movement proteins of MYMV DNA-B (MN602420), followed by 100% (MP) and 99.6% (NSP) identity to MYMV DNA-B (DQ865203), 99.6% (NSP) and 100% (MP) identity to MYMV DNA-B (MN698276), and 99.6% (NSP) and 98.4% (MP) identity to MYMV DNA-B (AF262064) (Supplementary Tables S5, S6).

Phylogenetic analysis of the isolate in the present study (MK317962-MYMV-ThC15) was performed with 46 DNA-B sequences, which were retrieved from the NCBI database, of which 23 nucleotide sequences were from Old World begomoviruses and 21 were from New World begomoviruses. An outgroup of Sugarcane streak virus (SSV) was used in the analysis. The phylogenetic distribution showed that two main groups diverged in the tree analysis. This indicates that the Old World begomovirus isolates were placed into the first major group and the New World begomovirus isolates were grouped into the second main branch. The isolate in the present study, DNA-B MK317962-MYMV-ThC15, was grouped in clade I of the first major branch, which is closely related to the other MYMV isolates (MN698283, MN602420, AF262064, and DQ865203) reported from Tamil Nadu, India (Figure 3B). In the case of the DNA-B component, the non-coding intergenic region is ~986 bp in length. In the case of DNA-B, one of the tandem repeats of iteron is ATTGGTGT. In the CR, TATA motifs were seen at nucleotide coordinates 2,681–2,684. The divergence between DNA-A and DNA-B included 22 deletions in DNA-A with respect to DNA-B and 12 SNPs between DNA-A and DNA-B.

3.3 Recombinant analysis

Recombination analysis for isolate MYMV in the present study was performed using the Recombinant Detection Programme (RDP 4.97) to identify the potential recombinant parental isolates and recombinant breakpoints. In the RDP analysis, DNA-A (MYMV-MK31791-ThCo3) along with 25 New World and 23 Old World begomovirus nucleotide sequences and DNA-B (MK317961-MYMV-ThC15) with the 21 New World and 23 Old World begomovirus nucleotide sequences retrieved from the NCBI database from different host plants were analyzed. The RDP results for DNA-A showed that 15 recombination events were detected in the analysis. Among the 15 recombination events, 11 were detected by more than three algorithms. Interestingly, only one recombination event was detected for DNA-A (MK317961-MYMV-ThC03) using three recombination methods (GENECONV, BOOTSCAN, and SiScan), which is a single recombination event of MYMV DNA-A with recombinant breakpoints at nucleotide locations 1,436–1,584 on the genome of MYMV-ORF AC2 (transcription activation protein) in the present isolate. The present isolate contributed to the recombination event as a potential major parent identified as MYMV-PA1 (KC911717) and as a potential minor parent, MYMV-Namakkal (DQ86520). Importantly, none of the other MYMV isolates exhibited any recombination events. Compared with MYMV and MYMIV, the other begomoviruses were prone to recombination, with the recombination analysis detecting several events. The *p*-values of the identified recombination events were given in GENECONV (4.823×10^{-02}), BOOTSCAN (7.813×10^{-03}), and SiScan (7.466×10^{-03}). The same event was also detected in other MYMV isolates, including MYMV-Namakkal (DQ8652), MYMV-VN15 (JX244181), MYMV-KA27 (AF262064), and MYMV-M167 (FM955607) (Figure 4A).

Similarly, RDP analysis of the DNA-B component detected 43 recombination events. Of these, 23 events were detected by more than three algorithms, and the *p*-values were found to be significant. The isolates of DNA-B in the present study (MK317962-MYMV-ThC15) revealed the presence of two recombination events. The first recombination event pans from the nucleotide coordinates of 472 to 2,560 nt coded for the movement protein and the nuclear shuttle protein, including the ori in the stem and loop sequences. This event was found to be significant for all the algorithms employed. The *p*-values for every algorithm are given in Table 1. Interestingly, this event involved MYMV-Vigna (AJ132574) as a minor parent and MYMIV-M120 (FM202447) as a major parent. It is also significant that the same recombinational event was observed in the DNA-B components of four more MYMV isolates: MYMV-Namakkal (DQ8652.1), MYMV-VN15(JX244181), MYMV-KA27 (AF262064), and MYMV-Soy (AJ582267). The second recombination event was observed in the segment from 2,126 to 2,216 and was found to be significant only in the algorithms MAXCHI ($p = 2.117\times 10^{-01}$) and SISCAN ($p = 8.045\times 10^{-04}$). This recombination event included HgYMV-LB (AM932430.1) as a potential major parent and VbSMV-Com (FN543426.1) as a minor parent (Figure 4B).

3.4 Infectivity assay of MYMV

To assess the infectivity of the MYMV isolates, agroinfectious constructs of both genomes were introduced into the overnight-sown seeds of 20 mung bean cultivars [i.e., VGGRU2, VGGRU3, VGGRU4, CO8, CO7, CO980, PUSA-118, PUSA-9871, VBN (Gg)2, PLS-316, LM469, Bapatla, VGGRU1, NDM 5–3, AVT/RMI-6/1, Maduramoong, SML119, PUSA-0672, PUSA-101, and VRM(Gg)1] using the agroinoculation technique. When both genomic components (DNA-A + DNA-B) were co-inoculated, typical yellow mosaic symptoms were observed in mung bean at 15–20 days post-inoculation (dpi). Among the tested cultivars, VGGRU1 and PUSA-0672 were found to be resistant; VGGRU2, VGGRU3, and VGGRU4 were found to be moderately susceptible; CO8, CO7, and CO980 were found to be susceptible; and PUSA-118, PUSA-9871, PUSA-101, PLS-316, LM469, Bapatla, NDM 5–3, AVT/RMI-6/1, Maduramoong, SML119, VRM (Gg)1, and VBN (Gg)2 were found to be highly susceptible (Figure 5A). The DNA-A or DNA-B genomic components individually failed to induce disease

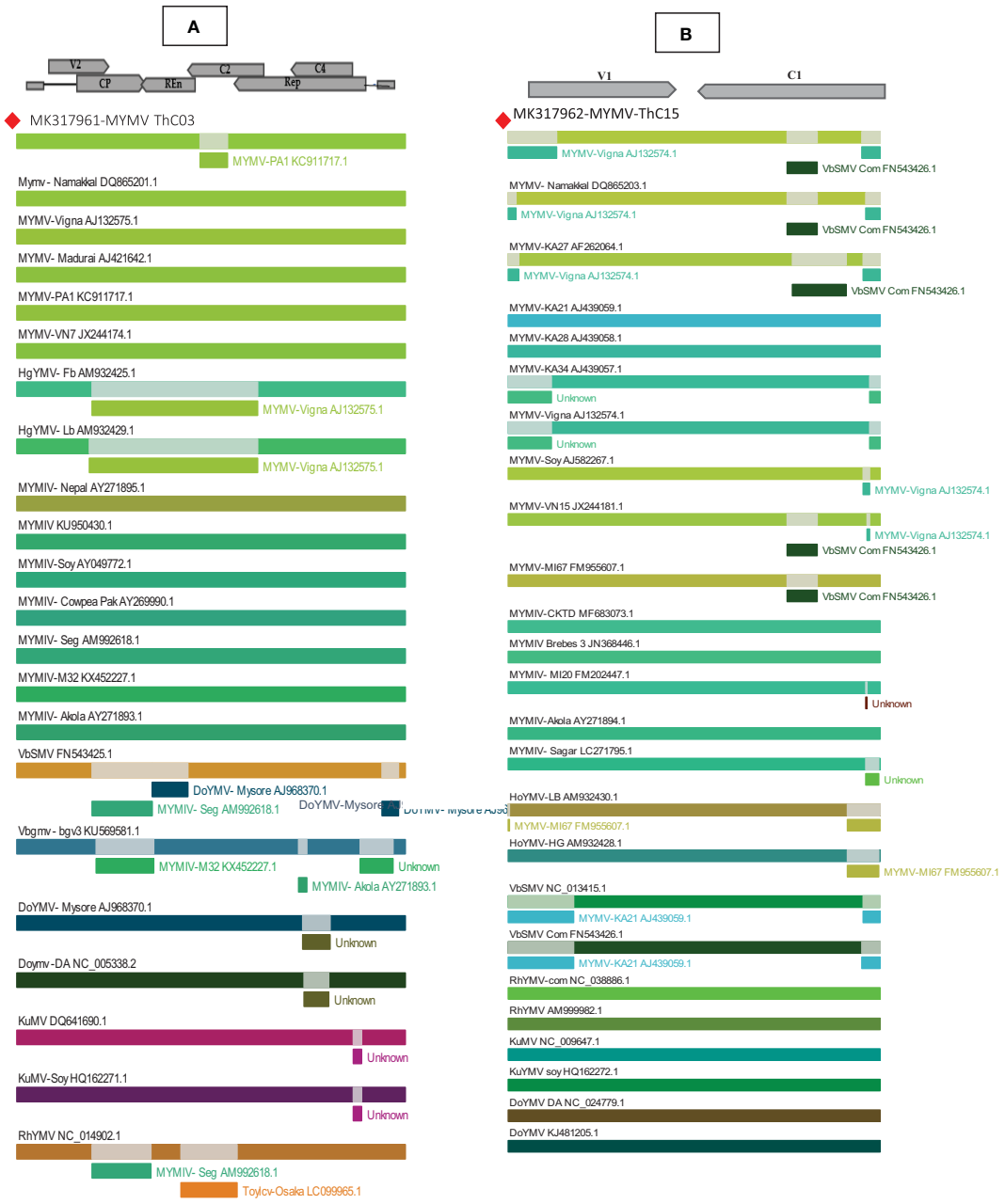

FIGURE 4
Recombination analyses of MYMV **(A)** MK317961 (DNA-A), **(B)** MK317962 (DNA-B) with other selected begomoviruses using RDP- 4.97. The top of the picture shows a linear genome map of begomoviruses, with arrows pointing in the direction of the genes to reveal recombinant segments.

symptoms. As expected, the empty vector pCAMBIA2300 (negative control) induced no disease symptoms in the test plants even after 180 dpi. The symptomatic plants were confirmed for the amplification of MYMV using PCR, with amplification on the CP region (703 bp) confirming the presence of MYMV; the resistant plants were observed with no amplification product (Figure 5B).

4 Discussion

Begomoviruses affect agricultural and horticultural crops, which include more than 300 species, and cause an estimated yield loss of as high as 100% (Nagendran et al., 2016; Zerbini et al., 2017). MYMV and MYMIV are known to cause YMD in various leguminous and non-leguminous crops (Usharani et al., 2004; Qazi et al., 2006; Biswas et al., 2008; Akhtar et al., 2011; Naimuddin et al., 2011; Shahid et al., 2012; Agnihotri et al., 2019). Madhumitha et al. (2019) surveyed the incidence of YMD in mung bean-growing areas of southern India (Coimbatore, Tamil Nadu, India) and observed severe YMD symptoms. A novel YMV isolate was identified in the survey, which was characterized by RCA (Inoue-Nagata et al., 2004), cloning, and sequencing. RCA by *phi*29 DNA polymerase offers an exclusive perspective to study the range of circular molecules of viral origin. John et al. (2008) suggested that

TABLE 1 Recombination breakpoint and major and minor parental sequences detected in MYMV DNA-B.

Recombinant isolate	Recombinant Break points		Parental isolate		Recombination Detection methods[c]	P-value[d]
	Begin	End	Major[b]	Minor[a]		
MK317962	472	2560	MYMIV-M120 (Vigna) (FM202447)	MYMV-Vigna (AJ132574)	R	1.127×10^{-08}
					G	6.857×10^{-05}
					B	$\mathbf{5.985 \times 10^{-10}}$
					M	6.220×10^{-03}
					C	2.306×10^{-0}
					S	4.632×10^{-06}
					3Seq	8.903×10^{-07}
MK317962	2126	2216	HgYMV-LB (AM932430.1)	VbSMV Com (FN543426.1)	M	2.117×10^{-01}
					S	$\mathbf{8.045 \times 10^{-04}}$

[a,b] Minor and major parental refer to isolates contributing the smaller and larger fractions of the recombinant's sequence, respectively. c, d Recombination detection methods and probability values, respectively.

RCA provides the opportunity to generate full genome-sized DNA fragments of the viruses for their characterization by utilizing *phi*29 DNA polymerase. The RCA of the YMD-infected mung bean sample from southern India identified two DNA molecules: DNA-A (2,726 bp) and DNA-B (2,679 bp). The sequence analysis revealed that the present isolate has the corresponding ORFs depicting an Old World begomovirus. Two genes are present in the virion sense (AV1 and AV2) and four in the complementary sense (AC1, AC2, AC3, and AC4) (Padidam et al., 1999; Paximadis et al., 1999; Qazi et al., 2007; Kamaal et al., 2015; Agnihotri et al., 2019; Ansar et al., 2021). The characteristic feature of the genome organization in the present study indicated that the presence of ORF AV2 in DNA-A was reported as absent in New World begomoviruses (Rybicki, 1994; Stanley et al., 2005). Interestingly, the species observed as MYMV based on their nomenclature were found to be associated with the findings of Brown et al. (2015). In general, begomoviruses of a geographical origin are grouped together due to their high degree of conservation in the coat protein region, which is required for the recognition and transmission of the virus by the whitefly genotype, which is prevalent in that region. This rule of thumb is not followed for legumoviruses (begomoviruses, especially those infecting leguminous crop species). However, the same whitefly genotypes actively transmit them and are not grouped with other begomoviruses (Fauquet et al., 2005). Exceptionally, within the legumoviruses, MYMV and MYMIV cluster together, and DoYMV occupies a separate clade (Bag et al., 2014; Akram et al., 2015; Malathi et al., 2017). The phylogenetic analysis of DNA-A and DNA-B confirmed that MYMV clustered with the other Old World legumoviruses and showed distinct variation from the cluster of New World begomoviruses.

In the present study, a major recombination event was identified *in silico* in the whole DNA-B, for which MYMIV-M120 (FM202447) and MYMV-Vigna (AJ132574) were identified as the event's major and minor parents, respectively, contributing to the inverted repeat (IR) region. This clearly indicates that the DNA-B of the MYMV-ThC15-India study is a recombinant, with the majority of the sequence derived from MYMV with a CR from MYMIV. This component exchange process, also known as pseudo-recombination for begomoviruses, has been reported for the recombinant DNA-B from India (Karthikeyan et al., 2004; John et al., 2008; Banerjee et al., 2018; Akram et al., 2020; Chowdary et al., 2022). Directly repeated sequences or short iterated elements called iterons, that are crucial to replication are present close to the TATA box and are crucial *cis*-elements in the ori that facilitate template recognition (Arguello-Astorga et al., 1994; Fontes et al., 1994). The putative Rep-binding iteron sequence, which consists of eight nucleotide repeats, was identified as ATCGGTGT, which occurs as one copy in the 5′ of the CR and as two tandem repeats upstream of the TATA box in DNA-A. In the case of DNA-B, one of the tandem repeats of the iteron is ATTGGTGT. However, DNA-B may have undergone recombination to circumvent the incompatibility between the iteron and the Rep proteins in the CR (Chowdary et al., 2022).

In disease resistance breeding programs, visual monitoring of the symptoms that occur on the plant, primarily after infection, is the main method of determining MYMV resistance. As MYMV symptoms may not always be present in the field, it can be challenging to identify the true resistant lines. These can be easily overcome by using the agroinoculation method. The primary advantage of agroinoculation is that it causes homogeneous disease symptoms that are simpler to measure than those of a natural infection (Sudha et al., 2015). To verify the infectivity and to determine the virus-resistant lines in the current study, agroinoculation screening was carried out by incubating the *Agrobacterium* cells at 28°C with a cell density of 1 (at OD_{600}), with the maximum infectivity of 100% being achieved. The agroinoculated samples, by co-delivering MYMV DNA-A and DNA-B, showed more efficacy in the identification of resistant sources compared with field screening, as reported by various

FIGURE 5
Infectivity and confirmation of cloned viral genomic component on mung bean cultivars **(A)** The symptomatic mung bean plants that were inoculated with agroinfectious constructs A. VRM(Gg)1, B. PUSA-101, C. PUSA-118, D. Maduramoong, E. VBN (Gg)2, F. PUSA-9871, G. LM 469, H. PLS-316, I. Bapatla, J. AVT/RMI-6/1, K. NDM 5-3, L. SML119, M. CO 8, N. CO7, O. CO 980, P. VGGRU2, Q. VGGRU3, R. VGGRU4, S. VGGRU1, T. PUSA – 0672, **(B)** Confirmation of MYMV resistance through MYMV coat protein primer on symptomatic B 39.50 25.29 A 39.50 25.29 plants, Lane M – 1kb marker, 1. VGGRU2, 2. VGGRU3, 3. VGGRU4, 4. CO8, 5. CO7, 6. CO980, 7. PUSA-118, 8. PUSA-9871, 9. VBN (Gg)2, 10. PLS- 316, 11. LM 469, 12. NDM 5-3, 13. VGGRU1, 14. AVT/RMI-6/1, 15. Maduramoong, 16. SML119, 17. PUSA-0672, 18. PUSA-101, 19. Bapatla, 20. VRM(Gg)1 (in this figure different gels are merged together as the gels contained many unpublished mung bean lines, the results for the cultivar in the present study were only shown and the original gels attached in Supplementary Figure (BI,BII,BIII).

researchers (Jacob et al., 2003; Usharani et al., 2004; Karthikeyan et al., 2011; Sudha et al., 2013; Bag et al., 2014; Madhumitha et al., 2022).

5 Conclusions

In future applications, breeders and plant pathologists can augment their screening techniques beyond reliance on whitefly-mediated assays by employing the agroinoculation method. This strategy presents a robust avenue for distinguishing between cultivars exhibiting resistance and susceptibility to YMD. This approach offers promising prospects, providing a reliable means to identify plant resistance, thereby enhancing breeding and disease management efforts.

Data availability statement

The original contributions presented in the study are included in the article/Supplementary Material. Further inquiries can be directed to the corresponding authors.

Author contributions

MB: Investigation, Methodology, Writing – original draft. TT: Formal analysis, Writing – review & editing. KA: Methodology, Writing – review & editing. SR: Writing – review & editing. VR: Writing – review & editing. MoS: Supervision, Writing – review & editing. SN: Writing – review & editing. SK: Conceptualization, Methodology, Writing – review & editing. RM: Investigation, Project administration, Resources, Methodology, Writing – review & editing. SM: Investigation, Supervision, Methodology, Writing – review & editing.

Funding

The author(s) declare financial support was received for the research, authorship, and/or publication of this article. The project was financial supported by DST SERB 2016–2019 (YSS/2015/000321).

Acknowledgments

We thank the Department of Biotechnology, Centre for Plant Molecular Biology and Biotechnology, Tamil Nadu Agricultural University, Coimbatore, for providing facilities during the research.

Conflict of interest

The authors declare that the research was conducted in the absence of any commercial or financial relationships that could be construed as a potential conflict of interest.

Publisher's note

All claims expressed in this article are solely those of the authors and do not necessarily represent those of their affiliated organizations, or those of the publisher, the editors and the reviewers. Any product that may be evaluated in this article, or claim that may be made by its manufacturer, is not guaranteed or endorsed by the publisher.

Supplementary material

The Supplementary Material for this article can be found online at: https://www.frontiersin.org/articles/10.3389/fpls.2024.1401526/full#supplementary-material

References

Agnihotri, A. K., Mishra, S. P., Ansar, M., Tripathi, R. C., Singh, R., and Akram, M. (2019). Molecular characterization of Mungbean yellow mosaic India virus infecting tomato (*Solanum lycopersicum* L.). *Australas. Plant Pathol.* 48, 159–165. doi: 10.1007/s13313-018-0611-7

Akhtar, K. P., Sarwar, G., Abbas, G., Asghar, M. J., Sarwar, N., and Shah, T. M. (2011). Screening of mungbean germplasm against *Mungbean Yellow Mosaic India Virus* and its vector *Bemisia tabaci*. *Crop Prot.* 30, 1202–1209. doi: 10.1016/j.cropro.2011.05.012

Akram, M., Kamaal, N., and Pratap, A. (2020). Molecular characterization of Begomoviruses causing yellow mosaic disease in *Vigna stipulacea* and evidence of recombination. *J. Food Legumes.* 33, 232–244.

Akram, M., Naimuddin,, Agnihotri, A. K., Gupta, S., and Singh, N. P. (2015). Characterisation of full genome of *Dolichos yellow mosaic virus* based on sequence comparison, genetic recombination, and phylogenetic relationship. *Ann. Appl. Biol.* 167, 354–363. doi: 10.1111/aab.2015.167.issue-3

Ansar, M., Agnihotri, A. K., Ranjan, T., Karn, M., Srinivasaraghavan, S. A., Kumar, R. R., et al. (2021). Nightshade (*Solanum nigrum*), an intermediate host between tomato and cucurbits of Tomato leaf curl New Delhi virus. *Phytopathol. Mediterr.* 60, 409–419. doi: 10.36253/phyto-12745

Arguello-Astorga, G. R., Guevara-González, R. G., Herrera-Estrella, L. R., and Rivera-Bustamante, R. F. (1994). Geminivirus replication origins have a group-specific organization of iterative elements: a model for replication. *Virology* 203, 90–100. doi: 10.1006/viro.1994.1458

Bag, M. K., Gautam, N. K., Prasad, T. V., Pandey, S., Dutta, M., and Roy, A. (2014). Evaluation of an Indian collection of black gram germplasm and identification of resistance sources to Mungbean yellow mosaic virus. *Crop Prot.* 61, 92–101. doi: 10.1016/j.cropro.2014.03.021

Banerjee, A., Umbrey, Y., Yadav, R. M., and Roy, S. (2018). Molecular evidence of an isolate of *mungbean yellow mosaic India virus* with a recombinant DNA B component occurring on mungbean from mid-hills of Meghalaya, India. *Virus dis.* 29, 68–74. doi: 10.1007/s13337-018-0429-5

Biswas, K. K., Malathi, V. G., and Varma, A. J. (2008). Diagnosis of symptomless yellow mosaic begomovirus infection in Pigeon pea by using cloned *Mungbean yellow mosaic India virus* as Probe. *Plant Biochem. Biotechnol.* 17, 9–14. doi: 10.1007/BF03263253

Boni, M. F., Posada, D., and Feldman, M. W. (2007). An exact nonparametric method for inferring mosaic structure in sequence triplets. *Genetics* 176, 1035–1047. doi: 10.1534/genetics.106.068874

Briddon, R. W., and Stanley, J. (2006). Subviral agents associated with plant single-stranded DNA viruses. *Virology* 344, 198–210. doi: 10.1016/j.virol.2005.09.042

Brown, J. K., Zerbini, F. M., Navas-Castillo, J., Moriones, E., Ramos-Sobrinho, R., Silva, J. C., et al. (2015). Revision of Begomovirus taxonomy based on pairwise sequence comparisons. *Arch. Virol.* 160, 1593–1619. doi: 10.1007/s00705-015-2398-y

Chowdary, V. T., Manoj Kumar, V., Kishore Varma, P., Sreekanth, B., Srinivas Rao, V., Selvarajan, R., et al. (2022). Characterization of *Mungbean yellow mosaic India virus* genome with a recombinant DNA-B in Southern Peninsular India. *Mol. Biol. Rep.* 49, 8587–8595. doi: 10.1007/s11033-022-07691-9

Ditta, G., Stanfield, S., Corbin, D., and Helinski, D. R. (1980). Broad host range DNA cloning system for gram-negative bacteria: construction of a gene bank of *Rhizobium meliloti*. *Proc. Natl. Acad. Sci. U.S.A.* 77, 7347–7351. doi: 10.1073/pnas.77.12.7347

Edgar, R. C. (2004). MUSCLE: multiple sequence alignment with high accuracy and high throughput. *Nucleic Acids Res.* 32, 1792–1797. doi: 10.1093/nar/gkh340

Fauquet, C., Briddon, R., Brown, J., Moriones, E., Stanley, J., Zerbini, M., et al. (2008). Geminivirus strain demarcation and nomenclature. *Arch. Virol.* 153, 783–821. doi: 10.1007/s00705-008-0037-6

Fauquet, C., Sawyer, S., Idris, A., and Brown, J. K. (2005). Sequence analysis and classification of apparent recombinant begomoviruses infecting tomato in the Nile and Mediterranean basins. *Phytopathology* 95, 549–555. doi: 10.1094/PHYTO-95-0549

Fontes, E. P., Eagle, P. A., Sipe, P. S., Luckow, V. A., and Hanley-Bowdoin, L. (1994). Interaction between a geminivirus replication protein and origin DNA is essential for viral replication. *J. Biol. Chem.* 269, 8459–8465. doi: 10.1016/S0021-9258(17)37216-2

Gibbs, M. J., Armstrong, J. S., and Gibbs, A. J. (2000). Sister scanning: A monte carlo procedure for assessing signals in recombinant sequences. *Bioinformatics* 16, 573–582. doi: 10.1093/bioinformatics/16.7.573

Girish, K. R., and Usha, R. (2005). Molecular characterization of two soybean-infecting begomoviruses from India and evidence for recombination among legume-infecting begomoviruses from South [corrected] South-East Asia. *Virus Res.* 108, 167–176. doi: 10.1016/j.virusres.2004.09.006

Habib, S., Shad, N., Javaid, A., and Iqbal, U. (2007). Screening of mungbean germplasm for resistance/tolerance against yellow mosaic disease. *Mycopath* 5, 89–94.

Hall, T. A. (1999). BioEdit: A user-friendly biological sequence alignment editor and analysis program for windows 95/98/NT. *Nucleic Acids Symp Ser.* 41, 95–98.

Hood, E. E., Gelvin, S. B., Melchers, L. S., and Hoekema, A. (1993). A New *Agrobacterium* helper plasmid for gene transfer to plants. *Transgenic Res.* 2, 208–218. doi: 10.1007/BF01977351

Inoue-Nagata, A. K., Albuquerque, L. C., and Rocha, W. B. (2004). A simple method for cloning the complete begomovirus genome using the bacteriophage *phi*29 DNA polymerase. *J. Virol. Methods* 116, 209–211. doi: 10.1016/j.jviromet.2003.11.015

Jacob, S., Vanitharani, R., Karthikeyan, A., Chinchore, Y., Thillaichidambaram, P., and Veluthambi, K. (2003). *Mungbean yellow mosaic virus*-Vi agroinfection by codelivery of DNA A and DNA B from one *Agrobacterium* strain. *Plant Dis.* 87, 247–251. doi: 10.1094/PDIS.2003.87.3.247

John, P., Sivalingam, P., Haq, Q., Kumar, N., Mishra, A., Briddon, R., et al. (2008). Cowpea golden mosaic disease in Gujarat is caused by a *Mungbean yellow mosaic India virus* isolate with a DNA B variant. *Arch. Virol.* 153, 1359. doi: 10.1007/s00705-008-0116-8

Kamaal, N., Akram, M., and Agnihotri, A. K. (2015). Molecular evidence for the association of tomato leaf curl Gujarat virus with a leaf curl disease of *Phaseolus vulgaris* L. *J. Phytopathol.* 163, 58–62. doi: 10.1111/jph.12255

Karthikeyan, A., Sudha, M., Pandiyan, M., Senthil, N., Shobana, V., and Nagarajan, P. (2011). Screening of MYMV resistant mungbean (*Vigna radiata* L. Wilczek) progenies through agroinoculation. *Int. J. Plant Pathol.* 2, 115–125. doi: 10.3923/ijpp.2011.115.125

Karthikeyan, A. S., Vanitharani, R., Balaji, V., Anuradha, S., Thillaichidambaram, P., Shivaprasad, P. V., et al. (2004). Analysis of an isolate of *Mungbean Yellow Mosaic Virus* (MYMV) with a highly variable DNA-B component. *Arch. Virol.* 149, 643–1652. doi: 10.1007/s00705-004-0313-z

Kumar, S., Stecher, G., and Tamura, K. (2016). MEGA7: molecular evolutionary genetics analysis version 7.0 for bigger datasets. *Mol. Biol. Evol.* 33, 1870–1874. doi: 10.1093/molbev/msw054

Madhumitha, B., Aiyanathan, K. E. A., Raveendran, M., and Sudha, M. (2022). Identification and confirmation of resistance in mungbean [*Vigna radiata* (L.) Wilczek] derivatives to *mungbean yellow mosaic virus* (MYMV). *Legume Res.* 45, 122–127. doi: 10.18805/LR-4437

Madhumitha, B., Aiyanathan, K. E. A., and Sudha, M. (2019). Coat protein-based characterization of *Mungbean yellow mosaic virus* in Tamil Nadu. *J. pharmacogn. phytochem.* 8, 2119–2123.

Maheshwari, R., Panigrahi, G., and Angappan, K. (2014). Molecular characterization of distinct YMV (*Yellow mosaic virus*) isolates affecting pulses in India with the aid of coat protein gene as a marker for identification. *Mol. Biol. Rep.* 41, 2635–2644. doi: 10.1007/s11033-014-3122-9

Malathi, V. G., Renukadevi, P., Chakraborty, S., Biswas, K. K., Roy, A., Sivalingam, P. N., et al. (2017). "Begomoviruses and their satellites occurring in India: distribution, diversity, and pathogenesis," in *Century of Plant Virology in India*. Eds. B. Mandal, G. Rao, V. Baranwal and R. Jain (Springer, Singapore), 75–177.

Mandal, B., Varma, A., and Malathi, V. G. (1997). Systemic infection of Vigna mungo using the cloned DNAs of the black gram isolate of mungbean yellow mosaic geminivirus through agroinoculation and transmission of the progeny virus by whiteflies. *J. Phytopathol.* 145, 505–510. doi: 10.1111/j.1439-0434.1997.tb00358.x

Martin, D. P., Murrell, B., Golden, M., Khoosal, A., and Muhire, B. (2015). RDP4: Detection and analysis of recombination patterns in virus genomes. *Virus Evol.* 1, vev003. doi: 10.1093/ve/vev003

Muhire, B. M., Varsani, A., and Martin, D. P. (2014). SDT: A virus classification tool based on pairwise sequence alignment and identity calculation. *PloS One* 9, e108277. doi: 10.1371/journal.pone.0108277

Nagendran, K., Satya, V. K., Mohankumar, S., and Karthikeyan, G. (2016). Molecular characterization of a distinct bipartite Begomovirus species infecting ivy gourd (*Coccinia grandis* L.) in Tamil Nadu, India. *Virus Genes* 52, 146–151. doi: 10.1007/s11262-015-1278-6

Naimuddin,, Akram, M., and Aditya, P. (2011). First report of natural infection of *mungbean yellow mosaic India virus* in two wild species of Vigna. *New Dis. Rep.* 23, 21–22. doi: 10.5197/j.2044-0588.2011.023.021

Padidam, M., Sawyer, S., and Fauquet, C. M. (1999). Possible emergence of new geminiviruses by frequent recombination. *Virol* 265, 218–225. doi: 10.1006/viro.1999.0056

Paximadis, M., Idris, A., Torres-Jerez, I., Villarreal, A., Rey, M., and Brown, J. K. (1999). Characterization of tobacco geminiviruses in the Old and New World. *Arch. Virol.* 144, 703–717. doi: 10.1007/s007050050537

Posada, D., and Crandall, K. A. (2001). "Evaluation of methods for detecting recombination from DNA sequences: computer simulations," *Proceedings of the National Academy of Sciences United States of America*. 98, p. 13757–62. doi: 10.1534/genetics.106.068874

Qazi, J., Ilyas, M., Mansoor, S., and Briddon, R. W. (2007). Legume yellow mosaic viruses: genetically isolated begomoviruses. *Mol. Plant Pathol.* 8, 343–348. doi: 10.1111/j.1364-3703.2007.00402.x

Qazi, J., Mansoor, S., Amin, I., Awan, M. Y., Briddon, R. W., and Zafar, Y. (2006). First report of Mungbean yellow mosaic India virus on mothbean in Pakistan. *New Dis. Rep.* 13, 16. doi: 10.1111/j.1365-3059.2006.01475.x

Ramesh, S. V., Chouhan, B. S., and Ramteke, R. (2017). Molecular detection of Begomovirus (family: Geminiviridae) infecting *Glycine max* (L.) Merr. *and* associated weed. *J. Crop Weed.* 13, 64–67.

Rathi, Y. P. S. (2002). "Epidemiology, yield losses and management of major diseases of Kharif pulses in India," in *Plant Pathology and Asian Congress of Mycology and Plant Pathology* (University of Mysore, Mysore, India).

Reddy, B. V. B., Obaiah, S., and Prasanthi, L. (2015). *Mungbean yellow mosaic India virus* is associated with yellow mosaic disease of blackgram (Vigna mungo L.) in Andhra Pradesh, India. *Arch. Phytopathol. Plant Prot.* 48, 345–353. doi: 10.1080/03235408.2014.888874

Rybicki, E. (1994). A phylogenetic and evolutionary justification for three genera of Geminiviridae. *Arch. Virol.* 139, 49–77. doi: 10.1007/BF01309454

Salminen, M. O., Carr, J. K., Burke, D. S., and McCutchan, F. E. (1995). Identification of breakpoints in intergenotypic recombinants of HIV type 1 by boot scanning. *AIDS Res. Hum. Retroviruses* 11, 1423–1425. doi: 10.1089/aid.1995.11.1423

Shahid, M. S., Pudashini, B. J., Khatri-Chhetri, G. B., Ikegami, M., and Natsuaki, K. T. (2012). First report of Mungbean yellow mosaic India virus on kidney bean in Nepal. *New Dis. Rep.* 25, 30. doi: 10.5197/j.2044-0588.2012.025.030

Singh, G., Sharma, Y. R., and Kaur, L. (1992). Method of rating *mungbean yellow mosaic virus* in mungbean and urdbean. *Plant Dis. Res.* 7, 1–6.

Smith, J. M. (1992). Analyzing the mosaic structure of genes. *J. Mol. Evol.* 34, 126–129. doi: 10.1007/BF00182389

Stanley, J., Bisaro, D. M., Briddon, R. W., Brown, J. K., Fauquet, C. M., Harrison, B. D., et al. (2005). "Family geminiviridae," in *Virus taxonomy, eighth report of the International Committee on Taxonomy of Viruses*, *1st edn* (Elsevier, London), 301–326.

Sudha, M. (2009). DNA isolation protocol for Vigna radiata with free of phenolics. *Protocol Exchange*. doi: 10.1038/nprot.2009.167

Sudha, M., Karthikeyan, A., Nagarajan, P., Raveendran, M., Senthil, N., Pandiyan, M., et al. (2013). Screening of mungbean (*Vigna radiata*) germplasm for resistance to mungbean yellow mosaic virus using agroinoculation. *Can. J. Plant Pathol.* 35, 424–430. doi: 10.1080/07060661.2013.827134

Sudha, M., Karthikeyan, A., Shobhana, V. G., Nagarajan, P., Raveendran, M., Senthil, N., et al. (2015). Search for Vigna species conferring resistance to *mungbean yellow mosaic virus* in mungbean. *Plant Genet. Resour.* 13, 162–167. doi: 10.1017/S1479262114000859

Thompson, J. D., Higgins, D. G., and Gibson, T. J. (1994). CLUSTAL W: improving the sensitivity of progressive multiple sequence alignment through sequence weighting, position-specific gap penalties and weight matrix choice. *Nucleic Acids Res.* 22, 4673–4680. doi: 10.1093/nar/22.22.4673

Usharani, K., Surendranath, B., Haq, Q., and Malathi, V. G. (2004). *Yellow mosaic virus* infecting soybean in northern India is distinct from the species infecting soybean in southern and western India. *Curr. Sci.* 86, 845–850.

Varma, A., and Malathi, V. G. (2003). Emerging geminivirus problems: a serious threat to crop production. *Ann. Appl. Biol.* 142, 145–164. doi: 10.1007/s13337-016-0358-0

Zerbini, F. M., Briddon, R. W., Idris, A., Martin, D. P., Moriones E, E., Castillo, J. N., et al. (2017). ICTV Virus taxonomy profile: Geminiviridae. *J. Gen. Virol.* 98, 131–133. doi: 10.1099/jgv.0.000738

frontiers | Frontiers in Plant Science

TYPE Original Research
PUBLISHED 16 August 2024
DOI 10.3389/fpls.2024.1428613

OPEN ACCESS

EDITED BY
Rachid Lahlali,
Ecole Nationale d'Agriculture de Meknès, Morocco

REVIEWED BY
David Vela-Corcia,
University of Malaga, Spain
Lucia Landi,
Marche Polytechnic University, Italy

*CORRESPONDENCE
Laura Vilanova
lavito82@gmail.com
Rosario Torres
rosario.torres@irta.cat

RECEIVED 06 May 2024
ACCEPTED 29 July 2024
PUBLISHED 16 August 2024

CITATION
López A, van Kan JAL, Beenen HG, Dolcet-Sanjuan R, Teixidó N, Torres R and Vilanova L (2024) Evaluation of cell death-inducing activity of *Monilinia* spp. effectors in several plants using a modified TRV expression system.
Front. Plant Sci. 15:1428613.
doi: 10.3389/fpls.2024.1428613

Evaluation of cell death-inducing activity of *Monilinia* spp. effectors in several plants using a modified TRV expression system

Anselmo López[1], Jan A. L. van Kan[2], Henriek G. Beenen[2], Ramon Dolcet-Sanjuan[3], Neus Teixidó[1], Rosario Torres[1]* and Laura Vilanova[1,2]*

[1]IRTA, Postharvest Programme, Edifici Fruitcentre, Parc Agrobiotech Lleida, Lleida, Catalonia, Spain, [2]Laboratory of Phytopathology, Wageningen University, Wageningen, Netherlands, [3]IRTA, Plant In Vitro Culture Laboratory, Fruticulture Program, Parc Agrobiotech Lleida, Lleida, Catalonia, Spain

Introduction: Brown rot is the most important fungal disease affecting stone fruit and it is mainly caused by *Monilinia fructicola*, *M. laxa* and *M. fructigena*. *Monilinia* spp. are necrotrophic plant pathogens with the ability to induce plant cell death by the secretion of different phytotoxic molecules, including proteins or metabolites that are collectively referred to as necrotrophic effectors (NEs).

Methods: We exploited the genomes of *M. fructicola*, *M. laxa* and *M. fructigena* to identify their common group of secreted effector proteins and tested the ability of a selected set of effectors to induce cell death in *Nicotiana benthamiana*, *Solanum lycopersicum* and *Prunus* spp. leaves.

Results: Fourteen candidate effector genes of *M. fructicola*, which displayed high expression during infection, were transiently expressed in plants by agroinfiltration using a modified *Tobacco Rattle Virus* (TRV)-based expression system. Some, but not all, effectors triggered leaf discoloration or cell death in *N. benthamiana* and *S. lycopersicum*, which are non-hosts for *Monilinia* and in *Prunus* spp., which are the natural hosts. The effector MFRU_030g00190 induced cell death in almost all *Prunus* genotypes tested, but not in the Solanaceous plants, while MFRU_014g02060, which is an ortholog to BcNep1, caused necrosis in all plant species tested.

Conclusion: This method provides opportunities for screening *Prunus* germplasm with *Monilinia* effector proteins, to serve as a tool for identifying genetic loci that confer susceptibility to brown rot disease.

KEYWORDS

***Monilinia fructicola*, *Prunus* spp., transient expression, NLPs, necrotrophic fungi**

1 Introduction

One of the most important fungal diseases affecting stone fruit is brown rot. It causes large economic losses, principally in peaches and nectarines, but also affects other stone fruit like cherries, apricots, and almonds (Ollero-Lara et al., 2019; Baró-Montel et al., 2019a). The infection occurs in the field, starting from overwintered mummies that generate the primary inoculum for emerging flowers and fruit during spring and summer (Villarino et al., 2010). Nevertheless, the main economic losses of brown rot appear during the postharvest handling, storage, and transportation (Casals et al., 2022).

The genus *Monilinia* are Ascomycetes included in the *Sclerotiniaceae* family and it contains 37 species, most of which are plant pathogens (Index Fungorum, 2023). The three species mainly responsible for stone fruit brown rot are *Monilinia fructicola*, *M. laxa* and *M. fructigena*. Out of these species, *M. fructicola* is considered to cause the most severe losses in stone fruit (Villarino et al., 2013). Occurrence and distribution of the three species has traditionally differed worldwide. While *M. laxa* and *M. fructigena* have long been the main causal agent of brown rot in stone fruit in Europe, *M. fructicola* has traditionally affected stone fruit in India, Japan, Oceania and the Americas. *M. fructicola* was first detected in Europe in fruit orchards in France in 2001 (Lichou et al., 2002) and it has since migrated into several European countries (Hrustić et al., 2015). In Spain it was first detected in Ebro Valley orchards in 2009 (De Cal et al., 2009).

Depending on the strategies developed to interact with the host, plant pathogenic fungi are classified as having either a necrotrophic, hemibiotrophic or biotrophic lifestyle (Tan et al., 2010). In a classical biotrophic lifestyle, the interaction between an effector (acting as an avirulence gene) and its specific plant receptor (encoded by an *R*-gene) leads to a defense response causing host cell death and stopping the infection process (Tan et al., 2015). By contrast, necrotrophic pathogens secrete cell death-inducing effectors with the capacity to trigger host programmed cell death (PCD), which is a key step in successful plant colonization and disease development (Tan et al., 2010; Kabbage et al., 2017; Faris and Friesen, 2020; Malvestiti and van Kan, in press).

Cell death-inducing effectors can either be secondary metabolites or relatively small proteins (Tan et al., 2010). Depending on their target in host plants, the effectors can be grouped as apoplastic or cytoplasmic effectors. Both are delivered into the plant, however, apoplastic effectors are secreted into the plant apoplast, where they interact with extracellular receptors, while cytoplasmic effectors are translocated inside the plant cell (Selin et al., 2016). In recent years, many studies have been devoted to host cell death-inducing effectors produced by necrotrophic pathogens affecting wheat, barley, and maize with the *Parastagonospora nodorum*-wheat pathosystem serving as a model for the interaction between necrotrophic fungi and their host (Friesen and Faris, 2021; Shao et al., 2021). Three fungal effector genes have been cloned along with their target genes in wheat: Tox1-*Snn1*, Tox3-*Snn3* and ToxA-*Tsn1* (Friesen and Faris, 2021). Three more effector genes (Tox4, Tox5 and Tox 267) have been cloned from *P. nodorum* and five wheat loci involved in recognition of these effectors were genetically mapped (reviewed in Malvestiti and van Kan, in press).

The best characterized necrotrophic pathogen from the Sclerotiniaceae family is *Botrytis cinerea*. A large number of cell death-inducing effectors have been studied and functionally characterized (Leisen et al., 2022; Bi et al., 2023). The availability of high-quality annotations of different *Monilinia* spp. genomes enables studies on effector proteins of these species (Landi et al., 2018; Naranjo-Ortíz et al., 2018; Rivera et al., 2018; De Miccolis Angelini et al., 2019; Marcet-Houben et al., 2021). Genome comparison among five *Monilinia* spp. highlighted the low variability in the CAZome, some common secondary metabolism clusters, and several potential candidate effector genes (Marcet-Houben et al., 2021). Despite the available genome information, molecular-genetic studies on the interaction between *Monilinia* spp. and *Prunus* spp. are in their infancy as compared to other Sclerotiniaceae. To investigate the role of *Monilinia* effectors in the infection process, it is desirable to have a tool to test their cell death-inducing capacity in *Prunus* spp. tissues. Previous studies in *B. cinerea* used heterologous expression in *Pichia pastoris* to produce a set of endopolygalacturonases (Kars et al., 2005), however, that is a time-consuming technique with relatively low efficiency. Functional screens with effector proteins of biotrophic pathogens often make use of transient expression systems using plant virus vectors as expression platform (Nasir et al., 2005; Vleeshouwers and Oliver, 2014). Potato Virus X (PVX) is often used for these purposes when screening germplasm of Solanaceae (Domazakis et al., 2017), however this virus was not reported to replicate in *Prunus* spp. *Tobacco Rattle Virus* (TRV), however, can replicate in a wide range of plant species, including *Prunus* spp. leaves (Bai et al., 2016) and this virus was considered to be potentially useful for expressing *M. fructicola* effector proteins in *Prunus* spp. leaves.

The aim of this study was to identify the common effectorome from the three most important species of *Monilinia* in stone fruit, *M. fructicola*, *M. laxa* and *M. fructigena*, and to study the cell death-inducing capacity of a subset of *M. fructicola* effectors using modified TRV constructs for expressing them in leaves of non-hosts and hosts of *Monilinia* spp.

2 Materials and methods

2.1 Identification of the common effectorome from three *Monilinia* species

The genomes of *M. fructigena* strain gena6 (BioProject Code PRJNA707424), *M. laxa* strain 8L (BioProject PRJNA433296; Naranjo-Ortíz et al., 2018) and *M. fructicola* strain CPMC6 (BioProject PRJNA503180; Vilanova et al., 2021) as well as the comparative genomic analysis (Marcet-Houben et al., 2021) were used for the identification of the effector genes for each species. Specifically, we used the effectorome data from Vilanova et al. (2021) for *M. fructicola* and the effectorome data from Marcet-Houben et al. (2021) for *M. laxa* and *M. fructigena*.

Each predicted effector gene from all three species was blasted to the other species one to one, using Genome Workbench and PhylomeDB (E-value cut-off 0.001 and query coverage ≥ 80%). The bidirectional best blast hits were listed and used for further analyses (Supplementary Table S1).

Transcriptionally inactive genes were eliminated based on RNA-Seq data from *M. laxa*- infected fruits (Balsells-Llauradó et al., 2020) and *M. fructicola*-infected leaves (Vilanova et al., unpublished).

2.2 Plant material and fungal culture

In this study, leaves from different plant species were used: *Nicotiana benthamiana*, *Solanum lycopersicum*, and *Prunus* spp. *N. benthamiana* and *S. lycopersicum* served as model plants to ensure the TRV system is well established. Additionally, *N. benthamiana* was used to detect non-host specific effectors while *S. lycopersicum* and *Prunus* spp. were used to identify host-specific effectors, with a particular focus on *Prunus* spp. as it is the actual host of *Monilinia* spp.

N. benthamiana plants were grown in a climate chamber located at IRTA Fruitcentre in Lleida at 25°C under a 16 h light/8 h dark cycle, *Solanum lycopersicum* var. Moneymaker plants were grown in the greenhouses located at University of Lleida. Furthermore, *Prunus* spp. were included due to their role as the pathogen host. Initially, *Prunus persica* plants derived from directed crosses were employed to assess the viability of agroinfiltration in this plant species. Subsequently, five well-characterized genotypes were selected for further investigation. These individuals included: *Cadaman* (*Prunus davidiana* × *Prunus persica*), *Prunus davidiana* and three different genotypes denotated 37p15-13, 37p15-16, and 37p15-17. These three genotypes are a BC1 population derived from a cross between the peach cultivar *Nectatop* and *Cadaman*. This population has been previously generated and genotyped (Zaracho-Echagüe et al., 2022). All *Prunus* spp. plants were *in vitro* clonally propagated as described (Cantabella et al., 2021). Briefly, *in vitro* shoot tip cultures were established from field grown plants, propagated by axillary branching in MS (Murashige & Skoog) medium supplemented with 5 µM benzylaminopurine (BAP). Shoot elongation was achieved adding liquid MS media, without hormones, to the semisolid multiplication medium. Root induction on *in vitro* elongated shoots was conducted in half-strength MS media supplemented with 10 µM indole-3-acetic acid (IAA), followed by transfer to auxin-free medium amended with vermiculite, and afterwards acclimated to greenhouse conditions.

The *M. fructicola* strain CPMC6 belongs to the collection of the Postharvest Pathology group of IRTA (Lleida, Spain) and is deposited in the Spanish Culture Type Collection (CECT 21105). For long-term storage, the isolate was kept as a conidial suspension in 20% glycerol at -80°C. Cultures were grown in malt extract plates (MEA) and incubated at 25°C in darkness for 10-12 days before use.

2.3 RNA isolation and cDNA synthesis

M. fructicola was grown on cellophane on MEA incubated at 24°C for 10-12 days, and RNA was extracted from freeze-dried mycelium using RNeasy® Plant Mini Kit (Qiagen, Hilden, Germany) according to manufacturer´s recommendations. RNA from *M. fructicola* decayed stone fruit tissue was extracted following the methodology described by Baró-Montel et al. (2019c). For elimination of genomic DNA, RNA was treated with TURBO™ DNase (Invitrogen, ThermoFisher Scientific, Carlsbad, CA, USA). First strand cDNA was synthesized using the SuperScript™ IV First-Strand Synthesis Kit (Invitrogen, ThermoFisher Scientific, Carlsbad, CA, USA) and used for gene amplification.

2.4 Amplification of candidate effector genes

All oligonucleotides used are listed in Supplementary Table S2. Primers were designed using the NEBuilder Assembly Tool (New England Biolabs, MA, USA) to amplify two fragments for each selected gene. The coding sequence of the signal peptide of the pathogenesis-related protein from *N. benthamiana* (PR1) and the coding sequence (CDS) of the mature candidate effector excluding the N-terminal signal peptide were amplified. Fragments for MFRU002g05260 and MFRU030g00580 genes were amplified directly from the plasmids obtained by Vilanova et al. (2021). Fragment amplification for cloning was performed in a volume of 50 µL containing 1µM of both forward and reverse primers, 0.2 mM of each dNTP, 1X PFU buffer (Promega, Leiden, The Netherlands), 1.5 U PFU polymerase (Promega), and 2 µL of template (100 ng of cDNA from *M. fructicola* or 100 ng of plasmid). PCR program for both fragments of MFRU004g02710, MFRU004g02720, MFRU014g02060, MFRU048g00370, MFRU004g00620 and MFRU005g00910 was 95°C for 2 min; 10 cycles of 95°C for 30 s, 55°C for 30 s and 72°C for 1 min and 25 cycles with an annealing temperature of 60°C instead of 55°C, ending with a final step at 72°C for 5 min. PCR program for the PR1 fragment of MFRU004g02090, MFRU008g03430, MFRU010g02580, MFRU018g01470, MFRU027g00340 and MFRU030g00190 was 95°C for 2 min; 35 cycles of 95°C for 15 s, 55°C for 30 s, and 72°C for 30 s, ending with a final step at 72°C for 5 min. PCR program for the other fragments was 95°C for 2 min; 35 cycles of 95°C for 15 s, 52°C for 30 s, and 72°C for 80 s, ending with a final step at 72°C for 5 min. PCR products were visualized in a range of 1-3% agarose gel.

2.5 Vector construction and cloning

pTRV2 VIGS vector pYL156 (Liu et al., 2002) (kindly provided by Laurens Deurhof, Wageningen University) was modified by removing remainders of the TRV2b protein coding sequence and inserting a sequence encoding a plant secretion signal peptide (derived from the tobacco pathogenesis-related protein PR1a), joint in frame to the coding sequence of a mature *Monilinia* effector gene, lacking the fungal secretion signal peptide sequence. Constructs were made using the NEBuilder® HiFi DNA Assembly Cloning kit (New England BioLabs, MA, USA). The pTRV2 vector was linearized using restriction enzymes (New England BioLabs, MA, USA), either PvuII,

EcoRI, AatII or BamHI (New England BioLabs, MA, USA) at 37°C, according to manufacturer's recommendations. Each digestion was done one by one followed by a purification step. Fragments and the linearized vector were incubated with Clonexpress II one step cloning kit (Vazyme, Nanjing, China) or NEBuilder HiFi DNA Assembly Master Mix (New England BioLabs, MA, USA) following manufacturer´s recommendations (Supplementary Figure S1). From 10 ng to 1000 ng of ligated plasmid was transformed into ultra-competent DH5α *E. coli* cells. Cells were selected on LB medium with kanamycin and incubated overnight at 37°C. Plasmids were isolated using the QIAprep Spin Miniprep kit (Qiagen, Hilden, Germany) according to manufacturer's recommendations. To check if the selected genes were integrated in the pTRV2 plasmids, PCR was performed using IBIAN®-Taq DNA Polymerase (Ibian Technologies, Zaragoza, Spain) in a total volume of 25 µL containing 0.5 µM of both forward and reverse primer, 0.2 mM of each dNTP, 1X IBIAN Buffer, 1.25 U IBIAN-Taq® DNA polymerase and 0.5 uL of the pTRV2 vector. PCR program was 94°C for 2 min; 30 cycles of 94°C for 10 s, 55°C for 20 s and 72°C for 1,5 min, ending with a final step of 72°C for 5 min. Those clones with similar size to the expected were sequenced for further confirmation.

2.6 *Agrobacterium tumefaciens* mediated-transient expression in *Nicotiana benthamiana*, *Solanum lycopersicum* and *Prunus* spp.

Fifty ng of plasmid were added to 50 µL of electro-competent *Agrobacterium tumefaciens* cells (strain GV3101). After electroporation, cells were plated in LB petri dishes supplemented with kanamycin and rifampicin and incubated at 28°C for two days. *Agrobacterium* cultures were transferred into 15 mL YEB medium containing 20 µM acetosyringone, 50 mg/L kanamycin and 20 mg/L rifampicin and they were grown during 22 h at 28°C and 200 rpm. Pellet was resuspended in MMAi (1 mM MES, 10 mM $MgCl_2$, 200 µM acetosyringone) buffer at OD600 = 1.6. Each solution of the different pTRV2 strains were mixed 1:1 with pTRV1 (Liu et al., 2002) and incubated during 1 h at room temperature. The different mixes were infiltrated using a needleless 1 mL syringe in leaves of 4-6 weeks old *N. benthamiana* plants, 5-6 weeks old *S. lycopersicum* and in *Prunus* spp. plants with at least 10 leaves. Pictures of responses in all *N. benthamiana* and *S. lycopersicum* plants were taken 5 and 7 days postinfiltration, and for *Prunus* spp. leaves, the symptoms were observed 10 days postinfiltration. This experiment was replicated three times, and each *Agrobacterium* suspension was infiltrated in three different leaves from three different plants.

3 Results

3.1 Identification of the common effectorome from three *Monilinia* spp.

The identification of the common effector genes shared between the three main *Monilinia* spp. was based on the analysis of Marcet-Houben et al. (2021). Bidirectional blast analysis was performed between effector genes in *M. fructicola*, *M. laxa* and *M. fructigena* in all possible combinations resulting in 76 effector genes shared among the three *Monilinia* spp. (Figure 1; Supplementary Tables S3, S4).

For these 76 common effectors, information about their expression during the infection of *M. fructicola* in leaves (Vilanova et al., 2021) and of *M. laxa* in nectarines (Balsells-Llauradó et al., 2020) was used to eventually select 14 effector genes for transient expression analysis of cell death-induction in different plant species (Table 1).

3.2 Response to transient expression in *Nicotiana benthamiana* and *Solanum lycopersicum*

The cell death-inducing capacity of each of the 14 candidate effector genes from *M. fructicola* was tested by ATTA using a modified binary vector containing the *Tobacco Rattle Virus* (pTRV2 mixed 1:1 with pTRV1) in three different plant species (Supplementary Figure S2). MFRU_014g02060 is an ortholog to BcNep1, which was previously shown to have a strong necrotizing activity in *N. benthamiana* leaves (Schouten et al., 2008), and it was used as a positive control. As negative control, we used an empty TRV2 vector combined with TRV1 (Figure 2).

In *N. benthamiana* leaves, six of the 14 candidate genes caused necrosis in the infiltrated area at five days postinfiltration (Table 2), with the genes MFRU_027g00340, MFRU_030g00580 and MFRU_005g00910 showing the strongest cell death-inducing activity (Figure 2).

Similar experiments were conducted in *S. lycopersicum* leaves and some differences were observed. Compared to *N. benthamiana*, the same number of candidate genes induced necrosis in the infiltrated area (Table 2), but these genes were different. MFRU_014g02060, MFRU_004g02710, MFRU_005g00910 and MFRU_027g00340 induced necrosis in the infiltrated area in both tomato and *N. benthamiana* leaves (Figure 2). No necrosis was observed in tomato leaves upon infiltration with the MFRU_030g00580 construct, while this produced significant necrosis in *N. benthamiana*. In contrast, clear necrosis was observed after infiltrating MFRU_002g05260 and MFRU_004g02710 in tomato, whereas no necrosis were noted in *N. benthamiana*. The cell death-inducing capacity of the MFRU_027g00340 construct exhibited the closest response to that of the positive control in both species.

3.3 Effect of transient gene expression in *Prunus* spp. leaves

As stone fruit is the real host of *M. fructicola*, the next step was to test the fourteen selected effector genes in host-specific tissues, specifically stone fruit leaves, using the transient TRV-mediated expression system developed in this work.

The constructs for the expression of the fourteen effector genes were tested in leaves of *Prunus persica*, and symptoms became apparent for some constructs 10 days postinfiltration (Supplementary

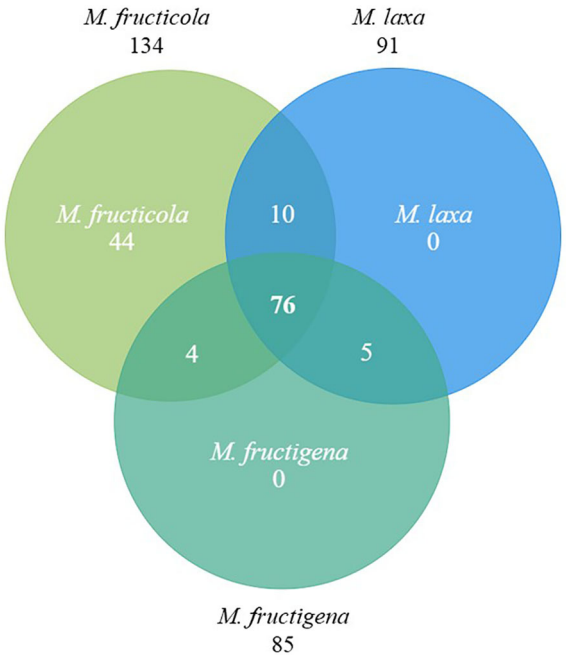

FIGURE 1
Venn diagram showing the effector genes shared among *Monilinia fructicola, M. laxa* and *M. fructigena*. Each circle represents the set of effectors for each species, with overlapping areas indicating shared effector genes between species.

Figure S2). Six of the fourteen genes induced necrosis in the infiltrated area and surroundings (Table 2). These genes were: MFRU_004g02710, MFRU_004g02720, MFRU_005g00910, MFRU_014g02060 (MFRU_Nep1), MFRU_027g00340, and MFRU_48g00370. In contrast with *N. benthamiana* and tomato, respectively, no necrosis symptoms were observed after the infiltration of MFRU_002g05260 construct and MFRU_030g00580 in *Prunus* leaves. The constructs that were able to induce necrosis

TABLE 1 *Monilinia fructicola* effector genes tested for cell death-induction by *Agrobacterium tumefaciens* transient expression (ATTA) in plants.

Protein	Ortholog in *M. laxa*	Ortholog in *M. fructigena*	Protein Size (aa)	#Cys	Description
MFRU_002g05260	Monilinia_093480	g5377	221	10	CFEM domain
MFRU_004g00620	Monilinia_063060	g1907	216	4	Hypothetical protein
MFRU_004g02090	Monilinia_028260	g4487	161	0	Hypothetical protein
MFRU_004g02710	Monilinia_064810	g1289	105	6	Hypothetical protein
MFRU_004g02720	Monilinia_064800	g1290	239	4	Hypothetical protein
MFRU_005g00910	Monilinia_024190	g6968	181	4	Hypothetical protein
MFRU_008g03430	Monilinia_059180	g6370	204	0	Hypothetical protein
MFRU_010g02580	Monilinia_060470	g5946	108	0	Hypothetical protein
MFRU_014g02060	Monilinia_013380	g6703	247	3	NEP1 Like Protein (NLP)
MFRU_018g01470	Monilinia_010100	g5286	342	0	Hypothetical protein
MFRU_027g00340	Monilinia_089850	g5226	273	0	Hypothetical protein
MFRU_030g00190	Monilinia_063010	g8181	126	6	Hypothetical protein
MFRU_030g00580	Monilinia_012000	g3324	160	6	Hypothetical protein
MFRU_048g00370	Monilinia_030790	g971	147	9	Hypothetical protein

10.3389/fpls.2024.1428613

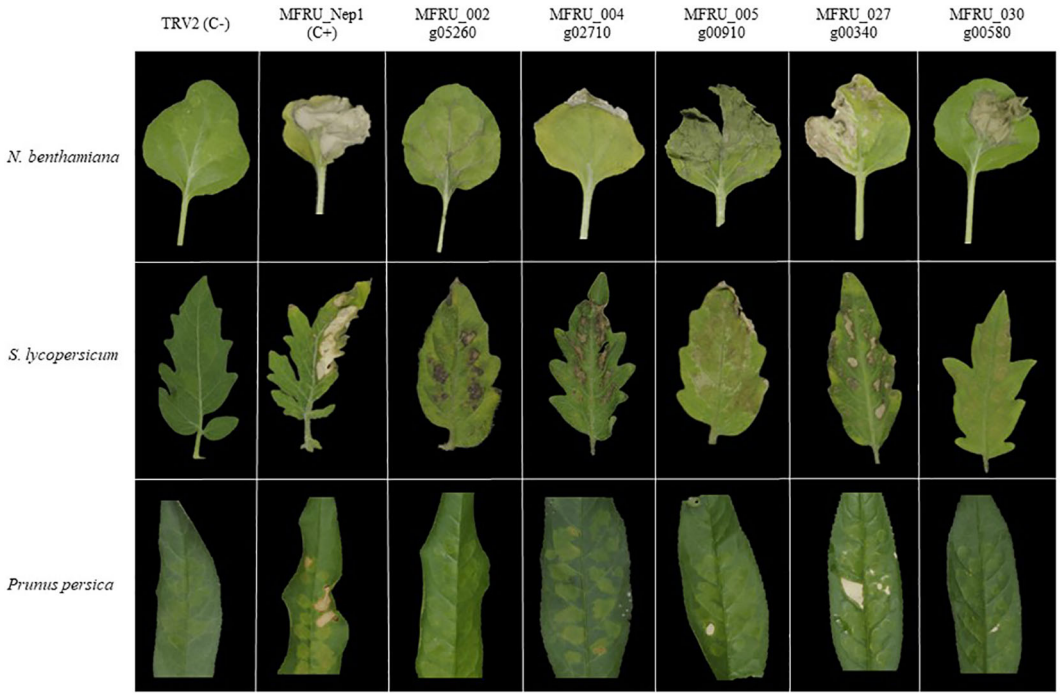

FIGURE 2
Agrobacterium tumefaciens mediated-transient expression (ATTA) using modified TRV binary vector for expressing several *Monilinia fructicola* candidate effector proteins in *N. benthamiana* (top row) and *S. lycopersicum* (middle row) and *Prunus persica* (bottom row). First column is the positive control, and the second column is the negative control. Pictures were taken 7 days postinfiltration.

TABLE 2 Summary of *Agrobacterium* infiltration and necrosis observation in various plant species for *Monilinia fructicola* proteins.

	N. benthamiana	*S. lycopersicum*	*P. persica*	Cadaman	*P. davidiana*	37p15.13	37p15.16	37p15.17
MFRU_002g05260	-	+	-	ND	ND	ND	ND	ND
MFRU_004g00620	-	-	-	ND	ND	ND	ND	ND
MFRU_004g02090	-	-	-	ND	ND	ND	ND	ND
MFRU_004g02710	+	+	+	-	-	+	-	+
MFRU_004g02720	-	+	+	-	ND	-	-	-
MFRU_005g00910	+	+	+	-	-	-	+	-
MFRU_008g03430	-	-	-	ND	ND	ND	ND	ND
MFRU_010g02580	-	-	-	ND	ND	ND	ND	ND
MFRU_014g02060	+	+	+	-	+	+	+	+
MFRU_018g01470	-	-	-	ND	ND	ND	ND	ND
MFRU_027g00340	+	+	+	-	-	-	+	-
MFRU_030g00190	-	-	-	-	+	+	+	+
MFRU_030g00580	+	-	-	ND	ND	ND	ND	ND
MFRU_048g00370	+	-	+	ND	ND	ND	ND	ND

Symbols "+" and "-" represent the presence or absence of necrosis, respectively. "ND" indicates cases where the experiment was not conducted.

symptoms in all three plant species after infiltration were MFRU_004g02710, MFRU_005g0910, MFRU_014g02060 and MFRU_027g00340 constructs (Table 2).

Subsequently, we tested the cell death-inducing capacity of six candidate effector genes in five different *Prunus* genotypes: Cadaman, *Prunus davidiana* and three genotypes called 37p15-13, 37p15-16, and 37p15-17 (Figure 3). Particularly, genotype 37p15-16 showed the most pronounced necrosis after the infiltration of all six candidate effector genes, except for MFRU_004g02710 and MFRU_004g02720, which only caused mild discoloration (Supplementary Figure S3, Table 2). In this genotype, the gene that produced more necrosis in the infiltrated area and surroundings was MFRU_005g00910, together with MFRU_014g02060 (Figure 3). On the other hand, no response was observed after the infiltration of any construct in the hybrid Cadaman. *P. davidiana* was the species in which symptoms of necrosis only appeared after the infiltration of MFRU_014g02060 and MFRU_030g00190. These 2 candidate effector genes, together with MFRU_004g02710, also induced necrosis and cell death in the leaves of the 37P15-17 and 37P15-13 genotypes (Figure 3).

4 Discussion

M. fructicola is considered to be the most economically damaging *Monilinia* spp. in stone fruit in Europe, even more than endemic *Monilinia* spp. such as *M. fructigena* and *M. laxa*. Its ability to produce more conidia than other *Monilinia* spp. may

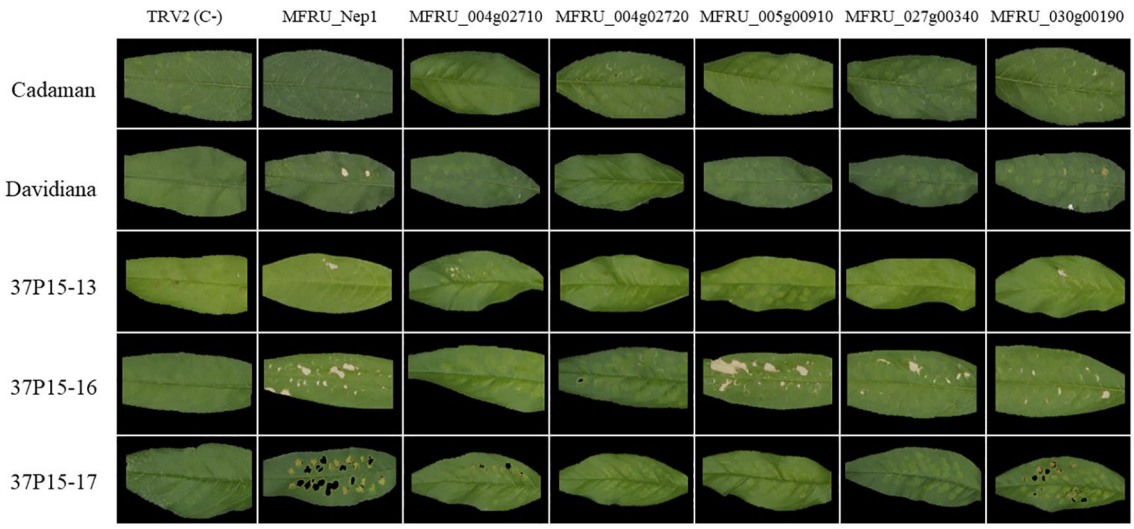

FIGURE 3
Agrobacterium mediated-transient expression (ATTA) using modified TRV construct for expressing several *M. fructicola* candidate effector proteins in different *Prunus* genotypes leaves. Columns contain the different gene constructs and rows contain are the different *Prunus* genotypes. Pictures were taken 10 days postinfiltration.

help it succeed as an invasive species (Villarino et al., 2013). In an effort to gain insights into the pathogenic mechanisms of *M. fructicola*, several groups have produced genome data for *Monilinia* spp. in recent years (Naranjo-Ortíz et al., 2018; Rivera et al., 2018; De Miccolis Angelini et al., 2019; Vilanova et al., 2021).

Valero-Jiménez et al. (2019) tried to identify species-specific effectors that were determinant in host specificity, by comparing the effector set of nine different *Botrytis* spp. No host-specific relation was found between the different genes found in the different species and its hosts, and furthermore, all effectors that were previously functionally characterized in *B. cinerea* were also present in the other species analyzed. Taking this into account, the approach of the present study was the opposite, identifying the common effectors shared among three *Monilinia* species responsible for causing brown rot in stone fruit. In the case of *M. fructicola*, the number of effector genes identified by Marcet-Houben et al. (2021) was different when compared to the number of effector genes defined by Vilanova et al. (2021). The numbers of effector genes that we used differ from the study by De Miccolis Angelini et al. (2022) which had fewer effector genes in all three species, and the study by Akhoon et al. (2023), which had significantly more effector genes in all three species. This discrepancy is due to the use of distinct criteria to determine what constitutes an effector and to differences in prediction tools and choices in the stringency of prediction parameters. Moreover, manual curation efforts as conducted by Vilanova et al. (2021) may further contribute to variability in gene numbers and lists. The strategy used in this study for identifying effectors shared between all three *Monilinia* species was based on bidirectional blasts of the effector repertoire of each species to the other species, one by one. After all comparisons, the number of effector genes shared among the three *Monilinia* spp. genomes in this study was 76. The effectors described by De Miccolis Angelini et al. (2022) and Akhoon et al. (2023) that are not represented in our effector lists might be excellent candidates for testing using the TRV-based expression system.

Viral vectors are used in effectoromic screenings, but those studies are mostly done with Potato Virus X on Solanaceae (Nasir et al., 2005; Vleeshouwers and Oliver, 2014). As PVX was not reported to infect *Prunus*, we decided to switch to a virus that is reported to infect and replicate in *Prunus*, namely Tobacco Rattle Virus (TRV). TRV-based expression systems are commonly used in plants for the purpose of achieving virus-induced gene silencing (VIGS). It serves as a high-throughput tool to investigate gene function in several plant species (Hartl et al., 2008). In this study, a TRV vector designed for VIGS (Liu et al., 2002) was modified to enable the transient expression of fungal effector genes in plants. The virus possesses a bipartite genome, with RNA2 encoding two proteins redundant for viral replication but essential for viral transmission by nematodes (Macfarlane, 2010). Liu et al. (2002) crafted a binary vector construct that includes T-DNA borders flanking an expression cassette containing TRV RNA2 sequences and a multiple cloning site for the insertion of desired sequences. *Agrobacterium tumefaciens* carrying this binary vector construct can be mixed with another *A. tumefaciens* containing TRV RNA1 sequences and then infiltrated into plants. The mixture of these *Agrobacterium* strains allows for the transformation of plant cells, facilitating the expression and subsequent replication of both viral RNAs. These RNAs can disperse throughout the host plant, enabling the expression of heterologous genes, particularly fungal effectors in this case.

With this modified virus construct, the cell death-inducing capacity of putative effector genes of *M. fructicola* could be tested in leaf tissues of different plants, including its host, *Prunus*. The development of a high-throughput screening method using a modified TRV expression vector offers a good perspective in disease resistance breeding against plant pathogens. The strategy

can be applied to study the response to fungal effector proteins in plants that can be infected by this virus such as strawberry, wheat, maize, and others (Zeng et al., 2019). This methodology provides an alternative strategy to heterologous protein production in bacteria or yeasts, which is more labour- and time-intensive. Besides this, these kind of effector assays could be complemented with infection assays and field trials (Vleeshouwers and Oliver, 2014) to test whether stone fruit, which do not show necrosis when infiltrating by fungal effectors, are less susceptible to *Monilinia* spp. In recent years, several genetic and quantitative genetic studies have revealed QTLs or markers related to brown rot resistance in peach (Baró-Montel et al., 2019b). In the case of *Monilinia* spp., knowledge about the capacity of its effectors to induce cell death and promote virulence can be exploited to genetically map and eventually clone susceptibility genes with the use of genomic tools (Martínez-García et al., 2013; Pacheco et al., 2014).

This study has identified several *M. fructicola* effector genes that induce cell death in its host plants leaf tissue. Necrosis was observed in leaves of almost all *Prunus* spp. tested upon infiltration of MFRU_030g00190, while neither *N. benthamiana* nor tomato responded to this protein. We hypothesize that the recognition of necrotrophic effectors (NEs) secreted by *Monilinia* species by receptor proteins of *Prunus* leads to host cell death and thereby confers susceptibility. If a pathogen does not produce a particular effector, or if the host does not express the susceptibility gene, the pathogen cannot invade the host, resulting in resistance (Faris and Friesen, 2020). This susceptibility mechanism is well-studied in the interaction between wheat and the necrotrophic fungi *Parastagonospora nodorum* and *Pyrenophora tritici-repentis* (Tan et al., 2012; Virdi et al., 2016; Faris and Friesen, 2020). Another well-characterized pathosystem involves fungi from the *Cochliobolus* genus, which produce cell death-inducing metabolites that are crucial for pathogenicity. In particular, *C. victoriae* produces victorin, conferring pathogenicity to oat genotypes carrying the *Vb* locus as a susceptibility determinant (reviewed in Malvestiti and van Kan, in press). Within the Sclerotiniaceae family, *Botrytis cinerea* stands out as the most extensively studied necrotrophic pathogen. It secretes several cell wall degrading enzymes (CWDEs) with NE activity, as well as NEs that lack an annotated enzymatic domain (for example BcNep1 and BcNep2), and secondary metabolites that contribute to virulence (Malvestiti and van Kan, in press; Bi et al., 2023).

In contrast with what it was observed with MFRU_030g00190, two genes (MFRU_005g00910 and MFRU_014g02060) were shown to cause necrosis in all three plant species tested. The MFRU_014g02060 protein is the ortholog to NEP1 proteins from *Botrytis* spp. NEP1-like proteins (NLPs) have been identified in plant pathogenic fungi, bacteria, and oomycetes, despite there has been ambiguity regarding their host range. While functionally characterized cytolytic NLPs have traditionally shown broad activity exclusively on dicotyledonous plant species (Seidl and Van den Ackerveken, 2019), recent reports revealed sensitivity of several monocotyledonous plants to NLPs as well (Steentjes et al., 2022). This underscores the importance of further investigating the host range and functional roles of these effectors. To do so, the generation of knockout mutants and even multigenic knockout mutants for the most interesting effectors identified in this study would be a promising approach. As demonstrated in *B. cinerea*, this approach would provide valuable insights into the function of each effector and its contribution to disease development (Leisen et al., 2022). By employing marker-free transformation methods using CRISPR/Cas and telomere vectors recently developed in *B. cinerea* (Leisen et al., 2020), we could systematically dissect the role of these effectors in the virulence of *M. fructicola*. This would enhance our understanding of the molecular mechanisms underlying pathogenicity and aid in the development of targeted strategies for disease management. As part of future experiments, it is also planned to produce pure effectors related to virulence to elucidate plant receptors and further enhance our understanding of plant-pathogen interactions.

The use of purified effectors is very promising as a base for genetic analysis allowing us to explore the complexities of plant responses and uncover the underlying mechanisms involved. This approach facilitates the identification of genetic loci associated with susceptibility to the disease, offering valuable insights into how plants interact with pathogens. Such insights are crucial for developing effective strategies to enhance crop resilience. This perspective aligns with successful instances, such as the *P. nodorum*-wheat interaction, where strategically excluding effector-sensitive genotypes from breeding programs has contributed to bolstering the partial resistance of wheat to *P. nodorum* (Friesen et al., 2007; Liu et al., 2012; Shi et al., 2016; Downie et al., 2018; Cowger et al., 2020) Emphasizing the parallels between these strategies, our study encourages the adoption of refined breeding approaches that exclude susceptible genotypes, providing breeders and growers with a powerful tool to fortify crops against the targeted disease. The methodology developed in this study, enables large-scale trials to be conducted, testing various effectors in non-model plants. This advancement opens the door to assessing germplasm for differences in cell death induction, which may serve as an indicator of susceptibility to brown rot. By employing advanced techniques such as marker-assisted selection breeders can more precisely identify and eliminate susceptible genotypes, resulting in the development of crop varieties with enhanced resistance.

Data availability statement

The original contributions presented in the study are included in the article/Supplementary Material. Further inquiries can be directed to the corresponding authors.

Author contributions

AL: Methodology, Writing – original draft, Writing – review & editing. JK: Conceptualization, Methodology, Supervision, Writing – review & editing. HB: Methodology, Writing – review & editing. RD-S: Methodology, Writing – review & editing. NT: Funding acquisition, Writing – review & editing. RT: Funding acquisition, Supervision, Writing – original draft, Writing – review & editing.

LV: Conceptualization, Funding acquisition, Methodology, Supervision, Writing – original draft, Writing – review & editing.

Funding

The author(s) declare financial support was received for the research, authorship, and/or publication of this article. This work was supported by national project PID2020-115702RB-C22/AEI/10.13039/501100011033 from the Spanish Government (MINECO) and by funding received from the CERCA Programme SGR-01477/Generalitat de Catalunya. LV received funding from the postdoctoral fellowships programme Beatriu de Pinós, funded by the Secretary of Universities and Research (Government of Catalonia) and by the Horizon 2020 programme of the European Union (MSCA grant 801370) and AL is recipient of a IRTA Sponsored Fellowship 2022.

Acknowledgments

The authors gratefully acknowledge Dr. Iban Eduardo for providing part of the plant material.

Conflict of interest

The authors declare that the research was conducted in the absence of any commercial or financial relationships that could be construed as a potential conflict of interest.

Publisher's note

Supplementary material

The Supplementary Material for this article can be found online at: https://www.frontiersin.org/articles/10.3389/fpls.2024.1428613/full#supplementary-material

References

Akhoon, B. A., Gupta, S. K., and Dhar, M. K. (2023). Dissecting the genome, secretome, and effectome repertoires of *Monilinia* spp.: The causal agent of brown rot disease: A comparative analysis. *Postharvest Biol. Technol.* 195, 112120. doi: 10.1016/j.postharvbio.2022.112120

Bai, S., Tuan, P. A., Tatsuki, M., Yaegaki, H., Ohmiya, A., Yamamizo, C., et al. (2016). Knockdown of carotenoid cleavage dioxygenase 4 (CCD4) via virus-induced gene silencing confers yellow coloration in peach fruit: evaluation of gene function related to fruit traits. *Plant Mol. Biol. Rep.* 34, 257–264. doi: 10.1007/s11105-015-0920-8

Balsells-Llauradó, M., Silva, C. J., Usall, J., Vall-llaura, N., Serrano-Prieto, S., Teixidó, N., et al. (2020). Depicting the battle between nectarine and *Monilinia* laxa: the fruit developmental stage dictates the effectiveness of the host defenses and the pathogen's infection strategies. *Hortic. Res.* 7, 167. doi: 10.1038/s41438-020-00387-w

Baró-Montel, N., Eduardo, I., Usall, J., Casals, C., Arús, P., Teixidó, N., et al. (2019a). Exploring sources of resistance to brown rot in an interspecific almond × peach population. *J. Sci. Food Agric.* 99, 4105–4113. doi: 10.1002/jsfa.9640

Baró-Montel, N., Torres, R., Casals, C., Teixidó, N., Segarra, J., and Usall, J. (2019b). Developing a methodology for identifying brown rot resistance in stone fruit. *Eur. J. Plant Pathol.* 154, 287–303. doi: 10.1007/s10658-018-01655-1

Baró-Montel, N., Vall-llaura, N., Giné-Bordonaba, J., Usall, J., Serrano-Prieto, S., Teixidó, N., et al. (2019c). Double-sided battle: The role of ethylene during *Monilinia* spp. infection in peach at different phenological stages. *Plant Physiol. Biochem.* 144, 324–333. doi: 10.1016/j.plaphy.2019.09.048

Bi, K., Liang, Y., Mengiste, T., and Sharon, A. (2023). Killing softly: a roadmap of *Botrytis cinerea* pathogenicity. *Trends Plant Sci.* 28, 211–222. doi: 10.1016/j.tplants.2022.08.024

Cantabella, D., Teixidó, N., Segarra, G., Torres, R., Casanovas, M., and Dolcet-Sanjuan, R. (2021). Rhizosphere microorganisms enhance in *vitro* root and plantlet development of *Pyrus* and *Prunus* rootstocks. *Planta* 253, 78. doi: 10.1007/s00425-021-03595-3

Casals, C., Torres, R., Teixidó, N., de Cal, A., Segarra, J., and Usall, J. (2022). Brown rot on stone fruit: From epidemiology studies to the development of effective control strategies. *Sci. Hortic.* 301, 111096. doi: 10.1016/j.scienta.2022.111096

Cowger, C., Ward, B., Brown-Guedira, G., and Brown, J. K. M. (2020). Role of effector-sensitivity gene interactions and durability of quantitative resistance to *Septoria nodorum* blotch in eastern U.S. wheat. *Front. Plant Scien.* 11. doi: 10.3389/fpls.2020.00155

De Cal, A., Usall, J., and Melgarejo, P. (2009). First report of brown rot caused by *Monilinia fructicola* in peach orchards in Ebro valley, Spain. *Plant Dise* 93, 763–763. doi: 10.1094/PDIS-93-7-0763A

De Miccolis Angelini, R. M., Landi, L., Raguseo, C., Pollastro, S., Faretra, F., and Romanazzi, G. (2022). Tracking of diversity and evolution in the brown rot fungi *Monilinia fructicola*, *Monilinia fructigena*, and *Monilinia laxa*. *Front. Microbiol.* 13, 854852. doi: 10.3389/fmicb.2022.854852

De Miccolis Angelini, R. M., Romanazzi, G., Pollastro, S., Rotolo, C., Faretra, F., and Landi, L. (2019). New high-quality draft genome of the brown rot fungal pathogen *Monilinia fructicola*. *Genome Biol. Evol.* 11, 2850–2855. doi: 10.1093/gbe/evz207

Domazakis, E., Lin, X., Aguilera-Galvez, C., Wouters, D., Bijsterbosch, G., Wolters J., P., et al. (2017). Effectoromics-based identification of cell surface receptors in potato. *Methods Mol. Biol.* 1578, 337–353. doi: 10.1007/978-1-4939-6859-6_29

Downie, R. C., Bouvet, L., Furuki, E., Gosman, N., Gardner, K. A., Mackay, I. J., et al. (2018). Assessing European wheat sensitivities to *Parastagonospora nodorum* necrotrophic effectors and fine-mapping the *Snn3-B1* locus conferring sensitivity to the effector SnTox3. *Front. Plant Sci.* 9. doi: 10.3389/fpls.2018.00881

Faris, J. D., and Friesen, T. L. (2020). Plant genes hijacked by necrotrophic fungal pathogens. *Curr. Opin. Plant Biol.* 56, 74–80. doi: 10.1016/j.pbi.2020.04.003

Friesen, T. L., and Faris, J. D. (2021). Characterization of effector-target interactions in necrotrophic pathosystems reveals trends and variation in host manipulation. *Annu. Rev. Phytopathol.* 59, 77–98. doi: 10.1146/annurev-phyto-120320

Friesen, T. L., Meinhardt, S. W., and Faris, J. D. (2007). The *Stagonospora nodorum*-wheat pathosystem involves multiple proteinaceous host-selective toxins and corresponding host sensitivity genes that interact in an inverse gene-for-gene manner. *Plant J.* 51, 681–692. doi: 10.1111/j.1365-313X.2007.03166.x

Hartl, M., Merker, H., Schmidt, D. D., and Baldwin, I. T. (2008). Optimized virus-induced gene silencing in *Solanum nigrum* reveals the defensive function of leucine aminopeptidase against herbivores and the shortcomings of empty vector controls. *New Phytol.* 179, 356–365. doi: 10.1111/j.1469-8137.2008.02479.x

Hrustić, J., Delibašić, G., Stanković, I., Grahovac, M., Krstić, B., Bulajić, A., et al. (2015). *Monilinia* spp. causing brown rot of stone fruit in Serbia. *Plant Dis.* 99, 709–717. doi: 10.1094/PDIS-07-14-0732-RE

Index Fungorum (2023). *Monilinia* species list. Available online at: http://www.indexfungorum.org.

Kabbage, M., Kessens, R., Bartholomay, L. C., and Williams, B. (2017). The life and death of a plant cell. *Annu. Rev. Plant Biol.* 68, 375–404. doi: 10.1146/annurev-arplant-043015

Kars, I., Krooshof, G. H., Wagemakers, L., Joosten, R., Benen, J. A. E., and van Kan, J. A. L. (2005). Necrotizing activity of five *Botrytis cinerea* endopolygalacturonases produced in *Pichia pastoris*. *Plant J.* 43, 213–225. doi: 10.1111/j.1365-313X.2005.02436.x

Landi, L., De Miccolis Angelini, R. M., Pollastro, S., Abate, D., Faretra, F., and Romanazzi, G. (2018). Genome sequence of the brown rot fungal pathogen *Monilinia fructigena*. *BMC Res. Notes* 11, 758. doi: 10.1186/s13104-018-3854-z

Leisen, T., Bietz, F., Werner, J., Wegner, A., Schaffrath, U., Scheuring, D., et al. (2020). CRISPR/Cas with ribonucleoprotein complexes and transiently selected telomere vectors allows highly efficient marker-free and multiple genome editing in *Botrytis cinerea*. *PloS Pathog.* 16, e1008326. doi: 10.1371/journal.ppat.1008326

Leisen, T., Werner, J., Pattar, P., Safari, N., Ymeri, E., Sommer, F., et al. (2022). Multiple knockout mutants reveal a high redundancy of phytotoxic compounds contributing to necrotrophic pathogenesis of *Botrytis cinerea*. *PloS Pathog.* 18, e1010367. doi: 10.1371/journal.ppat.1010367

Lichou, J., Mandrin, J. F., Breniaux, D., Mercier, V., Giauque, P., Desbrus, D., et al. (2002). A new, powerful monilia: *Monilia fructicola* chooses stone-fruit trees for its attacks. *Phytoma* 547, 22–25.

Liu, Y., Schiff, M., Marathe, R., and Dinesh-Kumar, S. P. (2002). Tobacco *Rar1*, *EDS1* and *NPR1/NIM1* like genes are required for *N*-mediated resistance to tobacco mosaic virus. *Plant J.* 30, 415–429. doi: 10.1046/j.1365-313X.2002.01297.x

Liu, Z., Zhang, Z., Faris, J. D., Oliver, R. P., Syme, R., McDonald, M. C., et al. (2012). The cysteine rich necrotrophic effector SnTox1 produced by *Stagonospora nodorum* triggers susceptibility of wheat lines harboring *Snn1*. *PloS Pathog.* 8, e1002467. doi: 10.1371/journal.ppat.1002467

Macfarlane, S. A. (2010). Tobraviruses—plant pathogens and tools for biotechnology. *Mol. Plant Pathol.* 11, 577–583. doi: 10.1111/j.1364-3703.2010.00617.x

Malvestiti, M. C., and van Kan, J. A. L. "Your death, my life: understanding the success story of necrotrophic plant pathogenic Ascomycota," in *The MYCOTA, Agricultural and Industrial Applications*. Eds. F. Kempken, S. Grüttner and K. Kollath-Leiss (Springer Nature Publishers). in press.

Marcet-Houben, M., Villarino, M., Vilanova, L., de Cal, A., van Kan, J. A. L., Usall, J., et al. (2021). Comparative genomics used to predict virulence factors and metabolic genes among *Monilinia* species. *J. Fungi* 7, 464. doi: 10.3390/jof7060464

Martínez-García, P. J., Parfitt, D. E., Bostock, R. M., Fresnedo-Ramírez, J., Vazquez-Lobo, A., Ogundiwin, E. A., et al. (2013). Application of genomic and quantitative genetic tools to identify candidate resistance genes for brown rot resistance in peach. *PloS One* 8, e78634. doi: 10.1371/journal.pone.0078634

Naranjo-Ortíz, M. A., Rodríguez-Píres, S., Torres, R., De Cal, A., Usall, J., and Gabaldón, T. (2018). Genome sequence of the brown rot fungal pathogen *Monilinia laxa*. *Geno. Announc.* 6, 10–1128. doi: 10.1128/genomeA.00214-18

Nasir, K. H., Takahashi, Y., Ito, A., Saitoh, H., Matsumura, H., Kanzaki, H., et al. (2005). High-throughput in planta expression screening identifies a class II ethylene-responsive element binding factor-like protein that regulates plant cell death and non-host resistance. *Plant J.* 43, 491–505. doi: 10.1111/j.1365-313X.2005.02472.x

Ollero-Lara, A., Agustí-Brisach, C., Lovera, M., Roca, L. F., Arquero, O., and Trapero, A. (2019). Field susceptibility of almond cultivars to the four most common aerial fungal diseases in southern Spain. *Crop Prot.* 121, 18–27. doi: 10.1016/j.cropro.2019.03.005

Pacheco, I., Bassi, D., Eduardo, I., Ciacciulli, A., Pirona, R., Rossini, L., et al. (2014). QTL mapping for brown rot (*Monilinia fructigena*) resistance in an intraspecific peach (*Prunus persica* L. Batsch) F1 progeny. *Tree Genet. Genmes.* 10, 1223–1242. doi: 10.1007/s11295-014-0756-7

Rivera, Y., Zeller, K., Srivastava, S., Sutherland, J., Galvez, M., Nakhla, M., et al. (2018). Draft genome resources for the phytopathogenic fungi *Monilinia fructicola*, *M. fructigena*, *M. polystroma*, and *M. laxa*, the causal agents of brown rot. *Phytopathology* 108, 1141–1142. doi: 10.1094/PHYTO-12-17-0418-A

Schouten, A., van Baarlen, P., and van Kan, J. A. L. (2008). Phytotoxic Nep1-like proteins from the necrotrophic fungus *Botrytis cinerea* associate with membranes and the nucleus of plant cells. *New Phytol.* 177, 493–505. doi: 10.1111/j.1469-8137.2007.02274.x

Seidl, M. F., and Van den Ackerveken, G. (2019). Activity and phylogenetics of the broadly occurring family of microbial Nep1-like proteins. *Annu.l Rev. Phytopathol.* 57, 367–386. doi: 10.1146/annurev-phyto-082718

Selin, C., de Kievit, T. R., Belmonte, M. F., and Fernando, W. G. D. (2016). Elucidating the role of effectors in plant-fungal interactions: Progress and challenges. *Front. Microbiol.* 7, 600. doi: 10.3389/fmicb.2016.00600

Shao, D., Smith, D. L., Kabbage, M., and Roth, M. G. (2021). Effectors of plant necrotrophic fungi. *Front. Plant Sci.* 12. doi: 10.3389/fpls.2021.687713

Shi, G., Zhang, Z., Friesen, T. L., Raats, D., Fahima, T., Brueggeman, R. S., et al. (2016). The hijacking of a receptor kinase-driven pathway by a wheat fungal pathogen leads to disease. *Sci. Adv.* 2, e1600822. doi: 10.1126/sciadv.1600822

Steentjes, M. B. F., Valderrama, A. L. H., Fouillen, L., Bahammou, D., Leisen, T., Albert, I., et al. (2022). Cytotoxic activity of Nep1-like proteins on monocots. *New Phytol.* 235, 690–700. doi: 10.1111/nph.18146

Tan, K.-C., Ferguson-Hunt, M., Rybak, K., Waters, O. D. C., Stanley, W. A., Bond, C. S., et al. (2012). Quantitative variation in effector activity of ToxA isoforms from *Stagonospora nodorum* and *Pyrenophora tritici-repentis*. *Mol. Plant Microbe Interact.* 25, 515–522. doi: 10.1094/MPMI

Tan, K. C., Oliver, R. P., Solomon, P. S., and Moffat, C. S. (2010). Proteinaceous necrotrophic effectors in fungal virulence. *Funct. Plant Biol.* 37, 907–912. doi: 10.1071/FP10067

Tan, K. C., Phan, H. T. T., Rybak, K., John, E., Chooi, Y. H., Solomon, P. S., et al. (2015). Functional redundancy of necrotrophic effectors – consequences for exploitation for breeding. *Front. Plant Sci.* 6, 501. doi: 10.3389/fpls.2015.00501

Valero-Jiménez, C. A., Veloso, J., Staats, M., and van Kan, J. A. L. (2019). Comparative genomics of plant pathogenic *Botrytis* species with distinct host specificity. *BMC Genomic.* 20, 203. doi: 10.1186/s12864-019-5580-x

Vilanova, L., Valero-Jiménez, C. A., and Van Kan, J. A. L. (2021). Deciphering the *Monilinia fructicola* genome to discover effector genes possibly involved in virulence. *Genes* 12, 568. doi: 10.3390/genes12040568

Villarino, M., Egüen, B., Lamarca, N., Segarra, J., Usall, J., Melgarejo, P., et al. (2013). Occurrence of *Monilinia laxa* and *M. fructigena* after introduction of *M. fructicola* in peach orchards in Spain. *Eur. J. Plant Pathol.* 137, 835–845. doi: 10.1007/s10658-013-0292-6

Villarino, M., Melgarejo, P., Usall, J., Segarra, J., and De Cal, A. (2010). Primary inoculum sources of *Monilinia* spp. in Spanish peach orchards and their relative importance in brown rot. *Plant Dis.* 94, 1048–1054. doi: 10.1094/PDIS-94-8-1048

Virdi, S. K., Liu, Z., Overlander, M. E., Zhang, Z., Xu, S. S., Friesen, T. L., et al. (2016). New insights into the roles of host gene-necrotrophic effector interactions in governing susceptibility of durum wheat to tan spot and *Septoria nodorum* blotch. *G3: Genes Genomes. Genet.* 6, 4139–4150. doi: 10.1534/g3.116.036525

Vleeshouwers, V. G. A. A., and Oliver, R. P. (2014). Effectors as tools in disease resistance breeding against biotrophic, hemibiotrophic, and necrotrophic plant pathogens. *Mol. Plant Microbe Interact.* 27, 196–206. doi: 10.1094/MPMI-10-13-0313-IA

Zaracho-Echagüe, N. H., Arús, P., and Eduardo, I. (2022). Construction of a NIL collection of *P. davidiana* into the peach genetic background. *Acta Hortic.* 1352, 263–270. doi: 10.17660/ActaHortic.2022.1352.35

Zeng, H., Xie, Y., Liu, G., Wei, Y., Hu, W., and Shi, H. (2019). *Agrobacterium*-mediated gene transient overexpression and tobacco rattle virus (TRV)-based gene silencing in cassava. *Int. J. Mol. Sci.* 20, 3976. doi: 10.3390/ijms20163976

frontiers | Frontiers in Plant Science

TYPE Original Research
PUBLISHED 16 August 2024
DOI 10.3389/fpls.2024.1446288

OPEN ACCESS

EDITED BY
Brigitte Mauch-Mani,
Université de Neuchâtel, Switzerland

REVIEWED BY
Hye-Seon Kim,
United States Department of Agriculture, United States
Sophie Trouvelot,
Université de Bourgogne, France

*CORRESPONDENCE
Ling Tian
tianling@szpu.edu.cn
Yan Xu
yan.xu@nwsuaf.edu.cn

RECEIVED 09 June 2024
ACCEPTED 24 July 2024
PUBLISHED 16 August 2024

CITATION
Dou M, Li Y, Hao Y, Zhang K, Yin X, Feng Z, Xu X, Zhang Q, Bao W, Chen X, Liu G, Wang Y, Tian L and Xu Y (2024) Histological and transcriptomic insights into the interaction between grapevine and *Colletotrichum viniferum*. *Front. Plant Sci.* 15:1446288. doi: 10.3389/fpls.2024.1446288

Histological and transcriptomic insights into the interaction between grapevine and *Colletotrichum viniferum*

Mengru Dou[1,2,3], Yuhang Li[1,2,3], Yu Hao[1,2,3], Kangzhuang Zhang[1,2,3], Xiao Yin[1,2,3], Zinuo Feng[1,2,3], Xi Xu[1,2,3], Qi Zhang[1,2,3], Wenwu Bao[1,2], Xi Chen[1,2,3], Guotian Liu[1,2,3], Yuejin Wang[1,2,3], Ling Tian[4]* and Yan Xu[1,2,3]*

[1]State Key Laboratory of Crop Stress Biology in Arid Areas, Northwest Agriculture & Forestry University, Yangling, Shaanxi, China, [2]College of Horticulture, Northwest A&F University, Yangling, Shaanxi, China, [3]Key Laboratory of Horticultural Plant Biology and Germplasm Innovation in Northwest China, Ministry of Agriculture, Yangling, Shaanxi, China, [4]School of Management, Shenzhen Polytechnic University, Shenzhen, Guangdong, China

Introduction: Grape is of high economic value. *Colletotrichum viniferum*, a pathogen causing grape ripe rot and leaf spot, threatens grape production and quality.

Methods: This study investigates the interplay between *C. viniferum* by Cytological study and transcriptome sequencing.

Results: Different grapevine germplasms, *V. vinifera* cv. Thompson Seedless (TS), *V. labrusca* accession Beaumont (B) and *V. piasezkii* Liuba-8 (LB-8) were classified as highly sensitive, moderate resistant and resistant to *C. viniferum*, respectively. Cytological study analysis reveals distinct differences between susceptible and resistant grapes post-inoculation, including faster pathogen development, longer germination tubes, normal appressoria of *C. viniferum* and absence of white secretions in the susceptible host grapevine. To understand the pathogenic mechanisms of *C. viniferum*, transcriptome sequencing was performed on the susceptible grapevine "TS" identifying 236 differentially expressed *C. viniferum* genes. These included 56 effectors, 36 carbohydrate genes, 5 P450 genes, and 10 genes involved in secondary metabolism. Fungal effectors are known as pivotal pathogenic factors that modulate plant immunity and affect disease development. *Agrobacterium*-mediated transient transformation in *Nicotiana benthamiana* screened 10 effectors (CvA13877, CvA01508, CvA05621, CvA00229, CvA07043, CvA05569, CvA12648, CvA02698, CvA14071 and CvA10999) that inhibited INF1 (infestans 1, *P. infestans* PAMP elicitor) induced cell death and 2 effectors (CvA02641 and CvA11478) that induced cell death. Additionally, transcriptome analysis of "TS" in response to *C. viniferum* identified differentially expressed grape genes related to plant hormone signaling (*TGA*, *PR1*, *ETR*, and *ERF1/2*), resveratrol biosynthesis genes (*STS*), phenylpropanoid biosynthesis genes (*PAL* and *COMT*), photosynthetic antenna proteins (*Lhca* and *Lhcb*), transcription factors (*WRKY*, *NAC*, *MYB*, *ERF*, *GATA*, *bHLH* and *SBP*), ROS (reactive oxygen species) clearance genes (*CAT*, *GSH*, *POD* and *SOD*), and disease-related genes (*LRR*, *RPS2* and *GST*).

10.3389/fpls.2024.1446288

Discussion: This study highlights the potential functional diversity of *C. viniferum* effectors. Our findings lay a foundation for further research of infection mechanisms in *Colletotrichum* and identification of disease response targets in grape.

KEYWORDS

grape, *Colletotrichum viniferum*, genome annotation, fungal infection strategy, grapevine response

1 Introduction

Grape (*Vitis vinifera* L.), an ancient and economically significant, is consumed worldwide (Dong et al., 2023). However, grapes are susceptible to various pathogens, including *Colletotrichum viniferum*, particularly under high temperatures and humidity. This pathogen affects grape cultivars such as Pione, Kyoho, Ives, and Merlot (Echeverrigaray et al., 2020; Yokosawa et al., 2020), resulting in significant economic losses of approximately 67% in the Mid-Atlantic region of the United States and around 37% in Northeast China (Cosseboom and Hu, 2022; Ji et al., 2021). *C. viniferum* infects grapevine leaves, shoots, stems, and berries, causing grape ripe rot and leaf spot, with particularly severe damage to berries (Pan et al., 2016).

Colletotrichum species are identified and categorized in China and globally according to morphological and molecular features. Pathogenic species identified include *C. acutatum*, *C. aenigma*, *C. capsici*, *C. fruticola*, *C. gloeosporioides*, and *C. viniferum*, among others (Lei et al., 2016; Oo and Oh, 2017; Echeverrigaray et al., 2020). With the continuous development of sequencing techniques, high-throughput sequencing technology has been widely adopted. Several *Colletotrichum* species from various host plants have had their complete genomes sequenced, including *C. lindemuthianum* (Gutiérrez et al., 2016), *C. acutatum* (Han et al., 2016), *C. graminicola* (Buiate et al., 2017), *C. sublineola* (Buiate et al., 2017), *C. asianum* (Meng et al., 2019), *C. higginsianum* (Ayako et al., 2019), and *C. fioriniae* (Xu et al., 2024). Fungal genome sequencing has greatly enhanced our understanding of the interactions between hosts and pathogens. However, the genomic sequencing of *C. viniferum* CvYL2a on grape has only recently been published (Dou et al., 2022).

Different grape varieties exhibit varying resistance levels to *Colletotrichum*. Researchers have classified the disease resistance abilities of various grape cultivars and their hybrids (Shiraishi et al., 2007). A comprehensive study of grape ripe rot resistance using natural field assessment, field inoculation, and indoor fruit *in vitro* analysis highlighted the exceptional resistance of Chinese wild grapes as valuable disease-resistant germplasm resources (He and Ren, 1990). Subsequent research revealed that cultivars such as Emerald Seedless, Tano Red, and Rem46-77 (Aestivalis GVIT 0970) are susceptible to grape ripe rot, while Agawan, Huangguan, and Xiangfei are resistant (Kim and Oh, 2019). The diversity in resistance levels provides valuable germplasm resources for investigating grape ripe rot resistance mechanisms, crucial for breeding and evaluating new resistant grapevine cultivars, and developing innovative disease control methods. Several investigations have analyzed the infection processes of various *Colletotrichum* spp. isolates in host fruits, such as apple infected by *C. fructicola*, Guava infected by *C. gloeosporioides*, blueberry, strawberry, and almond affected by *C. acutatum* (Arroyo et al., 2005; Diéguez-Uribeondo et al., 2005; Wharton and Schilder, 2008; Moraes et al., 2013; Shang et al., 2020). However, limited research has focused on grape pathogenesis and the histological differences between susceptible and resistant varieties. Currently, control of *Colletotrichum* spp. mainly relies on fungicide use, which negatively impacts soil, food safety, and the environment. Therefore, it's critical to develop more effective and environmentally friendly disease management strategies by studying potential plant-pathogen interactions with a more profound comprehensive approach.

Transcriptome sequencing is the most straightforward way to investigating gene expression levels, with numerous studies exploring transcriptome sequencing in host-pathogen interactions involving *Colletotrichum* species. Transcriptome analysis of the host included strawberry infected by *C. siamense*, sugarcane infected by *C. falcatum*, and Asian ginseng (*Panax ginseng*) infected by *C. panacicola* (Nandakumar et al., 2021; Zheng et al., 2022; Xia et al., 2023). Similarly, transcriptome analyses of *Colletotrichum* spp. have explored pathogenicity mechanisms in different host-pathogen interactions, such as *C. camelliae* on tea, *C. falcatum* on sugarcane, and *C. fructicola* on apple (Liang et al., 2018; Prasanth et al., 2022; He et al., 2023). However, real-time integration of transcriptomic data from both hosts and *Colletotrichum* spp. during infection remains limited. While several studies have investigated grapevine transcriptomes in response to *Colletotrichum* spp. infection, the transcriptomic dynamics of *Colletotrichum* itself are missing (Lei et al., 2022; Shen et al., 2022; Yu et al., 2023).

Colletotrichum spp. seriously threatens the yield and quality of grapes, especially affecting high-quality grape varieties with poor resistance. Fortunately, most wild grape germplasm resources in China are resistant to this fungus. Through histochemical staining and ultrastructural observation, *V. vinifera* cv. Thompson Seedless (TS), *V. labrusca* accession Beaumont (B) and *V. piasezkii* Liuba-8 (LB-8) were identified as highly sensitive, moderately resistant and

resistant to *C. viniferum*, respectively. The transient transformation assays in *Nicotiana benthamiana* showed that *Colletotrichum* spp. effectors CoNIS1, Cte1, Cg2LysM and CgCFEM1 inhibited plant immune response, CtNUDIX and ChCEC3 induced cell death similar to HR response (Bhadauria et al., 2013; Tsushima et al., 2021; Zhao et al., 2023; Feng et al., 2024; Yuan et al., 2024). Effectors play different roles during infection. Currently, there are no studies about *C. viniferum* effector on grape, and the infection mechanism remains unclear. To uncover the infection processes of *C. viniferum*, particularly the roles of effectors during infection and the responses of grapevine to *C. viniferum*, we conducted a study focusing on pathogenesis, selecting the susceptible grapes "TS" for transcriptome analysis. Our aim was to screen *C. viniferum* pathogenic genes by transcriptome sequencing, leading to the identification of 85 effectors. These effectors were subsequently screened on *Nicotiana benthamiana* to examine their roles in the infection process. Simultaneously, we analyzed the grapevines' responses to *C. viniferum*, providing insights into the interaction between *C. viniferum* and grapes and shedding light on its pathogenic mechanism.

2 Materials and methods

2.1 Fungal strain, plant materials, and inoculation

The *C. viniferum* strain CvYL2a, previously obtained and purified in our research facility, was cultured on potato dextrose agar (PDA) under dark conditions at 25°C. *C. viniferum* conidia were induced by transferring mycelia from PDA to a Carboxymethylcellulose (CMC) sodium fluid medium and incubating them at 150 rpm and 25°C for 3-5 days. Conidia were separated from mycelia by filtering with two-layer sterilization gauze and collected after centrifugation at 5000 rpm for 10 min. After two washes with sterile distilled water (SDW), the conidia were standardized to a 5×10^6 conidia/mL concentration, as determined using a hemocytometer and a light microscope.

For conidia inoculation, undamaged fully expanded leaves were collected from the apex of "TS", "B" and "LB-8" grown in the grapevine germplasm resource vineyard at Northwest A&F University in Yangling, Shaanxi, China. When inoculation was carried out in June 2020, average outdoor day/night temperature ranged between 32 and 15°C. The vineyard management is under regular management with fungicides and insecticides, and organic and compound fertilizers. After sterilizing the leaf surfaces spraying with 75% ethanol for 30 seconds and rinsing them three times with SDW, circular leaf discs with a diameter of 15 mm were prepared, and placed in sterile Petri dishes 90 mm in diameter with moist double-layer filter papers. These leaf discs were inoculated with 20 μL of the above concentration of conidia suspension, and incubated at 25°C with a relative humidity of 90% and a photoperiod of 16 h light/8 h dark. Leaves placed in trays were sprayed with the same concentration of conidial suspension under the same conditions. The experiment was conducted with nine leaf discs, the diameter of each leaf disc necrosis was measured three times. The experiment was repeated three times.

2.2 Staining and light microscope imaging

The leaf disks were immersed in a solution containing ethanol and trichloromethane (3:1, vol/vol) along with trichloroacetic acid (0.45% wt/vol) for 3 days, followed by clearing in chloral hydrate (250 g/100 mL water) for another 3 days.

For trypan blue staining, leaf discs underwent a 30-minute staining process using a solution comprising trypan blue (20 mg), lactic acid (20 mL), glycerol (20 mL), phenol (20 mL), and ddH_2O (20 mL). For DAB (Diaminobenzidine) staining, leaf discs were immersed in 5 mL centrifuge tubes filled with DAB staining Zsolution (1 mg DAB/mL ddH_2O, pH 3.8) for 20 min under vacuum in the dark, followed by incubation at 25°C for 8 h in tin foil bags, and examined with 200 × or 400 × magnification using a light microscope (BX-53, Olympus). The resolution of the photographs was 150 dpi.

2.3 Sample preparation and scanning electron microscopy

Grape leaves inoculated with *C. viniferum* CvYL2a were cut into 5 × 5 mm pieces and initially fixed in 4% (vol/vol) glutaraldehyde in 0.1 M phosphate buffer (pH 6.8) at 4°C overnight. After 4 × 10 min rises in the same buffer, the samples were subjected to dehydration in a series of ethanol solutions ranging from 30% to 90% (vol/vol), each step lasting for 15 min, followed by three cycles of absolute ethyl alcohol dehydration. Finally, these samples were dried using a CO_2 critical point dryer before being coated with gold and observed with SEM (Nano SEM-450, America).

2.4 Sample preparation and transmission electron microscopy

Grape leaves inoculated with *C. viniferum* CvYL2a were cut into 1 × 1 mm pieces and fixed in 4% (vol/vol) glutaraldehyde in 0.1 M phosphate buffer (pH 6.8) at 4°C overnight. After 4 × 10 min washes in the same buffer, the samples underwent post-fixation using a solution containing 1% osmium tetroxide (OsO_4) at 4°C for 2 h and were subjected to dehydration as described in Section 2.3. Next, these samples were infiltrated with London Resin Company Ltd (LR) White Resin (Basingstoke, UK) in a series of proportions, 3:1 (vol/vol) for 2 h, 1:1 (vol/vol) for 8 h, 1:3 (vol/vol) for 12 h, and pure resin for 48 h, with a change every 24 h. Finally, they were immersed in pure resin and polymerized at 55°C for 48 h.

For semi-thin sections of 1μm thickness, samples, cut using a glass knife, were treated with 0.3% aqueous toluidine blue in 1.89% sodium tetraborate and observed with bright-field microscope (Olympus BX-51, Japan). Ultra-thin sections (90 nm) were prepared using a diamond knife and treated with uranyl acetate

and lead citrate before being examined via a transmission electron microscope (HT7700, Japan).

2.5 Measurement of reactive oxygen species production rate

Plants rapidly produce reactive oxygen species (ROS) that directly inhibit the growth of pathogens during pathogens infection (Li et al., 2021). The DAB staining method is commonly used to detect H_2O_2 production (Huckelhoven et al., 1999; Ding et al., 2019). H_2O_2 production in both resistant and sensitive leaves was observed after DAB staining using a light microscopy. The rate was determined as the percentage of appressoria inducing H_2O_2 production in leaf cells to the overall count of appressoria. A total of 100 appressoria were randomly selected for assessment from each leaf, and this analysis was conducted on three blades at each time point. The experiment was performed with three independent biological replicates.

2.6 Gene family and phylogenetic evolution analyses

The gene sets of 14 fungal species were filtered, and similarity relationships between protein sequences of all species were analyzed using DIAMOND (Buchfink et al., 2015), which were further clustered using OrthoFinder2 (Emms and Kelly, 2019). To identify common single copy orthologous genes, multi-sequence alignment of genes within each single-copy homologous gene family was conducted using MUSCLE (Edgar, 2004). The evolutionary tree was constructed using RAxML with the maximum likelihood model (Stamatakis, 2014). Divergence times were estimated by integrating the constructed evolutionary tree with data from the TimeTree website and analyzed using the MCMCTree program in the software r8s and PAML software packages (Sanderson, 2003; Hedges et al., 2006). Data from 14 genomes used in comparative genomics can be found in the National Center for Biotechnology Information (NCBI) data library. These links and fungal strain names were shown in Supplementary Table 8.

2.7 RNA-seq and data analysis

Frozen tissue samples were obtained from *C. viniferum* CvYL2a-infested "TS" leaves at five different time points (0, 6, 12, 24, and 48 hours post inoculation (hpi)). Total RNA from these samples was extracted by Novogene Corporation Inc using the TRIzol Reagent (Invitrogen, Cat no. 15596026) and confirmed for integrity by 1% agarose gel electrophoresis. RNA purity and concentration were assessed using Nanodrop (Thermo Scientific, USA) and Agilent 5400 (Agilent Technologies, USA), respectively. Sequencing libraries of 150 bp paired-end reads were prepared and sequenced on an Illumina Novaseq platform. Clean reads were filtered by trimming the adapter sequences and low-quality reads of raw reads. High-quality reads were aligned to the *C. viniferum* CvYL2a (Dou et al., 2022) and the grapevine (12 × PN40024) reference genomes using HISAT2 (Mortazavi et al., 2008). Gene expression levels were quantified by calculating the fragments per kilobase of transcript per million mapped readings (FPKM). Differential expression genes (DEGs) were identified by comparing the inoculated samples at each infection time point with the 0 h samples using DESeq2 software (Love et al., 2014), with criteria set at $Log_2|(\text{fold change})| > 4$ and $P\text{-value} < 0.05$ via Benjamini and Hochberg's approach. The gene ontology (GO) terms were categorized using GOSeq (Joung et al., 2010), and KEGG (http://www.genome.jp/kegg/) was used to explore the metabolic pathways of DEGs. Visualization of the results was done using venn diagrams and heatmaps created using TBtools v0.664 software (Chen et al., 2018).

2.8 qRT-PCR analysis

45 total RNA from three different grape germplasms, five inoculation periods (0, 6, 12, 24, and 48 hpi) with *C. viniferum* infection, and three replicates per period were extracted following the manufacturer's instruction (R6827-01, Omega Bio-tek, USA). TransScript® One-Step gDNA Removal and cDNA Synthesis SuperMix (AT311-02, Trans gen, China) was used for the synthesis of first-strand cDNA. Primers are listed in Supplementary Table 2. Real-time PCR amplification was conducted using TransScript® II Green One-Step qRT-PCR SuperMix (AQ311-01, Trans gen, China).

2.9 Determination of endogenous hormone concentrations

According to the description of the method of extracting grape leaves hormones (Li et al., 2021b), 100 mg of TS leaves infected *C. viniferum* per period were promptly crushed in liquid nitrogen, followed by extraction with 1 mL of solvent (glacial acetic acid: methanol: isopropanol = 1: 20: 79 (v/v/v)). The concentration of hormones including salicylic acid (SA), ethylene (ET) synthesis precursor ACC and jasmonates (JA) in the extract was quantified by liquid chromatography-quadrupole ion trap-mass spectrometry (LC-QTRAP-MS, USA). There were three biological replicates for each hormone.

2.10 Plasmid construction and *Agrobacterium* transformation

SignalP and TMHMM software were used to select genes with signal peptide domain and TMHM without transmembrane domain as candidate effectors. 85 putative *C. viniferum* effectors were amplified, using cDNA as templates, with their predicted N-terminal signal sequences removed. The source of the cDNA was RNA extracted from grape leaves inoculated with *C. viniferum*. Specific primers designed (Supplementary Table 2) for each effector

10.3389/fpls.2024.1446288

can be found in Appendix T. Subsequently, these sequences were cloned into vector pCAMBIA2300-GFP (Green fluorescent protein). Recombinant plasmids were transformed into *Agrobacterium tumefaciens* strain GV3101 using the liquid nitrogen freezing-thawing method. *Agrobacteria* carrying effector-GFP constructs were cultured in LB liquid medium, collected after centrifugation at 5000 rpm for 3 min, and resuspended in infiltration buffer (10 mM $MgCl_2$, 10 mM MES (pH 5.7), 200μM acetosyringone) to achieve an OD_{600} of 0.6. The suspension was incubated for 3 h at 28°C in dark before infiltrating the leaves. Healthy leaves of 4 to 5 week-old *N. benthamiana* were infiltrated using a 1-mL needless syringe. INF1 (infestans 1, *P. infestans* PAMP elicitor) and GFP served as positive and negative controls, respectively. For experiments designed to suppress cell death triggered by INF1-GFP, leaves were infiltrated with effectors 12 h before INF1-GFP infiltration. Finally, leaf symptoms of cell death were evaluated through photography.

3 Results

3.1 Evolution of gene family in *C.viniferum* CvYL2a reveals unique features

To analyze the evolutionary relationships among *C. viniferum* CvYL2a and 13 other fungi, we clustered their proteins using OrthoFinder2. This process identified 16678 orthogroups containing 177914 proteins (Supplementary 1). From them, we selected 1155 single-copy orthologous families for phylogenetic analysis (Supplementary 2). Our findings indicate a close evolutionary relationship between *C. viniferum* CvYL2a and *C. viniferum* CGW01. CvYL2a appears to have diverged 3.2 million years ago within the genus *Colletotrichum*, which initially diverged approximately 45.2 million years ago (Figure 1). Additionally, we identified 33 specific genes in *C. viniferum* CvYL2a grouped into 13 categories. Notably, 20 of these genes (A08618, A10003, A09924, A08597, A01565, A09902, A09903, A09928, A11559, A09926, A09909, A01566, A10007, A09984, A09985, A10008, A14055, A10009, A11149 and A11147) lack significant homologous sequences in the NCBI database (Supplementary Table 1).

3.2 Symptoms of *C. viniferum* infection in three grape germplasms

C. viniferum infection on grape leaves results in necrotic lesions, a typical symptom of grape ripe rot disease. To study the differences in resistance among the three grape germplasm resources to *C. viniferum*, we used leaf disc assays to observe necrotic lesion development. Small necrotic lesions appeared on "TS" leaves within 24 hpi, progressively expanding to a diameter of 14.81 cm by 120 hpi (Figures 2A, C). In contrast, "B" showed smaller and milder lesions from 72 to 120 hpi. Remarkably, "LB-8" exhibited minimal or no lesions at 120 hpi. When leaves were sprayed with the spore suspension, similar symptoms were observed. Brown grape leaf spots initially appeared at 12 hpi on "TS", with spots enlarging and coalescing by 24 hpi, and large brown speckles became visible at 48 hpi. On the contrary, "B" and "LB-8" did not exhibit any disease necrotic spots before 24 hpi and small brown spots were observed only by 48 hpi (Figure 2B). Based on the grape ripe rot resistance grading standard (Gao et al., 2016), "TS", "B" and "LB-8" were classified as high-sensitive (HS), moderate resistance (MR) and resistant (R) to *C. viniferum*, respectively.

To study the differences in the infection process in three grape germplasms, we observed cytological changes under a light microscope after toluidine blue staining. From 6 to 24 hpi, conidia were distributed across the epidermal cells of "TS" leaves. By 48 hpi, epidermal cells began to collapse, reaching complete

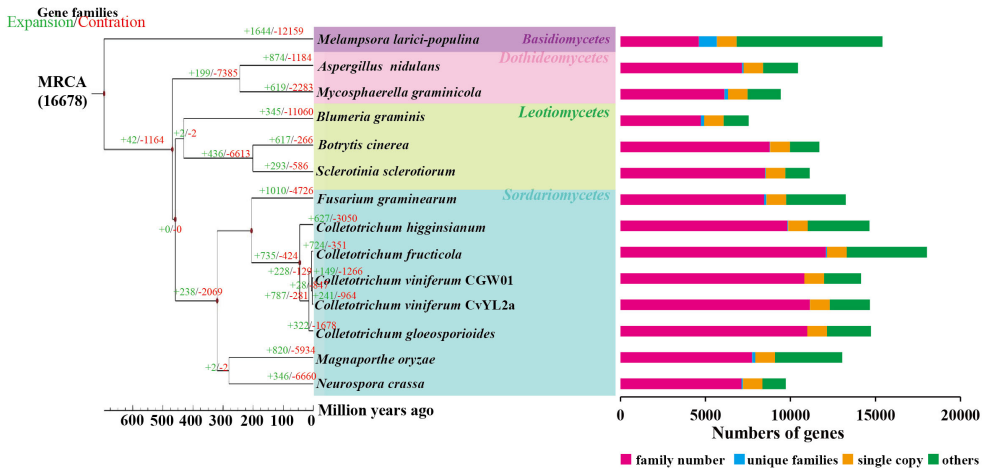

FIGURE 1
Phylogenetic relationship. The maximum likelihood phylogenetic tree was constructed using PhyML, based on the concatenated alignment of 1155 conserved single-copy orthologs from all species. Divergence time estimation for each species was performed utilizing the phylogenetic tree, software r8s, and the mcmctree program in the PAML software package. Time-correction points were obtained by integrating data from the TimeTree website.

10.3389/fpls.2024.1446288

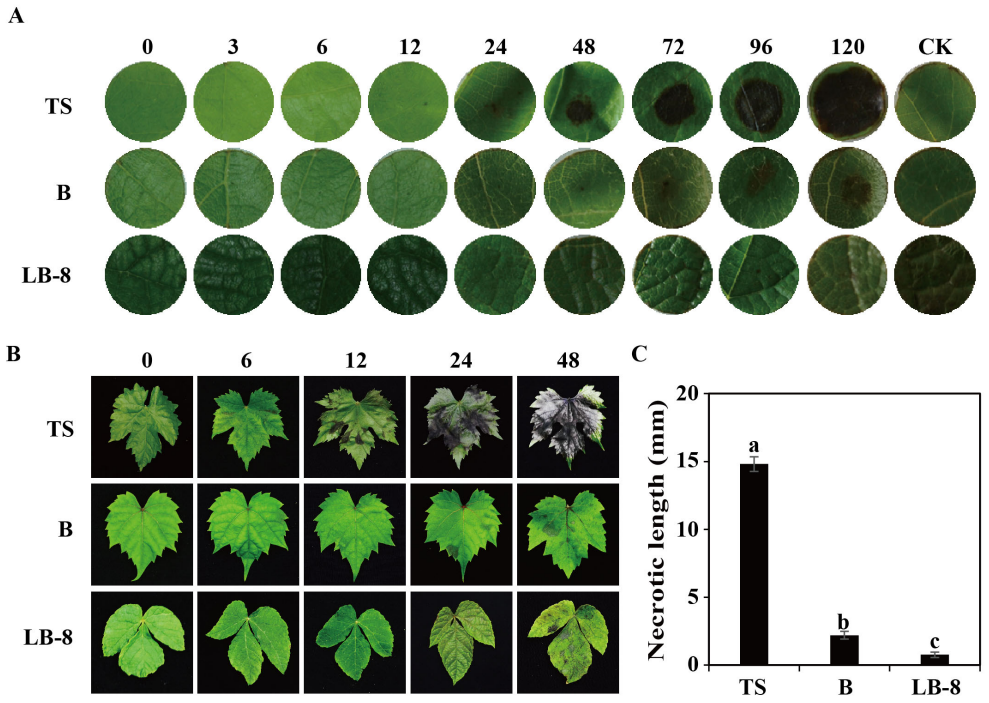

FIGURE 2
Ripe rot symptoms on three grapevine germplasms infected with *C. viniferum*. **(A)** Images captured at various time points [0, 3, 6, 12, 24, 48, 72, 96, and 120 hours post inoculation (hpi)] after applying 20 µl of fungi suspension (5 × 10^6 conidia/ml) and incubating at 25°C. **(B)** Images were taken at 0, 6, 12, 24, and 48 hpi. Minimal Lesions were observed on "B" and "LB-8", whereas necrosis rapidly developed on "TS" from 12 hpi. One representative leaf of three replicates is shown for each time point. **(C)** Symptoms evaluation through measurement of necrotic length at 120 hpi. Data represent the means ± SE of three independent experiments with three replicates taken from different plants, each containing ten replicates for each genotype. Distinct letters indicate significant differences (ANOVA test with Tukey's comparisons, $P < 0.05$). TS, "*V. vinifera* cv. Thompson Seedless"; B, "*V. labrusca* accession Beaumont"; LB-8, "*V. piasezkii* Liuba-8".

destruction at 72 hpi. At 96 hpi, the palisade mesophyll cells were also destroyed and leaf tissues had completely collapsed by 120 hpi. Compared to "TS", "B" exhibited delayed symptom onset, with epidermal cells becoming concave at 72 hpi, and noticeable damage observed by 120 hpi. Remarkably, the epidermal cells of "LB-8" remained intact at 120 hpi (Figure 3A).

3.3 Developmental differences of *C. viniferum* on the leaves of three grape germplasm resources

To study developmental differences of *C. viniferum* on the leaves of three grape genotypes, we performed scanning and transmission electron microscopy observations. Initially, conidia formed a central septum at 3 hpi, dividing the conidia into two equal-sized parts on the leaves of all three grapevines. Additionally, the conidia on "B" and "LB-8" leaves were surrounded by abundant white secretions compared to "TS" (Figure 3B). Previous studies of downy mildew infection have shown that resistant grape varieties also produced white secretions (Yin et al., 2017). Subsequently, these conidia germinated and formed germination tubes from one or both ends of the conidia (Figure 3B). Although conidial germination in all three grapevines started at 3 hpi and significantly increased by 6 hpi, "TS" exhibited the highest germination rate at 24 hpi (Figure 3D). Interestingly, at 72 hpi, "B" and "LB-8" elongated germination tubes were shorter compared to "TS", a difference that persisted even at 120 hpi (Figure 3B).

Next, appressoria developed from conidia, either directly or from the elongated germination tube, resulting in the production of several appressoria from a single conidium (Figure 3B). Appressorium formation became evident by 6 hpi on the leaves of all grape germplasms, with the highest appressorium formation rate occurring on "TS" by 24 hpi (Figure 3D). The shape of the appressoria is generally round or irregular in some cases (Velho et al., 2016). Irregular appressoria, such as downward concave hearts, gourds, and outward protruding convex morphology, were easily found with a proportion over 30% on "B" and "LB-8" (Figures 3D, E). This was possibly due to appressorium collapse caused by secretions from "B" and "LB-8" (Figure 3B) (Yin et al., 2017) or dense hair on grape leaves (Figure 3C; Supplementary Figure 1) (Kortekamp and Zyprian, 1999; Han et al., 2021). The paraxial surface of the B and LB-8 blades is covered with hairs, while the TS surface is hair-free.

The appressoria on "LB-8" appeared deflated and irregularly shaped compared to those on "TS".

Transmission electron microscopy revealed that on "TS", the appressoria formed penetration peg, infected vesicles and primary hyphae, and the primary hyphae further formed secondary hyphae

10.3389/fpls.2024.1446288

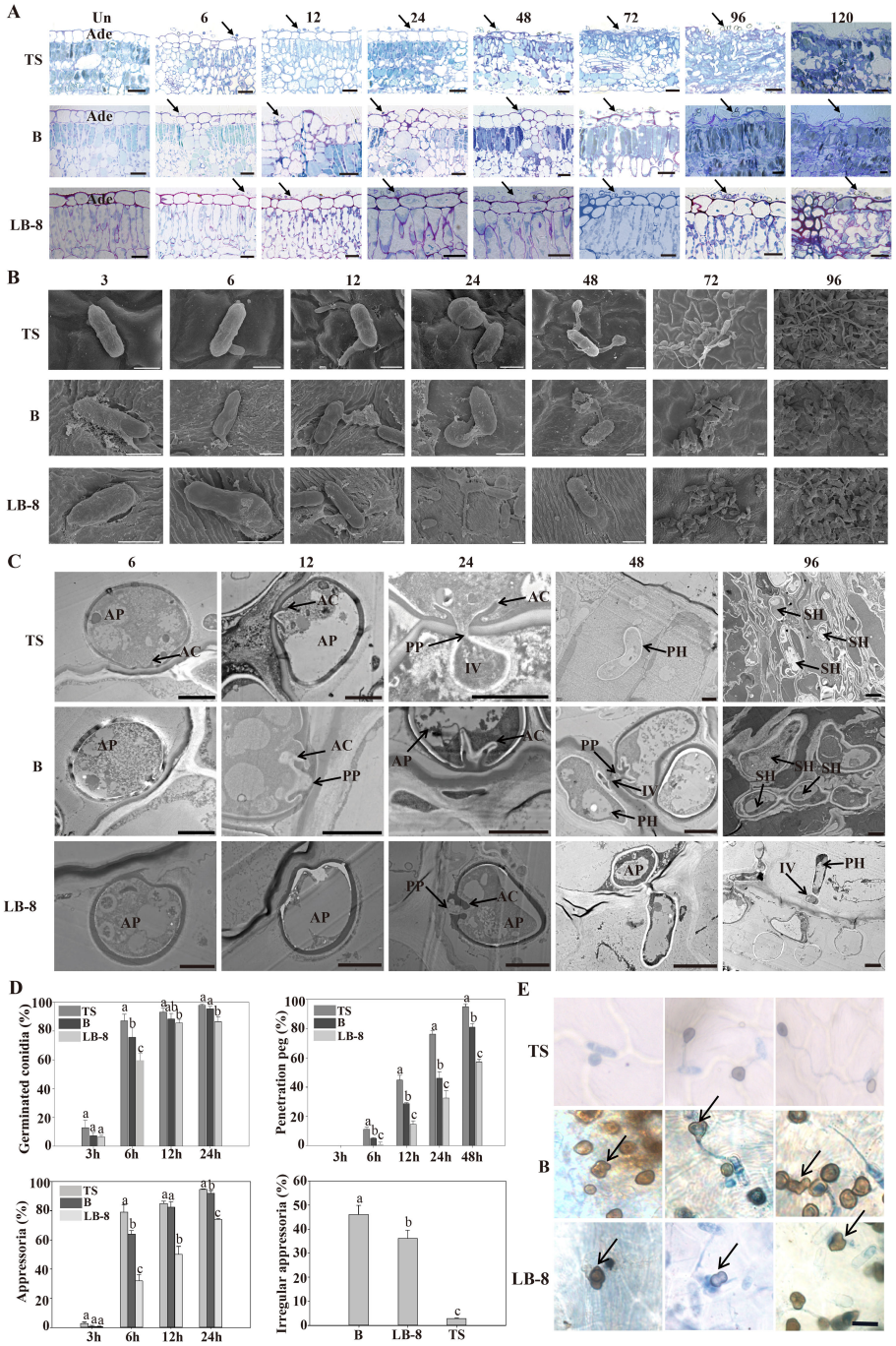

FIGURE 3
Histological and ultrastructural study of resistant and susceptible grapevine leaves infected by CvYL2a. **(A)** Cytological study of *C. viniferum* CvYL2a infected grape leaves. Un: Un-inoculated with *C. viniferum*; Ade, adaxial epidermis; scale bar, 20 µm. **(B)** SEM imaging of conidia development on leaves infected by *C. viniferum*. Scale bar = 5 µm **(C)** Ultrastructure of host-parasite interactions on "TS", "B", and "LB-8" leaves under TEM. AP, appressorium; AC, appressorial cone; Cu, cuticle; FCW, fungal cell wall; HCW, host cell wall; HPM, host plasma membrane; IV, infection vesicle; PP, penetration peg. Scale bar = 2 µm. **(D)** The percentages of *C. viniferum* germinated conidia, appressoria, and penetration peg on three grape germplasms at different time points post-inoculation, along with the presence of irregular appressoria on the three grape genotypes at 48 hpi, results are presented as mean ± SE, n=9. Different letters indicate significant differences (ANOVA test with Tukey's comparisons, $P < 0.05$). **(E)** Occurrence of more mature appressorium deformities on "TS", "B" and "LB-8" inoculated with *C. viniferum* CvYL2a. Deformed appressorium are marked by the arrow. Scal bar = 10 µm.

(Figure 3C). The formation of penetration pegs started at 6 hpi on all grapevines. However, the formation ratio was significantly lower on "LB-8" compared to the other two germplasms, with nearly half of the appressoria on "LB-8" failing to produce penetration pegs. Despite a similar developmental trend across different germplasms, penetration pegs formed more rapidly on "TS" than on "B" and "LB-8" at each time point post-inoculation (Figure 3D). While "B" closely resembled "TS" in the penetration process, "LB-8" exhibited distinctive characteristics.

10.3389/fpls.2024.1446288

"B" demonstrated a prolonged biotrophic stage compared to "TS", with no observable secondary hyphae on "LB-8" (Figure 3C).

3.4 Expression of pathogenicity genes

To analyze the expression dynamics of *C. viniferum* pathogenic genes, we selected the susceptible grape "TS" characterized by rapid *C. viniferum* development for transcriptome analysis. A total of 95.29 Gb of sequence data was produced, resulting in approximately 42 million clean readings from each sample (Figures 4E, F). The clean reads were then mapped to the *C. viniferum* CvYL2a genome, with percentages ranging from 0.43% to 16.19% (Supplementary Table 2). The shared DEGs among the 6, 12, 24, and 48 hpi samples increased over infection period. Specifically, compared to 0 hpi samples, there were 852, 1029, 1115, and 1141 up-regulated DEGs ($|\log_2$ (fold change)$| > 4$, $P < 0.05$), and 83, 78, 269, and 309 down-regulated DEGs detected at 6, 12, 24, and 48 hpi, respectively (Figure 4A; Supplementary Table 19–22). In addition, there exhibited 236 CvYL2a DEGs consistent differential expression across all infection time points (Figure 4C).

Transcriptome data was searched using SignalP, CAZy (Carbohydrate-Active Enzyme) database, AntiSMASH program, and the P450 database. All *C. viniferum* secondary metabolism gene clusters were shown in Supplementary Table 10. The transcriptome revealed significant differential expression of 56 effector genes, 36 Cazy genes, 5 P450 genes and 10 genes in secondary metabolism gene clusters at one or more infection stages (Supplementary Table 5). For further investigation into the functions of differentially expressed effectors, 20 cysteine-rich small effectors, 9 virulence-related effectors, and 28 effectors randomly chosen from the genome, along with 28 up-regulated effectors from both the genome and the transcriptome were selected (Supplementary Table 6) and assessed their abilities to induce or inhibit plant cell death. *Agrobacterium tumefaciens* carrying a GFP expression vector inserted with one of these 87 effectors was injected

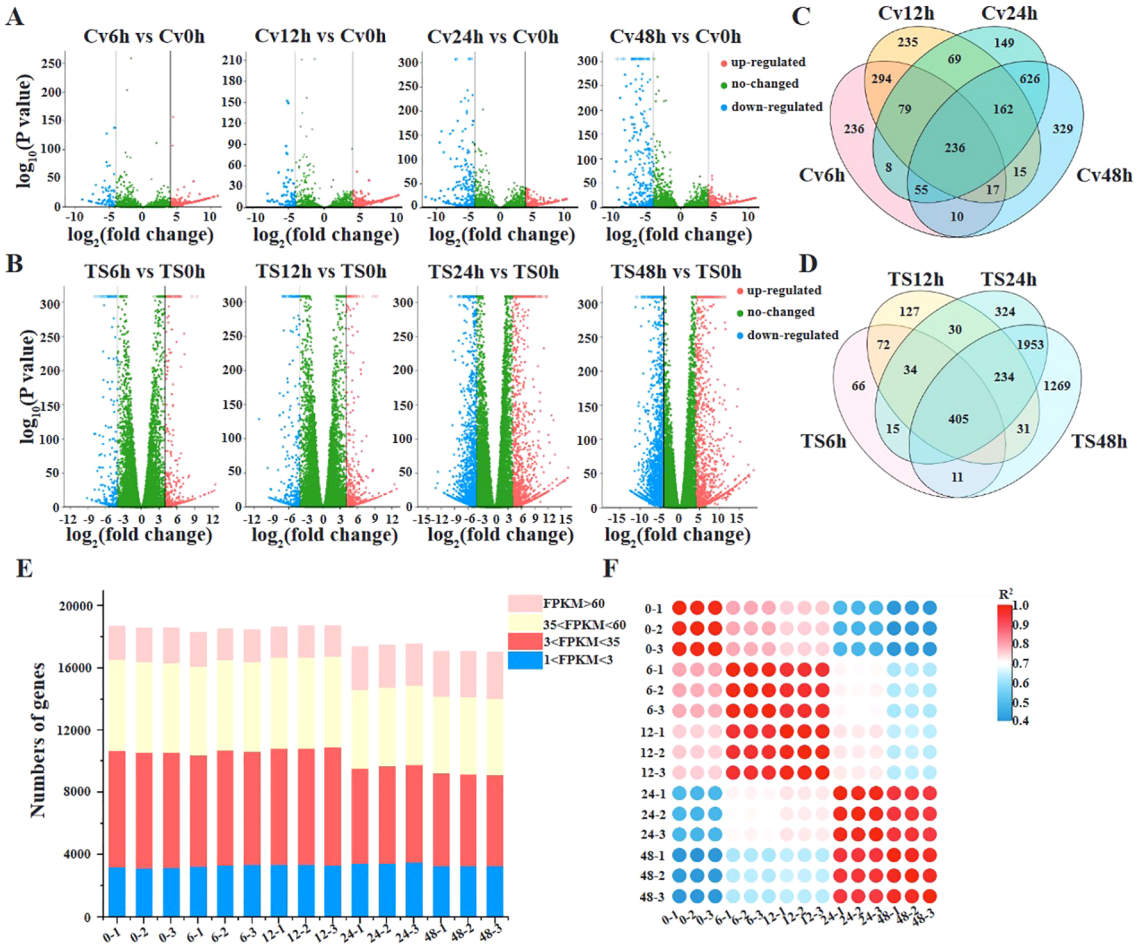

FIGURE 4
Transcriptome analyses of grapevines infected by *C. viniferum*. **(A, B)**Volcano plots displaying differentially expressed genes in *C. viniferum* and grapevine "TS", respectively. Cv0h, Cv6h, Cv12h, Cv24h and Cv48h represent *C. viniferum* transcriptome, while TS0h, TS6h, TS12h, TS24h and TS48h represent "TS" transcriptome prepared from grape leaves post-inoculation with *C. viniferum* at 0, 6, 12, 24 and 48 hpi, respectively. **(C)**, Overlap of upregulated and downregulated DEGs in *C. viniferum*. **(D)**, Overlap of upregulated and downregulated DEGs in "TS". **(E)**, Number of transcripts detected in 15 samples. Transcripts with an FPKM (fragments per kilobase of gene per million mapped reads) >1 are considered to be detected. Detected transcripts are further categorized as low (1<FPKM<3), moderated (3<FPKM<60), or high (FPKM>60) detection levels. **(F)**, Correlation of gene expression levels among grape leaves infected with *C. viniferum* at 0, 6, 12, 24, and 48 hpi.

10.3389/fpls.2024.1446288

into *N. benthamiana* leaves. 12 h later, the hypersensitive response-inducing INF1 was injected at the same location. Among the effectors, ten inhibited INF1-induced cell death, while two induced cell death in *N. benthamiana* leaves. Subcellular localizations of 12 effectors in *N. benthamiana* were shown in Supplementary Figure 2. These findings suggest that these 12 effectors play active roles in pathogen-host interactions (Figure 5G).

We compared the CAZyme library across 14 fungal species and identified 909 CAZymes in the predicted proteome of *C. viniferum* CvYL2a. These CAZymes were distributed across six major

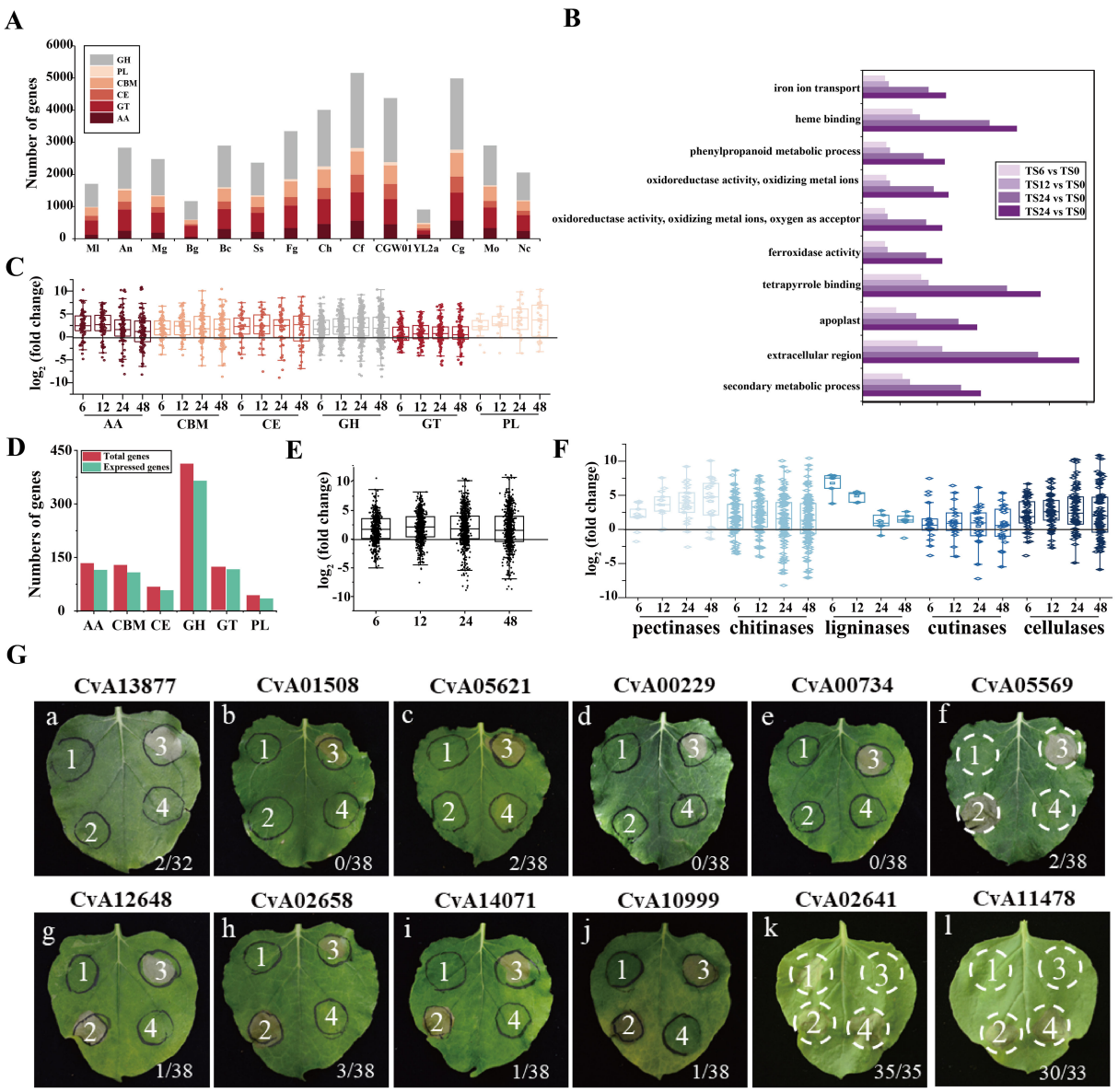

FIGURE 5
Gene Ontology and *C. viniferum* pathogenicity genes. **(A)** Repertoires of the carbohydrate-active enzymes (CAZymes) in *C. viniferum* and other 13 fungal genomes. GH, glycoside hydrolase; CE, carbohydrate esterase; AA, auxiliary activities; CBM, carbohydrate-binding module; PL, polysaccharide lyase. **(B)** Functional categorization of regulated differentially expressed genes (DEGs) in the *C. viniferum*-infected leaves of TS based on Gene Ontology (GO). *P*-value < 0.05. **(C)** Box plot of CAZymes gene expression of each family at 6, 12, 24, and 48 hpi. **(D)** CAZymes genes expressed post inoculation with *C. vinifera*. **(E)** Box plot displays expressed CAZymes (n = 530) in *C. viniferum* at 6, 12, 24, and 48 hpi. **(F)** Box plot of expressed CWDEs of *C. viniferum* in grape leaves at 6, 12, 24, and 48 hpi. **(G)** Cell death-suppression by INF1 and cell death-inducing activity of *C. viniferum* effectors on plant cell death induced. The label on the panel represents the name of the effector. a-j panels: the ability of 10 putative *C. viniferum* effectors to suppress cell death triggered by INF1. *A. tumefaciens* infiltration sites in *N. benthamiana* leaves expressing each of the 10 effectors were challenged with *A. tumefaciens* expressing the INF1 elicitin. *A. tumefaciens* strain carrying GFP was used as a control. Representative cell death symptoms were photographed at 7 days after INF1-GFP infiltration. k and l panels: 2 putative *C. viniferum* effectors CvA02641 and CvA11478 induced cell death. a-e panels received the following infiltration: 1, GFP; 2, effector-GFP; 3, GFP and INF1-GFP; 4, effector-GFP and INF1-GFP. f-j panels showed leaves infiltrated with 1, GFP; 2, INF1-GFP; 3, GFP and INF1-GFP; 4, effector-GFP and INF1-GFP. k and l panels were leaves infiltrated with 1, GFP; 2, effector-GFP; 3, GFP; 4, INF1-GFP. Ratios represent the proportion of infiltration sites displaying the cell death phenotype.

10.3389/fpls.2024.1446288

CAZymes superfamilies, including 413 glycoside hydrolases (GHs), 121 glycosyl transferases (GTs), 44 polysaccharide lyases (PLs), 68 carbohydrate esterases (CEs), 134 auxiliary activities (AAs), and 129 carbohydrate binding modules (CBMs). Compared to other fungi, CvYL2a had fewer genes distributed in each superfamily. The expressed carbohydrate genes in CvYL2a during infection account for 87.79% of the total carbohydrate genes (Figures 5C–E). Within the CAZyme library, we identified 316 cell wall degrading enzymes (CWDEs), including 29 pectinases, 148 chitinases, 6 ligninases 26 cutinases, and 107 cellulases. Of these CWDEs, 273 (86.39%) genes were expressed during infection, with 103 being up-regulated and 21 down-regulated (Figure 5F; Supplementary Table 9).

3.5 Grapevine responses to *C.viniferum* infection

To study the host response to *C. viniferum*, clean reads also were mapped to the *V. vinifera* PN40024 genome, with mapping percentages of 93.90 ± 0.06%, 93.82 ± 0.06%, 93.67 ± 0.12%, 91.59 ± 0.20%, and 77.90 ± 0.53%, respectively (Supplementary Table 3). In the *V. vinifera* transcriptome, we detected 422, 570, 1359, and 1503 up-regulated DEGs along with 261, 377, 1702, and 2480 down-regulated DEGs. Moreover, 405 common DEGs were identified throughout the infection process (Figures 4B, D). DEGs functional annotations with different time point were shown in Supplementary Tables 11–14. GO terms at different time point were analyzed (Supplementary Tables 15–18). Gene ontology analysis revealed their involvement in biological processes like iron ion transport, phenylpropane metabolism and secondary metabolism, cell components like apoplast and extracellular domain; and molecular functions including heme binding, tetrapyrrole binding and oxidoreductase activity (Figure 5B). Additionally, KEGG pathway enrichment analysis showed significant enrichment in phenylpropanoid-guided flavonoid and resveratrol biosynthesis (34 DEGs), phenylpropanoid biosynthesis (18 DEGs), photosynthesis antenna proteins (16 DEGs) (Figures 6–8).

Our analysis demonstrated distinct patterns of gene expression in several pathways, including phenylpropanoid-guided flavonoid and resveratrol biosynthesis, phenylpropanoid biosynthesis, and photosynthesis-antenna proteins. Notably, RNA-seq analysis showed downregulation of genes associated with anthocyanins synthesis, including flavonoid 3',10'-hydroxylase (*F3'5'H*), flavanone 3-hydroxylase (*F3H*), chalcone synthase (*CHS*), and leucoanthocyanidin dioxygenase (*LDOX*). Conversely, the stilbene synthase (*STS*) gene associated with the synthesis of resveratrol was significantly upregulated (Figure 6). In the phenylpropanoid biosynthesis pathway, while caffeoyl-CoA O-methyltransferase (*CCOAMT*) and phenylalanine ammonia-lyase (*PAL*) were upregulated, cinnamyl alcohol dehydrogenase (*CAD*), a gene related to lignin synthesis, was downregulated (Figure 7). Grape genes involved in the photosynthesis-associated pathway encoded light-harvesting chlorophyll a/b-binding proteins (Lhc). The Lhc superfamily contains eight subfamilies: early light-induced protein (ELIP), ferrochelatase II (FCII), Lhca, Lhcb, one-helix protein (OHP), photosystem II subunit S (PsbS), photosystem II protein 33 (Psb33), and stress-enhanced protein (SEP) (Klimmek et al., 2006). All differentially expressed photosynthesis antenna genes including 5 *Lhca* and 11 *Lhcb* were downregulated in susceptible *V. vinifera* "TS" (Figure 8).

Plant disease resistance is significantly influenced by the involvement of transcription factors. Recent research has highlighted the involvement of various transcription factor families in regulating signal transduction in plant SA, ET and JA pathways responding to different pathogen infections, such as WRKY (WRKY domain-containing transcription factors) family, MYB (v-myb avian myeloblastosis viral oncogene homolog) family, and ERF (thylene responsive factors) family (Liu et al., 2021; Gao et al., 2022; Zhou et al., 2022). Our study found that numerous transcription factors, including 10 WRKYs, 18 NACs (NAM, ATAF1/2, and CUC2), 38

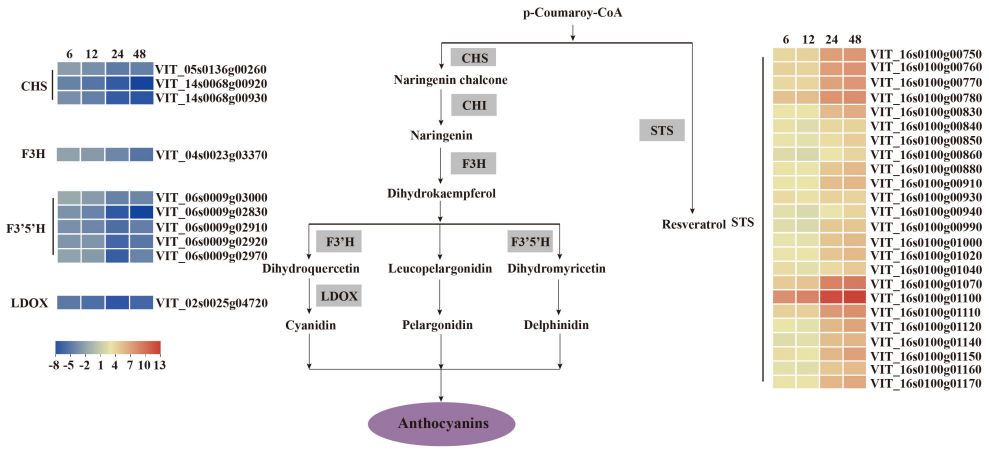

FIGURE 6
V. vinifera pathways and related gene expression for flavonoid biosynthesis in *C. viniferum*-infected leaves of *Vitis vinifera* cv. Thompson Seedless. Red indicates upregulation and blue indicates downregulation ($P < 0.05$) relative to the expression levels at 0 hpi. STS, stilbene synthase; CHS, chalcone synthase; CHI, chalcone isomerase; F3'H, flavonoid 3' hydroxylase; F3'5'H, flavonoid 3',10'-hydroxylase; F3H, flavanone 3-hydroxylase; LDOX, leucoanthocyanidin dioxygenase.

10.3389/fpls.2024.1446288

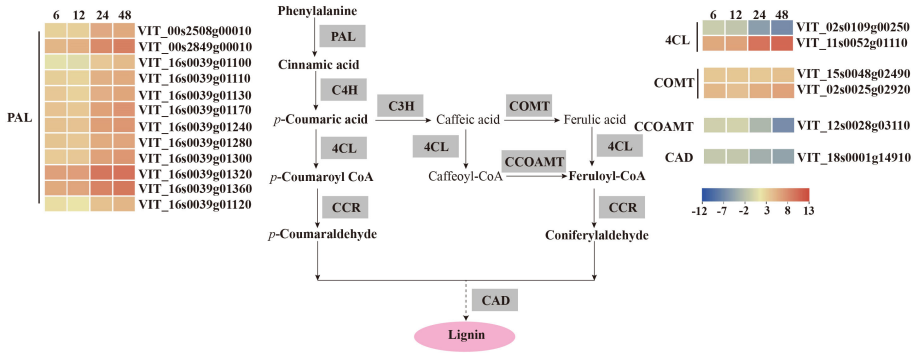

FIGURE 7
V. vinifera pathways and related gene expression for phenylpropanoid biosynthesis in *C. viniferum*-infected leaves of *Vitis vinifera* cv. Thompson Seedless. Red indicates upregulation and blue indicates downregulation, ($P < 0.05$) relative to the expression levels at 0 hpi. PAL, phenylalanine ammonia-lyase; C4H, cinnamate 4-hydroxylase; C3H, p-coumarate 3-hydroxylase; COMT, caffeic acid 3-O-methyltransferase; 4CL, 4 - coumarate -CoA ligase; CCOAMT, caffeoyl-CoA O-methyltransferase; CAD, cinnamyl alcohol dehydrogenase.

MYBs, 53 ERFs, 6 GATAs (GATA-binding transcription factors), 2 bHLHs (basic helix-loop-helix proteins), one SBP (quamosa promoter promoter binding proteins) were differentially expressed during *C.viniferum* infection at four stages (Figure 9). Gene expression associated with JA, SA, and ET signaling pathways significantly increased upon *C. viniferum* infection (Figure 10). Our results showed that the JA synthesis-related genes including *LOX* (VIT_00s0265g00170), AOS (VIT_03s0063g01820, VIT03s0063g01860 and VIT03s0063g01830), *AOC* (VIT_01s0011g03090, VIT_18s0041g02040, VIT_18s0041g02010, VIT_18s0041g02260, VIT_18s0041g02020, VIT_18s0041g02060, VIT_18s0041g02050), *OPCL* (VIT_00s0662g00010), and KAT (VIT_05s0051g00720), as well as the SA-synthesis-related genes *PAL* (VIT_16s0039g01170, VIT_00s2508g00010, VIT_16s0039g01280, VIT_00s2849g00010, VIT_16s0039g01100, VIT_16s0039g01300, VIT_16s0039g01110, VIT_16s0039g01130, VIT_16s0039g01240, VIT_16s0039g01320, VIT_16s0039g01120 and VIT_16s0039g01360) and *ACS* (VIT_15s0046g02220), a new transcript *AOC1* (novel.1296) for ethylene synthesis were upregulated during *C. viniferum* infection of grape leaves (Figure 10). We measured the hormones levels of *C. viniferum*

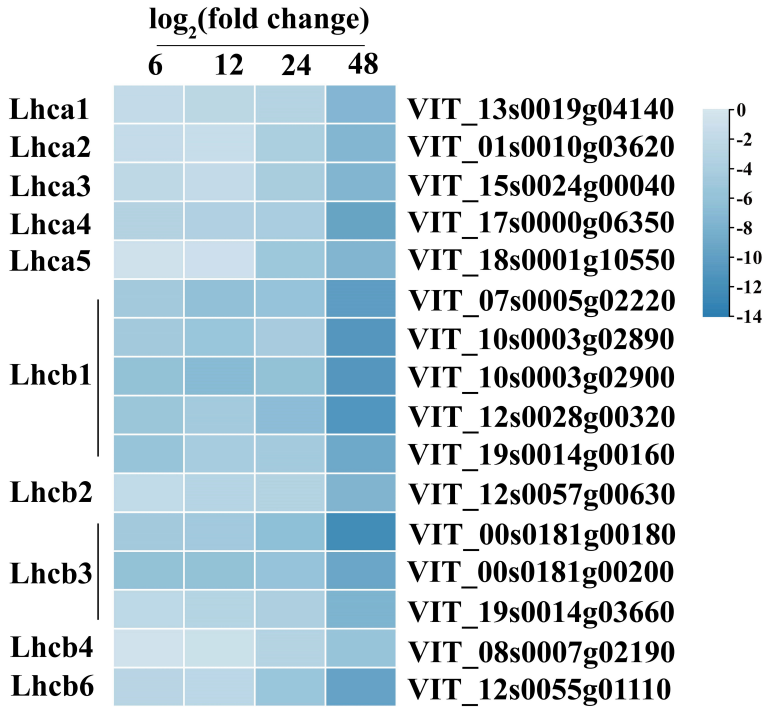

FIGURE 8
Gene expression of photosynthesis-antenna proteins in *C. viniferum*-infected leaves of *Vitis vinifera* cv. Thompson Seedless. Blue indicate downregulation, respectively; and unshaded represents no significant change ($P < 0.05$) relative to the expression levels at 0 hpi. Lhca, chlorophyll a binding protein of Light-harvesting chlorophyll; Lhcb, chlorophyll b binding protein of Light-harvesting chlorophyll.

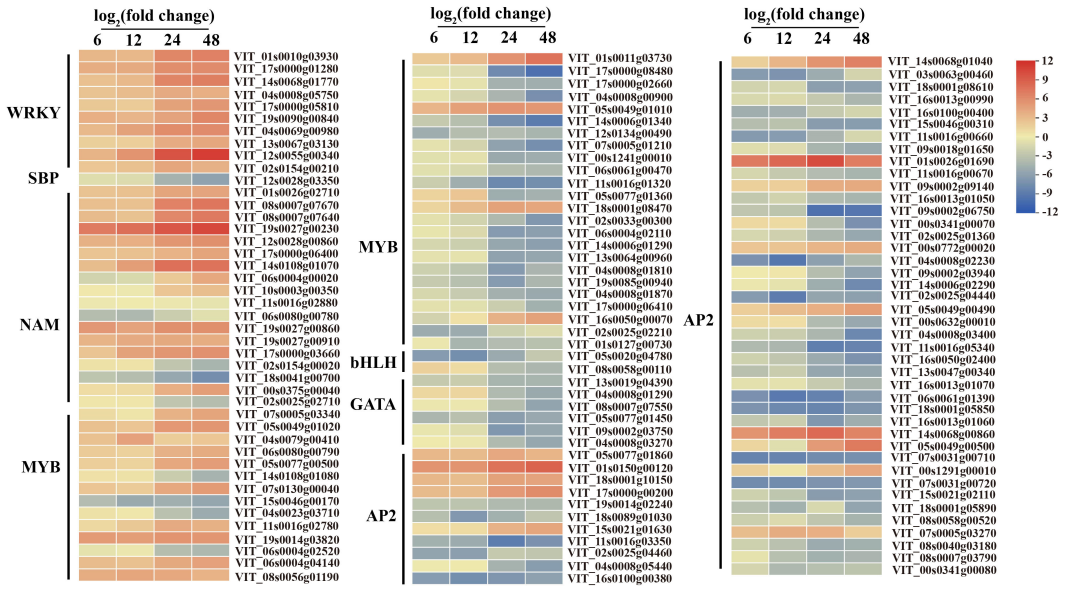

FIGURE 9
Expression patterns of differentially expressed transcription factors at 6, 12, 24, and 48 hpi in *C. viniferum*-infected *V. vinifera* leaves. WRKY, WRKY domain-containing transcription factors, SBP, quamosa promoter promoter binding proteins, NAM, No apical meristem, MYB, v-myb avian myeloblastosis viral oncogene homolog, bHLH, basic helix-loop-helix proteins, GATA, GATA-binding transcription factors, AP2, APETALA2 responsive factor. Red and blue indicate upregulation and downregulation, respectively, and yellow represents no significant change ($P < 0.05$) relative to the expression levels at 0 hpi.

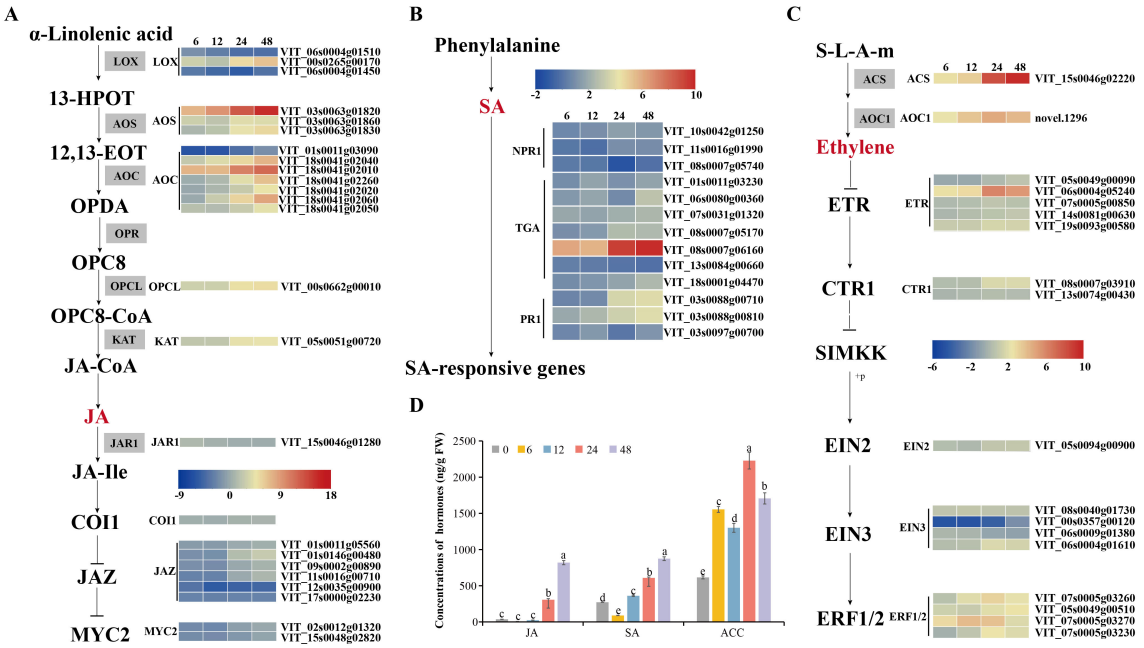

FIGURE 10
Hormonal content of grape leaves during infection and expression patterns of differentially expressed genes assigned to hormone signaling. **(A–C)** V. vinifera jasmonates (JA) biosynthesis, salicylic acid (SA) and ethylene (ET) pathways and related gene expression in C. viniferum-infected leaves at 6, 12, 24, and 48 hpi. Red and blue indicate upregulation and downregulation ($P < 0.05$), respectively, relative to the expression levels at 0 hpi. 12,13-EOT: 12,13(S)-epoxylinolenic acid; 13-HPOT: 13(S)-hydroperoxylinolenic acid; AOS: allene oxide synthase; LOX: lipoxygenase; AOC: allene oxide cyclase; OPR: 12-oxophytodienoate reductase; OPC:8, 3-oxo-2-(cis-29-pentenyl)-cyclopentane-1-octanoic acid; OPCL: 3-oxo-2-(cis-29-pentenyl)-cyclopentane-1-octanoic acid CoA Ligase; OPDA: 12-oxocis-10,15-phytodienoic acid; COI1, coronatine-insensitive protein 1; JAZ, jasmonate ZIM domain-containing protein; MYC2, transcription factor MYC2; ACS: 1-aminocyclopropane-1-carboxylate synthase 3; ACO1: 1-aminocyclopropane-1-carboxylate oxidase; ETR: ethylene receptor; CTR1: serine/threonine-protein kinase CTR1; EIN2: ethylene-insensitive protein 2; EIN3: ethylene-insensitive protein 3; EBF1/2: EIN3-binding F-box protein; ERF: ethylene-responsive transcription factor; NPR1: nonexpressor of pathogenesis-related genes 1; TGA: transcription factor TGA; PR1: pathogenesis-related protein 1. **(D)** Hormonal content of grape leaves in C. viniferum-infected leaves at 0, 6, 12, 24, and 48 hpi. Distinct letters indicate significant differences (ANOVA test with Tukey's comparisons, $P < 0.05$). ACC: 1-aminocyclopropane-1-carboxylic acid, precursor of ethylene.

10.3389/fpls.2024.1446288

infection and found that SA, JA, and ET synthesis precursor ACC significantly increased (Figure 10). The findings suggest the involvement of JA, SA, ET and ABA in regulating the response to *C. viniferum* during the late stage of infection.

To measure the production and accumulation of hydrogen peroxide (H_2O_2), we used diaminobenzidine (DAB) staining, which relies on the peroxidase-catalyzed oxidation of oxygen released by H_2O_2, resulting in tan deposits on the plant surface. Fewer cells produced H_2O_2 in "TS" leaves after *C. viniferum* inoculation. However, "B" and "LB-8" exhibited obvious browning due to DAB oxidation. "B" showed lighter staining and fewer stained cells after *C. viniferum* inoculation, while "LB-8" displayed the opposite pattern. At 6 hpi, none of the three grape leaves significantly produced H_2O_2. However, by 12 hpi, cells beneath the appressorium in "LB-8" exhibited tan staining, with a significant increase observed from 24 hpi to 48 hpi. In "B" leaves, the proportion increased from 6.00% to 12.12%, while "LB-8" reached 25.53%. "TS" leaves showed slight staining only at 48 hpi. These results suggest that *C. viniferum* invasion is more extensive during the initial 2 days after inoculation, with "TS" leaves exhibiting the lowest H_2O_2 production rate (Figures 11A–D). We identified 76 DEGs involved in antioxidation during *C. viniferum* infection in grapes. Among these, one-third (22) of the peroxidase (POD), and four-fifths of glutathione peroxidase (GSH) related

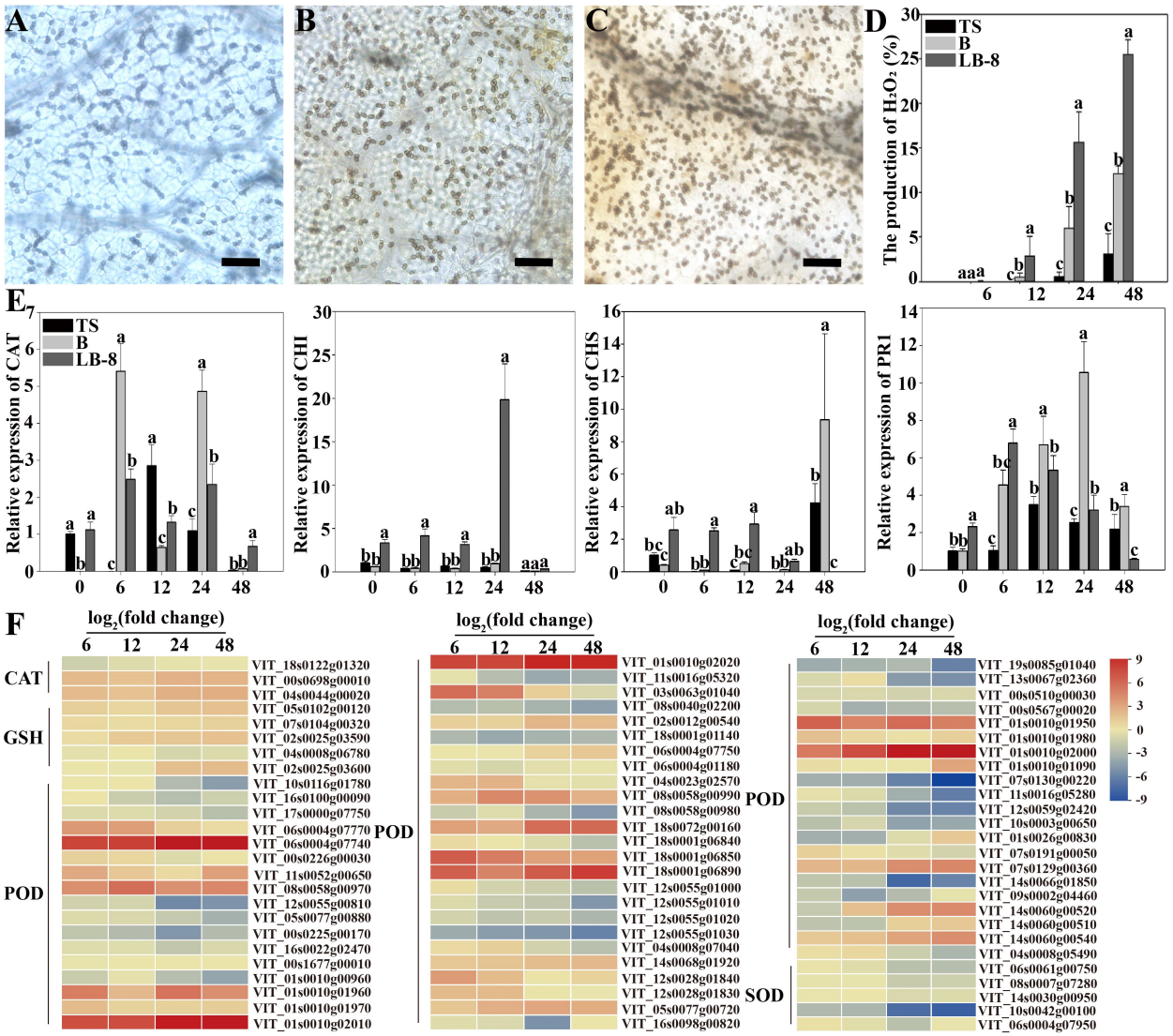

FIGURE 11
Responses of grapevines to *C viniferum* CvYL2a. **(A-C)** 2-day DAB staining of leaves from three grape varieties: **(A)** TS, **(B)** B, and **(C)** LB-8 inoculated with *C. viniferum* CvYL2a. Scal bar = 25 μm. **(D)** The production rate of H_2O_2 after inoculation of leaves from three grape varieties with *C. viniferum* CvYL2a, results are presented as mean ± SE, n = 9. Different letters indicate significant differences (ANOVA test with Tukey's comparisons, $P < 0.05$). **(E)** Quantitative analysis of defense-related genes in "TS", "B", and "LB-8" plants after inoculation with *C. viniferum*. The gene expression levels were analyzed using quantitative real-time polymerase chain reaction (RT-qPCR). The natural logarithm transformed normalized-expression values were plotted for each gene at five time points (0, 6, 12, 24 and 48 hpi). Results are presented as mean ± SE, n = 3. Different letters indicate significant differences (ANOVA test with Tukey's comparisons, $P < 0.05$). CAT, Catalase. CHI, Chalcone isomerase; CHS, Chalcone synthase; PR1, pathogenesis-related 1. **(F)** DEGs associated with reactive oxygen species (ROS) scavenging in *C viniferum*-infected "TS". CAT, Catalase; GSH, Glutathione peroxidase; POD, Peroxidase; SOD, Superoxide dismutase.

DEGs were up-regulated. Furthermore, three catalase (CAT) DEGs showed increased expression, and one was down-regulated. These findings underscore the significant role of ROS scavenging by POD, CAT and GSH in the grapevine responses to *C. viniferum* (Figure 11F).

One notable transcriptomic characteristic observed in grape leaves following *C. viniferum* infection is the up-regulation of defense-related genes. To further substantiate our transcriptome sequencing results, we performed qRT-PCR analysis of four defense-related genes at different time points post inoculation with *C. viniferum*. Two genes, CAT (Catalase) and PR1 (pathogenesis-related 1), showed higher expression levels at 6 hpi in "B" grape leaves. In "TS", the expression levels of defense-related genes increased slowly. In contrast, two other genes CHI (Chalcone isomerase) and CHS (Chalcone synthase) displayed rapid upregulation during infection in "LB-8" compared to "B" and "TS" (Figure 11E). Additionally, among 72 identified LRR (Leucine-rich repeat receptor) proteins in infected grape leaves, 23 were up-regulated. Two disease-resistant proteins (DRP) were detected, RPS2 (VIT_11s0016g01860) was upregulated and DRP (VIT_01s0026g01420) was down-regulated. Among two glutathione S-transferase (GST) genes, VIT_12s0028g00920 was up-regulated, whereas VIT_04s0079g00690 was down-regulated (Supplementary Table 8). These genes collectively play an important role in disease resistance responses.

4 Discussion

Colletotrichum spp. are highly destructive fungal pathogens to various plants, such as grapes, peppers, and lentils (Lei et al., 2016; Bhadauria et al., 2019; Huo et al., 2021). They can invade various parts of plants, including leaves, stems, shoots, tendrils, and berries Wang et al., 2021). Among these pathogens, *C. viniferum* poses a particularly serious risk to grape production. Previous research has demonstrated varying degrees of grapevine resistance to *C. viniferum*, indicating that different plant materials exhibit distinct reactions towards the same pathogen (Baroncelli et al., 2014; Echeverrigaray et al., 2020).

Histological observation is an effective method for studying the differences in cytology and ultrastructure of grapes infected with different germplasm resources by *C. viniferum*. Transcriptome analysis has become a common approach to studying pathogenic infection hosts. In this study, these two methods were used to reveal the interaction between grape and *C. viniferum*, providing a basis for the selection of candidate fungal pathogenic genes including CAZymes, effectors, P450 and grapevine response genes including plant hormone signaling, metabolite synthesis, expression of transcription factors, ROS clear genes and disease-associated genes.

4.1 *C. viniferum* developed rapidly on susceptible grapes

Current studies on *Colletotrichum* spp. in grapes have mainly focused on evolutionary and taxonomic aspects, with limited histological examination of the infection process of *Colletotrichum* spp., especially *C. viniferum* (Whitelaw-Weckert et al., 2010; Yan et al., 2015). Observations of *Colletotrichum* spp. on grape morphology, including conidia, appressorium, and hyphae, remain relatively scarce (Melksham et al., 2002; Peng et al., 2013; Oo and Oh, 2017). To evaluate the variance in *C. viniferum* infection on the differences of grapevines, the histopathology of the leaves of high-susceptible grape germplasm "TS", medium-resistant grape germplasm "B", and resistant grape germplasm "LB-8" were observed by transmission electron microscopy and scanning electron microscopy. By comparing the resistance levels of these three germplasm grapes to *C. viniferum*, the differences between susceptible grapes and resistant grapevine germplasm were studied. The results of this study can provide a theoretical basis for the later study of the pathogenesis of *C. viniferum*.

Our study revealed significant differences in the response of susceptible and resistant grapevines to *C. viniferum* infection. One notable distinction was the fast disintegration of upper epidermal cells in highly susceptible grapes compared to medium-resistant and resistant grapes. Additionally, visible damage on the leaf surface formed earlier in the susceptible grapevine (Figures 2, 3A). After *C. viniferum* infection, white secretions appeared on the leaves of "B" and "LB-8", while "TS" did not (Figure 3B), presumably a response, similar to previous studies on downy mildew infection of resistant grapes, which showed that "Langao-5" and "Liuba-8" resistant grape germplasms rapidly produced white secretion to limit downy mildew in the early stage of inoculation (Yin et al., 2017). We observed variations in the formation rate of appressoria and penetration pegs among different grapes. "TS" exhibited faster formation of appressoria and penetration pegs compared to "B" and "LB-8". This pattern is consistent with findings in other pathosystems, such as *C. acutatum*-almond pathosystem (Diéguez-Uribeondo et al., 2005). Interestingly, "B" and "LB-8" displayed more than 30% malformed appressoria, which we attribute to two factors. Firstly, the secretion from resistant grapes "B" and "LB-8" may interfere with appressorium formation (Figure 3B), a response observed in grapevines against downy mildew (Yu et al., 2012; Yin et al., 2017). Secondly, the dense hair on grapevine leaves may have compressed and deformed appressoria (Figure 3C), acting as a primary barrier against fungal infection (Kortekamp and Zyprian, 1999).

Colletotrichum spp. infections typically undergo a biotrophic phase in the early stage, followed by a necrotrophic stage after the emergence of secondary hyphae (Shang et al., 2020; Li et al., 2021a). The period of the brief biotrophic stage of *Colletotrichum* spp. infection varied by host and other factors. For instance, when *C. fructicola* infects apple leaves, its short biotrophic stage continues for at least 36 hpi, and then it transforms into the necrotrophic stage at 48 hpi (Shang et al., 2020). Similarly, our observations indicate variations in the duration of the biotrophic phase among grape germplasm resources. For "TS", the brief biotrophic phase lasted 24 h before transitioning to the necrotrophic phase by the emergence of secondary hyphae and the disintegration of epidermal cells. However, "B" exhibited a longer biotrophic stage than "TS" before progressing to the necrotrophic stage. Notably, secondary hyphae were not seen on "LB-8", indicating that *C. viniferum* infection on the resistant grape "LB-8" maintains in the biotrophic stage (Figure 3C).

4.2 *C. viniferum* pathogenicity genes may play an important role in infection

Transcriptome sequencing offers a direct way to explore gene expression levels, and numerous studies have investigated transcriptome sequencing of *Colletotrichum* spp.-infected hosts, encompassing both fungal and host transcriptomes. Transcriptome analyses of *Colletotrichum* spp. includes *C. fructicola* on apples (Liang et al., 2018), *C. falcatum* on sugarcane (Prasanth et al., 2022), and *C. camelliae* on tea (He et al., 2023). However, the transcriptome of *C. viniferum* on grapes has not been studied. To study the pathogenic mechanism of *C. viniferum*, we conducted transcriptome analysis using the susceptible grape "TS". Through transcriptome analysis, we identified a range of differentially expressed pathogenic factors, including 35 CAZymes, 56 effectors, and 5 P450 genes. Secondary metabolites are related to pathogenicity of fungi during infection. We also identified 67 secondary metabolic gene clusters, and only 10 genes (A01092, A01212, A01323, A07559, A08496, A11116, A13125, A13129, A13635, A13736) distributed in 9 secondary metabolite clusters (Cluster2, 21, 25, 26, 32, 33, 35, 57 and 65) had significant differences in expression levels during infection, these 10 genes may play core roles, and the remaining other genes on these 9 clusters may play accessory roles in fungal pathogenicity. (Supplementary Tables 4, 10).

The numbers of major CAZyme superfamilies and CAZymes in CvYL2a were lower than those in other fungi (Figure 5A). Some of these enzymes were responsible for plant cell wall degradation, such as pectinase and cellulase. During *C. viniferum* infection of "TS", the expression levels of these genes significantly increased, indicating their important roles in grape infection (Figure 5F). Furthermore, fungal and oomycete effectors are known as pivotal pathogenic factors that modulate plant immunity and affect disease development (Nie et al., 2019; Chen et al., 2021; Yin et al., 2022). In this study, two effectors induced HR responses in plants, potentially linked to plant resistance R genes in plants. Moreover, ten effectors were found to inhibit INF1-induced cell death, indicating their ability to evade immune recognition by grapevines and promote pathogen infection (Figure 5G).

4.3 Grape responses to *C. viniferum* include plant hormone signaling, metabolite synthesis, expression of transcription factors, ROS clear genes, and disease-associated genes

To explore grapevine responses to *C. viniferum*, we analyzed differentially expressed grapes genes involved in plant hormone signaling and metabolite synthesis, transcription factors, ROS clearance genes, and disease-associated genes. Plant hormones are important in plant responses to pathogens (Zhang et al., 2017; Li et al., 2019a). In this study, the level of SA increased at 6-12 hpi, JA increased at 24-48 hpi, and ACC, synthetic precursor of ET, increased at 12-24 hpi (Figure 10D). Our experiment indicated that the early stage of infection corresponds to the biotrophic stage, while the later stage corresponds to the necrotrophic stage. This is consistent with previous findings that SA-dependent responses are associated with biotrophic organisms, while ET and JA-dependent responses are associated with necrotic organisms (Glazebrook, 2005). The expression levels of hormone synthesis-related genes, downstream transcription factors (*MYC*, *ERF*, and *TGA*), and disease-related genes (*PR1*) were upregulated in the transcriptome. This finding suggests that these hormones may activate downstream transcription factors and disease-resistant genes. Hormonal networks that regulate downstream gene expression during plant-pathogen interactions have long been discovered. For example, SA activates TGA and PR1 (Shimizu et al., 2022), JA activates MYC (Schmiesing et al., 2016), and ethylene activates ERF (Broekaert et al., 2006). Additionally, other differentially expressed transcription factors (WRKY, SBP, NAM, MYB, and GATA) may also play critical roles in plant disease resistance and warrant further experimental studies (Figure 9). We hypothesize that the induction of JA, ET, and SA signaling pathways, along with the activation of transcription factors, are essential components of the grape response to *C. viniferum*.

Phenylpropanoid-guided flavonoid and resveratrol biosynthesis pathways, phenylpropanoid biosynthesis pathways, and photosynthetic antenna proteins have been implicated in plant resistance to pathogens (Jantasuriyarat et al., 2005; Manickavelu et al., 2010; Nabavi et al., 2020; Huang et al., 2021). Transcriptome analysis revealed upregulation of resveratrol synthesis genes during *C. viniferum* infection (Figure 6). Resveratrol is important in the fight against pathogen infections (Vestergaard and Ingmer, 2019; Zhou et al., 2024). This suggests a coordinated response wherein plants synthesize more resveratrol to resist *C. viniferum* infection. In phenylpropanoid biosynthesis, the downregulation of CAD genes, a key enzyme in lignin synthesis, was observed. CAD7, a negative regulator of plant immunity targeted by Avr3a effectors, promotes pathogen infection by inhibiting plant PAMP-triggered immunity (Li et al., 2019b). This raises the possibility that CAD could serve as a target protein for fungal effectors, leading to the loss of lignin synthesis activity and further promoting pathogen infection (Figure 7). Conversely, all differentially expressed photosynthetic antenna proteins were downregulated. Lhca/b-binding protein in the photosynthetic pathway is one of the most abundant proteins in plant chloroplasts. Genes encoding the Lhca/b protein have been identified in interaction between susceptible plants and pathogens (Jantasuriyarat et al., 2005; Manickavelu et al., 2010). The process of inducing plant response systems requires a lot of energy, which increases the need for photosynthesis in plants (Swarbrick et al., 2006). However, this study showed down regulation of Lhca and Lhcb during infection (Figure 8). Similarly, previous experiments have shown that tomato seedlings inoculated with DC3000 were also downregulated the expression of photosynthesis-related genes (Ishiga et al., 2009). This suggests that plants may limit the carbon sources available to pathogens or protect plant cells from oxidative damage by downregulating photosynthesis.

Earlier research has highlighted the diverse roles of plant response genes, such as chalcone synthase, pathogenesis-related proteins, catalase, and chitinase, in conferring resistance or

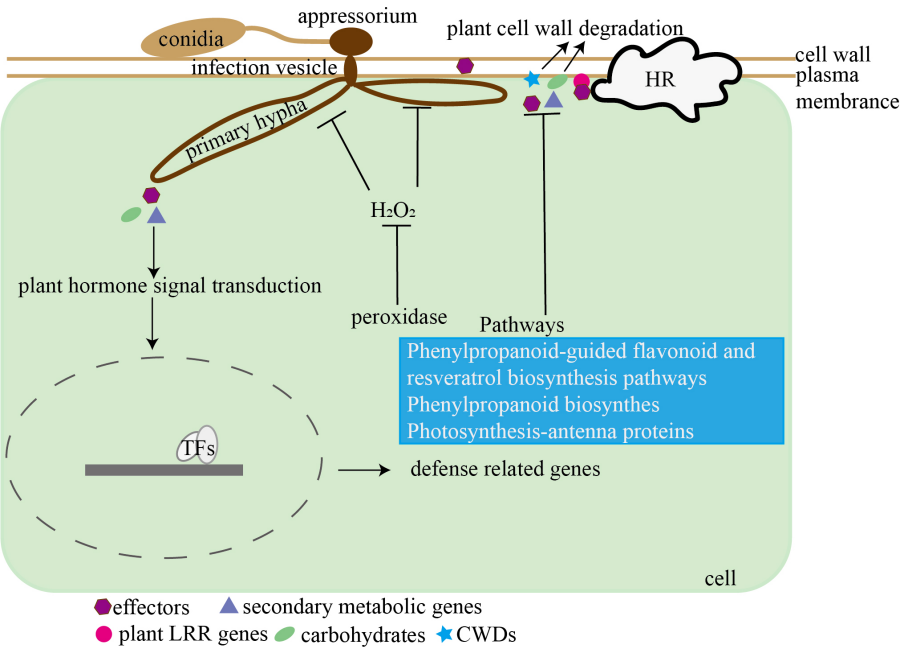

FIGURE 12
Hypothetical model of the interaction between *C. viniferum* and *V. vinifera*. *C. viniferum* infects grapevines through pathogenic genes including effectors, carbohydrates, secondary metabolites, and plant cell wall degradation enzymes, while grapes inhibit *C. viniferum* infection by LRRs recognizing pathogenic fungi and activating ROS accumulation.

tolerance to fungal pathogens (Nandeeshkumar et al., 2008; Jaulneau et al., 2010; Feng et al., 2011). In this study, we observed an earlier response in plants "LB-8" and "B" compared to "TS", characterized by higher expression levels of response genes (Figure 11E). Another notable difference is the accumulation of reactive oxygen species. Hydrogen peroxide increases significantly during host-pathogen interactions (Wang et al., 2010). Our results suggest that plant ROS clearance genes are upregulated during "TS" infection (Figure 11F), consistent with previous findings on pathogenic infections (Segal and Wilson, 2018). Peroxidase activity in grapes during *C. viniferum* infection may contribute to lignin breakdown and ROS scavenging (Figure 7). The most studied function of LRR protein in plants is to play an important role in disease resistance. LRR-encoding genes act as pattern recognition receptors (PRRs) to sense pathogen-associated molecular patterns (PAMPs) and as R genes involved in the immune responses of plants (Kunze et al., 2004; Meyers et al., 2005). Additionally, genes associated with grape response, including LRR, disease resistance genes, and glutathione S-transferase, were upregulated (Supplementary Table 6). Despite the elevated expression levels of these genes, susceptible grapevines remain infected with *C. viniferum* and develop lesions. This phenomenon parallels observations in susceptible grapevines *V. vinifera* cv. Red globe infected with *Elsinoë ampelina* (Li et al., 2021c).

Currently, only three grape transcriptome datasets related to *Colletotrichum* spp. infection are available (Lei et al., 2022; Shen et al., 2022; Yu et al., 2023). However, these three studies exclusively analyzed grape transcripts, leaving the changes in both *Colletotrichum* and grape transcriptomes during the infection process remain unexplored. Therefore, our research employed simultaneous transcriptome analyses to examine fungal genes associated with pathogenesis and grape genes associated with defense responses. We proposed a model depicting the interaction between grape and *C. viniferum* (Figure 12), providing a basis for further research on the pathogenesis of *C. viniferum* and the interaction between grapevines and *C. viniferum*.

5 Conclusion

In summary, our comparative analysis of susceptible and resistant grapevines through light and electron microscopy revealed distinct differences in infection dynamics. Notably, the diameter of *C. viniferum* lesions was the largest on "TS", followed by "B", and smallest on "LB-8". Susceptible grapes exhibited no white secretion, normal appressoria shape, and the formation of secondary hyphae, facilitating *C. viniferum* infection on grapes. We propose a model illustrating the interaction between grapes and *C. viniferum* (Figure 12). *C. viniferum* employs a variety of virulence strategies, including effectors, CWDEs, and secondary metabolites to target various cellular processes for nutrient acquisition. Conversely, grapevine responses to *C. viniferum* involves hormone signaling, disease-related genes expression, metabolic pathways activation, ROS accumulation, and transcription factors regulation. Our findings hold significance for the selection of candidate fungal pathogenic genes and plant disease response

genes. Furthermore, they laid the groundwork for further investigation into the pathogenic mechanisms of *C. viniferum* and the intricacies of the grape and *C. viniferum* interaction.

Data availability statement

All raw RNA-Seq read data in this study can be found in the National Center for Biotechnology Information (NCBI) Sequence Read Archive (SRA) with the accession numbers PRJNA1022593 and PRJNA1022588. The genomic datasets in this study can be found in online repositories. The names of the repository/repositories and accession number(s) can be found in the article/Supplementary Material.

Author contributions

MD: Data curation, Validation, Visualization, Writing – original draft, Writing – review & editing, Conceptualization, Formal analysis, Methodology, Investigation. YL: Validation, Writing – review & editing, Investigation. YH: Validation, Writing – review & editing. KZ: Validation, Writing – review & editing. XY: Writing – review & editing, Methodology. ZF: Validation, Writing – review & editing. XX: Validation, Writing – review & editing. QZ: Visualization, Writing – review & editing. WB: Visualization, Writing – review & editing. XC: Writing – review & editing, Visualization. GL: Writing – review & editing. YW: Writing – review & editing. LT: Writing – review & editing, Funding acquisition. YX: Funding acquisition, Writing – review & editing, Conceptualization, Project administration, Resources, Supervision.

Funding

The author(s) declare that financial support was received for the research, authorship, and/or publication of this article. This work was supported by the Project of Agricultural Breeding in Ningxia Hui Autonomous Region, China (NXNYYZ20210104), and Shenzhen Polytechnic University Research Project (6024330001K).

Conflict of interest

The authors declare that the research was conducted in the absence of any commercial or financial relationships that could be construed as a potential conflict of interest.

Publisher's note

Supplementary material

The Supplementary Material for this article can be found online at: https://www.frontiersin.org/articles/10.3389/fpls.2024.1446288/full#supplementary-material

References

Arroyo, F. T., Moreno, J., García-Herdugo, G., Santos, B. D. L., Barrau, C., Porras, M., et al. (2005). Ultrastructure of the early stages of *Colletotrichum acutatum* infection of strawberry tissues. *Can. J. Bot.* 83, 491–500. doi: 10.1139/b05-022

Ayako, T., Pamela, G., Naoyoshi, K., Mari, N., Yoshitaka, T., Yoshihiro, N., et al. (2019). Genomic plasticity mediated by transposable elements in the plant pathogenic fungus *Colletotrichum higginsianum*. *Genome Biol. Evol.* 11, 1487–1500. doi: 10.1093/gbe/evz087

Baroncelli, R., Sanz-Martín, J. M., Rech, G. E., Sukno, S. A., and Thon, M. R. (2014). Draft genome sequence of *Colletotrichum sublineola*, a destructive pathogen of Cultivated Sorghum. *Genome Announc.* 2, e00540–e00514. doi: 10.1128/genomeA.00540-14

Bhadauria, V., Banniza, S., Vandenberg, A., Selvaraj, G., and Wei, Y. (2013). Overexpression of a novel biotrophy-specific *Colletotrichum truncatum* effector, CtNUDIX, in hemibiotrophic fungal phytopathogens causes incompatibility with their host plants. *Eukaryot. Cell.* 12, 2–11. doi: 10.1128/EC.00192-12

Bhadauria, V., MacLachlan, R., Pozniak, C., Cohen-Skalie, A., Li, L., Halliday, J., et al. (2019). Genetic map-guided genome assembly reveals a virulence-governing minichromosome in the lentil anthracnose pathogen *Colletotrichum lentis*. *New Phytol.* 221, 431–445. doi: 10.1111/nph.15369

Broekaert, W. F., Delauré, S. L., De Bolle, M. F., and Cammue, B. P. (2006). The role of ethylene in host-pathogen interactions. *Annu. Rev. Phytopathol.* 44, 393–416. doi: 10.1146/annurev.phyto.44.070505.143440

Buchfink, B., Xie, C., and Huson, D. (2015). Fast and sensitive protein alignment using DIAMOND. *Nat. Methods* 12, 59–60. doi: 10.1038/nmeth.3176

Buiate, E. A. S., Xavier, K. V., Moore, N., Torres, M. F., Farman, M. L., Schardl, C. L., et al. (2017). A comparative genomic analysis of putative pathogenicity genes in the host-specific sibling species *Colletotrichum graminicola* and *Colletotrichum sublineola*. *BMC Genomics* 18, 67. doi: 10.1186/s12864-016-3457-9

Chen, C. J., Xia, R., Chen, H., and He, Y. H. (2018). TBtools, a toolkit for biologists integrating various biological data handling tools with a user-friendly interface. *Mol. Plant* 13, 1194–1202. doi: 10.1016/j.molp.2020.06.009

Chen, T. T., Peng, J., Yin, X., Li, M. J., Xiang, G. Q., Wang, Y. J., et al. (2021). Importin-αs are required for the nuclear localization and function of the *Plasmopara viticola* effector PvAVH53. *Hortic. Res-England.* 8, 46. doi: 10.1038/s41438-021-00482-6

Cosseboom, S. D., and Hu, M. (2022). Ontogenic susceptibility of grapevine clusters to ripe rot, caused by the Colletotrichum acutatum and C. *gloeosporioides species complexes. Phytopathol.* 112, 1956–1964. doi: 10.1094/PHYTO-01-22-0004-R

Diéguez-Uribeondo, J., Forster, H., Soto-Estrada, A., and Adaskaveg, J. E. (2005). Subcuticular-intracellular hemibiotrophic and intercellular necrotrophic development of *Colletotrichum acutatum* on almond. *Phytopathology* 95, 751–758. doi: 10.1094/PHYTO-95-0751

Ding, L. N., Li, M., Guo, X. J., Tang, M. Q., Cao, J., Wang, Z., et al. (2019). Arabidopsis GDSL1 overexpression enhances rapeseed *Sclerotinia sclerotiorum* resistance and the functional identification of its homolog in *Brassica napus*. *Plant Biotechnol. J.* 18, 1255–1270. doi: 10.1111/pbi.13289

Dong, Y., Duan, S., Xia, Q., Liang, Z., Dong, X., Margaryan, K., et al. (2023). Dual domestications and origin of traits in grapevine evolution. *Science* 379, 892–901. doi: 10.1126/science.add8655

Dou, M. R., Hao, Y., Yang, J., Yuan, X. J., Yin, X., Jiao, Y. T., et al. (2022). Genome sequence resource for *Colletotrichum viniferum*, the cause of grapevine ripe rot in China. *Mol. Plant Microbe In.* 35, 90–93. doi: 10.1094/MPMI-04-21-0077-A

Echeverrigaray, S., Scariot, F. J., Fontanella, G., Favaron, F., Sella, L., Santos, M. C., et al. (2020). *Colletotrichum* species causing grape ripe rot disease in *Vitis labrusca* and *V. vinifera* varieties in the highlands of southern Brazil. *Plant Pathol.* 69, 1504–1512. doi: 10.1111/ppa.13240

Edgar, R. C. (2004). MUSCLE: multiple sequence alignment with high accuracy and high throughput. *Nucleic Acids Res.* 32, 1792–1797. doi: 10.1093/nar/gkh340

Emms, D. M., and Kelly, S. (2019). OrthoFinder: phylogenetic orthology inference for comparative genomics. *Genome Biol.* 20, 238. doi: 10.1186/s13059-019-1832-y

Feng, L., Dong, M., Huang, Z., Wang, Q., An, B., He, C., et al. (2024). CgCFEM1 is required for the full virulence of *Colletotrichum gloeosporioides*. *Int. J. Mol. Sci.* 25, 2937. doi: 10.3390/ijms25052937

Feng, J. X., Cao, L., Li, J., Duan, C. J., Luo, X. M., Le, N., et al. (2011). Involvement of OsNPR1/NH1 in rice basal resistance to blast fungus Magnaporthe oryzae. *Eur. J. Plant Pathol.* 131, 221–235. doi: 10.1007/s10658-011-9801-7

Gao, X. M., Fan, X. C., Zhang, G. H., Zhang, Y., Jiang, J. F., Sun, H. S., et al. (2016). Identification and screening of hybrid progenies with resistance to grape anthracnose. *Acta Agriculturae Boreali-Occidentalis Sin.* 25, 882–888. doi: 10.7606/j.issn.1004-1389.2016.06.014

Gao, H., Jiang, L. Y., Du, B. H., Ning, B., Ding, X. D., Zhang, C. Z., et al. (2022). GmMKK4-activated GmMPK6 stimulates GmERF113 to trigger resistance to *Phytophthora sojae* in soybean. *Plant J.* 111, 473–495. doi: 10.1111/tpj.15809

Glazebrook, J. (2005). Contrasting mechanisms of defense against biotrophic and necrotrophic pathogens. *Annu. Rev. Phytopathol.* 43, 205–227. doi: 10.1146/annurev.phyto.43.040204.135923

Gutiérrez, P., Alzate, J., Yepes, M. S., and Marin, M. (2016). Complete mitochondrial genome sequence of the common bean anthracnose pathogen *Colletotrichum lindemuthianum*. *Mitochondrial DNA A* 27, 136–137. doi: 10.3109/19401736.2013.878912

Han, J. H., Chon, J. K., Ahn, J. H., Choi, I. Y., Lee, Y. H., and Kim, K. S. (2016). Whole genome sequence and genome annotation of *Colletotrichum acutatum*, causal agent of anthracnose in pepper plants in South Korea. *Genomics Data* 8, 45–46. doi: 10.1016/j.gdata.2016.03.007

Han, R., Yin, W., Ahmad, B., Gao, P., Li, Z., and Wang, X. (2021). Pathogenesis and immune response in resistant and susceptible cultivars of grapevine (Vitis spp.) against Elsinoë ampelina infection. *Phytopathology.* 111, 799–807. doi: 10.1094/PHYTO-03-20-0079-R

He, S., Qiao, X., Zhang, S., Xia, J., Wang, L., and Liu, S. (2023). Urate oxidase from tea microbe *Colletotrichum camelliae* is involved in the caffeine metabolism pathway and plays a role in fungal virulence. *Front. Nutr.* 9. doi: 10.3389/fnut.2022.1038806

He, P. C., and Ren, Z. B. (1990). Study on the resistances of wild Vitis species native to China to grape ripe rot. *J. Fruit Sci.* 7, 7–12. doi: 10.13925/j.cnki.gsxb.1990.01.002

Hedges, S. B., Dudley, J., and Kumar, S. (2006). TimeTree: a public knowledge-base of divergence times among organisms. *Bioinformatics* 22, 2971–2972. doi: 10.1093/bioinformatics/btl505

Huang, X. X., Wang, Y., Lin, J. S., Chen, L., Li, Y. J., Liu, Q., et al. (2021). The novel pathogen-responsive glycosyltransferase UGT73C7 mediates the redirection of phenylpropanoid metabolism and promotes *SNC1*-dependent Arabidopsis immunity. *Plant J.* 107, 149-165. doi: 10.1111/tpj.15280

Huckelhoven, R., Fodor, J., and Kogel, K. H. (1999). Hypersensitive cell death and papilla formation in barley attacked by the powdery mildew fungus are associated with hydrogen peroxide but not with salicylic acid accumulation. *Plant Physiol.* 119, 1251–1260. doi: 10.1104/pp.119.4.1251

Huo, J., Wang, Y., Hao, Y., Yao, Y., Wang, Y., Zhang, K., et al. (2021). Genome sequence resource for *Colletotrichum scovillei*, the cause of anthracnose disease of chili. *Mol. Plant Microbe In.* 34, 122–126. doi: 10.1094/MPMI-03-20-0055-A

Ishiga, Y., Uppalapati, S. R., Ishiga, T., Elavarthi, S., Martin, B., and Bender, C. L. (2009). The phytotoxin coronatine induces light-dependent reactive oxygen species in tomato seedlings. *New Phytol.* 181, 147–160. doi: 10.1111/j.1469-8137.2008.02639.x

Jantasuriyarat, C., Gowda, M., Haller, K., Hatfield, J., Lu, G. D., Stahlberg, E., et al. (2005). Large-scale identification of expressed sequence tags involved in rice and rice blast fungus interaction. *Plant Physiol.* 138, 105–115. doi: 10.1104/pp.104.055624

Jaulneau, V., Cazaux, M., Hoi, J. W. S., Fournier., S., Esquerré-Tugayé, M., Jacquet, C., et al. (2010). Host and nonhost resistance in Medicago-Colletotrichum interactions. *Mol. Plant Microbe Interact.* 23, 1107–1117. doi: 10.1094/MPMI-23-9-1107

Ji, T., Salotti, I., Dong, C., Li, M., and Rossi, V. (2021). Modeling the effects of the environment and the host plant on the ripe rot of grapes, caused by the Colletotrichum species. *Plants* 10, 2288. doi: 10.3390/plants10112288

Joung, J. G., Corbett, A. M., Fellman, S. M., Tieman, D. M., Klee, H. J., Giovannoni, J. J., et al. (2010). Plant MetGenMAP: an integrative analysis system for plant systems biology. *Plant Physiol.* 151, 1758–1768. doi: 10.1104/pp.109.145169

Kim, M. R., and Oh, S. K. (2019). Analysis of varietal difference and genetic diversity of grapevine cultivars through the leaf inoculation of Colletotrichum spp. *J. Agric. Life Sci.* 52, 49-60. doi: 10.14397/jals.2018.52.6.49

Klimmek, F., Sjödin, A., Noutsos, C., Leister, D., and Jansson, S. (2006). Abundantly and rarely expressed Lhc protein genes exhibit distinct regulation patterns in plants. *Plant Physiol.* 140, 793–804. doi: 10.1104/pp.105.073304

Kortekamp, A., and Zyprian, E. (1999). Leaf hairs as a basic protective barrier against downy mildew of grape. *J. Phytopathol.* 147, 453–459. doi: 10.1111/j.1439-0434.1999.tb03850.x

Kunze, G., Zipfel, C., Robatzek, S., Niehaus, K., Boller, T., and Felix, G. (2004). The N terminus of bacterial elongation factor Tu elicits innate immunity in *Arabidopsis* plants. *Plant Cell* 16, 3496–3507. doi: 10.1105/tpc.104.026765

Lei, Y., Tang, X. B., Jayawardena, R. S., Yan, J. Y., Wang, X. D., Liu, M., et al. (2016). Identification and characterization of *Colletotrichum* species causing grape ripe rot in southern China. *Mycosphere* 7, 1177–1191. doi: 10.5943/mycosphere/si/2c/8

Lei, Y., Yuan, X. J., Chen, T., Yuan, Y., Liu, X. M., Tang, X. B., et al. (2022). Transcriptome analysis of berries of spine grape (*Vitis davidii* Föex) infected by *Colletotrichum viniferum* during symptom development. *Horticulturae* 8, 843. doi: 10.3390/horticulturae8090843

Li, N., Han, X., Feng, D., Yuan, D. Y., and Huang, L. J. (2019a). Signaling crosstalk between salicylic acid and ethylene/jasmonate in plant defense: do we understand what they are whispering. *Int. J. Mol. Sci.* 20, 671. doi: 10.3390/ijms20030671

Li, Z. Q., Jiao, Y. T., Zhang, C., Dou, M. R., Weng, K., Wang, Y. J., et al. (2021b). VvHDZ28 positively regulates salicylic acid biosynthesis during seed abortion in Thompson Seedless. *Plant Biotechnol. J.* 19, 1824–1838. doi: 10.1111/pbi.13596

Li, M., Liu, J., and Zhou, G. Y. (2021a). Histopathological and ultrastructural observations of *Camellia oleifera* infected with *Colletotrichum fructicola*. *Australas. Plant Pathol.* 50, 523–531. doi: 10.1007/s13313-021-00811-2

Li, Z., Wang, Y., Fan, Y., Ahmad, B., Wang, X., Zhang, S., et al. (2021c). Transcriptome analysis of the grape-*Elsinoë ampelina* pathosystem reveals novel effectors and a robust defense response. *Mol. Plant Microbe In.* 34, 110–121. doi: 10.1094/MPMI-08-20-0227-R

Li, T. T., Wang, Q. H., Feng, R. R., Li, L. C., Ding, L. W., Fan, G. J., et al. (2019b). Negative regulators of plant immunity derived from cinnamyl alcohol dehydrogenases are targeted by multiple *Phytophthora* Avr3a-like effectors. *New Phytol.* doi: 10.1111/nph.16139

Li, P., Zhao, L., Qi, F., Htwe, N. M. P. S., Li, Q., Zhang, D., et al. (2021). The receptor-like cytoplasmic kinase RIPK regulates broad-spectrum ROS signaling in multiple layers of plant immune system. *Mol. Plant* 14, 1652–1667. doi: 10.1016/j.molp.2021.06.010

Liang, X., Shang, S., Dong, Q., Wang, B., Zhang, R., Gleason, M. L., et al. (2018). Transcriptomic analysis reveals candidate genes regulating development and host interactions of *Colletotrichum fructicola*. *BMC Genomics* 19, 557. doi: 10.1186/s12864-018-4934-0

Liu, T. L., Chen, T. Z., Kan, J. L., Yao, Y., Guo, D. S., Yang, Y. W., et al. (2021). The GhMYB36 transcription factor confers resistance to biotic and abiotic stress by enhancing PR1 gene expression in plants. *Plant Biotechnol. J.* 20, 722–735. doi: 10.1111/pbi.13751

Love, M. I., Huber, W., and Anders, S. (2014). Moderated estimation of fold change and dispersion for RNA-seq data with DESeq2. *Genome Biol.* 15, 550. doi: 10.1186/s13059-014-0550-8

Manickavelu, A., Kawaura, K., Oishi, K., Shin-I, T., Kohara, Y., Yahiaoui, N., et al. (2010). Comparative gene expression analysis of susceptible and resistant near-isogenic lines in common wheat infected by *Puccinia triticina*. *DNA Res.* 17, 211–222. doi: 10.1093/dnares/dsq009

Melksham, K. J., Weckert, M. A., and Steel, C. C. (2002). An unusual bunch rot of grapes in sub-tropical regions of Anstralia caused by *Colletotrichum acutatum*. *Australas. Plant Pathol.* 31, 193–194. doi: 10.1071/AP02013

Meng, Y. A., Gleason, M. L., Zhang, R., and Sun, G. Y. (2019). Genome sequence resource of the wide-host-range anthracnose pathogen *Colletotrichum siamense*. *Mol. Plant Microbe In.* 32, 931–934. doi: 10.1094/MPMI-01-19-0010-A

Meyers, B. C., Kaushik, S., and Nandety, R. S. (2005). Evolving disease resistance genes. *Curr. Opin. Plant Biol.* 8, 129–134. doi: 10.1016/j.pbi.2005.01.002

Moraes, S. R. G., Tanaka, F. A. O., and Massola, N. S. (2013). Histopathology of *Colletotrichum gloeosporioides* on guava fruits (*Psidium guajava* L.). *Rev. Bras. Frutic.* 35, 657–664. doi: 10.1590/S0100-29452013000200039

Mortazavi, A., Williams, B. A., McCue, K., Schaeffer, L., and Wold, B. (2008). Mapping and quantifying mammalian transcriptomes by RNA-Seq. *Nat. Methods* 5, 621–628. doi: 10.1038/nmeth.1226

Nabavi, S., Šamec, D., Tomczyk, M., Milella, L., Russo, D., Habtemariam, S., et al. (2020). Flavonoid biosynthetic pathways in plants: Versatile targets for metabolic engineering. *Biotechnol. Adv.* 38, 107316. doi: 10.1016/j.biotechadv.2018.11.005

Nandakumar, M., Malathi, P., Sundar, A. R., and Viswanathan, R. (2021). Expression analyses of resistance-associated candidate genes during sugarcane-*Colletotrichum falcatum* went interaction. *Sugar Tech* 23, 1056–1063. doi: 10.1007/s12355-021-00976-6

Nandeeshkumar, P., Ramachandrakini, K., Prakash, H. S., Niranjana, S. R., and Shekar Shetty, H. (2008). Induction of resistance against downy mildew on sunflower by rhizobacteria. *J. Plant Interact.* 3, 255–262. doi: 10.1080/17429140802245697

Nie, J. J., Yin, Z. Y., Li, Z. P., Wu, Y. X., and Huang, L. L. (2019). A small cysteine-rich protein from two kingdoms of microbes is recognized as a novel pathogen-associated molecular pattern. *New Phytol.* 222, 995–1011. doi: 10.1111/nph.15631

Oo, M. M., and Oh, S. K. (2017). Identification and characterization of new record of grape ripe rot disease caused by *Colletotrichum viniferum* in Korea. *Mycobiology* 45, 421–425. doi: 10.5941/MYCO.2017.45.4.421

Pan, F. Y., Huang, Y., Lin, L., Zhou, Y. M., Wei, R. F., Guo, W. F., et al. (2016). First report of *Colletotrichum capsici* causing grape ripe rot in Guangxi, China. *Plant Dis.* 100, 2531–2531. doi: 10.1094/PDIS-05-16-0691-PDN

Peng, L. J., Sun, T., Yang, Y. L., Cai, L., Hyde, K. D., Bahkali, A. H., et al. (2013). *Colletotrichum* species on citrus leaves in Guizhou and Yunnan provinces, China. *Mycoscience* 54, 29–41. doi: 10.1094/PDIS-06-23-1057-PDN

Prasanth, C. N., Viswanathan, R., Malathi, P., and Sundar, A. R. (2022). Carbohydrate active enzymes (CAZy) regulate cellulolytic and pectinolytic enzymes in *Colletotrichum falcatum* causing red rot in sugarcane. *3 Biotech.* 12, 48. doi: 10.1007/s13205-022-03113-6

Sanderson, M. J. (2003). r8s: inferring absolute rates of molecular evolution and divergence times in the absence of a molecular clock. *Bioinformatics* 19, 301. doi: 10.1093/bioinformatics/19.2.301

Schmiesing, A., Emonet, A., Gouhier-Darimont, C., and Reymond, P. (2016). Arabidopsis MYC transcription factors are the target of hormonal salicylic acid/jasmonic acid cross talk in response to *Pieris brassicae* egg extract. *Plant Physiol.* 170, 2432–2443. doi: 10.1104/pp.16.00031

Segal, L. M., and Wilson, R. A. (2018). Reactive oxygen species metabolism and plant-fungal interactions. *Fungal Genet. Biol.* 110, 1–9. doi: 10.1016/j.fgb.2017.12.003

Shang, S. P., Liang, X. F., Liu, G. L., Zhang, S., Lu, Z. X., Zhang, R., et al. (2020). Histological and ultrastructural characterization of the leaf infection events of *Colletotrichum fructicola* on *Malus domestica* 'Gala'. *Plant Pathol.* 69, 538–548. doi: 10.1111/ppa.13141

Shen, C. Q., Sun, L., Zhang, Y., Jiang, J. F., Liu, C. H., and Fan, X. C. (2022). Transcriptomic analysis of different resistant leaves infected by *Colletotrichum gloeosporioides* in grape. *J. Fruit Sci.* 39, 730–742. doi: 10.13925/j.cnki.gsxb.20210573

Shimizu, K., Suzuki, H., Uemura, T., Nozawa, A., Desaki, Y., Hoshino, R., et al. (2022). Immune gene activation by NPR and TGA transcriptional regulators in the model monocot *Brachypodium distachyon*. *Plant J.* 110, 470–481. doi: 10.1111/tpj.15681

Shiraishi, M., Koide, M., Itamura, H., Yamada, M., Mitani, N., and Ueno, T. (2007). Screening for resistance to ripe rot caused by *Colletotrichum acutatum* in grape germplasm. *Vitis* 46, 196–200. doi: 10.2503/jjshs.75.264

Stamatakis, A. (2014). RAxML version 8: a tool for phylogenetic analysis and post-analysis of large phylogenies. *Bioinformatics* 30, 1312–1313. doi: 10.1093/bioinformatics/btu033

Swarbrick, P. J., Schulze-Lefert, P., and Scholes, J. D. (2006). Metabolic consequences of susceptibility and resistance (race-specific and broad-spectrum) in barley leaves challenged with powdery mildew. *Plant Cell Environ.* 29, 1061–1076. doi: 10.1111/j.1365-3040.2005.01472.x

Tsushima, A., Narusaka, M., Gan, P., Kumakura, N., Hiroyama, R., Kato, N., et al. (2021). The conserved Colletotrichum spp. effector candidate CEC3 induces nuclear expansion and cell death in plants. *Front. Microbiol.* 3, 682155. doi: 10.3389/fmicb.2021.682155

Velho, A. C., Rockenbach, M. F., Mondino, P., and Stadnika, M. J. (2016). Modulation of oxidative responses by a virulent isolate of *Colletotrichum fructicola* in apple leaves. *Fungal Biol-UK.* 120, 1184–1193. doi: 10.1016/j.funbio.2016.07.001

Vestergaard, M., and Ingmer, H. (2019). Antibacterial and antifungal properties of resveratrol. *Int. J. Antimicrob. Ag.* 53, 716–723. doi: 10.1016/j.ijantimicag.2019.02.015

Wang, C. F., Huang, L. L., Zhang, H. C., Han, Q. M., Buchenauer, H., and Kang, Z. S. (2010). Cytochemical localization of reactive oxygen species (O_2 and H_2O_2) and peroxidase in the incompatible and compatible interaction of wheat-*Puccinia striiformis* f. sp. tritici. *Physiol. Mol. Plant P.* 74, 221–229. doi: 10.1016/j.pmpp.2010.02.002

Wang, M., Luo, X., and Wang, H. (2021). First draft genome sequence resource of Colletotrichum liriopes causing leaf anthracnose on Ophiopogon japonicus. *Plant Dis.* 105, 1179–1182. doi: 10.1094/PDIS-11-20-2326-A

Wharton, P. S., and Schilder, A. C. (2008). Novel infection strategies of *Colletotrichum acutatum* on ripe blueberry fruit. *Plant Pathol.* 57, 122–134. doi: 10.1111/j.1365-3059.2007.01698.x

Whitelaw-Weckert, M. A., Curtin, S. J., Huang, R., Steel, C. C., Blanchard, C. L., and Roffey, P. E. (2010). Phylogenetic relationships and pathogenicity of *Colletotrichum acutatum* isolates from grape in subtropical Australia. *Plant Pathol.* 56, 448–463. doi: 10.1111/j.1365-3059.2007.01569.x

Xia, J., Liu, N., Han, J., Sun, J., Xu, T., and Liu, S. (2023). Transcriptome and metabolite analyses indicated the underlying molecular responses of Asian ginseng (*Panax ginseng*) toward *Colletotrichum panacicola* infection. *Front. Plant Sci.* 14. doi: 10.3389/fpls.2023.1182685

Xu, X. W., Li, J. C., Hai, D., Wang, Y. X., Li, J. Y., and Zha, Y. P. (2024). Complete genome sequence of a novel alternavirus isolated from the phytopathogenic fungus *Colletotrichum fioriniae*. *Arch. Virol.* 169, 79. doi: 10.1007/s00705-024-06010-w

Yan, J. Y., Jayawardena, M. M. R. S., Goonasekara, I. D., Wang, Y., Zhang, W., Liu, M., et al. (2015). Diverse species of *Colletotrichum* associated with grapevine anthracnose in China. *Fungal Divers.* 71, 233–246. doi: 10.1007/s13225-014-0310-9

Yin, X., Fu, Q. Q., Shang, B. X., Wang, Y. J., Liu, R. Q., Chen, T. T., et al. (2022). An RxLR effector from *Plasmopara viticola* suppresses plant immunity in grapevine by targeting and stabilizing VpBPA1. *Plant J.* 112, 104–114. doi: 10.1111/tpj.15933

Yin, X., Liu, R. Q., Su, H., Su, L., Guo, Y. R., Wang, Z. J., et al. (2017). Pathogen development and host responses to *Plasmopara viticola* in resistant and susceptible grapevines: an ultrastructural study. *Hortic. Res-England.* 4, 17033. doi: 10.1038/hortres.2017.33

Yokosawa, S., Eguchi, N., and Sato, T. (2020). Characterization of the *Colletotrichum gloeosporioides* species complex causing grape ripe rot in Nagano Prefecture, Japan. *J. Gen. Plant Pathol.* 86, 163–172. doi: 10.1007/s10327-020-00907-5

Yu, D., Wei, W., Fan, Z. Q., Chen, J. Y., You, Y. L., Huang, W. D., et al. (2023). VabHLH137 promotes proanthocyanidin and anthocyanin biosynthesis and enhances resistance to *Colletotrichum gloeosporioides* in grapevine. *Hortic. Res-England.* 10, uhac261. doi: 10.1093/hr/uhac261

Yu, Y., Zhang, Y., Yin, L., and Lu, J. (2012). The mode of host resistance to *Plasmopara viticola* infection of grapevines. *Phytopathology* 102, 1094–1101. doi: 10.1094/PHYTO-02-12-0028-R

Yuan, X., Pan, S. H., Zhang, Q., Dai, F., and Zhang, J. X. (2024). A *Colletotrichum tabacum* effector Cte1 targets and stabilizes NbCPR1 to suppress plant immunity. *Mol. Plant Microbe Interact.* 37, 477-484. doi: 10.1094/MPMI-11-23-0197-R

Zhang, L., Zhang, F., Melotto, M., Yao, J., and He, S. Y. (2017). Jasmonate signaling and manipulation by pathogens and insects. *J. Exp. Bot.* 68, 1371–1385. doi: 10.1093/jxb/erw478

Zhao, L., Liao, Z., Feng, L., An, B., He, C., Wang, Q., et al. (2023). *Colletotrichum gloeosporioides* Cg2LysM contributed to virulence toward rubber tree through affecting invasive structure and inhibiting chitin-triggered plant immunity. *Front. Microbiol.* 14. doi: 10.3389/fmicb.2023.1129101

Zheng, R., Shu, B., and Luo, C. (2022). *Colletotrichum siamense* infection caused transcripts involved plant hormone signal transduction and phenylpropanoid biosynthesis varied in strawberry. *Not. Bot. Horti Agrobo.* 50, 12791. doi: 10.15835/nbha50312791

Zhou, R., Dong, Y. H., Liu, X., Feng, S., Wang, C. X., Ma, X. M., et al. (2022). JrWRKY21 interacts with JrPTI5L to activate the expression of JrPR5L for resistance to *Colletotrichum gloeosporioides* in walnut. *Plant J.* 111, 1152–1166. doi: 10.1111/tpj.15883

Zhou, J. W., Li, P. L., Ji, P. C., Yin, K. Y., Tan, X. J., Chen, H., et al. (2024). Carbon quantum dots derived from resveratrol enhances anti-virulence activity against *Pseudomonas aeruginosa*. *Surf. Interfaces* 44, 103662. doi: 10.1016/j.surfin.2023.103662

frontiers | Frontiers in Plant Science

TYPE Original Research
PUBLISHED 03 September 2024
DOI 10.3389/fpls.2024.1403226

OPEN ACCESS

EDITED BY
Brigitte Mauch-Mani,
Université de Neuchâtel, Switzerland

REVIEWED BY
Jiemeng Tao,
Zhengzhou Tobacco Research Institute of CNTC, China
Junliang Zou,
Beijing Academy of Agricultural and Forestry Sciences, China

*CORRESPONDENCE
Li Zhu
cdyc202112@163.com
Delong Meng
delong.meng@csu.edu.cn

†These authors have contributed equally to this work and share first authorship

RECEIVED 19 March 2024
ACCEPTED 15 July 2024
PUBLISHED 03 September 2024

CITATION
Liu W, Zhang Z, Zhang B, Zhu Y, Zhu C, Chen C, Zhang F, Liu F, Ai J, Wang W, Kong W, Xiang H, Wang W, Gong D, Meng D and Zhu L (2024) Role of bacterial pathogens in microbial ecological networks in hydroponic plants.
Front. Plant Sci. 15:1403226.
doi: 10.3389/fpls.2024.1403226

Role of bacterial pathogens in microbial ecological networks in hydroponic plants

Wenyi Liu[1,2†], Zhihua Zhang[3†], Bin Zhang[4†], Yi Zhu[3], Chongwen Zhu[3], Chaoyong Chen[3], Fangxu Zhang[3], Feng Liu[3], Jixiang Ai[3], Wei Wang[3], Wuyuan Kong[3], Haoming Xiang[3], Weifeng Wang[3], Daoxin Gong[1], Delong Meng[4*] and Li Zhu[3*]

[1]College of Environment and Ecology, Hunan Agricultural University, Changsha, China, [2]School of Minerals Processing and Bioengineering, Central South University, Changsha, China, [3]Changde Tobacco Company of Hunan Province, Changde, China, [4]College of Chemistry and Bioengineering, Hunan University of Science and Engineering, Yongzhou, China

Plant-associated microbial communities are crucial for plant growth and health. However, assembly mechanisms of microbial communities and microbial interaction patterns remain elusive across vary degrees of pathogen-induced diseases. By using 16S rRNA high-throughput sequencing technology, we investigated the impact of wildfire disease on the microbial composition and interaction network in plant three different compartments. The results showed that pathogen infection significantly affect the phyllosphere and rhizosphere microbial community. We found that the primary sources of microbial communities in healthy and mildly infected plants were from the phyllosphere and hydroponic solution community. Mutual exchanges between phyllosphere and rhizosphere communities were observed, but microbial species migration from the leaf to the root was rarely observed in severely infected plants. Moreover, wildfire disease reduced the diversity and network complexity of plant microbial communities. Interactions among pathogenic bacterial members suggested that Caulobacter and Bosea might be crucial "pathogen antagonists" inhibiting the spread of wildfire disease. Our study provides deep insights into plant pathoecology, which is helpful for the development of novel strategies for phyllosphere disease prediction or prevention.

KEYWORDS

***Pseudomonas*, wildfire disease, pathogen invasion, molecular ecological network, compartment niches, plant-microbe interactions**

1 Introduction

Pseudomonas is a common pathogenic bacterium found on Solanaceae crops (Höfte and De Vos, 2007). *Pseudomonas syringae* is a Gram-negative bacterium, and wildfire disease caused by *Pseudomonas syringae* is a major destructive bacterial leaf disease worldwide (Lucas, 1958). It affects various plants, including tobacco, tomato, citrus, and

beans (Morris et al., 2007; O'Brien et al., 2011), causing significant crop losses globally (Wang et al., 2013). Several studies suggest that microbes residing on plants without inducing disease may also contribute to host resistance against pathogens (Chapelle et al., 2016; Mendes et al., 2018). Therefore, a better understanding of the changes in the plant microbial community during the disease process is necessary for developing biological control strategies to manage wildfire disease.

Plants harbor complex bacterial communities in various plant parts, each exerting distinct roles (Dong et al., 2019). Diverse microorganisms inhabit different plant compartments, including roots, stems, leaves, flowers, and fruits (Lindow and Brandl, 2003; Hacquard et al., 2015). The phyllosphere, residing on plant surfaces, hosts numerous potentially beneficial, pathogenic, or antagonistic microorganisms (bacteria, fungi, and viruses), with the composition and diversity of leaf surface microbial communities influenced by plant diseases (Aleklett et al., 2014). The root system constitutes a crucial area for plant-microbe interactions (Edwards et al., 2015). Bacteria in the rhizosphere can induce or suppress diseases, produce plant growth regulators and other biologically active substances, or influence plant productivity by modulating the availability of nutrients and toxic elements (Saeed et al., 2021). The hydroponic solution for hydroponic plants consists primarily of inorganic ions providing essential elements for higher plants, obtained from the growth medium (Trejo-Téllez and Gómez-Merino, 2012). Despite prior research predominantly focusing on individual plant parts in wildfire disease, without exploration in a unified context involving all three compartments at varying severity levels, the shaping of microbial community assemblies and symbiotic patterns across the rhizosphere, phyllosphere, and endosphere remains largely unknown.

Infection by pathogens can have a significant impact on the resident microbial community. The pathogen may disrupt interactions among plant microbiota, leading to the restructuring of microbial communities (Van der Putten et al., 2007). However, current understanding of how pathogen infection in Solanaceae crops induces changes in microbial communities remains limited. Recent studies have suggested that during the invasion of bacterial wilt, the endophytic community was significantly affected by the invasion of the pathogen. Furthermore, interactions among pathogenic members suggested a positive correlation between pathogenic members and the presence of Delftia, Stenotrophomonas, and Bacillus in the infected plant roots (Hu et al., 2020). A recent study proposed that the pathogen Xanthomonas causing bacterial leaf spot disease in lettuce showed a significant positive correlation with the genus Alkanindiges, but exhibited negative correlations with the genera Bacillus, Erwinia, and Pantoea (Rastogi et al., 2012) Previous studies have shown that members of Botryosphaeria, Paraphoma, and Plectosphaerella in the phyllosphere fungal community of Solanaceae crops infected with leaf spot disease may act as crucial "pathogen facilitators" to exacerbate the severity of brown spot disease. Conversely, genera Pleospora and Ochrocladosporium could serve as significant "pathogen antagonists" to inhibit the expansion of pathogenic Alternaria (Tao et al., 2021). However, there have been limited studies investigating the interactions between microbial communities in plant leaves, roots, hydroponic solutions, and the pathogenic bacterium Pseudomonas. These relationships between microbial communities and Pseudomonas might uncover the roles played by various microbes in either inhibiting or promoting wildfire disease.

The objectives of this study were to (i) characterize the diversity and structure of phyllosphere, root and hydroponic solution bacteria communities at different disease severities of wildfire disease;(ii)The source of microbial migration from hydroponic solutions to endophytic communities under the influence of wildfire disease.;(iii) use association networks to examine the frequency of interactions within microbial communities associated with the disease severities and compartments of Solanceae crops and analyze the interactions between the pathogen and other microbiota through network analysis.

2 Materials and methods

2.1 Sample collection and processing

All 27 samples were collected in June 2022(the early stage of wildfire disease) from Kunming City, Yunnan Province, China (24° 23'N, 102°10'E), plants without any symptoms of wildfire disease were classified as healthy plants, while those showing symptoms were classified as diseased plants. The infection levels ranging from 3 to 9, and the severity classification standards for bacterial wildfire disease are based on the pest classification and survey methods (GB/T 23222–2008), P.R. China. Three plants were randomly selected from each category of the healthy, mildly infected, and severely infected plants for sampling. Subsequently, samples were collected from the phyllosphere, root and hydroponic solution of the same plants. All samples were transported to the laboratory on dry ice and labeled as H (healthy), S (slight infected), and I (severely infected). Each sample was a composite sample mixed from three subsamples taken from the same plant.

Gently stir the hydroponic solution to ensure even mixing. Using a sterile pipette, draw 50 mL of the hydroponic solution and store the obtained liquid at -80°C for subsequent DNA extraction. Roots and stems are washed separately with 75% ethanol, 2.5% sodium hypochlorite, and sterile water. Subsequently, the roots and stems are cut into small pieces and stored at -80°C for DNA extraction.

2.2 DNA extraction and amplicon sequencing

The DNA extraction was performed using the E.Z.N.A.®Soil DNA Kit (Omega, USA) according to the instructions, with 1.0 g of phyllosphere and root microbiota for DNA extraction. Additionally, the E.Z.N.A.®Water DNA Kit (Omega, USA)was employed to extract DNA from 5.00 ml of hydroponic solution. The 16S rRNA variable region (V3+V4) was amplified by PCR using primers 338F (5'-ACTCCTACGGGAGGCAGCAG-3') and 806R (5'-GGACTACHVGGGTWTCTAAT-3') (Srinivasan et al., 2012).

ThePCR conditions consisted of a 50 μL reaction system including 1.5 μL dNTP mix, 0.5 μL TaqDNA enzyme (Takara, Beijing, China), 5 μL 10× PCR buffer, 1.5 μL of 10 μM forward and reverse primers, and 20~30 ng of template. The thermal cycling operations was defined as: 94 for 1 minute, 30 cycles of 94 for 20 seconds, 57 for 25 seconds, 68 for 45 seconds, and a final elongation at 72 for 10 minutes, and finally stored at 4 . The PCR products were detected by 2% agarose gel electrophoresis, and the target fragments were recovered using the AxyPrep PCR Cleanup Kit. The purified PCR products were quantified using the Quant-iT PicoGreen dsDNA Assay Kit on the Qubit fluorescence quantification system. After gradient dilution of each qualified on-machine sequencing library (the Index sequence is not repeatable), they were mixed in corresponding proportions according to the required sequencing amount and denatured by NaOH into single strands for on-machine sequencing. These samples were performed to 2×300bp paired-end sequencing using the MiSeq sequencer from Hangzhou Lianchuan Biotechnology Co., Ltd. with the corresponding MiSeq Reagent Kit.

2.3 Sequence data preprocessing and statistical analysis

The raw gene sequences were analyzed using the QIIME 2 (Bolyen et al., 2019). Initially, DADA2 (Callahan et al., 2016) was employed to filter low-quality sequences (truncQ = 2, maxN = 0, maxEE = c(3, 5)). Then, sequences were clustered into Operational Taxonomic Units (OTUs) at a 97% similarity level, generating an operational taxonomic unit table. Subsequently, OTUs were taxonomically classified by comparing them with the silva-138-99-nb-classifier (Yilmaz et al., 2014) prokaryotic organism database. A systematic evolutionary tree was constructed using representative sequences of OTUs, and species annotations were performed.

All statistical analyses and computations were conducted using the R platform (version 4.1.1). The microeco 0.5.1 package (Liu et al., 2021) was employed for ecological data statistics and visualization of bacterial communities. The ggplot2 (Wickham et al., 2016) package was utilized to generate species abundance plots, and the α-diversity index (Shannon index) of bacterial communities was calculated. Kruskal-Wallis rank-sum tests and multiple comparisons of variance were performed to examine inter-group differences in alpha diversity of bacterial communities. Principal Coordinate Analysis (PCoA) was applied for dimensionality reduction of microbial communities. The Bray-Curtis distance was computed to assess community beta diversity. The Adonis (Dixon, 2003) function was employed for permutation multivariate analysis of variance (PERMANOVA) statistical tests, evaluating the relative contributions of different factors to community dissimilarities. The Linear Discriminant Analysis Effect Size (LEfSe) was used to identify statistically different biomarkers at various taxonomic levels between groups (Segata et al., 2011). The SourceTracker model was utilized to estimate the sources of bacterial communities in different parts of healthy and wildfire-infected plants.

2.4 Network construction

To elucidate the interactions of plant microbial communities during wildfire disease invasion, we constructed Molecular Ecological Networks (MENs) based on Sparcc correlation coefficients ($P < 0.05$). Greedy module optimization methods were employed for module separation. The optimal correlation coefficient threshold was determined using Random Matrix Theory (RMT). Additionally, a consistent threshold was selected to generate networks for comparison under the same conditions (Deng et al., 2012). The networks of phyllosphere, root, and hydroponic solution communities were analyzed using the mentioned approach. Subnetworks of interactions between pathogens and other microbial members were constructed in phyllosphere and root samples of slight infected plants. All networks were visualized using Gephi (Bastian et al., 2009). The calculated topological characteristics of bacterial networks included symbiotic (positive) and exclusion (negative) correlation numbers, average path length, network diameter, average clustering coefficient, average connectivity, and modularity.

3 Results

3.1 bacterial community structures diversity and composition of healthy and different disease severities infected samples

5403 OTUs were obtained from 27 bacterial samples. PERMANOVA analysis (Supplementary Table 1) suggested that the variation in bacteria was mainly influenced by compartment niches ($R2 = 38.97\%$, $P=0.001$) and disease severity ($R2 = 9.78\%$, $P=0.02$). PCoA of Bray–Curtis distance revealed that the phyllosphere, root and hydroponic solution formed three distinct clusters regardless of plant disease severity. The PCoA of each compartment microbiome indicated significant differences in the community structures of the phyllosphere, root and hydroponic due to wildfire disease. Compared to its effects on the bacterial communities in the phyllosphere and roots, the impact of wildfire disease on the bacterial community in the hydroponic solution was less pronounced (Figure 1; Supplementary Table 2; phyllosphere, root and hydroponic solution:$P<0.05$, $P<0.005$, $P<0.1$).

Bacterial communities in all compartment niches had a similar Shannon diversity index. The bacterial alpha diversity in each compartment niches was affected by disease severity (ANOVA; $P < 0.05$). Shannon diversity gradually decreased from healthy to slight to severe, indicating that diversity of bacteria communities did not change significantly in the early stage of disease infection but dramatically decreased in cases of severe infected disease. The variation in bacterial community diversity was more pronounced in the phyllosphere and root compartments compared to the hydroponic solution.

All OTUs were classified into 36 phyla. The top 10 most dominant OTUs (≥1.0% relative abundance) in the samples are

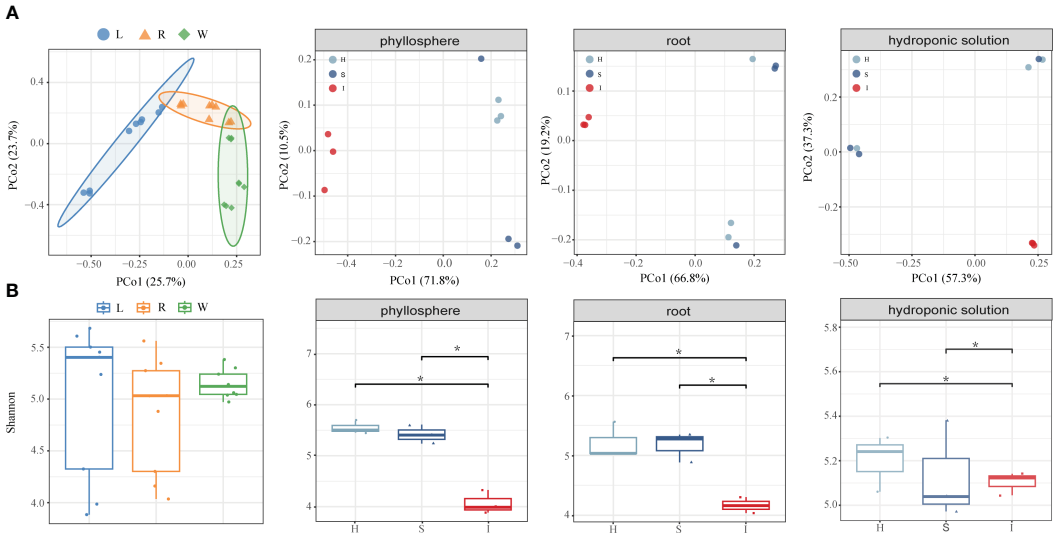

FIGURE 1
Assembly of phyllosphere, root and hydroponic solution bacterial communities. **(A)** Principal coordinate analysis (PCoA) of Bray–Curtis dissimilarity matrices showing the effects of compartment niches and bacterial wildfire disease on the community structure of the phyllosphere, root and hydroponic solution bacterial microbiomes. **(B)** Shannon diversity index of compartment niches and bacterial wildfire disease impact on the community structure of the phyllosphere, root, and hydroponic solution bacterial microbiomes, indicating significant differences (*P < 0.05).

shown in Supplementary Figure 1.The predominant phylum across all three compartment was Proteobacteria, accounting for no less than 38% of the relative abundance, followed by Bacteroidota, Firmicutes, and Actinobacteriota. In comparison to hydroponics, the proportions of Bacteroidota, Proteobacteria, and Firmicutes significantly increased on phyllosphere and roots, while Verrucomicrobiota, Planctomycetota, and Dependentiae were largely depleted. The compositional differences among the three compartments were more pronounced at the genus level, with all OTUs classified into 709 genera. The top 10 most abundant OTUs (≥1.0% relative abundance) were illustrated in Figure 2A. The compositions of phyllosphere, roots, and hydroponic solution were generally similar, with dominant genera including Chryseobacterium, Azospirillum, Vermiphilaceae, Allorhizobium, Brevundimonas, and Arcicella. The invasion of pathogenic wildfire disease altered the relative abundance of these genera in different compartment, with phyllosphere and roots experiencing more significant impacts than the hydroponic solution. In the phyllosphere, as the disease severity increased, the relative abundance of Chryseobacterium, Azospirillum, and Vermiphilaceae decreased, while Allorhizobium and Brevundimonas increased. In the roots, with the aggravation of wildfire disease, the relative abundance of Legionella and Allorhizobium decreased, and Chryseobacterium, Rhodobacter, and Brevundimonas significantly increased. Compared to healthy samples, the relative abundance of Vermiphilaceae decreased, while Allorhizobium, Azospirillum, Limnobacter, and other genera significantly increased In the hydroponic solution of severely diseased plants.

Considering the recruitment strategies of plants for beneficial microbes, we applied Lefse analysis to determine changes in the bacterial community composition of hydroponic plants under the invasion of wildfire disease in the phyllosphere, roots, and hydroponic solution. We identified enriched bacterial communities in severely diseased phyllosphere, roots, and hydroponic solution for each group using Lefse analysis. Linear Discriminant Analysis (LDA) scores were positively correlated with the significance of each bacterial biomarker in each group (see Figure 2B). In comparison, the phyllosphere exhibited a rich diversity of bacterial families, such as Allorhizobium(LDA=4.78), Stenotrophomonas (LDA=4.45), and Enterobacteriaceae (LDA=4.76). Meanwhile, the root system displayed elevated scores for Rhodobacteraceae (LDA=4.46), Flavobacteriales (LDA=5.27), and Chrysebacterium (LDA=5.27). In the hydroponic solution, bacterial enrichment was observed for families such as Chitinophagaceae (LDA=4.45), Azospirillales (LDA=4.47), and Sphingomonadaceae (LDA=4.57).

3.2 SourceTracker analysis of bacterial community of health and wildfire-diseased hydroponic plants

The SourceTracker program was used to study the proportion of endophytic bacterial communities originating from the hydroponic solution. The results revealed differences in microbial sources between healthy and wildfire-diseased hydroponic plants (Figure 3 and Supplementary Table 3). In healthy and mildly infected plants, the majority of the bacterial community in the roots originated from the phyllosphere (H:67.33%, S:62.33%), with a portion originating from the hydroponic solution (H:16.00%, S:23.67%), gradually filtering into the phyllosphere (H:74.00%, S:33.33%). The bacterial communities in the roots and leaves were found to migrate reciprocally. In severely infected plants with wildfire disease, the bacterial community in the roots

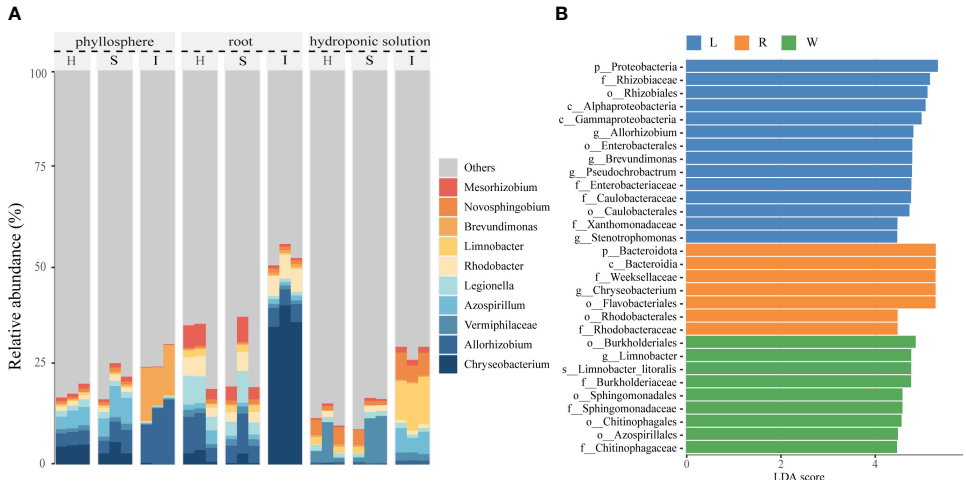

FIGURE 2
Comparison of phyllosphere, root and hydroponic solution community structures in healthy and infected samples **(A)** Relative abundance of bacterial genera of top 10 most dominant OTUs in healthy and infected phyllosphere, root and hydroponic solution. **(B)** The linear discriminant analysis effect size (LEfSe) analysis at species level of bacterial communities (with LDA score >3.1 and $p < 0.05$) among healthy and infected phyllosphere, root and hydroponic solution.

originated mainly from the hydroponic solution (31.67%). This suggests that the majority of microbial species can be traced back to the plant interior from both the phyllosphere and hydroponic solution.

3.3 Molecular ecological network analysis on phyllosphere, root and hydroponic solution communities

Molecular ecological networks (MENs) analyses were used to unravel interactions between phyllosphere, root, and hydroponic solution microbiota in hydroponic Solanaceae crops. The topological characteristics in Table 1 were consistent with the distinct visualization. The same threshold values were selected for the three compartments: phyllosphere (0.79), root (0.77), and hydroponic solution (0.71). The average connectivity was used to assess network complexity, which decreased progressively from the hydroponic solution (AVEK: 20.86) to the root (AVEK: 7.37) and further to the phyllosphere (AVEK: 4.47). The taxonomic composition of these networks varied among the phyllosphere, root, and hydroponic solution. In the phyllosphere, there were more nodes belonging to Acinetobacter and Stenotrophomonas; while in the root, there were more nodes belonging to

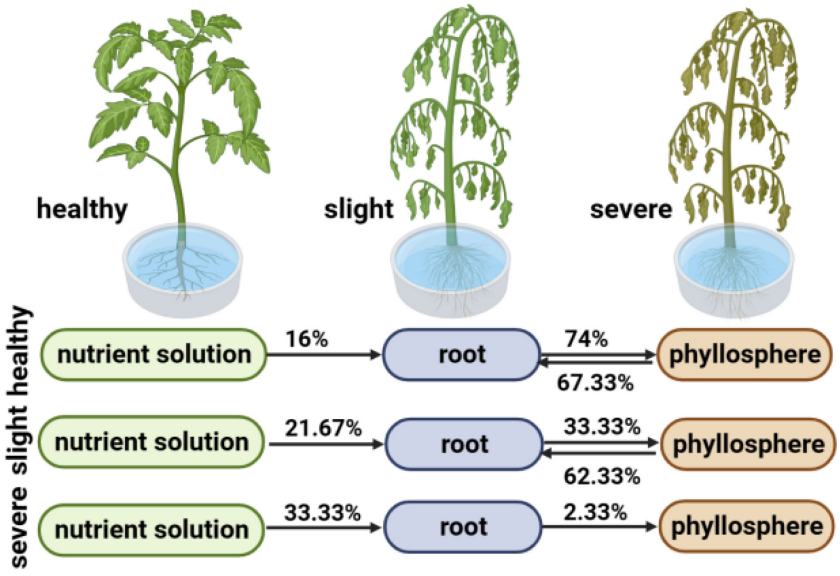

FIGURE 3
SourceTracker analysis results of healthy, slight infected and severely infected hydroponic plant.

TABLE 1 Topological properties of networks in phyllosphere, root and hydroponic solution communities of healthy and infected samples.

Compartment		Vertex	Edge	Average degree	Average path length	Clustering coefficient	Density	Modularity	positive links(%)
L	H	260	570	4.39	3.58	0.04	0.02	0.44	72.98
	S	258	580	4.5	3.55	0.04	0.02	0.45	72.93
	I	219	442	4.03	3.63	0.05	0.02	0.46	72.4
R	H	237	874	7.37	2.84	0.07	0.03	0.32	60.3
	S	234	862	7.37	2.84	0.07	0.03	0.31	60.21
	I	226	814	7.2	2.85	0.06	0.03	0.32	60.44
w	H	309	3155	20.42	2.17	0.11	0.1	0,19	64.63
	S	305	3046	19.97	2.18	0.11	0,1	0.2	64.62
	I	237	2064	17.42	2.18	0.11	0.1	0.19	64.15

Allorhizobium and Sphingobium. In the hydroponic solution, there were more nodes belonging to Novosphingobium and Sphingobium. Additionally, higher modularity and average path distance were observed in the phyllosphere and root compared to the hydroponic solution (see Supplementary Table 4 and Supplementary Figure 2).

To gain a deeper understanding of the interactions among plant phyllosphere, roots, and hydroponic solution microbiota under wildfire disease invasion, the nine networks were visualized, revealing significantly different network structures (Figure 4). Our results indicated that during the progression of wildfire disease, the trends in changes in the three compartments were consistent. In the phyllosphere, during the early stages of wildfire disease, there were no significant changes in nodes and links. However, as the disease severity increased, the number of nodes decreased dramatically from 258 to 219, and the links decreased from 580 to 442. In the roots, the network complexity for healthy plants (237 nodes and 874 links) exceeded that of severely diseased plants (226 nodes and 814 links). In the hydroponic solution, with the increasing severity of the disease, the number of nodes decreased from 309 to 305 and then to 237. Similarly, the number of links within the network exhibited a significant declining trend, decreasing from 3155 to 3046 and further to 2064. In summary, our results indicate that as the severity of Pseudomonas infection increases, the networks in different compartments, including the phyllosphere, rhizosphere, and hydroponic solution, are significantly simplified by the disease. Overall, these microbial networks tend to co-occur, and with the increasing wildfire disease severity, the percentage of positive correlation decreases, suggesting a reduction in cooperative relationships among microbial communities in phyllosphere, roots, and hydroponic solution of hydroponic plants.

Interactions between the pathogenic bacterium Pseudomonas and other bacterial members were observed in networks of healthy and wildfire-diseased samples across three different compartments. In both healthy and wildfire-diseased phyllosphere, four nodes of potential pathogenic bacterial OTUs were identified. In the root compartment, three nodes of potentially pathogenic bacteria OTUs were found in both healthy and slightly infected samples, which decreased to one as the disease severity increased. In the hydroponic solution, both healthy and diseased samples had one node for Pseudomonas OTUs. Based on the aforementioned network structures, further analysis of the networks in phyllosphere and roots invaded by pathogenic bacteria was conducted to verify which compartment played a more critical role in the invasion of pathogenic wildfire disease. In the network of mildly diseased phyllosphere, the number of links between potential pathogenic Pseudomonas OTUs and other microbial members (total of 30 links) was higher than in severely diseased plants (22 links). Similarly, In the network of mildly diseased roots, the number of links between potential pathogenic Pseudomonas OTUs and other microbial members (15 links) was higher than in severely diseased plants (5 links). This indicates that the invasion of pathogenic bacteria involves more interactions with other microbial members in the phyllosphere and root of slight infected plants.

3.4 Network of interactions among potential pathogenic *Pseudomonas* and other microbial members in slightly infected phyllosphere and root

To further elucidate which compartments microbes may play a crucial role in aiding or inhibiting wildfire disease, we analyzed subnetworks of interactions between the pathogenic Pseudomonas and other microbial members to identify the "inferred" key microbes in infected phyllosphere and root networks (see Figure 5). In the subnetwork of slightly infected phyllosphere, the pathogenic Pseudomonas showed positive correlations with genera such as *Ralstonia, Legionella, Bosea, and Dyella*, while exhibiting negative correlations with genera like *Chryseobacterium, Limnobacter, Methylobacterium, Zoogloea*, and *Arcicella*. In the subnetwork of mildly infected roots, the pathogenic *Pseudomonas* displayed positive correlations with *Arcicella, Caulobacter, Allorhizobium*, and negative correlations with genera like *Terrimonas, Azospirillum, Devosia*, and *Pedomicrobium*. These bacteria, positively or negatively correlated with the potential pathogenic *Pseudomonas*, may play crucial roles in assisting or inhibiting bacterial wilt infection. Our observations suggest that

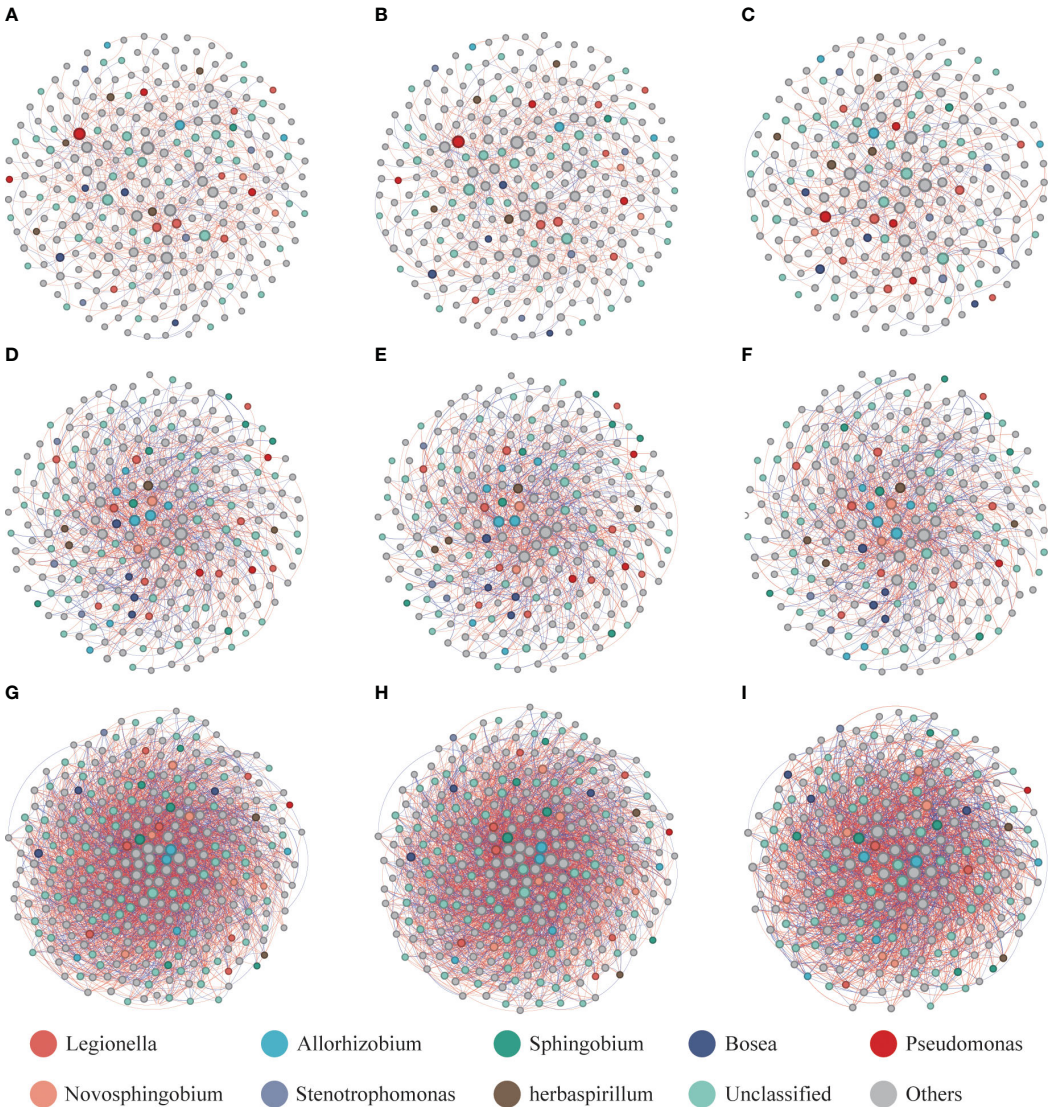

FIGURE 4
Network visualization of the bacterial communities of healthy and infected hydroponic plants. **(A)** phyllosphere of healthy plant, **(B)** phyllosphere of slight infected plant, **(C)** phyllosphere of severely infected plant, **(D)** root of healthy plant, **(E)** root of slight infected plant, **(F)** root of severely infected plant, **(G)** hydroponic solution of healthy plant, **(H)** hydroponic solution of slight infected plant, and **(I)** hydroponic solution of severely infected plant. A red line indicates a positive interaction between nodes, while a blue line indicates a negative interaction.

during the invasion of wildfire disease, the pathogenic *Pseudomonas* may receive assistance from locally correlated microbial members while being inhibited by some negatively correlated taxa, engaging in resource competition. Particularly noteworthy is *Caulobacter*, which exhibits a negative correlation with both pathogenic bacteria in the roots.

4 Discussion

Plant disease is traditionally considered as the product of the 'disease triangle': a susceptible host, a virulent pathogen, and an abiotic environment conducive to infection (Lucas, 2009). During plant disease invasion, the structural and assembly of plant-associated microbial communities are essential for advancing the co-evolutionary theory of plant-microbiome interactions (Tian et al., 2020). In this study, we linked the bacterial communities in the phyllosphere, root, and hydroponic solution of Solanaceae crops to the severity of bacterial wilt, gaining insights into the impact of bacterial wilt on these three compartments. Our results indicate that the microbial communities in all three compartments are simultaneously influenced by niches and disease. Pseudomonas infection is closely associated with the diversity and microbial interactions of the plant bacterial community. However, the microbial communities in the roots and phyllosphere exhibit greater sensitivity to plant disease compared to the microbial community in the hydroponic solution.

Our results indicate that, regardless of the plant's health status, distinct microbial communities form in the phyllosphere, root, and hydroponic solution. This suggests that plant compartments have a

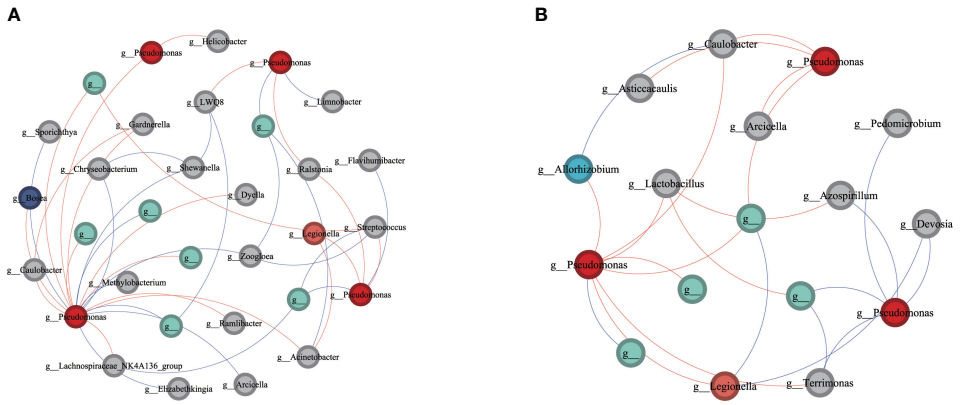

FIGURE 5
Network of interactions between the pathogen (Pseudomonas) and other bacteria species in bacteria communities of slightly infected **(A)** phyllosphere and **(B)** root. Each node is labeled at the genus level and unclassified OTUs are not labeled. A red line indicates a positive interaction between nodes, while a blue line indicates a negative interaction.

greater impact on the distribution of microbial communities than diseases and other environmental factors. This aligns with findings from studies on pepper with Fusarium wilt disease (Gao et al., 2021) and wheat under different fertilization regimes (Xiong et al., 2021). The pattern of microbial diversity (Shannon index) displays a clear gradient from the phyllosphere to the root and then to the hydroponic solution. All of these observations suggest that ecological niches play a dominant role in shaping the environmental factors governing the formation of plant microbial communities. We note that in the hydroponically grown plant, the abundance of Proteobacteria and Firmicutes is higher in both the phyllosphere and roots. This is similar to the composition observed in other hydroponically cultivated plants, such as lettuce, where Proteobacteria dominates the phyllosphere (Kyere et al., 2020), and in the roots of hydroponically grown cereal potatoes and wheat, where the dominant phyla are Proteobacteria and Firmicutes (Sheridan et al., 2017). Therefore, we hypothesize that the distribution of different bacterial phyla associated with the leaves and roots of hydroponically grown plants is likely similar across most hydrophytic plants.

We observed differential impacts of wildfire disease on the bacterial communities in the phyllosphere, roots, and hydroponic solution, with the phyllosphere and roots being more sensitive to the disease. Our results indicate that, during the early stages of pathogen invasion, the abundance of the pathogen is relatively low, exerting minimal impact on the bacterial community. The diversity of microbial communities in both the phyllosphere and roots remains relatively stable. However, as the infection intensifies and the plant's defense systems are compromised, the microbial communities in both the leaves and roots undergo an imbalance, leading to a significant decrease in community diversity. This aligns with previous findings (Tao et al., 2021), where the diversity of plant phyllosphere surface microbiota decreased with the progression of phyllosphere wildfire disease.

The analysis of bacterial communities in plants affected by wildfire disease through taxonomic classification reveals the impact of Pseudomonas infection on different plant compartments. We observed a low abundance of potential pathogenic Pseudomonas OTUs in all healthy samples, and We cannot technically confirm that all OTUs assigned to Pseudomonas are pathogenic just by ITS sequences. However, with the progression of disease severity, accompanied by changes in the abundance of other bacteria. In the phyllosphere, the abundance of Allorhizobium and Brevundimonas rapidly increases with disease severity, while Chryseobacterium significantly enriches in the infected roots. These compositional changes may be outcomes of pathogen invasion. Root bacteria form symbiotic relationships with plants, creating nodules to fix atmospheric nitrogen into plant-absorbable compounds. This enhances the plant's survival under environmental stress by improving soil conditions and degrading toxic substances (Siddiqui and Shaukat, 2002; Kuzmanović et al., 2022). Previous studies (Gutiérrez Mañero et al., 2003; Kumar et al., 2021) have identified Chryseobacterium as a Plant Growth-Promoting (PGP) bacterium, promoting seed germination and influencing root total nitrogen content and biological nitrogen fixation, and protecting plants from pathogenic invasion. Research by VOGEL et al. (Vogel et al., 2012; Asaf et al., 2020) indicated that Sphingomonas, a Gram-negative bacterium, produced plant hormones, protected plants through substrate competition against Pseudomonas syringae (wildfire pathogen) and various pathogenic fungi, and promoted plant growth under stressful conditions. LDA analysis demonstrates the enrichment of these three bacteria in the phyllosphere, roots, and hydroponic solution of severely diseased plants, suggesting a "call for help" strategy by plants under biotic stress (pathogen invasion). Pathogen invasion induces changes in the plant's immune system (Jones and Dangl, 2006), altering secretions to recruit beneficial microorganisms from the environment. This interaction, through competition or modulation of plant defense responses, endows the roots and leaves with the ability to resist wildfire disease. These results indicate that plant niches may create distinct ecological niches for specific microbial communities. When invaded by pathogens, plants demonstrate the ability to recognize signal molecules and adapt their immune systems in each niche (Cook

et al., 2015). The alterations in secretions recruit beneficial microorganisms, enabling the roots and leaves to develop resistance against wildfire disease.

Understanding the potential sources of crop-associated microbial communities provides a roadmap for the process of pathogenic invasion. Our study found that in healthy and slightly infected plants, the bacterial communities of hydroponically grown crops mainly originate from the phyllosphere. In severely diseased plants, the microbial sources differ, with the root bacterial community primarily originating from the hydroponic solution. This contrasts with previous study results where the soil was identified as the primary source of microbial species in plant root ecosystems, gradually occupying different niches (Lareen et al., 2016).For hydroponically grown plants, the main source of microbial communities is the plant phyllosphere. Therefore, the invasion of pathogenic bacteria may initiate from the phyllosphere, proliferating and subsequently transferring to the plant roots. In severely diseased plants, compared to healthy plants, the disruption of the plant's vascular system responsible for material transport in the phyllosphere (Sohrabi et al., 2023) implies higher proportions of unknown and hydroponic solution-derived microbial communities in the roots. This indicates that disease damage has altered the potential source pathways of microbial communities in hydroponically grown plants, disrupting material transport between the phyllosphere and roots.

Numerous studies have already revealed the cooperative and competitive interactions among microorganisms, as well as how network modularity can influence community stability (Faust and Raes, 2012; Coyte et al., 2015). However, it remains unclear how the interactions between pathogenic bacteria and bacterial communities in different plant compartments change under varying degrees of infection. In addition to analyzing changes in the composition of microbial communities in Solanaceae crops, the symbiotic network further illustrates the interactions between communities in different plant compartments, providing valuable information on the impact of microbial community changes on plant health. Our study reveals that networks in Solanaceae crops are significantly influenced by disease and plant compartments, with disease reducing network complexity. The network composition of the phyllosphere, roots, and hydroponic solutions differs, with hydroponic solutions having the most complex network. However, the patterns of change in phyllosphere, root, and hydroponic networks are similar. As the severity of pathogen invasion increases, network links and average degrees gradually decrease, and positive percentages decrease. This indicates that Pseudomonas syringae infection disrupts the existing interaction relationships between microbial communities and has irreversible effects. This is consistent with previous research findings that Pseudomonas syringae invasion results in the occupation of abundant resources on phyllosphere surfaces and roots, forcing other bacteria to develop negative interactions with Pseudomonas syringae in later stages to compete for resources (Alba et al., 2017). This competition relationship contributes to improving the stability of the microbial community

Additionally, we observed that in the network of slightly diseased phyllosphere surfaces, the number of connections between potential pathogenic Pseudomonas OTUs and other microbial members is 30, whereas in the case of severe disease, it is 22. In the network of mildly diseased root systems, the connections between potential pathogenic Pseudomonas OTUs and other microbial members amount to 15, while in the case of severe disease, it decreases to 5. Based on these findings and the results of our traceback analysis, we determine that in severely diseased plants, both the pathways from phyllosphere to roots and from roots to phyllosphere have been disrupted. Consequently, in mildly diseased plants, the interaction between Pseudomonas and other microbial members appears to be more intimate. Both the phyllosphere surfaces and root systems of the plants play crucial roles as migration hubs during the progression of bacterial wildfire.

The network analysis also reveals the relationships between the pathogen and other relevant bacterial species (Figure 5). Plant pathogens interact with other bacteria in both cooperative (negative) and competitive (positive) ways, and microorganisms with positive or negative connections to the pathogen are considered "pathogen antagonists" (Raghavendra and Newcombe, 2013) or "pathogen promoters" (Ridout and Newcombe, 2015), respectively. Therefore, Allorhizobium, Caulobacter, Dosea, and Ralstonia may act as pathogen antagonists, while Chryseobacterium, Azospirillum, Devosia, and Pedomicrobium may act as pathogen promoters. It is noteworthy that the potential "pathogen antagonist" Caulobacter, which shows a strong negative correlation with the pathogen Pseudomonas in diseased roots, may play a crucial role in inhibiting the growth of the pathogen. We found that beneficial bacteria, such as Chryseobacterium, Azospirillum, Devosia (Fibach-Paldi et al., 2012; Singh et al., 2013;53), closely collaborate with the pathogen. Through our source tracking results, it can be inferred that beneficial bacteria lead to the proliferation of bacteria on the phyllosphere and in the roots. They circulate mutually in phyllosphere and roots, triggering the outbreak of wildfire disease. This is consistent with previous research results (Lamichhane and Venturi, 2015) suggesting that harmless or beneficial bacteria may cause the invasion and proliferation of the pathogen. It has been demonstrated that pathogens do not operate independently, but their virulence is mediated by their interaction with other pathogens (Denny, 2006; Purahong et al., 2018). Ralstonia is a common plant pathogen (Luo et al., 2019), and the positive interaction between Ralstonia and Pseudomonas may be because Ralstonia also needs to reproduce by competing for substrates, thus inhibiting the growth of the wildfire disease pathogen Pseudomonas and decreasing the severity and development of wildfire disease. Caulobacter is a Gram-negative bacterium that can be isolated from various plant species such as Arabidopsis, watermelon, and maize (Yang et al., 2020; Berrios, 2021). Research (Luo et al., 2019) has shown that Caulobacter parasitizes both the roots and aboveground parts of Arabidopsis. It not only promotes lateral root formation and increases phyllosphere number and size but also protects plants from external stress and disease invasion (Carter, 2021). Currently, there is limited research on the antagonistic mechanism of Caulobacter against plant pathogens. Future studies should focus on the potential interactions between Caulobacter and pathogens.

5 Conclusions

Our study revealed significant differences in bacterial communities on the phyllosphere surface, roots, and hydroponic solution under varying degrees of wildfire disease conditions. The impact of host compartments on the assembly of bacterial microbiota was most pronounced, followed by the wildfire disease itself, with the phyllosphere and roots being more affected than the hydroponic solution. The invasion of the pathogen altered the composition of the plant's microbial community, resulting in reduced bacterial community diversity and network complexity. We also identified that the invasion of wildfire disease initiated from the phyllosphere surface. Chryseobacterium, Azospirillum, and Devosia may contribute to the severity and progression of wildfire disease, while Caulobacter might play a significant role in suppressing wildfire disease.

Data availability statement

The original contributions presented in the study are included in the article/Supplementary Material, further inquiries can be directed to the corresponding author/s.

Author contributions

WL: Data curation, Writing – original draft, Formal analysis, Visualization. ZZ: Methodology, Data curation, Writing – review & editing. BZ: Investigation, Conceptualization, Methodology, Writing – review & editing. YZ: Investigation, Resources, Writing – review & editing. CZ: Investigation, Writing – review & editing, Resources. CC: Visualization, Writing – review & editing. FZ: Data curation, Formal analysis, Resources, Writing – review & editing. FL: Resources, Writing – review & editing. JA: Resources, Investigation, Funding acquisition, Writing – review & editing. WW: Data curation, Writing – review & editing. WK: Data curation, Writing – review & editing. HX: Resources, Formal analysis, Writing – review & editing. WFW: Resources, Formal analysis, Writing – review & editing. DG: Data curation, Supervision, Writing – review & editing. DM: Resources, Visualization, Conceptualization, Funding acquisition, Project administration, Supervision, Writing – review & editing. LZ: Resources, Visualization, Conceptualization, Funding acquisition, Writing – review & editing.

Funding

The author(s) declare financial support was received for the research, authorship, and/or publication of this article. This project was supported by the Changde Tobacco Company of Hunan Province (CD2022KJ01).

Conflict of interest

ZZ, LZ, YZ, CZ, CC, FZ, WK, FL, JA, WW, WFW, HX, and FL were employed by Changde Tobacco Company of Hunan Province.

The remaining authors declare that the research was conducted in the absence of any commercial or financial relationships that could be construed as a potential conflict of interest.

Publisher's note

All claims expressed in this article are solely those of the authors and do not necessarily represent those of their affiliated organizations, or those of the publisher, the editors and the reviewers. Any product that may be evaluated in this article, or claim that may be made by its manufacturer, is not guaranteed or endorsed by the publisher.

Supplementary material

The Supplementary Material for this article can be found online at: https://www.frontiersin.org/articles/10.3389/fpls.2024.1403226/full#supplementary-material

References

Alba, C., NeSmith, J. E., Fahey, C., Angelini, C., and Flory, S. L. (2017). Methods to test the interactive effects of drought and plant invasion on ecosystem structure and function using complementary common garden and field experiments. *Ecol. Evol.* 7, 1442–1452. doi: 10.1002/ece3.2729

Aleklett, K., Hart, M., and Shade, A. (2014). The microbial ecology of flowers: an emerging frontier in phyllosphere research. *Botany* 92, 253–266. doi: 10.1139/cjb-2013-0166

Asaf, S., Numan, M., Khan, A. L., and Al-Harrasi, A. (2020). Sphingomonas: from diversity and genomics to functional role in environmental remediation and plant growth. *Crit. Rev. Biotechnol.* 40, 138–152. doi: 10.1080/07388551.2019.1709793

Bastian, M., Heymann, S., and Jacomy, M. (2009). Gephi: an open source software for exploring and manipulating networks. *Proceedings of the international AAAI conference on web and social media*. 3 (1), 361–362.

Berrios, L. (2021). Complete genome sequence of the plant-growth-promoting bacterium Caulobacter segnis CBR1. *Curr. Microbiol.* 78, 2935–2942. doi: 10.1007/s00284-021-02548-z

Bolyen, E., Rideout, J. R., Dillon, M. R., Bokulich, N. A., Abnet, C. C., Al-Ghalith, G. A., et al. (2019). Reproducible, interactive, scalable and extensible microbiome data science using QIIME 2. *Nat. Biotechnol.* 37, 852–857. doi: 10.1038/s41587-019-0209-9

Callahan, B. J., McMurdie, P. J., Rosen, M. J., Han, A. W., Johnson, A. J. A., and Holmes, S. P. (2016). DADA2: High-resolution sample inference from Illumina amplicon data. *Nat. Methods* 13, 581–583. doi: 10.1038/nmeth.3869

Carter, T. H. (2021). *Plasmids bring Novel Functions to Caulobacter Genomes* (Carolina, US: University of South Carolina).

Chapelle, E., Mendes, R., Bakker, P. A., and Raaijmakers, J. M. (2016). Fungal invasion of the rhizosphere microbiome. *ISME J.* 10, 265–268. doi: 10.1038/ismej.2015.82

Cook, D. E., Mesarich, C. H., and Thomma, B. P. (2015). Understanding plant immunity as a surveillance system to detect invasion. *Annu. Rev. Phytopathol.* 53, 541–563. doi: 10.1146/annurev-phyto-080614-120114

Coyte, K. Z., Schluter, J., and Foster, K. R. (2015). The ecology of the microbiome: networks, competition, and stability. *Science* 350, 663–666. doi: 10.1126/science.aad2602

Deng, Y., Jiang, Y.-H., Yang, Y., He, Z., Luo, F., and Zhou, J. (2012). Molecular ecological network analyses. *BMC bioinf.* 13, 1–20. doi: 10.1234/abcd.2012.0001

Denny, T. (2006). "Plant pathogenic Ralstonia species," in *Plant-associated bacteria* (Berlin, German: Springer), 573–644.

Dixon, P. (2003). VEGAN, a package of R functions for community ecology. *J. Veg. Sci.* 14, 927–930. doi: 10.1111/j.1654-1103.2003.tb02228.x

Dong, C.-J., Wang, L.-L., Li, Q., and Shang, Q.-M. (2019). Bacterial communities in the rhizosphere, phyllosphere and endosphere of tomato plants. *PLoS One* 14, e0223847. doi: 10.1371/journal.pone.0223847

Edwards, J., Johnson, C., Santos-Medellín, C., Lurie, E., Podishetty, N. K., Bhatnagar, S., et al. (2015). Structure, variation, and assembly of the root-associated microbiomes of rice. *Proc. Natl. Acad. Sci.* 112, E911–E920. doi: 10.1073/pnas.1414592112

Faust, K., and Raes, J. (2012). Microbial interactions: from networks to models. *Nat. Rev. Microbiol.* 10, 538–550. doi: 10.1038/nrmicro2832

Fibach-Paldi, S., Burdman, S., and Okon, Y. (2012). Key physiological properties contributing to rhizosphere adaptation and plant growth promotion abilities of Azospirillum brasilense. *FEMS Microbiol. Lett.* 326, 99–108. doi: 10.1111/fml.2011.326.issue-2

Gao, M., Xiong, C., Gao, C., Tsui, C. K., Wang, M.-M., Zhou, X., et al. (2021). Disease-induced changes in plant microbiome assembly and functional adaptation. *Microbiome* 9, 1–18. doi: 10.1186/s40168-021-01138-2

Gutiérrez Mañero, F. J., Probanza, A., Ramos, B., Colón Flores, J. J., and Lucas García, J. A. (2003). Effects of culture filtrates of rhizobacteria isolated from wild lupine on germination, growth, and biological nitrogen fixation of lupine seedlings. *J. Plant Nutr.* 26, 1101–1115. doi: 10.1081/PLN-120020078

Hacquard, S., Garrido-Oter, R., González, A., Spaepen, S., Ackermann, G., Lebeis, S., et al. (2015). Microbiota and host nutrition across plant and animal kingdoms. *Cell Host Microbe* 17, 603–616. doi: 10.1016/j.chom.2015.04.009

Höfte, M., and De Vos, P. (2007). ""Plant pathogenic Pseudomonas species,"," in *Plant-associated bacteria* (Berlin, German: Springer), 507–533.

Hu, Q., Tan, L., Gu, S., Xiao, Y., Xiong, X., Zeng, W.-A., et al. (2020). Network analysis infers the wilt pathogen invasion associated with non-detrimental bacteria. *NPJ Biofilms Microbiomes* 6, 8. doi: 10.1038/s41522-020-0117-2

Jones, J. D., and Dangl, J. L. (2006). The plant immune system. *nature* 444, 323–329. doi: 10.1038/nature05286

Kumar, M., Charishma, K., Sahu, K., Sheoran, N., Patel, A., Kundu, A., et al. (2021). Rice leaf associated Chryseobacterium species: An untapped antagonistic flavobacterium displays volatile mediated suppression of rice blast disease. *Biol. Control* 161, 104703. doi: 10.1016/j.biocontrol.2021.104703

Kuzmanović, N., Biondi, E., Overmann, J., Puławska, J., Verbarg, S., Smalla, K., et al. (2022). Genomic analysis provides novel insights into diversification and taxonomy of Allorhizobium vitis (ie Agrobacterium vitis). *BMC Genomics* 23, 1–17. doi: 10.1186/s12864-022-08662-x

Kyere, E. O., Palmer, J., Wargent, J. J., Fletcher, G. C., and Flint, S. (2020). Differences in nutrients concentration and microbiome community composition between hydroponically and soil grown lettuce leaves. *Colonisation of lettuce by Listeria monocytogenes and its biofilm formation*, 95.

Lamichhane, J. R., and Venturi, V. (2015). Synergisms between microbial pathogens in plant disease complexes: a growing trend. *Front. Plant Sci.* 6, 385. doi: 10.3389/fpls.2015.00385

Lareen, A., Burton, F., and Schäfer, P. (2016). Plant root-microbe communication in shaping root microbiomes. *Plant Mol. Biol.* 90, 575–587. doi: 10.1007/s11103-015-0417-8

Lindow, S. E., and Brandl, M. T. (2003). Microbiology of the phyllosphere. *Appl. Environ. Microbiol.* 69, 1875–1883. doi: 10.1128/AEM.69.4.1875-1883.2003

Liu, C., Cui, Y., Li, X., and Yao, M. (2021). microeco: an R package for data mining in microbial community ecology. *FEMS Microbiol. Ecol.* 97, fiaa255. doi: 10.1093/femsec/fiaa255

Lucas, G. B. (1958). *Diseases of tobacco*, (New York, US: Scarecrow Press).

Lucas, J. A. (2009). *Plant pathology and plant pathogens* (Hongkong, China: John Wiley & Sons).

Luo, D., Langendries, S., Mendez, S. G., De Ryck, J., Liu, D., Beirinckx, S., et al. (2019). Plant growth promotion driven by a novel Caulobacter strain. *Mol. Plant-Microbe Interact.* 32, 1162–1174. doi: 10.1094/MPMI-12-18-0347-R

Mendes, L. W., Raaijmakers, J. M., de Hollander, M., Mendes, R., and Tsai, S. M. (2018). Influence of resistance breeding in common bean on rhizosphere microbiome composition and function. *ISME J.* 12, 212–224. doi: 10.1038/ismej.2017.158

Morris, C. E., Kinkel, L. L., Xiao, K., Prior, P., and Sands, D. C. (2007). Surprising niche for the plant pathogen Pseudomonas syringae. *Infect. Genet. Evol.* 7, 84–92. doi: 10.1016/j.meegid.2006.05.002

O'Brien, H. E., Thakur, S., and Guttman, D. S. (2011). Evolution of plant pathogenesis in Pseudomonas syringae: a genomics perspective. *Annu. Rev. Phytopathol.* 49, 269–289. doi: 10.1146/annurev-phyto-072910-095242

Purahong, W., Orrù, L., Donati, I., Perpetuini, G., Cellini, A., Lamontanara, A., et al. (2018). Plant microbiome and its link to plant health: Host species, organs and Pseudomonas syringae pv. actinidiae infection shaping bacterial phyllosphere communities of kiwifruit plants. *Front. Plant Sci.* 9, 1563. doi: 10.3389/fpls.2018.01563

Raghavendra, A. K., and Newcombe, G. (2013). The contribution of foliar endophytes to quantitative resistance to Melampsora rust. *New Phytol.* 197, 909–918. doi: 10.1111/nph.12066

Rastogi, G., Sbodio, A., Tech, J. J., Suslow, T. V., Coaker, G. L., and Leveau, J. H. (2012). Leaf microbiota in an agroecosystem: spatiotemporal variation in bacterial community composition on field-grown lettuce. *ISME J.* 6, 1812–1822. doi: 10.1038/ismej.2012.32

Ridout, M., and Newcombe, G. (2015). The frequency of modification of Dothistroma pine needle blight severity by fungi within the native range. *For. Ecol. Manage.* 337, 153–160. doi: 10.1016/j.foreco.2014.11.010

Saeed, Q., Xiukang, W., Haider, F. U., Kučerik, J., Mumtaz, M. Z., Holatko, J., et al. (2021). Rhizosphere bacteria in plant growth promotion, biocontrol, and bioremediation of contaminated sites: A comprehensive review of effects and mechanisms. *Int. J. Mol. Sci.* 22, 10529. doi: 10.3390/ijms221910529

Segata, N., Izard, J., Waldron, L., Gevers, D., Miropolsky, L., Garrett, W. S., et al. (2011). Metagenomic biomarker discovery and explanation. *Genome Biol.* 12, 1–18. doi: 10.1186/gb-2011-12-6-r60

Sheridan, C., Depuydt, P., De Ro, M., Petit, C., Van Gysegem, E., Delaere, P., et al. (2017). Microbial community dynamics and response to plant growth-promoting microorganisms in the rhizosphere of four common food crops cultivated in hydroponics. *Microbial Ecol.* 73, 378–393. doi: 10.1007/s00248-016-0855-0

Siddiqui, I. A., and Shaukat, S. S. (2002). Mixtures of plant disease suppressive bacteria enhance biological control of multiple tomato pathogens. *Biol. Fertil. Soils* 36, 260–268. doi: 10.1007/s00374-002-0509-x

Singh, A. V., Chandra, R., and Goel, R. (2013). Phosphate solubilization by Chryseobacterium sp. and their combined effect with N and P fertilizers on plant growth promotion. *Arch. Agron. Soil Sci.* 59, 641–651. doi: 10.1080/03650340.2012.664767

Sohrabi, R., Paasch, B. C., Liber, J. A., and He, S. Y. (2023). Phyllosphere microbiome. *Annu. Rev. Plant Biol.* 74, 539–568. doi: 10.1146/annurev-arplant-102820-032704

Srinivasan, S., Hoffman, N. G., Morgan, M. T., Matsen, F. A., Fiedler, T. L., Hall, R. W., et al. (2012). Bacterial communities in women with bacterial vaginosis: high resolution phylogenetic analyses reveal relationships of microbiota to clinical criteria. *PLoS One* 7, e37818. doi: 10.1371/journal.pone.0037818

Tao, J., Cao, P., Xiao, Y., Wang, Z., Huang, Z., Jin, J., et al. (2021). Distribution of the potential pathogenic Alternaria on plant leaves determines foliar fungal communities around the disease spot. *Environ. Res.* 200, 111715. doi: 10.1016/j.envres.2021.111715

Tian, L., Lin, X., Tian, J., Ji, L., Chen, Y., Tran, L.-S. P., et al. (2020). Research advances of beneficial microbiota associated with crop plants. *Int. J. Mol. Sci.* 21, 1792. doi: 10.3390/ijms21051792

Trejo-Téllez, L. I., and Gómez-Merino, F. C. (2012). "Nutrient solutions for hydroponic systems," in *Hydroponics-a standard methodology for plant biological researches* (InTech), 1–22.

Van der Putten, W. H., Klironomos, J. N., and Wardle, D. A. (2007). Microbial ecology of biological invasions. *ISME J.* 1, 28–37. doi: 10.1038/ismej.2007.9

Vogel, C., Innerebner, G., Zingg, J., Guder, J., and Vorholt, J. A. (2012). Forward genetic in planta screen for identification of plant-protective traits of Sphingomonas sp. strain Fr1 against Pseudomonas syringae DC3000. *Appl. Environ. Microbiol.* 78, 5529–5535. doi: 10.1128/AEM.00639-12

Wang, H.-C., Wang, M.-S., Xia, H.-Q., Yang, S.-J., Guo, Y.-S., Xu, D.-Q., et al. (2013). First report of Fusarium wilt of tobacco caused by Fusarium kyushuense in China. *Plant Dis.* 97, 424–424. doi: 10.1094/PDIS-09-12-0835-PDN

Wickham, H., Chang, W., and Wickham, M. H. (2016). *Package 'ggplot2'. Create elegant data visualisations using the grammar of graphics*, Book of Abstracts, 2, 1–189. doi: 10.32614/CRAN.package.ggplot2

Xiong, C., Zhu, Y. G., Wang, J. T., Singh, B., Han, L. L., Shen, J. P., et al. (2021). Host selection shapes crop microbiome assembly and network complexity. *New Phytol.* 229, 1091–1104. doi: 10.1111/nph.16890

Yang, Y., Jin, C.-Z., Jin, F.-J., Li, T., Lee, J.-M., Kim, C.-J., et al. (2020). Caulobacter soli sp. nov., isolated from soil sampled at Jiri Mountain, Republic of Korea. *Int. J. Syst. Evol. Microbiol.* 70, 4158–4164. doi: 10.1099/ijsem.0.004264

Yilmaz, P., Parfrey, L. W., Yarza, P., Gerken, J., Pruesse, E., Quast, C., et al. (2014). The SILVA and "all-species living tree project (LTP)" taxonomic frameworks. *Nucleic Acids Res.* 42, D643–D648. doi: 10.1093/nar/gkt1209

frontiers | Frontiers in Plant Science

TYPE Brief Research Report
PUBLISHED 16 October 2024
DOI 10.3389/fpls.2024.1461896

OPEN ACCESS

EDITED BY
Brigitte Mauch-Mani,
Université de Neuchâtel, Switzerland

REVIEWED BY
Hosahatti Rajashekara,
Directorate of Cashew Research (ICAR), India
Thabiso Eric Motaung,
University of Pretoria, South Africa

*CORRESPONDENCE
Xuanjun Feng
xuanjunfeng@sicau.edu.cn

†These authors have contributed equally to this work

RECEIVED 09 July 2024
ACCEPTED 25 September 2024
PUBLISHED 16 October 2024

CITATION
Xiong H, Xing X, Liu M, Zhang Z, Wang Q, Zhang X, Gou X, Lu Y and Feng X (2024) Stalks and roots are the main battlefield for the coevolution between maize and *Fusarium verticillioides*. *Front. Plant Sci.* 15:1461896. doi: 10.3389/fpls.2024.1461896

Stalks and roots are the main battlefield for the coevolution between maize and *Fusarium verticillioides*

Hao Xiong[1†], Xiaobin Xing[1†], Muyuan Liu[1], Zhaoyu Zhang[2], Qingjun Wang[1], Xuemei Zhang[1], Xiangjian Gou[3], Yanli Lu[1,2] and Xuanjun Feng[1,2*]

[1]Maize Research Institute, Sichuan Agricultural University, Sichuan, Chengdu, China, [2]State Key Laboratory of Crop Gene Exploration and Utilization in Southwest China, Sichuan, Chengdu, China, [3]National Key Laboratory of Crop Genetic Improvement, Huazhong Agricultural University, Wuhan, Hubei, China

Fusarium species are the dominant cause of maize ear rot, but they also inflict serious damage to the roots and stalks. Theoretically, the organ where the host interacts with the pathogen most frequently should exhibit the highest degree of symptom-genotype correlation. Because that symptom-genotype correlation is an indicator reflecting the degree of coevolution between pathogen and its hosts. We wonder which organ is the main battlefield for the antagonism between maize and *Fusarium*. For this purpose, 43 isolates of *Fusarium* were isolated from infected maize ears. *Fusarium verticillioides* and *F. graminearum* are the two dominant pathogens, accounting for 44% and 30%, respectively. Furthermore, 14 elite maize inbreds were exposed to 43 *Fusarium* isolates and the symptoms of ear rot, stalk rot and root rot were investigated. In general, symptoms caused by *F. graminearum* were significantly more severe than those caused by other *Fusarium* species. Surprisingly, the genotype of *F. verticillioides* showed a strong correlation with stalk and root rot, but not with ear rot. Accordingly, our study may provide the first evidence that the stalk and root of maize, rather than the ear, is the main battlefield for the coevolution between maize and *F. verticillioides*.

KEYWORDS

pathogen-host interaction, coevolution, maize, fusarium, ear rot

1 Introduction

Maize (*Zea mays* L.) is a crucial global source of food, feed, and energy. In recent decades, the demand for increased maize yields has been a primary driver behind the ongoing development of commercial varieties. However, as maize yield gains have gradually slowed, the rise of destructive diseases has become the leading factor

propelling the renewal of commercial varieties (Ristaino et al., 2021). Therefore, understanding the interaction between pathogens and maize is important for maize production.

Maize ear rot is a destructive disease, mainly caused by *Fusarium* species, poses a significant threat to maize production and quality (Duan et al., 2016). *Fusarium* species overwinter in soil, seeds, and plant debris (Xia et al., 2022). They spread to maize grains through the roots, insects, and the air (Xia et al., 2022; Omotayo and Babalola, 2023). They also cause root and stalk rot, affecting overall plant health and yield (María I et al., 2017). In addition, *Fusarium* species can produce harmful mycotoxins such as deoxynivalenol (DONs), fumonisins (FBs) or Zearalenone (ZENs), which pose a risk to animal and human health if consumed in excessive amounts (María I et al., 2017). In China, significant yield losses and mycotoxin contamination problems have been associated with *Fusarium* species (Duan et al., 2016; Qin et al., 2020).

The pathogen-host-driven natural selection contributes to shape the genetic and phenotypic diversities and results in coevolution of both organisms (Sironi et al., 2015). Pathogens have a negative effect on host fitness, favoring selection for enhanced defense mechanisms in the affected hosts. Conversely, host defenses are detrimental to the pathogen, leading to selection for novel attack mechanisms. When the interaction persists over time, the ongoing cycles of antagonism can generate highly specific host-pathogen interaction patterns, which are intrinsically determined by specific genotype interaction and are manifested as lineage-specific invasion (Schneider et al., 2015; Delaux and Schornack, 2021). Symptom-genotype correlation, the manifestation of specific genotype interaction, is a simple and feasible indicator reflecting the degree of coevolution between pathogen and its hosts. Theoretically, the organ in which the host interacts with the pathogen most frequently should exhibit the highest degree of symptom-genotype correlation. Given the extensive research conducted on the interaction between *Fusarium* and maize ears, we subjectively think that ears are the main battlefield for the antagonism between maize and *Fusarium* species. However, our studies unexpectedly revealed that the genotype of *F. verticillioides* was more closely related to its pathogenicity to maize stalks and roots than to maize ears. Prior to this study, there was no direct evidence that the localized interactions between *Fusarium* species and maize were the main factor driving its coevolution. Our study may provide the first evidence that the stalk and root of maize, rather than the ear, is the main battlefield for the coevolution between maize and *F. verticillioides*.

2 Results

2.1 The isolation frequency of *F. verticillioides* from maize ear rot is the highest in China

Different isolates of *Fusarium* spp. were isolated from infected maize ears from 20 cornfields in 7 provinces in China (Supplementary Table S1). Forty-three isolates were isolated and grouped into 4 categories, *F. verticillioides* (44%), *F. graminearum* (30%), *F. proliferatum* (21%), and *F. fujikuroi* (5%) (Supplementary Table S1), which is consistent with that *F. verticillioides* was previously reported as the dominant ear rot pathogen (Logrieco et al., 2002; Folcher et al., 2009; Lanubile et al., 2017; Feng et al., 2022). Fumonisin production was high for most *F. verticillioides* and *F. proliferatum* isolates but low for *F. graminearum* isolates when grown on maize medium, and no T2 toxin was detected from any isolates (Figure 1; Supplementary Table S1).

2.2 The symptoms caused by *F. graminearum* are significantly more severe than that caused by *F. verticillioides and F. proliferatum*

The pathogenicity of 43 isolates was tested using 14 elite maize inbred lines. All 43 isolates could infect maize ears, stalks and roots, and pathogen-host interactions showed a wide range of symptom severity (Supplementary Table S2; Figure 2). The pathogenicity of *F. graminearum* was remarkably higher than that of *F. verticillioides* and *F. proliferatum*, and was comparable between *F. verticillioides and F. proliferatum* (Supplementary Table S2; Figures 2D-F). KN5585 and LH8012 exhibited strong resistance to ear rot caused by *F. graminearum* (Figure 2A). LX7531, ZNC442 and LX8581 displayed good resistance to ear rot caused by *F. verticillioides* (Figure 2A). CIMBL145, LH8012, and ZH14 showed effective resistance to most *Fusarium*-caused stalk rot, whereas Zheng58 was susceptible to most *Fusarium*-caused stalk rot (Figure 2B).

2.3 Stalks and roots are the main battlefield for the coevolution between maize and *F. verticillioides*

The relationship between fungal genotype, toxigenic capacity, and pathogenicity was further investigated. The correlation between the genotype of *F. verticillioides* and the symptom of stalk and root rot, but not ear rot, was notable (Figure 3A; Supplementary Tables S3-8). This implies that the coevolution of *F. verticillioides* and maize is mainly existed in the root and stalk, rather than the ear. The number of isolates of *F. graminearum* and *F. proliferatum* observed in this study was relatively low, which may explain why no significant correlation was found between the genotypes of these two pathogens and the different symptoms observed (Supplementary Tables S3-8). To test the effect of racial diversity on the genotype-symptom correlation, different numbers of *F. verticillioides* were progressively removed. With the decrease of racial diversity, the genotype-symptom correlation coefficient decreased, and the corresponding p value increased (Figure 3B). When the number of isolates was less than 17, the symptom-genotype correlation was no longer significant for both root and stalk rot (Figure 3B). To test the effect of maize diversity on the genotype-symptom correlation, different numbers of maize inbred lines were progressively removed. With the decrease of maize diversity, the genotype-symptom correlation coefficient decreased, and the corresponding p value increased (Figure 3C). These results indicated that in order to ascertain the correlation between genotype and

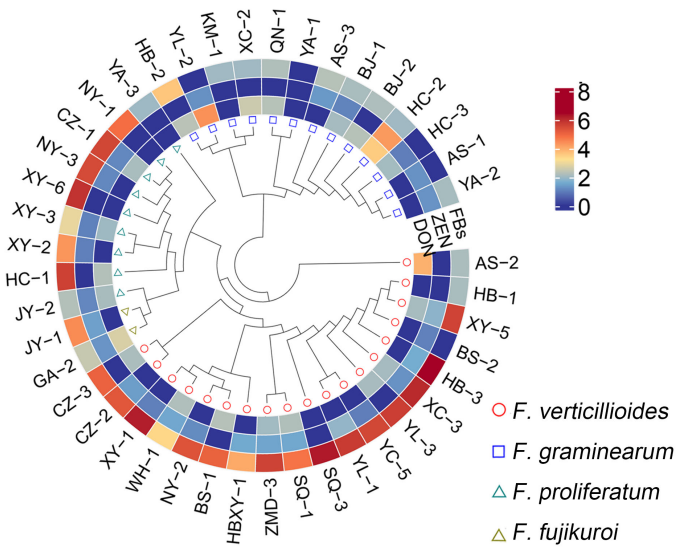

FIGURE 1
Topological phylogenetic tree of 43 *Fusarium* isolates and toxigenic capacity. The genetic distance matrix of 43 *Fusarium* isolates is showed as topological phylogenetic tree. The detail information was shown in Supplementary Table S4. The out layer heatmap represents the toxigenic capacity of different isolates grown in maize medium. The data used in heatmap are modified from Supplementary Table S1 by Log10 conversion. If the contents of FBs, T2 and DON were less than 100 μg/kg and of ZEN less than 10 μg/kg, the result was inaccurate and recorded as zero. FBs, Fumonisin; ZEN, zearalenone; DON, deoxynivalenol.

symptoms with sufficient clarity, it is necessary to ensure that the pathogens and hosts under consideration exhibit sufficient diversity. An expansion of the pathogen-host interacting population results in a heightened correlation between genotype and symptoms.

The toxigenic capacity is correlated well with fungal genotype in *F. verticillioides* and *F. proliferatum*, but not in *F. graminearum* (Figure 3A; Supplementary Table S3). The toxigenic capacity is not correlated with the symptom of ear rot, stalk rot, or root rot, indicating that the toxigenic capacity may not be a dominant determinate of pathogenicity.

3 Discussion

F. verticillioides and *F. graminearum* are the most widely reported causes of maize ear rot (Logrieco et al., 2002; Folcher et al., 2009; Gai et al., 2017; Lanubile et al., 2017; Feng et al., 2022). They also cause stalk, root and sheath rots (Duan et al., 2016; Lanubile et al., 2017; Wang et al., 2021). In this study, 44% of isolates are *F. verticillioides*, 30% are *F. graminearum* (30%), and 21% are *F. proliferatum* (21%). It is consistent with previous reports that *F. verticillioides* and *F. graminearum* are the dominant maize ear rot pathogens.

The distributions and pathogenicity of *F. verticillioides* and *F. graminearum* vary greatly in different environmental and climatic conditions (Ezrari et al., 2021; Liu et al., 2022). Although both *F. verticillioides* and *F. graminearum* can cause ear, stalk, and root rot in maize, there seems to be no studies that systematically compare the pathogenicity of the two pathogens at the population level. It was reported that the optimum temperature for growth of *F. verticillioides* is about 30°C, while cool growing conditions (20°C) promote the growth of *F. graminearum* (Samapundo et al., 2005; Hay et al., 2021; Ding et al., 2024). In this study, the field temperatures after inoculation were usually between 25 and 35°C, which may be more suitable for the growth of *F. verticillioides*. However, the results clearly showed that the severity of disease caused by *F. graminearum* to 14 elite maize inbred lines was significantly greater than that of *F. verticillioides*. This indicates that the pathogenicity of *F. graminearum* to maize is generally stronger than that of *F. verticillioides*.

F. verticillioides can survive in soil, seeds, and plant debris for extended periods. It is primarily a soil- and seed-borne fungus that moves from the root upward to the maize stalks and ears, causing stalk and ear rot (Omotayo and Babalola, 2023). It can also survive the winter as viable spores and is spread by airborne or insect vectors and rainfall (Omotayo and Babalola, 2023). The widespread existence of *F. verticillioides* in the soil made it necessary for maize roots to cope with the invasion of *F. verticillioides* at all times. Given the important economic attributes of maize ear, ear rot has received more attention than root and stalk rot. Thus, we subjectively think that ears may be the main battlefield for the antagonism between maize and *Fusarium* species before this study. To the best of our knowledge, there is currently no evidence can indicate the main organ in which the coevolution of maize and *F. verticillioides* has occurred. The organ where the pathogen frequently interacts with the host is expected to show the highest degree of symptom-genotype correlation (Schneider et al., 2015; Sironi et al., 2015; Delaux and Schornack, 2021). This correlation serves as a simple and feasible indicator of coevolution, as it is intrinsically shaped by the genotype interactions between pathogen and its hosts (Schneider et al., 2015; Sironi et al., 2015; Delaux and Schornack, 2021). Our findings indicate that the genotype of *F. verticillioides* is strongly associated with stalk and root rot, but not with ear rot. Consequently, this study may provide

10.3389/fpls.2024.1461896

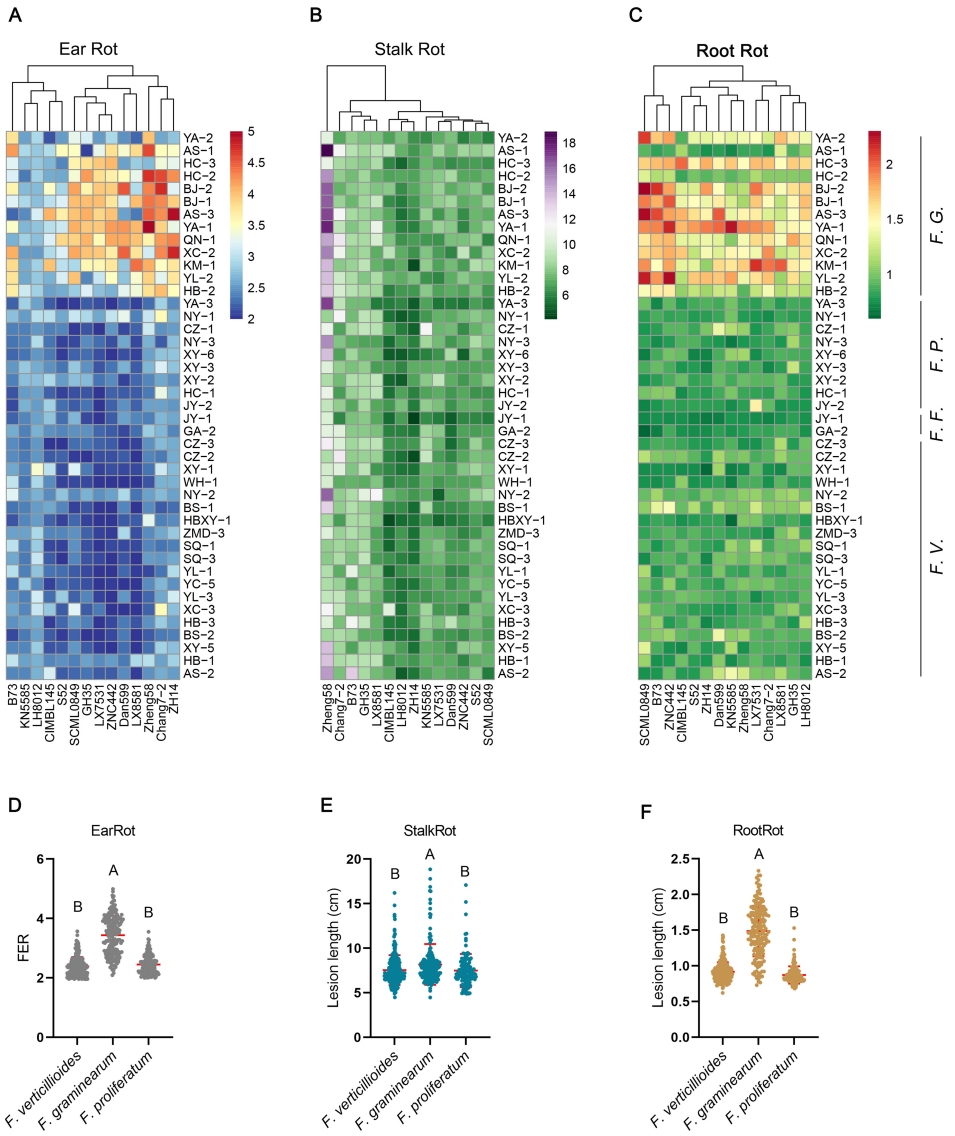

FIGURE 2
Severity of ear rot, stalk rot, and root rot of different pathogen-host pairwise interactions. **(A-C)** Severity of symptom for each pathogen-host pairwise was shown as heatmap. **(D-F)** Scatter plot of symptom severity caused by *F. verticillioides (F.V.)*, *F. graminearum* (*F.G.*) and *F. proliferatum (F.P.)*. *F.F.* is the abbreviation for *F. fujikuroi*. One point represents one pathogen-host interaction pairwise. The different capital letters above the scatter indicate that the difference between groups is significant at the level of *p*-value less than 0.01 using ANOVA analysis.

the first evidence that the stalk and root of maize, rather than the ear, is the main battlefield for the antagonism and coevolution between maize and *F. verticillioides*. The characteristics of the soil- and seed-borne form of *F. verticillioides* may explain why the antagonism and coevolution occurred mainly in the maize stalk and root.

Theoretically, a stronger long-term antagonism may result in a higher symptom-genotype correlation, while an increasing size of the pathogen-host interacting population may enhance this correlation (Schneider et al., 2015; Sironi et al., 2015; Delaux and Schornack, 2021). However, the specific size of the pathogen-host interacting population in which this correlation can be remarkably observed remains unclear. In previous studies, the correlation between genotype and symptoms was usually low or not statistically significant at all (Gai et al., 2017; Li et al., 2019; Han et al., 2020; Dong et al., 2022; Feng et al., 2022; Liu et al., 2024)(Supplementary Table S9). This may be due to the fact that the pathogen-host interacting populations were constructed with only one pathogen or host. In line with this, a decrease in the diversity of *F. verticillioides* or maize will decrease the genotype-symptom correlation coefficient and increase the corresponding *p*-value. In order to ascertain the correlation between genotype and symptoms with sufficient clarity, it is necessary to ensure that the pathogens and hosts under consideration exhibit sufficient diversity. Here, we suggested that the size of the pathogen-host interacting population is larger than a 20 × 15 matrix will be better. Our results showed that symptom-genotype correlation is a simple and feasible indicator of the degree of coevolution between pathogens and hosts, when the size of the pathogen-host interacting population is appropriate.

10.3389/fpls.2024.1461896

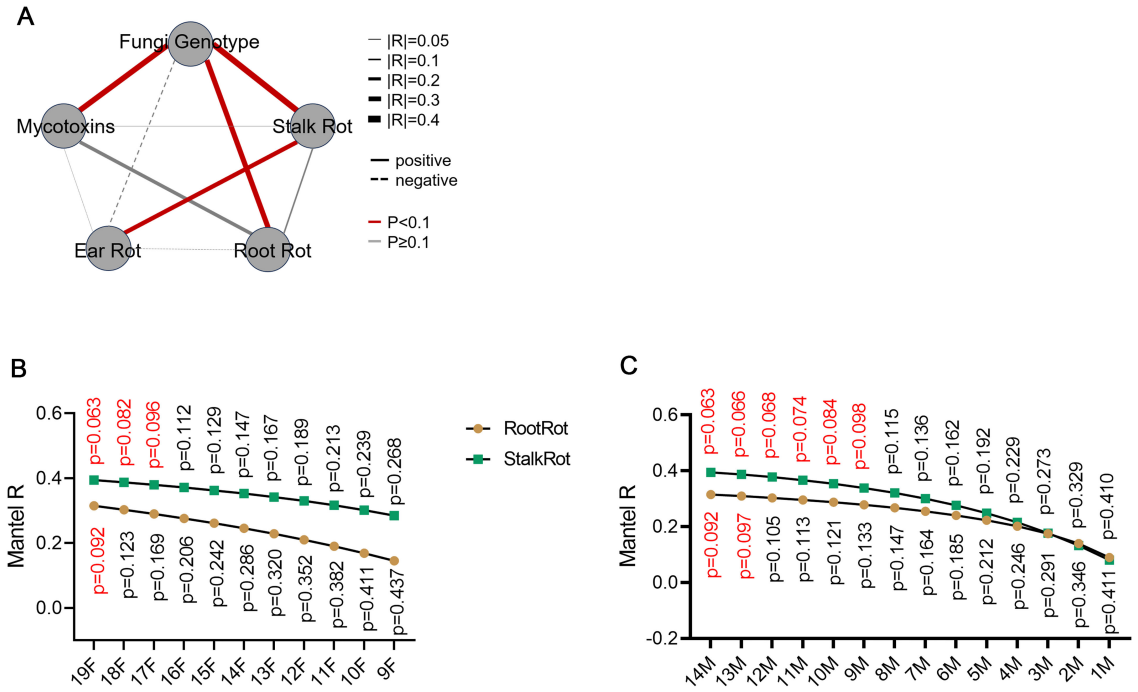

FIGURE 3
Stalks and roots are the main battlefield for the coevolution between maize and *F. verticillioides*. **(A)** Correlation between different traits of *F. verticillioides*. The correlation is considered statistically significant when the *p*-value is less than 0.1. The detail information of each trait was shown in Supplementary Tables S4-8. Mantel test was used to calculate the correlation and *p*-value between different traits. **(B)** The effect of pathogen diversity on the symptom-pathogenic genotype correlation was tested by retaining different numbers of *F. verticillioides* isolates. **(C)** The effect of maize diversity on the symptom-pathogenic genotype correlation was tested by retaining different numbers of inbred maize lines. For **(B, C)**, The distance matrix of different traits was used to calculate correlations using the Mantel test with 999 permutations.

4 Materials and methods

4.1 Isolation of *Fusarium* spp.

Infected maize ears were collected from 20 locations in 7 provinces in southwest China. Asymptomatic kernels adjacent to the infected aera were surface sterilized with 75% ethanol for 5 min and incubated on potato dextrose agar (PDA) medium at 25° C. Pure culture of pathogen was established by single spore isolation. Three housekeeping genes, the translation elongation factor *EF1α*, the largest (*RPB1*) and second largest (*RPB2*) subunits of RNA polymerase, were amplified by polymerase chain reaction (PCR) for resequencing. Sequences were aligned in the Fusarium database (https://fusarium.mycobank.org/) for species identification. Primers are listed in Supplementary Table S10.

4.2 Analysis of genetic distance

The sequences of three housekeeping genes (*EF1α, RPB1, and RPB2*) were used for phylogenetic analysis and computing of pairwise genetic distance. Analyses were conducted using the Maximum Composite Likelihood model in MEGA7 (Kumar et al., 2016). Pairwise genetic distance was further used for correlation analysis with other phenotypes.

4.3 Determination of the content of four mycotoxins

As previous reported, *Fusarium* species were cultured in solid maize sand medium at 28 °C in the dark for 5 days. The contents of fumonisins (FBs), deoxynivalenol (DON), T-2, and zearalenone (ZEN) in the medium were determined with FD-600 (Femdetection, China) using immunofluorescence-based rapid quantitative test strips (Feng et al., 2022).

4.4 Artificial inoculation and symptom investigation of ear, stalk and root rots

To investigate the severity of ear and stalk rots, 14 elite inbred maize lines were planted in 2022 in Xishuangbanna (21° 53′ N, 100° 59′ E) and in 2023 in Chongzhou, China (30° 33′ N, 103° 39′ E). Seedlings were planted with 3.5 m single rows and 0.8 m row widths. Approximately 60 days after planting, a hole about 1 cm deep was made in the middle of the second stalk node using a 1 mm diameter electric drill. The hole was inoculated with 200 µL of spore suspension (5×10^6 spores/mL) and the lesion length was measured when the seed was mature. Fourteen days after silking for each inbred maize line, 200 µL of spore suspension (5×10^6 spores/mL) was inoculated into the ears using the side-needle syringe method. The severity of ear rot was assessed as in our previous report, based

on the agricultural industry standard of the People's Republic of China (NY/T1248.8-2016) (Feng et al., 2022). For each pathogen-host interaction, 20 ears or stalks from each replicate and two replicates at each location were investigated.

To assess the severity of root rot, healthy seeds were soaked in water overnight and incubated on wet seed germination paper at 25°C for about 2 days in the dark. Seeds with uniform growth were selected and transferred to fresh wet seed germination paper in a 13 × 13 cm Petri dish for 3 days of continuous growth. A wound was created by needle at the root position at about 4 cm from the seed, and then a hyphae-covered clump of PDA (0.3 cm diameter) was touched to induce root rot. The seeds were covered with wet germination paper to keep them moist and to ensure that the roots grew straight. About 4 days after inoculation, the lesion length was measured to reflect the severity of root rot. The best linear unbiased prediction (BLUP) values for each trait from two years were used to calculate symptoms distance matrix. Representative photos illustrating the inoculation site and symptoms of ear rot, stem rot, and root rot are presented in Supplementary Figure S1.

4.5 Correlation analysis between different traits

The vegdist function of the vegan package (https://CRAN.R-project.org/package=vegan) (Dixon, 2003) was used to construct the distance matrix of different isolates for the toxin production, the symptoms of ear, stalk and root rot. The mantel function was then used to calculate the correlation and *p*-value between different traits. To test the effect of pathogen and host diversity on the correlation, different numbers of pathogens or hosts were removed and the corresponding correlation and *p* value was calculated. For example, if three of the fourteen inbred maize lines were removed, 364 combinations and 364 correlation and *p*-values would be generated. Therefore, the correlation and *p* value would be calculated from the mean of the 364 values when the host diversity was eleven.

Data availability statement

The datasets presented in this study can be found in online repositories. The names of the repository/repositories and accession number(s) can be found in the article/Supplementary Material.

Author contributions

XF: Conceptualization, Data curation, Funding acquisition, Visualization, Writing – original draft, Writing – review & editing. HX: Data curation, Formal analysis, Investigation, Methodology, Resources, Validation, Writing – original draft. XX: Data curation, Formal analysis, Investigation, Validation, Writing – original draft. ML: Data curation, Formal analysis, Investigation, Writing – original draft. ZZ: Formal analysis, Investigation, Validation, Writing – original draft. QW: Investigation, Methodology, Validation, Writing – original draft. XZ: Data curation, Formal analysis, Validation, Writing – original draft. XG: Formal analysis, Methodology, Visualization, Writing – original draft. YL: Project administration, Resources, Supervision, Writing – review & editing, Writing – original draft.

Funding

The author(s) declare that financial support was received for the research, authorship, and/or publication of this article. We acknowledge funding from the Scientific and Technological Innovation 2023-Major Project of Biological Breeding of the Ministry of Agriculture (2023ZD04029), the National Key R&D Program of China (2021YFD1200700), the Natural Science Foundation of Sichuan Province (2023NSFSC0221), and the key Research Program of the Department of Science and Technology of Sichuan province (2021YFN0034).

Conflict of interest

The authors declare that the research was conducted in the absence of any commercial or financial relationships that could be construed as a potential conflict of interest.

Publisher's note

Supplementary material

The Supplementary Material for this article can be found online at: https://www.frontiersin.org/articles/10.3389/fpls.2024.1461896/full#supplementary-material

References

Delaux, P.-M., and Schornack, S. (2021). Plant evolution driven by interactions with symbiotic and pathogenic microbes. *Science* 371. doi: 10.1126/science.aba6605

Ding, Y., Ma, N., Haseeb, H. A., Dai, Z., Zhang, J., and Guo, W. (2024). Genome-wide transcriptome analysis of toxigenic Fusarium verticillioides in response to variation of temperature and water activity on maize kernels. *Int. J. Food Microbiol.* 410, 110494. doi: 10.1016/j.ijfoodmicro.2023.110494

Dixon, P. (2003). VEGAN, a package of R functions for community ecology. *J. Veget. Sci.* 14, 927–930. doi: 10.1111/j.1654-1103.2003.tb02228.x

Dong, S., Jiang, K., Huai, B., Ye, L., You, J., Ma, Y., et al. (2022). Genetic variability and pathogenicity of Fusarium verticillioides isolates from the summer-sown maize regions in China. *Plant Pathol.* 72, 582–592. doi: 10.1111/ppa.13673

Duan, C., Qin, Z., Yang, Z., Li, W., Sun, S., Zhu, Z., et al. (2016). Identification of pathogenic Fusarium spp. Causing maize ear rot and potential mycotoxin production in China. *Toxins (Basel)* 8. doi: 10.3390/toxins8060186

Ezrari, S., Radouane, N., Tahiri, A., Amiri, S., Lazraq, A., and Lahlali, R. (2021). Environmental Effects of Temperature and Water Potential on Mycelial Growth of Neocosmospora solani and Fusarium spp. Causing Dry Root Rot of Citrus. *Curr. Microbiol.* 78, 3092–3103. doi: 10.1007/s00284-021-02570-1

Feng, X., Xiong, H., Zheng, D., Xin, X., Zhang, X., Wang, Q., et al. (2022). Identification of Fusarium verticillioides resistance alleles in three maize populations with teosinte gene introgression. *Front. Plant Sci.* 13, 942397. doi: 10.3389/fpls.2022.942397

Folcher, L., Jarry, M., Weissenberger, A., Ge´Rault, F., Eychenne, N., Delos, M., et al. (2009). Comparative activity of agrochemical treatments on mycotoxin levels with regard to corn borers and Fusarium mycoflora in maize (Zea mays L.) fields. *Crop Prot.* 28, 302–308. doi: 10.1016/j.cropro.2008.11.007

Gai, X. T., Xuan, Y. H., and Gao, Z. G. (2017). Diversity and pathogenicity of Fusarium graminearum species complex from maize stalk and ear rot strains in northeast China. *Plant Pathol.* 66, 1267–1275. doi: 10.1111/ppa.2017.66.issue-8

Han, G., Li, C., Xiang, F., Zhao, Q., Zhao, Y., Cai, R., et al. (2020). Genome-wide association study leads to novel genetic insights into resistance to Aspergillus flavus in maize kernels. *BMC Plant Biol.* 20. doi: 10.1186/s12870-020-02404-5

Hay, W. T., Mccormick, S. P., and Vaughan, M. M. (2021). Effects of atmospheric CO2 and temperature on wheat and corn susceptibility to Fusarium graminearum and deoxynivalenol contamination. *Plants* 10, 2582. doi: 10.3390/plants10122582

Kumar, S., Stecher, G., and Tamura, K. (2016). MEGA7: molecular evolutionary genetics analysis version 7.0 for bigger datasets. *Mol. Biol. Evol.* 33, 1870–1874. doi: 10.1093/molbev/msw054

Lanubile, A., Maschietto, V., Borrelli, V. M., Stagnati, L., Logrieco, A. F., and Marocco, A. (2017). Molecular basis of resistance to Fusarium ear rot in maize. *Front. Plant Sci.* 8. doi: 10.3389/fpls.2017.01774

Li, N., Lin, B., Wang, H., Li, X., Yang, F., Ding, X., et al. (2019). Natural variation in ZmFBL41 confers banded leaf and sheath blight resistance in maize. *Nat. Genet.* 51, 1540–1548. doi: 10.1038/s41588-019-0503-y

Liu, N., Chen, Y., Liu, J., Su, Q., Zhao, B., Sun, M., et al. (2022). Transcriptional differences between major Fusarium pathogens of maize, Fusarium verticillioides and Fusarium graminearum with different optimum growth temperatures. *Front. Microbiol.* 13. doi: 10.3389/fmicb.2022.1030523

Liu, C., He, S., Chen, J., Wang, M., Li, Z., Wei, L., et al. (2024). A dual-subcellular localized β-glucosidase confers pathogen and insect resistance without a yield penalty in maize. *Plant Biotechnol. J.* 22, 1017–1032. doi: 10.1111/pbi.14242

Logrieco, A., Mule, G., Moretti, A., and Bottalico, A. (2002). Toxigenic Fusarium species and mycotoxins associated with maize ear rot in Europe. *Eur. J. Plant Pathol.* 108, 597–609. doi: 10.1023/A:1020679029993

María I, D., Eliana, C., and Sebastián A, S. (2017). Fusarium–plant interaction: state of the art – a review. *Plant Prot. Sci.* 53, 61–70. doi: 10.17221/182/2015-pps

Omotayo, O. P., and Babalola, O. O. (2023). Fusarium verticillioides of maize plant: Potentials of propitious phytomicrobiome as biocontrol agents. *Front. Fungal Biol.* 4. doi: 10.3389/ffunb.2023.1095765

Qin, P. W., Xu, J., Jiang, Y., Hu, L., van der Lee, T., Waalwijk, C., et al. (2020). Survey for toxigenic Fusarium species on maize kernels in China. *World Mycotoxin J.* 13, 213–224. doi: 10.3920/WMJ2019.2516

Ristaino, J. B., Anderson, P. K., Bebber, D. P., Brauman, K. A., Cunniffe, N. J., Fedoroff, N. V., et al. (2021). The persistent threat of emerging plant disease pandemics to global food security. *Proc. Natl. Acad. Sci. U.S.A.* 118, e2022239118. doi: 10.1073/pnas.2022239118

Samapundo, S., Devliehgere, F., De Meulenaer, B., and Debevere, J. (2005). Effect of Water Activity and Temperature on Growth and the Relationship between Fumonisin Production and the Radial Growth of Fusarium verticillioides and Fusarium proliferatum on Corn. *J. Food Prot.* 68, 1054–1059. doi: 10.4315/0362-028X-68.5.1054

Schneider, D. S., Masri, L., Branca, A., Sheppard, A. E., Papkou, A., Laehnemann, D., et al. (2015). Host–pathogen coevolution: the selective advantage of Bacillus thuringiensis virulence and its cry toxin genes. *PloS Biol.* 13, e1002169. doi: 10.1371/journal.pbio.1002169

Sironi, M., Cagliani, R., Forni, D., and Clerici, M. (2015). Evolutionary insights into host–pathogen interactions from mammalian sequence data. *Nat. Rev. Genet.* 16, 224–236. doi: 10.1038/nrg3905

Wang, W., Wang, B., Sun, X., Qi, X., Zhao, C., Chang, X., et al. (2021). Symptoms and pathogens diversity of Corn Fusarium sheath rot in Sichuan Province, China. *Sci. Rep.* 11. doi: 10.1038/s41598-021-82463-2

Xia, Y., Wang, B., Zhu, L., Wu, W., Sun, S., Zhu, Z., et al. (2022). Identification of a Fusarium ear rot resistance gene in maize by QTL mapping and RNA sequencing. *Front. Plant Sci.* 13. doi: 10.3389/fpls.2022.954546

frontiers | Frontiers in Plant Science

TYPE Review
PUBLISHED 23 October 2024
DOI 10.3389/fpls.2024.1481650

OPEN ACCESS

EDITED BY
Choong-Min Ryu,
Korea Research Institute of Bioscience and Biotechnology (KRIBB), Republic of Korea

REVIEWED BY
Gabriel Castrillo,
University of Nottingham, United Kingdom
April Hastwell,
The University of Queensland, Australia

*CORRESPONDENCE
Satoru Nakagami
snakagami@mail.hzau.edu.cn

RECEIVED 16 August 2024
ACCEPTED 02 October 2024
PUBLISHED 23 October 2024

CITATION
Nakagami S, Kajiwara T, Tsuda K and Sawa S (2024) CLE peptide signaling in plant-microbe interactions. *Front. Plant Sci.* 15:1481650. doi: 10.3389/fpls.2024.1481650

CLE peptide signaling in plant-microbe interactions

Satoru Nakagami[1,2,3]*, Taiki Kajiwara[4], Kenichi Tsuda[1,2,3] and Shinichiro Sawa[4,5,6,7]

[1]National Key Laboratory of Agricultural Microbiology, Hubei Hongshan Laboratory, Hubei Key Laboratory of Plant Pathology, College of Plant Science and Technology, Huazhong Agricultural University, Wuhan, China, [2]Shenzhen Institute of Nutrition and Health, Huazhong Agricultural University, Wuhan, China, [3]Shenzhen Branch, Guangdong Laboratory of Lingnan Modern Agriculture, Genome Analysis Laboratory of the Ministry of Agriculture and Rural Affairs, Agricultural Genomics Institute at Shenzhen, Chinese Academy of Agricultural Sciences, Shenzhen, Guangdong, China, [4]Graduate School of Science and Technology, Kumamoto University, Kumamoto, Japan, [5]International Research Center for Agricultural and Environmental Biology, Kumamoto University, Kumamoto, Japan, [6]International Research Organization for Advanced Science and Technology (IROAST), Kumamoto University, Kumamoto, Japan, [7]Institute of Industrial Nanomaterial (IINA), Kumamoto University, Kumamoto, Japan

Cell-cell communication is essential for both unicellular and multicellular organisms. Secreted peptides that act as diffusive ligands are utilized by eukaryotic organisms to transduce information between cells to coordinate developmental and physiological processes. In plants, The *CLAVATA3/EMBRYO SURROUNDING REGION-RELATED* (*CLE*) genes encode a family of secreted small peptides which play pivotal roles in stem cell homeostasis in various types of meristems. Accumulated evidence has revealed that CLE peptides mediate trans-kingdom interactions between plants and microbes, including pathogens and symbionts. This review highlights the emerging roles of CLE peptide signaling in plant-microbe interactions, focusing on their involvement in nodulation, immunity, and symbiosis with arbuscular mycorrhizal fungi. Understanding these interactions provides insights into the sophisticated regulatory networks to balance plant growth and defense, enhancing our knowledge of plant biology and potential agricultural applications.

KEYWORDS

peptide, plant-microbe interaction, systemic signaling, plant immunity, nodulation, phytoparasitic nematode, AM symbiosis

1 Introduction

Cell-to-cell communication is essential for multicellular organisms to coordinate their growth and development. Plants transmit information between cells through phytohormones, proteins/peptides, small RNAs, and metabolites. Secreted peptides acting as ligands are defined as extracellular proteins (less than 100 amino acids in length) derived from precursor proteins called prepropeptides (Tavormina et al., 2015). Peptide ligands are typically recognized by receptor kinases localized at the plasma membrane, thereby provoking

an intracellular signal transduction cascade that changes the activity of downstream genes to modify cellular programs. The CLAVATA3 (CLV3)/EMBRYO SURROUNDING REGION-RELATED (CLE) gene family is one of the largest signaling peptide families in plants, with model plant *Arabidopsis thaliana* (hereafter Arabidopsis) genome containing 32 *CLE* genes. Canonical CLE prepropeptides possess a signal peptide at the N-terminus, a highly conserved motif at the C-terminus called the CLE domain, and a variable domain between the signal peptide and the CLE domain (Betsuyaku et al., 2011) (Figure 1). It is thought that CLE prepropeptides are cleaved by an endoplasmic reticulum-localized signal peptide peptidase to remove their signal peptide, resulting in a propeptide (Figure 1A). Propeptides are processed by post-translational modifications and are proteolytically cleaved at the N- and C- termini of the CLE domain by subtilases to generate a mature peptide in length of 12-14 amino acids (Betsuyaku et al., 2011; Stührwohldt et al., 2020). For instance, the mature CLV3 peptide has been identified as two distinct forms; (1) a 12 amino acids peptide with hydroxyproline (Hyp) residues in the 4th and 7th positions; (2) a 13 amino acids peptide that, with Hyp at the 4th position and tri-arabinosylated Hyp at the 7th position, contains an additional histidine residue at the 13th position (Figure 1B), those two forms can directly bind to extracellular domain of the plasma membrane-localized leucine-rich repeat receptor-like kinase (LRR-RLK) AtCLV1 (Kondo et al., 2006; Ohyama et al., 2009). The tri-arabinosylation is catalyzed by the Hyp O-arabinosyltransferases (HPATs) localized at Golgi (Ogawa-Ohnishi et al., 2013). This modification is critical for the binding affinity with CLV1, and therefore important for the bioactivity of the CLV3 peptide.

Secreted mature CLE peptides are perceived by LRR-RLKs and coreceptors such as CLV1 and CLV3 INSENSITIVE RECEPTOR KINASEs (CIKs), LRR receptor-like protein (LRR-RLP) CLV2, and RLK CORYNE (CRN), which lacks the extracellular domain and acts with CLV2 and CIKs (Hu et al., 2018; Fletcher, 2020; Jones et al., 2021) (Figure 1A). CLV-type receptor complexes have been well characterized for their role in shoot apical meristem (SAM) maintenance, where CLE peptides are recognized by their cognate receptors, reading to the activation of an intracellular signaling cascade such as the receptor-like cytoplasmic kinases (RLCKs) PBS1-LIKEs (PBLs), the protein phosphatases POLTERGEIST (POL) and POLTERGEIST-LIKE1 (PLL1), MAP kinases, and the heterotrimeric GTP binding proteins (Yamaguchi et al., 2016; Wang et al., 2021c). In the SAM, the expression of the homeodomain transcription factor *WUSCHEL* (*WUS*) that promotes stem cell activity is suppressed by the CLV3-receptors module, thereby maintaining stem cell homeostasis. CLE-receptor modules also regulate stem cell homeostasis in inflorescence meristem, root apical meristem, and vascular meristem, and some physiological responses (Fletcher, 2020; Bashyal et al., 2023).

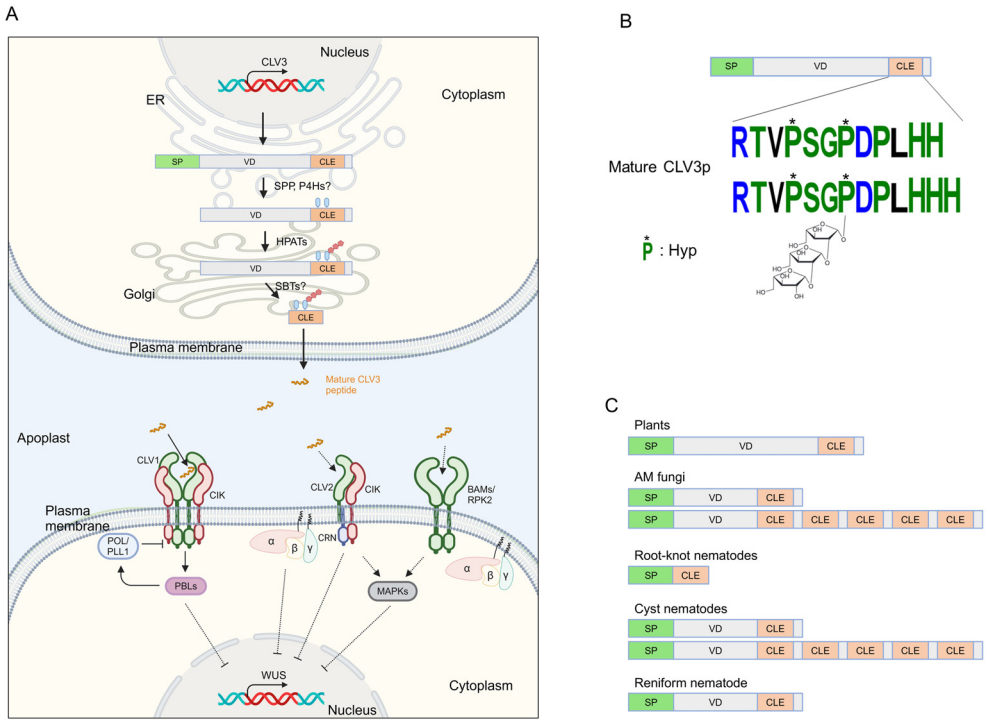

FIGURE 1
Illustrating signaling components of the CLAVATA pathway. **(A)** CLV3 signaling in the shoot apical meristem. The CLV3 prepropeptide is processed by hydroxyproline (Hyp) O-arabinosyltransferases (HPATs), and presumably by a signal peptide peptidase (SPP), prolyl-4-hydroxylases (P4Hs) and subtilases (SBTs) in ER-Golgi, and then mature CLV3 peptide is secreted to the apoplast. The CLV3 peptide is recognized by plasma membrane-associated receptor complexes, which in turn, WUSCHEL (WUS) is repressed through heterotrimeric G proteins, receptor-like cytoplasmic kinases (RLCKs) PBS1-LIKEs (PBLs), phosphatases POLTERGEIST (POL) and POL-LIE 1 (PLL1), and MAPKs. Dashed lines indicate putative or indirect pathways. **(B)** A model of the CLV3 prepropeptide and CLV3 peptide. The CLV3 prepropeptide consists of the N-terminal signal peptide (SP), the C-terminal CLE domain, and the variable domain (VD) between SP and CLE. **(C)** Representative structures of CLE prepropeptides produced by plants and microbes. Figure adapted from images created with BioRender.com.

In nature, plants are associated with various microbes including bacteria, fungi, oomycetes, viruses, and nematodes. Plant-associated microbes affect host developmental processes and physiological responses as infection outcomes; in turn, host plants regulate microbial associations and behaviors to shape optimal interactions between plants and microbes. Accumulating evidence has depicted the emerging roles of CLE signaling in plant-microbe interactions. In this review, we describe CLE signaling pathways participating in plant-microbe interaction regulation and how CLE peptides and their receptors may respond to biotic and abiotic stimuli and culminate in changes to downstream signal transduction.

2 Regulation of nodule formation by host CLE signaling

The relationship between legume plants (members of the family Fabaceae) and nitrogen-fixing bacteria, so-called rhizobia, is one of the most successful symbioses in nature. Endosymbiotic rhizobia inhabiting nodules which are lateral organs formed on the legume roots supply ammonia converted from atmospheric nitrogen to the host, while the host supplies malate converted from sucrose as the primary source of carbon (Udvardi and Poole, 2013). Excessive nodule formation can be detrimental to the host growth since plants lose carbon sources assimilated by photosynthesis. Therefore, legume plants have evolved a sophisticated regulatory mechanism called autoregulation of nodulation (AON) to prevent excess nodulation (Chaulagain and Frugoli, 2021). AON is a complex mechanism modulated through long-distance signaling between roots and shoots and is highly conserved across legume plants (Chaulagain and Frugoli, 2021; Li et al., 2022). Here, we focus on the role of signaling components constituted by CLE peptides and their cognate receptors mainly in *Lotus japonicus* and *Medicago truncatula* (Figure 2A).

CLE peptides act as root-derived mobile signals in AON. In *L. japonicus*, a model legume plant, the expression of *LjCLE-ROOT SIGNAL 1* (*LjCLE-RS1*), *LjCLE-RS2*, and *LjCLE-RS3* is induced in the roots where rhizobia infect (Okamoto et al., 2009; Nishida et al., 2016). Experiments using transgenic hairy roots revealed that constitutive expression of these genes suppressed nodulation on not only transgenic hairy roots but also untransformed roots (Okamoto et al., 2009; Nishida et al., 2016). The mature LjCLE-RS2 peptide was detected in xylem sap collected at the hypocotyl of the plants that have transgenic hairy roots transformed with *LjCLE-RS2*, indicating that LjCLE-RS2 peptide is a root-derived mobile signal (Okamoto et al., 2013). As well as the mature form of AtCLV3 peptide, mature LjCLE-RS2 peptide is a 13 amino acids peptide that is derived from the C-terminal region of the precursor polypeptide and the 7th Hyp residue of this peptide is modified with three residues of arabinose (Ohyama et al., 2009; Okamoto et al., 2013). These *CLE* genes that act as a negative regulator on AON are evolutionarily conserved in other legumes, such as *M. truncatula*, *Glycine max* (soybean), *Pisum sativum* (pea), and *Phaseolus vulgaris* (common bean). It has been shown that *CLE* genes of *M. truncatula* (*MtCLE12*, *MtCLE13*, *MtCLE34*, and *MtCLE35*), *G. max* (*RHIZOBIA-INDUCED CLE 1*: *GmRIC1* and *GmRIC2*), *P. sativum* (*PsCLE12*, *PsCLE13*, and other ten *PsCLEs*) and *P. vulgaris* (*PvRIC1* and *PvRIC2*) are upregulated by rhizobial infection (Mortier et al., 2010; Lim et al., 2011; Reid et al., 2011; Ferguson et al., 2014; Alves-Carvalho et al., 2015; Kassaw et al., 2017; Samorodova et al., 2018; Lebedeva et al., 2020; Mens et al., 2021). Constitutive expression of these genes in transgenic hairy roots leads to suppression of nodulation on systemic roots. However, the mature forms of most of these CLE peptides have yet to be elucidated. In *L. japonicus*, *M. truncatula*, and *G. max*, upregulation of *CLE* genes (*LjCLE-RS1*, *LjCLE-RS2*, *MtCLE13*, *GmRIC1*, and *GmRIC2*) in AON requires NODULE INCEPTION (NIN), which is an indispensable transcription factor for multiple aspects of rhizobial symbioses and is consistently lost in non-nodulating species (Soyano et al., 2014; Wang et al., 2019; Laffont et al., 2020; Shen and Feng, 2024). NIN has evolved from NIN-LIKE PROTEINs (NLPs) which control the expression of nitrate-responsive genes (Konishi and Yanagisawa, 2013; Marchive et al., 2013), suggesting that the regulation of CLE gene expression on AON may have evolved from the mechanism for fine-tuning in planta nitrogen status.

Post-translational modification of CLE peptides is critical for AON. An *M. truncatula* mutant lacking *ROOT DETERMINED NODULATION 1* (*MtRDN1*) gene that encodes HPAT exhibits hyper nodulation phenotype (Schnabel et al., 2011; Kassaw et al., 2017). Through a combination of biochemical and genetic analyses to test functional implications of arabinosylation on AON, Imin and colleagues demonstrated that chemically synthesized MtCLE12 and MtCLE13 peptides with tri-arabinosylation at the 7th Hyp residue exerted nodulation inhibition in the wild-type and *rdn1* mutant when they were applied to the roots or the cotyledons, but these oligopeptides without this modification no longer inhibited nodulation (Imin et al., 2018). Consistent with this, tri-arabinosylated LjCLE-RS1/2/3 and GmRIC1/2 peptides can weaken the hyper nodulation phenotype of mutants lacking LjPLENTY and PsNOD3, which are orthologs to MtRDN1 (Hastwell et al., 2019; Yoro et al., 2019). The MtRDN1 and LjPLENTY are localized to the Golgi (Kassaw et al., 2017; Yoro et al., 2019). Indeed, tri-arabinosylated LjCLE-RS2 peptide was detected in shoot xylem sap collected from soybean plants that developed transformed hairy roots having the genomic region of *LjCLE-RS2*; its modification significantly impacts binding affinity to the receptor mentioned below (Okamoto et al., 2013). These observations indicate that HPATs-mediated tri-arabinosylation of CLE peptides plays a key role in AON. As Kassaw and coauthors have provided evidence that MtRDN1 is required for the function of MtCLE12, but not MtCLE13 (Kassaw et al., 2017), further studies would reveal substrate preferences/specificities of HPATs for individual CLE peptides in each legume.

CLE-mediated AON requires shoot-acting cognate receptors. Grafting experiments and genetic assays showed that the LjCLE-RS peptides were recognized by shoot-acting LRR-RLKs HYPERNODULATION ABERRANT ROOT FORMATION 1 (LjHAR1) and KLAVIER (LjKLV) and LRR-RLP LjCLV2, which have high similarity to AtCLV1, RECEPTOR-LIKE PROTEIN KINASE 2 (AtRPK2) and AtCLV2, respectively (Wopereis et al., 2000; Krusell et al., 2002, 2011; Nishimura et al., 2002; Oka-Kira

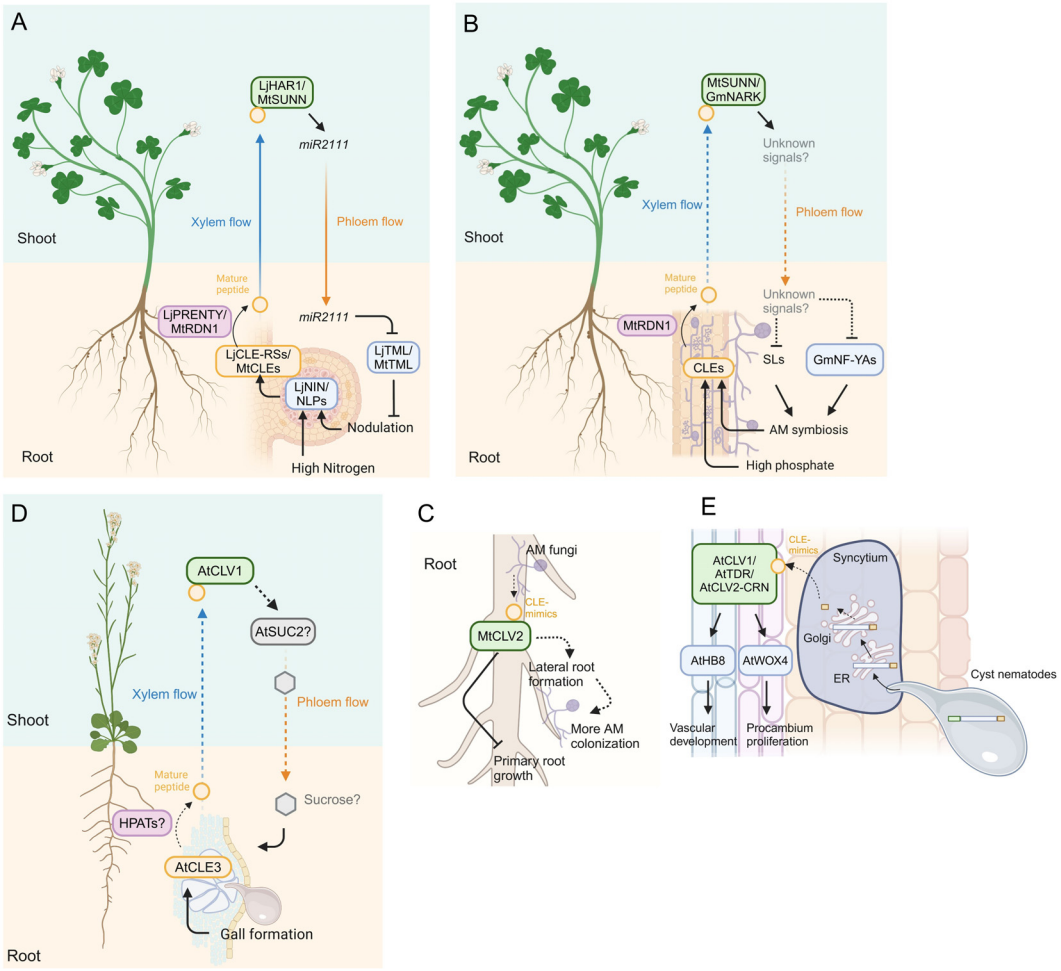

FIGURE 2
Model of CLE signaling in plant-microbe interactions. **(A)** Model of systemic signals mediated by CLE signaling in legume-rhizobium interactions. The transcription factors NODULE INCEPTION (NIN) and NIN-LIKE PROTEINs (NLPs) induce *CLE* gene expression in response to nodulation and high nitrogen conditions, respectively. Mature CLE peptides are post-translationally modified by HPATs LjPRENTY or MtRDN1 and translocate to the shoot via xylem, where the cognate receptors recognize the mature peptides. The *miR2111* translocates from the shoot to the root via phloem and suppresses excessive nodulation by downregulating *TOO MUCH LOVEs* (*TMLs*) expression. **(B)** Model of systemic signals mediated by CLE signaling in plant-AM fungi interactions. AM colonization and high phosphate conditions induce the accumulation of CLE peptides, which are post-translationally modified by RDN1 and translocated to the shoot, where the cognate receptors recognize the mature CLE peptides. Strigolactones (SLs) and NUCLEAR FACTOR-YA transcription factors (NF-YAs) accumulation is suppressed through yet unknown long-distance signals translocating from the shoot to the root downstream of the CLE peptides perception, thereby suppressing additional AM symbiosis. **(C)** Model of local signal mediated by CLE peptide mimics in *M. truncatula*. AM fungi produce CLE mimics that inhibit primary root growth partially dependent on CLV2. The AM-CLE mimics also induce more AM colonization probably due to their induction effect of lateral root formation. **(D)** Model of systemic signal mediated by CLE signaling in plant and root-knot nematode interaction in Arabidopsis. The *CLE3*, which is upregulated in root-knot nematode-induced galls, regulates gall formation in a shoot-expressed CLV1-dependent manner, presumably via SUCROSE-PROTON SYMTORTER 2 (SUC2)-regulated sucrose translocation from the shoot to the root. **(E)** Model of local signal mediated by CLE peptide mimics in plant-cyst nematode interaction in Arabidopsis. Mature CLE mimics are secreted to the apoplast via the host ER-Golgi network. The host receptors recognize the mimics and induce expression of *WUSCHEL-RELATED HOMEOBOX 4* (*WOX4*) and *HOMEOBOX GENE 8* (*AtHB8*) which regulate procambium activity and vascular formation, thereby supporting cynsytium formation. Dashed lines indicate putative or indirect pathways. Figure adapted from images created with BioRender.com.

et al., 2005; Okamoto et al., 2009, 2013; Miyazawa et al., 2010; Nishida et al., 2016). Indeed, synthetic tri-arabinosylated LjCLE-RS1 and -RS2 peptides directly bind to the extracellular domain of LjHAR1 (Okamoto et al., 2013). Akin to AtCLV1, LjHAR1, LjKLV, and LjCLV2 can form isoforms, with homo- and hetero-dimerization (Miyazawa et al., 2010; Krusell et al., 2011). Since AtCLV2 acts with RLK AtCRN through a protein-protein interaction manner, LjCLV2 may also heterodimerize with an unidentified *L. japonicus* CRN orthologue (Bleckmann et al., 2009; Krusell et al., 2011). AtCLV1 and AtCLV2 like receptors have been characterized as negative regulators of nodulation in other legume plants: SUPER NUMERIC NODULES (MtSUNN, an AtCLV1 paralog) and MtCLV2 in *M. truncatula*, NODULE AUTOREGULATION RECEPTOR KINASE (GmNARK/PvNARK, an AtCLV1 paralog) in *G. max* and *P. vulgaris*, and PsSYM29 and PsSYM28 (AtCLV1 and AtCLV2 paralog, respectively) in *P. sativum* (Krusell et al., 2002, 2011; Searle et al., 2003; Schnabel et al., 2005; Ferguson et al., 2014). In *M. truncatula*,

MtCLV2 and MtCRN can form heteromers, in heterologous expression system in tobacco leaf cells, and they act as a negative regulator on AON downstream of MtCLE12 and MtCLE13 peptides (Crook et al., 2016; Nowak et al., 2019). Interestingly, unlike *AtCLV1*, a mutant lacking *LjHAR1* does not show any shoot phenotypes, whereas *klv* mutant of *L. japonicus* shows *clv1*-like shoot phenotypes such as fasciated stems, suggesting that AtCLV1 orthologs of legumes have evolved to control nodulation in shoots (Oka-Kira et al., 2005; Miyazawa et al., 2010).

CLE-mediated regulation of nodule formation is exerted by not only rhizobial infection but also several abiotic conditions. For instance, *LjCLE-RS2*, *LjCLE-RS3*, *LjCLE40*, *MtCLE34*, *MtCLE35*, and *NITRATE-INDUCED CLE* (*GmNIC1*) are induced in response to high nitrogen conditions, and among them, overexpression of *LjCLE-RS2*, *LjCLE-RS3*, *MtCLE35*, and *GmNIC1* suppresses nodulation through their cognate receptors (Okamoto et al., 2009; Reid et al., 2011; Nishida et al., 2016; Lebedeva et al., 2020; Lebedeva et al. 2022; Mens et al., 2021; Moreau et al., 2021). Recent studies have shown that LjNLP1, LjNLP4, MtNLP1, GmNLP1, and GmNLP4, which are homologs of NIN transcription factors, are required to induce these nitrogen-responsive *CLEs* by directly binding to their promoter regions (Luo et al., 2021; Moreau et al., 2021; Nishida et al., 2021; Fu et al., 2024). Phosphate is another abiotic factor that controls nodulation mediated by CLE signaling. *PvRIC1* and *PvRIC2* are upregulated under low phosphate conditions as well as rhizobial infection (Isidra-Arellano et al., 2018; Isidra-Arellano et al., 2020). Suppression of nodulation by low phosphate is not observed in the *NARK* mutants of *G. max* and *P. vulgaris*, suggesting that the peptides-receptors module required for phosphate-responsive nodule regulation is shared with AON pathway.

As described above, root-derived CLE peptides travel to the shoot where they are perceived by shoot-acting receptor complexes, and, in turn, downstream signals suppress excessive nodule formation in roots. Therefore, there should be the signaling molecule(s) that, downstream of CLE perception, translocates from shoots to roots. To regulate nodule numbers during rhizobial infection, two shoot-to-root mobile signals have been proposed by studies of *L. japonicus* and *M. truncatula* to date: (1) phytohormone cytokinin and (2) micro-RNA *miR2111* (Sasaki et al., 2014; Tsikou et al., 2018; Gautrat et al., 2020; Okuma et al., 2020; Zhang et al., 2021). Rhizobial infection activates the cytokinin production in the shoot by inducing a cytokinin biosynthesis gene *LjIPT3* in a LjHAR1-dependent manner, which can suppress nodule formation (Sasaki et al., 2014). An experiment using isotope-labeled cytokinin demonstrated that cytokinin fed to leaves was transported to roots in *L. japonicus*, probably via phloem, suggesting cytokinin is a shoot-to-root mobile signal downstream of LjHAR1 on AON. On the contrary to cytokinin, an *miR2111* has been characterized as a positive regulator of nodulation. Mature *miR2111*s were highly accumulated in uninfected plants to repress nodule suppressor *TOO MUCH LOVE* (*TML*) in roots. In contrast, the expression level of *miR2111s* in leaf phloem was downregulated depending on the signaling module constituted by LjCLE-RS peptides and LjHAR1 in infected plants, thereby derepressing *TML* to inhibit excessive nodulation (Tsikou et al., 2018; Okuma et al., 2020). The *miR2111* expression in shoots was required for *TML* repression in roots, suggesting *miR2111* acts as a shoot-to-root mobile signal on AON. This *miR2111*-mediated systemic AON through the CLE signaling is conserved in *M. truncatula* and *G. max* as well (Gautrat et al., 2020; Moreau et al., 2021; Zhang et al., 2021).

Collectively, these conserved peptide-receptor pairs of legumes function in AON during rhizobial colonization in the same context. Interestingly, some parts of these signaling components are often utilized for regulation of lateral organ formations such as lateral root formation in both leguminous and non-leguminous plants (Araya et al., 2014; Huault et al., 2014; Soyano et al., 2019; Zhang et al., 2021; Hayashi-Tsugane and Kawaguchi, 2022; Kang et al., 2022; Lebedeva et al., 2023; Nakagami et al., 2023a; Sexauer et al., 2023). Therefore, it seems that organogenesis-regulating molecular network mediated by CLE signaling shares with the lateral organ developmental pathway, which is regulated in response to changing nutritional status. Nevertheless, our knowledge of CLE signaling components on AON is still insufficient, necessitating further investigation.

3 Regulation of fungal colonization by CLE signaling

The interaction between plants and Arbuscular Mycorrhizal (AM) fungi that belong to the phylum Glomeromycotina is often recognized as mutualistic because host plants receive phosphorus and some other micronutrients from AM fungi, with the hosts providing carbohydrates and lipids to the fungus (Shi et al., 2023). The host plants suppress excessive AM colonization to prevent excess loss of the photosynthetic products. Similar to AON, the hosts exert a long-distance negative feedback regulation that controls AM symbiosis in already colonized roots, called autoregulation of mycorrhization (AOM). Here, we introduce a molecular mechanism involved in AOM mediated by the CLE signaling pathway (Figure 2B).

AM colonization induces *CLE* genes in roots of *L. japonicus* (*LjCLE7* and other 5 *LjCLEs*), *M. truncatula* (*MtCLE53*), *Solanum lycopersicum* (tomato) (*SlCLE11*), and a monocotyledon *Brachypodium distachyon* (*Bd1g49027* and *Bd2g50170*) (Handa et al., 2015; Müller et al., 2019; Karlo et al., 2020; Wulf et al., 2023). *M. truncatula* plants ectopically overexpressing *MtCLE53* in the roots showed low colonization levels of the AM fungus, while a mutant lacking *MtCLE53* was more colonized than the wild-type plant (Müller et al., 2019; Karlo et al., 2020). Overexpression of *MtCLE33*, which is not induced by AM colonization but phosphate-inducible, also reduced AM colonization, suggesting the CLE signaling negatively controls AM symbiosis responding to both AM colonization and the nutritional status (Müller et al., 2019). In *S. lycopersicum* plants, loss- and gain-of-function studies showed that *SlCLE11* repressed AM symbiosis by responding to AM infection (Wulf et al., 2023). Akin to the function of the CLE peptides on AON, genes encoding HPATs are required for the function of the CLEs involving AOM. The mutant lacking *MtRDN1* showed high levels of AM colonization, with overexpression of *MtCLE53* in the roots showing no change in AM colonization in the *rdn1*, suggesting that MtCLE53 requires HPAT for AOM (Karlo et al.,

2020). Corresponding with the effect of HPAT on the CLE function in *M. truncatula*, a defect of *FASCIATED INFLORESCENCE* (*SlFIN*), which encodes HPAT in *S. lycopersicum*, caused an increase in AM colonization levels and lost the low colonization phenotype caused by *SlCLE11* overexpression (Wang et al., 2021a; Wulf et al., 2023). Although genetic studies have revealed that the *HPATs* are required for *MtCLE53* and *SlCLE11* function, whether mature forms of these peptides are indeed arabinosylated has not been identified yet. Furthermore, how *CLE* genes are induced during AM symbioses is still elusive, which necessitates further investigation.

Recognition of CLE peptides involved in AOM requires its cognate receptors, and accumulating evidence indicates that orthologs of *AtCLV1* or *AtCLV2* are signaling components of AOM. It has been shown that mutants defective in *LjHAR1*, *MtSUNN*, *GmNARK*, *PsNARK*, *SlCLV2*, *FASCIATED AND BRANCHED* (*SlFAB*), and *FLORAL ORGAN NUMBER 1* (*BdFON1*) exhibit more colonization phenotypes (Morandi et al., 2000; Zakaria Solaiman et al., 2000; Meixner et al., 2005; Müller et al., 2019; Karlo et al., 2020; Wang et al., 2021a). The suppressive effect of *MtCLE53* overexpression on AM symbiosis is MtSUNN dependent, suggesting MtSUNN is a cognate receptor for MtCLE53p (Karlo et al., 2020); however, a receptor required for MtCLE33 peptide recognition in AOM has not been characterized. Considering the observation that *MtCLE53* and *MtCLE33* are expressed in the root vascular tissues and MtSUNN is expressed in the vasculatures of both the root and shoot (Schnabel et al., 2012; Müller et al., 2019), the MtCLEs-MtSUNN module could act locally and/or systemically on AOM. Further investigations using grafting and split-root system would be valuable in distinguishing between these possibilities. Grafting experiments showed that shoot-expressed GmNARK controlled AM colonization systemically (Sakamoto and Nohara, 2009). Genetic studies revealed that SlCLE11 required neither SlFAB nor SlCLV2 (Wulf et al., 2023), suggesting the possibility that there are other CLE peptides involved in AOM and other receptor(s) that can perceive SlCLE11. Grafting experiments showed that SlFAB acts only in roots, while SlCLV2 acts in both roots and shoots (Wang et al., 2021a); whether regulation of AOM mediated by distinct CLE-receptor modules is exerted locally or systemically remains unclear.

Several nutritional conditions also trigger CLE-mediated regulation of AM symbiosis. As described above, *MtCLE33* is not induced by AM colonization but phosphate-inducible, with *MtCLE33* overexpression reducing AM colonization in a MtSUNN-dependent manner (Müller et al., 2019). Similarly, *SlCLE10* is upregulated in responding to high nitrogen and phosphate, and *SlCLE10* overexpression suppresses AM colonization (Wulf et al., 2023); however, its cognate receptor has not been identified yet. Although other *CLE* genes (two *LjCLEs*, four *MtCLEs*, three *SlCLEs*, and three *BdCLEs*) that respond to phosphate and some other nutrition status have been characterized in several plant species (Funayama-Noguchi et al., 2011; Handa et al., 2015; Müller et al., 2019; Karlo et al., 2020; Wulf et al., 2023), there is a lack of evidence as to whether these *CLEs* control AM symbioses.

Following CLE perception by their receptor modules, its downstream signaling regulates AM colonization in roots. Gene expression analyses revealed that biosynthesis genes of phytohormone strigolactones that promote AM colonization were downregulated both in *MtCLE53* and *MtCLE33* overexpressing roots in an MtSUNN-dependent manner, in consequence, strigolactones content was reduced in the roots (Müller et al., 2019). Exogenous treatment of a strigolactone analog GR24 to the *MtCLEs* overexpressing roots rendered AM colonization levels, indicating that strigolactone signaling is downstream of the MtCLE-MtSUNN module on AM symbiosis. Other factors downstream of the CLE-receptor module are transcription factor *NUCLEAR FACTOR-Y* (*NF-Y*) genes. Gene expression studies using split-root experiments showed that *GmNF-YA1a* and *GmNF-YA1b* were systemically downregulated in non-infected roots GmNARK-dependently, with knocking down of these two genes weakening hyper AM colonization phenotype of *nark* mutants (Schaarschmidt et al., 2013). Considering that the CLE peptides are perceived by their cognate receptors in the shoot during AM symbiosis, a shoot-derived descending signal is required for the downstream factors acting in the roots. Further investigation would identify yet unknown shoot-to-root factors. Previous studies have identified two shoot-to-root mobile factors involved in AM symbiosis regulation, ELONGATED HYPOCOTYL 5 (HY5) transcription factor that regulates strigolactone levels in roots, and micro RNAs such as *miR399* that induces phosphate transporter genes in response to phosphate starvation (Wu et al., 2013; Müller and Harrison, 2019; Ge et al., 2022). It would be interesting to investigate whether these mobile factors are downstream of CLE signaling.

Plant-associated microbes also produce phytohormones or their mimics that manipulate phytohormone signaling networks in plants, thereby supporting their colonization of the hosts (Nakano et al., 2022). Le Marquer et al. (2019) identified *CLE*-like genes in the genome of five AM species. The prepropeptides of four *Rhizophagus* species were comprised of a predicted signal peptide at the N-terminus, a relatively shorter variable domain, and a CLE domain at the C-terminus as well as that of plants, while that of *Gigaspora rosea* possessed five CLE domains (Figure 1C). Expression of the fungal *CLE*-like genes of *Rhizophagus irregularis* and *G. rosea* (*RiCLE1* and *GrCLE1*) was induced during symbiotic conditions. Exogenous application of synthetic RiCLE1 peptide on roots of *M. truncatula*, *P. sativum* and *A. thaliana* reduced primary root growth (Le Marquer et al., 2019). Consistent with a previous study in AtCLE peptides, this effect was partially dependent on CLV2 type receptor but not CLV1 (Fiers et al., 2005; Le Marquer et al., 2019), suggesting that RiCLE1 peptide is perceived by the host receptors. In addition, RiCLE1 peptide application to *M. truncatula* roots increased lateral root branching and AM colonization (Le Marquer et al., 2019). Since AM colonization often leads to an increase in lateral root formation and lateral roots are preferentially colonized by AM fungi (Sukumar et al., 2013), these observations raise the possibility that their increased abundance mediated by the fungal CLE peptides may lead to an enlarged interface for the plant-AM fungi interaction (Figure 2C). However, there is the possibility that increasing lateral

root growth may merely be caused by the inhibition of primary root growth (Potters et al., 2009), further studies should investigate the biological implications of the fungal CLE peptides on AM symbiosis.

4 Roles of CLE signaling in plant-nematode interactions

Phytoparasitic nematodes are obligate parasitic animals, which are recognized to cause severe economic losses in agriculture worldwide (Jones et al., 2013). Accumulating evidence has shown that the CLE signaling pathway is utilized for successful infection. Here, we introduce the roles of CLE signaling in plant-nematode interactions.

4.1 Root-knot nematodes

Root-knot nematodes (RKN; *Meloidogyne* spp.) parasite most vascular plants and are distributed worldwide. Infective juveniles move toward plant roots in the soil and invade through the root meristematic zone. After invasion, they inject an effector cocktail into the host procambial cells that suppresses host defense responses and manipulates host developmental pathways, thereby triggering the formation of their feeding sites called galls or root-knots on the host root by modulating the host auxin pathway (Favery et al., 2016; Olmo et al., 2020; Suzuki et al., 2022; Abril-Urias et al., 2023; Noureddine et al., 2023). Gene expression analyses in *M. incognita*-infected Arabidopsis showed that *AtCLE1*, *AtCLE3*, *AtCLE4*, and *AtCLE7*, which are orthologs of the symbiosis-induced *CLEs* described above, were upregulated in galls (Yamaguchi et al., 2017; Nakagami et al., 2023b). Single mutants lacking *AtCLE1*, *AtCLE3*, or *AtCLE7* exhibited reduced gall numbers, and the higher-order mutant of *AtCLE1* to *AtCLE7* (*cle1~7*) showed an additive effect on the reduction of gall formation, whereas CLE overexpression led to increased gall formation, showing that these *CLE* genes positively regulate gall formation (Nakagami et al., 2023b). Grafting and split-root experiments revealed that the CLE-mediated regulation of gall formation required shoot-expressed AtCLV1, with synthetic AtCLE3 peptide directly binding to the extracellular domain of AtCLV1, indicating that AtCLE1~7-AtCLV1 module is the systemic pathway. Consistent with this, MtSUNN positively controls gall formation during *M. javanica* infection (Costa et al., 2020). These results raise the question of how shoot-expressed AtCLV1 regulates gall formation on roots after AtCLE peptides perception. A recent study showed that *AtCLE2* and *AtCLE3* were induced in roots when the roots were exposed to sucrose starvation (Okamoto et al., 2022). Root-expressed *AtCLE1~AtCLE7* maintained *SUCROSE-PROTON SYMTORTER 2* (*SUC2*) expression in the leaves, thereby balancing the root sucrose levels and growth. Indeed, exogenous sucrose application to the *M. incognita*-infected roots compensated the gall-reducing phenotype of the *cle1~7* and *clv1* mutants (Nakagami et al., 2023b), suggesting that maintenance of sucrose levels in roots mediated by leaf-expressed SUC2 is a possible downstream mechanism of AtCLE peptides/CLV1 on RKN infection (Figure 2D). Therefore, *M. incognita* may manipulate host sucrose homeostasis to acquire sucrose as a nutrient efficiently and/or allocate sucrose as an energy source for gall formation.

Our knowledge of AtCLE/CLV1 on plant-nematode interactions is still fragmented. For instance, there is a lack of explanation for how *M. incognita* induces these *AtCLEs* in the host roots, whether these AtCLEs require arabinosylation for their function, and if so, which HPAT arabinosylates these AtCLEs. In another aspect of CLE signaling in plant-RKN interactions, like cyst nematodes (see below), *M. incognita* possesses a gene harboring a ligand-like motif somewhat similar to the CLE motif, named *16D10*, that is required for RKN parasitism, and the 16D10 peptide can interact with host transcription factors, not receptor-like proteins, making it unique among secreted peptides (Huang et al., 2006b, 2006a; Yang et al., 2013). In addition, RKNs harbor *CLE*-like genes constituted by only a signal peptide domain and a CLE domain, but their function is unknown (Mitchum and Liu, 2022) (Figure 1C). However, several studies provide evidence that RKNs possess functional peptide mimics to facilitate their successful infection (Kim et al., 2018; Zhang et al., 2020; Mishra et al., 2023; Yimer et al., 2023). Investigating the functions of *CLE*-like genes of RKN will underscore the ecological significance of CLE signaling in plant-RKN interactions. Moreover, the ways which RKN and rhizobia infect host plants share similarities even though RKNs and rhizobia are parasites and symbionts, respectively (Costa et al., 2021). Advancing our knowledge about plant-rhizobia interactions may help to reveal the mechanisms of plant-RKN interactions.

4.2 Cyst nematodes

Parasitic cyst nematodes (CN; *Heterodera* and *Globodera* spp.) are obligate parasites to vascular plants including economically important crops (Jones et al., 2013). They penetrate their host roots and inject various effectors into the host procambial cells to establish their feeding site called syncytium in the root (Davis et al., 2008). Like AM fungi, CNs possess functional *CLE*-like genes in their genome as effectors. The prepropeptides of *Hterodera* species were similar to that of plants, while that of *Globodera* species possessed five CLE domains in addition to a signal peptide and a variable domain (Mitchum and Liu, 2022) (Figure 1C). Several studies in *H. glycines*, and *G. rostochiensis* showed that transcript of *GrCLE1* and *GrCLE4* was accumulated in dorsal gland secretory cells of the infective and parasitic juveniles, while immunolocalization experiments revealed that HgCLE peptides were localized in dorsal gland cells of parasitic juveniles (Wang et al., 2005, 2010; Bakhetia et al., 2007; Lu et al., 2009). Neither *HsCLEs* nor *HgCLEs* were expressed in pre-parasitic juveniles, implying that CN *CLE*-like genes act only in parasitic stages (Wang et al., 2010; Fosu-Nyarko et al., 2016). Heterologous expression of CN *CLE*-like genes (*HsCLE1*, *HsCLE2, HgCLE1*, *HgCLE2, GrCLE1*, and *GrCLE4*) that have high similarities of *AtCLE1~AtCLE7* mimicked *AtCLE* function; exogenous application of the 12 amino acids form of them inhibited primary root growth of *Arabidopsis* as well as AtCLE peptides (Wang et al.,

2005, 2010, 2011; Lu et al., 2009; Replogle et al., 2011, 2013; Chen et al., 2015). Moreover, in planta-expressed *GrCLE1* was post-translationally processed, producing a 12 amino acids triarabinosylated GrCLE1 peptide which had high structural similarity to mature plant-CLE peptides, and this can directly bind to CLV2 of potato (Chen et al., 2015). The effect of *CLE*-like genes and peptides depends on the host receptor complexes such as AtCLV1 and AtCLV2 (Replogle et al., 2011, 2013; Chen et al., 2015; Guo et al., 2015, 2017), suggesting that the CN CLE-like peptides are recognized by receptors of the host plants. So, how do CN-CLE peptides injected into the host cells translocate to the apoplast to be perceived by the extracellular receptors? It has been shown that the variable domain of the CN CLE-like proteins has the function of a translocation signal that enables the CN CLE-like peptides to be delivered from the cytoplasm of syncytial cells to the apoplast through the host endoplasmic reticulum (Wang et al., 2010, 2021b).

The host receptor complexes also play a role in syncytium formation and CN fecundity. Mutants of AtCLV1, AtCLV2/AtCRN, AtRPK2, GmCLV2, and GmRPK2 exhibit defects of syncytium formation and low levels of CN fecundity (Replogle et al., 2011, 2013; Guo et al., 2015). In addition, exogenous treatment of HsCLEB, which is similar to TRACHEARY ELEMENT DIFFERENTIATION INHIBITORY FACTOR (AtTDIF), induces the expression of *WUSCHEL-RELATED HOMEOBOX 4* (*WOX4*) transcription factor, which promotes procambial cell proliferation, through TDIF-RECEPTOR (TDR) in roots, thereby facilitating syncytium formation (Guo et al., 2017). Gene expression profiles and genetic studies revealed that *HOMEOBOX GENE 8* (*AtHB8*), which controls vascular cell differentiation as well as *WOX4*, is a downstream component of CLE signaling during CN infection (Smetana et al., 2019; Liu and Mitchum, 2024). Also, direct binding of several CN CLE-like peptide/plant receptor pairs has been shown (Guo et al., 2011, 2015; Chen et al., 2015). Thus, it has been proposed that CNs co-opt the host developmental programs through CLAVATA pathways to support their infection (Figure 2E). However, whether CN CLE-like peptides injected into the host cells are processed during infection is not yet clear (Frei dit Frey and Favery, 2021).

4.3 Reniform nematode

Reniform nematodes (RN) also possess *CLE*-like genes. An RN, *Rotylenchulus reniformis*, is an obligate semi-endoparasite of more than 300 plant species. Three *RrCLE* genes were identified in the *R. reniformis* genome and consisted of a signal peptide at the N-terminus, a cryptic signal peptide within a variable domain, and a CLE domain at the C-terminus (Wubben et al., 2015) (Figure 1C). The *RrCLE* transcripts were detected in parasitic juveniles and localized in their dorsal gland. Another study in *G. max* infected by *R. reniformis* showed that several *GmCLE* genes were upregulated in the roots similarly to in the RKN-induced galls (Redding et al., 2018; Nakagami et al., 2023b). Therefore, RNs may use their CLE mimics and/or host-endogenous CLE peptides for their infection.

5 Involvement of CLE signaling in insect-induced gall formation

Some phytoparasitic insects induce gall formation on their host tissues where they acquire nutrients and are protected from enemies and environments (Favery et al., 2020). Phyloxera (*Daktulosphaira vitifoliae*), which parasitizes wild grapevine (*Vitis riparia*), induces the formation of flower-like gall on the host leaf. A transcriptomic analysis has found that the CLE signaling pathway in regulating cambial cell homeostasis is activated in *D. vitifoliae*-inducing galls (Schultz et al., 2019). For instance, *VrCLE44*, *VrTDR*, and *VrWOX4* are up-regulated in insect-inducing galls, as well as in RKN- and CN-inducing galls/syncytia (Yamaguchi et al., 2017; Schultz et al., 2019). Gall-forming insects may therefore use the mechanism for the cambial cell maintenance of their hosts.

6 Involvement of CLE signaling in plant-pathogen interactions

Plants employ RKs and RLPs as pattern recognition receptors (PRRs) to recognize pathogen-associated molecular patterns (PAMPs), damage-associated molecular patterns (DAMPs), and phytocytokines (Zhang et al., 2023b). PRRs induce pattern-triggered immunity (PTI) by recognizing PAMPs. One of the best-studied PRRs is FLAGELLIN SENSITIVE 2 (FLS2) which recognizes bacterial flagellin with the co-receptor BAK1 via a 22 amino acids epitope (flg22) (DeFalco and Zipfel, 2021). Emerging evidence suggests that CLE signaling is involved in plant immune responses and signaling by CLEs-CLV1/BAMs in development and flg22-FLS2 in immunity uses similar downstream factors (DeFalco et al., 2022) (Figure 3A). Here we discuss the current knowledge on the contribution of CLE signaling to plant immunity.

AtCLV1 and AtCLV2 participate in susceptibility to bacterial, fungal, and oomycete pathogens (Figure 3B). The *clv1* and *clv2* mutants exhibited increased resistance against the bacterial pathogen *Ralstonia solanacearum* and the oomycete pathogen *Hyaloperonospora arabidopsidis* compared to the wild-type plant (Hanemian et al., 2016). Conversely, *clv1* was more susceptible to the bacterial pathogen *Pseudomonas syringae* pv. *tomato* DC3000 and the fungal pathogens *Plectosphaerella cucumerina* and *Botrytis cinerea*. Multiple *NF-YA* genes were upregulated in *clv1* and *clv2* mutants infected with *R. solanacearum* in an *miR169*-dependent manner. The overexpression of *miR169* that suppresses the *NF-YA* genes facilitated susceptibility of *clv1* and *clv2* to *R. solanacearum* (Sorin et al., 2014; Hanemian et al., 2016). In contrast to the more susceptible phenotype of *clv1* to *B. cinerea*, the mutant lacking AtACR4, which recognizes CLE40p coordinately with AtCLV1, was more resistant to this fungal pathogen (E-Zereen and Ingram, 2012; Czyzewicz et al., 2016). On the one hand, work by Lee et al. (2011) has proposed that AtCLV3 peptide is recognized by AtFLS2 leading to activation of immune response in the SAM. On the other hand, work by Segonzac et al. (2012) has provided experimental evidence that AtFLS2 does not recognize AtCLV3 peptide and that the immunity of the SAM to DC3000 is independent of AtCLV3

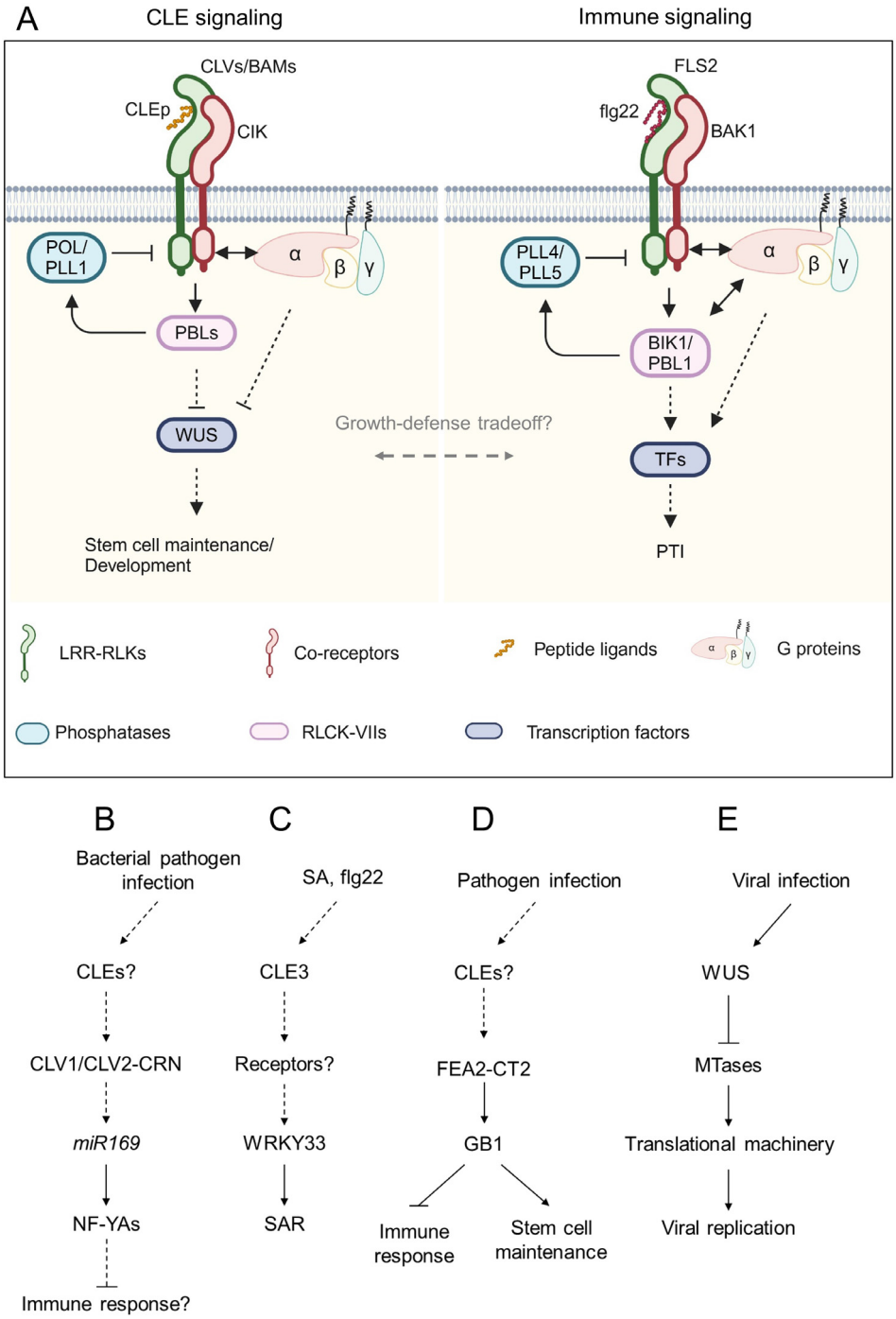

FIGURE 3
Schematic model of CLE signaling involved in immune response. **(A)** Representative model of the conserved signaling pathway between CLE signaling and immune signaling. Peptide ligands are recognized by leucine-rich repeat receptor-like kinases (LRR-RLKs) with their co-receptors. The signals are transduced via receptor-like cytoplasmic kinases (RLCKs) and G proteins and dampened by phosphatases to regulate downstream transcription factors. **(B-E)** Schematic flowcharts of CLE signaling involving plant-pathogen interactions. **(B-D)** Involvement of CLE signaling in plant-bacterial pathogen interactions in Arabidopsis **(B, C)** and maize **(D)**. **(E)** Involvement of WUS in plant-virus interaction in Arabidopsis. Dashed lines indicate putative or indirect pathways. Figure adapted from images created with BioRender.com.

peptide perception. Another study focused on gene expression analyses of *AtCLE* genes has revealed that *AtCLE3* expression is induced in the roots by exogenous treatments of flg22, Pep2, which is a 23 amino acids peptide known as a DAMP, and the defense phytohormone salicylic acid (SA) (Ma et al., 2022). Root-expressing *AtCLE3* is required for upregulation of shoot-expressed *WRKY33* that contributes to systemic acquired resistance (Wang et al., 2018; Ma et al., 2022), suggesting that the AtCLE3 peptide may act as a systemic signal to transduce SA signaling from roots to shoots (Figure 3C). However, it has not been tested yet whether AtCLE3

peptide contributes to immune response, particularly affecting pathogen growth in planta. Therefore, careful investigation of whether and how the CLE signaling is involved in plant immunity is necessary.

Recent studies have also provided evidence that downstream components of the CLE-receptor modules are involved in plant immunity. Genetic studies have shown that Arabidopsis G proteins AtAGB1 (Gβ), AtAGG1, and AtAGG2 (Gγ) are required for FLS2-mediated immune response (Liu et al., 2013). Furthermore, AtAGB1 and EXTRA-LARGE GTP BINDING PROTEIN 2 (AtXLG2), a noncanonical Gα, directly interact with FLS2 and BOTRYTIS-INDUCED KINASE 1 (BIK1), conferring stability on the receptor complex (Liang et al., 2016). AtAGB1 also interacts with AtRPK2, which maintains meristem activity in the SAM (Ishida et al., 2014), suggesting that G proteins control both meristem development and immune response. A recent study found that the *Zea mays Gβ subunit 1* (*ZmGB1*) mutants showed seedling-lethal phenotype due to autoimmunity (Wu et al., 2020b). A viable *ZmGB1* mutant *fea*183* was identified from ethyl methanesulfonate-mutagenesis screen and showed striking inflorescence defects, reminiscent of mutants lacking ZmCT2 (Gα) (Bommert et al., 2013; Wu et al., 2020b). *ZmFEA2*, an ortholog of *AtCLV2*, and *ZmCT2* were epistatic to *ZmGB1*, suggesting that the CLE-CLV-G protein signaling circuit may balance the tradeoff between growth and defense (Figure 3D). The SAM-specific transcription factor WUS protects the SAM from infection by cucumber mosaic virus (CMV) (Wu et al., 2020a; Lopes et al., 2021). WUS inhibits transcript levels of *S*-adenosyl-Lmethionine-dependent methyltransferases (MTases), which are involved in rRNA processing and ribosome stability, by responding to CMV infection, thereby sabotaging CMV replication and its invasion ability to the SAM (Wu et al., 2020a) (Figure 3E).

Apart from the CLE signaling pathway, plant endogenous signaling peptides play roles in plant immunity, abiotic stress response, and growth regulation (Fitrianti et al., 2022; Liu et al., 2022; Rzemieniewski and Stegmann, 2022; Rzemieniewski et al., 2022; Taleski et al., 2024). In addition, a recent study has revealed that a RALF-FERONIA signaling module that modulates the formation of FLS2-BAK1 receptor complex affects the rhizosphere microbiome (Song et al., 2021). This suggests that peptide-receptor modules are central regulators of diverse aspects of plant physiology, and their roles in immunity, development, and beyond are mechanistically coupled. Yet, how the CLE signaling harmonizes multiple aspects of plant immunity, development, and physiology is still elusive.

7 Conclusion

Peptide ligand and its receptor pairs play important roles in plant development and plant-microbe interactions. The CLE gene family is one of the largest among those that encode peptide ligands, and they are conserved across green algae to higher plants (Olsson et al., 2019). Plants have evolved the CLE signaling to develop more complex multicellular bodies and be adapted to environmental nutritional status that is constantly changing. Both developing *de novo* organs induced by plant-associated microbes and coping with the nutritional status of their host are pivotal for microbial colonization. Thus, plant-associated microbes may utilize the host-CLE signaling to achieve those.

Secreted peptides are perceived by distinct receptors in the apoplast, in consequence, their signals are transduced into the cell. In this process, post-translational modifications to form mature peptides are required. However, the mature form of most CLE peptides involved in plant-microbe interactions remains uncharacterized. In addition, most of the knowledge about peptide-receptor pairs has been brought by genetic studies, it is still largely unknown whether distinct peptides bind their cognate receptors. Interestingly, it has been shown that AI-based prediction to identify peptide ligand and receptor pairs is a powerful tool for structure-function analysis of peptide-receptor pairs (Snoeck et al., 2024). Applying this in silico method to CLE peptides and their postulated receptors holds the potential to identify bona fide peptide-receptor pairs more and distinguish functions of different peptides.

While there are increasing studies on plant-microbe interactions, such efforts still lag behind those on plant development and physiology due to more complex phenomena and technical obstacles. Recently, several studies have tackled unraveling molecular mechanisms underlying plant-microbe interactions by using the co-transcriptomics of plants inoculated with microbes and the microbes in planta (Roux et al., 2014; Hacquard et al., 2016; Nobori et al., 2018, 2022; Sauviac et al., 2022; Siddique et al., 2022; Zhang et al., 2023a), spacial transcriptomics (Frank et al., 2023; Nobori et al., 2023; Schnabel et al., 2023; Tang et al., 2023; Verbon et al., 2023; Zhu et al., 2023), and the technique that is combined with both (Serrano et al., 2024a, 2024b), which will identify yet unknown upstream and downstream components of the CLE-receptor modules, and accelerate our understanding of ecological implications of the plant-microbe interactions.

Author contributions

SN: Conceptualization, Funding acquisition, Visualization, Writing – original draft, Writing – review & editing. TK: Writing – original draft, Writing – review & editing. KT: Supervision, Writing – review & editing. SS: Conceptualization, Writing – review & editing.

Funding

The author(s) declare that financial support was received for the research, authorship, and/or publication of this article. Research on this topic is supported by Human Resources Department of Huazhong Agricultural University (Fellowship ID: TH9009350) to SN and KAKENHI (Grant Numbers: 20H00422, 20KK0135, 21K19273, and 23H04748) to SS.

Acknowledgments

SN thanks members of the Kenichi Tsuda and Xiaowei Han laboratories (Huazhong Agricultural University) and members of

the Shinichiro Sawa laboratory (Kumamoto University) for useful discussions.

Conflict of interest

The authors declare that the research was conducted in the absence of any commercial or financial relationships that could be construed as a potential conflict of interest.

Publisher's note

References

Abril-Urias, P., Ruiz-Ferrer, V., Cabrera, J., Olmo, R., Silva, A. C., Díaz-Manzano, F. E., et al. (2023). Divergent regulation of auxin responsive genes in root-knot and cyst nematodes feeding sites formed in Arabidopsis. *Front. Plant Sci* 14. doi: 10.3389/fpls.2023.1024815

Alves-Carvalho, S., Aubert, G., Carrère, S., Cruaud, C., Brochot, A., Jacquin, F., et al. (2015). Full-length *de novo* assembly of RNA-seq data in pea (*P isum sativum* L.) provides a gene expression atlas and gives insights into root nodulation in this species. *Plant J* 84, 1–19. doi: 10.1111/tpj.12967

Araya, T., Miyamoto, M., Wibowo, J., Suzuki, A., Kojima, S., Tsuchiya, Y. N., et al. (2014). CLE-CLAVATA1 peptide-receptor signaling module regulates the expansion of plant root systems in a nitrogen-dependent manner. *Proc. Natl. Acad. Sci* 111, 2029–2034. doi: 10.1073/pnas.1319953111

Bakhetia, M., Urwin, P. E., and Atkinson, H. J. (2007). QPCR analysis and RNAi define pharyngeal gland cell-expressed genes of Heterodera glycines required for initial interactions with the host. *Mol. Plant-Microbe Interact* 20, 306–312. doi: 10.1094/MPMI-20-3-0306

Bashyal, S., Gautam, C. K., and Müller, L. M. (2023). CLAVATA signaling in plant-environment interactions. *Plant Physiol* 194, 1336–1357. doi: 10.1093/plphys/kiad591

Betsuyaku, S., Sawa, S., and Yamada, M. (2011). The function of the CLE peptides in plant development and plant-microbe interactions. *Arabidopsis Book* 9, e0149. doi: 10.1199/tab.0149

Bleckmann, A., Weidtkamp-Peters, S., Seidel, C. A. M., and Simon, R. (2009). Stem cell signaling in arabidopsis requires CRN to localize CLV2 to the plasma membrane. *Plant Physiol* 152, 166–176. doi: 10.1104/pp.109.149930

Bommert, P., Je, B. I., Goldshmidt, A., and Jackson, D. (2013). The maize Gα gene COMPACT PLANT2 functions in CLAVATA signalling to control shoot meristem size. *Nature* 502, 555–558. doi: 10.1038/nature12583

Chaulagain, D., and Frugoli, J. (2021). The regulation of nodule number in legumes is a balance of three signal transduction pathways. *Int. J. Mol. Sci* 22, 1117. doi: 10.3390/ijms22031117

Chen, S., Lang, P., Chronis, D., Zhang, S., De Jong, W. S., Mitchum, M. G., et al. (2015). In planta processing and glycosylation of a nematode CLAVATA3/ENDOSPERM SURROUNDING REGION-Like effector and its interaction with a host CLAVATA2-Like receptor to promote parasitism. *Plant Physiol* 167, 262–272. doi: 10.1104/pp.114.251637

Costa, S. R., Chin, S., and Mathesius, U. (2020). Infection of medicago truncatula by the root-knot nematode meloidogyne javanica does not require early nodulation genes. *Front. Plant Sci* 11. doi: 10.3389/fpls.2020.01050

Costa, S. R., Ng, J. L. P., and Mathesius, U. (2021). Interaction of symbiotic rhizobia and parasitic root-knot nematodes in legume roots: From molecular regulation to field application. *MPMI* 34, 470–490. doi: 10.1094/MPMI-12-20-0350-FI

Crook, A. D., Schnabel, E. L., and Frugoli, J. A. (2016). The systemic nodule number regulation kinase SUNN in Medicago truncatula interacts with MtCLV2 and MtCRN. *Plant J* 88, 108–119. doi: 10.1111/tpj.13234

Czyzewicz, N., Nikonorova, N., Meyer, M. R., Sandal, P., Shah, S., Vu, L. D., et al. (2016). The growing story of (ARABIDOPSIS) CRINKLY 4. *J. Exp. Bot* 67, 4835–4847. doi: 10.1093/jxb/erw192

Davis, E. L., Hussey, R. S., Mitchum, M. G., and Baum, T. J. (2008). Parasitism proteins in nematode–plant interactions. *Curr. Opin. Plant Biol* 11, 360–366. doi: 10.1016/j.pbi.2008.04.003

DeFalco, T. A., Anne, P., James, S. R., Willoughby, A. C., Schwanke, F., Johanndrees, O., et al. (2022). A conserved module regulates receptor kinase signalling in immunity and development. *Nat. Plants* 8, 356–365. doi: 10.1038/s41477-022-01134-w

DeFalco, T. A., and Zipfel, C. (2021). Molecular mechanisms of early plant pattern-triggered immune signaling. *Mol. Cell* 81, 3449–3467. doi: 10.1016/j.molcel.2021.07.029

E-Zereen, J., and Ingram, G. (2012). A possible involvement of ACR4, a receptor like kinase, in plant defence mechanism. *Bangladesh Pharm. J* 15, 127–130. doi: 10.3329/bpj.v15i2.12576

Favery, B., Dubreuil, G., Chen, M.-S., Giron, D., and Abad, P. (2020). Gall-inducing parasites: convergent and conserved strategies of plant manipulation by insects and nematodes. *Annu. Rev. Phytopathol* 58, 1–22. doi: 10.1146/annurev-phyto-010820-012722

Favery, B., Quentin, M., Jaubert-Possamai, S., and Abad, P. (2016). Gall-forming root-knot nematodes hijack key plant cellular functions to induce multinucleate and hypertrophied feeding cells. *J. Insect Physiol* 84, 60–69. doi: 10.1016/j.jinsphys.2015.07.013

Ferguson, B. J., Li, D., Hastwell, A. H., Reid, D. E., Li, Y., Jackson, S. A., et al. (2014). The soybean (Glycine max) nodulation-suppressive CLE peptide, GmRIC1, functions interspecifically in common white bean (Phaseolus vulgaris), but not in a supernodulating line mutated in the receptor PvNARK. *Plant Biotechnol. J* 12, 1085–1097. doi: 10.1111/pbi.12216

Fiers, M., Golemiec, E., Xu, J., van der Geest, L., Heidstra, R., Stiekema, W., et al. (2005). The 14-amino acid CLV3, CLE19, and CLE40 peptides trigger consumption of the root meristem in Arabidopsis through a CLAVATA2-dependent pathway. *Plant Cell* 17, 2542–2553. doi: 10.1105/tpc.105.034009

Fitrianti, A. N., Mai, T. L., Phuong, L. T., Monden, H., Shiiba, N., Matsui, H., et al. (2022). CEP peptide induces susceptibility of Arabidopsis thaliana to non-adapted pathogens. *J. Gen. Plant Pathol* 88, 287–292. doi: 10.1007/s10327-022-01077-2

Fletcher, J. C. (2020). Recent advances in arabidopsis CLE peptide signaling. *Trends Plant Sci* 25, 1005–1016. doi: 10.1016/j.tplants.2020.04.014

Fosu-Nyarko, J., Nicol, P., Naz, F., Gill, R., and Jones, M. G. K. (2016). Analysis of the transcriptome of the infective stage of the beet cyst nematode, H. schachtii. *PloS One* 11, e0147511. doi: 10.1371/journal.pone.0147511

Frank, M., Fechete, L. I., Tedeschi, F., Nadzieja, M., Nørgaard, M. M. M., Montiel, J., et al. (2023). Single-cell analysis identifies genes facilitating rhizobium infection in lotus japonicus. *Nat. Commun* 14, 7171. doi: 10.1038/s41467-023-42911-1

Frei dit Frey, N., and Favery, B. (2021). Plant-parasitic nematode secreted peptides hijack a plant secretory pathway. *New Phytol* 229, 11–13. doi: 10.1111/nph.16842

Fu, M., Yao, X., Li, X., Liu, J., Bai, M., Fang, Z., et al. (2024). GmNLP1 and GmNLP4 activate nitrate-induced CLE peptides NIC1a/b to mediate nitrate-regulated root nodulation. *Plant J* 119, 783–795. doi: 10.1111/tpj.16795

Funayama-Noguchi, S., Noguchi, K., Yoshida, C., and Kawaguchi, M. (2011). Two CLE genes are induced by phosphate in roots of Lotus japonicus. *J. Plant Res* 124, 155–163. doi: 10.1007/s10265-010-0342-5

Gautrat, P., Laffont, C., and Frugier, F. (2020). Compact Root Architecture 2 Promotes Root Competence for Nodulation through the miR2111 Systemic Effector. *Curr. Biol* 30, 1339–1345.e3. doi: 10.1016/j.cub.2020.01.084

Ge, S., He, L., Jin, L., Xia, X., Li, L., Ahammed, G. J., et al. (2022). Light-dependent activation of HY5 promotes mycorrhizal symbiosis in tomato by systemically regulating strigolactone biosynthesis. *New Phytol* 233, 1900–1914. doi: 10.1111/nph.17883

Guo, X., Chronis, D., de la Torre, C. M., Smeda, J., Wang, X., and Mitchum, M. G. (2015). Enhanced resistance to soybean cyst nematode *Heterodera glycines* in transgenic soybean by silencing putative CLE receptors. *Plant Biotechnol. J* 13, 801–810. doi: 10.1111/pbi.12313

Guo, Y., Ni, J., Denver, R., Wang, X., and Clark, S. E. (2011). Mechanisms of molecular mimicry of plant CLE peptide ligands by the parasitic nematode Globodera rostochiensis. *Plant Physiol* 157, 476–484. doi: 10.1104/pp.111.180554

Guo, X., Wang, J., Gardner, M., Fukuda, H., Kondo, Y., Etchells, J. P., et al. (2017). Identification of cyst nematode B-type CLE peptides and modulation of the vascular stem cell pathway for feeding cell formation. *PloS Pathog* 13, e1006142. doi: 10.1371/journal.ppat.1006142

Hacquard, S., Kracher, B., Hiruma, K., Münch, P. C., Garrido-Oter, R., Thon, M. R., et al. (2016). Survival trade-offs in plant roots during colonization by closely related beneficial and pathogenic fungi. *Nat. Commun* 7, 11362. doi: 10.1038/ncomms11362

Handa, Y., Nishide, H., Takeda, N., Suzuki, Y., Kawaguchi, M., and Saito, K. (2015). RNA-seq transcriptional profiling of an arbuscular mycorrhiza provides insights into regulated and coordinated gene expression in *Lotus japonicus* and *Rhizophagus irregularis*. *Plant Cell Physiol* 56, 1490–1511. doi: 10.1093/pcp/pcv071

Hanemian, M., Barlet, X., Sorin, C., Yadeta, K. A., Keller, H., Favery, B., et al. (2016). Arabidopsis CLAVATA1 and CLAVATA2 receptors contribute to *Ralstonia solanacearum* pathogenicity through a miR169-dependent pathway. *New Phytol* 211, 502–515. doi: 10.1111/nph.13913

Hastwell, A. H., Corcilius, L., Williams, J. T., Gresshoff, P. M., Payne, R. J., and Ferguson, B. J. (2019). Triarabinosylation is required for nodulation-suppressive CLE peptides to systemically inhibit nodulation in *Pisum sativum*: Tri-arabinosylated CLE peptides in nodulation. *Plant Cell Environ* 42, 188–197. doi: 10.1111/pce.13325

Hayashi-Tsugane, M., and Kawaguchi, M. (2022). Lotus japonicus HAR1 regulates root morphology locally and systemically under a moderate nitrate condition in the absence of rhizobia. *Planta* 255, 95. doi: 10.1007/s00425-022-03873-8

Hu, C., Zhu, Y., Cui, Y., Cheng, K., Liang, W., Wei, Z., et al. (2018). A group of receptor kinases are essential for CLAVATA signalling to maintain stem cell homeostasis. *Nat. Plants* 4, 205–211. doi: 10.1038/s41477-018-0123-z

Huang, G., Allen, R., Davis, E. L., Baum, T. J., and Hussey, R. S. (2006a). Engineering broad root-knot resistance in transgenic plants by RNAi silencing of a conserved and essential root-knot nematode parasitism gene. *Proc. Natl. Acad. Sci* 103, 14302–14306. doi: 10.1073/pnas.0604698103

Huang, G., Dong, R., Allen, R., Davis, E. L., Baum, T. J., and Hussey, R. S. (2006b). A root-knot nematode secretory peptide functions as a ligand for a plant transcription factor. *MPMI* 19, 463–470. doi: 10.1094/MPMI-19-0463

Huault, E., Laffont, C., Wen, J., Mysore, K. S., Ratet, P., Duc, G., et al. (2014). Local and systemic regulation of plant root system architecture and symbiotic nodulation by a receptor-like kinase. *PloS Genet* 10, e1004891. doi: 10.1371/journal.pgen.1004891

Imin, N., Patel, N., Corcilius, L., Payne, R. J., and Djordjevic, M. A. (2018). CLE peptide tri-arabinosylation and peptide domain sequence composition are essential for SUNN-Dependent autoregulation of nodulation in *Medicago Truncatula*. *New Phytol* 218, 73–80. doi: 10.1111/nph.15019

Ishida, T., Tabata, R., Yamada, M., Aida, M., Mitsumasu, K., Fujiwara, M., et al. (2014). Heterotrimeric G proteins control stem cell proliferation through CLAVATA signaling in *Arabidopsis*. *EMBO Rep* 15, 1202–1209. doi: 10.15252/embr.201438660

Isidra-Arellano, M. C., Pozas-Rodríguez, E. A., Del Rocío Reyero-Saavedra, M., Arroyo-Canales, J., Ferrer-Orgaz, S., Del Socorro Sánchez-Correa, M., et al. (2020). Inhibition of legume nodulation by Pi deficiency is dependent on the autoregulation of nodulation (AON) pathway. *Plant J* 103, 1125–1139. doi: 10.1111/tpj.14789

Isidra-Arellano, M., Reyero-Saavedra, M., Sánchez-Correa, M., Pingault, L., Sen, S., Joshi, T., et al. (2018). Phosphate deficiency negatively affects early steps of the symbiosis between common bean and rhizobia. *Genes* 9, 498. doi: 10.3390/genes9100498

Jones, J. T., Haegeman, A., Danchin, E. G. J., Gaur, H. S., Helder, J., Jones, M. G. K., et al. (2013). Top 10 plant-parasitic nematodes in molecular plant pathology: Top 10 plant-parasitic nematodes. *Mol. Plant Pathol* 14, 946–961. doi: 10.1111/mpp.12057

Jones, D. S., John, A., VanDerMolen, K. R., and Nimchuk, Z. L. (2021). CLAVATA signaling ensures reproductive development in plants across thermal environments. *Curr. Biol* 31, 220–227.e5. doi: 10.1016/j.cub.2020.10.008

Kang, J., Wang, X., Ishida, T., Grienenberger, E., Zheng, Q., Wang, J., et al. (2022). A group of CLE peptides regulates *de novo* shoot regeneration in *Arabidopsis thaliana*. *New Phytol* 235, 2300–2312. doi: 10.1111/nph.18291

Karlo, M., Boschiero, C., Landerslev, K. G., Blanco, G. S., Wen, J., Mysore, K. S., et al. (2020). The CLE53–SUNN genetic pathway negatively regulates arbuscular mycorrhiza root colonization in medicago truncatula. *J. Exp. Bot* 71, 4972–4984. doi: 10.1093/jxb/eraa193

Kassaw, T., Nowak, S., Schnabel, E., and Frugoli, J. (2017). ROOT DETERMINED NODULATION1 Is Required for M. truncatula CLE12, But Not CLE13, Peptide Signaling through the SUNN Receptor Kinase. *Plant Physiol* 174, 2445–2456. doi: 10.1104/pp.17.00278

Kim, J., Yang, R., Chang, C., Park, Y., and Tucker, M. L. (2018). The root-knot nematode meloidogyne incognita produces a functional mimic of the arabidopsis INFLORESCENCE DEFICIENT IN ABSCISSION signaling peptide. *J. Exp. Bot* 69, 3009–3021. doi: 10.1093/jxb/ery135

Kondo, T., Sawa, S., Kinoshita, A., Mizuno, S., Kakimoto, T., Fukuda, H., et al. (2006). A plant peptide encoded by CLV3 identified by in *situ* MALDI-TOF MS analysis. *Science* 313, 845–848. doi: 10.1126/science.1128439

Konishi, M., and Yanagisawa, S. (2013). Arabidopsis NIN-like transcription factors have a central role in nitrate signalling. *Nat. Commun* 4, 1617. doi: 10.1038/ncomms2621

Krusell, L., Madsen, L. H., Sato, S., Aubert, G., Genua, A., Szczyglowski, K., et al. (2002). Shoot control of root development and nodulation is mediated by a receptor-like kinase. *Nature* 420, 422–426. doi: 10.1038/nature01207

Krusell, L., Sato, N., Fukuhara, I., Koch, B. E. V., Grossmann, C., Okamoto, S., et al. (2011). The Clavata2 genes of pea and Lotus japonicus affect autoregulation of nodulation. *Plant J* 65, 861–871. doi: 10.1111/j.1365-313X.2010.04474.x

Laffont, C., Ivanovici, A., Gautrat, P., Brault, M., Djordjevic, M. A., and Frugier, F. (2020). The NIN transcription factor coordinates CEP and CLE signaling peptides that regulate nodulation antagonistically. *Nat. Commun* 11, 3167. doi: 10.1038/s41467-020-16968-1

Lebedeva, M., Azarakhsh, M., Yashenkova, Y., and Lutova, L. (2020). Nitrate-induced CLE peptide systemically inhibits nodulation in medicago truncatula. *Plants* 9, 1456. doi: 10.3390/plants9111456

Lebedeva, M. A., Dobychkina, D. A., Yashenkova, Y., Romanyuk, D. A., and Lutova, L. A. (2023). Local and systemic targets of the MtCLE35-SUNN pathway in the roots of Medicago truncatula. *J. Plant Physiol* 281, 153922. doi: 10.1016/j.jplph.2023.153922

Lebedeva, M., Dvornikova, K., and Lutova, L. (2022). Nitrate-induced mtCLE34 gene lacks the ability to reduce symbiotic nodule number and carries nonsense mutation in a few accessions of medicago truncatula. *Agronomy* 12, 842. doi: 10.3390/agronomy12040842

Lee, H., Chah, O.-K., and Sheen, J. (2011). Stem-cell-triggered immunity through CLV3p–FLS2 signalling. *Nature* 473, 376–379. doi: 10.1038/nature09958

Le Marquer, M., Bécard, G., and Frei dit Frey, N. (2019). Arbuscular mycorrhizal fungi possess a CLAVATA3/embryo surrounding region-related gene that positively regulates symbiosis. *New Phytol* 222, 1030–1042. doi: 10.1111/nph.15643

Li, Y., Pei, Y., Shen, Y., Zhang, R., Kang, M., Ma, Y., et al. (2022). Progress in the self-regulation system in legume nodule development-AON (Autoregulation of nodulation). *Int. J. Mol. Sci* 23, 6676. doi: 10.3390/ijms23126676

Liang, X., Ding, P., Lian, K., Wang, J., Ma, M., Li, L., et al. (2016). Arabidopsis heterotrimeric G proteins regulate immunity by directly coupling to the FLS2 receptor. *eLife* 5, e13568. doi: 10.7554/eLife.13568

Lim, C. W., Lee, Y. W., and Hwang, C. H. (2011). Soybean nodule-enhanced CLE peptides in roots act as signals in GmNARK-Mediated nodulation suppression. *Plant Cell Physiol* 52, 1613–1627. doi: 10.1093/pcp/pcr091

Liu, X., and Mitchum, M. (2024). A major role of class III HD-ZIPs in promoting sugar beet cyst nematode syncytium formation in *Arabidopsis*. *bioRxiv*. doi: 10.1101/2024.02.15.580549

Liu, J., Ding, P., Sun, T., Nitta, Y., Dong, O., Huang, X., et al. (2013). Heterotrimeric G proteins serve as a converging point in plant defense signaling activated by multiple receptor-like kinases. *Plant Physiol* 161, 2146–2158. doi: 10.1104/pp.112.212431

Liu, L., Song, W., Huang, S., Jiang, K., Moriwaki, Y., Wang, Y., et al. (2022). Extracellular ph sensing by plant cell-surface peptide-receptor complexes. *Cell* 185, 3341–3355.e13. doi: 10.1016/j.cell.2022.07.012

Lopes, F. L., Galvan-Ampudia, C., and Landrein, B. (2021). WUSCHEL in the shoot apical meristem: old player, new tricks. *J. Exp. Bot* 72, 1527–1535. doi: 10.1093/jxb/eraa572

Lu, S.-W., Chen, S., Wang, J., Yu, H., Chronis, D., Mitchum, M. G., et al. (2009). Structural and functional diversity of CLAVATA3/ESR (CLE)-like genes from the potato cyst nematode Globodera rostochiensis. *Mol. Plant-Microbe Interact* 22, 1128–1142. doi: 10.1094/MPMI-22-9-1128

Luo, Z., Lin, J., Zhu, Y., Fu, M., Li, X., and Xie, F. (2021). NLP1 reciprocally regulates nitrate inhibition of nodulation through SUNN-CRA2 signaling in medicago truncatula. *Plant Commun* 2, 100183. doi: 10.1016/j.xplc.2021.100183

Ma, D., Endo, S., Betsuyaku, E., Fujiwara, T., Betsuyaku, S., and Fukuda, H. (2022). Root-specific CLE3 expression is required for WRKY33 activation in arabidopsis shoots. *Plant Mol. Biol.* 108, 225–239. doi: 10.1007/s11103-021-01234-9

Marchive, C., Roudier, F., Castaings, L., Bréhaut, V., Blondet, E., Colot, V., et al. (2013). Nuclear retention of the transcription factor NLP7 orchestrates the early response to nitrate in plants. *Nat. Commun* 4, 1713. doi: 10.1038/ncomms2650

Meixner, C., Ludwig-Müller, J., Miersch, O., Gresshoff, P., Staehelin, C., and Vierheilig, H. (2005). Lack of mycorrhizal autoregulation and phytohormonal changes in the supernodulating soybean mutant nts1007. *Planta* 222, 709–715. doi: 10.1007/s00425-005-0003-4

Mens, C., Hastwell, A. H., Su, H., Gresshoff, P. M., Mathesius, U., and Ferguson, B. J. (2021). Characterisation of *Medicago truncatula* CLE34 and CLE35 in nitrate and rhizobia regulation of nodulation. *New Phytol* 229, 2525–2534. doi: 10.1111/nph.17010

Mishra, S., Hu, W., and DiGennaro, P. (2023). Root-knot-nematode-encoded CEPs increase nitrogen assimilation. *Life* 13, 2020. doi: 10.3390/life13102020

Mitchum, M. G., and Liu, X. (2022). Peptide effectors in phytonematode parasitism and beyond. *Annu. Rev. Phytopathol* 60, 97–119. doi: 10.1146/annurev-phyto-021621-115932

Miyazawa, H., Oka-Kira, E., Sato, N., Takahashi, H., Wu, G.-J., Sato, S., et al. (2010). The receptor-like kinase KLAVIER mediates systemic regulation of nodulation and non-symbiotic shoot development in lotus japonicus. *Development* 137, 4317–4325. doi: 10.1242/dev.058891

Morandi, D., Sagan, M., Prado-Vivant, E., and Duc, G. (2000). Influence of genes determining supernodulation on root colonization by the mycorrhizal fungus Glomus mosseae in Pisum sativum and Medicago truncatula mutants. *Mycorrhiza* 10, 37–42. doi: 10.1007/s005720050285

Moreau, C., Gautrat, P., and Frugier, F. (2021). Nitrate-induced CLE35 signaling peptides inhibit nodulation through the SUNN receptor and miR2111 repression. *Plant Physiol* 185, 1216–1228. doi: 10.1093/plphys/kiaa094

Mortier, V., Den Herder, G., Whitford, R., Van de Velde, W., Rombauts, S., D'haeseleer, K., et al. (2010). CLE peptides control *Medicago truncatula* nodulation locally and systemically. *Plant Physiol* 153, 222–237. doi: 10.1104/pp.110.153718

Müller, L. M., Flokova, K., Schnabel, E., Sun, X., Fei, Z., Frugoli, J., et al. (2019). A CLE–SUNN module regulates strigolactone content and fungal colonization in arbuscular mycorrhiza. *Nat. Plants* 5, 933–939. doi: 10.1038/s41477-019-0501-1

Müller, L. M., and Harrison, M. J. (2019). Phytohormones, miRNAs, and peptide signals integrate plant phosphorus status with arbuscular mycorrhizal symbiosis. *Curr. Opin. Plant Biol* 50, 132–139. doi: 10.1016/j.pbi.2019.05.004

Nakagami, S., Aoyama, T., Sato, Y., Kajiwara, T., Ishida, T., and Sawa, S. (2023a). CLE3 and its homologs share overlapping functions in the modulation of lateral root formation through CLV1 and BAM1 in *Arabidopsis thaliana*. *Plant J* 113, 1176–1191. doi: 10.1111/tpj.16103

Nakagami, S., Notaguchi, M., Kondo, T., Okamoto, S., Ida, T., Sato, Y., et al. (2023b). Root-knot nematode modulates plant CLE3-CLV1 signaling as a long-distance signal for successful infection. *Sci. Adv.* 9, eadf4803. doi: 10.1126/sciadv.adf4803

Nakano, M., Omae, N., and Tsuda, K. (2022). Inter-organismal phytohormone networks in plant-microbe interactions. *Curr. Opin. Plant Biol* 68, 102258. doi: 10.1016/j.pbi.2022.102258

Nishida, H., Handa, Y., Tanaka, S., Suzaki, T., and Kawaguchi, M. (2016). Expression of the CLE-RS3 gene suppresses root nodulation in Lotus japonicus. *J. Plant Res* 129, 909–919. doi: 10.1007/s10265-016-0842-z

Nishida, H., Nosaki, S., Suzuki, T., Ito, M., Miyakawa, T., Nomoto, M., et al. (2021). Different DNA-binding specificities of NLP and NIN transcription factors underlie nitrate-induced control of root nodulation. *Plant Cell* 33, 2340–2359. doi: 10.1093/plcell/koab103

Nishimura, R., Hayashi, M., Wu, G.-J., Kouchi, H., Imaizumi-Anraku, H., Murakami, Y., et al. (2002). HAR1 mediates systemic regulation of symbiotic organ development. *Nature* 420, 426–429. doi: 10.1038/nature01231

Nobori, T., Cao, Y., Entila, F., Dahms, E., Tsuda, Y., Garrido-Oter, R., et al. (2022). Dissecting the cotranscriptome landscape of plants and their microbiota. *EMBO Rep* 23, e55380. doi: 10.15252/embr.202255380

Nobori, T., Monell, A., Lee, T. A., Zhou, J., Nery, J. R., and Ecker, J. R. (2023). Time-resolved single-cell and spatial gene regulatory atlas of plants under pathogen attack. *bioRxiv*. doi: 10.1101/2023.04.10.536170

Nobori, T., Velásquez, A. C., Wu, J., Kvitko, B. H., Kremer, J. M., Wang, Y., et al. (2018). Transcriptome landscape of a bacterial pathogen under plant immunity. *Proc. Natl. Acad. Sci. U.S.A* 115, E3055–E3064. doi: 10.1073/pnas.1800529115

Noureddine, Y., Da Rocha, M., An, J., Médina, C., Mejias, J., Mulet, K., et al. (2023). AUXIN RESPONSIVE FACTOR8 regulates development of the feeding site induced by root-knot nematodes in tomato. *J. Exp. Bot* 74, 5752–5766. doi: 10.1093/jxb/erad208

Nowak, S., Schnabel, E., and Frugoli, J. (2019). The Medicago truncatula CLAVATA3-LIKE CLE12/13 signaling peptides regulate nodule number depending on the CORYNE but not the COMPACT ROOT ARCHITECTURE2 receptor. *Plant Signaling Behav* 14, 1598730. doi: 10.1080/15592324.2019.1598730

Ogawa-Ohnishi, M., Matsushita, W., and Matsubayashi, Y. (2013). Identification of three hydroxyproline O-arabinosyltransferases in arabidopsis thaliana. *Nat. Chem. Biol* 9, 726–730. doi: 10.1038/nchembio.1351

Ohyama, K., Shinohara, H., Ogawa-Ohnishi, M., and Matsubayashi, Y. (2009). A glycopeptide regulating stem cell fate in arabidopsis thaliana. *Nat. Chem. Biol* 5, 578–580. doi: 10.1038/nchembio.182

Oka-Kira, E., Tateno, K., Miura, K., Haga, T., Hayashi, M., Harada, K., et al. (2005). Klavier (klv), a novel hypernodulation mutant of lotus japonicus affected in vascular tissue organization and floral induction: Klavier, a novel hypernodulation mutant of lotus. *Plant J* 44, 505–515. doi: 10.1111/j.1365-313X.2005.02543.x

Okamoto, S., Kawasaki, A., Makino, Y., Ishida, T., and Sawa, S. (2022). Long-distance translocation of CLAVATA3/ESR-related 2 peptide and its positive effect on roots sucrose status. *Plant Physiol* 189, 2357–2367. doi: 10.1093/plphys/kiac227

Okamoto, S., Ohnishi, E., Sato, S., Takahashi, H., Nakazono, M., Tabata, S., et al. (2009). Nod Factor/Nitrate-Induced CLE genes that drive HAR1-Mediated systemic regulation of nodulation. *Plant Cell Physiol* 50, 67–77. doi: 10.1093/pcp/pcn194

Okamoto, S., Shinohara, H., Mori, T., Matsubayashi, Y., and Kawaguchi, M. (2013). Root-derived CLE glycopeptides control nodulation by direct binding to HAR1 receptor kinase. *Nat. Commun* 4, 2191. doi: 10.1038/ncomms3191

Okuma, N., Soyano, T., Suzaki, T., and Kawaguchi, M. (2020). MIR2111-5 locus and shoot-accumulated mature miR2111 systemically enhance nodulation depending on HAR1 in Lotus japonicus. *Nat. Commun* 11, 5192. doi: 10.1038/s41467-020-19037-9

Olmo, R., Cabrera, J., Díaz-Manzano, F. E., Ruiz-Ferrer, V., Barcala, M., Ishida, T., et al. (2020). Root-knot nematodes induce gall formation by recruiting developmental pathways of post-embryonic organogenesis and regeneration to promote transient pluripotency. *New Phytol* 227, 200–215. doi: 10.1111/nph.16521

Olsson, V., Joos, L., Zhu, S., Gevaert, K., Butenko, M. A., and De Smet, I. (2019). Look closely, the beautiful may be small: precursor-derived peptides in plants. *Annu. Rev. Plant Biol* 70, 153–186. doi: 10.1146/annurev-arplant-042817-040413

Potters, G., Pasternak, T. P., Guisez, Y., and Jansen, M. A. K. (2009). Different stresses, similar morphogenic responses: integrating a plethora of pathways. *Plant Cell Environ* 32, 158–169. doi: 10.1111/j.1365-3040.2008.01908.x

Redding, N. W., Agudelo, P., and Wells, C. E. (2018). Multiple nodulation genes are up-regulated during establishment of reniform nematode feeding sites in soybean. *Phytopathology* 108, 275–291. doi: 10.1094/PHYTO-04-17-0154-R

Reid, D. E., Ferguson, B. J., and Gresshoff, P. M. (2011). Inoculation- and nitrate-induced CLE peptides of soybean control NARK-Dependent nodule formation. *MPMI* 24, 606–618. doi: 10.1094/MPMI-09-10-0207

Replogle, A., Wang, J., Bleckmann, A., Hussey, R. S., Baum, T. J., Sawa, S., et al. (2011). Nematode CLE signaling in arabidopsis requires CLAVATA2 and CORYNE: Nematode CLE receptors. *Plant J* 65, 430–440. doi: 10.1111/j.1365-313X.2010.04433.x

Replogle, A., Wang, J., Paolillo, V., Smeda, J., Kinoshita, A., Durbak, A., et al. (2013). Synergistic interaction of CLAVATA1, CLAVATA2, and RECEPTOR-LIKE PROTEIN KINASE 2 in cyst nematode parasitism of Arabidopsis. *Mol. Plant-Microbe Interact* 26, 87–96. doi: 10.1094/MPMI-05-12-0118-FI

Roux, B., Rodde, N., Jardinaud, M.-F., Timmers, T., Sauviac, L., Cottret, L., et al. (2014). An integrated analysis of plant and bacterial gene expression in symbiotic root nodules using laser-capture microdissection coupled to RNA sequencing. *Plant J* 77, 817–837. doi: 10.1111/tpj.12442

Rzemieniewski, J., Leicher, H., Lee, H. K., Broyart, C., Nayem, S., Wiese, C., et al. (2022). CEP signaling coordinates plant immunity with nitrogen status. *Plant Biol*. doi: 10.1101/2022.12.20.521212

Rzemieniewski, J., and Stegmann, M. (2022). Regulation of pattern-triggered immunity and growth by phytocytokines. *Curr. Opin. Plant Biol* 68, 102230. doi: 10.1016/j.pbi.2022.102230

Sakamoto, K., and Nohara, Y. (2009). Soybean (Glycine max [L.] Merr.) shoots systemically control arbuscule formation in mycorrhizal symbiosis. *Soil Sci. Plant Nutr* 55, 252–257. doi: 10.1111/j.1747-0765.2009.00358.x

Samorodova, A. P., Tvorogova, V. E., Tkachenko, A. A., Potsenkovskaya, E. A., Lebedeva, M.A., Tikhonovich, I. A., et al. (2018). Agrobacterial tumors interfere with nodulation and demonstrate the expression of nodulation-induced CLE genes in pea. *J. Plant Physiol* 221, 94–100. doi: 10.1016/j.jplph.2017.12.005

Sasaki, T., Suzaki, T., Soyano, T., Kojima, M., Sakakibara, H., and Kawaguchi, M. (2014). Shoot-derived cytokinins systemically regulate root nodulation. *Nat. Commun* 5, 4983. doi: 10.1038/ncomms5983

Sauviac, L., Rémy, A., Huault, E., Dalmasso, M., Kazmierczak, T., Jardinaud, M., et al. (2022). A dual legume-rhizobium transcriptome of symbiotic nodule senescence reveals coordinated plant and bacterial responses. *Plant Cell Environ* 45, 3100–3121. doi: 10.1111/pce.14389

Schaarschmidt, S., Gresshoff, P. M., and Hause, B. (2013). Analyzing the soybean transcriptome during autoregulation of mycorrhization identifies the transcription factors GmNF-YA1a/b as positive regulators of arbuscular mycorrhization. *Genome Biol* 14, R62. doi: 10.1186/gb-2013-14-6-r62

Schnabel, E., Journet, E.-P., De Carvalho-Niebel, F., Duc, G., and Frugoli, J. (2005). The Medicago truncatula SUNN gene encodes a CLV1-like leucine-rich repeat receptor kinase that regulates nodule number and root length. *Plant Mol. Biol* 58, 809–822. doi: 10.1007/s11103-005-8102-y

Schnabel, E., Karve, A., Kassaw, T., Mukherjee, A., Zhou, X., Hall, T., et al. (2012). The M. truncatula SUNN gene is expressed in vascular tissue, similarly to RDN1, consistent with the role of these nodulation regulation genes in long distance signaling. *Plant Signaling Behav* 7, 4–6. doi: 10.4161/psb.7.1.18491

Schnabel, E. L., Kassaw, T. K., Smith, L. S., Marsh, J. F., Oldroyd, G. E., Long, S. R., et al. (2011). The ROOT DETERMINED NODULATION1 gene regulates nodule number in roots of Medicago truncatula and defines a highly conserved, uncharacterized plant gene family. *Plant Physiol* 157, 328–340. doi: 10.1104/pp.111.178756

Schnabel, E., Thomas, J., El-Hawaz, R., Gao, Y., Poehlman, W. L., Chavan, S., et al. (2023). Laser capture microdissection transcriptome reveals spatiotemporal tissue gene expression patterns of *medicago truncatula* roots responding to rhizobia. *Mol. Plant-Microbe Interact* 36, 805–820. doi: 10.1094/MPMI-03-23-0029-R

Schultz, J. C., Edger, P. P., Body, M. J. A., and Appel, H. M. (2019). A galling insect activates plant reproductive programs during gall development. *Sci. Rep* 9, 1833. doi: 10.1038/s41598-018-38475-6

Searle, I. R., Men, A. E., Laniya, T. S., Buzas, D. M., Iturbe-Ormaetxe, I., Carroll, B. J., et al. (2003). Long-distance signaling in nodulation directed by a CLAVATA1-like receptor kinase. *Science* 299, 109–112. doi: 10.1126/science.1077937

Segonzac, C., Nimchuk, Z. L., Beck, M., Tarr, P. T., Robatzek, S., Meyerowitz, E. M., et al. (2012). The shoot apical meristem regulatory peptide CLV3 does not activate innate immunity. *Plant Cell* 24, 3186–3192. doi: 10.1105/tpc.111.091264

Serrano, K., Bezrutczyk, M., Goudeau, D., Dao, T., O'Malley, R., Malmstrom, R. R., et al. (2024a). Spatial co-transcriptomics reveals discrete stages of the arbuscular mycorrhizal symbiosis. *Nat. Plants* 10, 673–688. doi: 10.1038/s41477-024-01666-3

Serrano, K., Tedeschi, F., Andersen, S. U., and Scheller, H. V. (2024b). Unraveling plant–microbe symbioses using single-cell and spatial transcriptomics. *Trends Plant Sci* 10, 1360–1385. doi: 10.1016/j.tplants.2024.06.008

Sexauer, M., Bhasin, H., Schön, M., Roitsch, E., Wall, C., Herzog, U., et al. (2023). A micro RNA mediates shoot control of root branching. *Nat. Commun* 14, 8083. doi: 10.1038/s41467-023-43738-6

Shen, L., and Feng, J. (2024). NIN—at the heart of NItrogen-fixing Nodule symbiosis. *Front. Plant Sci* 14. doi: 10.3389/fpls.2023.1284720

Shi, J., Wang, X., and Wang, E. (2023). Mycorrhizal symbiosis in plant growth and stress adaptation: from genes to ecosystems. *Annu. Rev. Plant Biol* 74, 569–607. doi: 10.1146/annurev-arplant-061722-090342

Siddique, S., Radakovic, Z. S., Hiltl, C., Pellegrin, C., Baum, T. J., Beasley, H., et al. (2022). The genome and lifestage-specific transcriptomes of a plant-parasitic nematode and its host reveal susceptibility genes involved in trans-kingdom synthesis of vitamin B5. *Nat. Commun* 13, 6190. doi: 10.1038/s41467-022-33769-w

Smetana, O., Mäkilä, R., Lyu, M., Amiryousefi, A., Sánchez Rodríguez, F., Wu, M.-F., et al. (2019). High levels of auxin signalling define the stem-cell organizer of the vascular cambium. *Nature* 565, 485–489. doi: 10.1038/s41586-018-0837-0

Snoeck, S., Lee, H. K., Schmid, M. W., Bender, K. W., Neeracher, M. J., Fernández-Fernández, A. D., et al. (2024). Leveraging coevolutionary insights and AI-based structural modeling to unravel receptor-peptide ligand-binding mechanisms. *Proc. Natl. Acad. Sci* 121, e2400862121. doi: 10.1073/pnas.2400862121

Song, Y., Wilson, A. J., Zhang, X.-C., Thoms, D., Sohrabi, R., Song, S., et al. (2021). FERONIA restricts pseudomonas in the rhizosphere microbiome via regulation of reactive oxygen species. *Nat. Plants* 7, 644–654. doi: 10.1038/s41477-021-00914-0

Sorin, C., Declerck, M., Christ, A., Blein, T., Ma, L., Lelandais-Brière, C., et al. (2014). A mi R 169 isoform regulates specific NF - YA targets and root architecture in A rabidopsis. *New Phytol* 202, 1197–1211. doi: 10.1111/nph.12735

Soyano, T., Hirakawa, H., Sato, S., Hayashi, M., and Kawaguchi, M. (2014). NODULE INCEPTION creates a long-distance negative feedback loop involved in homeostatic regulation of nodule organ production. *Proc. Natl. Acad. Sci* 111, 14607–14612. doi: 10.1073/pnas.1412716111

Soyano, T., Shimoda, Y., Kawaguchi, M., and Hayashi, M. (2019). A shared gene drives lateral root development and root nodule symbiosis pathways in lotus. *Science* 366, 1021–1023. doi: 10.1126/science.aax2153

Stührwohldt, N., Ehinger, A., Thellmann, K., and Schaller, A. (2020). Processing and formation of bioactive CLE40 peptide are controlled by posttranslational proline hydroxylation. *Plant Physiol* 184, 1573–1584. doi: 10.1104/pp.20.00528

Sukumar, P., Legué, V., Vayssières, A., Martin, F., Tuskan, G. A., and Kalluri, U. C. (2013). Involvement of auxin pathways in modulating root architecture during beneficial plant–microorganism interactions. *Plant Cell Environ* 36, 909–919. doi: 10.1111/pce.12036

Suzuki, R., Kanno, Y., Abril-Urias, P., Seo, M., Escobar, C., Tsai, A. Y.-L., et al. (2022). Local auxin synthesis mediated by YUCCA4 induced during root-knot nematode infection positively regulates gall growth and nematode development. *Front. Plant Sci* 13. doi: 10.3389/fpls.2022.1019427

Taleski, M., Jin, M., Chapman, K., Taylor, K., Winning, C., Frank, M., et al. (2024). CEP hormones at the nexus of nutrient acquisition and allocation, root development, and plant–microbe interactions. *J. Exp. Bot* 75, 538–552. doi: 10.1093/jxb/erad444

Tang, B., Feng, L., Hulin, M. T., Ding, P., and Ma, W. (2023). Cell-type-specific responses to fungal infection in plants revealed by single-cell transcriptomics. *Cell Host Microbe* 31, 1732–1747. doi: 10.1016/j.chom.2023.08.019

Tavormina, P., De Coninck, B., Nikonorova, N., De Smet, I., and Cammue, B. P. A. (2015). The plant peptidome: an expanding repertoire of structural features and biological functions. *Plant Cell* 27, 2095–2118. doi: 10.1105/tpc.15.00440

Tsikou, D., Yan, Z., Holt, D. B., Abel, N. B., Reid, D. E., Madsen, L. H., et al. (2018). Systemic control of legume susceptibility to rhizobial infection by a mobile microRNA. *Science* 362, 233–236. doi: 10.1126/science.aat6907

Udvardi, M., and Poole, P. S. (2013). Transport and metabolism in legume-rhizobia symbioses. *Annu. Rev. Plant Biol* 64, 781–805. doi: 10.1146/annurev-arplant-050312-120235

Verbon, E. H., Liberman, L. M., Zhou, J., Yin, J., Pieterse, C. M. J., Benfey, P. N., et al. (2023). Cell type-specific transcriptomics reveals that root hairs and endodermal barriers play important roles in beneficial plant-rhizobacterium-interactions. *Mol. Plant* 16, 1160–1177. doi: 10.1016/j.molp.2023.06.001

Wang, J., Dhroso, A., Liu, X., Baum, T. J., Hussey, R. S., Davis, E. L., et al. (2021b). Phytonematode peptide effectors exploit a host post-translational trafficking mechanism to the ER using a novel translocation signal. *New Phytol* 229, 563–574. doi: 10.1111/nph.16765

Wang, W., Hu, C., Li, X., Zhu, Y., Tao, L., Cui, Y., et al. (2021c). Receptor-like cytoplasmic kinases PBL34/35/36 are required for CLE peptide-mediated signaling to maintain shoot apical meristem and root apical meristem homeostasis in arabidopsis. *Plant Cell* 34, 1289–1307. doi: 10.1093/plcell/koab315

Wang, J., Lee, C., Replogle, A., Joshi, S., Korkin, D., Hussey, R., et al. (2010). Dual roles for the variable domain in protein trafficking and host-specific recognition of Heterodera glycines CLE effector proteins. *New Phytol* 187, 1003–1017. doi: 10.1111/j.1469-8137.2010.03300.x

Wang, X., Mitchum, M. G., Gao, B., Li, C., Diab, H., Baum, T. J., et al. (2005). A parasitism gene from a plant-parasitic nematode with function similar to CLAVATA3/ESR (CLE) of Arabidopsis thaliana. *Mol. Plant Pathol* 6, 187–191. doi: 10.1111/j.1364-3703.2005.00270.x

Wang, J., Replogle, A., Hussey, R., Baum, T., Wang, X., Davis, E. L., et al. (2011). Identification of potential host plant mimics of CLAVATA3/ESR (CLE)-like peptides from the plant-parasitic nematode heterodera schachtii: Beet cyst nematode CLEs. *Mol. Plant Pathol* 12, 177–186. doi: 10.1111/j.1364-3703.2010.00660.x

Wang, Y., Schuck, S., Wu, J., Yang, P., Döring, A.-C., Zeier, J., et al. (2018). A MPK3/6-WRKY33-ALD1-Pipecolic acid regulatory loop contributes to systemic acquired resistance. *Plant Cell* 30, 2480–2494. doi: 10.1105/tpc.18.00547

Wang, L., Sun, Z., Su, C., Wang, Y., Yan, Q., Chen, J., et al. (2019). A gmNINa-miR172c-NNC1 regulatory network coordinates the nodulation and autoregulation of nodulation pathways in soybean. *Mol. Plant* 12, 1211–1226. doi: 10.1016/j.molp.2019.06.002

Wang, C., Velandia, K., Kwon, C.-T., Wulf, K. E., Nichols, D. S., Reid, J. B., et al. (2021a). The role of CLAVATA signalling in the negative regulation of mycorrhizal colonization and nitrogen response of tomato. *J. Exp. Bot* 72, 1702–1713. doi: 10.1093/jxb/eraa539

Wopereis, J., Pajuelo, E., Dazzo, F. B., Jiang, Q., Gresshoff, P. M., de Bruijn, F. J., et al. (2000). Short root mutant of lotus japonicus with a dramatically altered symbiotic phenotype. *Plant J* 23, 97–114. doi: 10.1046/j.1365-313x.2000.00799.x

Wu, H., Qu, X., Dong, Z., Luo, L., Shao, C., Forner, J., et al. (2020a). WUSCHEL triggers innate antiviral immunity in plant stem cells. *Science* 370, 227–231. doi: 10.1126/science.abb7360

Wu, P., Shou, H., Xu, G., and Lian, X. (2013). Improvement of phosphorus efficiency in rice on the basis of understanding phosphate signaling and homeostasis. *Curr. Opin. Plant Biol* 16, 205–212. doi: 10.1016/j.pbi.2013.03.002

Wu, Q., Xu, F., Liu, L., Char, S. N., Ding, Y., Je, B. I., et al. (2020b). The maize heterotrimeric G protein β subunit controls shoot meristem development and immune responses. *Proc. Natl. Acad. Sci* 117, 1799–1805. doi: 10.1073/pnas.1917577116

Wubben, M. J., Gavilano, L., Baum, T. J., and Davis, E. L. (2015). Sequence and spatiotemporal expression analysis of CLE-Motif containing genes from the reniform nematode (rotylenchulus reniformis linford & oliveira). *J. Nematol* 47, 159–165.

Wulf, K., Sun, J., Wang, C., Ho-Plagaro, T., Kwon, C.-T., Velandia, K., et al. (2023). The role of CLE peptides in the suppression of mycorrhizal colonization of tomato. *Plant And Cell Physiol* 65, 107–119. doi: 10.1093/pcp/pcad124

Yamaguchi, Y. L., Ishida, T., and Sawa, S. (2016). CLE peptides and their signaling pathways in plant development. *J. Exp. Bot* 67, 4813–4826. doi: 10.1093/jxb/erw208

Yamaguchi, Y. L., Suzuki, R., Cabrera, J., Nakagami, S., Sagara, T., Ejima, C., et al. (2017). Root-knot and cyst nematodes activate procambium-associated genes in arabidopsis roots. *Front. Plant Sci* 8. doi: 10.3389/fpls.2017.01195

Yang, Y., Jittayasothorn, Y., Chronis, D., Wang, X., Cousins, P., and Zhong, G.-Y. (2013). Molecular characteristics and efficacy of 16D10 siRNAs in inhibiting root-knot nematode infection in transgenic grape hairy roots. *PloS One* 8, e69463. doi: 10.1371/journal.pone.0069463

Yimer, H. Z., Luu, D. D., Coomer Blundell, A., Ercoli, M. F., Vieira, P., Williamson, V. M., et al. (2023). Root-knot nematodes produce functional mimics of tyrosine-sulfated plant peptides. *Proc. Natl. Acad. Sci* 120, e2304612120. doi: 10.1073/pnas.2304612120

Yoro, E., Nishida, H., Ogawa-Ohnishi, M., Yoshida, C., Suzaki, T., Matsubayashi, Y., et al. (2019). PLENTY, a hydroxyproline O-arabinosyltransferase, negatively regulates root nodule symbiosis in Lotus japonicus. *J. Exp. Bot* 70, 507–517. doi: 10.1093/jxb/ery364

Zakaria Solaiman, M., Senoo, K., Kawaguchi, M., Imaizumi-Anraku, H., Akao, S., Tanaka, A., et al. (2000). Characterization of Mycorrhizas Formed by Glomus sp. on Roots of Hypernodulating Mutants of Lotus japonicus. *J. Plant Res* 113, 443–448. doi: 10.1007/PL00013953

Zhang, L., Hua, C., Janocha, D., Fliegmann, J., and Nürnberger, T. (2023b). Plant cell surface immune receptors-novel insights into function and evolution. *Curr. Opin. Plant Biol* 74, 102384. doi: 10.1016/j.pbi.2023.102384

Zhang, X., Peng, H., Zhu, S., Xing, J., Li, X., Zhu, Z., et al. (2020). Nematode-encoded RALF peptide mimics facilitate parasitism of plants through the FERONIA receptor kinase. *Mol. Plant* 13, 1434–1454. doi: 10.1016/j.molp.2020.08.014

Zhang, M., Su, H., Gresshoff, P. M., and Ferguson, B. J. (2021). Shoot-derived miR2111 controls legume root and nodule development. *Plant Cell Environ* 44, 1627–1641. doi: 10.1111/pce.13992

Zhang, D., Wu, Q., Zhao, Y., Yan, Z., Xiao, A., Yu, H., et al. (2023a). Dual RNA-Seq Analysis Pinpoints a Balanced Regulation between Symbiosis and Immunity in Medicago truncatula-Sinorhizobium meliloti Symbiotic Nodules. *Int. J. Mol. Sci* 24, 16178. doi: 10.3390/ijms242216178

Zhu, J., Lolle, S., Tang, A., Guel, B., Kvitko, B., Cole, B., et al. (2023). Single-cell profiling of arabidopsis leaves to pseudomonas syringae infection. *Cell Rep* 42, 112676. doi: 10.1016/j.celrep.2023.112676

frontiers | Frontiers in Plant Science

TYPE Original Research
PUBLISHED 12 November 2024
DOI 10.3389/fpls.2024.1481165

OPEN ACCESS

EDITED BY
Choong-Min Ryu,
Korea Research Institute of Bioscience and Biotechnology (KRIBB), Republic of Korea

REVIEWED BY
Rosalba Troncoso,
Centro de Investigación en Alimentación y Desarrollo A.C. (CIAD), Mexico
Romain Berruyer,
Université d'Angers, France

*CORRESPONDENCE
Jianjun Hao
jianjun.hao1@maine.edu
Xia Liu
liuxia_0213@163.com
Yanli Yang
yangyanliyyl@foxmail.com

RECEIVED 15 August 2024
ACCEPTED 24 October 2024
PUBLISHED 12 November 2024

CITATION
Deng L, Huang X, Dao J, Xu Y, Zhou K, Wang W, Liu C, Chen M, Zhang S, Zhang Y, Hao J, Liu X and Yang Y (2024) Pectinesterase activity and gene expression correlate with pathogenesis of *Phytophthora infestans*. *Front. Plant Sci.* 15:1481165. doi: 10.3389/fpls.2024.1481165

Pectinesterase activity and gene expression correlate with pathogenesis of *Phytophthora infestans*

Linmei Deng[1], Xun Huang[1], Jian Dao[1], Yajin Xu[1], Kunyan Zhou[1], Wenping Wang[1], Chunjiang Liu[1], Meng Chen[1], Shunhong Zhang[1], Yue Zhang[1], Jianjun Hao[2]*, Xia Liu[1]* and Yanli Yang[1]*

[1]Key Laboratory for Agro-biodiversity and Pest Control of Ministry of Education, College of Plant Protection, Yunnan Agricultural University, Kunming, China, [2]School of Food and Agriculture, The University of Maine, Orono, ME, United States

Late blight caused by *Phytophthora infestans* is the most devastating disease of potato. *Phytophthora infestans* produces many secondary metabolites and effector proteins, involved in the pathogenesis, which compromise host defense mechanisms. Pectinesterase (PE) is a cell wall degrading enzyme secreted by *P. infestans* to infect the host. To examine the role of PE in *P. infestans*, 15 strains of *P. infestans* were isolated from infected potato leaves in Yunnan, China. We analyzed the biological effects of exogenously added PE on *P. infestans* and its activity and gene expression after infection of potato using quantitative real-time polymerase chain reaction (RT-PCR). It was found that PE significantly promotes the growth of *P. infestans*, increases the weight of mycelium and the number of sporangia, and promotes the sporangial germination. PE accelerated the infection process of *P. infestans* on potato. The pathogenicity of *P. infestans* was positively correlated with PE activity and gene expression. PE is a key to the virulence difference of potato late blight.

KEYWORDS

potato late blight, pathogen-host interaction, gene expression, physiological race, cell wall degrading enzyme

Introduction

Potato (*Solanum tuberosum*) is one of the three top food crops in the world (Naumann et al., 2020). Due to its short growth period and strong adaptability to the environment, it has been cultivated in more than 120 countries and regions in the world. According to the Food and Agriculture Organization of the United Nations (FAO) (http://www.fao.org/), in 2021, the world's potato planted area was more than 18 million hectares, with a total yield

of 376 million tons, of which China ranked the first. Late blight caused by *Phytophthora infestans* is the most devastating disease of potato. At present, the use of chemical products and the cultivation of disease-resistant varieties are commonly used and effective means to control potato late blight (Najdabbasi et al., 2022; Rogozina et al., 2021). However, due to the adaptability of *P. infestans* to environmental changes, new physiological races are continuously evolving, resulting in the loss of variety resistance and difficulty in disease control (Ivanov et al., 2021). *Phytophthora infestans* produces many secondary metabolites and effector proteins to deactivate the host's defense while infecting the host, thereby promoting infection (Yang et al., 2021; Li et al., 2020), which is common in many other plant pathogens (Kubicek et al., 2014).

Pectinase is an enzyme complex that consists of several different types of enzymes that collectively act on pectin, a polysaccharide found in plant cell walls. The primary compounds or types of enzymes that make up pectinase includes polygalacturonase, pectin methylesterase, and pectin lyase. These compounds are cell-wall-degrading enzymes secreted by plant pathogens during host infection and are pathogenicity factors (Bravo et al., 2016). Pectinesterase (PE) is one of the crucial cell wall degrading enzymes secreted by plant pathogens, including pathogenic fungi, oomycetes and bacteria (Xue et al., 2018). In 1979, Krátká and Veselý (1979) first detected the activity of PE from *Pythium ultimum*, *Pythium oligandrum* and *Pythium debaryanum*. Several decades later, Ospina-Giraldo et al. (2010) found highly complex CAZy homologs in the genomes of *P. infestans*, *P. sojae*, and *P. ramorum*. A large number of CAZy homologs play an important role in pathogenicity by participating in the degradation of plant cell walls. respectively, of which pectinase accounted for about 25% (Blackman et al., 2014). Since then, this gene has been further investigated in it roles. Pectinesterase has also been studied in *P. infestans*, it can contribute to the breakdown of plant tissues, which can facilitate infection by degrading pectin (Sabbadin et al., 2021). Research into pectinesterase in *P. infestans* often focuses on understanding how the enzyme helps the pathogen invade and colonize host plants. The enzyme's activity can be crucial for the pathogen's ability to overcome plant defenses and establish an infection, but requires further investigations. The objective of this study was to investigate the effects of exogenous addition of PE on *P. infestans* and its infection of potato, and to clarify the role of PE activity and expression in the pathogenesis of *P. infestans*. The outcome would provide foundation for understanding plant-host interactions and advancing plant breeding efforts.

Materials and methods

Effects of PE on *P. infestans in vitro*

A total of 15 strains of *P. infestans* with different pathogenicity were isolated from potato leaves showing late blight symptoms in Yunnan, China (Table 1). The pathogenicity data in the table were determined according to method of detached-leaf inoculation (Raza et al., 2019) in the early stage. For pathogen inoculation, compound leaves from the top to the third leaf position were chosen from potato 'S88' grown for 45 days. PE (30,000 U/g, Yien Chemistry, Shanghai, China), derived from *Aspergillus niger*, was initially dissolved in 99.7% ethanol subsequently diluted with ddH_2O to achieve a final concentration of 1,000 U/mL PE, containing 0.1% ethanol, which was used as a stock solution for later use.

TABLE 1 Measurement of disease lesion on potato leaves inoculated with different strains of *Phytophthora infestans*.

Strain	Location of isolation	Virulence	Lesion area (%)
HS03	Huize	Weak	3.77 ± 4.25h
JCZ29	Huize	Weak	10.42 ± 3.67gh
HZ02	Huize	Weak	12.66 ± 4.90g
HS02	Huize	Weak	19.79 ± 3.86f
DSPQ006	Dali	Medium	20.04 ± 3.28f
MLS13418-2	Malong	Medium	23.79 ± 7.9f
DQ01	Diqing	Medium	38.46 ± 6.89e
MLS8802	Malong	Medium	48.49 ± 7.36d
NLL605	Lijiang	Medium	56.27 ± 3.17c
HJG02	Dali	Strong	60.43 ± 5.22c
LJ04	Lijiang	Strong	61.49 ± 6.08c
XDL601	Xundian	Strong	64.36 ± 16.65c
ZTQ907	Zhaotong	Strong	70.63 ± 10.42b
DL04	Dali	Strong	76.26 ± 5.66b
ML01-2018	Malong	Strong	90.10 ± 6.44a

Different letters indicate significant differences between treatments ($p < 0.05$).

In a petri plate, rye tomato agar (Qian et al., 2021) was amended with PE stock solution at series of concentrations including 0, 10, 100, and 1,000 U/mL. Four strains of *P. infestans* (HZ02, DL04, HJG02, and ML01-2018) was inoculated onto the plate and grown for 8 days of incubation at 19 °C in the dark. The colony diameter was measured perpendicularly on days 4, 6, and 8. Mycelia were scraped off from the plate and weighed, and then homogenized with water. Sporangia were counted using a hemocytometer. According to the method of Zhu et al. (2015), DL04 sporangia suspension was mixed with different concentrations of PE solution at a ratio of 1:1 to prepare a sporangia suspension containing 8,000 sporangia per mL and various concentrations of PE. Five microliters were pipetted onto the concave slide, and the cover glass was placed in a dark incubator at 19°C for 48 h. Both zoosporic and sporangial germinations were observed under a biomicroscope (E200MV, Nikon, Nanjing, China). Each treatment contained three replicates.

Effect of PE on *P. infestans* in planta

The mycelia of *P. infestans* DL04 and HJG02 cultured for 10 days were collected using toothpicks, and ground with sterilized water in a mortar with pestle. The sporangium was obtained by filtration through a 300-mesh filter. The sporangia were transferred into 100 U/mL or 1,000 U/mL PE solutions and adjusted to a

concentration of 8,000 sporangia per mL, which were used as inocula. According to method of detached-leaf inoculation (Raza et al., 2019), compound potato leaves were cut from the third leaf position and washed three times using sterilized water. Potato tubers were cut into one centimeter disks. Each leaf and tuber was a replicate with six replicates per treatment. Both the leaves and tuber disks were placed on 0.8% water agar. The *P. infestans*-PE mixture (25 µL) was inoculated onto both sides of the leaf or the center of the tuber disk. Inoculation of sporangium suspension was used as control. One day after the inoculation, the leaves were flipped over and placed in an incubator set to a 12 h light/dark cycle at 19 °C, along with the tuber disk. Disease was evaluated three days after the treatment. The ratio of leaf and tuber lesion area to total leaf and tuber area was used to evaluate the incidence of the disease.

Measurement of PE activity

Enzymatic analysis was performed using a pectinesterase kit (Suzhou Grace Biotechnology Co., Ltd., Suzhou, China) to determine the enzymatic activity of *P. infestans* strains and infected potato leaves. Briefly, 0.15 g *P. infestans* mycelia were ground with 1.5 mL of the pectinesterase kit in a mortar with a pestle in an ice bath and centrifuged at 12,000 g at 4°C for 15 min. An aliquot of 1 mL of the supernatant was transferred into a centrifuge tube, and 25 µL of reagent 2 and 4 mL of reagent 1 were added in order and mixed well. Subsequently, reagent 3 was added to adjust pH to 7.8 (pink). The tubes were incubated at 37°C in a water bath for 60 min. The pH was maintained to 7.8 (pink) with reagent 4 every 20 minutes. At the same time, the volume V2 (mL) of the consumed reagent 4 was recorded. PE activity (µmoL/min/g) was calculated as = 30 × V2 ÷ W × D (V2: the amount of reagent 4 consumed by titration; D: sample dilution factor; W: sample weight) (Wang et al., 2023).

Cloning and real-time absolute quantification of the PE gene *pipme1* in *P. infestans*

The DNA of each *P. infestans* strain was extracted using the Ezup Column Fungal Genomic DNA Extraction Kit (B518259, Sangon Biotech, Shanghai, China). DNA quality was examined on a 1.5% agarose gel using electrophoresis. Pectinesterase nucleotide sequence (XM_ 002907416.1) was used as a template. Polymerase chain reaction (PCR) was performed using the primer pair for *pipme1*: Pipme1-F1 (5' CGGTGTCGGAAGGGGTAG 3') and Pipme1-R1 (5' TAAGCAGCAGCGTGGTCG 3'). The PCR reaction was prepared in a 25 µL system, containing 2 µL of 10X PCR buffer, 0.5 µL of primer F (10 µM), 0.5 µL of primer R (10 µM), 0.5 µL of dNTP (10 mM), 2 µL of MgCl2 (25 mM), 0.5 µL of Taq Plus DNA Polymerase (5 U/µL), 2 µL of DNA, and 17 µL of ddH_2O. The thermal cycler conditions were as follows: pre-denaturation at 95°C for 3 min, 35 cycles of denaturation at 95°C for 30 s, annealing at 57°C for 30 s, and extension at 72°C for 30 s, followed by a final extension at 72°C for 8 min. The PCR products were examined through 1.5% agarose gel using electrophoresis and the target band was cut off and recovered with SanPrep column DNA gel recovery kit (B518259, Sangon Biotech, Shanghai, China).

The PCR product was ligated with the pMD ® 18-T vector (1000328, TAKARA, Dalian, China). An aliquot of 5 µL of ligation high Solution I, 0.2 µL of pMD ® 18-T vector, 4.8 µL of PCR product, and total volume were combined. After one hour of ligation at 16°C, the resulting product was transformed using the One-step Rapid Competent Cell Preparation Kit (B529307, Sangon Biotech, Shanghai, China). Subsequently, the plasmid was extracted using a SanPrep column plasmid DNA small extraction kit (B518191, Sangon). The constructed plasmid was confirmed by DNA sequencing. The value of plasmid OD_{260} was measured using a microspectrophotometer and converted into copy number (copies/µL).

The standard curve of plasmids were constructed by 10-fold gradient dilution, including 90 µL diluent and 10 µL plasmid. The product was added into X SG Fast qPCR Master Mix (B639271, BBI, Roche, Rotkreuz, Switzerland), and analyzed using quantitative PCR on a LightCycler480 II fluorescence quantitative PCR instrument (Roche, Rotkreuz, Switzerland). The 10 µL PCR reaction mixture included 5 µL of 2X SybrGreen qPCR Master Mix, 0.2 µL of 10 µM primer F, 0.2 µL 10 µM R, 3.6 µL of ddH_2O, 1.0 µL of DNA. The thermal cycle was 95°C 3min, 95°C 15 s, 60°C 30 s, 45 cycles. The products were placed in a 96-well plate and incubated in LightCycler480 II. After the reaction, the exact copies of *pipme1* gene in *P. infestans* was calculated according to the regression equation established by the standard curve.

RNA extraction from potato leaves infected by *P. infestans* and reverse transcription

Sporangial suspension of *P. infestans* was inoculated on both sides of potato leaves, and the diseased parts of potato leaves were collected at 0, 12, 24, 36, 48, 60, and 72 h after inoculation, respectively, and frozen in liquid nitrogen and stored at -80°C. RNA was extracted using the UNIQ-10 column Trizol total RNA extraction kit (B511321, Sangon Biotech, Shanghai, China). The integrity and purity of RNA were determined using 1% agarose gel electrophoresis and the ultraviolet spectrophotometer (SMA4000, Merinton Instrument, Inc. Beijing, China). A total of 1200 ng of total RNA was added to the nuclease-free PCR tube on ice, with 1 µL Random Primer p $(dN)_6$ (100 pmol), 1 µL dNTP Mix (0.5 mM final concentration), and RNase-free ddH_2O to bring the volume up to 14.5 µL. The mixture was gently mixed and briefly centrifuged for 3 to 5 s. The reaction mixture was incubated at 65°C for 5 min, ice bathed for 2 min, and centrifuged for 3 to 5 s. A test tube was placed in an ice bath, then 4 µL 5X RT Buffer, 0.5 µL Thermo Scientific RiboLock RNase Inhibitor (20 U), and 1 µL Maxima Reverse Transcriptase (200 U) were added. The tube was gently shaken and centrifuged for 3 to 5 s. A reverse transcription reaction was carried out on a PCR instrument. The obtained cDNA template was used for subsequent expression analysis.

Real-time relative quantification of *pipme1*

Fluorescence quantitative PCR was performed using cDNA as the template, with the actin housekeeping gene as the target for amplification. PCR primers were actin-F2 (5' TGCCTGATGGACAAGTTATTACC 3') and actin-R2 (5' CCACTGAGCACAATGTTACCG 3'). Fluorescence quantitative real-time PCR (RT-qPCR) was performed using 2X SG Fast qPCR Master Mix (B639271, BBI, Roche) on a LightCycler 480 II fluorescence quantitative PCR instrument. The reaction mixture contained 1.0 µL cDNA, 5 µL SYBR Green qPCR Master Mix, and 0.2 µL 10 µmol/L primers, and 3.6 µL RNase-free water. The thermal cycle consistent with the above. The relative quantitation of gene expression between samples was analyzed using the $2^{-\Delta\Delta CT}$ method (Livak and Schmittgen, 2001), comparing the cycle threshold (CT) values of the housekeeping gene *actin* and the CT value of the *pipme1* gene.

Statistical analysis

SPSS version 17.0 software (SPSS Inc., Chicago, IL) and Prism 7.0 software (GraphPad Inc., USA) were used for general statistical analyses. The normality of distribution and homogeneity of variance were evaluated before statistical analysis was conducted. Mean separation among treatments was analyzed by oneway analysis of variance and Duncan's multiple range test ($p < 0.05$).

Results

Effects of PE on *P. infestans in vitro*

Mycelial weight, sporangia concentration, and spore germination of four strains of *P. infestans* were measured on a PE-amended agar medium. Results showed that PE increased the growth of *P. infestans* to various degrees (Figure 1). PE at 10 U/mL significantly increased the weight of mycelia of ML01-2018 and HJG02 (Figure 1E). PE at 10 U/mL significantly increased the number of sporangia of all four strains (Figure 1F). PE at 10 U/mL and 500 U/mL significantly promoted the sporangial germination but not zoosporic germination of strain DL04 (Figure 1G). Therefore, PE promotes the growth of *P. infestans*, increases the weight of mycelium, the number of sporangia, and promotes the sporangial germination of *P. infestans* under certain conditions.

PE accelerated *P. infestans* infection on potato leaves and tubers

Compared with the control, the central lesion area on potato leaves and tubers, inoculated with strains DL04 and HJG02, was largest after adding 1,000 U/mL PE solution, indicating that a high concentration of PE can accelerate the infection of the leaf by *P. infestans* (Figure 2). However, this result was not observed at a lower PE concentration (100 U/mL). It is speculated that the pathogenicity of the two strains may be relatively strong, and they can secrete PE themselves. A low concentration of PE is not sufficient to produce a significant infection. It indicated a low concentration of PE had no promoting effect on the infection of potato leaves and tubers by *P. infestans*.

Measurement of PE activity

There were significant differences in PE activity among different *P. infestans* strains after 8 d of culture. Combining with pathogenicity, it was found that ML01-2018 had the strongest pathogenicity, followed by DL04, HJG02 and MLYWS8802; while HZ02 and HS03 had the weakest pathogenicity (Figure 3A), the results of PE activity were consistent with the pathogenicity. The correlation between PE activity and pathogenicity of six *P. infestans* was analyzed by Pearson (Supplementary Table S1). There were high positive correlations between the PE activity and pathogenicity of *P. infestans*, the *r* value was 0.94, the linear equation was y = 0.5089x - 8.014 ($R^2 = 0.88$, $p = 0.006$), the difference was highly significant ($p < 0.01$). It indicating that *P. infestans* with high PE activity had strong pathogenicity (Figure 3B).

The enzymatic activity in potato leaves inoculated with DL04 and HZ02 was determined at different time points (Figure 3C). The enzymatic activity increased with the extension of infection time and decreased after reaching the highest point. The enzymatic activity of DL04 was highest at 24 h after infection, and that of HZ02 was highest at 48 h after infection. The enzymatic activity of DL04 was significantly higher than that of HZ02 at 24 h and 72 h after infection, which was consistent with the pathogenicity results. It indicated that the activity of PE could affect the pathogenicity of *P. infestans* to potato leaves.

Pipme1 expression in *P. infestans*

PE genes were expressed in different pathogenic strains, and the expression levels of the gene product were significantly different. The gene product level of HS03 and JCZ29 was the lowest (Figure 4), while the pathogenicity of four strains of *P. infestans* isolated from Huize, including HS03 and JCZ29, was consistently low. The *pipme1* gene product level of *P. infestans* varied depending on the region of isolation. The level of gene product was in the order from high to low: HS03 (Huize) < MLS13418 (Malong) < LJ04 (Lijiang) < ZTQ907 (Zhaotong) < DQ01 (Diqing). The level of *P. infestans* gene products isolated from the same region was also different. The *pipme1* expression of *P. infestans* strains from Huize varied from high to low: HS03 < JCZ29 < HS02 < HZ02. The level of PE gene product in the strains with strong pathogenicity in the test materials was relatively high. The level of ML01-2018 gene product was higher than that of DL04, HJG02, MLYWS8802, while HZ02 and HS03 had the lowest level, which was consistent with the results of the enzyme activity assay. The correlation between copies of *pipme1* DNA and pathogenicity of 15 strains of *P. infestans* was analyzed (Supplementary Table S2). There were positive correlations between the DNA copies of the pectinesterase gene *pipme1* and pathogenicity, the *r* value was 0.65, the linear equation was y = 0.01x + 10.20 ($R^2 = 0.42$; $p = 0.009$), the difference was highly

10.3389/fpls.2024.1481165

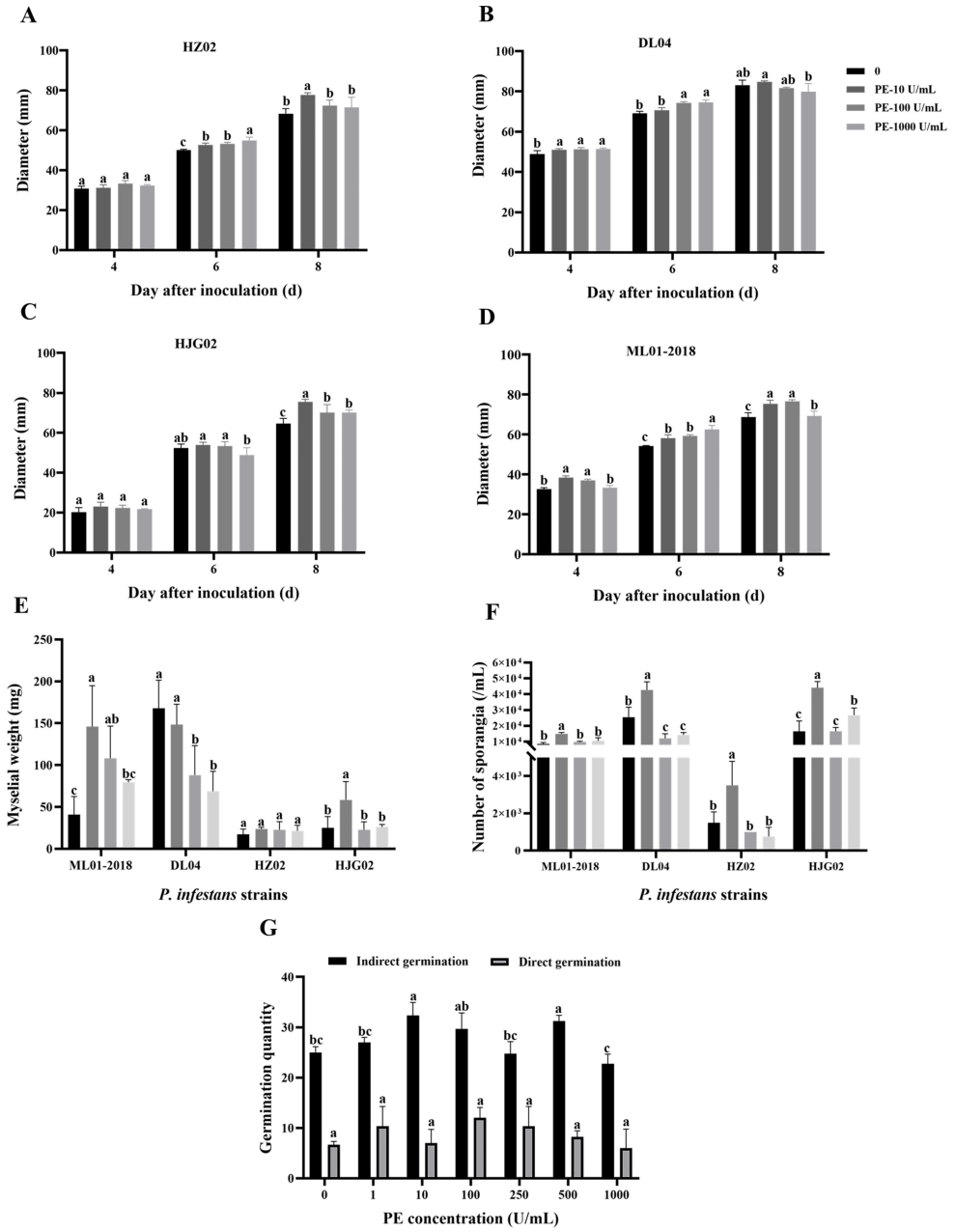

FIGURE 1
Effects of exogenous addition of pectinesterase (PE) at various concentrations on the colony size of *Phytophthora infestans* strains HZ02 **(A)**, DL04 **(B)**, HJG02 **(C)**, and ML01-2018 **(D)**, mycelial weight of the four strains **(E)**, sporangial production of the four strains **(F)**, and spore germination of DL04 **(G)**. Different letters on the bars indicate significant differences between treatments ($p < 0.05$).

significant ($p < 0.01$). It indicating that the expression of the pectinesterase gene *pipme1* could affect the pathogenicity of *P. infestans* to potato leaves.

Pipme1 expression in potato leaves infected by *P. infestans*

The level of PE gene product was determined using fluorescence quantitative PCR in potato leaves infected by *P. infestans* after 0 h, 12 h, 24 h, 36 h, 48 h, 56 h and 72 h. The level of *pipme1* product in HZ02 and DL04 increased with the extension of infection time, which was consistent with the pathogenicity test (Figure 5). There was a significant difference in gene product level between HZ02 and DL04 at the same time point after infection. The expression levels of the genes were consistent across different strains. After 48 hours of infection with HZ02, the *pipme1* gene expression was observed, and the expression level increased significantly, reaching the highest at 72 hours post inoculation. The *pipme1* of DL04 began to express at 24 h after infection, and the expression level increased significantly, reaching the highest at 56 h post inoculation. Although the two strains had the same trend of *pipme1* expression after infection, the

10.3389/fpls.2024.1481165

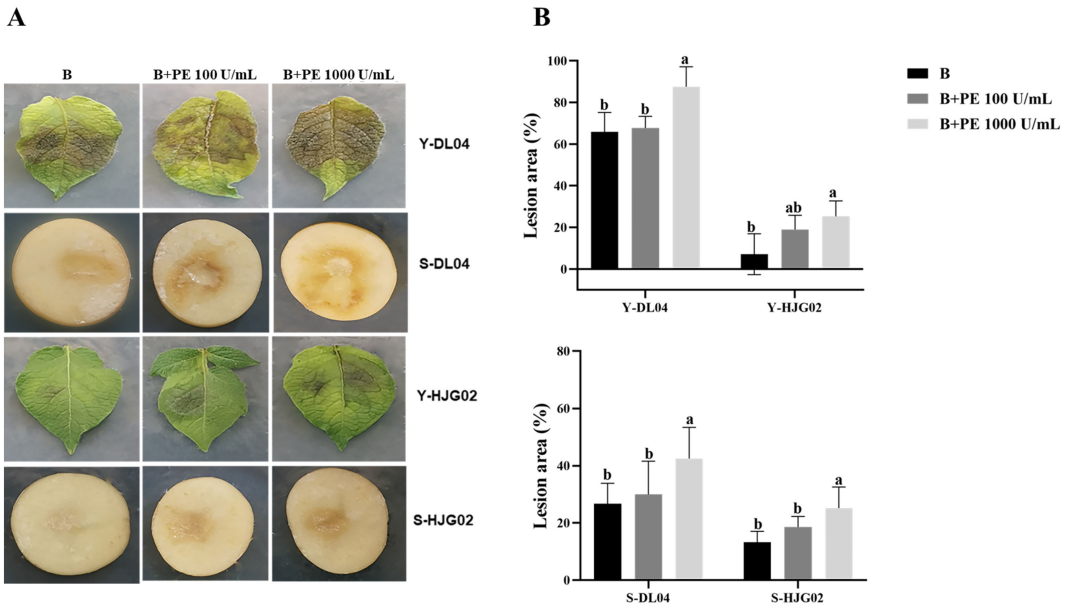

FIGURE 2
Effects of pectinesterase (PE) treatment and *Phytophthora infestans* DL04 and HJG02 inoculation on potato leaves and tubers. **(A)** Visualization of potato leaf and tuber inoculation; **(B)** Lesion area of infected potato leaves and tubers. B: sporangial suspension of *P. infestans* at 8,000/mL, Y: leaf, S: tuber. Different letters on the bars indicate significant differences between treatments ($p < 0.05$).

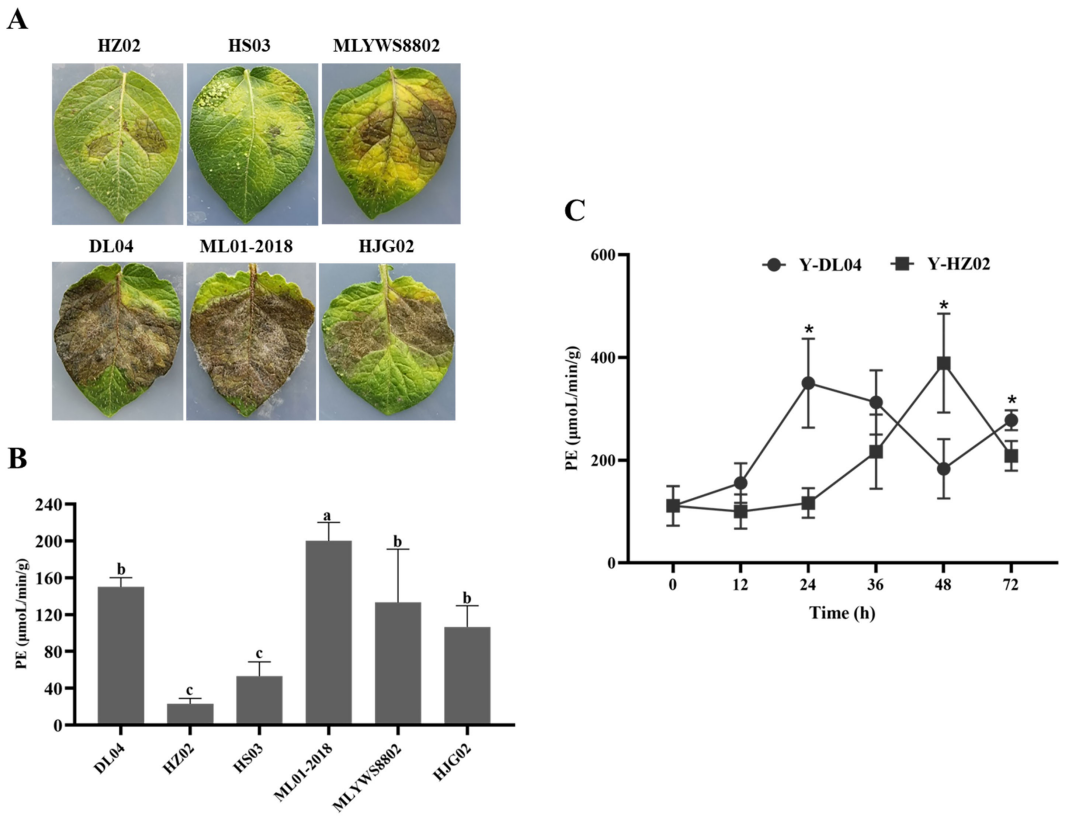

FIGURE 3
Infection of potato leaves inoculated with *Phytophthora infestans* strains HZ02, DL04, HS03, ML01-2018, MLYWS8802, and HJG02 **(A)**, activities of pectinesterase (PE) in *P. infestans* **(B)**, and enzymatic activities of PE in potato leaves infected by *P. infestans* DL04 and HZ02 **(C)**. Different letters on the bars and the asterisks on the line chart indicate significant differences between treatments ($p < 0.05$).

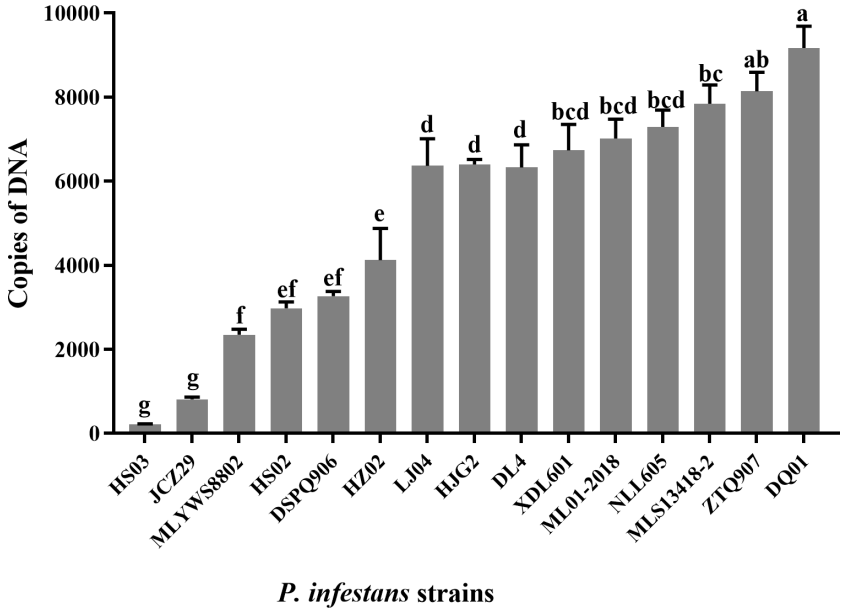

FIGURE 4
Expression levels (copies of DNA) of the pectinesterase gene in *Phytophthora infestans* strains. Different letters on the bars indicate significant differences between treatments ($p < 0.05$).

expression patterns were different. Therefore, the gene expression of DL04 strain with strong pathogenicity was faster than that of HZ02, indicating that the gene was a major factor leading to the pathogenic difference and the speed of leaf disease development.

Discussion

Plant pathogenic fungi produce multiple cell wall-degrading enzymes, which aid in degrading host cell walls to obtain essential nutrients and facilitate pathogen invasion and colonization, contributing to pathogenicity in plant tissues (Ramezani et al., 2019; Kikot et al., 2009). This activity is a crucial criterion for determining their pathogenicity and defining the infection or pathogenicity of plant pathogens (Esquerre-Tugaye et al., 2000). A higher enzymatic activity correlates with increased pathogenicity in the pathogen (Gawade et al., 2017; Joshi, 2018). Studies have shown that cell wall-degrading enzyme activities vary in *Macrophomina phaseolina* depending on the strains infecting corn, sunflower, and watermelon seeds, leading to different pathogenicity (Ramos et al., 2016). This has also been confirmed in *Colletotrichum gloeosporioides* infecting coffee trees (Armesto et al., 2019) and *Colletotrichum oxysporum* causing rubber tree anthracnose (Fernando et al., 2001). In *Heterobasidion annosum* (Johansson, 1988) and *Pellicularia filamentosa* (Mwenje and Ride, 1997), the pathogenicity is directly related to the activity of their pectinases. By measuring the enzymatic activity in *P. infestans* and *P. infestans*-

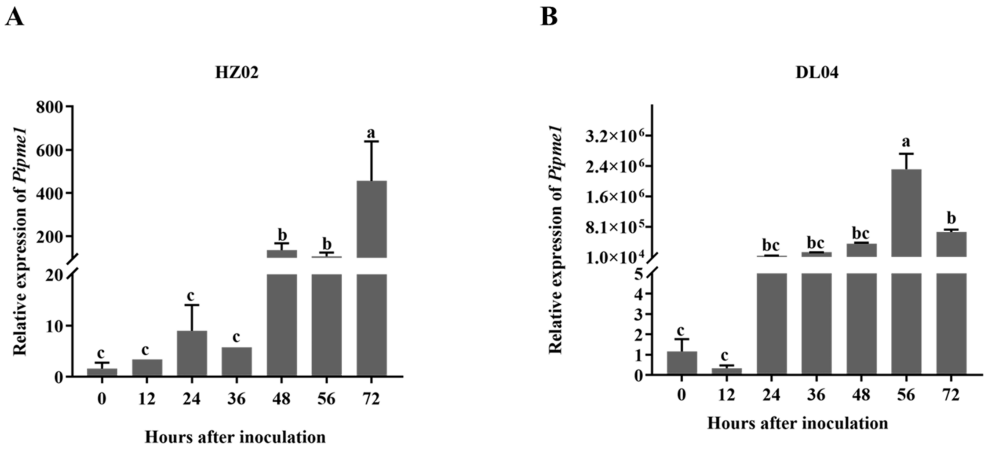

FIGURE 5
Expression of the pectinesterase gene *pipme1* in potato leaves infected by *Phytophthora infestans* strains HZ02 **(A)** and DL04 **(B)**. Different letters on the bars indicate significant differences between treatments ($p < 0.05$).

infected potatoes, we have found that the PE activity is positively correlated with pathogenicity but significantly varied depending on *P. infestans* strains. With the extension of infection time, the PE activity of DL04 was significantly higher than that of HZ02 at 24 h and 72 h. These indicate that pectinesterase activity correlates with pathogenesis of *P. infestans*. Pectinase plays an important role in the early pathogenesis of pathogens (Dallai et al., 2016). For example, the pectin methylesterase *Pcpme6* of *P. capsici* exhibits strong virulence and diversity of transcription when infecting different hosts (Feng et al., 2010). The pectin lyases can induce plant cell death, with *PcPL1*, *PcPL16*, and *PcPL20* being the most aggressive (Fu et al., 2015). Pectin acetylesterase *PlPAE5* of *Peronophythora litchii* plays an significant role in the infection process (Kong et al., 2019). Furthermore, the expression levels of four PG genes vary at different infection stages shown in *C. gloeosporioides* (Jing et al., 2024). In this study, the level of the PE gene *pipme1* expression in *P. infestans* varies significantly with pathogenicity. The expression pattern of *pipme1* after infection is associated with the pathogenicity level, indicating that this gene plays an important role in the progression of late blight. More and more genetic methods are used to study pathogenic factors. The pathogenicity of *Botrytis cinerea* was significantly reduced by knocking out the pectin methylesterase *Bcpme1* gene (Valette-Collet et al., 2003). *Alternaria citri* and *Alternaria alternata* produce polygalacturonases with similar physiological and biochemical characteristics. Knockout of the highly homologous *Acpg1* significantly reduced the pathogenicity of the pathogen, indicating that the virulence of polygalacturonases to the pathogen is related to different pathogenic methods (Isshiki et al., 2001). The site of action will be determined by subcellular localization, and the mechanism of action will be investigated using gene knockout or gene silencing techniques in our future work.

Although PE has been identified as a key factor in the pathogenesis of *P. infestans*, the pathogenesis is complex, because PE is likely one of several cell wall-degrading enzymes contributing to this process (Ramos et al., 2010). Kagda et al. (2020) found that the invertase expression during leaf infection was linked to a decline in apoplastic sucrose, consistent with a role of the enzymes in plant pathogenesis. Hu et al. (2007) found that the mutation of the cellulase gene *eglXoB* in the *Xanthomonas oryzae* pv. *oryzae* PXO99A strain resulted in a decrease in the virulence of the pathogen by about 87% compared to the wild type. Zou et al. (2012) identified the only extracellular protease EcpA from Xoc RS105 strain. After *ecpA* mutation, the protease activity of the strain was completely lost, and the pathogenicity was also significantly reduced compared with the wild type. Hsiao et al. (2010) found that the mannanase activity of Xcc Xc17 strain was completely lost after the mutation of endo-β-mannanase *manA* gene.In this study, we solely focused on PE, excluding other cell wall-degrading enzymes. Therefore, the roles of these enzymes in the pathogenesis of *P. infestans* and their interaction mechanisms require further investigation (Oeser et al., 2002). Further analysis of the redundancy within the multi-gene family will aid in identifying the specificity of different members and exploring their roles in the pathogen-host interactions.

PE can promote the biological characteristics of *P. infestans* and accelerate the infection of *P. infestans* on potato. The pathogenicity of *P. infestans* is related to the enzymatic activity of PE and the expression level of gene *pipme1*. The higher the enzymatic activity and the higher the expression level, the stronger the pathogenicity. Therefore, the pectinesterase activity and expression correlates with pathogenesis of *P. infestans*.

Data availability statement

The original contributions presented in the study are included in the article/Supplementary Material. Further inquiries can be directed to the corresponding authors.

Author contributions

LD: Writing – original draft, Formal analysis, Data curation, Conceptualization. XH: Writing – original draft, Methodology, Investigation. JD: Writing – original draft, Visualization, Resources. YX: Writing – original draft, Investigation, Data curation. KZ: Writing – original draft, Validation, Data curation. WW: Writing – original draft, Validation, Software. CL: Writing – original draft, Resources, Investigation. MC: Writing – original draft, Methodology, Investigation. SZ: Writing – original draft, Investigation. YZ: Writing – original draft, Formal analysis. JH: Writing – review & editing, Data curation. XL: Writing – review & editing, Resources, Project administration, Funding acquisition. YY: Writing – review & editing, Supervision, Project administration.

Funding

The author(s) declare financial support was received for the research, authorship, and/or publication of this article. This work was supported by the Modern Agricultural Potato Industry Technology System in Yunnan Province (2023KJTX004), the Major Science and Technology Projects in Yunnan Province (202402AE090017), the Bian Chunsong Expert Workstation in Yunnan Province (202205AF150053).

Conflict of interest

The authors declare that the research was conducted in the absence of any commercial or financial relationships that could be construed as a potential conflict of interest.

Publisher's note

Supplementary material

The Supplementary Material for this article can be found online at: https://www.frontiersin.org/articles/10.3389/fpls.2024.1481165/full#supplementary-material

References

Armesto, C., Maia, F. G., Monteiro, F. P., and Abreu, M. S. (2019). Exoenzymes as a pathogenicity factor for Colletotrichum gloeosporioides associated with coffee plants. *Summa Phytopathol.* 45, 368–373. doi: 10.1590/0100-5405/191071

Blackman, L. M., Cullerne, D. P., and Hardham, A. R. (2014). Bioinformatic characterisation of genes encoding cell wall degrading enzymes in the *Phytophthora parasitica* genome. *BMC Genom.* 15, 785. doi: 10.1186/1471-2164-15-785

Bravo, R. G., Di Pietro, A., and Roncero, M. I. (2016). Combined action of the major secreted exo- and endopolygalacturonases is required for full virulence of *Fusarium oxysporum*. *Mol. Plant Pathol.* 17, 339–353. doi: 10.1111/mpp.12283

Dallai, R., Paoli, F., Mercati, D., and Lupetti, P. (2016). The centriole adjunct of insects: Need to update the definition. *Tissue Cell* 48, 104–113. doi: 10.1016/j.tice.2016.02.001

Esquerre-Tugaye, M. T., Boudart, G., and Dumas, B. (2000). Cell wall degrading enzymes, inhibitory proteins and oligosaccarides participate in the molecular dialogue between plants and pathogens. *Plant Physiol. Biochem.* 38, 157–163. doi: 10.1016/S0981-9428(00)00161-3

Feng, B. Z., Li, P. Q., Wang, H. M., and Zhang, X. G. (2010). Functional analysis of *pcpme6* from oomycete plant pathogen *Phytophthora capsici*. *Microb. Pathog.* 49, 23–31. doi: 10.1016/j.micpath.2010.03.004

Fernando, T. H. P. S., Jayasinghe, C. K., and Wijesundera, R. L. C. (2001). Cell wall degrading enzyme secretion by *Colletotrichum acutatum* the causative fungus of secondary leaf fall of Hevea brasiliensis. *Mycological Res.* 105, 195–201. doi: 10.1017/S0953756200003324

Fu, L., Zhu, C. Y., Ding, X. M., Yang, X. Y., Morris, P. F., Tyler, B. M., et al. (2015). Characterization of Cell-Death-Inducing members of the pectate lyase gene family in *Phytophthora capsici* and their contributions to infection of pepper. *Mol. Plant Microbe Interact.* 28, 766–775. doi: 10.1094/MPMI-11-14-0352-R

Gawade, D. B., Perane, R. R., Suryawanshi, A. P., and Deokar, C. D. (2017). Extracellular enzymes activity determining the virulence of *Rhizoctonia bataticola*, causing root rot in soybean. *Physiol. Mol. Plant P.* 100, 49–56. doi: 10.1016/j.pmpp.2017.06.003

Hsiao, Y. M., Liu, Y. F., Fang, M. C., and Tseng, Y. H. (2010). Transcriptional regulation and molecular characterization of the *manA* gene encoding the biofilm dispersing enzyme mannan *endo*-1,4-β-mannosidase in *Xanthomonas campestris*. *J. Agric. Food Chem.* 58, 1653–1663. doi: 10.1021/jf903637s

Hu, J., Qian, W., and He, C. Z. (2007). The *Xanthomonas oryzae* pv. *oryzae eglXoB* endoglucanase gene is required for virulence to rice. *FEMS Microbiol. Lett.* 269, 273–279. doi: 10.1111/j.1574-6968.2007.00638.x

Isshiki, A., Akimitsu, K., Yamamoto, M., and Yamamoto, H. (2001). Endopolygalacturonase is essential for citrus black rot caused by *Alternaria citri* but not brown spot caused by Alternaria alternata. *Mol. Plant-Microbe interactions: MPMI* 14, 749–757. doi: 10.1094/MPMI.2001.14.6.749

Ivanov, A. A., Ukladov, E. O., and Golubeva, T. S. (2021). *Phytophthora infestans*: An overview of methods and attempts to combat late blight. *J. Fungi* 7, 1071. doi: 10.3390/jof7121071

Jing, M. J., Yang, C. D., Li, T. H., Richard, O. S. E. I., Cai, F. F., and Ma, T. (2024). The role of cell wall degrading enzymes of *colletotrichum coccodes* during its infection. *Plant Prot.* 50, 88–98. doi: 10.16688/j.zwbh.2023263

Johansson, M. (1988). Pectic enzyme activity of spruce (S) and pine (P) strains of *Heterobasidion annosum* (Fr) Bref. *Physiol. Mol. Plant Pathol.* 33, 333–349. doi: 10.1016/0885-5765(88)90002-1

Joshi, R. (2018). A Review on *Colletotrichum* spp. Virulence mechanism against host plant defensive factors. *J. Medicinal Plants Stud.* 6, 64–67. doi: 10.22271/PLANTS.2018.V6.I6B.02

Kagda, M. S., Martínez-Soto, D., Ah-Fong, A. M. V., and Judelson, H. S. (2020). Invertases in *phytophthora infestans* localize to haustoria and are programmed for infection-specific expression. *mBio* 11, e01251–e01220. doi: 10.1128/mBio.01251-20

Kikot, G. E., Hours, R. A., and Alconada, T. M. (2009). Contribution of cell wall degrading enzymes to pathogenesis of *Fusarium graminearum*: a review. *J. Basic Microbiol.* 49, 231–241. doi: 10.1002/jobm.200800231

Kong, G. H., Wan, L., Deng, Y. Z., Yang, W. S., Li, W., Jiang, L. Q., et al. (2019). Pectin acetylesterase *PAE5* is associated with the virulence of plant pathogenic oomycete *Peronophythora litchii*. *Physiol. Mol. Plant P.* 106, 16–22. doi: 10.1016/j.pmpp.2018.11.006

Krátká, J., and Veselý, D. (1979). Activity of pectinases, amylases, and saccharase in *Pythium* spp. *Zentralblatt fur Bakteriologie Parasitenkunde Infektionskrankheiten und Hygiene. Zweite naturwissenschaftliche Abteilung: Mikrobiologie der Landwirtschaft der Technologie und Des. Umweltschutzes.* 134, 627–632. doi: 10.1016/s0323-6056(79)80114-7

Kubicek, C. P., Starr, T. L., and Glass, N. L. (2014). Plant cell wall-degrading enzymes and their secretion in plant-pathogenic fungi. *Annu. Rev. Phytopathol.* 52, 427–451. doi: 10.1146/annurev-phyto-102313-045831

Li, Q., Wang, J., Bai, T., Zhang, M., Jia, Y. L., Shen, D. Y., et al. (2020). A *Phytophthora capsici effector* suppresses plant immunity via interaction with EDS1. *Mol. Plant Pathol.* 21, 502–511. doi: 10.1111/mpp.12912

Livak, K. J., and Schmittgen, T. D. (2001). Analysis of relative gene expression data using real-time quantitative PCR and the $2^{-\Delta\Delta CT}$ method. *Methods* 25, 402–408. doi: 10.1006/meth.2001.1262

Mwenje, E., and Ride, J. P. (1997). Pectic enzymes in the characterization of tropical Armillaria. *Plant Pathol.* 46, 341–354. doi: 10.1046/j.1365-3059.1997.d01-30.x

Najdabbasi, N., Mirmajlessi, S. M., Dewitte, K., Mänd, M., Landschoot, S., and Haesaert, G. (2022). Combination of potassium phosphite and reduced doses of fungicides encourages protection against *Phytophthora infestans* in potatoes. *Agriculture* 12, 189. doi: 10.3390/agriculture12020189

Naumann, M., Koch, M., Thiel, H., Gransee, A., and Pawelzik, E. (2020). The importance of nutrient management for potato production part II: plant nutrition and tuber quality. *Potato Res.* 63, 121–137. doi: 10.1007/s11540-019-09430-3

Oeser, B., Heidrich, P. M., Müller, U., Tudzynski, P., and Tenberge, K. B. (2002). Polygalacturonase is a pathogenicity factor in the Claviceps purpurea/rye interaction. *Fungal Genet. Biol.* 36, 176–186. doi: 10.1016/s1087-1845(02)00020-8

Ospina-Giraldo, M. D., Griffith, J. G., Laird, E. W., and Mingora, C. (2010). The cazyome of *Phytophthora* spp.: a comprehensive analysis of the gene complement coding for carbohydrate-active enzymes in species of the genus *Phytophthora*. *BMC Genom.* 11, 525. doi: 10.1186/1471-2164-11-525

Qian, H. J., Liu, X., Guo, L., Zhang, Z., Li, G. J., Yang, L., et al. (2021). Sensitivity determination of *P. infestans* to metalaxyl in spring potato planting area of Yunnan Province. *Acta Agriculturae Boreali-occidentalis Sin.* 30, 1083–1088. doi: 10.7606/j.issn.1004-1389.2021.07.016

Ramezani, Y., Taheri, P., and Mamarabadi, M. (2019). Identifica-tion of *Alternaria* spp. associated with tomato early blight in I-ran and investigating some of their virulence factors. *J. Plant Pathol.* 101, 647–659. doi: 10.1007/s42161-019-00259-w

Ramos, A. M., Gally, M., García, M. C., and Levin, L. (2010). Pectinolytic enzyme production by colletotrichum truncatum, causal agent of soybean anthracnose. *Rev. Iberoam Micol.* 27, 186–190. doi: 10.1016/j.riam.2010.06.002

Ramos, A. M., Gally, M., Szapiro, G., Itzcovich, T., Carabajal, M., and Levin, L. (2016). *In vitro* growth and cell wall degrading enzyme production by Argentinean isolates of *Macrophomina phaseolina*, the causative agent of charcoal rot in corn. *Rev. Argent Microbiol.* 48, 267–273. doi: 10.1016/j.ram.2016.06.002

Raza, W., Ghazanfar, M. U., and Hamid, M. I. (2019). Pathotype determination of *Phytophthora infestans* isolates on detached potato leaves under laboratory conditions. *Int. J. Bot. Stud.* 4, 7–12. Available online at: https://www.researchgate.net/publication/333032568.

Rogozina, E. V., Beketova, M. P., Muratova, O. A., Kuznetsova, M. A., and Khavkin, E. E. (2021). Stacking resistance genes in multiparental interspecific potato hybrids to anticipate late blight outbreaks. *Agronomy* 11, 115. doi: 10.3390/agronomy11010115

Sabbadin, F., Urresti, S., Henrissat, B., Avrova, A. O., Welsh, L. R. J., Lindley, P. J., et al. (2021). Secreted pectin monooxygenases drive plant infection by pathogenic oomycetes. *Science* 373, 774–779. doi: 10.1126/science.abj1342

Valette-Collet, O., Cimerman, A., Reignault, P., Levis, C., and Boccara, M. (2003). Disruption of *Botrytis cinerea* pectin methylesterase gene *Bcpme1* reduces virulence on several host plants. *Mol. Plant-Microbe interactions: MPMI.* 16, 360–367. doi: 10.1094/MPMI.2003.16.4.360

Wang, Y., Ma, L., Ma, Y., Tian, T., Zhang, J., Wang, H., et al. (2023). Comparative physiological and transcriptomic analyses provide insights into fruit softening in Chinese cherry [*Cerasus pseudocerasus* (Lindl.) G.Don. *Front. Plant Sci.* 14. doi: 10.3389/fpls.2023.1190061

Xue, C. Y., Zhou, R. J., Li, Y. J., Xiao, D., and Fu, J. F. (2018). Cell-wall-degrading enzymes produced in *vitro* and in *vivo* by *Rhizoctonia solani*, the causative fungus of peanut sheath blight. *Peer J.* 6, e5580. doi: 10.7717/peerj.5580

Yang, B., Yang, S., Guo, B. D., Wang, Y. Y., Zheng, W. Y., Tian, M. J., et al. (2021). The *Phytophthora* effector Avh241 interacts with host NDR1-like proteins to manipulate plant immunity. *J. Integr. Plant Biol.* 63, 1382–1396. doi: 10.1111/jipb.13082

Zhu, L. D., Xu, J., Yang, Z. H., Zhu, J. H., and Zhao, D. M. (2015). Inhibition effect of five fungicides on spore germination of *phytophthora infestans*. *Hubei Agric. Sci.* 54, 1097–1101. doi: 10.14088/j.cnki.issn0439-8114

Zou, H. S., Song, X., Zou, L. F., Yuan, L., Li, Y. R., Guo, W., et al. (2012). EcpA, an extracellular protease, is a specific virulence factor required by *Xanthomonas oryzae* pv. *oryzicola* but not by *X. oryzae* pv. *oryzae* in rice. *Microbiol. (Reading England)* 158, 2372–2383. doi: 10.1099/mic.0.059964-0

frontiers | Frontiers in Plant Science

TYPE Brief Research Report
PUBLISHED 04 December 2024
DOI 10.3389/fpls.2024.1472536

OPEN ACCESS

EDITED BY
Choong-Min Ryu,
Korea Research Institute of Bioscience and Biotechnology (KRIBB), Republic of Korea

REVIEWED BY
Erik H. A. Rikkerink,
The New Zealand Institute for Plant and Food Research Ltd, New Zealand
Huamin Chen,
Chinese Academy of Agricultural Sciences, China

*CORRESPONDENCE
Ofere Francis Emeriewen
ofere.emeriewen@julius-kuehn.de

RECEIVED 29 July 2024
ACCEPTED 30 October 2024
PUBLISHED 04 December 2024

CITATION
Emeriewen OF, Zetzsche H, Wöhner TW, Flachowsky H and Peil A (2024) A putative gene-for-gene relationship between the *Erwinia amylovora* effector gene *eop1* and the *FB_Mar12* resistance locus of *Malus* ×*arnoldiana* accession MAL0004. *Front. Plant Sci.* 15:1472536. doi: 10.3389/fpls.2024.1472536

A putative gene-for-gene relationship between the *Erwinia amylovora* effector gene *eop1* and the *FB_Mar12* resistance locus of *Malus* ×*arnoldiana* accession MAL0004

Ofere Francis Emeriewen[1]*, Holger Zetzsche[2], Thomas Wolfgang Wöhner[1], Henryk Flachowsky[1] and Andreas Peil[1]

[1]Julius Kühn-Institut (JKI), Federal Research Centre for Cultivated Plants, Institute for Breeding Research on Fruit Crops, Dresden, Germany, [2]Julius Kühn-Institut (JKI), Federal Research Centre for Cultivated Plants, Institute for Resistance Research and Stress Tolerance, Quedlinburg, Germany

The bacterial pathogen *Erwinia amylovora* causes fire blight on rosaceous plants, including apples and their wild relatives. The pathogen uses the type III secretion pathogenicity island to inject effector proteins, such as Eop1, into host plants, leading to disease phenotypes in susceptible genotypes. In contrast, resistant genotypes exhibit quantitative resistance associated with genomic regions and/or R-gene-mediated qualitative resistance to withstand the pathogen. In *Malus*, strong resistance is observed in some wild species accessions, for example, in *Malus xarnoldiana* accession MAL0004. The resistance locus *FB_Mar12*, previously identified on linkage group 12 (LG12) of MAL0004, is one of two gene loci in *Malus* proven to withstand highly virulent North American strains of *E. amylovora*. This suggests the influence of a major gene, with a few candidate genes proposed within the *FB_Mar12* region. In this report, we provide evidence that this gene locus is completely broken down by a mutant strain of the *E. amylovora* effector protein Eop1 (Δ*eop1*) following artificial shoot inoculations of an 'Idared' × MAL0004 F_1 progeny set, indicating a gene-for-gene interaction. Interestingly, Δ*eop1* does not overcome the resistance of the *FB_Mar12* donor MAL0004 itself, but only the QTL on LG12, an indication that other resistance factors, possibly QTLs/genes are contributing to the fire blight resistance of MAL0004.

KEYWORDS

apple wild species, fire blight, resistance QTL, resistance-breakdown, *Malus* hosts

Introduction

Fire blight is the most destructive bacterial disease of apples (*Malus domestica* Borkh.) and other rosaceous plants, causing huge economic losses (Norelli et al., 2003; Hasler et al., 2002). The causal pathogen, *Erwinia amylovora* (Burrill) (Winslow et al., 1920), enters hosts through flowers or wounds on vegetative tissues and deposits effectors via the hypersensitive response and pathogenicity (*hrp*) type III secretion system (T3SS), resulting in disease in susceptible hosts (Oh et al., 2005; Oh and Beer, 2005; Yuan et al., 2021). Effector proteins secreted and translocated by *E. amylovora* via the T3SS include DspA/E, AvrRpt2$_{EA}$, HopPtoC$_{EA}$, Eop1, and Eop3 (Oh and Beer, 2005; Zhao, 2014; McNally et al., 2015) among other virulence factors and helper proteins (Piqué et al., 2015; Yuan et al., 2021). From the host perspective, genomic regions associated with fire blight resistance have been described in both wild and cultivated apple genotypes (Peil et al., 2021). However, wild apple genotypes exhibit the strongest resistance effects against *E. amylovora* in *Malus*, with candidate resistance genes underlying these regions identified only in wild species (Emeriewen et al., 2019). For example, resistance has been associated with linkage group 3 (LG3) of *Malus xrobusta* 5 (Mr5) (Peil et al., 2007; Fahrentrapp et al., 2013), on LG12 of the ornamental cultivar 'Evereste' (Durel et al., 2009; Parravicini et al., 2011), on LG10 of *Malus fusca* MAL0045 (Emeriewen et al., 2014, 2018, 2022), and on LG12 of *Malus xarnoldiana* MAL0004 (Emeriewen et al., 2017, 2021).

Furthermore, resistance to *E. amylovora* is strain-dependent (Vogt et al., 2013; Wöhner et al., 2018). Vogt et al. (2013) demonstrated that strains with a single nucleotide polymorphism (SNP) at position 156 of the amino acid sequence of the *E. amylovora* effector AvrRpt2$_{EA}$ differ in virulence on Mr5. For example, Ea222, which carries cysteine at this position, is avirulent on Mr5, whereas Ea3049, which carries serine, is virulent and can break down the resistance of Mr5. Peil et al. (2011) also showed that Ea3049 completely broke down the resistance QTL on LG3 of Mr5. Similarly, the deletion of the *E. amylovora* effector gene *avrRpt2$_{EA}$* in a wild-type strain, Ea1189 (Δ*avrRpt2$_{EA}$*), led to the breakdown of Mr5 resistance (Vogt et al., 2013) and the resistance gene *FB_MR5*, which underlies the resistance region on LG3 of Mr5 (Broggini et al., 2014). This provided the first evidence of a gene-for-gene relationship between a *Malus* host and the *E. amylovora* pathosystem (Vogt et al., 2013). Furthermore, Wöhner et al. (2018) demonstrated that the wild-type strain Ea1189 did not lead to disease symptoms on 'Evereste', *M. floribunda* 821 (Mf821), and *M. xarnoldiana* MAL0004—three donors of fire blight resistance that map to the distal end of LG12 (Durel et al., 2009; Emeriewen et al., 2017). Nevertheless, the deletion of the *E. amylovora* effector gene *eop1* (Δ*eop1*) in this wild-type strain led to considerable disease symptoms on 'Evereste' and Mf821, but not on *M. xarnoldiana* MAL0004. This suggests gene-for-gene relationships between *eop1* of *E. amylovora* and the fire blight resistance genes of 'Evereste' and Mf821, respectively (Wöhner et al., 2018).

In this brief research report, we confirm that the deletion mutant strain, Δ*eop1*, causes disease on Mf821 but not on MAL0004. However, we report that inoculating the F_1 progeny of MAL0004, derived from crosses with the apple cultivar 'Idared' (Emeriewen et al., 2017), with Δ*eop1* leads to the complete breakdown of the resistance QTL of LG12 of MAL0004. We discuss the implications of these results.

Methods

Plant material

As previously reported, 'Idared' was crossed with MAL0004 to establish an F_1 progeny designated as the 07240 population, which was used to identify the resistance region on LG12 associated with the fire blight resistance of MAL0004 (Emeriewen et al., 2017, 2021). This population, maintained in the orchard of the Julius Kühn Institute, Institute for Breeding Research on Fruit Crops in Dresden-Pillnitz (Germany), served as the basis for this study.

Artificial shoot inoculations

We inoculated the 07240 progeny with the same Δ*eop1*-deletion mutant strain reported in Wöhner et al. (2018). Between six and 10 replicates of 102 individuals from the 07240 population were grafted on rootstock M111 and grown in the greenhouse under conditions of 25°C–27°C during the day, 20°C at night, and 85% air humidity, with normal day and night lighting conditions. Inoculation was performed on plants by cutting the youngest leaves with a pair of scissors dipped in an inoculum with a bacterial concentration of 10^9 cfu/ml. Both parents of the 07240 population, 'Idared' and MAL0004, as well as Mf821, were included as controls. Shoot length and lesion length (in cm) of the replicates for each genotype were measured 28 days postinoculation (dpi). The percent lesion length (PLL) per shoot was calculated from the data, and the average PLL for each genotype was determined for further analysis.

Mapping analyses

We employed the molecular marker data of the 07240 individuals for LG12 previously reported (Emeriewen et al., 2017, 2021) for mapping analyses. The genetic map of LG12 of MAL0004 was recreated with 114 F_1 individuals using JoinMap 4.0 (Van Ooijen, 2018). The phenotypic data of these same individuals for the Δ*eop1* strain generated in this study and data for two other strains, Ea222 and Ea3049 (Emeriewen et al., 2017), as well as their LG12 marker data, were used for QTL analysis via Kruskal–Wallis analysis and interval mapping on MapQTL software 5 (Van Ooijen, 2004).

Results

Artificial shoot inoculations

We observed and recorded an average lesion length of 1.7% for MAL0004, the resistant parent, based on five replicates, which showed

no disease symptoms and one replicate with disease symptoms of 10.4%. 'Idared', the susceptible parent, on the other hand, showed 90.9% average disease, with most replicates showing 100% lesions. The other control genotype, Mf821, showed 23.2% average disease. Figure 1A shows the phenotype distribution of 102 progeny of the 07240 population that were phenotyped with Δ*eop1*. Of these individuals, only two displayed no disease symptoms, while the overall average PLL was 35.7. To compare the results of Δ*eop1* and two other strains (Ea222 and Ea3049) previously used to inoculate the progeny, we used 77 progeny that possessed phenotypic data for the three strains. The direct comparison showed that only one individual showed no symptom to Δ*eop1*, whereas for Ea222 and Ea3049 (data from Emeriewen et al., 2017), 11 and seven individuals, respectively, showed no symptoms (Figure 1B). For these 77 individuals, the average PLL with Δ*eop1* was 35.9, whereas it was 32.0 and 69.9 for Ea222 and Ea3049, respectively (Figure 1B).

Mapping analyses

The 14 markers that map to LG12 of MAL0004 (Emeriewen et al., 2017), along with two additional markers used for fine mapping the *FB_Mar12* region (Emeriewen et al., 2021), totaled 16 markers for recreating the LG12 genetic map of MAL0004. The recreated genetic map measured 36.74 cM, compared to 34.29 cM reported by Emeriewen et al. (2017), attributed to the inclusion of the two additional markers and different progeny sizes used in the analyses. However, the order of the markers remained the same.

The genotypic data from the 114 individuals used to generate the map, along with the phenotypic data for 102 of these individuals that included Δ*eop1* data, as well as data for Ea222 and Ea3049 (Emeriewen et al., 2017), were used for marker-phenotype analyses and QTL mapping. The Kruskal–Wallis analysis (Table 1) revealed a significant correlation between the LG12 markers and resistance to Ea222 and Ea3049, but not to Δ*eop1*. The strongest significance (*K*-value = 57.2) for Ea222 was observed for markers flanking and co-segregating with *FB_Mar12*, specifically CHFBE01, CHFBE02, and CHFBE08 (Emeriewen et al., 2021). The strength of the significance of these markers weakened but remained relevant with Ea3049 (*K*-value = 31.9) and completely disappeared for Δ*eop1* (*K*-value = 1.2).

QTL analysis via interval mapping (Figure 2) showed that the major QTL on LG12 of MAL0004 was detected using data from Ea222 and Ea3049, but not with Δ*eop1*. The markers that significantly correlated with resistance to Ea222 and Ea3049 showed a LOD score of > 16 for both strains, while they showed almost zero for Δ*eop1*. All markers on LG12, including those within the *FB_Mar12* region, had < 1 LOD score (Figure 2), confirming the complete breakdown of the QTL and associated genes in this region by Δ*eop1*.

Discussion

Inoculation of host plants with mutant strains of *E. amylovora* where T3SS effector genes are disrupted is an effective approach to determine several putative interactions between the pathogen and its hosts (Zhao et al., 2006; Vogt et al., 2013; Wöhner et al., 2014, 2018). The deletion of the entire T3SS in a wild-type strain of *E. amylovora* (Δ*T3SS*) proved its loss of function, as virulence was abolished in this mutant, resulting in no disease in known susceptible apple hosts and thereby confirming the T3SS as essential for *E. amylovora* pathogenicity (Wöhner et al., 2018). Similarly, the deletion of *E. amylovora* effector genes provides evidence of gene-for-gene relationships (Flor, 1971), as it reveals dominant avirulence genes in the pathogen that correspond to dominant resistance genes in the host. The absence of these avirulence genes is required for a compatible relationship between pathogen and host. For instance, the *E. amylovora* mutant strain ZYRKD3-1, with a disrupted $avrRpt2_{EA}$ effector gene, resulted in an average disease necrosis of 52.4% on Mr5, whereas a wild-type strain caused zero necrosis on Mr5 (Vogt et al., 2013). This breakdown of Mr5 resistance confirms a gene-for-gene relationship within the Mr5–*E. amylovora* pathosystem, with $avrRpt2_{EA}$ acting as the avirulence gene. Broggini et al. (2014) further validated this relationship by showing that transgenic 'Gala' plants overexpressing *FB_MR5*—the fire blight resistance gene of Mr5—were resistant to wild-type strains Ea222 and Ea1189 (with average necrosis between 0% and 4%), yet became susceptible to the $avrRpt2_{EA}$ effector mutant ZYRKD3-1 (average necrosis between 26.9% and 49.9%).

In a previous study, Wöhner et al. (2018) showed that the wild-type strain Ea1189 caused no disease on MAL0004 and Mf821, with both genotypes showing 0 and 0.3% average disease; however, an Δ*eop1* mutant of this same strain caused disease (35.1%) on Mf821 but not on MAL0004 (0.1%). Mf821 and MAL0004 are both donors of fire blight resistance QTLs located at the distal end of LG12 (Durel et al., 2009; Emeriewen et al., 2017). In the current study, we inoculated the 07240 F_1 progeny of 'Idared' × MAL0004 with Δ*eop1* including both parents and Mf821 as controls. The results obtained confirmed the results of Wöhner et al. (2018) as Δ*eop1* caused disease on Mf821 but not on MAL0004. This confirms that the mechanism of fire blight resistance in both wild genotypes is different. Although MAL0004 was very resistant to Δ*eop1*, only two individuals of the entire F_1 progeny showed no disease symptoms (strong resistant phenotype) in comparison to inoculation results from this same F_1 progeny with Ea222 and Ea3049, where 11 and seven individuals, respectively, showed no disease symptoms (Emeriewen et al., 2017).

Interestingly, the Δ*eop1* strain resulted in the complete breakdown of the fire blight resistance QTL of MAL0004 on LG12, which was previously identified by Emeriewen et al. (2017) following artificial shoot inoculation of 116 F_1 progeny with *E. amylovora* strains Ea222 and Ea3049. The QTL region was delimited from a 5.6 cM region to 0.67 cM in fine mapping studies using 892 progeny, leading to the identification of candidate genes within this locus, designated as *FB_Mar12* (Emeriewen et al., 2021). Using data from Emeriewen et al. (2017), we detected the locus on LG12 with Ea222 and Ea3049 in 114 progeny in the current study. However, the complete

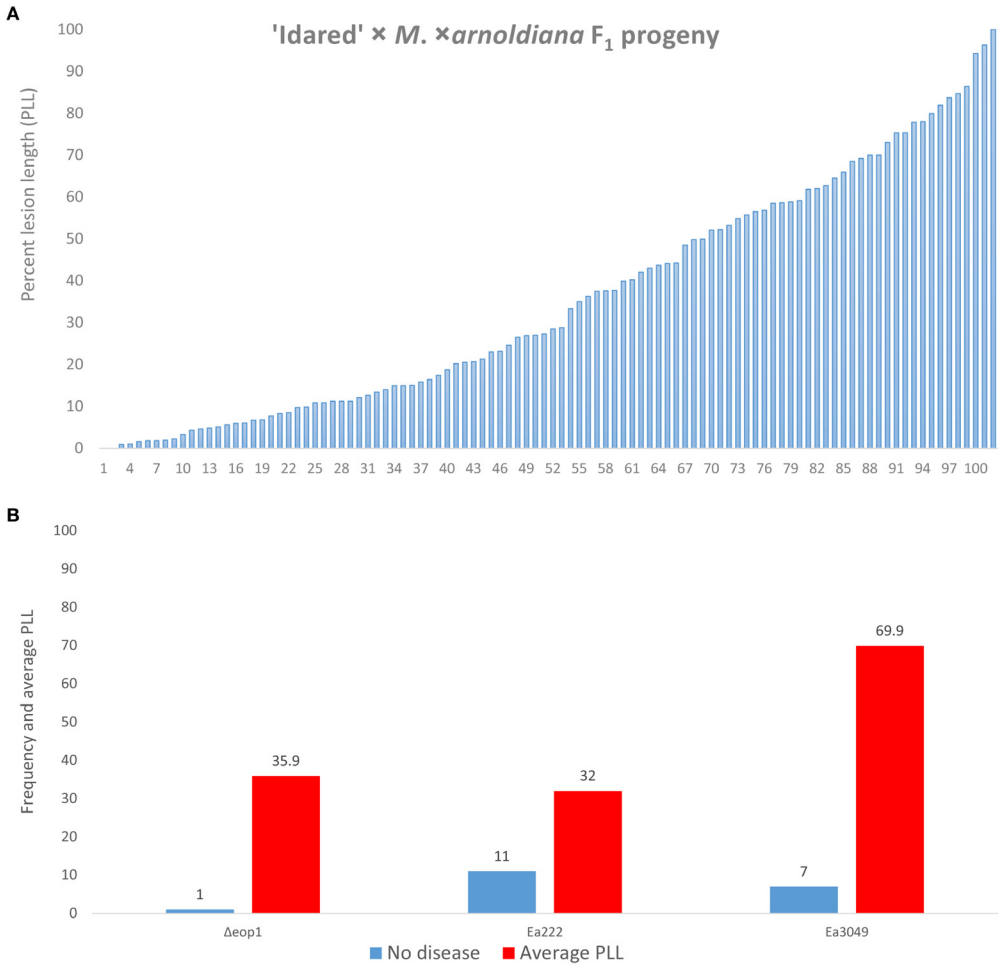

FIGURE 1
Distribution of resistance/susceptibility of 102 'Idared' × *M. xarnoldiana* progeny inoculated with *E. amylovora* Δ*eop1* **(A)**. A direct comparison of 77 progeny with phenotypic data for Δ*eop1* (current study) and Ea222 and Ea3049 (data from Emeriewen et al., 2017) showing the number of individuals exhibiting complete resistant phenotype (no disease) and the average percent lesion for these individuals **(B)**.

breakdown of this locus by Δ*eop1* strongly indicates a gene-for-gene interaction between the Eop1 effector of *E. amylovora* and the resistance gene underlying the *FB_Mar12* locus. In addition, the fact that Δ*eop1* does not overcome the resistance of MAL0004 itself, yet completely breaks down *FB_Mar12*, suggests that other resistance factors may play key and/or contributory roles in the resistance of MAL0004. This hypothesis is supported by the findings of Durel et al. (2009), who found a minor QTL on LG15 in addition to the major QTL on LG12 in 'Evereste'. A genome-wide saturated genetic map of MAL0004 is required to further elucidate its fire blight resistance.

The putative gene-for-gene interaction identified in this study differs from that described between Mr5 and the *avrRpt2*$_{EA}$ effector gene of *E. amylovora* in that the resistance donor, Mr5, was also overcome, along with the responsible resistance gene (Vogt et al., 2013; Broggini et al., 2014). The situation with Mr5 provides a strong precedent, suggesting that since the resistance of Mf821 is broken down by Δ*eop1*, as initially shown by Wöhner et al. (2018) and supported in the current study, it is highly probable that the responsible resistance gene locus on LG12 (Durel et al., 2009) could also be broken down. A similar situation may apply to the ornamental cultivar 'Evereste', whose resistance was also overcome by Δ*eop1* (Wöhner et al., 2018). This suggests that the resistance QTLs described in all three wild genotypes are overcome by Δ*eop1*, raising the question of whether the QTLs on LG12 are the same or allelic. All three QTLs are located within the same region on LG12, below the SSR marker Hi07f01 (Figure 2), which is a common marker shared in their respective genetic maps (Durel et al., 2009; Emeriewen et al., 2017). In addition, *FB_Mar12* co-segregates with CHFBE02, which also co-segregates with the 'Evereste' gene locus, *FB_E*, and is closely associated with CHFBE01 and CHFBE08 (Parravicini et al., 2011; Emeriewen et al., 2021). Mf821 possesses the same allele sizes as the alleles of the markers linked to resistance (data not shown). Therefore, it is plausible that MAL0004, 'Evereste', and Mf821 share the same resistance allele on LG12. However, our results clearly indicate that

10.3389/fpls.2024.1472536

TABLE 1 Kruskal–Wallis analysis of linkage group 12 of *Malus xarnoldiana* using two wild-type *Erwinia amylovora* strains and the Δ*eop1* mutant.

Map position	Locus	Ea222		Ea3049		*Δeop1*	
		K[a]	Signif.	K[a]	Signif.	K[a]	Signif.
0	CH04g04	13.8	******	9.6	****	3.1	*
6.41	CH01g12	20.9	*******	14.2	******	4.3	**
16.78	CH01f02	27.8	*******	19.5	*******	0.5	–
19.25	CH03c02	33.3	*******	22.5	*******	1.9	–
28.08	FRMb251	37.5	*******	20.7	*******	0.3	–
30.67	Hi07f01	46.6	*******	21.3	*******	0.3	–
30.67	FRMb103x	46.6	*******	21.3	*******	0.3	–
30.67	FRMb108y	46.6	*******	21.3	*******	0.3	–
34.95	FRMb31M87	54.7	*******	31.9	*******	1.2	–
34.95	FRMb32M04b	54.7	*******	31.9	*******	1.2	–
35.84	CHFBE08	57.2	*******	31.9	*******	1.2	–
35.84	CHFBE02	57.2	*******	31.9	*******	1.2	–
35.84	CHFBE01	57.2	*******	31.9	*******	1.2	–
36.73	FRMb533	53.2	*******	30.5	*******	1.4	–
36.73	FRMb197	53.2	*******	30.5	*******	1.4	–
36.75	FRMb199	52.5	*******	29.7	*******	1.2	–

[a]Value of Kruskal–Wallis analysis (significance levels: **0.05, ****0.005, *******0.0001). *LOD*, logarithm of the odds.

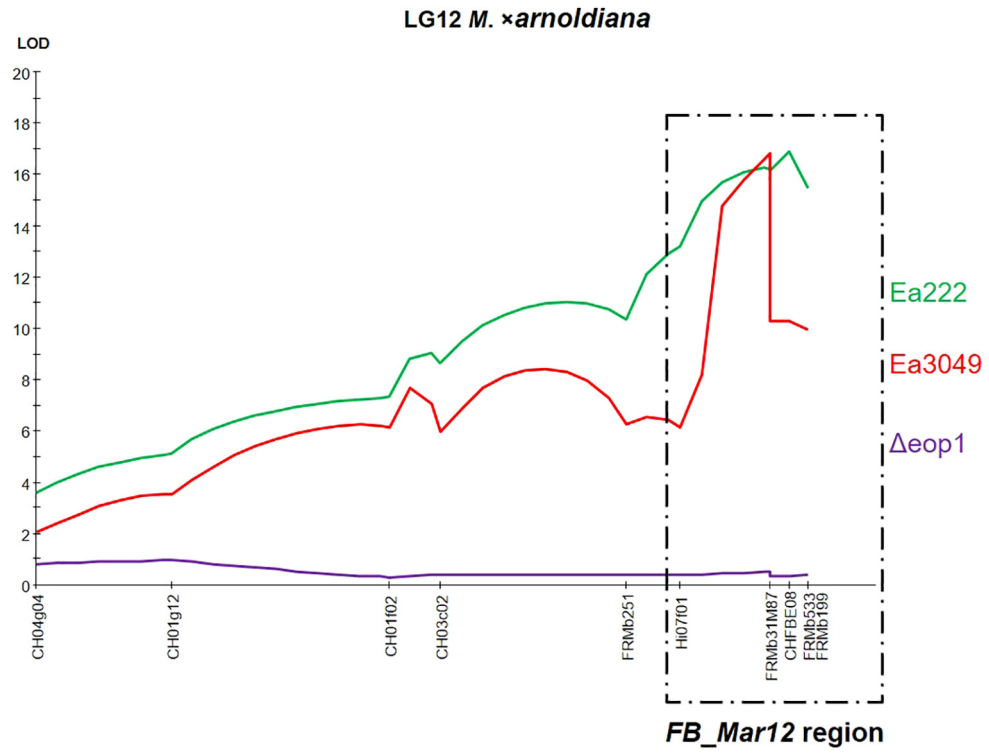

FIGURE 2
LOD score plot for the necrosis trait along LG12 of *M. xarnoldiana*, based on phenotypic data from the F_1 progeny of 'Idared' × *M. xarnoldiana* MAL0004 inoculated with Ea222 and Ea3049 (Emeriewen et al., 2017), and Δ*eop1* (current study), as determined by interval mapping. The *FB_Mar12* region is highlighted with a dotted box at the distal end of the linkage group.

there is another resistance factor expressed in MAL0004 but not in Mf821 or Evereste, which makes MAL0004 itself resistant to Δ*eop1*.

In summary, while we present strong evidence of a gene-for-gene interaction between the *E. amylovora* effector gene *eop1* and *FB_Mar12* on LG12, several missing links remain in fully elucidating the resistance mechanisms of *M. xarnoldiana* MAL0004 and the other donors of resistance at the distal end of LG12. Several open and interesting research questions remain concerning *E. amylovora* and host interactions (Rezzonico et al., 2024), not least the implications for the management of the disease and host resistance breeding (Zeng et al., 2024).

Data availability statement

The original contributions presented in the study are included in the article/supplementary material. Further inquiries can be directed to the corresponding author.

Author contributions

OFE: Conceptualization, Data curation, Formal analysis, Investigation, Methodology, Writing – original draft, Writing – review & editing. HZ: Formal analysis, Validation, Writing – review & editing. TWW: Conceptualization, Formal analysis, Writing – review & editing. HF: Conceptualization, Resources, Writing – review & editing. AP: Conceptualization, Data curation, Investigation, Resources, Validation, Writing – review & editing.

Funding

The author(s) declare that no financial support was received for the research, authorship, and/or publication of this article.

Acknowledgments

We are grateful to the orchard and greenhouse staff of JKI at the Dresden-Pillnitz and Quedlinburg locations for their technical assistance.

Conflict of interest

The authors declare that the research was conducted in the absence of any commercial or financial relationships that could be construed as a potential conflict of interest.

Publisher's note

References

Broggini, G. A., Wöhner, T., Fahrentrapp, J., Kost, T. D., Flachowsky, H., Peil, A., et al. (2014). Engineering fire blight resistance into the apple cultivar 'Gala' using the *FB_MR5* CC-NBS-LRR resistance gene of *Malus* x*robusta* 5. *Plant Biotechnol. J.* 12, 728–733. doi: 10.1111/pbi.12177

Durel, C. E., Denance, C., and Brisset, M. N. (2009). Two distinct major QTL for resistance to fire blight co-localize on linkage group 12 in apple genotypes 'Evereste' and *Malus floribunda* clone 821. *Genome* 52, 139–147. doi: 10.1139/G08-111

Emeriewen, O., Richter, K., Killian, A., Zini, E., Hanke, M.-V., Malnoy, M., et al. (2014). Identification of a major quantitative trait locus for resistance to fire blight in the wild apple species Malus fusca. *Mol. Breed.* 34, 407–419. doi: 10.1007/s11032-014-0043-1

Emeriewen, O. F., Peil, A., Richter, K., Zini, E., Hanke, M.-V., and Malnoy, M. (2017). Fire blight resistance of *Malus* ×*arnoldiana* is controlled by a quantitative trait locus located at the distal end of linkage group 12. *Eur. J. Plant Pathol.* 148, 1011–1018. doi: 10.1007/s10658-017-1152-6

Emeriewen, O. F., Piazza, S., Cestaro, A., Flachowsky, H., Malnoy, M., and Peil, A. (2022). Identification of additional fire blight resistance candidate genes following MinION Oxford Nanopore sequencing and assembly of BAC clone spanning the Malus fusca resistance locus. *J. Plant Pathol.* 104, 1509–1516. doi: 10.1007/s42161-022-01223-x

Emeriewen, O. F., Richter, K., Flachowsky, H., Malnoy, M., and Peil, A. (2021). Genetic analysis and fine mapping of the fire blight resistance locus of *Malus* ×*arnoldiana* on linkage group 12 reveal first candidate genes. *Front. Plant Sci.* 12, 667133. doi: 10.3389/fpls.2021.667133

Emeriewen, O. F., Richter, K., Piazza, S., Micheletti, D., Broggini, G. A. L., Berner, T., et al. (2018). Towards map-based cloning of *FB_Mfu10*: Identification of a receptor-like kinase candidate gene underlying the *Malus fusca* fire blight resistance locus on linkage group 10. *Mol. Breed.* 38, 106. doi: 10.1007/s11032-018-0863-5

Emeriewen, O. F., Wöhner, T., Flachowsky, H., and Peil, A. (2019). *Malus* hosts–*Erwinia amylovora* interactions: strain pathogenicity and resistance mechanisms. *Front. Plant Sci* 10. doi: 10.3389/fpls.2019.00551

Fahrentrapp, J., Broggini, G. A. L., Kellerhals, M., Peil, A., Richter, K., Zini, E., et al. (2013). A candidate gene for fire blight resistance in *Malus* × *robusta* 5 is coding for a CC-NBS-LRR. *Tree Genet. Genomes* 9, 237–251. doi: 10.1007/s11295-012-0550-3

Flor, H. H. (1971). Current status of the gene-for-gene concept. *Annu. Rev. Phytopathol.* 9, 275–296. doi: 10.1146/annurev.py.09.090171.001423

Hasler, T., Schaerer, H. J., Holliger, E., Vogelsanger, J., Vignutelli, A., and Schoch, B. (2002). Fire blight situation in Switzerland. *Acta Hortic.* 590, 73–79. doi: 10.17660/ActaHortic.2002.590.8

McNally, R. R., Zhao, Y., and Sundin, G. W. (2015). Towards understanding fire blight: virulence mechanisms and their regulation in *Erwinia amylovora*. *Bacteria-plant interactions: advanced Res. Future Trends*, 61–82. doi: 10.21775/9781908230584

Norelli, J. L., Jones, A. L., and Aldwinkle, H. S. (2003). Fire blight management in the twenty-first century – using new technologies that enhance host resistance in apple. *Plant Dis.* 87, 756–765. doi: 10.1094/PDIS.2003.87.7.756

Oh, C.-S., and Beer, S. V. (2005). Molecular genetics of *Erwinia amylovora* involves in the development of fire blight. *FEMS Microbio. Lett.* 253, 185–192. doi: 10.1016/j.femsle.2005.09.051

Oh, C. S., Kim, J. F., and Beer, S. V. (2005). The Hrp pathogenicity island of *Erwinia amylovora* and identification of three novel genes required for systemic infection. *Mol. Plant Pathol.* 6, 125–138. doi: 10.1111/j.1364-3703.2005.00269.x

Parravicini, G., Gessler, C., Denance, C., Lasserre-Zuber, P., Vergne, E., Brisset, M. N., et al. (2011). Identification of serine/threonine kinase and nucleotide-binding-site-leucine-rich repeat (NBS-LRR) genes in the fire blight resistance quantitative trait locus of apple cultivar 'Evereste'. *Mol. Plant Pathol.* 12, 493–505. doi: 10.1111/j.1364-3703.2010.00690.x

Peil, A., Emeriewen, O. F., Khan, A., Kostick, S., and Malnoy, M. (2021). Status of fire blight resistance breeding in *Malus*. *J. Plant Pathol.* 103, 3–12. doi: 10.1007/s42161-020-00581-8

Peil, A., Flachowsky, H., Hanke, M.-V., Richter, K., and Rode, J. (2011). Inoculation of *Malus* ×*robusta* 5 progeny with a strain breaking resistance to fire blight reveals a minor QTL on LG5. *Acta Hortic.* 896, 357–362. doi: 10.17660/ActaHortic.2011.896.49

Peil, A., Garcia-Libreros, T., Richter, K., Trognitz, F. C., Trognitz, B., Hanke, M. V., et al. (2007). Strong evidence for a fire blight resistance gene of *Malus robusta* located on linkage group 3. *Plant Breed.* 126, 270–475. doi: 10.1111/j.1439-0523.2007.01408.x

Piqué, N., Miñana-Galbis, D., Merino, S., and Tomás, J. M. (2015). Virulence factors of *Erwinia amylovora*: a review. *Int. J. Mol. Sci.* 16, 12836–12854. doi: 10.3390/ijms160612836

Rezzonico, F., Emeriewen, O. F., Zeng, Q., Peil, A., Smits, T. H., and Sundin, G. W. (2024). Burning questions for fire blight research: I. Genomics and evolution of *Erwinia amylovora* and analyses of host-pathogen interactions. *J. Plant Pathol.* 106, 1–14. doi: 10.1007/s42161-023-01581-0

Van Ooijen, J. W. (2004). *MapQTL® 5 Software for the mapping of quantitative trait loci in experimental populations* (Wageningen, the Netherlands: Plant Research International).

Van Ooijen, J. W. (2018). *JoinMap ® 5, software for the calculation of genetic linkage maps in experimental populations of diploid species* (Wageningen, Netherlands: Kyazma B.V).

Vogt, I., Wöhner, T., Richter, K., Flachowsky, H., Sundin, G. W., Wensing, A., et al. (2013). Gene-for-gene relationship in the host-pathogen system *Malus* x*robusta* 5-*Erwinia amylovora*. *New Phytol.* 197, 1262–1275. doi: 10.1111/nph.12094

Winslow, C. E. A., Broadhurst, J., Buchanan, R. E., Krumwiede, C., Rogers, L. A., and Smith, G. H. (1920). The families and genera of the bacteria. Final report of the Committee of the Society of American Bacteriologists on the characterization and classification of bacterial types. *J. Bacteriol.* 5, 191–229. doi: 10.1128/jb.5.3.191-229.1920

Wöhner, T. W., Flachowsky, H., Richter, K., Garcia-Libreros, T., Trognitz, F., Hanke, M. V., et al. (2014). QTL mapping of fire blight resistance in *Malus*× *robusta* 5 after inoculation with different strains of *Erwinia amylovora*. *Mol. Breed.* 34, 217–230. doi: 10.1007/s11032-014-0031-5

Wöhner, T., Richter, K., Sundin, G. W., Zhao, Y., Stockwell, V. O., Sellmann, J., et al. (2018). Inoculation of *Malus* genotypes with a set of *Erwinia amylovora* strains indicates a gene-for-gene relationship between the effector gene *Eop1* and both *Malus floribunda* 821 and *Malus* 'Evereste'. *Plant Pathol.* 67, 938–947 doi: 10.1111/ppa.12784

Yuan, X., Hulin, M. T., and Sundin, G. W. (2021). Effectors, chaperones, and harpins of the Type III secretion system in the fire blight pathogen *Erwinia amylovora*: a review. *J. Plant Pathol.* 103, 25–39. doi: 10.1007/s42161-020-00623-1

Zeng, Q., Emeriewen, O. F., Rezzonico, F., Sundin, G. W., and Peil, A. (2024). Burning questions for fire blight research: II. Critical next steps in disease management and in host resistance breeding of apple and pear. *J. Plant Pathol* 106, 811–822. doi: 10.1007/s42161-024-01678-0

Zhao, Y. (2014). "Genomics of *Erwinia amylovora* and related *Erwinia* species associated with pome fruit trees," in *Genomics of plant-associated bacteria* (Springer Berlin Heidelberg, Berlin, Heidelberg), 1–36.

Zhao, Y. F., He, S. Y., and Sundin, G. W. (2006). The *Erwinia amylovora avrRpt2*(EA) gene contributes to virulence on pear and AvrRpt2(EA) is recognized by *Arabidopsis* RPS2 when expressed in *Pseudomonas syringae*. *Mol. Plant–Microbe Interact.* 19, 644–654. doi: 10.1094/MPMI-19-0644

Frontiers in Plant Science

Cultivates the science of plant biology and its applications

The most cited plant science journal, which advances our understanding of plant biology for sustainable food security, functional ecosystems and human health.

Discover the latest Research Topics

See more →

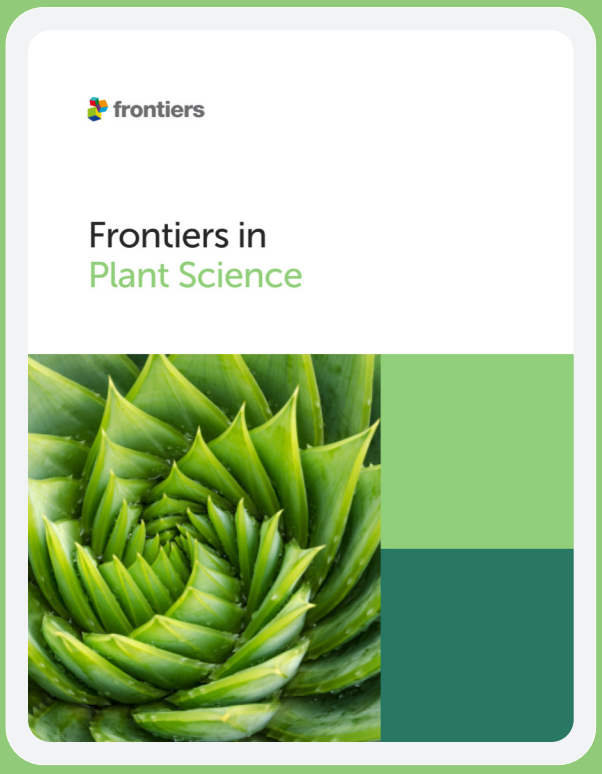

Frontiers

Avenue du Tribunal-Fédéral 34
1005 Lausanne, Switzerland
frontiersin.org

Contact us

+41 (0)21 510 17 00
frontiersin.org/about/contact